

Technical Report 2037 April 2015

A Methodology for Assessing the Impact of Sea Level Rise on Representative Military Installation in the Southwestern United States (RC-1703)

Bart Chadwick P. F. Wang Marissa Brand SSC Pacific

In Collaboration with

TerraCosta Consulting Group UCSD San Diego Supercomputing Center U.S. Geological Survey Moffatt & Nichol

Approved for public release.

SSC Pacific San Diego, CA 92152-5001

SSC Pacific San Diego, California 92152-5001

K. J. Rothenhaus, CAPT, USN Commanding Officer

C. A. Keeney Executive Director

ADMINISTRATIVE INFORMATION

The work described in this report work was prepared for the Strategic Environmental Research and Development Program, Alexandria, VA, by the Environmental Sciences Branch (Code 71750) of the Advanced Systems and Applied Sciences Division (Code 71700), Space and Naval Warfare Systems Center (SSC Pacific), San Diego, CA.

Released by C. Katz, Head Environmental Sciences Branch Under authority of A. Ramirez, Head Advanced Systems & Applied Sciences Division

This is a work of the United States Government and therefore is not copyrighted. This work may be copied and disseminated without restriction.

The citation of trade names and names of manufacturers in this report is not to be construed as official government endorsement or approval of commercial products or services referenced in this report.

MATLAB® is a registered trademark of The MathWorks, Inc. Arcview GIS® is a registered trademark of Environmental Systems Research Group.

ACKNOWLEDGEMENTS

This project was supported by a grant from the Department of Defense Strategic Environmental Research and Development Program (SERDP). We are indebted to the program, the guidance of our SERDP program manager Dr. John Hall, the helpful efforts of his support staff, and the critical reviews of the SERDP review panel and Scientific Advisory Board.

The project was truly made possible by the cooperation of the installations at Naval Base Coronado (NBC) and Marine Corps Base Camp Pendleton (MCBCP), both of which went out of their way to support the project and provide underlying data for the installations that supported key aspects of the project. We particularly recognize General Michael Lehnert, Mr. Lupe Armas, Mr. Stan Norquist, Mr. Jeff Paul, Ms. Megan Sayles, Mr. Mark Bonsavage and Mr. Beven Harris of MCBCP, and Captain Gary Mayes, Mr. Tim Latas, Mr. Nate Mendenhall, Mr. Terrance Smalls, Mr. Rich Johnston, Mr. Patrick McCay, and Mr. Bruce Shaffer of Naval Base Coronado (NBC) for supporting the project and providing a pathway of access to this information, as well as opportunities to communicate our findings to the installation communities. The project was also broadly facilitated by support from Commander, Navy Region Southwest, including Mr. Rene Trevino, Mr. Chris Stathos, and Mr. John Crow.

Beyond the report authors, a number of people provided contributions and support to the effort. At SSC Pacific, Bill Wild and Ernie Arias provided key administrative and contracting support to keep the effort moving forward, and Janessa McDonald and Ripan Barua provided invaluable technical assistance on the Geographic Information System (GIS) and numerical modeling efforts. A number of student interns also made contributions to the effort including Ralph Till, Olivier Frei, David Boiano, Bradley Peters, Karen Chu, Chantry Davis, and Joe Fabiana. Early stages of the development of the project and the project approach were supported by Dr. Walter Oechel of the San Diego State University Global Change Research Group, and Dr. Kevin Knuuti, Technical Director, ERDC Cold Regions Research and Engineering Laboratory. Dan Cayan, and Mary Tyree provided projections for future precipitation conditions that were used in the analysis of subaerial erosion.

EXECUTIVE SUMMARY

OBJECTIVE

The objective of the project was to develop an analysis framework and methodologies for evaluation of coastal military installation vulnerabilities and test them under prescribed scenarios of increased local mean sea level (0.5, 1.0, 1.5, and 2.0 m) over the next century. Methodologies were developed to assess the potential scope and magnitude of impacts from physical effects of flooding (wetting that occurs infrequently), inundation (wetting occurs regularly), erosion, seawater intrusion, and alteration of tidal flows. Assessment methodologies targeted potential vulnerabilities of buildings, civil infrastructure, training areas, and waterfront and coastal structures. The project focused on conditions in the southwestern United States (U.S.) and utilized the key coastal military installations at Naval Base Coronado (NBC) and Marine Corps Base Camp Pendleton (MCBCP) to test the approach.

TECHNICAL APPROACH

The technical approach for the project was organized around five tasks. The first task focused on development of a generalized sea level rise (SLR) vulnerability assessment framework for application to coastal military installations. The second task encompassed developing methods to project future trends in sea level and sea level variability, and then combining these underlying sea level characteristics into realistic assessment scenarios for a range of regional sea level conditions. In the third task, methods were developed to compile, analyze, and integrate critical biogeophysical and infrastructure data for each installation within a three-dimensional Geographic Information System (GIS) modeling environment. Using the range of scenarios developed under task two as test cases, task four focused on the development of methods to characterize the expected physical effects of SLR within the Southwest region. These results were then incorporated into the GIS modeling framework. Finally, the framework and tools developed under the first four tasks were then used in task five to explore the application of these methods to assess SLR vulnerability at the two installations.

RESULTS

The assessment framework adopted a source-pathway-receptor conceptual model in which a source is a sea-level related hazard, a pathway is the process that links a sea level related hazard and a military installation element that is subject to harm from that hazard, and a receptor is a military installation element or class of elements that is subject to harm from a sea-level related hazard. The framework reflects the evolution of the field from strategies to support broad-scale, qualitative screening assessments, toward application at regional and local scales. This enables more quantitative assessment of specific vulnerability questions at Department of Defense installations, evaluation of a range of plausible future scenarios, and identification of potential responses at the source, pathway, and receptor level.

Sea level rise projection methods were successfully developed based on a superposition of mean sea level rise (MSLR) scenarios with increases of 0.5, 1.0, 1.5, and 2.0 m by 2100 relative to 2000, astronomical tide heights, non-tide residual (NTR) water level variability from general circulation models (GCMs), and wave-driven run-up on beaches. Using these time series, robust regional scenarios were developed for water level extremes at MCBCP and NBC using extreme value methods. Geospatial basemodels of the terrestrial and marine topography were constructed for both of the installations. This included development of methods to accommodate future conditions by superimposing revised beach or beach/cliff elevation sub-models into the changed domain of the basemodel using the results of physical response models. An infrastructure model defining six key

receptor categories of training areas, buildings, civil infrastructure, waterfront structures, and coastal structures was integrated with the terrain model such that accurate locations and elevations for the infrastructure could be extracted to evaluate interactions with erosion, inundation, and flooding.

Physical response models were developed to describe exposure pathways including inundation, flooding, erosion, and seawater intrusion. Primary pathways for this study were classified by exposure under categories for exposed shorelines, protected shorelines, and groundwater. New modeling systems were developed that enabled the long-term topographic response of these beach and cliff/beach systems to SLR to be integrated with short-term storm wave response changes. Evaluation of inundation and flooding along exposed shorelines incorporated changes to the underlying elevation model due to erosion, spatially varying total water level exposures, and requirements for complete hydraulic connectivity. A density-dependent groundwater-flow and solute-transport model was used to explore the influence of seawater intrusion in the Santa Margarita River Basin at MCBCP and the resulting potential impacts to water quality and future extraction capacity.

Sea level rise vulnerability at NBC and MCBCP was assessed through application of these methodologies using two levels of analysis: receptor-level and component-level. The receptor-level methodology encompassed the breadth of the data compilation, modeling, and analysis methods and included installation- and exposure-specific SLR source scenarios, pathway-specific physical response of the coastal system, and characteristic sensitivities and operational thresholds for the installation receptors. The analysis illustrated the ability of these methods to resolve the increasing level of vulnerability of the installation to erosion as a function of increasing sea level, as well as the sensitivity of some receptors to short-term wave driven erosion events. At NBC training areas this translated into frequent (weekly return period) conditions with remaining available area reduced to about 53% of baseline for 1.0-m SLR, and further reductions to a remaining area of about 23% of baseline for 2.0-m SLR. Training areas at MCBCP are generally backed by erodible cliffs, and the landward boundary of the beach training area was allowed to retreat inland (autonomous adjustment) at the rate of retreat of the cliff base. MCBCP also had a higher underlying sand imbalance, and together these factors resulted in frequent (weekly return period) conditions with remaining area reduced to about 41% of baseline for 1.0-m SLR and further reductions to a remaining area of 27% of baseline for 2.0-m SLR. Component-level assessment examples were illustrated for NBC training areas, building, waterfront structures, coastal structures, and civil infrastructure receptor classes.

BENEFITS

Based on our objective to develop a robust analysis methodology that provides a reliable means to identify and plan for vulnerabilities under both currently projected sea level scenarios, and scenarios that may be considered in the future, a number of key accomplishments were successfully achieved. We successfully demonstrated new methodologies for the development of Southwest U.S.-relevant SLR scenarios and cyclical events and a capability to project these at 100-m increments along the shoreline. These scenarios were successfully applied to the development and application of a range of "beyond the bathtub" pathway response models that link these sea level scenarios to potential vulnerabilities to coastal military installations. Based on the projection of these physical responses, we were able to illustrate their application to an assessment of the responses of two key Southwest U.S. military installations, with an emphasis on military-specific receptors including beach training areas and waterfront infrastructure, and to contrast the results. As part of this research and development effort, a number of products were developed that served to advance the research and provided a testing ground for our methodologies. In addition, these products may serve future uses, particularly for the installations where the analysis was conducted, but also potentially as models for application to other areas with similar requirements and conditions.

CONTENTS

		IVE SUMMARY	
		/MS	
		RDS	
		BUTING AUTHORS	
1. OB	JE	CTIVE	1
2. BA	CK	GROUND	3
	2.1	VULNERABILITY FRAMEWORK	3
		2.1.1 Review of Existing Frameworks	6
		2.1.2 Framework Review Summary	
		2.1.3 Vulnerability Assessment Framework for DoD Installations	
		2.1.4 Components of the Framework	
	2.2	COASTAL SETTING	
		2.2.1 Marine Corps Base Camp Pendleton	
		2.2.2 Naval Base Coronado	
	2.3	COASTAL PROCESSES IDENTIFICATION	
		2.3.1 Sea Level	
		2.3.3 Historical Shoreline Position	
		2.3.4 Historical Cliff Erosion and Gullying	
3. MA	TF	RIALS AND METHODS	119
		SEA LEVEL RISE PROJECTIONS	
	. .	3.1.1 Mean Sea Level	
		3.1.2 Tides	
		3.1.3 Sea Level Fluctuations	
		3.1.4 Waves	128
;	3.2	DELINEATION OF THE COASTAL SYSTEM	151
		3.2.1 Terrain Data and Methods	
		3.2.2 Installation Data and Methods	
		3.2.3 Receptor Categories	
	2 2	PHYSICAL RESPONSE TO SEA LEVEL RISE	
,	ა.ა	3.3.1 Exposed Beach Shoreline Erosion – Long-Term Response	
		3.3.2 Exposed Cliff/Beach Shoreline Erosion – Long-Term Response	172 181
		3.3.3 Exposed Beach Erosion – Short-Term Response	
		3.3.4 Exposed Shorelines - Modification of Terrain Models	
		3.3.5 Exposed Shorelines – Inundation and Flooding	
		3.3.6 Protected Bays	
	. .	3.3.7 Seawater Intrusion	
į	3.4	METHOD FOR ASSESSMENT OF VULNERABILITY	
		3.4.1 Receptor-Level Vulnerability Assessment Methods	
4 55	٠	•	
		LTS AND DISCUSSION	
•	4.1	SEA LEVEL RISE PROJECTIONS	
		4.1.1 Total Water Levels	263

		4.1.2 Future Sea Level Scenarios	264
	4.2	DELINEATION OF THE COASTAL SYSTEM	274
		4.2.1 Baseline Terrain Models	274
		4.2.2 Installation Infrastructure Models	
		4.2.3 Integrated Terrain and Infrastructure Models	
	4.3	PHYSICAL RESPONSE TO SEA LEVEL RISE	
		4.3.1 Exposed Shoreline Response	328
		4.3.2 Protected Bay Response	
		4.3.3 Groundwater Response	
	4.4	APPLICATION TO THE ASSESSMENT OF VULNERABILITY	
		4.4.1 Receptor-Level Assessment – Naval Base Coronado	
		4.4.2 Receptor-Level Assessment - Marine Corps Base Camp Pendleton 4.4.3 Component-Level Assessment Examples	
		·	
5. C		LUSIONS AND IMPLICATIONS FOR FUTURE RESEARCH	
		VULNERABILITY FRAMEWORK	
	5.2	SEA LEVEL RISE PROJECTIONS	524
	5.3	COASTAL SYSTEM DELINEATION	525
	5.4	PHYSICAL RESPONSE OF THE SYSTEM	526
	5.5	ASSESSMENT OF VULNERABILITY	527
		5.5.1 Naval Base Coronado	527
		5.5.2 Marine Corps Base Camp Pendleton	529
	5.6	SUMMARY OF KEY ACCOMPLISHMENTS	529
	5.7	REMAINING GAPS	530
	5.8	SUMMARY OF KEY PRODUCTS	531
REFI	ERE	NCES	532
		ICES	
AFF		PENDIX A: SUPPORTING DATA	
	API		
		Appendix A1. Sea Level Scenarios	
		Appendix A3. Installation Infrastructure Models	
		Appendix A4. Exposed Shoreline Response – Erosion Footprints	
		Appendix A5. Exposed Shoreline Response – Elevation Models	
		Appendix A6. Exposed Shoreline Response – Inundation and Flooding	
		Footprints	550
		Appendix A7. Protected Shoreline Response – Inundation and Flooding	EEO
		Footprints	550 550
		Appendix A9. Receptor Level Response – Naval Base Coronado	
		Appendix A10. Receptor Level Response – Marine Corps Base Camp	
		Pendleton	
	API	PENDIX B: LIST OF SCIENTIFIC/TECHNICAL PUBLICATIONS	551
		Publications – Published or Submitted	551
		In Preparation	
		Planned	
	ΔΡΙ	PENDIX C: GLOSSARY	553

Figures

 2-1. Typical scales of vulnerability assessments (adapted from Nichols and Mimura, 2-2. Vulnerability analysis framework of the Common Methodology (adapted from IPCC, 1992) 2-3. The seven steps of climate impact assessment from the IPCC Technical Guidel (adapted from Carter et al., 1994) 2-4. Framework diagram for selection of methods to assess land at risk from erosior inundation (adapted from Klein and Nicholls, 1999) 2-5. Example of the six coastal subsystem index-based assessments in the South P Methodology (adapted from Center for Global Environmental Research, 1996). 2-6. Integrated vulnerability framework (adapted from Dolan and Walker, 2006) 2-7. A conceptual framework for sea level rise vulnerability (adapted from Sterr et al.) 2-8. A risk assessment and management framework for climate change impacts (ad from Jones, 2001) 2-9. The source, pathway, receptor framework for assessing sea level rise vulnerabil (adapted from NCDEM, 2009) 2-10. Ecological risk assessment framework (adapted from U.S. EPA, 1998) 2-11. A sea level rise vulnerability assessment framework for DoD Installations 2-12. Problem formulation components for ecological risk assessment (adapted from U.S. EPA, 1998) 2-13. Increasing levels of uncertainty associated with the complexity of the sea level vulnerability assessment process (adapted from Hulme and New, 2001) 2-14. Time span and time slices for the North Carolina study (adapted from NCDEM 2-15. Measured local mean sea level from the tide gauge record at Fort Point, San Fernance 	12
 2-2. Vulnerability analysis framework of the Common Methodology (adapted from IPCC, 1992)	12
 2-3. The seven steps of climate impact assessment from the IPCC Technical Guidel (adapted from Carter et al., 1994)	12
 (adapted from Carter et al., 1994)	1
 2-4. Framework diagram for selection of methods to assess land at risk from erosion inundation (adapted from Klein and Nicholls, 1999) 2-5. Example of the six coastal subsystem index-based assessments in the South P Methodology (adapted from Center for Global Environmental Research, 1996). 2-6. Integrated vulnerability framework (adapted from Dolan and Walker, 2006) 2-7. A conceptual framework for sea level rise vulnerability (adapted from Sterr et al.) 2-8. A risk assessment and management framework for climate change impacts (ad from Jones, 2001) 2-9. The source, pathway, receptor framework for assessing sea level rise vulnerability (adapted from NCDEM, 2009) 2-10. Ecological risk assessment framework (adapted from U.S. EPA, 1998) 2-11. A sea level rise vulnerability assessment framework for DoD Installations 2-12. Problem formulation components for ecological risk assessment (adapted from U.S. EPA, 1998) 2-13. Increasing levels of uncertainty associated with the complexity of the sea level vulnerability assessment process (adapted from Hulme and New, 2001) 2-14. Time span and time slices for the North Carolina study (adapted from NCDEM 2-15. Measured local mean sea level from the tide gauge record at Fort Point, San Fort	
inundation (adapted from Klein and Nicholls, 1999)	
 2-5. Example of the six coastal subsystem index-based assessments in the South P Methodology (adapted from Center for Global Environmental Research, 1996). 2-6. Integrated vulnerability framework (adapted from Dolan and Walker, 2006) 2-7. A conceptual framework for sea level rise vulnerability (adapted from Sterr <i>et al</i> 2-8. A risk assessment and management framework for climate change impacts (ad from Jones, 2001)	
Methodology (adapted from Center for Global Environmental Research, 1996). 2-6. Integrated vulnerability framework (adapted from Dolan and Walker, 2006) 2-7. A conceptual framework for sea level rise vulnerability (adapted from Sterr <i>et al</i> 2-8. A risk assessment and management framework for climate change impacts (ad from Jones, 2001)	
 2-6. Integrated vulnerability framework (adapted from Dolan and Walker, 2006)	
 2-7. A conceptual framework for sea level rise vulnerability (adapted from Sterr et al 2-8. A risk assessment and management framework for climate change impacts (ad from Jones, 2001) 2-9. The source, pathway, receptor framework for assessing sea level rise vulnerability (adapted from NCDEM, 2009) 2-10. Ecological risk assessment framework (adapted from U.S. EPA, 1998) 2-11. A sea level rise vulnerability assessment framework for DoD Installations 2-12. Problem formulation components for ecological risk assessment (adapted from U.S. EPA, 1998) 2-13. Increasing levels of uncertainty associated with the complexity of the sea level vulnerability assessment process (adapted from Hulme and New, 2001) 2-14. Time span and time slices for the North Carolina study (adapted from NCDEM 2-15. Measured local mean sea level from the tide gauge record at Fort Point, San F 	
 2-8. A risk assessment and management framework for climate change impacts (ad from Jones, 2001)	14
from Jones, 2001)	<i>I.</i> , 1999) 15
 2-9. The source, pathway, receptor framework for assessing sea level rise vulnerabin (adapted from NCDEM, 2009) 2-10. Ecological risk assessment framework (adapted from U.S. EPA, 1998) 2-11. A sea level rise vulnerability assessment framework for DoD Installations 2-12. Problem formulation components for ecological risk assessment (adapted from U.S. EPA, 1998) 2-13. Increasing levels of uncertainty associated with the complexity of the sea level vulnerability assessment process (adapted from Hulme and New, 2001) 2-14. Time span and time slices for the North Carolina study (adapted from NCDEM 2-15. Measured local mean sea level from the tide gauge record at Fort Point, San F 	dapted
(adapted from NCDEM, 2009)	15
(adapted from NCDEM, 2009)	ility
 2-10. Ecological risk assessment framework (adapted from U.S. EPA, 1998)	
 2-11. A sea level rise vulnerability assessment framework for DoD Installations 2-12. Problem formulation components for ecological risk assessment (adapted from U.S. EPA, 1998)	17
 2-12. Problem formulation components for ecological risk assessment (adapted from U.S. EPA, 1998) 2-13. Increasing levels of uncertainty associated with the complexity of the sea level vulnerability assessment process (adapted from Hulme and New, 2001) 2-14. Time span and time slices for the North Carolina study (adapted from NCDEM 2-15. Measured local mean sea level from the tide gauge record at Fort Point, San F 	18
U.S. EPA, 1998)	
 2-13. Increasing levels of uncertainty associated with the complexity of the sea level vulnerability assessment process (adapted from Hulme and New, 2001) 2-14. Time span and time slices for the North Carolina study (adapted from NCDEM 2-15. Measured local mean sea level from the tide gauge record at Fort Point, San F 	20
vulnerability assessment process (adapted from Hulme and New, 2001)	l rise
2-14. Time span and time slices for the North Carolina study (adapted from NCDEM 2-15. Measured local mean sea level from the tide gauge record at Fort Point, San F	
2-15. Measured local mean sea level from the tide gauge record at Fort Point, San F	
	•
showing the trend over the last century (based on Cayan et al., 2006)	
2-16. Combination of the observed and projected mean sea level for Fort Point, San	
extending to the year 2100 (based on Cayan <i>et al.</i> , 2008a)	
2-17. El Niño and winter storm events in 1982 co-occurring with neap tides, and in 1	
event co-occurring with spring tides (adapted from Flick, 1986)	
2-18. Tiered assessment approach from the Australian framework (adapted from	29
Commonwealth of Australia, 2006)	25
•	33
2-19. Generic conceptual model for vulnerability assessment of coastal military	27
installations.Note that local mean sea level includes vertical land movements	
2-20. Schematic of southern California fault systems that form the boundary betwee	
North American and Pacific tectonic plates located to the east and west, respectively	
MCBCP is located along the coast north of San Diego and west of Escondido,	
NBC lies just south of San Diego (adapted from Flick and Sterrett, 1984; image	
Google, SIO, NOAA, U.S. Navy, NGA, GEBCO, LDEO-Columbia, NSF, Landsa	•
2-21. Geological fault map of the southern San Diego region showing the alternating	•
high (H) and low (L) tectonically- formed topographic features including Point L	
Mission Bay, Pont Loma, and San Diego Bay (overlay courtesy of D. Inman, So	
Institution of Oceanography, University of California, San Diego; image data: G	•
SIO, NOAA, U.S. Navy, NGA, GEBCO, LDEO-Columbia, NSF, Landsat)	44
2-22. Map showing the Oceanside, Mission Bay, and Silver Strand littoral cells of	
the San Diego region. MCBCP is located in the northern part of the Oceanside	Cell,
between San Mateo Point and Oceanside Harbor. NBC is in the Silver Strand of	
the southern end of San Diego (ædapted from Flick and Sterrett, 1984; image d	
Google, SIO, NOAA, U.S. Navy, NGA, GEBCO, LDEO-Columbia, NSF, Landsa	nata:

2-23. Schematic map of MCBCP showing the major divisions of the coastline, Sections A-F and potentially vulnerable coastal facilities (adapted from U.S. Government, 2002; image data: Google, SIO, NOAA, U.S. Navy, NGA, GEBCO, DigitalGlobe, CSUMB,	
2-24. Google Earth image taken 25 May 2009 of Section A, Green Beach located about 1.5 km from the (coastal) northern boundary of MCBCP and available for recreational	47
2-25. Google Earth image taken 1 June 1994 and covering the same area of Section A,	<u>148</u>
2-26. Aerial photo of San Onofre State Beach in 1986 shows remnant beach width up to several kilometers north of SONGS from 20-years of construction activity that ended in 1985 (scale 1:12,000 California Department of Boating and Waterways Photo 220 available as California Coastal Records Project image 198610220; Copyright (C) 2002–2014 Kenneth & Gabrielle Adelman, California Coastal Records Project,	40
 www.Californiacoastline.org) 2-27. Composite of four aerial photographs of SONGS Units 2 and 3 taken near the end of construction between 4 December 1984, just before removal of the Units 2 and 3 laydown pad began (left), and 12 December 1985 (right) after beach had begun narrowing. The pad had been in place from 1974–1984. (courtesy of Southern California Edison Company; see Flick et al., 2010; note the photo orientation with ocean on the right) 	49 50
2-28. Google Earth image taken 25 May 2009 of about 4 km of coast at SONGS shows the greatly reduced beach widths at and adjacent to the power plant (see text). Note the	50
2-29. Google Earth image taken 1 February 2008 of 2 km of coast south of SONGS shows narrow, cliff-backed beach with landslides and several large gullies associated with drainage culverts and channels (see text)	51
2-30. Google Earth image taken 25 May 2009 of about 7.5 km of coast extending from north edge of Section B to Section D (see Figure 2-23) showing four helipads pads and strips	
 2-31. Google Earth image taken 3 October 1995 covering reach shown in Figure 2-30 2-32. Google Earth image taken 25 May 2009 of the LCAC facility in Section E (see text for discussion; image data: Google, USDA Farm Service Agency) 	
2-33. Oblique air photo of LCAC ramp taken 23 October 2004 and showing rough surface conditions at the end of the ramp, and a ditch from uncontrolled runoff (bottom center) in front of the tower (California Coastal Records Project Image 200407314; Copyright (C) 2002–2014 Kenneth & Gabrielle Adelman, California Coastal Records Project,	
2-34. Google Earth photo taken 25 May 2009 and showing Sections F, G, and H between the LCAC facility (upper left) and Del Mar Boat Basin including the Del Mar Beach and the adjacent recreation and housing complex, and Oceanside Harbor, (lower center) at the southern boundary of MCBCP. The Santa Margarita River (center) flows through	56
2-35. Watersheds at MCBCP (overlay original art; Image: Google, U.S. Geolocical Survey) 2-36. Groundwater sub-basins of the Santa Margarita lower basin at MCBCP (adapted from	
2-37. Geology of the Santa Margarita lower basin (adapted from San Diego State University, http://www.geology.sdsu.edu/kmlgeology/california_geology.html)	

2-38. Schematic map shows North Island, Coronado, Silver Strand, Imperial Beach, and	
Border Field facilities with amphibious boat lane (number) and beach (color)	
designations (adapted from U.S. Navy 2010; Image data: Google, SIO, NOAA, U.S.	
Navy, NGA, GEBCO, LDEO-Columbia, NSF)	61
2-39. Google Earth photo taken 25 May 2009 of NASNI including about 3.5 km of shoreline	
eastward of San Diego Bay entrance and Zuniga Jetty. Note numerous naval facilities	
along the low-lying, south-facing Breakers Beach	62
2-40. (left) Oblique developer's 1880's view of North and South Coronado in the distance	
from San Diego showing Spanish Bight wetland separating North Island from Coronad	0
(courtesy of The Bancroft Library, University of California, Berkeley); (right) Chart of	
San Diego Bay from 1857 showing North Island ("The Island") in its pre-fill condition	
with the two main island areas separated by the "Spanish Bight" (Coast Survey Office;	
http://www.coronado.ca.us/library/)	63
2-41. Google Earth photo taken 25 May 2009 showing 2.8 km of Coronado City Beach,	
Hotel Del Coronado, and the Coronado Shores high-rise condominiums	63
2-42. View to the northwest from the Hotel Del Coronado after large wave storm from the	
south caused massive beach erosion in 1905 (courtesy of the Center for Coastal	
Studies, Scripps Institution of Oceanography, University of California, San Diego)	64
2-43. Google Earth photo (25 May 2009) showing 4 km of shoreline from Hotel Del Coronac	
(upper left) to Fiddler's Cove (lower right). Note NAB Coronado bayside peninsula and	
beach development including the training areas along Silver Strand State Beach	
2-44. (left) Photo of NAB ocean-front facilities taken in 1972 (Cal Boating Image 958012	
from California Coastal Records Project); (right) photo of same area taken 19 Septemb	oer
2008 with additional construction on back beach (black boxes) and denser bayside	,
housing (California Coastal Records Project Image 200805108; Copyright (C)	
2002–2014 Kenneth & Gabrielle Adelman, California Coastal Records Project,	
www.Californiacoastline.org)	66
2-45. Photo taken from the Hotel Del Coronado cupola looking south over Silver Strand	00
in 1898 (courtesy the U.S. Grant IV collection). Note the narrow ocean beach (right)	
and over-wash fans on the bayside (left)	67
2-46. Google Earth photograph taken 25 May 2009 shows about 14 km of the southern Silv	
Strand shoreline (refer also to Figure 2-38)	69
2-47. MSLR in the past 20,000 years associated with ice-cap retreat and global warming	00
of about 8 °C (Rohde, 2013)	70
2-48. Long-term tide gauge data from Amsterdam, Brest, and Swinoujscie (Poland) indicate	
sea level rise over the past 300 years (IPCC, 2001)	 71
2-49. Annual MSL at SIO pier, La Jolla, CA (1926–2009) is representative of MCBCP and	
NBC	71
2-50. Monthly relative mean sea levels at the SIO La Jolla, CA, tide gauge station adjusted	, ,
for the inverse barometer effect (see text)	72
2-51. Map showing high rates of MSLR in the western Pacific and low rates or actual drops	
MSL in the eastern Pacific off the west coast of the Americas (Aviso, 2010)	
2-52. Relative sea level from satellite altimetry for different regions (Aviso, 2010). Note that	
1 cm/yr = 10 mm/yr = 1 m/cy (see text and Figure 2-5)	
2-53. Number of winter (November-March) hours that water levels exceed given percentile	<i>1</i> 3
	7/
thresholds (see text)	/ 4
the 95th percentile (the binomial-filtered event count, cyan curve) for at least 6 consecutive hours	7.
CONSECUTIVE HOURS	/ C

2-55.	. Duration (hours) of the 63 extreme NTR events that exceeded the 99.5th percentile	
	during the full year (red) and non-winter (April-September, blue)	76
2-56.	. PDF of NTR fluctuations relative to MSL from the La Jolla tide gauge for winter	
	(November-March) 1924–2005. Solid line is the mean and dashed lines are ±1	
	standard deviation bounds. Gray curves show individual years	76
2-57.	. Correlations of satellite altimetry sea level height monthly anomalies (AVISO) with	
	(a) the multivariate ENSO index (MEI), (b) the Pacific decadal oscillation (PDO),	
	(c) the Pacific-North America (PNA) index, and (d) the North Pacific index (see text)	78
	Schematic summary showing offshore wave exposure for the San Diego region of	
	the Southern California Bight (overlay adapted from USACE, 1988a; image data:	
	Google, SIO, NOAA, U.S. Navy, NGA, GEBCO, Landsat, LDEO-Columbia, NSF)	80
	. Oblique conceptual view of a typical California cliff-backed beach (upper A). Cross-	
	section illustrating wave-cut platform (terrace), sea cliff, and typical effects of winter	
	and summer waves on beach width (lower B) (courtesy of D.L. Inman, Scripps	
	Institution of Oceanography, University of California, San Diego)	85
	. Illustration (adapted from Gutierrez <i>et al.</i> , 2009) showing the basic parameters used	
	in the Bruun Rule (see text)	85
	Summary of the sediment budget of the Oceanside littoral cell (overlay adapted from	00
	Inman and Masters, 1991; image data: Google, SIO, NOAA, U.S. Navy, NGA, GEBCO,	
	Landsat, LDEO-Columbia, NSF). MCBCP occupies the North and Central sub-cells	
	(see text)	90
	. Summary of the sediment budget of the Silver Strand littoral cell (overlay adapted from	
	Inman and Masters 1991; image data: Google, USGS, SIO, NOAA, U.S. Navy, NGA,	
	GEBCO, LDEO-Columbia, NSF). NBC occupies most of this cell (see text)	91
	Schematic map of MCBCP shoreline shows locations and designations of available	0 1
	historical beach profile data. See Table 4-1 for profile range information (image data:	
	Google, SIO, NOAA, U.S. Navy, NGA, GEBCO, DigitalGlobe, CSUMB, SFML,	
	CA-OPC)	93
2-64	Beach profiles from MCBCP Range SO1530 (see text)	
	Shoreline position history for 1983–1989 at MCBCP Range SO1530.	
	Beach profiles from MCBCP Range SO1470	
	Shoreline position history for 1983–1989 at MCBCP Range SO1470.	
	Beach profiles from MCBCP Range PN1340	
	Shoreline position history for 1984–1989 at MCBCP Range PN1340	
	Beach profiles from MCBCP Range PN1290	
	Shoreline position history for 1984–1989 at MCBCP Range PN1290	
2-72	Beach profiles from MCBCP Range PN1280	100
	Shoreline position history for 1972–1989 at MCBCP Range PN1280	
2-74	Beach profiles from MCBCP Range PN1240	101
	Shoreline position history for 1972–1989 at MCBCP Range PN1240	
	Beach profiles from MCBCP Range PN1180	
2-70.	Shoreline position history for 1972–1989 at MCBCP Range PN1180	102
2-71.	Google Earth image shows location of SCBPS beach surveys near Range PN1180,	102
	between LCAC facility and Del Mar Boat Basin (Image data: Google, Digital Globe)	103
	. MSL shoreline position versus time for 2007–2010 about 0.5 km south of LCAC	103
		102
2.20	facility	100
2-0U.	. Unadjusted shoreline position history 1950–1989 at MCBCP Range PN1110	104
2-01.	. Adjusted shoreline position history 1950–1969 at MCBCP Range PN1110 (see text)	104
Z-0Z.	. Adjusted shoreline position history 1800–1808 at MODOF Nange FIVELIO (See text)	100

2-83	3. Schematic map of Silver Strand and Coronado shows locations of available historical	
	beach profile data.NBC, including the Naval Amphibious Base, is located at North Island	
	and along Coronado and Silver Strand. Profile range information in Table 4-2 (image date	ta:
	Google, SIO, NOAA, U.S. Navy, NGA, GEBCO, LDEO-Columbia, NSF)	106
2-84	I. Beach profile data from NBC Range SS0160	
2-85	5. Shoreline position history from 1983–2009 at NBC Range SS0160	109
2-86	6. Beach profile data from NBC Range SS0125. Note the sand borrow pit from 500 to	
_ 00	900 m offshore (see text)	109
2-87	'. Shoreline position history from 1984–1989 at NBC Range SS0125	
	B. Beach profile data from NBC Range SS0090	
	D. Shoreline position history from 1983–2009 at NBC Range SS0090	
2.00	b. Shoreline position history from 1983–2009 at NBC Range 330090	111
	. Shoreline position history from 1983–2009 at NBC Range SS0077	
	2. Early 1954–1987 beach profile data from NBC Range SS0050 (see text)	
	3. Later 2001–2009 beach profile data from NBC Range SS0050 (see text)	
	Unadjusted shoreline position from 1954–2009 at NBC Range SS0050 (see text)	
	5. Adjusted shoreline position from 1954–2009 at NBC Range SS0050 (see text)	114
2-96	6. Schematic map showing coastal cliff setting and general composition, and place	
	names (adapted from Young et al., 2014)	115
2-97	'. Map shows extent of relic and active deep-seated landslides south of SONGS. Note	
	that coastal drainages under I5 develop into gullies through the terrace to the west 1	116
2-98	B. Photo of large, deep gully at San Onofre State Beach area of MCBCP (see Figure	
	2-97 for location; California Coastal Records Project Image 200407227, October	
	2004; Copyright (C) 2002–2014 Kenneth & Gabrielle Adelman, California Coastal	
	Records Project, www.Californiacoastline.org)	117
2-99	9. Estimates of cliff retreat and gully erosion from previous studies normalized alongshore	
	A - Everts (1991) with rates adapted from USACE (1988b). B - Everts (1991) with	
	modeled toe retreat rates for 1954–1988. C - USACE (1990) adapted from USACE	
	(1988b) including some cliff erosion. D - USACE (1990) adapted from USACE (1988b)	
	and excludes cliff erosion and fine sediments	118
3-1	Flow chart of sea level rise projection components	
	Schematic of approximate amplitudes of MSLR, tides, non-tide residual (NTR) variations	
0 2.	and wave-driven runup during 21st century	
3-3	MSLR curves considered in this study plotted relative to NAVD88	121
	Typical seasonal tide curves in the San Diego region (see text)(adapted from Flick and	121
J- 4 .		127
2 5	Sterrett, 1984)	
	Time and height of predicted peak high and low tides at La Jolla 2000–2050	121
3-6.	Monthly maximum tide predictions at La Jolla 2000–2050 illustrating the important	
	periodicities1	128
3-7.	Mean (solid) and 1-sigma (dashed) non-tide water level probability density function for	
	A2 (upper) and B1 (lower) from three climate models and observations	129
3-8.	Extreme (98th percentile) non-tide fluctuations for A2 (upper) and B1 (lower), and tide	
	gauge observations at La Jolla, CA (SIO) (offset 100 years). Only the CNRM A2 trend	
	(upper, green) is statistically significant from zero at 95% confidence level	130
3-9.	Hours non-tide projections during winter (November-March) exceed 95th (9.3 cm), 98th	
	(12.2 cm), and 99.5th (16.4 cm) percentile thresholds. A2 scenario (left), B1 (right) 1	131
3-10	D. Positive non-tide sea level fluctuations relative to MSL with 3-year running mean (red)	
	and least squares trend (green) superimposed	132

3-11. Hindcast of January 1998 North Pacific swell - offshore wave height 3.5 m (11.4 ft) I shadows appear as areas with lower wave height (yellow-green) in lee of islands. Re areas along coast are locations with strong refractive focusing from underwater	ed
escarpments, relic sediment fans off river mouths, and submarine canyons (courtesy of the Coastal Data Information Program http://cdip.ucsd.edu)	
3-12. Wave exposure at central MCBCP (Range PN1290)Colors show ratio of nearshore wave height (H) to deep water (Ho) as a function of offshore direction and period	Э
3-13. Same as Figure 4-11 for Coronado City Beach (Range SS0160) representative of west-facing Coronado portion of NBC	
3-14. Wave height and direction for CCSM3-A2 scenario winter wave conditions in deep water SW of Pt. Conception, CA for 2000–2099. Black lines are least square fit trend. The mean annual significant wave height (blue, upper panel) trends down only slight while maximum annual winter wave height (red, upper panel) trends downward by approximately 1 m over coming century. Incoming peak wave directions trend northwells and the state of the state o	ly, vard
(lower panel)	re
3-16. Model (green) and observed (blue) wave height (upper), peak period (middle), and peak direction (lower) at MCBCP during December 2009	139
3-17. Model (green) and data (blue) comparisons of wave height (upper), peak period (middle), and peak direction at NBC during December 2009	140
3-18. Same as Figure 5-17. Mean (green) and extreme (red and asterisks) alongshore was height statistics for a 10-year (January 2000–December 2009) wave hindcast spanni	ave
3-19. Same as Figure 5-21. Mean and extreme alongshore wave height statistics for 100-year CCSM3-A2 GCM-derived nearshore wave height projection at MCBCP beach profile ranges. Green bars show mean significant wave height, black asterisks show means of annual wave height maxima, and red bars give range of annual maximum wave height.	8
3-20. Same as Figure 5-22. Annual GCM-derived nearshore wave statistics for MCBCP Range PN1290 including annual significant wave height mean (blue) and maximum (red)	143
3-21. Same as Figure 5-20. Mean (green) and extreme (red and asterisks) along shore wave height statistics for a 10-year (January 2000 to December 2009) wave hindcas at NBC	t
3-22. Same as Figure 5-26. Mean and extreme along shore wave height statistics for 100-year CCSM3-A2 GCM-derived near-shore wave height projection at NBC beach profile ranges. Green bars show mean significant wave height, black asterisks show means of annual wave height maxima, and red bars give range of annual maximum wave height	
3-23. Same as Figure 5-27. Annual GCM-derived nearshore wave statistics for NBC Range SS0160 including annual significant wave height mean (blue) and maximum (red)	ge
3-24. Extreme (98th percentile) runup projection at MCBCP Range SO1470 for winters (Nov–Mar) 2000–2100 using the A2 CCSM3 scenario and the slope independent	
formulation of Stockdon <i>et al.</i> (2006)	et al.
3-26. Same as Figure 3-24 but at NBC Range SS0160	

3-27.	. Same as Figure 3-25 for NBC Range SS0160	148
3-28.	. XBeach coordinate system	
3-29.	. Comparison of constant-slope runup testing results from XBeach and the slope	
	dependent and independent estimates from Stockdon et al, 2006	149
3-30.	. Beach profile at MOP station 970 at MCBCP with reference to NAVD88, and	
	adjustments for underlying MSL, Tide, and Non-Tidal Residuals for yearly wave	150
3-31.	. An example of XBeach simulated water surface elevations on MCBCP breach profile	
	MOP 970 for the week (A), year (B), and decade (C) return period wave and total water	
	level conditions	153
	. Comparison of runup from Stockdon et al. (2006) versus the XBeach results at NBC.	
	The dashed line is a polynomial best fit	154
	. Comparison of runup from Stockdon et al. (2006) versus the XBeach results at	
	MCBCP. The dashed line is a polynomial best fit	154
	. Best-fit beach slopes for concurrence between the XBeach simulated runup values	
	and the Stockdon et al. (2006) slope dependent runup estimates	155
	. Overall data processing workflow for producing calibrated, interoperable data products	
	from source data	157
	. Tile index for fused USACE LiDAR (calibrated) with SIO coastal LiDAR for Camp	
	Pendleton locale	160
	. Tile index for USGS regional basemap	
	: Illustration of littoral-zone modeling using field-measures beach profiles as fiducial	
	transects in combination with MOP lines	162
	Mission Dependency Index rating system used by NAVFAC ESC	
	Condition Index ratings used by NAVFAC ESC for waterfront structures	
	Typical beach training area profile at NBC (adapted from U.S. Navy, 2010)	
	Typical training patterns for beach training areas at NBC. Rectangles indicate the	
	approximate area of the beach zone in a training lane, and lines and shading indicate	
	training traffic patterns (adapted from U.S. Navy, 2010)	166
	Amphibious training at MCBCP Red Beach (courtesy of Marine Corps Base Camp	
	Pendleton, http://www.pendleton.marines.mil)	167
	Naval Amphibious Base Coronado buildings (image data: Google)	
	Buildings concentrated in the Del Mar area of MCBCP (image data: Google)	
	. Waterfront structures at NBC including the Carrier Wharves (far left) and the Ammuni-	
	tion Pier (far right) (red arrows). Shore protection coastal structures can also be seen	
	along the bay shoreline (yellow arrows) (Image data: Google)	169
	. Methodology for integration of the terrain and infrastructure data	
	Pathway response modeling approach.	
	Schematic of the fully accreted summer. dry equilibrium profile	
	The nearshore sand volume is calculated relative to the PFA reference frame	177
	(green box)	175
	Schematic flow chart of the implementation of the Cross-Shore Profile Equilibrium	175
	Model	170
	The theoretical volume conserving shoreline migration path with sea level rise is	173
	along the mean slope of the fully accreted equilibrium profile	120
	Example of beach profile adjustments and (a and b), and beach retreat (c) for a	100
	100-year simulation with 2-m MSLR.Profiles in (a) include the sand budget deficit,	
	while profiles in (b) assume zero deficit and retreat driven only by sea level rise	101
	General geometric parameters of sand balance models	
	Schematic flow chart of the conditionally decoupled profile sand balance model	
~ ~~.	. Somethand how shall of the somalibiliany accounted biblic datia balance inclici	

3-56. Model profile adjustments considering sea level rise. (a) Initial profile and active beach bounded by total water level and closure depth. The active beach profile shifts (b) verti- cally equal to the amount of sea level rise and (c) landward to obtain (d) sand balance.	-
3-57. Example of decadal (a) active beach and cliff profile adjustments and (b) cliff retreat and back beach width for a 100-year simulation with 2-m MSLR.In this example, initial cliff erosion is exclusively subaerial and then becomes marine-dominated toward the end of the simulation	. 189
3-58. Cliff and gully airborne LiDAR change detection, May 2002–March 2009, southern MCBCP	
3-59. Subaerial eroded cliff and gully sand volumes and interval precipitation, southern MCBCP	. 191
3-60. (a) The four MSLR curves considered in this study and current (1983–2001) MSL elevation. (b) Modeled mean and range of cliff retreat versus time for the zero deficit and four MSLR scenarios	. 192
3-61. Beach width (shoreline position) comparison for the YGOR model and beach data (top, left scale), and wave energy derived from hindcasts (bottom, right scale) at	
Coronado City Beach, Range SS0160	. 195
red), and projected wave energy (lower, grey)	. 195
the baseline elevation model to create the future elevation models	
3-65. Selected station for model output analysis (image data: Google, SIO, NOAA, U.S. Navy, NGA, GEBCO).	. 201
3-66. Figure showing study area, cross-section trace, location of wells used for cross section and offshore bathymetry, Santa Margarita River Basin, CA (image data: Google, Digital Globe)	
3-67. Lithologic geometry for conceptual model, Santa Margarita River Basin used in SUTRA with an inland freshwater boundary condition located at well 010S005W07J001S	
(7J1)	. 202
3-68. 10-meter bathymetry contour lines (blue lines)	. 204
3-69. Sutra Model Element size refinement scheme. The white area has a nominal size of 5 x 100 m, red a nominal size of 2 x 40 m, and blue a nominal size of 1 x 20 m	
3-70. SUTRA finite element layout used in the model simulation	8
the ocean due to sea level rise	
3-73. Total monthly pumpage for all wells in the SMR model in acre-ft (blue line) with a 5-year moving average (black line).*Note that pumping for WY 1950 to 1959 is a repea of the pumping values reported for WY 1961	ıt
3-74. Total pumping in acre-ft during water years 1961 and 2000 of wells located in the model.	. 207
3-75. Location of observation and pumping wells within the model. The pumping wells only show the screening interval of the well. The short names of each well are provided	000
either above or below each location	. 208

3-76	. Mean monthly discharge from the Santa Margarita River from USGS Gauge 11046000	
		208
	7 . 3 . 4	210
		211
	, ,	212
3-80	. 10S005W35K005S (35K5) observed and simulated hydrograph from 1950 to 2000	212
3-81	. 10S005W14R001S (14R1) observed and simulated hydrograph from 1950 to 2000	213
3-82	. 11S005W09J001S (9J1) observed and simulated breakthrough curves from 1950	
		213
3-83	. 11S005W10B001S (10B1) observed and simulated breakthrough curves from 1950	
		214
3-84	. 11S005W02N004S (2N4) observed and simulated breakthrough curves from 1950	
		214
3-85	. 10S005W35K005S (35K5) observed and simulated breakthrough curves from 1950	
		215
3-86	. Observed and simulated chloride levels in 1962 for selected wells arranged by	
		215
3-87	. Observed and simulated chloride levels in 1965 for selected wells arranged by	
		216
3-88	. Comparison of the 11S005W10B001S (10B1) hydrograph produced by a homogeneou	S
	system that has the properties of the alluvium layer with the original calibrated model	
		217
3-89	. Comparison of the 10S005W35K005S (35K5) hydrograph produced by a homogeneou	S
	system that has the properties of the alluvium layer with the original calibrated model	
		217
3-90	. Comparison of the 11S005W10B001S (10B1) breakthrough curve produced by a	
	homogeneous system that has the properties of the alluvium layer with the original	
		218
3-91	. Comparison of the 10S005W35K005S (35K5) breakthrough curve produced by a	
	homogeneous system that has the properties of the alluvium layer with the original	
		218
3-92	. Comparison of the 11S005W10B001S (10B1) hydrograph produced by a reversed	
		219
3-93	. Comparison of the 10S005W35K005S (35K5) hydrograph produced by a reversed	
		219
	. Comparison of the 11S005W10B001S (10B1) breakthrough produced by a reversed	
	system with the original calibrated model and observations	220
3-95	. Comparison of the 10S005W35K005S (35K5) breakthrough produced by a reversed	
	system with the original calibrated model and observations	
	. Four scenarios for mean sea level rise including tidal variability	
	. Overview of the receptor-level assessment methodology	223
3-98	. General process approach for the component-level vulnerability assessment	
	approach	231
3-99	. Beach Training Area, MCBCP. A view looking north at the beach zones from	
		234
	0. Existing conditions checklist for the component-level assessment of training areas	
	Existing conditions checklist for the component-level assessment of buildings	236
3-10	2. The groundwater table location influences the bearing capacity and settlement of	
	shallow foundations.(a) The groundwater table is above bottom of the footing; (b)	
	the groundwater table is at the bottom of the footing; (c) the groundwater table is	
	below the bottom of the footing. (Das, 2002)	237

3-103. Existing conditions checklist for the component-level assessment of waterfro structures.	ont 242
3-104. Typical pier fender system with floating fenders and concrete reaction piles a	
close spacing for bearing	243
3-105. Foam filled fenders shown at high tide. With less than 1.0 m of SLR, "roll-ove	
could occur	243
3-106. Partial pier section showing a floating fender system at low tide. The compress	
fender (dashed) is fully supported by the fender piles	
3-107. Partial pier section showing a floating fender system at high tide. The top of the	
fender system is below the top of the fender pile. The compressed fender (das	
is fully supported by the fender piles	•
3-108. Partial pier section showing a floating fender system subjected to SLR. The fe	
is at the critical elevation where it becomes susceptible to "roll-over"	
3-109. Pier with utility pipes located below deck in the tidal zone.he pipes are subm	
during high tides and collect kelp and other debris	-
3-110. Pier with water pipe located below deck. The pipe and hangers may not be de	
for wav \e and curent loading	247
3-111. Process of steel corrosion-related concrete damage (adapted from American	1
Galvanizers Association, http://archive.galvanizeit.org/about-hot-dip-galvanizin	g/how-
long-does-hdg-last/in-concrete)	
3-112. Effects of sea level rise on a typical pier	248
3-113. Waterfront structure that has excessive deterioration from chloride contamination	
and corrosion of the reinforcing steel (courtesy of Blaylock Willis and Associate	es) 248
3-114. Existing conditions checklist for the component-level assessment of coastal	
structures	252
3-115. Wave breaking on the rubble-mound structure at Oceanside Harbor (Californ	
Coastal Records Project Image 8921042; Copyright (C) 2002. 2014 Kenneth &	
Gabrielle Adelman, California Coastal Records Project, www.Californiacoastlin	•
3-116. Typical rubble-mound revetment section (adapted from USACE. 2006)	
3-117. Typical Seawall or Bulkhead Section (adapted from USACE, 2006)	
3-118. Typical rubble-mound jetty section (adapted from USACE, 2006)	254
3-119. Existing conditions checklist for the component-level assessment of civil	050
infrastructure	256
3-120. The photo shows a below-grade electrical vault partly full of water. A connec	
panel is visible above the water. The vault remains operational	260
3-121. The photo shows an electrical vault with older equipment that has exposed connections and is susceptible to flood damage	260
4-1. Winter 98-percentile combined total winter water level projections not including	260
runup	
4-2. Return period from monthly extreme order statistics (dark curve) with two-slope	
(broken lines), and from joint probability convolution method with runup beach	
of 0.04 and 0.02 (upper and lower dotted curves, respectively) for MCBCP Rar	•
PN1180 with respect to the NAVD88 Datum	
4-3. Same as Figure 4-2 for NBC Range SS0160 (Coronado City Beach)	
4-4. Total water level scenarios for NBC using the XBeach runup results. Line colors	
return periods as follows: black = week; green = month; blue = year; magenta =	
red = century	
4-5. Total water level scenarios for MCBCP using the XBeach runup results. Line co	
are return periods as follows: black = week; green = month; blue = year; mage	
decade; red = century	

4-6. The baseline digital terrain model for NBC.Red outline show the primary areas of NBC	
that were evaluated in this study	. 275
4-7. The baseline digital terrain model for MCBCP. The red outline shows the primary areas	
of MCBCP that were evaluated in this study	. 276
4-8. Cumulative histogram of the terrain model elevations at NBC and MCBCP	
4-9. Training area receptor category for NBC	. 280
4-10. Detailed view of the training areas at SSTC North (left) and South (right)	
4-11. Training area receptor category for MCBCP.	
4-12. Detailed view of the training areas for Blue Beach (bottom left), White Beach (upper	
left), and Red Beach (right)	. 283
4-13. Detailed view of the training areas for Gold Beach (left), and San Onofre Beach	
(right)	. 284
4-14. Building receptor category for NBC	
4-15. Detail view of the buildings at North Island (left) and NAB (right)	
4-16. The Navy housing complex at Silver Strand	
4-17. Histogram of building perimeter elevations for NBC and MCBCP	207
	. 201
4-18. NBC building category characteristics including non-zero MDI, replacement cost and	200
building area	
4-19. Building receptor category for MCBCP	
4-20. Detailed view of the buildings for southern (left) and central (right) MCBCP	
4-21. Detailed view of the buildings for northern MCBCP	. 291
4-22. MCBCP building category characteristics including non-zero MDI, replacement cost	
and building area	. 292
4-23. Waterfront structures receptor category for NBC	
4-24. Detail views of the waterfront structures at North Island	
4-25. Detailed view of the waterfront structures at NAB	
4-26. Waterfront structure receptor category for MCBCP	
4-27. Coastal structure receptor category for NBC	
4-28. Detailed view of the coastal structures along North Island	
4-29. Detailed view of the coastal structures at NAB	
4-30. Coastal structure receptor category for MCBCP	. 301
4-31. Detailed view of coastal structures at the Del Mar basin (left) and SONGS (right)	
areas of MCBCP	
4-32. Civil infrastructure - airfields receptor category for NBC	303
4-33. Civil infrastructure – airfields receptor category for MCBCP	304
4-34. Detail view of Landing Strip Victor coastal airfield at MCBC.	
4-35. Civil infrastructure – recreation areas receptor category for NBC	306
4-36. Detailed view of the recreation areas at North Island (left) and NAB and Silver Strand	
(right)	307
4-37. Civil infrastructure - recreation areas receptor category for MCBCP	308
4-38. Detailed view of the recreation areas at Del Mar (left) and NAB and San Onofre	
(right)	309
4-39. Civil infrastructure - roads receptor category for NBC	310
4-40. Detailed view of the roadways at North Island (left) and NAB and Silver Strand North	
(right)	311
4-41. Detailed view of the roadways at Silver Strand South	
4-42. Civil infrastructure - roads receptor category for MCBCP	. 313
4-43. Detail view of the roads for the southern (left) and northern (right) areas of MCBCP	
4-44. Civil infrastructure – storm water system receptor category for NBC	
4-45. Detailed view of the storm water system at North Island (left) and NAB (right)	
4-46. Detailed view of the storm water system at Silver Strand South	
	-

4-47. Civil infrastructure – stormwater system receptor category for MCBCP	
4-48. Detail view of the storm water system in the Del Mar (left) and SONGS (right) area	
of MCBCP	319
4-49. Integrated terrain and infrastructure model for NBC	320
4-50. Detailed view of the integrated model for North Island Naval Air Station	
4-51. Detailed view of the integrated model for NAB/SSTC North (right)	
4-52. Detailed view of the integrated model at SSTC South	
4-53. Integrated terrain and infrastructure model for MCBCP	
4-54. Detailed view of the integrated model for the Del Mar area of MCBCP	
4-55. Detailed view of the integrated model for the Red beach training area of MCBCP	
4-56. Detailed view of the integrated model for the San Onofre area of MCBCP	
4-57. Alongshore variation in beach retreat at NBC for the zero sand deficit (above) and	
Inman and Masters, 1991 sand deficit scenarios	330
4-58. Comparison of retreat profiles for the year 2100 with no sand deficit at MOP	
station 155 for active profile boundaries defined by a range of return period condition	ns
(above), and retreat curves for the corresponding conditions from 2000–2100	331
4-59. Erosion footprint for the baseline (SLR = 0 m) scenario at NBC. The overall green	
shaded band spans the 100-year return period wave condition from the YGOR mod	del,
and the fine grey lines indicate the shorter return periods ranging from week to	
decade	334
4-60. Detailed view of the erosion footprint for the baseline (SLR = 0 m) scenario at Nort	th
IslanThe overall green shaded band spans the 100-year return period wave condition	on
from the YGOR model, and the fine grey lines indicate the shorter return periods	
anging from week to decade	335
4-61. Detailed view of the erosion footprint for the baseline (SLR = 0 m) scenario at	
NAB/SSTC North. The overall green shaded band spans the 100-year return period	I
wave condition from the YGOR model, and the fine grey lines indicate the shorter	
return periods ranging from week to decade	335
4-62. Detailed view of the erosion footprint for the baseline (SLR = 0 m) scenario at SST	C
South. The overall green shaded band spans the 100-year return period wave	
condition from the YGOR model, and the fine grey lines indicate the shorter return	
periods ranging from week to decade	337
4-63. Erosion footprint for the SLR = 1.0-m scenario at NBC. The overall green shaded	
band spans the 100-year return period wave condition from the YGOR model, and	
the fine grey lines indicate the shorter return periods ranging from week to decade.	338
4-64. Detailed view of the erosion footprint for the SLR = 1.0-m scenario at North Island.	
The overall green shaded band spans the 100-year return period wave condition from	
the YGOR model, and the fine grey lines indicate the shorter return periods ranging	•
from week to decade	339
4-65. Detaied view of the erosion footprint for the SLR = 1.0-m scenario at NAB/SSTC N	
The overall green shaded band spans the 100-year return period wave condition from	
the YGOR model, and the fine grey lines indicate the shorter return periods ranging	J
from week to decade	340
4-66. Detailed view of the erosion footprint for the SLR = 1.0-m scenario at SSTC South	
The overall green shaded band spans the 100-year return period wave condition from	
the YGOR model, and the fine grey lines indicate the shorter return periods ranging	
from week to decade	341
4-67. Erosion footprint for the SLR = 2.0-m scenario at NBC. The overall green shaded	
band spans the 100-year return period wave condition from the YGOR model, and	
the fine grey lines indicate the shorter return periods ranging from week to decade.	342

The overall green shaded band spans the 100-year return period wave condition from	
the YGOR model, and the fine grey lines indicate the shorter return periods ranging from week to decade	343
4-69. Detailed view of the erosion footprint for the SLR = 2.0-m scenario at NAB/SSTC	343
North.The overall green shaded band spans the 100-year return period wave	
· · · · · · · · · · · · · · · · · · ·	
condition from the YGOR model, and the fine grey lines indicate the shorter return	244
	344
4-70. Detailed view of the erosion footprint for the SLR = 2.0-m scenario at SSTC South.	
The overall green shaded band spans the 100-year return period wave condition from	
the YGOR model, and the fine grey lines indicate the shorter return periods ranging	- · -
	345
4-71. CDPM - Zero deficit scenario: (a) initial back beach width, (b) initial cliff height, and	
	346
4-72. Comparison of modeled 100-year cliff retreat (n = 207) of 5-m bin width retreat	
	347
	349
4-74. Time series of subaerial beach width change for (upper panel) the zero deficit and	
(lower panel) negative 15 m^3/m-yr deficit scenarios. Both upper and lower panels	
show 100-year color coded decadal beach widths for the four MSLR scenarios	350
4-75. Erosion footprint for the baseline (SLR = 0 m) scenario at MCBCP. The overall light	
green shaded band spans the 100-year return period wave condition from the YGOR	
model, and the fine grey lines indicate the shorter return periods ranging from week	
to decade	353
4-76. Detailed view of the erosion footprint for the baseline (SLR = 0 m) scenario at Del Mar.	
The overall light green shaded band spans the 100-year return period wave condition	
from the YGOR model, and the fine grey lines indicate the shorter return periods	
	354
4-77. Detailed view of the erosion footprint for the baseline (SLR = 0 m) scenario at Red	
Beach. The overall light green shaded band spans the 100-year return period wave	
condition from the YGOR model, and the fine grey lines indicate the shorter return	
	355
4-78. Detailed view of the erosion footprint for the baseline (SLR = 0 m) scenario at San	200
Onofre. The overall light green shaded band spans the 100-year return period wave	
condition from the YGOR model, and the fine grey lines indicate the shorter return	
	356
4-79. Erosion footprint for the SLR = 1.0-m scenario at MCBCP. The overall light green	550
shaded band spans the 100-year return period wave condition from the YGOR model,	
and the fine grey lines indicate the shorter return periods ranging from week to decade.	
The dark green shaded band indicates the extent of cliff erosion	
	337
4-80. Detail view of the erosion footprint for the SLR = 1.0-m scenario at Del Mar. The	
overall light green shaded band spans the 100-year return period wave condition from	
the YGOR model, and the fine grey lines indicate the shorter return periods ranging	
from week to decade. The dark green shaded band indicates the extent of cliff	
	358
4-81. Detailed view of the erosion footprint for the SLR = 1.0-m scenario at Red Beach. The	
overall light green shaded band spans the 100-year return period wave condition from	
the YGOR model, and the fine grey lines indicate the shorter return periods ranging	
from week to decade. The dark green shaded band indicates the extent of cliff erosion	359

4-82. Detailed view of the erosion footprint for the SLR = 1.0-m scenario at San Onofre. The overall light green shaded band spans the 100-year return period wave condition from the YGOR model, and the fine grey lines indicate the shorter return periods ranging from week to decade. The dark green shaded band indicates the extent of clif erosion	f 360
4-83. Erosion footprint for the SLR = 2.0-m scenario at MCBCP. The overall light green shaded band spans the 100-year return period wave condition from the YGOR model, and the fine grey lines indicate the shorter return periods ranging from week to decade	
The dark green shaded band indicates the extent of cliff erosion	
from week to decade. The dark green shaded band indicates the extent of cliff erosion	362
The overall light green shaded band spans the 100-year return period wave condition from the YGOR model, and the fine grey lines indicate the shorter return periods ranging from week to decade. The dark green shaded band indicates the extent of clif	
erosion	
erosion	364
4-88. Inundation and flooding for the baseline (SLR = 0 m) scenario at NBC. The blue shaded zones represent week (dark blue), year (medium blue), and century (light blue) return periods	367
4-89. Detailed view of inundation and flooding for the baseline (SLR = 0 m) scenario at North Island. The blue shaded zones represent week (dark blue), year (medium blue), and century (light blue) return periods	368
4-90. Detailed view of inundation and flooding for the baseline (SLR = 0 m) scenario at NAB/STTC North. The blue shaded zones represent week (dark blue), year (medium blue), and century (light blue) return periods	369
4-91. Detailed view of inundation and flooding for the baseline (SLR = 0 m) scenario at STTC South. The blue shaded zones represent week (dark blue), year (medium blue) and century (light blue) return periods	
4-92. Inundation and flooding for the SLR,=1.0 m scenario at NBC. The blue shaded zones represent week (dark blue), year (medium blue), and century (light blue) return periods	i
4-93. Detailed view of -and flooding for the SLR = 1.0-m scenario at North Island. The blue shaded zones represent week (dark blue), year (medium blue), and century (light blue) return periods	372
4-94. Detailed view of inundation and flooding for the SLR = 1.0 m scenario at NAB/STTC North. The blue shaded zones represent week (dark blue), year (medium blue), and century (light blue) return periods	373
4-95. Detailed view of inundation and flooding for the SLR = 1.0-m scenario at STTC South. The blue shaded zones represent week (dark blue), year (medium blue), and century (light blue) return periods	374

4-96. Inundation and flooding for the SLR = 2.0-m scenario at NBC. The blue shaded zones represent week (dark blue), year (medium blue), and century (light blue) return periods	.375
4-97. Detailed view of inundation and flooding for the SLR = 2.0-m scenario at North Island. The blue shaded zones represent week (dark blue), year (medium blue), and	
century (light blue) return periods	.376
century (light blue) return periods	.377 .378
blue) return periods	.380
4-101. Inundation and flooding for the baseline (SLR = 0 m) scenario at MCBCP. The blue shaded zones represent week (dark blue), year (medium blue), and century (light blue)	
4-102. Detailed view of inundation and flooding for the baseline (SLR = 0 m) scenario at Del Mar. The blue shaded zones represent week (dark blue), year (medium blue), and century (light blue) return periods	.382
4-103. Detailed view of inundation and flooding for the baseline (SLR = 0 m) scenario at Red Beach. The blue shaded zones represent week (dark blue), year (medium blue), and century (light blue) return periods	.383
4-104. Detailed view of inundation and flooding for the baseline (SLR = 0 m) scenario at San Onofre. The blue shaded zones represent week (dark blue), year (medium blue), and century (light blue) return periods	.384
4-105. Inundation and flooding for the SLR = 1.0-m scenario at MCBCP. The blue shaded zones represent week (dark blue), year (medium blue), and century (light blue) return periods	.385
4-106. Detailed view of inundation and flooding for the SLR = 1.0-m scenario at Del Mar. The blue shaded zones represent week (dark blue), year (medium blue), and century (light blue) return periods	.386
4-107. Detailed view of inundation and flooding for the SLR = 1.0-m scenario at Red Beach. The blue shaded zones represent week (dark blue), year (medium blue), and century	
4-108. Detailed view of inundation and flooding for the SLR = 1.0-m scenario at San Onofre. The blue shaded zones represent week (dark blue), year (medium blue) and century (light blue) return periods	<u>-</u>
4-109. Inundation and flooding for the SLR = 2.0-m scenario at MCBCP. The blue shaded zones represent week (dark blue), year (medium blue), and century (light blue) return	
4-110. Detailed view of inundation and flooding for the SLR = 2.0 m scenario at Del Mar. The blue shaded zones represent week (dark blue), year (medium blue) and century	
(light blue) return periods	
(light blue) return periods	•
(light blue) return periods	. აყ∠

4-113. Inundation and flooding for the baseline (SLR = 0 m) bay-exposure scenario at NBC. The blue shaded zones represent week (dark blue), year (medium blue), and century	004
	394
4-114. Detailed view of inundation and flooding for the baseline (SLR = 0 m) bay-exposure scenario at North Island. The blue shaded zones represent week (dark blue), year	
\	395
4-115. Detailed view of inundation and flooding for the baseline (SLR = 0 m) bay-exposure scenario at NAB/SSTC North. The blue shaded zones represent week (dark blue),	
, , , , , , , , , , , , , , , , , , , ,	396
4-116. Detailed view of inundation and flooding for the baseline (SLR = 0 m) bay-exposure scenario at SSTC South. The blue shaded zones represent week (dark blue), year	
, , , , , , , , , , , , , , , , , , , ,	397
4-117. Inundation and flooding for the 1.0-m SLR bay-exposure scenario at NBC. The blue	
shaded zones represent week (dark blue), year (medium blue), and century (light blue) return periods	398
4-118. Detailed view of inundation and flooding for the 1.0-m SLR bay-exposure scenario at	
North Island. The blue shaded zones represent week (dark blue), year (medium blue),	200
	399
4-119. Detailed view of inundation and flooding for the 1.0-m SLR bay-exposure scenario at NAB/SSTC North. The blue shaded zones represent week (dark blue), year	
(medium blue), and century (light blue) return periods	400
4-120. Detailed view of inundation and flooding for the 1.0-m SLR bay-exposure scenario	
at SSTC South. The blue shaded zones represent week (dark blue), year (medium	
,, , , , , , , , , , , , , , , , , , ,	401
4-121. Inundation and flooding for the 2.0-m SLR bay-exposure scenario at NBC. The	
blue shaded zones represent week (dark blue), year (medium blue), and century	
	402
4-122. Detailed view of inundation and flooding for the 2.0-m SLR bay-exposure scenario	
at North Island. The blue shaded zones represent week (dark blue), year (medium blue), and century (light blue) return periods	, 403
4-123. Detailed view of inundation and flooding for the 2.0-m SLR bay-exposure scenario	
at NAB/SSTC North. The blue shaded zones represent week (dark blue), year (medium	
	404
4-124. Detailed view of inundation and flooding for the 2.0-m SLR bay-exposure scenario	
at SSTC South. The blue shaded zones represent week (dark blue), year (medium	
blue), and century (light blue) return periods	405
4-125. Station locations for the model simulations shown in Figure 4-126 to Figure 4-1354	408
4-126. Simulated current amplitudes at Bravo Pier (#1)for the five sea level rise scenarios:	
baseline, 0.5, 1, 1.5, and 2 m for a spring-neap tide cycle	408
4-127. Simulated current amplitudes at Bravo Pier (#1)for the five sea level rise scenarios:	
baseline, 0.5, 1, 1.5, and 2 m for a 48-hour period	409
4-128. Simulated current amplitudes at Turning Basin (#2) for the five sea level rise	
	409
4-129. Simulated current amplitudes at Glorietta Bay (#3) for the five sea level rise	
scenarios: baseline, 0.5, 1m, 1.5, and 2 m for a 48-hour period	410
4-130. Simulated current amplitudes at Silver Strand (#4) for the five sea level rise	
scenarios: baseline, 0.5, 1, 1.5, and 2 m for a 48-hour period	410
4-131. Simulated bottom shear stress at Bravo Pier (#1)for the five sea level rise	
scenarios: baseline, 0.5, 1, 1.5, and 2 m for a spring-neap tide cycle	411
4-132. Simulated bottom shear stress at Bravo Pier (#1)for the five sea level rise	
	411

scenarios: baseline, 0.5, 1, 1.5, and 2 m for a 48-hour period	4-133. Simulated bottom shear stress at Turning Basin (#2) for the five sea level rise	
scenarios: baseline, 0.5, 1, 1.5, and 2 m for a 48-hour period	scenarios: baseline, 0.5, 1, 1.5, and 2 m for a 48-hour period	.412
4-135. Simulated current amplitudes at Silver Strand (#4) for the five sea level rise scenarios: baseline, 0.5, 1, 1.5, and 2 m for a 48-hour period		
scenarios: baseline, 0.5, 1, 1.5, and 2 m for a 48-hour period	scenarios: baseline, 0.5, 1, 1.5, and 2 m for a 48-hour period	.412
4-136. RMS velocity differences over a complete spring-neap tidal cycle with 1.0 m SLR at NBC. Blue indicates velocities lower than current day conditions (-) red indicates velocities higher than current day conditions (+), and yellow indicates little change. The range of the differences are from about -5.1 to 4 cm/s		
at NBC Blue indicates velocities lower than current day conditions (-) red indicates velocities higher than current day conditions (+), and yellow indicates little change. The range of the differences are from about -5.1 to 4 cm/s	scenarios: baseline, 0.5, 1, 1.5, and 2 m for a 48-hour period	.413
velocities higher than current day conditions (+), and yellow indicates little change. The range of the differences are from about -5.1 to 4 cm/s	4-136. RMS velocity differences over a complete spring-neap tidal cycle with 1.0 m SLR	
The range of the differences are from about -5.1 to 4 cm/s	at NBC.Blue indicates velocities lower than current day conditions (-) red indicates	
4-137. RMS velocity differences over a complete spring-neap tidal cycle with 2.0 m SLR at NBC. Blue indicates velocities lower than current day conditions (-) red indicates velocities higher than current day conditions (+), and yellow indicates little change. The range of the differences are from about -7.3 to 7.3 cm/s		
at NBC.Blue indicates velocities lower than current day conditions (-) red indicates velocities higher than current day conditions (+), and yellow indicates little change. The range of the differences are from about -7.3 to 7.3 cm/s		.414
velocities higher than current day conditions (+), and yellow indicates little change. The range of the differences are from about -7.3 to 7.3 cm/s		
The range of the differences are from about -7.3 to 7.3 cm/s		
4-138. RMS bottom shear differences over a complete spring-neap tidal cycle with 1.0-m SLR at NBC.Blue indicates bottom shear lower than current day conditions (-) red indicates bottom shear higher than current day conditions (+), and yellow indicates little change. The range of the differences are from about -0.6 to 0.9 Dyne/cm²		
SLR at NBC.Blue indicates bottom shear lower than current day conditions (-) red indicates bottom shear higher than current day conditions (+), and yellow indicates little change. The range of the differences are from about -0.6 to 0.9 Dyne/cm²		.415
indicates bottom shear higher than current day conditions (+), and yellow indicates little change. The range of the differences are from about -0.6 to 0.9 Dyne/cm²		
little change. The range of the differences are from about -0.6 to 0.9 Dyne/cm²		
4-139. RMS bottom shear differences over a complete spring-neap tidal cycle with 2.0-m SLR at NBC. Blue indicates bottom shear lower than current day conditions (-) red indicates bottom shear higher than current day conditions (+), and yellow indicates little change. The range of the differences are from about -1.1 to 1.5 Dyne/cm²		
SLR at NBC.Blue indicates bottom shear lower than current day conditions (-) red indicates bottom shear higher than current day conditions (+), and yellow indicates little change. The range of the differences are from about -1.1 to 1.5 Dyne/cm²		.416
indicates bottom shear higher than current day conditions (+), and yellow indicates little change. The range of the differences are from about -1.1 to 1.5 Dyne/cm²		
little change. The range of the differences are from about -1.1 to 1.5 Dyne/cm²	, , ,	
4-140. 11S005W09J001S (9J1) simulated hydrograph from 1950 to 2100 with no sea level rise. The sharp changes in the water levels occur from monthly changes in pumping. The same annual pump schedule is used from 2001 to 2100, causing the water levels to oscillate		
rise.The sharp changes in the water levels occur from monthly changes in pumping. The same annual pump schedule is used from 2001 to 2100, causing the water levels to oscillate		.417
The same annual pump schedule is used from 2001 to 2100, causing the water levels to oscillate		
to oscillate		
4-141. 10S005W35K005S (35K5) simulated hydrograph from 1950 to 2100 with no sea level rise		440
level rise		.418
4-142. 11S005W02N004S (2N4) simulated hydrograph from 1950 to 2100 with no sea level rise		440
level rise		.418
4-143. 11S005W10B001S (10B1) simulated hydrograph from 1950 to 2100 with no sea level rise		440
level rise		.419
4-144. 11S005W09J001S (9J1) simulated breakthrough curve from 1950 to 2100 with no sea level rise		440
sea level rise		.419
4-145. 11S005W10B001S (10B1) simulated breakthrough curve from 1950 to 2100 with no sea level rise		420
sea level rise		.420
4-146. 11S005W02N004S (2N4) simulated breakthrough curve from 1950 to 2100 with no sea level rise	· · · · · · · · · · · · · · · · · · ·	420
sea level rise		.420
4-147. 10S005W35K005S (35K5) simulated breakthrough curve from 1950 to 2100 with no sea level rise	` ,	421
sea level rise		. 72 1
 4-148. Final chloride of the base case at December 31, 2099, for selected wells arranged by distance from the coastline compared with the chloride at September 31, 2000		421
distance from the coastline compared with the chloride at September 31, 2000	4-148 Final chloride of the base case at December 31, 2099, for selected wells arranged by	. /
 4-149. Four scenarios for mean sea level rise including tidal variability		
4-150. 11S005W09J001S (9J1) simulated Hydrograph during the sea level rise time frame 2000 to 2100 for the four scenarios		
2000 to 2100 for the four scenarios		. 120
4-151. 11S005W10B001S (10B1) simulated hydrograph during the sea level rise time		.423
		0
frame 2000 to 2100 for the four scenarios424		424
4-152. 11S005W02N004S (2N4) simulated hydrograph during the sea level rise time		
frame 2000 to 2100 for the four scenarios		
4-153. 10S005W35K005S (35K5) simulated hydrograph during the sea level rise time		.424
	4-153. 10S005W35K005S (35K5) simulated hydrograph during the sea level rise time	.424

4-154. 11S005W09J001S (9J1) simulated breakthrough curves during the sea level rise	
	425
4-155. 11S005W10B001S (10B1) simulated breakthrough curves during the sea level rise	
time frame 2000 to 2100 for the four scenarios	426
4-156. 11S005W02N004S (2N4) simulated breakthrough curves during the sea level rise	
	426
4-157. 10S005W35K005S (35K5) simulated Breakthrough curves during the sea level rise	
	427
4-158. Final chloride for Scenario 1 and 4 for selected wells arranged by distance from the	
	427
4-159. Location of the 250 mg/L Chloride contour at year 2100 For the four sea level rise	
scenarios with the average inland boundary condition. The contour lines are	
indistinguishable because the distance between the four lines is approximately	
	429
4-160. Comparison between Scenario 4 and the base case without sea level rise from 2000	720
to 2100. The white area on the right of the image is freshwater with 0 mg/L chloride,	
the blue region has chloride levels between 0 and 250 mg/L, the red region contains	
concentrations greater than 10,000 mg/L and small white area on the bottom left of	
the figure contains chloride concentrations greater than 19,000 mg/L. The black vertical	
line is where the ocean line is located at the start of the sea level rise at year 2000	430
4-161. Location of the 250 mg/L Chloride contour line and water table at year 2100 for	
different 2000 to 2100 constant boundary conditions (BC) for Scenario 4. Note that	
this image has been scaled 1:50 in the vertical direction and that the 27.3 m BC is the	
and the state of t	431
4-162. This image is identical to Figure 4-161, except the water table has been removed	
and it is now a 1:1 scale to illustrate the density lens that is formed from the seawater	
	431
4-163. 11S005W09J001S (9J1) simulated hydrograph for different future pumping rates	
with no sea level rise compared with Scenario 4.P110% means that the pumping rate	
from WY 2000 is increased by 10% and then used from 2000 to 2100	432
4-164. 11S005W10B001S (10B1) simulated hydrograph for different future pumping rates	
with no sea level rise compared with Scenario 4.P110% means that the pumping rate	
from WY 2000 is increased by 10% and then used from 2000 to 2100	432
4-165. 11S005W02N004S (2N4) simulated hydrograph for different future pumping rates	
with no sea level rise compared with Scenario 4. P110% means that the pumping rate	
from WY 2000 is increased by 10% and then used from 2000 to 2100	433
4-166. 10S005W35K005S (35K5) simulated hydrograph for different future pumping rates	
with no sea level rise compared with Scenario 4.P110% means that the pumping rate	
from WY 2000 is increased by 10% and then used from 2000 to 2100	433
4-167. 11S005W09J001S (9J1) simulated breakthrough curve for different future pumping	
rates with no sea level rise compared with Scenario 4. P110% means that the pumping	
rate from WY 2000 is increased by 10% and then used from 2000 to 2100	434
4-168. 11S005W10B001S (10B1) simulated breakthrough curve for different future pumping	
rates with no sea level rise compared with Scenario 4. P110% means that the pumping	
rate from WY 2000 is increased by 10% and then used from 2000 to 2100	434
4-169. 11S005W02N004S (2N4) simulated breakthrough curve for different future pumping	.5 1
rates with no sea level rise compared with Scenario 4.P110% means that the pumping	
rate from WY 2000 is increased by 10% and then used from 2000 to 2100	1 25
4-170. 10S005W35K005S (35K5) simulated breakthrough curve for different future pumping	+55
rates with no sea level rise compared with Scenario 4.P110% means that the pumping	
	12E
rate from WY 2000 is increased by 10% and then used from 2000 to 2100	435

4-189. Total replacement cost of buildings within the exposed shoreline inundation/flooding footprint at NBC with water depth exceeding 1 m	449
4-190. Inundation and flooding pathway analysis for buildings exposed via the protected	449
shoreline of NBC showing the quantity of buildings within the inundation and flooding	
footprint with water depth exceeding 1 m for each SLR scenario and return period	
event	450
4-191. Receptor-level estimate of the quantity of piers and wharves overtopped at NBC.	+30
No impacts were projected for the baseline or 0.5-m SLR scenario	452
4-192. Receptor-level estimate of the ROM replacement costs of Piers and wharves	+52
overtopped at NBC. No impacts were projected for the baseline or 0.5-m SLR	
scenarioscenario	452
4-193. Receptor-level estimate of the quantity of piers and wharves with operational impacts	
at NBC.Operational impacts are expected for each SLR scenario except the baseline	
4.404 Evenuela alavatian autoratian formatian DEM	4 55
4-194. Example elevation extraction from the DEM4-195. Receptor-level estimate of the ROM replacement cost of the bay-side coastal	+5+
structures overtopped at NBC. No impacts were projected for the baseline, 0.5, or	
40.015	455
4-196. Roadway erosion at NBC showing the estimated roadway replacement cost for each	
SLR scenario for the erosion pathway	456
4-197. Roadway inundation and flooding at exposed shorelines of NBC.The length of	430
roadway flooded increases for each return period event, with major flooding occurring	
for all SLR scenarios	457
4-198. Roadway inundation and flooding at protected shorelines of NBC. The length of	457
roadway flooded increases for each return period event for the 1.5- and 2.0-m	
	457
scenarios. The roadways do not flood significantly for the 0.5- or 1.0-m scenarios 4-199. Inundation and flooding pathway assessment of airfields for exposed shorelines at	437
NBC.The total flooded area increases for each SLR scenario and is approximately	
···	458
10 times greater than for the protect shorelines4-200. Inundation and flooding pathway assessment of airfields for protected shorelines	450
at NBC. Minor flooding occurs for the 1.5- and 2.0-m SLR scenarios. No flooding	
occurs for the 0.5- or 1.0-m SLR scenarios	459
4-201. Exposed shoreline erosion pathway assessment of storm water conveyance system at NBC	460
	400
4-202. Inundation and flooding pathway assessment of stormwater drainage system at	
exposed shoreline of NBC. The quantity of stormwater inlets with flood depths greater	461
than 0.3 m is shown	401
4-203. Erosion pathway assessment for recreational areas at NBC determined the	460
percentage of recreational area within the erosion footprint	462
4-204. Exposed shoreline inundation and flooding pathway assessment for recreational	400
areas of NBC determined the percentage of recreational area flooded	462
4-205. Protected shoreline inundation and flooding pathway assessment for recreational are	
of NBC determined the percentage of recreational area flooded	463
4-206. Erosion pathway assessment of average beach width impacts to training areas at	
MCBCP.The average beach width decreases by approximately 10 m for each SLR	474
scenario	471
4-207. Erosion pathway assessment of beach width impacts to individual beach training	4
areas at MCBCP for the monthly return period condition	471
4-208. The sand replenishment volume required for both SLR and the sand deficit at	
MCBCP beaches. The associated costs are to maintain the existing baseline beach	470
width	472
4-209. Assessment of inundated/flooded beach width for beach training areas at MCBCP	4/2

4-210. Inundation and flooding pathway assessment of beach width remaining for beach	
	.473
4-211. View of the northern coastline of MCBCP showing buildings, transportation corridors	
and recreational areas potentially vulnerable to erosion under future SLR scenarios	
(from California Coastal Records Project Image 200803818, Copyright (C) 2002–2014	
Kenneth & Gabrielle Adelman, California Coastal Records Project,	
	.473
4-212. Erosion pathway analysis of buildings at the exposed shoreline of MCBCP.The	170
quantity of buildings within the beach erosion footprint for each SLR scenario and	
return period event	171
4-213. Total replacement cost of buildings within the beach erosion footprint at MCBCP	171
4-214. Inundation and flooding pathway analysis for buildings via the exposed shoreline of	. – , –
MCBCP showing the quantity of buildings within the inundation and flooding footprint	476
with water depth exceeding 1 m for each SLR scenario and return period event	4/0
4-215. Total replacement cost of buildings within the exposed shoreline inundation/flooding	470
footprint at MCBCP with water depth exceeding 1 m	4/6
4-216. Receptor-level estimate of the number of coastal structures impacted by inundation	
and flooding along the exposed shorelines at MCBCP	4/8
4-217. Receptor-level estimate of the number of coastal structures impacted by SLR along	
the protected shorelines at MCBCP	.478
4-218. Roadway erosion at MCBCP showing the estimated roadway eroded area for each	
	.479
,	.480
4-220. Exposed shoreline erosion pathway assessment of storm water conveyance system	
	.481
4-221. Inundation and flooding pathway assessment of stormwater drainage system at	
exposed shoreline of MCBCP. The quantity of stormwater inlets with flood depths	
greater than 0.3 m is shown	.482
4-222. Erosion pathway assessment for recreational areas at MCBCP determined the	
percentage of recreational area within the erosion footprint	.483
4-223. Exposed shoreline inundation and flooding pathway assessment for recreational	
areas of MCBCP determined the percentage of recreational area flooded	.483
4-224. Elevated Causeway System training activity. The causeway is anchored to shore,	
and extends beyond the surf zone (U.S. Navy photo by Mass Communication	
Specialist 2nd Class Bryan Niegel)	.489
4-225. Estimated activity footprint for the elevated causeway training activity at STTC,	
including typical beach profile (above), planview of a training lane (middle), and	
activity footprint (bottom left) (adapted from U.S. Navy, 2010)	489
4-226. Average beach width remaining for all training areas at SSTC as a function of SLR	
	490
4-227. Beach width remaining by training lane at SSTC for the monthly return period	
flood event	.490
4-228. A portion of Berth Juliet at NAS Coronado is shown. The yellow outline indicates	
	.492
4-229. The CVN Warehouse at NBC showing a cross-section through the building. Note the	
truck ramp on the right and an office/lounge area on the left side of the figure	402
4-230. An excerpt from the Record Drawings grading plan for the construction of the Berth	.02
Juliet wharf, buildings and other improvements. The red lines indicate elevation	
contours in meters relative to MLLW. The green dashed lines indicate a below grade	
· · · · · · · · · · · · · · · · · · ·	.493
Storm water drainage system	- -

4-232. Operational limits for the CVN Warehouse, NBC in comparison to the 1.0-m SLR scenarios. 4-233. Operational limits for the CVN Warehouse, NBC in comparison to the 1.5 m SLR scenarios. 4-234. Operational limits for the CVN Warehouse, NBC in comparison to the 2.0 m SLR scenarios. 4-235. Naval Base Coronado looking north at the Helicopter Training Facility. The building is located approximately 70 ft from San Diego Bay 4-236. Naval Base Coronado with the Helicopter Training Facility as seen from Moffett Road. The exterior surface (lawn) berms up towards the building to lessen the impact of the wall elevation. The interior finish floor is approximately 30-in. below adjacent exterior grade. 4-237. View from San Diego Bay looking south, the Helicopter Training Facility can be seen in the background. A concrete seawall provides shore protection. 497. 4-238. View from San Diego Bay looking south, the Helicopter Training Facility can be seen in the background. A concrete seawall provides shore protection. 498. 4-239. Operational limits for the Helicopter Training Facility, NBC in comparison to the 0.5-m SLR scenarios. 498. 4-240. Operational limits for the Helicopter Training Facility, NBC in comparison to the 1.0-m SLR scenarios. 499. 4-241. Operational limits for the Helicopter Training Facility, NBC in comparison to the 1.5-m SLR scenarios. 499. 4-242. Operational limits for the Helicopter Training Facility, NBC in comparison to the 2.0-m SLR scenarios. 499. 4-243. Google Earth photo showing the configuration of Ammunition Pier Bravo at NBC (image: Google). 499. 4-244. Typical section through Pier Bravo. The major components that are vulnerable to SLR are indicated. 499. 4-245. View of floating fender and concrete piles at Ammunition Pier Bravo, NBC. This system is vulnerable to "roll-over" with 0.5 m of SLR. 499. 4-246. Operational limits for Ammunition Pier Bravo, NBC in comparison to the 1.5-m SLR scenarios. 490. 4-247. Operational limits for Ammunition Pier Bravo, NBC in comparison to the 1.5		. Operational limits for the CVN Warehouse, NBC in comparison to the 0.5-m SLR scenarios	494
scenarios			- 5-
4-234. Operational limits for the CVN Warehouse, NBC in comparison to the 2.0 m SLR scenarios	5	scenarios	494
4-235. Naval Base Coronado looking north at the Helicopter Training Facility. The building is located approximately 70 ft from San Diego Bay		·	495
4-235. Naval Base Coronado looking north at the Helicopter Training Facility. The building is located approximately 70 ft from San Diego Bay. 4-236. Naval Base Coronado with the Helicopter Training Facility as seen from Moffett Road. The exterior surface (lawn) berms up towards the building to lessen the impact of the wall elevation. The interior finish floor is approximately 30-in. below adjacent exterior grade. 4-237. View from San Diego Bay looking south, the Helicopter Training Facility can be seen in the background. A concrete seawall provides shore protection. 4-238. View from San Diego Bay looking south, the Helicopter Training Facility can be seen in the background. A concrete seawall provides shore protection. 4-238. View from San Diego Bay looking south, the Helicopter Training Facility can be seen in the background. A concrete seawall provides shore protection. 4-238. View from San Diego Bay looking south, the Helicopter Training Facility. NBC in comparison to the 0.5-m SLR scenarios. 4-240. Operational limits for the Helicopter Training Facility, NBC in comparison to the 1.0-m SLR scenarios. 4-241. Operational limits for the Helicopter Training Facility, NBC in comparison to the 2.0-m SLR scenarios. 4-243. Google Earth photo showing the configuration of Ammunition Pier Bravo at NBC (image: Google). 4-244. Typical section through Pier Bravo.The major components that are vulnerable to SLR are indicated. 4-245. View of floating fender and concrete piles at Ammunition Pier Bravo, NBC. This system is vulnerable to "roll-over" with 0.5 m of SLR. 4-246. The fire suppression piping and electrical conduits at Ammunition Pier Bravo are located below the pier deck. 4-247. Operational limits for Ammunition Pier Bravo, NBC in comparison to the 0.5-m SLR scenarios. 4-248. Operational limits for Ammunition Pier Bravo, NBC in comparison to the 1.0-m SLR scenarios. 4-249. Operational limits for Ammunition Pier Bravo, NBC in comparison to the 1.5-m SLR scenarios. 4-249. Operational limits for Ammunitio			
is located approximately 70 ft from San Diego Bay			495
4-236. Naval Base Coronado with the Helicopter Training Facility as seen from Moffett Road. The exterior surface (lawn) berms up towards the building to lessen the impact of the wall elevation. The interior finish floor is approximately 30-in. below adjacent exterior grade			496
Road. The exterior surface (lawn) berms up towards the building to lessen the impact of the wall elevation. The interior finish floor is approximately 30-in. below adjacent exterior grade			
exterior grade	F	Road. The exterior surface (lawn) berms up towards the building to lessen the impact	
4-237. View from San Diego Bay looking south, the Helicopter Training Facility can be seen in the background. A concrete seawall provides shore protection			407
in the background. A concrete seawall provides shore protection			491
4-238. View from San Diego Bay looking southeast at the seawall that protects Moffett Road and the Helicopter Training Facility. 4-239. Operational limits for the Helicopter Training Facility, NBC in comparison to the 0.5-m SLR scenarios. 4-240. Operational limits for the Helicopter Training Facility, NBC in comparison to the 1.0-m SLR scenarios. 4-241. Operational limits for the Helicopter Training Facility, NBC in comparison to the 1.5-m SLR scenarios. 4-242. Operational limits for the Helicopter Training Facility, NBC in comparison to the 2.0-m SLR scenarios. 4-243. Google Earth photo showing the configuration of Ammunition Pier Bravo at NBC (image: Google). 4-244. Typical section through Pier Bravo. The major components that are vulnerable to SLR are indicated. 4-245. View of floating fender and concrete piles at Ammunition Pier Bravo, NBC. This system is vulnerable to "roll-over" with 0.5 m of SLR. 5-24-246. The fire suppression piping and electrical conduits at Ammunition Pier Bravo are located below the pier deck. 5-24-247. Operational limits for Ammunition Pier Bravo, NBC in comparison to the 0.5-m SLR scenarios. 5-24-249. Operational limits for Ammunition Pier Bravo, NBC in comparison to the 1.0-m SLR scenarios. 5-24-249. Operational limits for Ammunition Pier Bravo, NBC in comparison to the 1.5-m SLR scenarios. 5-24-250. Operational limits for Ammunition Pier Bravo, NBC in comparison to the 1.5-m SLR scenarios. 5-24-250. Operational limits for Ammunition Pier Bravo, NBC in comparison to the 1.5-m SLR scenarios. 5-24-251. An aircraft carrier moored at Berth Kilo, NBC. 5-252. Typical section at berths Juliet and Kilo, NBC. The wharf has crane rails, a utility tunnel, and a fender system designed for aircraft carriers. Steam and deionized water are located outside of the utility tunnel, on the face of the wharf at Carrier Wharf Berth Kilo, NBC. These utilities are not designed for saltwater submersion. The			407
Road and the Helicopter Training Facility		·	497
4-239. Operational limits for the Helicopter Training Facility, NBC in comparison to the 0.5-m SLR scenarios		· · · · · · · · · · · · · · · · · · ·	
0.5-m SLR scenarios			498
0.5-m SLR scenarios	4-239	D. Operational limits for the Helicopter Training Facility, NBC in comparison to the	
1.0-m SLR scenarios			498
1.0-m SLR scenarios	4-240	. Operational limits for the Helicopter Training Facility, NBC in comparison to the	
4-241. Operational limits for the Helicopter Training Facility, NBC in comparison to the 1.5-m SLR scenarios			499
1.5-m SLR scenarios			
4-242. Operational limits for the Helicopter Training Facility, NBC in comparison to the 2.0-m SLR scenarios			499
2.0-m SLR scenarios			
4-243. Google Earth photo showing the configuration of Ammunition Pier Bravo at NBC (image: Google)			500
(image: Google)			000
4-244. Typical section through Pier Bravo. The major components that are vulnerable to SLR are indicated			5 ∩1
SLR are indicated			JU 1
4-245. View of floating fender and concrete piles at Ammunition Pier Bravo, NBC. This system is vulnerable to "roll-over" with 0.5 m of SLR			E01
system is vulnerable to "roll-over" with 0.5 m of SLR			5U I
4-246. The fire suppression piping and electrical conduits at Ammunition Pier Bravo are located below the pier deck		·	
located below the pier deck			502
4-247. Operational limits for Ammunition Pier Bravo, NBC in comparison to the 0.5-m SLR scenarios			
scenarios			502
4-248. Operational limits for Ammunition Pier Bravo, NBC in comparison to the 1.0-m SLR scenarios	4-247	. Operational limits for Ammunition Pier Bravo, NBC in comparison to the 0.5-m SLR	
scenarios	-		503
 4-249. Operational limits for Ammunition Pier Bravo, NBC in comparison to the 1.5-m SLR scenarios	4-248	3. Operational limits for Ammunition Pier Bravo, NBC in comparison to the 1.0-m SLR	
scenarios	5	scenarios	503
scenarios	4-249	Operational limits for Ammunition Pier Bravo, NBC in comparison to the 1.5-m SLR	
 4-250. Operational limits for Ammunition Pier Bravo, NBC in comparison to the 2.0-m SLR scenarios			504
scenarios	4-250		
 4-251. An aircraft carrier moored at Berth Kilo, NBC			504
 4-252. Typical section at berths Juliet and Kilo, NBC. The wharf has crane rails, a utility tunnel, and a fender system designed for aircraft carriers. Steam and deionized water are located outside of the utility tunnel, on the face of the wharf	<i>1</i> _251		
tunnel, and a fender system designed for aircraft carriers. Steam and deionized water are located outside of the utility tunnel, on the face of the wharf			500
are located outside of the utility tunnel, on the face of the wharf			
4-253. Steam and deionized water lines are located at the edge of the wharf at Carrier Wharf Berth Kilo, NBC. These utilities are not designed for saltwater submersion. The			EOO
Wharf Berth Kilo, NBC. These utilities are not designed for saltwater submersion. The			၁ပဗ
utility tunnel is located behind these utilities 507			
duity turner is located bernira triese duities	ι	utility tunnel is located behind these utilities	507

4-254. An aircraft carrier separator is a floating platform that provides clearance between the aircraft carrier and the wharf fender system, shown moored at Carrier Wharf Berth	50 7
Kilo, NBC4-255. Operational limits for Berths Juliet and Kilo, NBC in comparison to the 0.5-m SLR	.507
scenarios	.508
4-256. Operational limits for Berths Juliet and Kilo, NBC in comparison to the 1.0-m SLR scenarios	. 508
4-257. Operational limits for Berths Juliet and Kilo, NBC in comparison to the 1.5-m SLR scenarios	.509
4-258. Operational limits for Berths Juliet and Kilo, NBC in comparison to the 2.0-m SLR	.509
	.511
 4-260. Small Craft Pier No.2, NAB Coronado. The pier is representative of 13 piers at NAB. The piers have fender systems for small craft, potable water service, and lighting	.511
elevation is low to accommodate small craft berthing	.512
4-262. Operational limits for the small craft piers, NBC in comparison to the 0.5-m SLR scenarios	.512
4-263. Operational limits for the small craft piers, NBC in comparison to the 1.0-m SLR scenarios	.513
4-264. Google Earth photo showing the configuration of Pier Bravo and the Pier Bravo Revetment, NBC (image: Google)	.513
4-265. Pier Bravo Revetment, NBC	.514
4-266. Typical cross section for the Pier Bravo Revetment. The major components that are vulnerable to SLR are indicated	.514
4-267. Operational limits for the Pier Bravo Revetment, NBC in comparison to the 0.5-m SLR scenarios	.515
4-268. Operational limits for the Pier Bravo Revetment, NBC in comparison to the 1.0-m SLR scenarios.	.515
4-269. Operational limits for the Pier Bravo Revetment, NBC in comparison to the 1.5-m SLR scenarios	.516
4-270. Operational limits for the Pier Bravo Revetment, NBC in comparison to the 2.0-m	.516
	.517
4-272. Bulkhead No.2 at NAB typical cross section. The major components that are vulnerable to SLR are indicated	.518
4-273. Operational limits for Bulkhead No.2, NBC in comparison to the 0.5-m SLR	.518
4-274. Operational limits for Bulkhead No.2, NBC in comparison to the 1.0-m SLR	.519
4-275. Operational limits for Bulkhead No.2, NBC in comparison to the 1.5-m SLR	.519
4-276. Operational limits for Bulkhead No.2, NBC in comparison to the 2.0-m SLR	.520
4-277. Google Earth aerial view showing the configuration of Berth Lima and Quay Road, NBC.The dashed yellow line indicates the approximate location of the storm drain	. 520
	.521
	.521

4-279. A section through Berth Lima between Quay Road and San Diego Bay showing	500
the stormwater system with 1.0 m of SLR at a 10-year return period	522
4-280. Operational limits for Berth Lima Storm Water System, NBC in comparison to the 0.5-m SLR scenarios	522
4-281. Operational limits for Berth Lima Storm Water System, NBC in comparison to the	522
1.0-m SLR scenarios	523
1.0-III OLIV SCETIATIOS	525
Tables	
i abies	
2-1. Summary of sea level rise assessment frameworks reviewed for this study	Q
2-2. Key to variables used in Figures 3-23 and 3-24	
2-3. MCBCP beach profile range information	
2-4. NBC beach profile range information	
3-1. Quadratic sea level rise formula coefficients	
3-2. Tidal datum relationships (1983–2001)	
3-3. Tidal datum relationships (1991–2009)	
3-4. Tide prediction constituents	
3-5. Input datasets for Naval Base Coronado and surrounding area of San Diego Bay	
as shown in Figure 3-37. Dataset names reflect the sequence of processing that	
has been applied to produce the data layer	158
3-6. Input datasets for Marine Corps Base Camp Pendleton as shown in Figure 3-36	
3-7. Comparison of coastal calibration points at specified locations within the SIO	
March 2006 coastal LiDAR with data from the USGS Seamless, High-resolution	
dataset for Southern California (Barnard and Hoover, 2010)	159
3-8. Comparison of coastal calibration points at specified locations within the SIO	
March 2006 coastal LiDAR with data from the USACE 2002 LiDAR	159
3-9. Relationship with USGS well name with this documents short name	
3-10. Soil properties used in the SMR SUTRA model	210
3-11. Inundation/flood depth ranges, scenarios, and operational impacts to buildings.	
Actual damage and impacts will depend on building structure type and usage	
3-12. MDI groupings associated with building usage descriptions	
3-13. Building interior finishes and susceptibility to SLR damage	238
3-14. Comparison of the uplift force on a 36-in. diameter pipe in various materials:	
reinforced concrete (RCP), corrugated metal (CMP), high-density polyethylene	
(HDPE), and polyvinyl chloride (PVC)	261
3-15. Buoyancy force on reinforced concrete pipes per linear foot	
4-1. Extreme water levels as a function of return period and MSLR	267
4-2. Parameters for five wave scenarios (week, month, year, decade and century) at the	000
six range stations of NBC	268
4-3. Parameters for five wave scenarios (week, month, year, decade and century) at the	270
eight range stations of MCBCP	270
4-4. Cumulative histogram percentile bands for terrain model elevations at NBC and MCBCP. All values are in meters NAVD88	277
4-5. Beach training area characteristics at NBC	
4-6. Beach training area characteristics at MCBCP	
4-7. Beach retreat comparison for different sand deficit assumptions	
4-8. MCBCP 100-year cliff retreat projection summary	
4-9. Comparison of DEM and Construction Record Drawing Elevations at NBC	
4-10. Receptor-level vulnerability assessment summary for Naval Base Coronado based	. 1 01
on the exposed shoreline erosion pathway	466
on the expected enterential enterior patrivaly	100

4-11. Receptor-level vulnerability assessment summary for Naval Base Coronado based	
on the exposed shoreline inundation and flooding pathway	467
4-12. Receptor-level vulnerability assessment summary for Naval Base Coronado based	
on the protected shoreline inundation and flooding pathway	468
4-13. Receptor-level vulnerability assessment summary for MCBCP based on the exposed	
shoreline erosion pathway	487
4-14. Receptor-level vulnerability assessment summary for MCBCP based on the exposed	
shoreline inundation and flooding pathway	488

ACRONYMS

AAV Assault Amphibious Vehicle

AC Alternating Current

AR4 Fourth Assessment Report

ASCII American Standard Code for Information Interchange

AVISO Archiving, Validation and Interpretation of Satellite Oceanographic Data

BC Before Christ

BCCA Bias-Correction and Constructed Analogs

CA California

CNA Center for Naval Analysis

CCSM3 Community Climate System Model Version 3

CDIP Coastal Data Information Program

CDPM Conditionally Decoupled Profile Model

CE Common Era

CI Condition Index

CMP Corrugated Metal Pipe

CNIC Commander Naval Installations Command

CNRM Centre National de Recherches Météorologique

CO2 Carbon Dioxide

CSPEM Cross-Shore Profile Equilibrium Model

CVN Aircraft Carrier, Nuclear Powered

CZMS Coastal Zone Management Subgroup

DEM Digital Elevation Model

DoD Department of Defense

DoN Department of the Navy

ELCAS Elevated Causeway System

ENSO El Niño-Southern Oscillation

ESC Engineering Service Center

FEMA Federal Emergency Management Agency

FORTRAN Formula Translator

GCM General Circulation Models

GEBCO General Bathymetric Chart of the Oceans

GFDL Geophysical Fluid Dynamics Laboratory

GHG Green House Gas

GIS Geographic Information System

GMT Generic Mapping Tools

GPS Global Positioning System

GRASS Geographic Resources Analysis Support System

HDPE High Density Polyethylene

ICCE International Conference on Coastal Engineering

ID Inside Diameter

IE Invert Elevation

INFADS Internet Facility Real Estate Data Store

INLS Improved Navy Lighterage System

INSAR Interferometric Synthetic Aperture Radar

IPCC Intergovernmental Panel on Climate Change

JONSWAP Joint North Sea Wave Project

LCAC Landing Craft Air Cushion

LDEO Lamont-Doherty Earth Observatory

LiDAR Light Detection and Ranging

MB Megabyte

MCBCP Marine Corps Base Camp Pendleton

MCTSSA Marine Corps Tactical Systems Support Activity

MDI Mission Dependency Index

MEI Multivariate ENSO Index

MHW Mean High Water

MLLW Mean Lower Low Water

MLW Mean Low Water

MOP Monitoring and Prediction

MSLR Mean Sea Level Rise

MWL Mean Water Level

NAB Naval Amphibious Base

NAD83 North American Datum 1983

NASNI Naval Air Station North Island

NAVD88 North American Vertical Datum of 1988

NAVFAC Naval Engineering Facilities Command

NBC Naval Base Coronado

NCAR National Center for Atmospheric Research

NCDEM North Carolina Division of Emergency Management

NE Northeast

NetCDF Network Common Data Form

NGA National Geospatial-Intelligence Agency

NGVD National Geodetic Vertical Datum

NOAA National Oceanic and Atmospheric Administration

NOLF Navy Outlying Field

NOS National Ocean Service

NPGO North Pacific Gyre Oscillation

NPI North Pacific Index

NRC National Research Council

NSF National Science Foundation

NTDE National Tidal Datum Epoch

NTR Non-Tidal Residual

NW Northwest

NWIS National Water Information System

OD Outside Diameter

OPC Ocean Protection Council

OPDES Offshore Petroleum Discharge System

OUB Offshore Petroleum Discharge System [OPDES] Utility Boat

PA Planning Assessment

PDF Probability Distribution Function

PDO Pacific Decadal Oscillation

PN Pendleton

PNA Pacific North America

PVC Polyvinylchloride

RCP Reinforced Concrete Pipe

RMS Root Mean Square

ROM Rough Order of Magnitude

RRDF Roll On/Roll Off Discharge Facility

RWQCB Regional Water Quality Control Board

SA Screening Assessment

SANDAG San Diego Association of Governments

SC South Carolina

SCAPE Soft Cliff and Platform Erosion

SCB Southern California Bight

SCBPS Southern California Beach Processes Study

SEAL Sea Air and Land

SERDP Strategic Environmental Research and Development

SIO Scripps Institution of Oceanography

SL Sea Level

SLH Sea Level Height

SLP Sea Level Pressure

SLR Sea Level Rise

SMCL Secondary Maximum Contaminant Level

SMR Santa Margarita River

SO San Onofre

SON Statement of Need

SONGS San Onofre Nuclear Generating Station

SPAWAR Space and Naval Warfare

SPR Source-Pathway-Receptor

SRES Special Report on Emission Scenarios

SSC SPAWAR Systems Center

SST Sea Surface Temperature

SSTC Silver Strand Training Complex

SUTRA Saturated Unsaturated Transport Model

SW Southwest

TAR Third Assessment and Report

TO Technical Objective

TRIM Tidal Residues Inter-tidal Mudflat
UCSD University of California San Diego

UFC Unified Facilities Criteria

UNEP United Nations Environment Program

UNFCCC United Nations Framework Convention on Climate Change

US United States

USACE United States Army Corps of Engineers

USCSP United States Country Studies Program

US EPA United States Environmental Protection Agency

USGS United States Geological Survey
UTM Universal Transverse Mercator

VA Vulnerability Assessment

VCP Vitrified Clay Pipe

WFI Waterfront Facility Inspection

WY Water Year

YGOR Yates, Guza, and O'Reilly

KEYWORDS

Airfields Pacific Ocean
Aquifers Pathways
Assessment Physical effects

Bathymetry Planning
Beach replenishment Precipitation
Beaches Receptors

Bottom shear Recreational areas

Buildings Regional

Civil infrastructure Replacement value

Cliffs Resilience
Coastal structures Return period
Conceptual model Roadways
Currents San Diego Bay

Damage Santa Margarita River Basin

Department of Defense Scenarios

Deposition Screening assessment

Digital elevation model Sea level rise

El Niño Sea level variability Erosion Seawater intrusion

Exposure pathway Sediment Extreme value methods Sensitivity

Flooding Shoreline erosion

Framework Sources

Geographic information system Southwestern United States

General circulation model Storm drain systems

Groundwater Tidal flows Hazard Tides

Impacts Total water level

Infrastructure Training
Inundation Training area
LiDAR Transport
Littoral Vulnerability

Marine Corps Base Camp Pendleton Vulnerability assessment
Military infrastructure Waterfront structures

Naval Base Coronado Wave models Non-tide residuals Wave run-up

Operational threshold Waves

CONTRIBUTING AUTHORS

SPAWAR Systems Center Pacific

Dr. Bart Chadwick

Dr. Pei Fang Wang

Ms. Marrisa Brand

TerraCosta Consulting Group

Dr. Reinhard Flick

Dr. Adam Young

Dr. William O'Reilly

Dr. Peter Bromirski

Mr. Walter Crampton

Dr. Robert Guza

University of California, San Diego: San Diego Supercomputer Center

Dr. John Helly

U.S. Geological Survey

Dr. Tracey Nishikawa

Mr. Scott Boyce

Mr. Matthew Landon

Moffatt & Nichol Blaylock

Mr. Matthew Martinez, S.E.

Mr. Isaac Canner, P.E.

Mr. Brian Leslie

1. OBJECTIVE

This project directly addresses the objective of the Strategic Environmental Research and Development (SERDP) Statement of Need (SON) to develop analysis methods to assess the impacts of local mean sea level rise (SLR) and associated phenomena on United States (U.S.) military infrastructure. Our vision was to develop a rigorous and robust analysis methodology that provides a reliable means to identify and plan for vulnerabilities under both currently projected sea level rise scenarios, and emerging scenarios in the future. We developed analysis methods that can be applied to military installations using available data to assess the potential impacts of sea level rise of a range of magnitudes. The methodology serves to address potential mission readiness impacts, support critical policy and implementation decisions for response actions, and to identify and leverage other essential research needs in this area. Our project utilized a strong team of regional scientists and managers to provide a focused and rigorous regional vulnerability assessment methodology for representative southwestern U.S. coastal military installations. While responding directly to the SON, the application of our methodology focused uniquely on the potential ramifications of these changing conditions on military installations in the Southwestern U.S. including, Naval Base Coronado (NBC) and Marine Corps Base Camp Pendleton (MCBCP). This regional focus built on and enhanced general strategies that have been applied over larger scales in previous efforts. The motivations for this focus include recognition that:

- To achieve meaningful and useful vulnerability assessments, a significant degree of installation-specific detail is required; thus the scope of the effort was carefully focused. The methodology and analysis tools are exportable to other regions and can be applied with regional forcing.
- Regional sea level forcing scenarios were generally applicable across the two installations in the study.
- While limited previous analysis and experience suggests a very high vulnerability to SLR, the southwest was a region that had received relatively little assessment compared, for example, to the southeastern and gulf coasts.
- The region has a high concentration of critical coastal military installations poised across a range of coastal topographies.
- A regional effort allowed more meaningful direct interaction with local scientists, facilities and resource managers, and policy makers, and allowed application of the enormous amount of scientific data, analysis and understanding, and visualization technologies, that were available at Scripps Institution of Oceanography, University of California San Diego (UCSD), and SPAWAR Systems Center Pacific (SSC Pacific).

The objective of this effort was to develop an analysis framework and methodologies to support the evaluation of regional military installation vulnerabilities and test them under prescribed scenarios of four increases in mean sea level (0.5, 1.0, 1.5, and 2.0 m) with coinciding water level variations associated with tide, wave, storm, El Niño-Southern Oscillation (ENSO), and other regional-specific climatic responses as projected over the next century. Methodologies were developed to assess the scope and magnitude of the following five physical effects of these joint SLR scenarios: flooding, inundation, erosion, seawater intrusion, and alteration of tidal flows. Based on projected physical effects, strategies for assessing key installation vulnerabilities were evaluated for their ability to support future planning and recommendations for possible mitigation. Vulnerability assessment methodologies were structured around potential vulnerabilities for receptor categories that included buildings, civil infrastructure, training and testing lands, waterfront structures, and

coastal structures. The project was organized around five specific technical objectives (TO) (Figure 1-1):

- TO1. Vulnerability Framework: Develop a generalized sea level rise vulnerability assessment framework for application to coastal military installations.
- TO2. Delineation of Regional Sea Level Rise and Climate Change: Develop methods to project future trends in sea level and sea level variability. Further, develop methodologies to combine these underlying sea level characteristics into realistic assessment scenarios based on the probability of occurrence for a range of regional sea level conditions
- TO3. Delineation of the Coastal System: Develop methods to compile analyze and integrate critical biogeophysical and infrastructure data for each installation within a three-dimensional Geographic Information System (GIS) modeling environment.
- TO4. Assessment of Physical Effects and Responses: Using the range of scenarios develop under T02 as test cases, develop methods to characterize the expected physical effects of SLR within the southwest region, and to compile these results into the GIS modeling framework.
- TO5. Assessment of Vulnerability: Integrate the analytical methods developed under T02-T04 within the vulnerability framework of T01 to explore the application of these methods to assess vulnerability at the two installations.

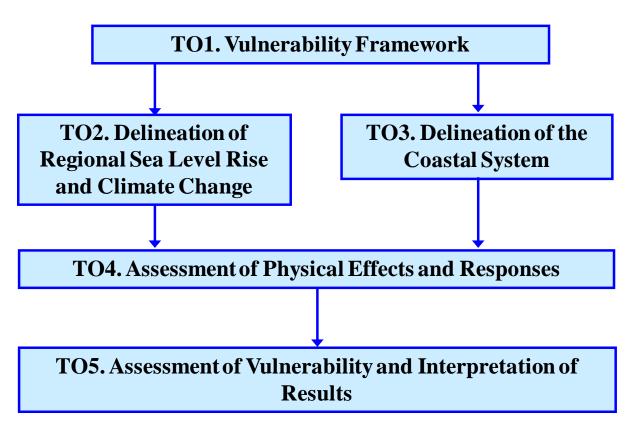


Figure 1-1. Components of the project technical objectives.

2. BACKGROUND

Climate change has potential ramifications for national security. This has been recently recognized in legislation that directs the Department of Defense (DoD) to provide guidance to military planners to assess the risks of potential climate change, and in a study directed by a board of senior retired military officers that recommended DoD conduct assessments of the impact on U.S. military installations of rising sea levels, extreme weather events, and other projected climate change impacts over the next 30 to 40 years (Center for Naval Analysis, 2010).

Installation vulnerabilities include:

- Loss or damage to mission-essential infrastructure including coastal development and beaches;
- Loss or degradation of mission capabilities;
- Loss of training and testing lands, including beaches;
- Loss of transportation means, facilities, and/or corridors;
- Loss of habitat and associated natural resources;
- Increased risk of storm damage; and,
- Increased potential for loss of life.

These concerns are reinforced by the recent projections from the fourth assessment of the IPCC (2007a) and other studies, especially those dealing with the potential for increased contributions to mean sea level rise (MSLR) from melting ice caps. Observations indicate that global mean sea level (MSL) rose at an average rate of 0.15 to 0.20 meters per century (m/cy) over the 20th century, and that this rate has increased since about 1992 to over 0.30 m/cy. The acceleration is confirmed in both tide gauge and satellite data (Merrifield *et al.*, 2009; U.S. EPA, 2010) and appears distinct from decadal variability since it is uncorrelated with standard climate indexes. Most of the acceleration appears to be the result of tropical and southern ocean warming associated with upper-ocean heat content and ice melt. MSLR scenarios specified and considered in this study ranged from global MSL end-points of 0.5, 1.0, 1.5, and 2.0 m by year 2100, which were assumed to apply to the study area.

The focus of this effort was to develop and exercise analysis methods to assess the impacts of local mean SLR and associated phenomena on military infrastructure in the Southwest U.S. The application of our methodology focused uniquely on the potential ramifications of these changing conditions on military installations in the southwestern U.S., including NBC and MCBCP. To achieve this, we developed an analysis framework and applied it to determine regional military installation vulnerabilities under the four specified scenarios of increased mean sea level (0.5, 1.0, 1.5, and 2.0 m) with coinciding water level variations associated with tide, wave, storm, ENSO, and other regional-specific climatic responses as projected over the next century. Methodologies were developed to assess the potential scope and magnitude of the following five physical effects of these joint SLR scenarios: flooding, inundation erosion seawater intrusion, and alteration of tidal flows. Based on projected physical effects, key installation vulnerabilities were evaluated to support future planning and recommendations for possible mitigation. Vulnerability assessment methodologies were structure around potential impacts to receptor categories that included buildings, civil infrastructure, training and testing lands, waterfront structures, and coastal structures. The framework for the methodology, the coastal setting at the two coastal installations, and an overview of key coastal processes in the region are described below.

2.1 VULNERABILITY FRAMEWORK

Climate change vulnerability is defined by Intergovernmental Panel on Climate Change (IPCC) as "the degree of inability to cope with the consequences of climate change and accelerated sea-level

rise" (IPCC, 1992). This concept of vulnerability assessment embraces the assessment of both anticipated impacts and available adaptation options (Smith *et al*, 1996; Tol *et al.*, 1998; Klein and Nicholls, 1999), and encompasses biogeophysical, socio-economic, and political factors (Bijlsma *et al.*, 1996; Klein, 2002; Turner *et al.*, 2003). In this context, adaptive capacity represents the "ability of a system to adjust to climate change (including climate variability and extremes) to moderate potential damages, to take advantage of opportunities, or to cope with the consequences" (McCarthy *et al.*, 2001). Because research under the statement of need for this project did not focus significantly on adaptation, in the context of this project we also use vulnerability to describe the combination of exposure and sensitivity without full consideration of adaptive capacity.

In general, climate change vulnerability in coastal areas is magnified by exposure to oceanic forces including increases in sea level, storm surge, and wave heights, as well as limitations on adaptive capacity. Limitations on adaptive capacity in these areas may stem from physical, economic, and institutional constraints and may be particularly acute in highly developed coastal areas where natural buffers such as dunes and wetlands have already been lost, and there is a high density of costly fixed infrastructure near the shoreline (Parry *et al.*, 2007).

Vulnerability analysis of SLR for coastal areas has been conducted over varying scales including local area studies, country studies, and global studies (Figure 2-1; Nichols and Mimura, 1998; Nicholls, 1995; Nicholls and de la Vega-Leinert, 2008). Larger scale analyses are generally more qualitative and comparative (e.g., which areas of the world are most vulnerable), whereas regional studies are generally more quantitative and focus more on specific planning initiatives (Dolan and Walker, 2006). Various frameworks have been proposed and applied for SLR vulnerability assessment and adaptation over these spatial scales, including the IPCC Common Method (IPCC, 1992), the U.S. Country Studies Methodology (Benioff et al., 1996), the United Nations Environment Program (UNEP) Handbook Methodology (Burton et al., 1998), the United States Agency for International Development guidance manual for Adapting to Climate Variability and Change (USAID, 2007), and the South Pacific Islands Methodology (Yamada et al., 1995). While these frameworks bear similarities, they all have recognized limitations and criticisms (Dolan and Walker, 2006). The Common Method has been most widely applied, particularly at larger scales (country and global), and incorporates the following objectives within its framework: (1) identify and assess physical, ecological, and socio-economic vulnerabilities to accelerated SLR and other coastal impacts of global climate change; (2) understand how development and other socio-economic factors affect vulnerability; (3) clarify how possible responses can mitigate vulnerability, and assess their residual effects; and (4) evaluate capacity for implementing a response within a broad coastal zone management framework.

While these objectives are not specifically targeted to military installations, they do provide a point of departure for adaptation to a military installation specific framework. The Common Method is structured around a seven-step framework that links research, monitoring, and policy making processes to assist policy-makers to make informed decisions (IPCC, 1992). While previous assessments have been carried out, there are still significant barriers including: limited understanding of relevant processes affected by sea-level rise; insufficient data on existing conditions; difficulty in developing the local and regional scenarios of future change; and lack of appropriate analytical methodologies for some impacts (Nicholls and Klein, 2000). Within these frameworks, adaptation is generally considered in terms of retreat (minimize impacts by pulling back from the coast), accommodation (minimize impacts by adjusting human use of the coastal zone), and protection (impacts are controlled by soft or hard engineering) (IPCC, 1990; Bijlsma *et al.*, 1996). For coastal military bases, these responses must be also weighed in consideration of critical readiness, training and support missions of the installation (Center for Naval Analysis, 2010).

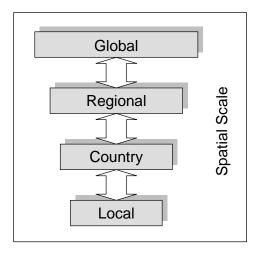


Figure 2-1. Typical scales of vulnerability assessments (adapted from Nichols and Mimura, 1988).

While these objectives are not specifically targeted to military installations, they do provide a point of departure for adaptation to a military installation specific framework. The Common Method is structured around a seven-step framework that links research, monitoring, and policy making processes to assist policy-makers to make informed decisions (IPCC, 1992). While previous assessments have been carried out, there are still significant barriers, including limited understanding of relevant processes affected by sea level rise, insufficient data on existing conditions, difficulty in developing the local and regional scenarios of future change, and lack of appropriate analytical methodologies for some impacts (Nicholls and Klein, 2000). Within these frameworks, adaptation is generally considered in terms of retreat (minimize impacts by pulling back from the coast), accommodation (minimize impacts by adjusting human use of the coastal zone), and protection (impacts are controlled by soft or hard engineering) (IPCC, 1990; Bijlsma *et al.*, 1996). For coastal military bases, these responses must be also weighed in consideration of critical readiness, training and support missions of the installation (Center for Naval Analysis, 2010).

More recently, climate change assessments have embraced risk assessment paradigms to evaluate sea level rise vulnerability (Patz and Balbus, 1996; NCDEM, 2009; Leggett *et al.*, 2003; Cartwright, 2008; Kasperson *et al.*, 2001; Liverman, 2001; van Westen and Georgiadou 2001; Scheitlin *et al.*, 2011; Kuleli, 2010). In these approaches, vulnerability is cast in the risk assessment nomenclature of exposure and effects, with changes in sea level and storminess representing sources or stressors which are manifested through pathways such as shoreline response, erosion, inundation, and seawater intrusion, which in turn result in risk to receptors (or sometimes referred to as sectors such as buildings and structures, natural resources, transportation, and so on (Snover *et al.*, 2007). These risk assessment strategies have generally been applied on regional or smaller scales (NCDEM, 2009; Cartwright, 2008; Kuleli, 2010; Scheitlin *et al.*, 2011), and provide a framework for addressing specific vulnerability questions at a relatively quantitative level. In these frameworks, risk conceptually incorporates both the likelihood of a given event and the consequence of the event (Kasperson et al., 2001; Liverman, 2001; Westen and Georgiadou, 2001), reflecting the notion that the same sea level rise scenario may result in different risks in different places because some people and places are more sensitive and less able to adapt than others (Cartwright, 2008).

A general review of existing frameworks was conducted to appraise the state of the science for vulnerability assessment, and to create a credible basis for a DoD-relevant framework that builds on the strategies already developed and utilized in other applications. A cross-section of existing

frameworks and strategies were identified and reviewed. These are summarized in Table 2-1, and briefly described below.

2.1.1 Review of Existing Frameworks

IPCC Common Methodology

The IPCC Common Methodology was developed primarily to assist countries in making first-order assessments of vulnerability to sea-level rise (Klein and Nicholls, 1999). The framework was first proposed in 1991 and was designed to assist the user in estimating impacts from sea level rise, including the value of lost land and wetlands. The methodology incorporates expert judgment and data analysis of socioeconomic and physical characteristics, but does not explicitly instruct the user on how to perform the analyses. Information from this methodology, including the identification of priority regions and their possible adaptation measures, is generally used on a screening basis for the development of more detailed analysis and modeling for biophysical and socio-economic impacts and adaptations. The user follows seven steps: (1) delineate the case study area, (2) inventory study area characteristics, (3) identify the relevant socioeconomic development factors, (4) assess the physical changes, (5) formulate response strategies, (6) assess the vulnerability profile, and (7) identify future needs (Figure 2-2). Adaptation focuses around three generic options: retreat, accommodate or protect.

The Common Methodology has been for assessments in at least 46 countries including quantitative results for 22 country case studies and eight sub-national studies (Nicholls, 1995). While the approach is most useful as an initial, baseline analysis for country level studies where little is known about coastal vulnerability, it can be applied at a range of scales including sub-national, national, regional and global. The output of the assessment is generally a vulnerability profile indicating a range of impacts of sea level rise, such as land loss and associated value and uses and a list of future policy needs to adapt both physically and socio-economically. Application requires delineation of physical and socioeconomic characteristics of the study area, and considerable knowledge on a range of techniques for estimating biophysical and socioeconomic impacts of sea level rise and adaptation (UNFCCC, 1999).

IPCC Technical Guidelines for Assessing Climate Change Impacts and Adaptations

IPCC published the Technical Guidelines for Assessing Climate Change Impacts and Adaptations in 1994 to provide a consistent framework for the assessment of climate impacts and adaptations across a range of regions and geographical areas (Carter et al., 1994). The report reviews methods and outlines an analytical framework for assessing the impacts of climate change. The guidelines are structured around a seven-step procedure that includes: (1) definition of the problem, (2) selection of the methodology, (3) testing the method, (4) selection of scenarios, (5) assessment of the biophysical and socio-economic impacts, (6) assessment of autonomous adjustments, and (7) evaluation of adaptation strategies (Figure 2-3). Guidance is provided for a range of techniques that may be applied in each step of the process. The problem definition step identifies the goal of the assessment, the exposure unit, the spatial and temporal scope, and the data requirements. Selection of methods encompasses a range of possible techniques including experimentation, impact projections, empirical studies, and expert judgment. Method testing serves as a precursor to the main evaluation, and encompasses feasibility studies, data acquisition, and model testing. Scenarios development relies on the specification of a range of plausible future climate conditions. Assessment of impacts describes the differences between the environmental and socio economic baseline, and the projected conditions under the selected climate change scenarios. The guidance incorporates the assessment of both autonomous adjustments and adaptation strategies.

UNEP Handbook Methodology

The UNEP Handbook on Methods (Feenstra, Brton, Smith, and Tol, 1998; Klein and Nicholls, 1998) was developed to provide a detailed application strategy for the IPCC Technical Guidelines for Assessing Climate Change Impacts and Adaptations (Carter, Parry, Harasawa, and Nishioka, 1994). It provides a generic framework for conducting assessments of sea-level rise and climate change. The general procedure includes seven guiding steps including: (1) define the problem, (2) select the method, (3) test the method, (4) select scenarios, (5) assess the biogeophysical and socioeconomic impacts, (6) assess the autonomous adjustments, and (7) evaluate adaptation strategies. A range of methods are suggested for each of the steps with selection of the best approach left up to the user (Figure 2-4). The approach is applicable to situations ranging from regional to national level studies, and can be used at both screening and more detailed levels of analysis. General input requirements include physical and socioeconomic characteristics of the coastal zone, and the resulting outputs include potential impacts of sea level rise and corresponding adaptation strategies according to both socioeconomic and physical characteristics. The methodology has been applied in several countries, including the Cameroon, Antigua and Barbuda, Estonia, Pakistan, and Cuba (UNFCCC, 1999).

U.S. Country Studies Methodology

The U.S. Country Studies Methodology was tailored to meet the needs of developing countries in assessing their vulnerability to climate change and identifying opportunities for adaptation (USCSP, 1999; Benioff, Guill, and Lee, 1996). The general approach centers on the evaluation of biophysical effects and involves six primary steps, including: (1) define scope of assessment process, (2) select scenarios, (3) conduct biophysical and economic impact assessments, (4) integrate impact results, (5) analyze adaptation policies and programs, and (6) document and present results to decision makers. The method is flexible in that relatively simple methods can be applied when an analysis of biophysical impacts of climate change is the central goal. It is broadly applicable to coastal resources, agriculture, grasslands/ livestock, water resources, forestry, human health, fisheries, and wildlife. Inputs to the method include climate change and socioeconomic scenarios and outputs tend to focus on climate change impacts and, to limited extent, adaptation options (UNFCCC, 1999).

The South Pacific Island Methodology

The South Pacific Island Methodology was developed in response to factors that restricted the direct application of the IPCC Common Methodology such as a lack of data, such as topographic maps with precise contours, historical records of climate and mean sea level, and land use patterns, a common constraint in developing countries (Mimura, 1999). The South Pacific Island Methodology is an index-based approach that applies relative scores to assess a variety of scenarios and take advantage of traditional knowledge and memories of the local people to overcome the shortage of empirical data (Kay and Hay, 1993). The method utilizes six classes of coastal subsystems including natural, human, infrastructural, economic, institutional, and cultural (Figure 2-5). These are further divided into subsystems to which a vulnerability score and a resilience score is assigned based on expert judgment under a range of scenarios. The two values are then combined to produce a sustainable capacity index for each scenario. The method is particularly useful in coastal settings with limited quantitative data but considerable experience and qualitative knowledge. It is generally viewed as a screening level analysis that should be followed by a more quantitative analysis (UNFCCC, 1999). The method is generally applied at the island or regional scale and requires little quantitative data, but significant background knowledge of physical, social, and economic characteristics of the area.

Table 2-1. Summary of sea level rise assessment frameworks reviewed for this study.

Framework or Methodology	Description/Purpose	Assessment Type	Reference
IPCC Common Methodology	Assist countries in making first-order assessments of vulnerability to sealevel rise.	Vulnerability Assessment	Klein and Nicholls, 1999
IPCC Technical Guidelines for Assessing Climate Change Impacts and Adaptations	Provide a consistent framework for the assessment of climate impacts and adaptations across a range of regions and geographical areas.	Vulnerability Assessment	Carter et al., 1994
UNEP Handbook Methodology	Provide a detailed application strategy for the IPCC Technical Guidelines for Assessing Climate Change Impacts and Adaptations.	Impact Assessment	Feenstra et al., 1998; Klein and Nicholls, 1998
US Country Studies Methodology	Tailored to meet the needs of developing countries in assessing their vulnerability to climate change and identifying opportunities for adaptation.	Vulnerability Assessment	USCSP, 1999; BenioffÉA Õ 利益的 åÆ^^, F996
The South Pacific Island Methodology	Developed in response to factors that restricted the direct application of the IPCC Common Methodology such as a lack of data, such as topographic maps with precise contours, historical records of climate and mean sea level, and land use patterns, a common constraint in developing countries.	Index-Based Vulnerability Assessment	Mimura, 1999
Understanding Vulnerability of Coastal Communities to Climate Change Related Risks	Describes a framework for assessing adaptive capacity which addresses the inherent susceptibilities of human environment systems exposed to climate variability and change in contrast to typical impact assessments that focus largely on reducing economic impacts.	Vulnerability Assessment	Dolan and Walker (2004)
Climate Change and Coastal Zones: An Overview of the State of the Art on Regional and Local Vulnerability Assessment	Provides an overview of methodologies for assessing the vulnerability of coastal zones, present a conceptual framework for vulnerability assessment, and outline the steps that are required for the actual assessment of coastal vulnerability	Vulnerability Assessment	Sterr et al., 1999
An Environmental Risk Assessment/Management Framework for Climate Change Impact Assessments	Presents a risk assessment and mangement framework for climate change impacts with a focus on individual exposure units. Incorporates stakeholder involvement and links key climate variables with impact thresholds.	Blend of Vulnerability and Risk Assessment	Jones, 2001
North Carolina Sea Level Rise Risk Management Study	Describes a risk assessment and mitigation strategy demonstration of the potential impacts of sea level rise in that state associated with long-term climate change.	Blend of Vulnerability and Risk Assessment	North Carolina Division of Emergency Management, 2009

Understanding Vulnerability of Coastal Communities to Climate Change Related Risks

This paper by Dolan and Walker (2006) presents a framework for assessing adaptive capacity which addresses the inherent susceptibilities of human environment systems exposed to climate variability and change in contrast to typical impact assessments that focus largely on reducing economic impacts. The framework incorporates differential exposures and vulnerabilities based on a range of determinants including access and distribution of resources, technology, information, and wealth; risk perceptions; social capital, and community structure; and institutional frameworks that address climate change hazards (Figure 2-6). This broader approach contrasts typical impact assessments that focus largely on reducing economic detriments of change. The framework is generally applicable on the local scale as a community-based or bottom-up approach and incorporates short-term exposure to variability as an important source of vulnerability superimposed on long-term change. Similar to the South Pacific Island Methodology, the framework utilizes community level perceptions and experiences to identify the characteristics that influence response, recovery and adaptation, focusing on locally relevant outcomes that promote more effective decision-making, planning and management. The framework was applied to study sea level rise impacts on northeast Graham Island, Haida Gwaii (Queen Charlotte Islands).

Climate Change and Coastal Zones: An Overview of the State of the Art on Regional and Local Vulnerability Assessment

Sterr et al., 1999, provide an overview of methodologies for assessing the vulnerability of coastal zones, present a conceptual framework for vulnerability assessment, and outline the steps that are required for the actual assessment of coastal vulnerability. The conceptual framework distinguishes between natural-system vulnerability and socio-economic vulnerability to climate change and defines many of the concepts involved in vulnerability assessment (Figure 2-7). They identify the most important biogeophysical effects of sea level rise as increasing flood-frequency probabilities and enhancement of extreme flood-level risks, erosion and sediment deficits, gradual inundation of lowlying areas and wetlands, rising water tables, seawater intrusion, and biological effects. Socioeconomic vulnerability resulting from these biogeophysical effects is categorized in terms of direct loss of economic, ecological, cultural, and subsistence values through loss of land, infrastructure, and coastal habitats; increased flood risk of people, land, and infrastructure; and impacts related to water management, salinity, and biological activity. Within the framework, analysis of coastal vulnerability starts with the natural system's susceptibility to the biogeophysical effects of sea level rise, and of its natural capacity to cope with these effects. These effects are interpreted in the context of socioeconomic vulnerability as determined by society's technical, institutional, economic and cultural ability to prevent or cope. The framework provides an acknowledgement of the concepts of exposure and risk in defining the relationship between biogeophysical effects and socio-economic vulnerability and impact. Implementation is described as three levels of increasingly complex assessment including screening assessment (SA), vulnerability assessment (VA), and planning assessment (PA). The three-level approach relates to the issue of scale as more specific planning-level assessment results at smaller scales. Thus the approach can be viewed as a tiered approach, or a scaled approach, depending on the questions that are to be considered in the assessment.

An Environmental Risk Assessment/Management Framework for Climate Change Impact Assessments

Jones (2001) presents a risk assessment and management framework for climate change impacts with a focus on individual exposure units that incorporates stakeholder involvement and links key climate variables with impact thresholds. The framework reflects modern risk assessment and management methodologies while maintaining consistency with the IPCC Technical Guidelines for

Assessing Climate Change Impacts and Adaptations. This framework introduces the important notion of critical response thresholds in the context of conditional probabilities of exceedance. Risks are managed during "windows of adaptation," through a combination of mitigation and adaptation strategies. The framework developed consists of seven steps with a central focus on stakeholder involvement. The steps include (1) identification of key climate variables affecting exposure units; (2) creation of scenarios or expected ranges of these variables; (3) a sensitivity analysis of the relationship between climate variables and impacts; (4) identification of impact thresholds through interaction with stakeholders; (5) implementation of the risk analysis; (6) Evaluation of risk, feedbacks, and autonomous adaptations; and (7) consultation with stakeholders, analysis of adaptations, and recommendations (Figure 2-8). While the linkage of these steps is not prescriptive, the order presented here is a logical progression.

North Carolina Sea Level Rise Risk Management Study

The State of North Carolina has initiated risk assessment and mitigation strategy demonstration of the potential impacts of sea level rise in that state associated with long-term climate change. The assessment is structured around four principal questions: (1) What changes to coastal flooding hazards will possibly occur between 2009 and 2100 due to storminess and sea level rise? (2) What built and living systems will be exposed to coastal flooding from increased storminess and sea level rise? (3) What possible impacts/consequences (system-wide, financial) will occur on the exposed built and living systems? (4) What short-term and long-term strategies will result in efficient and effective prevention and/or alleviation of exposure and consequences from sea level rise and increased storminess? (NCDEM, 2009). The assessment is scenario-based, utilizing potential sea level rise and demographic conditions in four "time slices" through 2100, including near term (2025), medium term (2050), long term (2075), and end of the century (2100). The approach for assessment is based on the source-pathway-receptor (SPR) model in which "sources" are climate or weather conditions that drive flood hazards, "pathways" are the mechanisms by which sources influence receptors, and "receptors" are the people, industries, infrastructure, and natural resources that may be affected by the hazard (Figure 2-9). Potential advantages of the SPR framework include the ability to break down the assessment process into constituent parts, and support for the targeted development of approaches that address vulnerability at the source, pathway and/or receptor level.

2.1.2 Framework Review Summary

Across these frameworks, there are commonalities and differences, as well as an evolution and refinement in approaches over time. All of the frameworks share common requirements to define the problem, its scale and boundaries, and characterize the biogeophysical and resulting socioeconomic impacts. Many of the earlier applications of the general frameworks, such as the Common Method and the UNEP Handbook Method were applied at larger scales and in a more qualitative way, often as a result of limited data and/or resources to conduct the assessment. Evolving approaches such as the South Pacific Island Method and the U.S Country Studies Method have recognized the importance of local knowledge and experience to supplement data limitations in the assessment of sea level rise vulnerability. Frameworks are also evolving to incorporate both the concept of tiered assessment, such as that described by Sterr et al., 1999, as well as acknowledging the importance of scale to the level of quantitative analysis that can be achieved in the assessment. More recently, frameworks such as the one adopted for the North Carolina Sea Level Rise Study (NCDEM, 2009) have formalized the application of risk assessment methodologies within the vulnerability assessment, and in particular made use of risk-based conceptual frameworks such as the sourcepathway-receptor model. Overall, sea level rise vulnerability frameworks appear to be evolving from strategies to support large-scale, qualitative screening assessments for specific future conditions, toward strategies that can be applied at regional and local scales to more quantitatively respond to

specific vulnerability questions, evaluate a range of possible scenarios, take and identify potential responses to vulnerability at the source, pathway, and/or receptor level.

In a general sense, the approaches reviewed above can be viewed as complementary, with the traditional approaches such as the Common Methodology providing a flexible procedural strategy for a relatively qualitative assessment, and the emerging methodologies focusing more on defining and quantifying the conceptual linkages between stressors and receptors and the resulting consequences. For the purpose at hand, we adopt a hybrid approach which incorporates aspects and nomenclature of the risk-based paradigm into the procedural strategies of the IPCC Common Method and the Technical Guidelines to provide a vulnerability framework that can be generalized to a broad range of potential climate impacts to coastal military installations, while providing sufficient conceptual, qualitative and quantitative strategies to develop meaningful assessments for specific questions at individual installations. This strategy is also consistent with frameworks developed for ecological risk assessment by US EPA (Figure 2-10; US EPA, 1998). In addition, as emphasized in the US Country Studies Method and the South Pacific Island Method, as well as Jones (2001), we recognize the critical importance of local knowledge and expertise in achieving meaningful vulnerability assessments for these installations. While a general framework is necessary to provide a level of consistency and comparability among assessments, a top-down, prescriptive strategy is likely to underutilize this local knowledge and expertise and result in a less satisfying assessment. Finally, we recognize and incorporate the key concept of sensitivity thresholds in the assessment as a means of focusing the effort on critical characteristics of the installation.

In the context of sea level rise vulnerability, military installations share many commonalities with other coastal communities. These include increased risk of loss or damage infrastructure, buildings, and natural resources, as well as potential increased risk for injury or loss of life. In contrast to typical coastal communities, however, military installations serve critical national defense missions that are generally not considered in other previous sea level rise vulnerability assessments. Thus an important aspect of developing this framework was to identify the important military-specific receptors that could be subject to increased vulnerabilities, and to develop strategies to quantify these vulnerabilities based on metrics that were meaningful to the military planning community. This will allow meaningful vulnerability assessments to be conducted more consistently at the regional level, while still supporting prioritization and planning at national and global scales.

2.1.3 Vulnerability Assessment Framework for DoD Installations

Strategy for the Framework

In the context of sea level rise vulnerability, military installations share many commonalities with other coastal communities. These include increased risk of loss or damage infrastructure, buildings, and natural resources, as well as potential increased risk for injury or loss of life. In contrast to typical coastal communities however, military installations serve critical national defense missions that are generally not considered in other previous sea level rise vulnerability assessments. Thus an important aspect of developing this framework was to identify the important military-specific receptors that could be subject to increased vulnerabilities, and to develop strategies to quantify these vulnerabilities based on metrics that were meaningful to the military planning community. This will allow meaningful vulnerability assessments to be conducted more consistently at the regional level, while still supporting prioritization and planning at national and global scales.

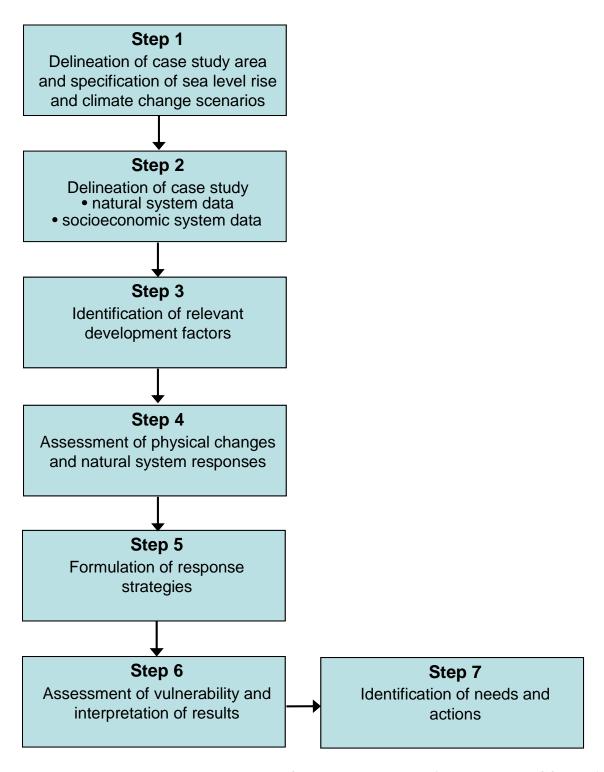


Figure 2-2. Vulnerability analysis framework of the Common Methodology (adapted from IPCC, 1992).

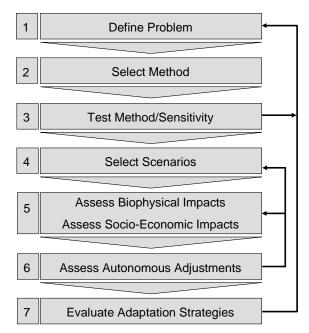


Figure 2-3. The seven steps of climate impact assessment from the IPCC Technical Guidelines (adapted from Carter et al., 1994).

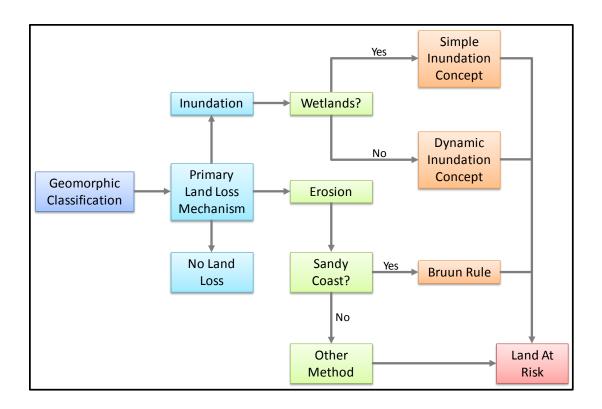


Figure 2-4. Framework diagram for selection of methods to assess land at risk from erosion and inundation (adapted from Klein and Nicholls, 1999).

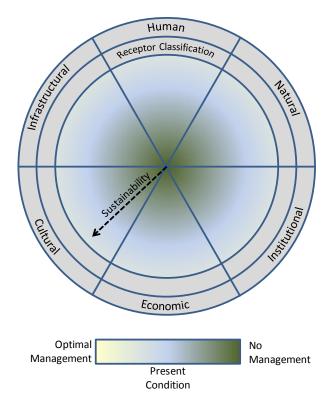


Figure 2-5. Example of the six coastal subsystem index-based assessments in the South Pacific Island Methodology (adapted from Center for Global Environmental Research, 1996).

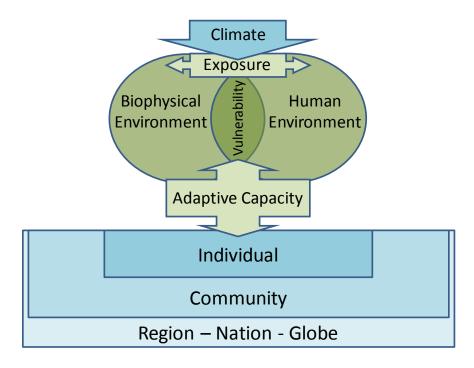


Figure 2-6. Integrated vulnerability framework (adapted from Dolan and Walker, 2006).

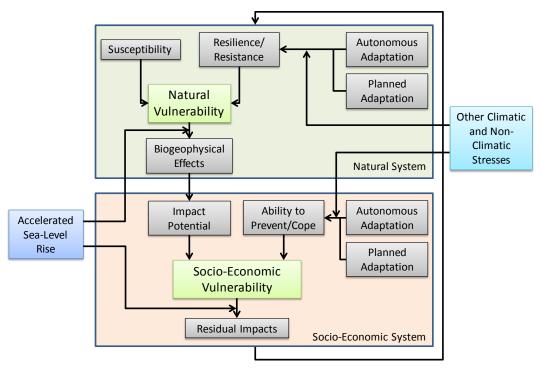


Figure 2-7. A conceptual framework for sea level rise vulnerability (adapted from Sterr et al., 1999).

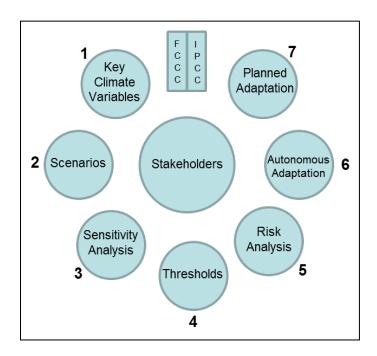


Figure 2-8. A risk assessment and management framework for climate change impacts (adapted from Jones, 2001).

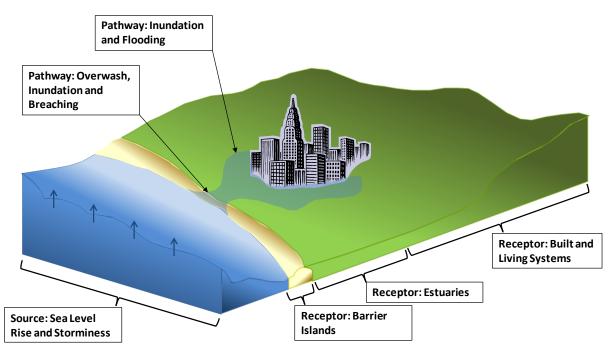


Figure 2-9. The source, pathway, receptor framework for assessing sea level rise vulnerability (adapted from NCDEM, 2009).

Overview of the Framework

The proposed sea level rise vulnerability assessment framework for DoD installations is shown in Figure 2-11. The framework is quite general, and is consistent with typical systematic planning strategies for risk assessment frameworks that have been applied to human health and ecological risk assessment (U.S. EPA, 1998; U.S. Navy, 2008; U.S. EPA, 1991), while building on the key elements of traditional vulnerability assessment frameworks. The general nature of the framework means that it can be adapted for application to a broad range of climate related vulnerability assessment applications well beyond the specific goal here that focuses on sea level rise. The framework was structured around six primary components: (1) problem formulation and scoping, (2) conceptual model development, (3) defining and validating data and modeling requirements, (4) conducting the vulnerability assessment, (5) communication of vulnerabilities, and (6) management of vulnerability. These components were structured in a roughly sequential arrangement that anticipates the potential for successive iterations. These iterations can serve to refine the assessment, can represent a progression from screening level assessment to more quantitative vulnerability or planning level assessments, or can incorporate future updates or reassessments. The framework incorporates a continuing communication with stakeholders and experts to capture and address critical concerns as well as to leverage local knowledge and expertise. The framework culminates in a management component where needs and actions are identified, and recommended response and adaptation strategies are formulated. Components of the framework are described in more detail in the following section.

2.1.4 Components of the Framework

In the sections below, we outline the common components of the vulnerability assessment framework described in Figure 2-11. These components are described in both a general sense for the structure and elements that should be considered, and also in a detailed sense in following sections for the case study applications to MCBCP and NBC.

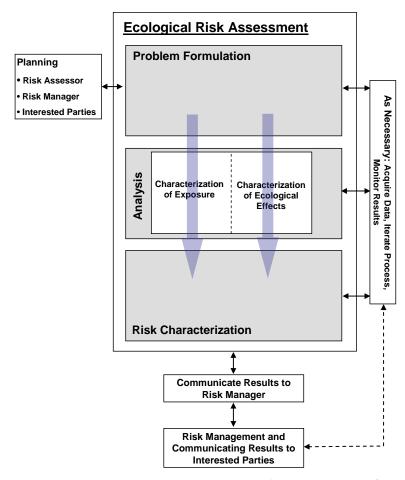


Figure 2-10. Ecological risk assessment framework (adapted from U.S. EPA, 1998).

Problem Formulation and Scoping

Problem formulation and scoping encompasses a clear development of the installation and environmental setting, the questions to be addressed, identification of the desired end products, and definition of the environmental setting, assessment scale, spatial boundaries, time span, and time resolution (U.S. EPA, 1998, NCDEM, 2009; IPCC, 1992; Carter *et al.*, 1994). Early definition of the problem and scope is critical to the success of the assessment, and provides the basis for development of the conceptual model (Figure 2-11; Figure 2-12; U.S. EPA, 1998). Vulnerability assessment for sea level rise is a highly complex and potentially costly proposition, reinforcing the need to focus the study on the critical questions to be addressed, and limiting the analysis to the aspects required to address those questions.

Identification of Stakeholders

Because stakeholder input is an essential element of the problem formulation, identifying stakeholders early in the process is important. For DoD coastal installations, there may be a broad range of both installation and non-installation personnel that should be included in the process. In general, the identification of stakeholders should be an installation-led process starting with the base commander and leading from there to constituents that either have a key interest in the assessment, or are critical to developing the assessment itself. At the installation level, this may include public

Problem Formulation & Scoping Describe the installation and environmental setting Identify question and desired end products Define the temporal and spatial scales **Management Activities** Identification of needs & actions **Conceptual Model** Formulation and Define the sources, pathways & receptors implementation of response Define the scenarios to be evaluated strategies Define the level of the assessment to be performed Develop the conceptual model Stakeholder Input Communicate the Vulnerabilities **Data Requirements & Development** Develop the assessment products Communicate the results to stakeholders Define the data/data quality requirements Develop the sea level scenarios Develop the digital elevation/installation models Develop the sensitivity thresholds **Conduct the Vulnerability Assessment** Characterize source-pathway-receptor relationships Evaluate relative to defined metrics and thresholds Assess autonomous and planned adaptation

Figure 2-11. A sea level rise vulnerability assessment framework for DoD Installations.

affairs, planning, operations, facilities, environmental, natural resources, and other key stakeholders. For non-installation stakeholders, often the installation will already have relationships that can be drawn on with interested entities such as cities, counties, ports, other state and federal agencies, as well as industry and non-governmental agencies, and the public, and it is important to work with the installation to utilize these existing relationships. In addition, the installation can help to determine the extent to which other local or regional DoD stakeholders should be involved in the process. The degree and mechanisms for involvement for this range of stakeholders should be mapped out early in the process in collaboration with the installation.

Describe the Installation and Environmental Setting

A general understanding of the installation and its environmental setting is critical to the problem formulation for the assessment. The relationship of the installation to its environmental setting provides a context for defining the conditions that will control vulnerability for a given installation. In general, this will include both a historical perspective, a description of current day conditions, and a projection of future conditions.

Identify Questions and the Desired End Products

The development of questions should be structured in a manner consistent with the Source-Pathway-Receptor model. In other words, the question should specify the source of the vulnerability, the receptor that is impacted, and the pathway of impact. Formulation of the questions in this way supports the clear communication of the connections between stressors and impacts, and provides a direct basis for the development of the conceptual model while allowing flexibility to address a broad range of climate change related questions. While the questions that drive the assessment will vary across applications, the assessments summarized in the previous section provide a general basis for common questions associated with sea level rise vulnerability. Typical general questions may include:

- What will be the vulnerability of coastal habitat and infrastructure to permanent inundation associated with climate change related sea level rise?
- How will increased flooding associated with accelerating sea level rise and increased storminess drive vulnerability to coastal built and living systems?
- How will erosion driven by sea level rise and increased storminess drive vulnerability to coastal beaches, bluffs, and barrier islands?

In the context of coastal military installations, these questions may remain general, or be refined and focused to specific receptors. For example, a general question could be formulated as:

• What is the vulnerability of MCBCP to erosion caused by the combined effects of accelerating sea level and changing storm, precipitation and wave regimes?

Or focused to a specific receptor as

• What is the vulnerability of amphibious training at MCBCP to erosion caused by the combined effects of accelerating sea level and changing storm, precipitation and wave regimes?

Clearly as the questions become refined, the applicability becomes narrower but the answers are likely to become more specific and quantitative. The important aspect at this stage is to work closely with stakeholders to formulate the questions as clearly as possible so that the assessment can be carefully tailored to answer them directly and specifically to the extent possible.

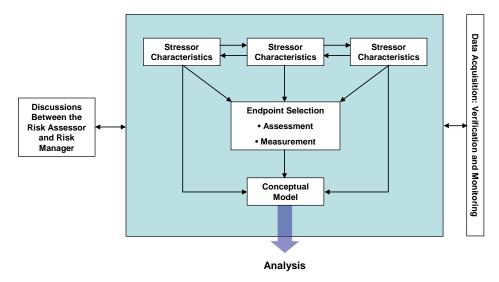


Figure 2-12. Problem formulation components for ecological risk assessment (adapted from U.S. EPA, 1998).

Specifying the desired assessment products is also a process that should rely strongly on stakeholder interaction. Because vulnerability assessments may be carried out over different scales, in different locales, and for different purposes, the desired end products will vary accordingly. As a general rule, the primary product of most vulnerability assessments is a report (U.S. EPA, 2009). In addition, while the media for a typical assessment product may culminate in a report, there are a range of other potential product media such as GIS layers, animations, models, and maps that may be critical tools for the communication and management of risk (Titus and Richman, 2001). Specific education and communication products may be useful in the form of flyers, websites, and mailers. In many cases, data and literature compiled, strategies developed and lessons learned during the course of an assessment may also serve as a template or product to improve or streamline future studies. Potential products to consider in the development are summarized below.

- Assessment Reports
- · Vulnerability Matrices
- Study Templates
- Data Repositories
- Literature Reviews & Bibliographies
- · GIS layers and tools
- Animations
- Maps
- Education & communication materials

Define the Temporal and Spatial Scales

Defining the scale and boundaries of the spatial domain requires consideration of two conceptual aspects of the system. The first consideration is the domain that encompasses the land, shoreline, infrastructure and other resources that are the subject of the assessment (e.g., Heberger *et al.*, 2009). The IPCC technical guidance (Carter *et al.*, 1994) defines this as the exposure unit and its scale is linked to the receptors of the study. The second consideration is the scale of the processes that must be accounted for to conduct the assessment. These scales are linked to the sources and pathways of the assessment. Clearly, these two scales may be considerably different, and the factors that will constrain them will be based on divergent requirements.

For a military installation, the legal boundaries of the installation itself provide one context for defining the boundaries of the assessment. Certainly the bulk of the actual vulnerability assessment may focus within these boundaries. However, to characterize the relevant biogeophysical processes, the boundaries may need to encompass broader scales such as the scale of the coastal littoral cell, or the regional watershed, and the scales of erosion, flooding, inundation, and seawater intrusion may be quite different for a given installation. Also, most military installations are highly interdependent with other regional infrastructure such as roads, power, communications, water, sewer, and many of the installations personnel may reside outside the boundaries of the base itself. Thus, sea level rise impacts that affect the regional infrastructure and communities around the installation could result in vulnerabilities to the mission and personnel of the installation.

For these reasons, selection of the spatial domain for the assessment should be considered carefully. In particular, consideration should be given to utilizing existing regional studies or collaborating with other regional programs that may be examining civilian issues in the same general area. In defining the boundaries of the area to be assessed, the coast-wise extent of the installation should provide a starting point. This extent can be expanded to include bordering areas that may support critical external access, buffers, infrastructure, or other interdependencies, or may be contracted to focus on particular aspects of the installation that are predetermined to be the focus of the assessment. In the early stages of the assessment, when uncertainty remains high, it is advisable to delineate the boundaries more broadly until further analysis allows for more refinement (Heberger *et al.*, 2009; Carter *et al.*, 1994). As a general rule, the inland extent of the assessment should be defined so that it extends somewhat beyond all areas that could be physically affected by the contemplated sea level rise scenarios. This inland scale should consider all of the contemplated pathways of impact including potentially flooding, erosion, inundation, and seawater intrusion. The offshore boundary may extend to incorporate offshore infrastructure such as piers or jetties, as well as navigation channels, mooring areas, and training areas.

For process-based boundaries, the process scales will dictate the domain. However, in the case of sea level rise, many of the relevant processes such as waves, tides, surge, wind, etc. have very large scales relative, for example, to the scale of an individual military installation. Practical application may require either the use of nested models, or more localized process estimates or boundary conditions. In considering the location of study boundaries for process analysis, the availability of data or modeling results to define the conditions at those boundaries should also be considered. Clear physical barriers may also serve as boundary locations, for example the coastal canyons along the California coast, which interrupt long-shore sand transport and distinguish the various coastal littoral cells (Hapke *et al.*, 2006). Watershed drainages and aquifer confining layers are other examples of process-based boundaries that may be useful in certain cases. While the technical nature of these process boundaries means that their final definition will not be determined in the problem formulation stage, the general requirements should be considered to the extent that they will influence the overall scope of the assessment.

Definition of the time span and resolution of the assessment is another central aspect of determining the scope of the study. The starting point of the assessment is generally grounded in the best possible delineation of the current or baseline condition, or may hindcast some historical period to provide a measure of validation for the methods to be applied. In contrast, selection of the end point of the time span for the assessment should be considered in the balance of the underlying climate drivers, the response, planning and management time scales of the target receptors, and the level of uncertainty associated with long-term projections. For a military installation, the time span must encompass relevant planning projections for mission-critical infrastructure and training requirements. In addition to the overall time span, the assessment may also require various levels of

time resolution to establish scenarios that incorporate sea level variability at different frequencies, to support modeling analysis of time varying biophysical pathways, and to evaluate receptors at certain time slices along the trajectory (NCDEM, 2009; Heberger *et al.*, 2009).

The starting or baseline condition for assessment is commonly selected as the beginning of the decade in which the assessment is conducted (e.g., Cayan et al., 2009). A primary consideration for the selection of the starting time is the availability of data to accurately delineate the baseline condition because, in most assessments, vulnerability is measured relative to this baseline. Thus, the start of the assessment generally coincides with a time as close to the current condition as possible at which the best description of the sources, pathways and receptors is available. However, because of the strong reliance of vulnerability assessments on the development of future scenarios, consideration should also be given to selection of a historical starting time that will provide a significant overlap between the range of modeled conditions and the range of available measurements. This overlap can provide a critical validation of the modeling methods that will help to define the level of uncertainty as well as to support communication with stakeholders. For example, for validation of sea level conditions, tide gauge records may be available extending back as much as 100 years, a time scale comparable to many of the forecasting requirements (Cayan et al., 2009). Similarly, historical shoreline change rates have been cataloged for many areas over similar time frames (Hapke et al., 2006). An assessment methodology that can show reasonable correspondence to these historical measurements over an extended period will provide more confidence in developing future scenarios. It may also be possible to incorporate this validation as a separate step in the assessment, as a precursor to the actual assessment.

In considering the time span for the assessment, the underlying sources of the sea level rise and variability must also be considered. Most current projections suggest that sea level rise will accelerate with the strongest rate of increase later in the 21st century. Because these projected increases are not linear, the degree of sea level rise that is evaluated depends to a significant degree on the time span of the assessment. Time spans extending 50 years may reflect sea level rise scenarios that are largely linear projections of current day trends, while time spans extending 100 years or beyond will generally reflect a much stronger degree of non-linearity and hence significantly higher sea level scenarios (Figure 2-14). While uncertainties in the projections of the magnitude and frequency of storms are more variable, the same considerations should be included, as well as considering the time span required to capture meaningful statistical representations of storms as a function of return period (Cayan *et al.*, 2009; Heberger *et al.*, 2009).

Most vulnerability assessments consider a range of potential receptors (Van Westen and Georgiadou, 2001; NCDEM, 2009). These receptors may have different response characteristics that require consideration of different time scales. Also, since the magnitude of sea level rise is expected to accelerate over time, different receptors may come into play at different time spans. For example, impact of sea level rise for buildings is likely to be linked to the frequency and magnitude of extreme events. Buildings closest to the shoreline may be significantly exposed or impacted within only 10 to 20 years, while infrastructure that is set back further from the coast may not be significantly exposed or impacted for 50 to 100 years. Given these potential differences, the life cycle of built infrastructure will also influence the time span of the assessment. From this standpoint, the time span should encompass long-term planning cycles for construction, maintenance, upgrade, and decommissioning of built infrastructure. This should be consistent with the projections and time scales of the base master plan, and other regional and national planning requirements. Training areas and natural resource receptors are likely to be controlled more by response times dictated by their associated biophysical systems. That is, while an increase in the frequency of storms may reduce the number of training days slightly, it may be the loss of the training area or capability that drives the

major concern. For example, impacts to beachfront amphibious training areas will occur over time scales associated with the shoreline erosion rates of the beach, to the extent that this erosion would significantly preclude the use of the beach for training.

A final consideration in adopting a time span for the assessment is the increasing level of uncertainty associated with increasing length of future projections of sources, pathways, and receptors (Figure 2-13; Cartwright, 2008). This uncertainty manifests in virtually every aspect of the assessment, including the characteristics of the source climate change and variability drivers; the biophysical pathways of erosion, flooding, inundation, and seawater intrusion; and the response of receptors including built and natural resources. For this reason, the time span of the assessment should be limited to the extent necessary to answer the questions to be addressed, and the formulation of these questions should be tempered by the knowledge of this uncertainty.

Along with the overall time span, the assessment may also require various levels of time resolution to establish scenarios that incorporate sea level variability at different frequencies, to support modeling analysis of time varying biophysical pathways, and to evaluate receptors at certain time slices along the trajectory. In particular, the time resolution of the source terms for sea level must accommodate the range of variability of the underlying components. This may range from relatively high frequency terms such as waves and tides, to inter-annual events such as El Niño, as well as the long-term average trend of the regional sea level. In some cases the mechanics of the assessment may dictate requirements for time resolution. For example, time domain modeling may require a minimum time resolution to accurately simulate the physics of a particular pathway such as erosion or flooding. While impacts to specific receptors are not likely to be assessed at this level of resolution, these considerations may play into the selection of appropriate assessment tools because time resolution must generally be balanced against the time span of the simulations.

A final and important consideration in time resolution is the selection of intermediate time horizons or "slices" along the trajectory of the assessment (Figure 2-13; NCDEM, 2009). In general, these slices represent relatively discrete time windows (as opposed to years or decades), and should be selected at times that are dictated by the potential vulnerability of selected receptors in the context of typical planning cycles and horizons for the installation. Because the assessment is primarily a management tool for future planning and management decisions, these time slices can help to guide a progression of response over time, rather than planning for a single condition a century in the future. For this reason, along with consideration of the potential receptors, selection of the time slices should consider planning cycles and link closely to the master planning process for the base.

Conceptual Model

The conceptual model serves as a roadmap for the assessment, defining the sources, pathways. and receptors, outlining the scenarios to be evaluated, and specifying the level of the assessment to be performed. The conceptual model should follow logically from the problem formulation by characterizing the critical components and linkages required to answer the questions to be addressed.

Define the Sources, Pathways, and Receptors

Identification of the relevant sources, pathways, and receptors for the assessment should follow directly from the problem formulation if the questions for the study are structured in a manner consistent with the Source-Pathway-Receptor (SPR) model. The conceptual model is based on the SPR framework in which "sources" are climate or weather conditions that drive hazards, "pathways" are the mechanisms by which sources influence receptors, and "receptors" are the people, industries, infrastructure, and natural resources that may be affected by the hazard. Definition of these components provides the ability to break down the assessment process into constituent parts.

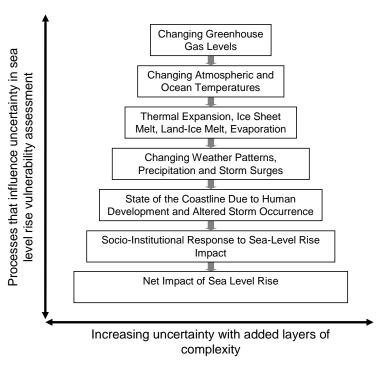


Figure 2-13. Increasing levels of uncertainty associated with the complexity of the sea level rise vulnerability assessment process (adapted from Hulme and New, 2001).

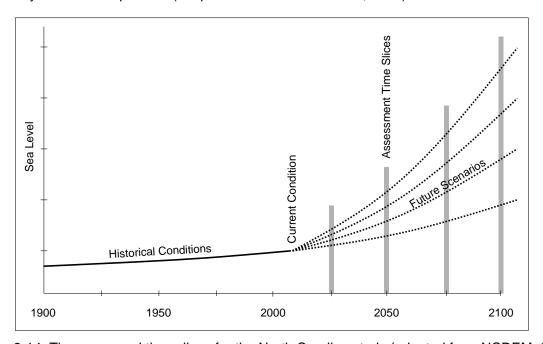


Figure 2-14. Time span and time slices for the North Carolina study (adapted from NCDEM, 2009).

Sources

Source terms that are relevant to the assessment of sea level rise vulnerability are reasonably consistent across studies, although the relative importance of individual terms may vary considerably depending on regional conditions. The importance of a given source term is also dependent on the receptor of interest. For instance, increased seawater intrusion into coastal aquifers is expected to be driven primarily by long-term changes in mean sea level, while increased rates of erosion on exposed coastlines are expected to be driven by the interaction of sea level rise with waves. Typical sources that should be considered include potential climate-related changes and interactions of local mean sea level (including uplift and subsidence), atmospheric—oceanic processes such as ENSO, storm surge, precipitation, tides, and waves. These sources are defined with respect to their potential contribution to sea level rise vulnerability below. While described separately, impacts are generally the result of interaction among several sources, and this must be accounted for in formulating sources and scenarios.

Local Mean Sea Level. Local mean sea level represents the near-field manifestation of global sea level change and is defined as the height of the sea with respect to a land benchmark, averaged over a long enough period of time to remove short-term fluctuations caused by waves and tides. While it is thus driven primarily by the same factors that influence global sea level, including thermal expansion and the release of water stored on land as glaciers and ice caps, it may also be influenced by atmospheric pressure, ocean currents, local ocean temperature changes, and vertical land movement. The magnitude of sea level response to these processes varies considerably from one location to the next, so that the global average is not always applicable on a local basis. Instead, local mean sea level is generally assumed to follow the same general trend as global mean sea level, but may be modified in accordance with local tide gauge measurements (Figure 2-15; Cayan et al., 2006; USACE, 2009). The character of these sea level rise curves generally include a linear trend, derived from the local historical trend, and an acceleration term that may be used to account for different future climate scenarios that result in different rates of thermal expansion and melting of glaciers and ice caps (US Army Corps of Engineers, 2009). Alternately, changes in local mean sea level may be linked to global mean sea level changes, which in turn are estimated from relationships with global mean surface air temperature (Figure 2-16; Cayan et al., 2008a). Significant increases in local mean sea level can lead to permanent inundation of coastal areas. The extent of inundation will depend on the degree of sea level rise and the elevation and slope of the local shoreline. In addition, while local mean sea level as such does not cause flooding, damage or erosion, secular increase in local mean sea level results in the exposure of higher coastal elevations to more frequent and progressively stronger hydrodynamic forces with the potential for increasingly severe impacts (Cayan et al., 2006).

Subsidence and Uplift. Subsidence is a component of local mean sea level caused by localized displacements of the land generally as a result of tectonic motions, consolidation and compaction of sediments, and/or withdrawal of subsurface fluids. Uplift generally results from tectonic motions and/or isostatic rebound due to the retreat of the glaciers. In some areas, the local rate of subsidence or uplift may be a source of comparable magnitude to the rate of change of local mean sea level (Burkett et al., 2003; Milliman and Haq, 1996). This may either compound or negate to some extent the potential effects of global sea level rise (Hammar-Klose and Thieler, 2001). Rates of subsidence and uplift are generally derived from geodetic differential leveling, borehole extensometers, Global Positioning System (GPS), Light Detection and Ranging (LiDAR), and Interferometric Synthetic Aperture Radar (INSAR). Rates typically range from ±5 mm/year along the west coast of the U.S., with extreme cases ranging much higher, usually in response to specific localized effects of water or oil extraction (Gornitz, 1997). Thus, the localized source effects of subsidence and uplift may be an important consideration in the long-term changes in local mean sea level at some locations.

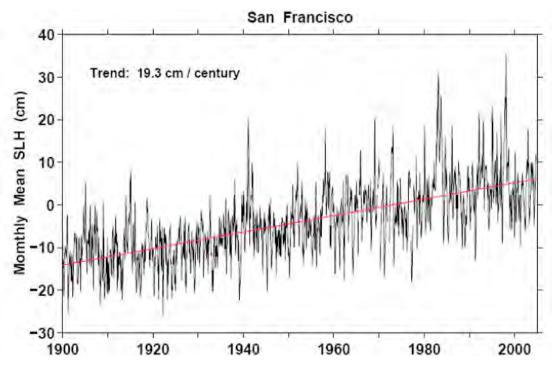


Figure 2-15. Measured local mean sea level from the tide gauge record at Fort Point, San Francisco showing the trend over the last century (based on Cayan et al., 2006).

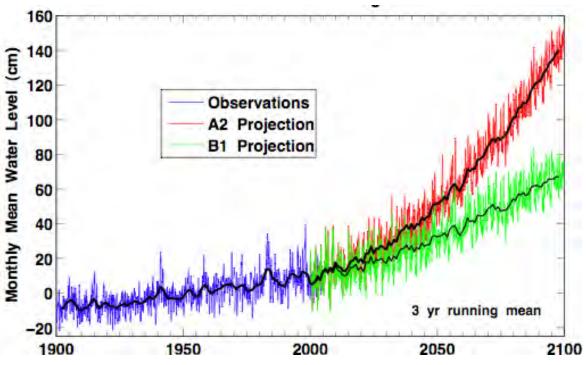


Figure 2-16. Combination of the observed and projected mean sea level for Fort Point, San Francisco extending to the year 2100 (based on Cayan *et al.*, 2008a).

Atmospheric-Oceanic Processes. Coupled atmospheric-oceanic processes including El Niño-Southern Oscillation (ENSO) or the North Atlantic Oscillation are a source of significant inter-annual variability in sea level (Nerem, 1999; Hurrell, 1995). For example, ENSO is characterized by a longperiod change in the atmosphere and ocean of the tropical Pacific region, occurring irregularly every 3 to 8 years. ENSO is a source associated with effects to both weather and ocean conditions including floods, droughts, ocean warming, and elevated sea level. ENSO cycles drive fluctuations in local sea level due to both changes in large-scale wind patterns, and surface water warming. For example, sea level increases along the west coast of the U.S. during recent El Niño events ranged from 10 to 30 cm, and significant damage occurs when El Niño events coincide with storm surge and spring tides (Figure 2-17; Flick and Cayan, 1984; Andrews et al., 2004). Historical trends indicate an increase in the frequency of El Niño events since about 1976. However, the potential interaction of ENSO with climate change is still not well defined. It is hypothesized that a warmer earth would produce more and stronger El Niños, and there is evidence that El Niños have been more frequent during the recent period of warming. While recent modeling simulations do not indicate and increase in the frequency or the intensity of ENSO, they do exhibit continued ENSO activity within the 21st century (Cubash and Meehl, 2001; Cayan et al., 2006). In any case, the interaction of El Niño effects on sea level, precipitation, and storminess with increasing local mean sea level is an important source of vulnerability. Above average sea levels also occur in the southeastern U.S. during the positive phase of the North Atlantic Oscillation.

Storm Surge. Storm surge is a source of increase in local sea level characterized as a long period wave and associated with the combined effects of storm driven wind and low atmospheric pressure weather. Sometimes the elevation of sea level due to waves and wave- induced surges is also included in storm surge. Storm surge is generally strongest when storms move onto shallow coastal waters in areas such as the North Sea, the Gulf of Mexico, the Bay of Bengal, and the Adriatic Sea. Surge height and duration is influenced by a range of factors including the translational velocity and duration of the storm, the speed, intensity, radius of the wind field, track angle to the coastline, coastal topography, offshore bathymetry, as well as wave effects (NOAA, 2011; Lin et al., 2010; Fleming et al., 2008). Duration may range from hours to days, and magnitude from centimeters to several meters. Because they both derive from storms, the co-occurrence of storm surge and high waves may be particularly damaging. For example, wave-induced surge on a beach can reach 40% of the significant offshore wave height, which has been observed to reach 10 m on the southwest U.S. coast in rare extreme storm events. The impact of storm surge is likely to be enhanced by increasing mean sea level; however, climate change may also influence the frequency and magnitude of storminess and storm surge for a given location (IPCC, 2007b). Climate factors that potentially contribute to more intense storms include increases in ocean heat content and atmospheric water vapor which have both increased over the past several decades (NOAA, 2011).

<u>Precipitation.</u> While direct influence of precipitation and evaporation cycles plays a role in the large scale water balance and level of the oceans, the localized effects of precipitation and its contribution to runoff, river flow, ground saturation and subsequent flooding and erosion are of principal concern. Because high levels of precipitation accompany storms that may also result in high waves and storm surge, the interaction of these events with increasing local means sea level is of particular concern. While this source is expected to be most critical in areas of rivers and estuaries, these events may also be significant in bluff erosion and in straining the abilities of storm water conveyance infrastructure in a broad range of coastal military installations.

<u>Tides.</u> In many areas, tides are the source of the largest variability in sea level on all time scales of practical interest, short of the millennial time scales associated with glaciations and de-glaciations (Cayan et al., 2008a). Peak tides may be particularly important to flooding and beach erosion, since

coastal problems tend to occur when large waves coincide with peak tides and enhanced sea levels due to storm surges and El Niño (Flick and Cayan, 1984; Flick, 1986, 1998, 2000; Flick and Badan-Dangon, 1989). Where reliable data records exist, tidal fluctuations are highly predictable over extended periods of time. However, there is evidence that tidal characteristics in some areas may be changing over time (Flick et al., 2003) although the cause is not yet known. There is also the potential for changes in tidal conditions with changes in local mean sea level because the amplification and propagation of tides near the coast is highly dependent on topography and water depth, both of which are likely to change with accelerating sea level rise.

<u>Waves.</u> Wind-generated waves are surface waves that occur on the free surface of oceans, seas, lakes, and rivers as a result of wind blowing over a significant length of fluid surface. Ranging in size from centimeters to tens of meters, waves may be generated locally or may travel as swells for thousands of miles before reaching land. Waves provide nearly all of the energy input that drives shoreline processes along the exposed portions of the coast. Understanding the interaction of local sea level rise with wave impacts is a key element to understanding and dealing with coastal processes, especially flooding and erosion. Wave setup can also induce enhanced flows through tidal inlets resulting in increased flooding in bays and harbors (Nguyen et al., 2007).

Pathways

Pathways represent the process or mechanism by which sea level rise sources act on receptors to cause impact. Pathways of action for sea level rise generally include inundation, flooding, erosion, and seawater intrusion. Often, a given pathway may be governed by the combined action of multiple sources and may influence a range of potential receptors. A solid conceptual understanding of these pathways is critical to establishing a meaningful vulnerability assessment, as well as to formulating response and adaptation strategies. Primary pathways are defined with respect to their associated mode of action and relationship to exposure below.

Inundation. In the context of this framework, inundation is considered as an exposure pathway resulting from a long-term increase in local mean sea level, in contrast to the short-term exposure that may occur in association with flooding. Thus, inundation is primarily linked to the local mean sea level source, and its importance is strongly influenced by the elevation and topography of the coastline. If the increase in local mean sea level is severe enough, coastal areas that were previously dry will become permanently submerged, potentially resulting in significant loss of land, infrastructure, and habitat.

Flooding. Flooding is an exposure pathway that interacts with increases in local mean sea level to increase the frequency and magnitude of short-term impacts to coastal areas. In addition, climate change may also lead directly to increases in storminess relative to current conditions, thus compounding the influence of sea level rise increase. Flooding often results through the interaction of multiple sources including storm surge, waves, and precipitation. These impacts may be exacerbated if storms co-occur with high tides or El Niño conditions. As with inundation, the sensitivity of coastal areas to increased impacts from storminess and the interaction of storms with sea level rise are highly dependent on the topography and geology of the shoreline.

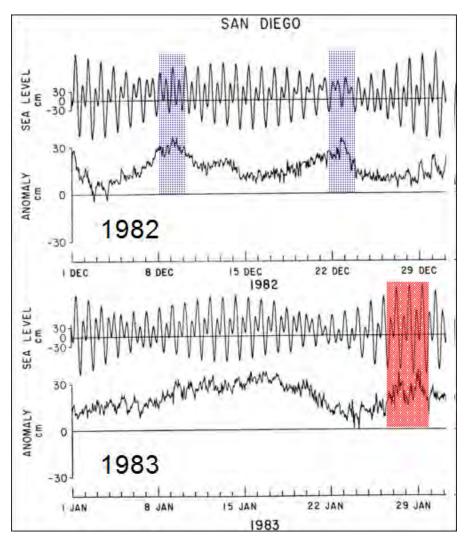


Figure 2-17. El Niño and winter storm events in 1982 co-occurring with neap tides, and in 1983 an event co-occurring with spring tides (adapted from Flick, 1986).

Erosion. Erosion is another significant pathway of exposure for sea level rise vulnerability. In the broadest sense, coastlines tend to recede as sea level increases, and this recession occurs partially through erosion. Erosion is often varies considerably over annual cycles with offshore transport during the winter and onshore transport in the summer. Local net erosion is generally controlled by transport and a balance of sources and sinks, including sea cliffs, rivers, gullies, dunes, nourishment, and coastal canyons. Increases in erosion are fundamentally linked to the interaction of waves with local sea level rise. Sea level rise combined with storm-driven wave and storm surge may drive significant increases in wave-induced erosion of coastal landforms. With higher local mean sea level, increases in erosion will also depend on potential changes in wave height, wave direction, and changes in the frequency and duration of storms, and the extent to which this erosion is balanced by other sources.

Seawater Intrusion. Seawater intrusion in surface water and groundwater due to increases of local mean sea level is another exposure pathway for vulnerability. These impacts can be exacerbated by drought cycles, changes in storminess and precipitation, and increasing demands on water supplies due to population growth. Salinity intrusion into rivers and estuaries can also impact sensitive aquatic plants and animals that do not tolerate high salinity. **Receptors**

Common receptors for sea level rise vulnerability have been identified in a range of previous assessments (US EPA, 1989; Titus et al., 1991; FEMA, 1991; Van Westen and Georgiadou, 2001; Nichols, 2002; NCDEM, 2009). Nichols (2002) summarized a range of potential receptors to include property, coastal habitats, human life, coastal protection works and other infrastructure, renewable and subsistence resources, tourism, recreation, transportation functions, cultural resources, agriculture and aquaculture. The North Carolina study defined similar receptors including ecological, agriculture, and aquaculture, buildings/coastal structures, critical infrastructure, and societal. In the risk assessment of natural disasters, "high potential loss facilities" such as nuclear reactors, dams, and military installations are generally not included unless supplemental studies specific to these facilities are carried out (Van Westen and Georgiadou, 2001). Thus, there is a need to identify receptors that are applicable for the assessment of military installations. SERDP (2007) defined a range of military-relevant receptors that may be vulnerable to sea level rise to varying degrees including mission essential infrastructure, mission capabilities, training and testing lands, transportation means, facilities and/or corridors, storm damage, increased potential for loss of life. For purposes of this framework, we have adapted these previous definitions to align with general categories more commonly used by planners, engineers and facilities personnel at military installations. These receptor categories include:

- Training and Testing Lands
- Buildings
- Waterfront Structures
- Coastal Structures
- Civil Infrastructure
- Military and Civilian Personnel
- Protective Buffers and Natural Resources

These categories serve as fundamental generalized receptors that span a reasonable cross section of the potential endpoints of interest for coastal military installations. In general, receptors will be identified on a site-specific basis and may encompass broad categories such as these or specific subcomponents, depending on the requirements of the assessment, the questions to be addressed, and input from key stakeholders. In the course of the assessment and through stakeholder interaction, receptors may be added or screened out, or potentially weighted at different levels depending on their value and criticality to the installation. As a starting point, these generalized receptors are defined below, and more site-specific examples are given in the case study sections for MCBCP and NBC that follow. Characterization of these receptors requires an understanding of both their potential sensitivity to sea level related exposure pathways, as well as their adaptive capacity through autonomous adjustment and planned adaptations.

Training and Testing Lands. Training and testing lands are a category of receptors that encompass the coastal land areas that support training and testing missions. In many instances, testing and training require a broad range of coastal terrain and conditions and thus this category can span many different land forms such as beaches, bays, estuaries, rivers, barrier islands, wetlands, bluffs, and lagoons. These areas support many types of training and testing missions including amphibious

assault training, coastal components of maneuver corridors, amphibious landing beaches, airfields, and beach/bay training areas. On exposed shorelines, these receptors are particularly susceptible to erosion, while broader areas of exposed and protected lands may be impacted by inundation and flooding.

Buildings. This category includes a range of buildings that support operations and missions of the installation. This could include buildings for housing, logistics, training, testing, operations, and security. These receptors are susceptible to sea level rise sources through all major pathways including inundation, flooding, erosion, and seawater intrusion. Of particular interest are building structures that are already close (e.g. within 200 ft horizontally) to the high tide line, and the relationship of building foundation and finish floor elevation to projected sea level elevations. Autonomous adaptive capacity for buildings is generally limited, while planned adaptation can range from shoreline protection to retreat strategies.

Waterfront Structures. This category includes a range of structures that support waterfront operations and missions of the installation. This category encompasses structures such as piers, wharves, quay walls, floating docks, and graving docks. These receptors are susceptible to sea level rise sources through all major pathways including inundation, flooding, erosion, and seawater intrusion. Of particular interest for waterfront structures are vulnerabilities associated with overtopping, sea levels that obstruct mooring and berthing, loss of function for dockside utilities, and increased physical loading from water uplift or current forces in relation to the structural capacity. As with buildings, autonomous adaptive capacity for waterfront structures is limited, while planned adaptation can involve strategies ranging from structural modifications to extend operational life, to planned replacement with more resilient structures.

Coastal Structures. This category includes a range of coastal structures whose primary purpose is to protect the shoreline from erosion and thus sustain operations and missions of the installation. This category encompasses structures such as jetties, groins, and revetments, which are used to protect the shoreline and dredged improvements. These receptors are susceptible to sea level rise sources, particularly through inundation, flooding, and erosion. Of particular interest for coastal structures are vulnerabilities associated with changes in currents, wave climate, and water levels that may influence the functionality and performance of coastal structures under various sea level rise scenarios. Autonomous adaptation is limited, and adaptation strategies for these structures are generally interlinked with the infrastructure that they are designed to protect.

Civil Infrastructure. This receptor category describes a broad category of built infrastructure that is critical to the day-to-day operations and mission of the installation. The category includes receptors ranging from critical utility infrastructure such as buried utilities, fuel transfer/supply, transportation corridors, potable water systems, and storm water conveyance systems. These receptors are susceptible to sea level rise sources through all major pathways, including inundation, flooding, erosion, and seawater intrusion. Of particular interest for infrastructure are vulnerabilities associated with overtopping, buoyancy effect on underground infrastructure, and seawater immersion and/or spray on low-lying electrical and communication utilities. We include in this category groundwater aquifers that support potable water extraction for the installations. As with other built infrastructure, autonomous adaptation is limited.

Military and Civilian Personnel. Increasing sea level poses the prospect for injury and loss of life at coastal military installations, both from the prospect of increased flood frequency similar to civilian communities, but also from the tension between these increasing physical impacts and the requirements of the military to carry out its mission anyway. In both cases, increased vulnerability of military and supporting personnel is predominantly linked to the potential for more frequent and

severe flood events that are likely to result from the co-occurrence of storm surge, high waves, high tides, and increasing local mean sea level. While this potential is not viewed as being severe, potential vulnerabilities do exist, particularly in association with severe storm impacts at the human interface on military bases, and due to more dangerous conditions in coastal training grounds such as swimmer/diver training areas and amphibious landing zones. Severe erosion along seaward bluffs pose a threat to military personnel in near shore facilities, as does severe flooding that may occur in association with combined effects of high sea level with strong storm water runoff flows. Adaptation in this context could include strategies from heightened awareness and warning systems for storm conditions, to incorporation of sea level condition and safety analysis in operational planning.

Protective Buffers and Natural Resources. Protective buffers are generally classified as non-engineered coastal areas that provide a natural means of protection for coastal installations from changes in sea level. These can include receptors such as beaches, dunes, and wetlands that are generally in the first line of exposure to changing sea level. Along with protecting the coastal installation, these buffer areas often serve as critical habitat for natural resources that are under the management of the installation. Thus, impacts to these protective buffers may go hand-in-hand with impacts to natural resources that are dependent on this habitat. These receptors are susceptible to sea level rise sources, particularly with respect to inundation, flooding, and erosion. Autonomous adaptation capacity of these receptors is often a function of their ability to adjust landward at a rate that is sustainable in the face of sea level rise.

Define the Scenarios to be Evaluated

Future estimates of sea level rise vulnerability depend on a broad range of biophysical and socioeconomic variables. This, combined with the complexity of the interactions of these systems makes the prediction of future conditions highly uncertain. For this reason, sea level rise vulnerability assessments are generally developed based on a limited set of scenarios for both the driving source terms, as well as for the receptors. In establishing source scenarios, IPCC (1994) identifies three general strategies including synthetic, analog, and general circulation model scenarios. Synthetic strategies generally utilize a range of adjustments to a baseline condition to establish assessment scenarios. This is exemplified by the scenarios from SERDP (2007), where four specified increases in mean sea level (0.5, 1.0, 1.5, and 2.0 m) were identified for the assessment of sea level rise vulnerability at coastal military installations. The magnitude of these adjustments should be consistent with a range of modeled or published future scenarios. Analog strategies utilize identified historical climatic regimes to serve as models for future climate scenarios. Thus, historical records of transitions from low to high stands of sea level could serve as analogs for future scenarios of increasing sea level. The third strategy utilizes climate models, combined with plausible future assumptions for emissions, to develop a range of potential scenarios for sea level rise assessment.

For the purposes of this project, we utilized the synthetic SERDP scenarios as estimates of local mean sea level (assuming negligible vertical land movement), but incorporated climate modeling results primarily for the purpose of evaluating future sea level variability associated with changing wave and oceanographic conditions. The initial application of this method in this project focused on available results from a single climate model and a single emission scenario rather than ensemble results due to project limitations in generating multiple outcomes through the entire climate and wave modeling process. Where available, results from multiple models were evaluated to determine the consistency of the model used for the project. In addition, even under the relatively high emission scenario used for this study, future wave condition did not vary substantially from current day conditions. However, ongoing efforts are underway to expand the range of available modeling results and future analyses and assessments should consider this broader range of conditions to better bound the uncertainty of the methods.

In addition, scenario development for assessment of sea level rise at coastal military installations must consider the projected future development in and around the installation itself. Although developmental changes in and around the installation are not likely to have a measureable global impact, they may be critical to the assessment to the degree that they influence exposure and vulnerability, as well as for the opportunities they present for implementation of adaptation measures. Clearly, the location and characteristics of future development on the installation will influence its future vulnerability to sea level rise. Thus, scenarios for future development at the installation should be a key element of the scenario development process.

Define the Level of the Assessment to be Performed

A final consideration prior to the development of the conceptual model is the level of the assessment to be performed. As described in the framework, vulnerability assessment is often an iterative process, and the complexity of sea level rise vulnerability analysis dictates that different levels of assessment may be appropriate depending in the scope of the project and the resources and data available. In many cases, preliminary screening analysis may be important to even framing what the critical questions for a more detailed assessment will be, or which spatial areas may be most sensitive (e.g. Hammar-Klose and Thieler, 2001). While the need for screening or subsequent iterations will be a site specific decision, a common construct is to consider at least two levels of analysis. The first level is often termed a screening level assessment, and the subsequent level a baseline or detailed assessment. For the purposes of this study, we adopt the "detailed assessment" terminology to avoid confusion with the use of the term baseline to describe the starting condition of the assessment. This strategy is commonly applied in ecological risk assessment, and has recently been adopted by the Australian Department of the Environment and Heritage (Commonwealth of Australia, 2006; Figure 2-18) and others in climate change vulnerability assessment as well.

Screening Assessment

Both levels of assessment grow out of the conceptual model, but the screening level analysis will be more simplistic, and should generally be more conservative. The goal of the screening level assessment will often be to determine if more detailed analyses or data are required, and if so, for what areas, sources, pathways, and receptors. Historically, screening level assessments for sea level rise vulnerability have focused on inundation. These assessments generally assume a static coastline (no erosion), which is inundated to varying degrees under prescribed local mean sea level rise scenarios. Short-term flooding events with lower probability but higher magnitude have also been assessed with these static inundation approaches. When attempted, screening level analysis of shoreline erosion has usually been limited to beaches, and generally assessed with simple analytical methods such as the Bruun rule (Bruun, 1962). In an alternative approach, Hammar-Klose and Thieler (2001) applied a regional screening method to the coast of California using information on coastal geomorphology, rate of SLR, past shoreline evolution, and other factors to identify areas where physical changes were more likely to occur due to SLR. Similar screening strategies such as the Ghyben-Herzberg principle (Herzberg, 1961) have been applied for analysis of seawater intrusion into groundwater, as well as estuaries. While these methods may be less than quantitative, or may carry a high degree of uncertainty, they are still often quite useful in guiding the effort to the critical questions, and focusing resources on the important areas, sources, pathways and receptors for more quantitative analysis and reduction of uncertainty. For these reasons, screening level analysis is an important component of sea level rise vulnerability assessment.

Detailed Assessment

The detailed assessment is generally used to identify and characterize current and potential impacts to receptors associated with sea level rise sources. If the detailed assessment follows a screening level cycle, it will generally focus on refinement of the assumptions, methods, and data used during the screening assessment to provide a more quantitative analysis and reduce uncertainties. In the context of sea level rise, detailed assessment may require moving from the use of limited available data to extensive data collection. It may also require the application of more sophisticated models, extending beyond simple inundation analysis to include, for example, more rigorous shoreline evolution modeling, dynamic flood modeling and mapping, and two- or three-dimensional groundwater modeling. The detailed assessment may also adopt more rigorous methods for projecting socioeconomic conditions.

Develop the Conceptual Model

The conceptual model should be viewed as an evolving tool that is updated as the assessment progresses, and in the end captures a simplified yet accurate representation of the vulnerability assessment. In risk assessment, the conceptual model generally combines a written description and visual representation of hypothesized relationships between sources, pathways, and receptors (U.S. EPA, 1998). As we have seen, a conceptual model for sea level rise must also describe the spatial and temporal context of the assessment, and layout plausible future scenarios for both biophysical and socioeconomic systems. Visual representations of conceptual models may take on a range of different forms, depending on which aspects of these relationships are described. Typical representations include source-pathway-receptor diagrams that illustrate which sources potentially drive vulnerability for a given receptor and though which pathway or pathways. Spatial models are also useful for illustrating the juxtaposition of sources and receptors within the assessment domain.

Temporal representations are also useful to illustrate the hypothesized or assumed evolution of the system through time. Clearly, the construction of the conceptual model will be site specific, and the level of detail will evolve over time as the model is updated to capture the results of the assessment. However, at least to some level, conceptual models for the assessment of sea level rise vulnerability should capture the relationships between sources, pathways, and receptors, and illustrate the spatial and temporal dimensions of the assessment.

Source-Pathway-Receptor Relationships

Sea level rise sources terms are linked to receptors by process-based pathways that describe the mechanism of impact. A conceptual model provides a means to map these relationships and provide a roadmap for assessing vulnerability to the selected receptors. For a specified receptor, a SPR linear flow chart can be used to illustrate the source or combination of sources that act through a given pathway to impact that receptor. Multiple combinations of sources, pathways, and receptors can be mapped in this way to construct a conceptual model that addresses all of the identified questions to be addressed by the assessment. Figure 2-19 shows a generic example, mapping the combined source impacts of local mean sea level rise and subsidence via the inundation pathway to mission essential infrastructure receptors.

Spatial Relationships

While conceptual models of SPR illustrate how sources act through pathways to impact receptors, they don't provide a spatial context for these relationships. A spatially oriented conceptual model can help to establish the physical proximity and connectivity that enables these interactions in a way that is often more intuitive for stakeholder communication. Two-dimensional illustrations of shoreline erosion hypothesized littoral transport pathways, sand mass balance, inundation, and flood zones are

all examples of processes that can be captured in spatial conceptual models. Spatially oriented conceptual models may also be useful in illustrating the potential study domain and boundaries for a given assessment. These spatial descriptions should still be consistent with the SPR framework, and may need to focus on a limited number of receptors at a time to avoid becoming overly complex.

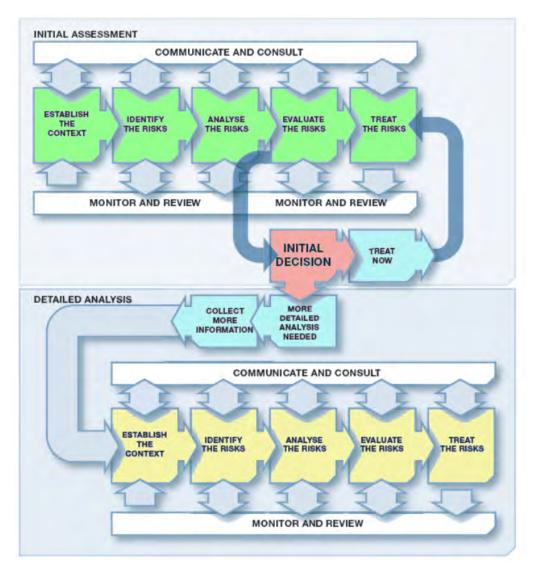


Figure 2-18. Tiered assessment approach from the Australian framework (adapted from Commonwealth of Australia, 2006).

Temporal Relationships

Finally, the temporal nature of the sea level rise vulnerability assessment dictates that conceptual models may also be useful in the time domain. A temporal conceptual model should illustrate hypothesized time slices or trajectories over the period of interest for the assessment. This could be as simple as a before vs. after cross section of the shoreline, a series of conceptual time slices, or the continuous trajectory of a particular parameter over time. This can be particularly useful for illustrating the overall time domain for the assessment, as well as representing the selected time slices that have been selected.

Data Requirements and Development

Data requirements and development for the vulnerability assessment focuses on defining what data is required, characterizing the quality of the data in the context of uncertainty, and developing these data into the products required to perform the assessment (Basher, 1999; NOAA, 2009).

Define The Data/Data Quality Requirements

Data and data quality requirements can be defined in the context of the source-pathway-receptor conceptual framework. In this context, sea level rise vulnerability assessments will share the same general data requirements for most coastal military installations. Installation-specific requirements will vary to some degree as a function of geographical location, site-specific coastal processes, and the type, character, and mission of the installation. Typical data requirements based on the installations studied in this project are summarized below, and described in additional detail in subsequent sections.

Sources

Data requirements for sea level source terms are developed based on the key contributing subcomponents that govern short- and long-term regional trends and fluctuations. For the southwest U.S. where this project was focused, the primary sea level source terms are mean sea level, tides, and waves, along with non-tidal residuals, which include effects of storm surge, El Niño, and other largescale oceanographic phenomenon. A range of methods exist for establishing mean sea level trends (e.g., Rahmstorf, 2007; USACE, 2009) that require different data. For this study, we utilized the SERDP prescribed scenarios and followed the USACE (2009) approach for which the data requirements to establish future mean sea level conditions include the historical regional trend, the mean sea level for the tidal epoch centered on the starting year, and the sea level at the end-year condition. In some cases, data may be required to establish local subsidence or uplift rates as well. The majority of this data (regional trends, starting conditions) are determined from local tide gauge data. Future tides are generally predictable from harmonic analysis of historical data, and data sources for these predictions are broadly available. For non-tide residuals, there are two approaches, one using historical tide data, and the other using general circulation models. The use of historical data requires an adequately long historical tide gage record, and presumes that future non-tide residuals will be similar to historical conditions. Because many of these fluctuations are low frequency (decades), historical tide gage data must be adequately long to resolve and quantify the return period and magnitude. Alternatively, non-tide residuals can be estimated using general circulation models, in which case an extensive range of data (not described here) is required to parameterize the model. Many of these model runs for a range of climate futures exist and can be mined for application to quantifying this source term. Similarly, for wave simulations, these conditions can be developed from historical data or from climate model winds. Wave records are often no longer than a few decades, and so it may be difficult to accurately estimate the magnitude of episodic events (e.g., 100-year storm waves). Detailed examples of the compilation and analysis of these data sources are presented in Section 3.1.

Pathways

Data requirements for the assessment of physical exposure pathways can be extensive. Quantifying these responses often requires a range of historical data and model parameterization. For erosion on exposed shorelines, long-term response models generally require information on the shore profile and substrate, as well as information on the sea level rise trajectory. Additional information for beaches such as sand budgets and transport patterns may also be required. Because episodic events may

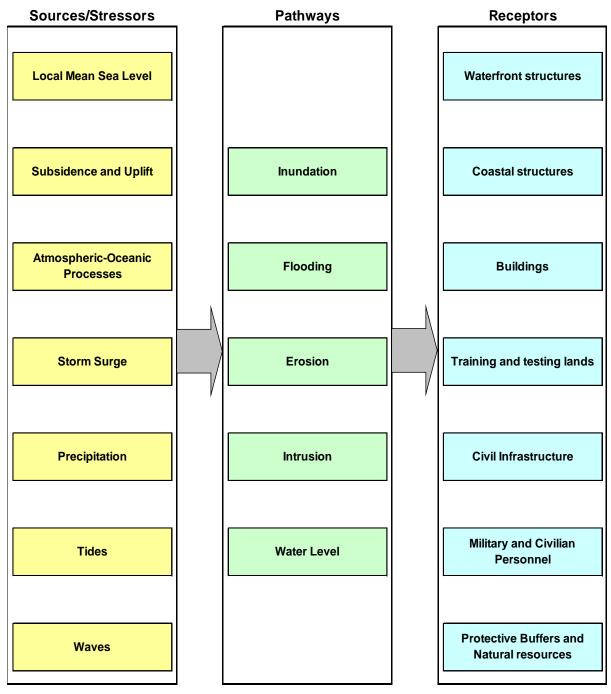


Figure 2-19. Generic conceptual model for vulnerability assessment of coastal military installations. Note that local mean sea level includes vertical land movements.

influence the long-term change, data that reveal the relationship between these events and shoreline response can also be important. For these short-term episodic events, empirical or modeling approaches may be used to estimate the shore response. Empirical estimates generally rely on measured relationships between wave/storm conditions and beach profile change. Modeling approaches will generally require information for the starting condition of the shore along with time series conditions for the wave and water level forcing, along with historical shoreline and wave data for hindcast and validation.

Flooding and inundation pathways require data to simulate the movement of water into upland areas as water levels rise. This generally requires high-resolution elevation maps, benchmarks for vertical datum conversions, land cover and shore protection, uplift or subsidence rates, and water level scenarios. For the southwest U.S. where storm surge is a minor component of total water level, static analysis may be sufficient, while in other areas where hurricane impacts are dominant, dynamic analysis of storm surge may be required with additional data requirements.

For protected harbor and bay areas, assessment of changes in water levels and currents required data to support hydrodynamic modeling. These data generally include high-resolution bathymetric and shoreline elevation data, water levels at the forcing boundaries (e.g., ocean and river), and water level and currents measured within the harbor for validation purposes.

General data requirements for the seawater intrusion pathway will include land elevations, lithology of the aquifer, water levels at the ocean and upland boundary, other source and loss terms within the domain, and water levels and salinity data within the domain for model validation. Detailed descriptions of data requirements for the range of exposure pathways assessed in this study are provided in subsequent sections.

Receptors

The receptor categories described previously provide a framework for establishing data requirements. Building, civil infrastructure and waterfront structure data for a given installation are often available through the public works officer at the installation or region. In general, this data is represented in GIS layers that may or may not correspond to the categories defined here. Coastal structures and natural buffers may not be described in the GIS, but may be available through natural resource management plans or other regional sources. Often these items can be cataloged from imagery or national wetland inventory data if they are not present in the installation GIS. Although not specifically addressed in this study, data to support evaluation of the adaptive capacity of receptors are also fundamental to the vulnerability assessment. A detailed description of the receptor data used in this study is provided in subsequent sections.

Develop the Sea Level Scenarios

Sea level scenarios represent future conditions on the basis of the integration of source terms, spatial and time scales as defined in the conceptual model. The scenarios can be constructed in a variety of ways where the emphasis on different source terms may be a function of their importance to a particular installation. In the end, the goal is to produce a cross-section of conditions that represent the expected range of future conditions. In addition, to the extent possible, the scenarios should incorporate estimates of the uncertainty associated with these conditions.

In the general approach used for this study, water level sources are determined through a range of modeling and empirical methods, and then integrated to construct a range of scenarios which are exposure dependent. Thus, different scenarios were developed for exposed shorelines, protected bays, and groundwater systems because these exposures are subject to different combinations of sea level sources. SERDP-prescribed mean sea level conditions at 2100 were translated to mean sea level curves for the next century through an empirical model. IPCC future climate scenarios were used to parameterize general circulation models, which in turn were used to generate atmospheric and oceanographic conditions. These conditions were applied directly to estimate local non-tidal fluctuations in sea level (non-tide residuals), as well as to drive wave models to simulate run-up. Finally, empirical harmonic models were used to predict tides, and the various source terms are integrated (in a statistical sense) to create exposure-dependent scenarios for exposed shorelines, protected bays, and groundwater. Detailed examples of this procedure for the MCBCP and NBC installations are presented in subsequent sections.

Develop the Digital Elevation and Installation Models

A fundamental aspect of conducting the vulnerability assessment is developing an integrated model of the terrain elevation and installation infrastructure. This integrated model serves as the backbone for the analysis, starting with assessment of the physical response of the shoreline, and building toward the analysis of inundation and flooding. This model also provides the basis for understanding the basic sensitivity of the installation receptors to different magnitudes of sea level exposure. Just as in ecological risk assessment, we can define dose-response curves for receptors to physical or chemical stressors, with an integrated terrain and installation model, we can define the dose-response of our installation components to the physical impacts of water level, erosion, seawater intrusion and other exposures associated with sea level rise.

In developing this integrated model, the terrain data is compiled, generally to the best degree possible from available sources. The data are integrated to provide a complete representation of the terrain at the installation for the baseline (current day) condition. For analysis purposes, the shoreline data must be classified with respect to erodability. In some cases, this may be a distinction between a hardened shoreline (coastal structure) and a natural buffer, while in other cases it could be the distinction between a rocky coast and a sandy beach. As a parallel effort, the data describing the built infrastructure of the installation must be compiled. Integration of these data sets then allows for an accurate representation of the vertical elevation of the infrastructure, as well as the lateral location with respect to the shoreline. This vertical and horizontal registration then allows for analysis of exposure with respect to water level, erosion, and seawater intrusion pathways. Often, it is useful to filter the data at this point to limit the assessment to areas and infrastructure that is within a reasonable range of the expected exposure scenarios. Detailed examples for MCBCP and NBC are provided in subsequent sections.

Develop the Sensitivity Thresholds

Determining sensitivity thresholds for the range of receptors at an installation provides a means of streamlining the vulnerability assessment, and targeting limited resources for adaptation to the most critical vulnerabilities. Sensitivity thresholds are generally specific to a given installation and represent the exposure to a given stressor that will bring about a rapidly accelerating rate of response. Threshold elevations are a characteristic of most installations where, due for instance to a leveling of the terrain combined with a density of infrastructure, when sea level reaches that level the potential for damage to the installation can increase dramatically. Similarly, for seawater intrusion, increasing sea level may increase salinity levels inland, but a threshold occurs when the allowable level of chloride is exceeded in potable water production wells. Sensitivity curves, developed as described above from the integrated terrain and installation model, provide the means to identify these thresholds and incorporate them into the assessment.

Conducting the Assessment

Conducting the vulnerability assessment requires a characterization of complete source-pathway-receptor scenarios. With the conceptual model as a guide, and defined scenarios and baseline conditions, assessment consists of determining the pathway responses of the system, and quantifying the associated vulnerabilities in the context of the installation sensitivity.

Characterize Source-Pathway-Receptor Relationships

To assess vulnerability, the response of the system to estimated future conditions must be determined. The specific methods for characterizing various response pathways may vary for different studies and locations, but in general will require the application of a range of biophysical response models that provide a simulation of the response of the coastal system. These can range

from hydrodynamic and morphological models, to groundwater transport and flood routing models and may be theoretically or empirically based. To reduce uncertainty, the response models should be grounded in the context of historical data and well proven, at least under current conditions. The goal of using these models is then to create plausible representations of future conditions at the installation with respect to water levels, currents, shoreline locations, and other sea level controlled conditions.

In the strategy adopted here, exposure-specific future sea level scenarios are used to drive a range of pathway-specific models. For exposed shorelines, we examined both long-term response to mean sea level, and short-term response to episodic events. These response models are used to develop modified terrain models that account for erosion and accretion, and quantify the potential for inundation and flooding. Protected harbor areas are assessed under scenarios that exclude wave exposures, but account for sea level rise, tides, and non-tide residuals. Hydrodynamic models are applied to evaluate the expected changes in water levels, currents and bottom shear. For groundwater, a cross-sectional transport model was constructed through a critical section of MCBCP to account for potential responses of the freshwater aquifer to elevated ocean boundary conditions. The scenarios for this exposure utilize monthly average to correspond to the typical time step of the model, and because the long-term groundwater response is highly filtered by the low permeability of the soils. Response is measured in terms of changes in groundwater flow patterns, and landward migration distance of the saltwater front. Detailed analyses following this strategy are described in subsequent sections of the report.

Evaluate Relative to Defined Metrics and Sensitivity Thresholds

The final characterization of vulnerability incorporates the three primary products of scenarios, pathway response assessment, and receptor sensitivity and adaptive capacity. Scenarios associated with a given exposure at the installation provide total water level conditions linked to a given mean sea level and statistical return period associated with the sea level variability and associated high water level events. Using the pathway modeling for these scenarios, future conditions at the installation are estimated. These future conditions provide the basis for adjusting the underlying terrain model at the installation, and evaluating vulnerability based on the sensitivity and adaptive capacity of the exposed installation infrastructure. These vulnerabilities are quantified using various damage, operational, and cost functions that translate the infrastructure sensitivity into specific metrics such as dollars, training days lost, etc. Based on this procedure, an integrated suite of products are generated including installation response curves, sea level vulnerability matrices, and scenario visualizations that provide both quantitative and descriptive assessments of vulnerability.

Communicate the Vulnerabilities

An important component of the framework includes the development of actionable products and the communication of these results to vulnerability assessment results to key stakeholders. As described above, these products are defined early in the process and communication throughout the development of the assessment to allow adjustment and input is required. Although this project focused primarily on method development, and was not in itself a vulnerability assessment, we did rely on these communication strategies to shape the project direction and to provide feedback to the installations during the evolution of the project. For example, we conducted formal stakeholder input meetings with the installations at the inception, mid-point and end stages of the project. We also communicated regularly with key installation personnel throughout the study to identify and refine important inputs and analysis methods for the project. These meetings and communications were invaluable in guiding the project development, focusing the development of methodologies, and populating the example cases that are presented later in this report

Management Activities

Although not explored in the methods developed in this study, active management decisions play a key role in the vulnerability assessment and response cycle. Based on the vulnerability assessment and subsequent communication to installation personnel, needs and actions can be developed by planning, facilities, and operational personnel most familiar with the vulnerable receptors, providing a basis for the formulation and implementation of response strategies. Within the cycle of the vulnerability framework, these strategies can then be assessed to evaluate their potential effectiveness in reducing vulnerability and protecting the infrastructure and operational capabilities of the installation.

2.2 COASTAL SETTING

MCBCP and NBC were selected as model test sites because they lie at opposite ends of San Diego County, California, and have significantly different coastal settings and vulnerabilities to erosion, flooding, and damage related to future storminess and sea level rise. The settings of MCBCP and NBC are strongly influenced by the location, distribution, and shape of the faults (Figure 2-20) that form the boundary between the North American and Pacific tectonic plates in southern California (Greene and Kennedy, 1978; Inman and Nordstrom, 1971).

MCBCP is configured similarly to most of the California coast, and consists of a narrow sand and cobble beach lying on a wave-cut marine terrace backed by steep, erodible cliffs. NBC, on the other hand, lies on sand spit formed from material discharged by the Tijuana River. This material was moved alongshore by wave action and now forms North Island, Coronado, and Silver Strand, the barrier island complex fronting San Diego Bay. The sources of sand, both natural and anthropogenic at the two locations are considerably different, both as to the primary sources and in the quantity and rates of supply. Beaches at both installations rely on natural sand supply. However, NBC has benefitted from massive public works projects that have provided sand at rates far in excess of the natural supply over the past century. Furthermore, coastal structures stabilize this fill. The Silver Strand-Coronado coast is one of the most heavily modified in southern California (Flick, 1993).

The coastal processes that alter this basic geographical setting and measured changes to beaches and cliffs are presented in Section 2.3.

Today's coastal topography began to be established when the North American Plate overrode the Pacific Plate, forming the San Andreas Fault system and the beginnings of the Gulf of California in the last half of the Tertiary, starting about 25 million years ago. The result was a massive block tilting that uplifted the coastal margins of southern California, eventually forming the steep coastal mountains, sea cliffs and headlands. These cliffs were in turn composed of huge volumes of sediment eroded and transported seaward as early as the Cretaceous (135 million years ago) or as late as the various Tertiary epochs (60 million years old) and the Quaternary (the last 2 million years).

The sea cliffs and beaches along the California coast on average have retreated landward together by at least several kilometers as sea level rose about 125 m since the end of the last glacial period about 18,000 years ago. However, there is an important difference between cliff and beach behavior. On any time scale shorter than millions of years, the sea cliffs can at best be stable or erode; there is no mechanism for them to accrete and build seaward. Beaches, on the other hand, can erode or accrete as sand is removed or added by wave action. Beaches in southern California undergo sizeable seasonal cycles of erosion in winter and accretion in summer, as well as more subtle changes in long-term width. There are no comparable seasonal cycles in cliff position, which can only remain fixed or retreat.

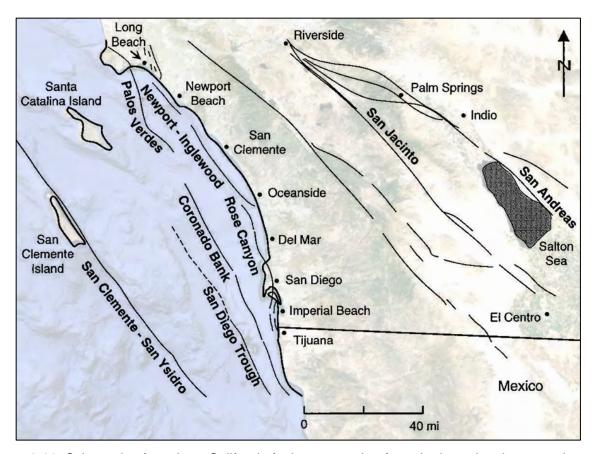


Figure 2-20. Schematic of southern California fault systems that form the boundary between the North American and Pacific tectonic plates located to the east and west, respectively. MCBCP is located along the coast north of San Diego and west of Escondido, while NBC lies just south of San Diego (adapted from Flick and Sterrett, 1984; image data: Google, SIO, NOAA, U.S. Navy, NGA, GEBCO, LDEO-Columbia, NSF, Landsat).

The sea cliffs and beaches along the California coast on average have retreated landward together by at least several kilometers as sea level rose about 125 m since the end of the last glacial period about 18,000 years ago. However, there is an important difference between cliff and beach behavior. On any time scale shorter than millions of years, the sea cliffs can at best be stable or erode; there is no mechanism for them to accrete and build seaward. Beaches, on the other hand, can erode or accrete as sand is removed or added by wave action. In fact, beaches in southern California undergo sizeable seasonal cycles of erosion in winter and accretion in summer, as well as more subtle changes in long-term width. There are no comparable seasonal cycles in cliff position, which can only remain fixed or retreat.

Even so, sea cliffs provide a relatively stable and high-relief shoreline anchor on most of the California coast. This relief and relative on-offshore stability of shoreline position is a key difference between this coast and the low-relief shorelines on much of the U.S. east coast and Gulf of Mexico.

Wave-cut marine terraces were formed during extended periods of relative sea level still-stand, such as the current one. The terraces are prominent features in the region and provide the flat, easily accessible mesa lands. The marine terraces near the shoreline include the submerged, low tide terrace now being cut by wave action. Formation of this terrace began about 6,000 years ago, during the beginning of the latest relative still-stand of sea level. It comprises the flat, rocky, shallow part of the

foreshore common along southern California and is often visible during low tide. This relatively stable bedrock platform erodes slowly and limits the seasonal vertical excursion of the beach profile in many places. Most of the region's sandy beaches, including at MCBCP, are thin veneers of sand only a few meters thick over the low-tide terrace.

Rivers and streams flowing toward the coast dissected the uplifted terrain during past lower stands of sea level, forming valleys, flood plains, and wetlands. In these areas, erosion has formed gaps in the cliffs and underlying terraces and beach sand depths are much greater than over the low tide terrace. River channels filled with sand were drowned as sea level rose during the latest inter-glacial. This setting—narrow beaches with relatively thin veneers of sand, backed by steep cliffs that form the seaward edges of an uplifted terraces, incised with valleys and coastal wetlands—describes most of coastal San Diego County, including MCBCP.

The Rose Canyon section of the Newport-Inglewood Fault largely provides the setting of the southern San Diego coast (Figure 2-21). The coastal area between La Jolla and the Mexican border, including Mission Bay, San Diego Bay, Point Loma, and Coronado and Silver Strand was shaped by tectonic motions along the Rose Canyon and other nearby fault zones (Abbott, 1999; Kennedy and Tan, 2008). Lateral motion along the faults has formed extension basins and uplifted collision features as a result of the right-lateral movement along these alternating right- and left-stepping, sinuous fault systems, both onshore and offshore.

Figure 2-21 shows a fault map of the southern part of San Diego, including the Coronado, Silver Strand, and San Diego Bay locations of NBC. Movement along the Rose Canyon fault and numerous other sinuous, sub-parallel faults dominate this area, resulting in the distinct alternating up-and-down topography, which is one feature that makes the San Diego area so attractive. Coronado—Silver Strand is the barrier island spit of land that fronts San Diego Bay, which is an extension basin associated with fault movement along the sinuous "S-shaped" Rose Canyon fault zone. In contrast, Point Loma, which forms the western boundary of San Diego Bay, is an uplift feature that resulted from the collision of fault blocks on the opposite side of the "S" curve. From south to north, Mission Bay, Point La Jolla, and the La Jolla submarine canyon system are similar, alternating high and low features.

As sections of the faults pulled apart, the areas between the steps opened and dropped, forming the low-lying areas of Mission and San Diego bays that were then flooded by the ocean. North Island, Coronado, and Silver Strand are essentially large, low-lying, sand spit accretion features that accumulated as a barrier island fronting San Diego Bay from the prodigious historical sand supply provided by the Tijuana River (Abbott, 1999; Moore and Kennedy, 1970).

The headlands of Point La Jolla and Point Loma, and others in southern California¹, naturally divide the coast into a series of coastal compartments called littoral cells, as shown in Figure 2-22 (Inman and Frautschy, 1965). Each littoral cell is from several tens of km up to almost 200-m long. Sand contributions from rivers, cliffs, and anthropogenic sources in varying proportions provide each littoral cell with sand. This sand is moved cross-shore and alongshore, thus sustaining the beaches.²

¹ Point Conception, Point Dume, Palos Verdes, and Dana Point

² Recent work by O'Reilly (unpublished) at Scripps Institution of Oceanography suggests that nearshore topography alters wave patterns to create littoral sub-cells, only a few kilometers long, with boundaries often located at lagoon mouths.

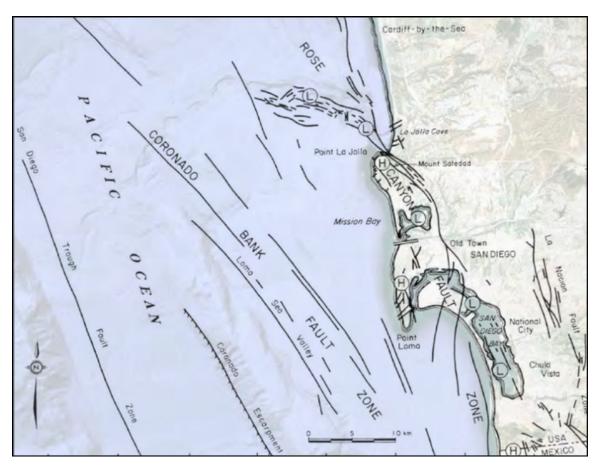


Figure 2-21. Geological fault map of the southern San Diego region showing the alternating high (H) and low (L) tectonically- formed topographic features including Point La Jolla, Mission Bay, Pont Loma, and San Diego Bay (Overlay courtesy of D. Inman, Scripps Institution of Oceanography, University of California, San Diego; image data: Google, SIO, NOAA, U.S. Navy, NGA, GEBCO, LDEO-Columbia, NSF, Landsat).

2.2.1 Marine Corps Base Camp Pendleton

Camp Pendleton is one of the Department of Defense's busiest installations with a broad spectrum of training facilities for many active and reserve Marine, Army, and Navy units, as well as national, state, and local agencies. The base is home to the I Marine Expeditionary Force, 1st Marine Division, 1st Marine Logistics Group and many tenant units, including Marine Corps Installation-West, 1st Marine Special Operations Battalion, Wounded Warriors Battalion-West, Marine Corps Air Station at Munn Field, Marine Aircraft Group 39, Marine Corps Tactical Systems Support Activity, Marine Corps Recruit Depot San Diego's Weapons & Field Training Battalion, Marine Corps and Army Reserve Forces, the Navy's Assault Craft Unit 5, a Naval Hospital and Dental Battalion.³

_

³ http://www.cpp.usmc.mil/information/basefacts/introduction.asp

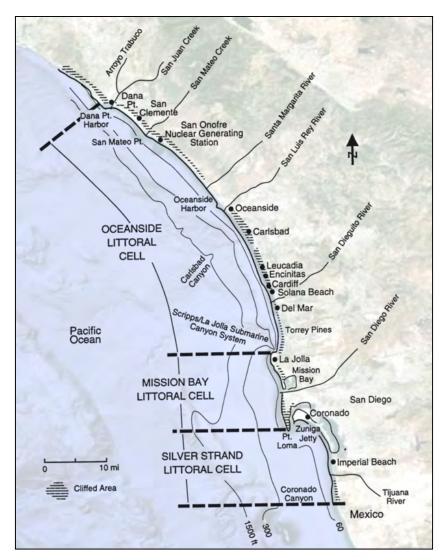


Figure 2-22. Map showing the Oceanside, Mission Bay, and Silver Strand littoral cells of the San Diego region. MCBCP is located in the northern part of the Oceanside Cell, between San Mateo Point and Oceanside Harbor. NBC is in the Silver Strand cell at the southern end of San Diego (adapted from Flick and Sterrett, 1984; image data: Google, SIO, NOAA, U.S. Navy, NGA, GEBCO, LDEO-Columbia, NSF, Landsat).

The Camp Pendleton ecosystem includes beaches, bluffs, mesas, canyons, mountains, and southern California's least regulated river, the Santa Margarita. There are more than 1,000 species of plants, fish, and animals, some of which are either threatened or endangered. Wildlife and habitat protection is a top concern at Camp Pendleton. The coastal and mountain terrain support a variety of military training. Fleet Marine Force units use Camp Pendleton's ranges and training areas to maintain combat readiness. MCBCP also provides specialized schools and training. These schools include Assault Amphibian School Battalion, School of Infantry, Field Medical Service School, and Marine Corps University.

Exposed and Protected Shorelines

MCBCP occupies essentially the entire northern half of the Oceanside littoral cell, the 84-km long coastal compartment lying between Dana Point in Orange County, California, and Point La Jolla in San Diego County (Figure 2-22). MCBCP stretches from San Mateo Point on the coast in the north to the Del Mar Boat Basin in the Oceanside Harbor complex in the south. The base encompasses 125,547 acres (420 km²) with about 28 km of shoreline (Byrd and Berryman, 2006) and contains the largest undeveloped portion of coastal land in southern California. The U.S. government purchased the camp in 1942 to develop the base. The ranch was originally a Mexican land grant deeded to Pio and Andres Pico in 1841 that, with some additional parcels, was named *Rancho Santa Margarita y Las Flores*.

Camp Pendleton is divided into scores of special segments (U.S. Government, 2002) including training areas, harbor and airport facilities, housing areas, recreation facilities, and real estate on long-term lease as a state beach and for the San Onofre Nuclear Generating Station (SONGS). As shown schematically in Figure 2-23, the coastline of MCBCP is divided into a number of beach areas designated as Sections A through F, not including the areas designated as a state beach or SONGS.

The northern (coastal) border of MCBCP lies at San Mateo Point, which is also the mouth of San Mateo Creek, an ephemeral river. Section A, also called San Onofre Beach and historically known as Crescent Beach, lies about 1.5 km south of San Mateo Point and provides one of the two coastal recreational facilities available to MCBCP personnel (Figure 2-24 and Figure 2-25). San Onofre State Beach lies on both sides of Section A. San Onofre Creek empties into the northern part of Section A. Together, these two creeks supply about 20,000 m³/yr of sand to this coastal segment. Section A is southwest-facing and lays in the wave shadows of Catalina and San Clemente islands, and is therefore substantially sheltered from northwest Pacific swell waves prominent in winter. Nevertheless, this beach is vulnerable to erosion and flooding during high tide and wave storms.

A large fraction of the available width at Section A has been paved and otherwise improved for parking, mobile homes, cabanas, and related beach recreational facilities. Using the scale tool in Google Earth it is reasonably simple to measure the distance from a fixed back-beach feature and the wetted line in each photo to an accuracy of a few meters⁴. This suggests that the beach width decreased by about 35 m in the 15 years between 1994 and 2009. Both photos were taken in the early-summer beach profile transition period, usually a time of rapid accretion, differences in which may account for some of the apparent change. Differences in tide height or wave-driven run-up were also not considered and could account for the differences observed. Nevertheless, the photos show a substantial amount of important coastal infrastructure that will be increasingly vulnerable in the future. Further work on the beach changes available from aerial photos at MCBCP and comparison with the beach profile data will be carried out in Year 2 of this program.

The entrance to San Onofre State Beach lies south of Section A and about 1.5 km north of SONGS (Figure 2-23). San Onofre State Beach north of SONGS is sandy and there are beach-level restroom facilities and parking areas that serve a popular and historical surf spot. This section of beach was much wider than its natural state from the late 1960s to the mid-1980s as a result of the prolonged construction activity at SONGS, as described by Flick *et al.* (2010), and as seen in Figure 2-26. SONGS was built as three units in a large space about 0.75-km long excavated out of the cliffs between 1964 and 1985. More than 1 million m³ of sand were produced by construction activities that included the cliff excavation and trenching for several massive cooling water pipes over 4 m in

⁻

⁴ The precision of scaling dimensions in the 10's to a few 100's of meters range off Google Earth photos was determined by repeatedly measuring the length of fixed features at different scales and in photos taken on different dates. Repeatability was 0.5 to 3.0 m.

diameter extending over 1 km offshore. Laydown pads used as construction staging areas from 1964-68 and 1975-85 (Figure 2-27) stabilized the fill on the north side, greatly benefiting the state park beach width for several decades.



Figure 2-23. Schematic map of MCBCP showing the major divisions of the coastline, Sections A-F and potentially vulnerable coastal facilities (overlay adapted from U.S. Government 2002; image data: Google, SIO, NOAA, U.S. Navy, NGA, GEBCO, DigitalGlobe, CSUMB, SFML, CA-OPC).

The state beach is accessible south of SONGS laterally along the shore by transiting in front of SONGS through the double-seawall arrangement built to maintain plant security. Access is also possible vertically from above via a number of trails winding down the cliffs or through gullies locally known as "barancas." Beach amenities are sparse, but parking with camping and restroom facilities are located along the cliff-top on the old, abandoned coast highway. This reach is vulnerable to beach and cliff erosion, although data is sparse (see Section 2.3 for details of historical erosion rates). SONGS facilities are protected from erosion or flooding in the foreseeable future by the seawall. The adjacent beaches, however, have narrowed greatly and essentially disappeared adjacent to the power plant in the 25 years since the Units 2 and 3 laydown was removed in 1985, as shown in Figure 2-28.



Figure 2-24. Google Earth image taken 25 May 2009 of Section A, Green Beach located about 1.5 km from the (coastal) northern boundary of MCBCP and available for recreational use by base personnel.



Figure 2-25. Google Earth image taken 1 June 1994 and covering the same area of Section A, Green Beach as Figure 2-24.

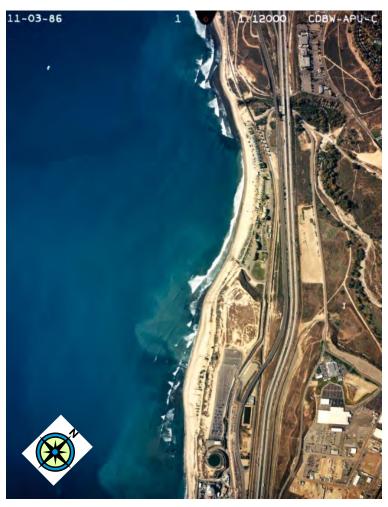


Figure 2-26. Aerial photo of San Onofre State Beach in 1986 shows remnant beach width up to several kilometers north of SONGS from 20-years of construction activity that ended in 1985 (scale 1:12,000 California Department of Boating and Waterways Photo 220 available as California Coastal Records Project Image 198610220; Copyright (C) 2002–2014 Kenneth & Gabrielle Adelman, California Coastal Records Project, www.Californiacoastline.org).

The San Onofre State Beach coastal reach extends about 6 km south of SONGS to the vicinity of Horno Canyon and the beginning of Section B (Figure 2-23). This state beach area has a narrow sandy beach backed by steep 20- to 30-m high cliffs with numerous large gullies and several massive landslides, as seen in Figure 2-29. Sand for beach formation is mainly provided by the erosion of large gullies and the cliff-face along almost the entire length. The concentration of runoff in culverts underlying Interstate 5 (I5) and the railroad enhances episodic erosion through the loosely consolidated terrace sediments during heavy rains. This process can quickly produce large volumes of sediment. In one case a canyon was lengthened over 60 m in 24 hours, contributing about 38,000 m³ of sand to the adjacent beach (Kuhn and Shepard 1991). Gully and cliff face erosion provides sand to this reach and the entire MCBCP keeping the beaches intact. However, depending on future erosion rates in the face of accelerated rates of MSLR, it is only a matter of time until the cliff face reaches the railroad tracks and then I5.



Figure 2-27. Composite of four aerial photographs of SONGS Units 2 and 3 taken near the end of construction between 4 December 1984, just before removal of the Units 2 and 3 laydown pad began (left), and 12 December 1985 (right) after beach had begun narrowing. The pad had been in place from 1974–1984 (courtesy of Southern California Edison Company; see Flick *et al.*, 2010; note the photo orientation with ocean on the right).



Figure 2-28. Google Earth image taken 25 May 2009 of about 4 km of coast at SONGS shows the greatly reduced beach widths at and adjacent to the power plant (see text). Note the railroad tracks that lie coastward of I5.



Figure 2-29. Google Earth image taken 1 February 2008 of 2 km of coast south of SONGS shows narrow, cliff-backed beach with landslides and several large gullies associated with drainage culverts and channels (see text).

Figure 2-30 and Figure 2-31 show 2009 and 1995 Google Earth photos of the 7.5-km reach from the northern end of Section B to Section D (see Figure 2-23). Note there are four helipad and other landing strips visible in the 2009 photo, including the one just south of Horno Canyon (second from the north) that was built after 1995. Rough measurements done as before of the change in distance between the western end of each pavement area and the head of the nearest gully revealed a decrease in this distance of only about 7 m between the earlier and later photographs. Infrastructure like these pads can be moved for the foreseeable future if threatened from erosion, but eventually must be relocated landward of I5 as the gullies grow and the cliffs retreat. The distance from the pads to the edge of the nearest cliff or gully ranges from about 80 to 120 m.

A training beach does not necessarily have to be composed only of sand, but may consist of bedrock formations, or cobbles and rocks. However, a relatively low-slope and flat portion of beach between the water and the cliff needs to be present for the amphibious vehicles to land on. Depending on the sand supply and the recession rate of the beach in the face of future sea level rise, there may or may not be sufficient beach area during normal ranges of tide to accommodate all the training needs at MCBCP.



Figure 2-30. Google Earth image taken 25 May 2009 of about 7.5 km of coast extending from north edge of Section B to Section D (see Figure 2-23) showing four helipads pads and strips.

The MCBCP Landing Craft Air Cushion (LCAC) ⁵ facility in Section E is shown in Figure 2-32, a Google Earth photo taken on 25 May 2009. As indicated, the facility is already squeezed up against the southbound lanes of I5, while its southwest corner is only about 170 m from the cliff line. This represents a 50-m decrease since 1994, when the earliest vertical photo that is available on Google Earth (not shown) was taken. Clearly, continued cliff and gully retreat will eventually encroach on this critical facility. Eventual encroachment is not the only problem at the LCAC facility. Figure 2-33 shows an oblique beach view of the LCAC ramp end where it hits the beach. In this photo, the beach surface is uneven due to wave scour. These particular conditions are probably not limiting to LCAC operations, but more severe scour and high scarp formation, which is common during winter wave storm-driven beach retreat, could be. Additionally, uncontrolled surface runoff has formed a trench through the beach, which may hasten erosion. Diverting this kind of runoff is a relatively easy and inexpensive erosion prevention measure.

_

⁵ LCAC stands for Landing Craft Air Cushion. The unit motto is "No Beach out of Reach."



Figure 2-31. Google Earth image taken 3 October 1995 covering reach shown in Figure 2-30.

The relatively undeveloped coastline along Sections F, G, and H may be seen in the Google Earth photo taken 25 May 2009 and shown in Figure 2-34. The Santa Margarita River flows through Section G just north of the Del Mar Boat Basin and Oceanside Harbor. The Santa Margarita is the last free-flowing river in southern California with no flood control or water storage dams along its length downstream of Temecula. Several major tributaries do, however, have dams and associated reservoirs, including Vail Lake on Temecula Creek and Lake Skinner on Tucalota Creek. The Santa Margarita watershed is about 44-km long with an area of 1,940 km² (194,000 ha). A relatively wide sandy beach backed by dunes and marsh lies across its mouth. The Santa Margarita provides on average from 9,000 to 18,000 m³/yr of sediment to the coast, depending on which study is cited (Flick, 1993), but also has been known to build large deltas that persisted for years after major floods.

-

⁶ http://www.usbr.gov/lc/socal/reports/SMappend_A.pdf.



Figure 2-32. Google Earth image taken 25 May 2009 of the LCAC facility in Section E (see text for discussion; image data: Google, USDA Farm Service Agency).

Section H, the 1-km long Del Mar Recreation Beach adjacent to the Del Mar Beach housing area comprises the southern-most beach segment of MCBCP. It lies against the north side of the Oceanside Harbor jetty, which protects the Del Mar Boat Basin (Figure 2-23) and Oceanside Harbor. These harbors' development histories, influence on the coast, and long-term federal involvement in maintenance and sand dredging and bypassing, has been reviewed many times (see for example, Inman and Masters, 1991; Flick, 1993).

The harbor structures at Oceanside were built in stages starting with the Del Mar Boat Basin in 1942 at the beginning of U.S. involvement in World War II. The boat basin was urgently needed for amphibious training, with "the environment" not much considered. Construction was essentially complete by 1968 when the adjacent recreational small craft harbor was finished, with the exception of a few later additions and improvements to the breakwaters. Beach accretion to the north and erosion to the south were noted soon after harbor construction began since the jetties interrupted the southward flow of sand, probably deflecting some offshore, with the harbor trapping up to 200,000 m³/yr. Erosion south of Oceanside Harbor has been a vexatious problem ever since.



Figure 2-33. Oblique air photo of LCAC ramp taken 23 October 2004 and showing rough surface conditions at the end of the ramp, and a ditch from uncontrolled runoff (bottom center) in front of the tower (California Coastal Records Project Image 200407314; Copyright (C) 2002–2014 Kenneth & Gabrielle Adelman, California Coastal Records Project, www.Californiacoastline.org).

Some mitigation is presented, since the federal government has accepted responsibility for maintenance dredging, which essentially amounts to bypassing sand around the harbor. However, the harbor breakwater in effect cuts the Oceanside littoral cell (Figure 2-22) in half and seems to divert substantial quantities of sand offshore. This has caused a serious mal-distribution of sand that may be related to chronic sand shortages as far south as Solana Beach and Del Mar (SANDAG, 1993).

Overall, the northern half of the Oceanside littoral cell seems to have a net surplus of beach sand supply of 230,000 m³/yr for the period beginning in 1983, according to the analysis of Inman and Masters (1991). This suggests that the beaches will be relatively stable for the foreseeable future, even if MSLR resumes or accelerates modestly. More discussion of the littoral cell sand budget and the shoreline changes observed along the MCBCP shoreline are reviewed in Section 2.3.

Groundwater

The Santa Margarita River Basin spans 744 square miles of drainage area in San Diego and Riverside counties, separated in to two watersheds referred to as the Upper Basin and Lower Basin (Figure 2-35). The portion bordering on MCBCP is the Lower Basin, and the occurrence of ground water is found in the alluvial basin located below the confluence of the Santa Margarita River and De Luz Creek, where the basin is further divided into three separate sub-basins: the Upper Ysidora, Chappo, and Lower Ysidora sub-basins (Figure 2-36). The Upper Ysidora sub-basin is the most upstream of the three basins and is characterized by coarse sediments, followed by the Chappo sub-basin consisting of sands, gravels and clays, and then the Lower Ysidora sub-basin, consisting predominately of sands and clays.



Figure 2-34. Google Earth photo taken 25 May 2009 and showing Sections F, G, and H between the LCAC facility (upper left) and Del Mar Boat Basin including the Del Mar Beach and the adjacent recreation and housing complex, and Oceanside Harbor, (lower center) at the southern boundary of MCBCP. The Santa Margarita River (center) flows through Section G (Figure 2-23).

Through MCBCP, the Santa Margarita River Basin is typified by a relatively flat alluvial floodplain that drains the watershed from the northeast to the southwest bordered by terraces and gently to steeply sloping hillsides while the topography flattens as the river enters the Pacific Ocean (Figure 2-37). Surface and groundwater is largely restricted to the alluvial regions that are bounded by rock units that form the sloped borders to the north and to the south of the alluvium. Alluvial deposits, the principal source of groundwater in the lower Santa Margarita River Basin, are made up of three distinct geologic units: the Upper Alluvium, Lower Alluvium, and Terrace Deposits. The Lower Alluvium is generally more coarse-grained than the Upper and these two units are the main groundwater bearing formations. The total thickness of the alluvium increases downstream from about 120 feet at the De Luz Creek confluence to about 200 ft at the coast.

MCBCP's water supply is produced primarily from underground aquifers that are recharged by percolation from overlying rivers and streams. Santa Margarita River wells provide about 65% of the total water consumed on the base while Las Flores Creek, San Onofre Creek, and San Mateo Creek wells combine to supply the remaining requirement (MCBCP, 1993). Agricultural wells supply

irrigation water for leased sites of about 700 ac in the Stuart Mesa area. Since records began in 1944, total annual water use has ranged from 5,850 ac-feet (1991) to 10,656 ac-feet (1979) with an average of 8,066 ac-feet (MCBCP, 2007). There is concern about potential seawater intrusion into the base wells from water extraction exceeding the safe yield of the individual basins. In 1952, the wells in the Santa Margarita River basin showed evidence of seawater advance 3 miles upstream due to pumping in the basin (California Department of Water Resources 1956). While frequent monitoring and extraction control of key wells has helped prevent such contamination from occurring in recent years, future sea level rise could exacerbate this issue.

Through MCBCP, the Santa Margarita River Basin is typified by a relatively flat alluvial floodplain that drains the watershed from the northeast to the southwest bordered by terraces and gently to steeply sloping hillsides while the topography flattens as the river enters the Pacific Ocean (Figure 2-37). Surface and ground water is largely restricted to the alluvial regions that are bounded by rock units that form the sloped borders to the north and to the south of the alluvium. Alluvial deposits, the principal source of ground water in the lower Santa Margarita River Basin, are made up of three distinct geologic units: the Upper Alluvium, Lower Alluvium, and Terrace Deposits. The Lower Alluvium is generally more coarse-grained than the Upper and these two units are the main ground-water bearing formations. The total thickness of the alluvium increases downstream from about 120 feet at the De Luz Creek confluence to about 200 feet at the coast.

MCBCP's water supply is produced primarily from underground aquifers that are recharged by percolation from overlying rivers and streams. Santa Margarita River wells provide about 65% of the total water consumed on the Base while Las Flores Creek, San Onofre Creek, and San Mateo Creek wells combine to supply the remaining requirement (MCBCP, 1993). Agricultural wells supply irrigation water for leased sites of about 700 ac in the Stuart Mesa area. Since records began in 1944, total annual water use has ranged from 5,850 ac-feet (1991) to 10,656 ac-feet (1979) with an average of 8,066 ac-feet (MCBCP, 2007). There is concern about potential seawater intrusion into the Base wells from water extraction exceeding the safe yield of the individual basins. In 1952 the wells in the Santa Margarita River basin showed evidence of seawater advance 3 miles upstream due to pumping in the basin (California Department of Water Resources 1956). While frequent monitoring and extraction control of key wells has helped prevent such contamination from occurring in recent years, future sea level rise could exacerbate this issue.

2.2.2 Naval Base Coronado

Naval Base Coronado (NBC) lies in the Silver Strand littoral cell (Figure 2-22), which is likely the most highly altered stretch of coast in southern California. NBC comprises a number of installations including the following in the Coronado, Silver Strand, and Imperial-Beach areas that are the subjects of this study:

- Naval Air Station North Island
- Naval Amphibious Base Coronado
- Fiddler's Cove Marina
- Silver Strand Training Complex
- Naval Outlying Landing Field Imperial Beach



Figure 2-35. Watersheds at MCBCP (overlay original art; image: Google, U.S. Geological Survey).

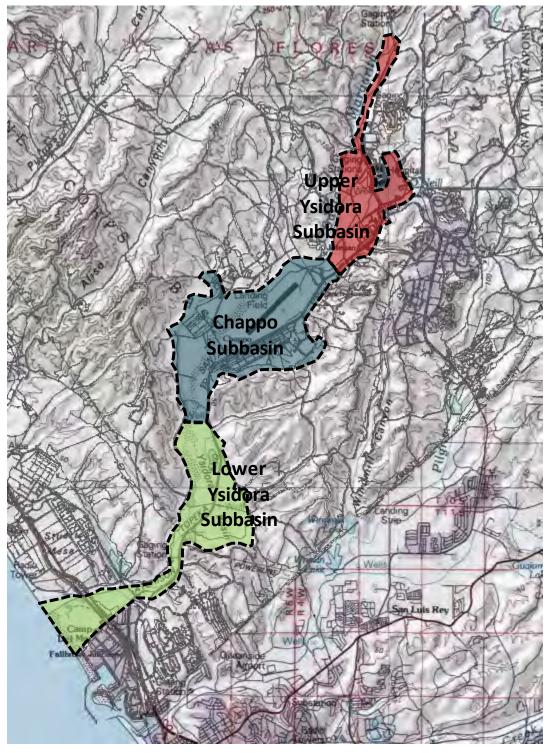


Figure 2-36. Groundwater sub-basins of the Santa Margarita lower basin at MCBCP (adapted from Stetson Engineering, 2001).

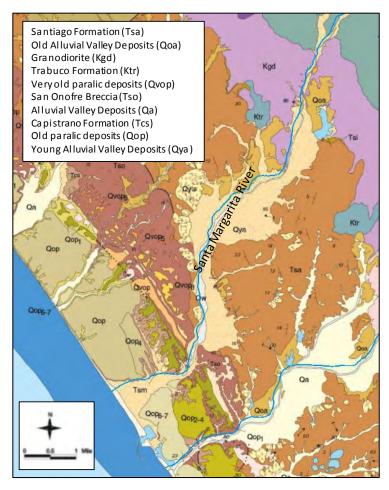


Figure 2-37. Geology of the Santa Margarita lower basin (adapted from San Diego State University, http://www.geology.sdsu.edu/kmlgeology/california_geology.html).

Exposed and Protected Shorelines

Figure 2-38 shows a schematic map of the North Island, Coronado, Silver Strand, and Imperial Beach coastal areas, and also includes Point Loma, San Diego Bay (with the Naval Amphibious Base), and several other location names. The map delineates coastal features that are potentially vulnerable to erosion and flooding and from accelerated rise in MSL. The entire coastal segment forms the Silver Strand littoral cell (Figure 2-22), which extends from the tip of Point Loma to a point in Baja south of the international border.

Naval Air Station North Island

NASNI (Figure 2-39) is part of the largest aerospace-industrial complex in the Navy. The complex's 2,000 ha in San Diego and 130 commands bracket the city of Coronado from the entrance to San Diego Bay to the Mexican border. North Island itself is host to 23 squadrons and 75 additional tenants. North Island was commissioned a naval air station in 1917. In 1963, the station, which was originally called the Naval Air Station, San Diego until 1955, was granted official recognition as the "Birthplace of Naval Aviation" by resolution of the House Armed Services Committee. ⁷

7 1

⁷ http://www.globalsecurity.org/military/facility/north-island.htm

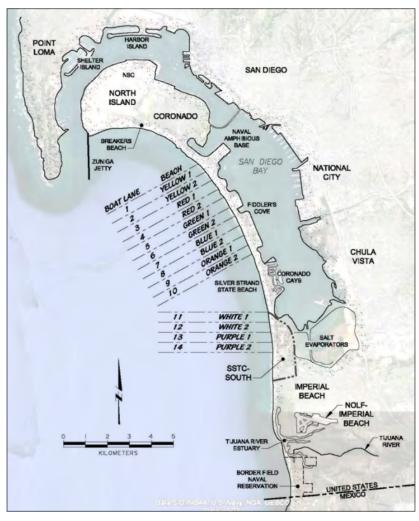


Figure 2-38. Schematic map shows North Island, Coronado, Silver Strand, Imperial Beach, and Border Field facilities with amphibious boat lane (number) and beach (color) designations (adapted from U.S. Navy, 2010; image data: Google, SIO, NOAA, U.S. Navy, NGA, GEBCO, LDEO-Columbia, NSF).

A substantial number of facilities at NASNI are located on relatively low-lying terrain, both on the ocean and the San Diego Bay sides, including runways, weapons and munitions storage facilities, aircraft and ship maintenance facilities and berthing, medical and dental clinics, fueling and arming stations, commissaries, officer and enlisted housing and dining areas, and numerous other buildings. Recreational and other amenities such as a golf course, beach club, pool, skeet range, naval lodge, and the Navy Band building are located on or near the beach along the relatively vulnerable southern shoreline (Figure 2-39)⁸.

North Island derived its name from the original geography, which included Spanish Bight a waterway and wetland that separated the two parts of Coronado, as shown in Figure 2-40. In the 19th century, it was referred to as North Coronado Island. In 1886, North and South Coronado Island were purchased for development as a residential resort. South Coronado became famous as the city of Coronado, but North Coronado was never developed. Instead, Glen Curtiss opened a flying school

-

⁸ http://www.hsl49.navy.mil/nasnimap.pdf

and held a lease to the property until the beginning of World War I. In 1917, Congress appropriated the land and two airfields were commissioned on its sandy flats. One of history's most famous aviation feats was the flight of Charles A. Lindbergh from New York to Paris in May,1927. That flight originated at North Island on May 9, 1927, when Lindbergh began the first leg of his journey.



Figure 2-39. Google Earth photo taken 25 May 2009 of NASNI including about 3.5 km of shoreline eastward of San Diego Bay entrance and Zuniga Jetty. Note numerous naval facilities along the low-lying, south-facing Breakers Beach.

Coronado

Until the mid-20th Century, this coast was mostly in a natural state except for some decrease in sand supply because of flood control and water storage dam projects on the Tijuana River, and shoreline stabilization provided by Zuniga Jetty along the eastern side of the entrance to San Diego Bay (Figure 2-40). Figure 2-41 shows Coronado City Beach in its current, highly modified, and relatively wide (200-m) condition. In sharp contrast, Figure 2-42 shows the beach at Coronado almost completely removed by southerly storm waves in January and February 1905 that washed out the coastal road, and threatened to destroy the Hotel Del Coronado, which was completed in 1888. The hotel was saved only with placement of thousands of sand bags (Kuhn and Shepard 1991).



Figure 2-40. (left) Oblique developer's 1880's view of North and South Coronado in the distance from San Diego showing Spanish Bight wetland separating North Island from Coronado (courtesy of The Bancroft Library, University of California, Berkeley); (right) Chart of San Diego Bay from 1857 showing North Island ("The Island") in its pre-fill condition with the two main island areas separated by the "Spanish Bight" (Coast Survey Office: http://www.coronado.ca.us/library/).



Figure 2-41. Google Earth photo taken 25 May 2009 showing 2.8 km of Coronado City Beach, Hotel Del Coronado, and the Coronado Shores high-rise condominiums.

Beginning in 1946, massive dredging in San Diego Bay was needed to make room for the Pacific Fleet returning after the end of WW II. This produced about 26 million m³ of sand, most of which was pumped unto Silver Strand, then migrating north to Coronado. This widened these beaches by hundreds of meters (Kuhn and Shepard, 1991; Flick, 1993).

Coronado City Beach to the west and Coronado Shores to the southwest are now highly modified, relatively wide, sandy beaches with excellent access. Coronado City Beach is backed by a 1.5-km long, continuous rip-rap revetment built after the 1905 storms. Zuniga Jetty and a curved groin built adjacent to the hotel in 1900 to create a small craft anchorage (Figure 2-41) essentially created a long, stable pocket beach. This stability is aided by the generally northward along shore sand transport that prevails along this section of coast owing to the sheltering effect of Point Loma on waves approaching from the northwest and west.

The capacity of San Diego Bay to berth U.S. Navy ships returning from the Pacific after World War II was increased in 1946 by the dredging of about 26 million m³ of bay sand, which was deposited on Coronado and Silver Strand Beaches. As a direct result of this dredging and the stabilizing effects of the aforementioned coastal structures, Coronado City Beach and Coronado Shores, the area just south of the Hotel Del Coronado, are some of the widest beaches in southern California (Flick, 1993).



Figure 2-42. View to the northwest from the Hotel Del Coronado after large wave storm from the south caused massive beach erosion in 1905 (courtesy of the Center for Coastal Studies, Scripps Institution of Oceanography, University of California, San Diego).

Coronado Shores does not appear to be wide since the large Coronado Shores high-rise condominium development was built directly on the accreted beach beginning about 1967 (see Figure 2-43). This development was one "poster-child" that galvanized public opinion and led to passage of the California Coastal Act and creation of the California Coastal Commission. The towers are fronted by a large rip-rap revetment, but are still subject to wave overtopping during large storm wave events.

Naval Amphibious Base Coronado

The Secretary of the Navy authorized the establishment of the Amphibious Training Base in the San Diego area in June 1943 to meet wartime needs for trained landing craft crews. The Naval Amphibious Base (NAB), located within the City of Coronado, was commissioned in 1944, providing a base for operations, training, and support of naval amphibious units on the West Coast. It is one of only two amphibious training bases in the U.S. (Figure 2-43).

The base has also provided training for underwater demolition teams, U.S. Navy SEALs, brownwater Navy personnel, and Naval Reserve Officer Training Corps midshipmen. The base conducts research and tests of newly developed amphibious equipment. NAB Coronado is also home to over 27 tenant commands with approximately 5,000 personnel.

NAB occupies about 4 km² (400 ha) and encompasses a main base located on a peninsula in San Diego Bay, amphibious training beaches, a least tern preserve, a recreational marina at Fiddler's Cove, housing, and Silver Strand State Beach (Figure 2-38). The majority of training activity takes place on about 1 km² (100 ha) of beachfront leased from the State of California (Figure 2-38).

The NAB Coronado bayside and oceanfront facilities, which are separated by Hwy 75 that runs along an elevated berm (Figure 2-43), were built on 70% of the available beach. The apparent beach width (about 65 m, seaward of the developments) is only about 30% of the actual width (220 m). While wider than the beach adjacent to the Coronado Shores high-rises, which is only about 50 m; it is obviously much narrower than the accessible beach area to the south along Silver Strand State Beach. Comparison of the earliest available oblique photographs of NAB taken in 1972 (Figure 2-44) and the latest from 2008 (Figure 2-44, CA Coastal Records Project) show that beach encroachment was already significant by 1972, but has increased dramatically since then.

Silver Strand

Historically, Silver Strand was a narrow, marginal sand spit that was occasionally overtopped by ocean waves (Figure 2-45). Silver Strand is now a moderately wide barrier sand beach separating the southern portion of San Diego Bay from the Pacific Ocean, and stretches from Coronado to Imperial Beach. Like Coronado, this is another highly modified shoreline (Flick, 1993). The ocean side has benefited from the 26 million m³ of sand dredged from the bay beginning in 1946 and deposited between Silver Strand and Coronado. The bay side has also been altered by filling, including the area occupied by the NAB peninsula, and the Coronado Cays residential development (Figure 2-38).

The southern part of the Silver Strand from Fiddler's Cove to the International Border with Mexico (Figure 2-46) includes the South Silver Strand Training Facility (SSTS) and the Naval Outlying Landing Field Imperial Beach (NOLF), adjacent to the Tijuana River and Estuary (Figure 2-38). The low-lying areas around the river and wetland are subject to flooding from both the ocean and the river during high-flow periods.

The Tijuana River supplies sand to the entire Silver Strand littoral cell, albeit at a rate reduced to about one-half or less from the natural supply rate owing to dams on both sides of the border. Estimates for the rate of sand supply from the Tijuana River vary by a factor of about eight under pre-dam conditions (66,000 to 535,000 m³/yr), and a factor of 3.5 with the dams (32,000 to 115,000 m³/yr, Flick, 1993).

_

⁹ http://www.globalsecurity.org/military/facility/coronado.htm



Figure 2-43. Google Earth photo (25 May 2009) showing 4 km of shoreline from Hotel Del Coronado (upper left) to Fiddler's Cove (lower right).Note NAB Coronado bayside peninsula and beach development including the training areas along Silver Strand State Beach.



Figure 2-44. (left) Photo of NAB ocean-front facilities taken in 1972 (Cal Boating Image 958012 from California Coastal Records Project); (right) photo of same area taken 19 September 2008 with additional construction on back beach (black boxes) and denser bayside housing (California Coastal Records Project Image 200805108; Copyright (C) 2002–2014 Kenneth & Gabrielle Adelman, California Coastal Records Project, www.Californiacoastline.org).

Regardless of the present rate of sand supply, it is dwarfed by the 26 million m³ of sand placed starting in 1946, which annualized over the past 65 years amounts to 400,000 m³/yr. This does not include the approximately 115,000 m³/yr now placed on the Imperial Beach shore from dredging of San Diego Bay. Without additional and constant nourishment, the Silver Strand littoral cell will have a net sand deficit of about 200,000 m³/yr (Inman and Masters, 1991). The littoral cell sand budget and the shoreline changes observed along the NBC shoreline are reviewed in Section 2.3.



Figure 2-45. Photo taken from the Hotel Del Coronado cupola looking south over Silver Strand in 1898 (courtesy the U.S. Grant IV collection). Note the narrow ocean beach (right) and over-wash fans on the bayside (left).

Groundwater

Groundwater on NBC, because of its proximity to San Diego Bay and the Pacific Ocean, is too saline for potable uses (RWQCB, 2007; DoN, 1992). Well data at various areas on the base suggest elevations in the range of 6 and 7 ft above mean lower low water (MLLW), which translates to a depth of about 24 to 25 feet bgs in the interior regions of the base, with temporal fluctuation on the order of 1 ft. North Island is underlain by an unconfined aquifer in the unconsolidated Bay Point Formation, consisting of a fresh to brackish water lens overlying more saline water, which is recharged by infiltration of precipitation and irrigation water. Because of limited resources, and the lack of direct groundwater use at NBC, we have not assessed the potential impact of future SLR scenarios on this pathway. However, changes in groundwater levels can be expected to be comparable to changes in sea level, which depending on the magnitude, could create vulnerabilities for upland structures and infrastructure.

2.3 COASTAL PROCESSES IDENTIFICATION

Three basic physical processes that are important to shoreline evolution in southern California are discussed in this section:

Sea Level – Including MSL and sea level fluctuations on many time scales; Ocean Waves – Including sources, shoaling, refraction, sheltering, and run-up; Beach Processes – Including the budget of sand.

2.3.1 Sea Level

Sea level changes on time scales ranging from days to a century that are relevant to coastal erosion, flooding, and inundation on these same time scales. Tides are particularly important because they are large – the local open-coast extreme range is nearly 3 m, larger than any sea level changes since the last ice age. Sea level observations and analyses of data from local tide gauges as well as satellites are discussed. Future MSLR scenarios are considered in the Section 3.1.

Wave-driven run-up can reach 40% of the offshore significant wave height, which can be as large as 10 m. Thus, vertical wave run-up at the shore can reach up to 4 m in rare, extreme cases. Mean sea level rise, even for the most pessimistic future scenario considered herein, is not expected to exceed 2 m by 2100. In other words, sea level fluctuations from tides and wave run-up will greatly exceed the contribution of MSLR for the foreseeable future. This means that while the long-term trend in MSL is important, and will shift the frequency and return period of extreme events, these events will still be controlled by the co-occurrence of high tides and high waves and the notion that MSLR in itself will cause flooding is misleading.

The cumulative effects of MSLR will over time gradually worsen the effects of high waves occurring during peak tides. In effect, MSLR will gradually reduce the recurrence intervals of given elevations of sea level. What are now once-in-100-year events, for example, will become once-in-10-year occurrences, and so on. This will progressively increase the severity of coastal flooding and beach erosion.

El Niño-related sea level fluctuations and storm surges, also discussed below, are smaller than about 0.3 m. However, this modest enhancement of total sea level can be important when large storm waves coincide with extreme high tides.

Regional mean sea levels may for several decades change at rates far different than the average "global" rate as a result of inter-decadal fluctuations that are described below. These are strongly influenced by broad-scale ocean circulation patterns dynamically driven by surface winds associated with persistent climate regimes over the North Pacific Ocean. Changes in the spatial patterns of wind stress curl before and after the mid-1970's regime shift (Miller *et al.*, 1994), together with wind stress curl correlations with tide gauge and satellite altimetry data, suggest that the persistent atmospheric regimes that produce the Pacific Decadal Oscillation (PDO, Mantua *et al.*, 1997) and the North Pacific Gyre Oscillation (NPGO, Di Lorenzo *et al.*, 2008) sea surface temperature (SST) and sea level height (SLH) spatial patterns may have also changed the North Pacific subtropical and subarctic (Alaskan) gyre circulation. This affected upwelling along the eastern Pacific boundary and appears to have suppressed the rate of sea level rise to essentially zero along the west coast of the Americas for the last 30 years (Bromirski, Cayan, Helly, and Wittman, 2013).

Mean Sea Level Rise

Over the past 2 million years, earth's climate has periodically warmed and cooled with periods of around 100,000, 40,000, and 20,000 years, set respectively by the ellipticity, tilt, and precession perturbations of the earth's orbit around the sun caused by the other planets (Milankovitch, 1920). The orbital fluctuations produce small changes in high-latitude solar power, which then pace the periodic warming and cooling that are amplified by feedbacks related to albedo and greenhouse gas concentrations. These temperature cycles of global warming and cooling range up to about 10° C and drive glacial retreat and advance (Hays *et al.*, 1976). The temperature and related ice volume changes together cause rises and falls in global MSL of up to about 200 m.



Figure 2-46. Google Earth photograph taken 25 May 2009 shows about 14 km of the southern Silver Strand shoreline (refer also to Figure 2-38).

Over the past 20,000 years, there was a general, if erratic global warming of about 8° C and associated ocean water expansion and glacial and icecap melting that raised global MSL by about 130 m (Figure 2-47). The relatively rapid MSLR of about 110 m from about 15,000 to 7,000 years ago averaged 1.4 meters per century (m/cy), and occurred in brief episodes of rapid rise and longer periods of slower rise. For example, "Meltwater Pulse 1A," approximately 14,000 years ago (Figure 2-47), raised sea level by 20 m in only 500 years, an average MSLR rate of 4 m/cy. The rate of sea level rise slowed to an average of about 0.1 m/cy for the past 5,000 years, and to an even slower rate of about 0.02 m/cy for the past 2,000 years. Even during the past 2,000 years, however, MSLR rates have varied, increasing during the medieval warming period (from about 800 to 1300 CE), and slowing during the Little Ice Age (from about 1500 to the mid-1800s).

Historical Sea Level Observations

Long-term tide gauge records such as the ones from Amsterdam (Holland, 1700–1930), Brest (France, 1810–1995), and Swinoujscie (Poland, 1810–2000 indicate that MSL has been risen over the last 300 years (Figure 2-48). Furthermore, the records suggest that the rate of MSLR has increased since at least 1870 (see Amsterdam record in Figure 2-48), and probably earlier (Church and White, 2006). For the past 100–150 years sea level in California has been accurately measured by tide

gauges. For example, the tide gauge at San Francisco has recorded water levels at least hourly since 1855 (Flick *et al.*, 2003). Because sea levels are well correlated on spatial scales of 100 km and more (Chelton and Davis, 1982; Enfield and Allen, 1980), water level data from the tide gauge at the SIO pier (Figure 2-49), located between MCBP and NBC, give a good estimate of historical short- and long-term sea level variability for MCBCP and NBC.

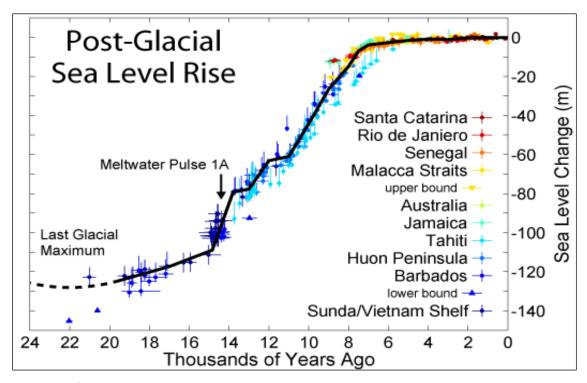


Figure 2-47. MSLR in the past 20,000 years associated with ice-cap retreat and global warming of about 8 °C (Rohde, 2013).

The MSL trend over the entire SIO record is close to the accepted upward trend in global MSL of 0.15 to 0.20 m/cy (Flick *et al.*, 2003; White *et al.*, 2005; IPCC 2007). However, there are 2 to 3 decade periods where the trend in MSL is relatively flat, or even decreasing. This is particularly noticeable since about 1980, but also from about 1940–1950, and the late 1950s to the mid-1970s (Figure 2-49 and Figure 2-50). The latest 30-year flat (or even downward) trend off the west coast of the Americas is consistent with global satellite data.

The downward trend at SIO since 1992 (green, Figure 2-50) is consistent with the satellite altimetry data. Periods when global sea level rise is locally suppressed appear to follow strong El Niños including the 1940–1941, 1957–1958, and 1982–1983 events, consistent with such events possibly initiating or being associated with persistent changes in ocean circulation. The satellite data allow linkage of coastal MSL variability with broad-scale SLH patterns across the North Pacific, as well as with other important oceanographic parameters such as SST and surface winds.

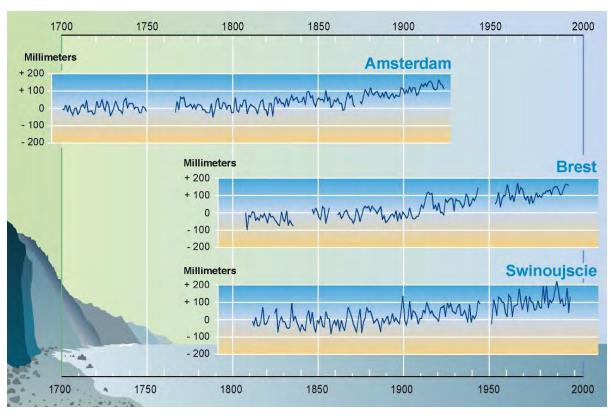


Figure 2-48. Long-term tide gauge data from Amsterdam, Brest, and Swinoujscie (Poland) indicates sea level rise over the past 300 years (IPCC, 2001).

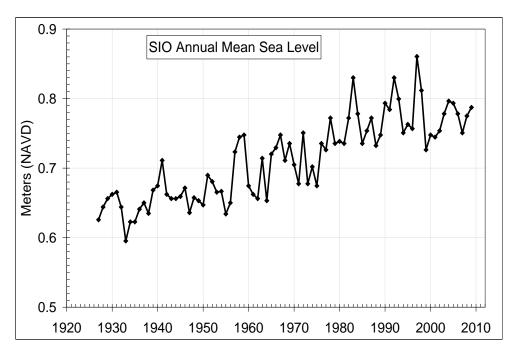


Figure 2-49. Annual MSL at SIO pier, La Jolla, CA (1926–2009) is representative of MCBCP and NBC.

Decadal-scale MSLR variability is also evident (Figure 2-50, cyan), with peaks coinciding with strong ENSO episodes. Perhaps surprisingly, the highest decadal peak is not associated with either the 1982–1983 or 1997–1998 great El Niños, but occurred during a series of moderate ENSO events in the early 1990's (Trenberth and Hoar, 1996). While current MSLR projections indicate only moderate increases in global MSL over the next two to three decades, local MSL increases from potential changes in ocean circulation could be larger.

Rates of sea level rise are highest in the western Pacific (warm, yellow and red colors in Figure 2-51). Rates are much lower, and often zero, in the eastern Pacific (cool, blue and green colors) since at least 1992. Fletcher (2009) shows recent annual global and regional MSL values. Globally, an upward trend (blue) of 0.28 m/cy (0.28 cm/yr) and a western Pacific trend (red) of 0.47 m/cy are statistically significant at the 97.5% level (Figure 2-52). There is no significant west coast (eastern Pacific) trend (green) in the satellite data, a result similar to that indicated by the tide gauge data shown in Figure 2-50.

Satellite records suggest that the global average rate of MSLR is now about 0.3 m/cy (Figure 2-52). It is not known if this higher global rate is a new symptom of the awaited global acceleration of sea level rise due to the "greenhouse effect." However, there is now evidence of acceleration in the rate of sea level rise commencing as early as 1870, coinciding with the Industrial Revolution, and related to anthropogenic global warming (Church and White, 2006).

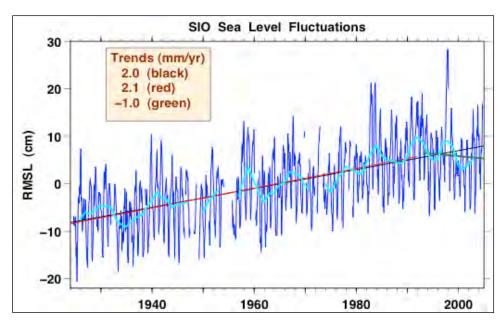


Figure 2-50. Monthly relative mean sea levels at the SIO La Jolla, CA, tide gauge station adjusted for the inverse barometer effect (see text).

The increase in flooding potential (frequency and duration of local sea level extremes) from MSLR is illustrated by an upward trend in the number of hours water levels exceed the 95th (2.22 m), 98th (2.39 m), and the 99.5th (2.58 m) percentile thresholds during winter (November to March), relative to the start of the record (Figure 2-53). Compared to the time prior to 1940, the incidence of extreme winter sea level fluctuations since 1980 has at least doubled in the SIO record.

Projected global sea level rise will cause a geometric increase in the occurrence of extreme sea levels (Cayan et al., 2008a), resulting in an ever-increasing likelihood of adverse coastal impacts.

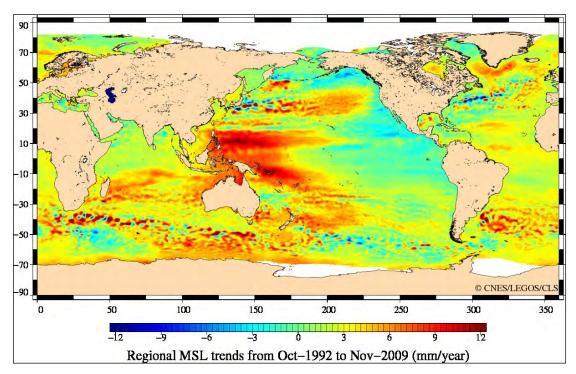


Figure 2-51. Map showing high rates of MSLR in the western Pacific and low rates or actual drops in MSL in the eastern Pacific off the west coast of the Americas (Aviso, 2010).

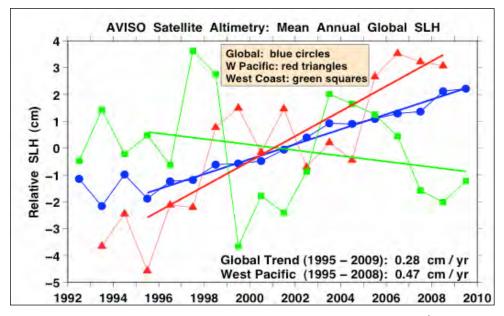


Figure 2-52. Relative sea level from satellite altimetry for different regions (AX $\hat{\mathbf{Q}}$ U, 2010). Note that 1 cm/yr = 10 mm/yr = 1 m/cy (see text and Figure 2-5).

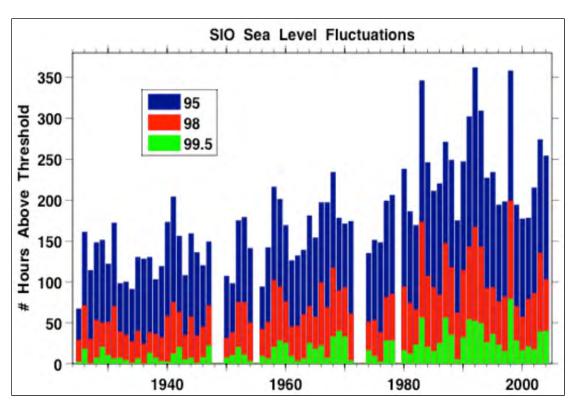


Figure 2-53. Number of winter (November–March) hours that water levels exceed given percentile thresholds (see text).

Non-Tide Sea Level Fluctuations

MSLR is important because it determines the base-level on which shorter-duration sea level fluctuations and wave run-up are superimposed. Sea level fluctuations include tides, weather-induced storm-surges, and climate-related fluctuations related to El Niño and longer-term Pacific Ocean changes characterized by the Pacific Decadal Oscillation (PDO).

Because astronomical tides are predictable, the occurrence and duration of NTR fluctuations are the independent-variable associated with short-term climate processes, including storm surges. Positive NTR fluctuations, obtained from the SIO tide gauge record using the spectral method of Bromirski *et al.* (2003), are less than about 30 cm. A very small 0.002 m/cy upward trend in NTR at SIO since 1924 is statistically significant. The 3-year running-mean (red) indicates that NTR levels are elevated during El Niños, similar to the decadal variability (Figure 2-50). The association of non-tide extremes with El Niño in the San Diego region also is indicates that the number of hours that NTR levels exceed the 95th (0.093 m), 98th (0.122 m), and 99.5th (0.164 m) percentile thresholds peaks during strong El Niños.

Decadal peaks in NTR extremes occur during strong El Niño events (Figure 2-54), similar to that observed for total sea levels (Figure 2-50) and mean NTR levels (Figure 2-53), with the early 1990s similarly the most prominent. Strong events are at least twice as likely during strong El Niños. The duration of extreme events is important because the longer an event lasts, the larger will be the chance that it coincidences with a high tide. Since the NTR levels include an El Niño component, there is a tendency for longer duration events during El Niño Figure 2-55; e.g., the 1997–98 event). The most extreme non-tide events (> 99.5th percentile) by definition occur infrequently, although concentrations of these events occurred near the 1940–1941 and 1982–1983 great El Niños (Figure

2-55). Note that extreme events occasionally occur outside the typical November-March winter period, but only in the adjacent months of October or April. Occasionally, lulls as long as five years with no events exceeding the 99.5% level occur.

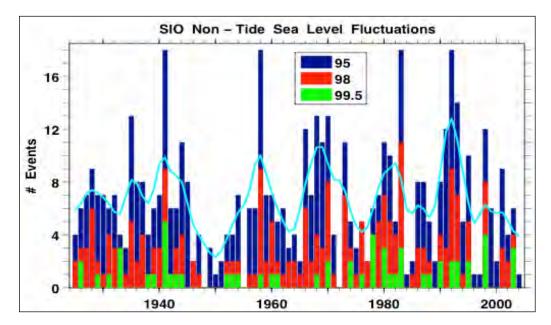


Figure 2-54. Number of NTR events during winter months (November–March) that exceed the 95th percentile (the binomial-filtered event count, cyan curve) for at least 6 consecutive hours.

Historical NTR variability in the San Diego region is characterized with the probability density function distributions of water level observations from the La Jolla tide gauge in Figure 2-56. All winter (November–March) data are shown with gray curves giving the full range of variability. The dashed lines are 1-standard deviation bounds. The Probability Distribution Function (PDF) indicates that NTR levels exceeding 10 cm occur only about 4% or the time during winter months.

MSL and Climate Indexes

MSL along the San Diego region is likely affected by gyre-scale circulation patterns that have resulted in suppression of local MSLR below the global average value (Figure 2-51 and Figure 2-52). This suppression of MSLR is probably related to the dynamical steric response of the ocean to a combination of surface warming and changes in wind stress patterns, key factors that affect gyre circulation (Bromirski et al., 2011). The ocean's response to wind forcing produces what is commonly referred to as the PDO pattern in SST and SLH across the basin. If and when the component of the ocean dynamics that is responsible for the rate of MSLR along the Pacific coast of North America ever relaxes or reverses, the San Diego region could see rates of sea level rise above the increasing global average rate.

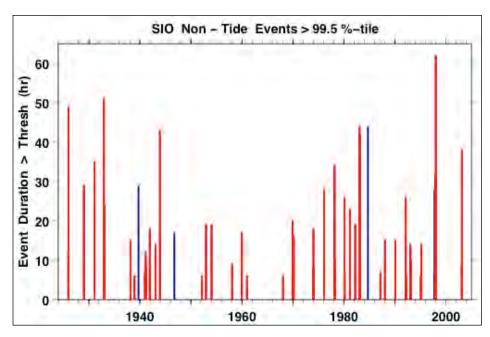


Figure 2-55. Duration (hours) of the 63 extreme NTR events that exceeded the 99.5th percentile during the full year (red) and non-winter (April–September, blue).

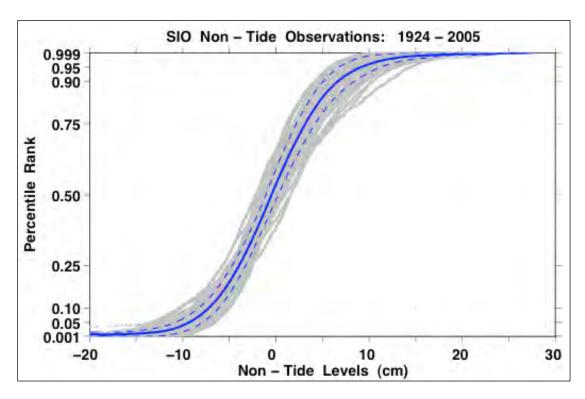


Figure 2-56. PDF of NTR fluctuations relative to MSL from the La Jolla tide gauge for winter (November-March) 1924–2005. Solid line is the mean and dashed lines are ±1 standard deviation bounds. Gray curves show individual years.

The wind stress patterns of variability across the Pacific that affect gyre circulation are related to climate variability. Climate indices commonly used to describe the modes of climate variability across the North Pacific Ocean include:

- The Pacific Decadal Oscillation (PDO, Mantua et al., 1997) is the leading principal component of monthly SST anomalies in the North Pacific;
- The Multivariate ENSO Index (MEI) is the first principal component of several atmosphereocean parameters (sea and air temperatures along with wind, pressure, and cloud cover) across the tropical Pacific;
- The Pacific North America (PNA) pattern (Wallace and Gutzler, 1981) is the difference in 500 hPa geopotential height "Z" over the North Pacific between 160-165W and over North America between 245-275W as follows: 0.25*[Z(20N,190W) Z(45N,195W) + Z(55N,245W) Z(30N,275W)];
- The North Pacific Index (NPI) pattern¹⁰ is the area-weighted sea level pressure over the midlatitude region 30-65N, 160-220W (Trenberth and Hurrell, 1994).

Monthly sea level anomalies from Archiving, Validation and Interpretation of Satellite Oceanographic Data (AVISO, 2010) satellite altimetry are correlated with these four Pacific climate indexes (Figure 2-57, a-d). Moderate to strong correlations exist between sea level along the west coast of the Americas and the major climate indexes. Correlation of the indices with altimetry SLH monthly anomalies gives similar PDO-like patterns of variability across the basin (Figure 2-57(b)), with the region south of the Aleutians anti-correlated with coastal SLH. Note that this pattern is similar to that observed in the SLH trends across the basin. Also note that sea levels in the San Diego region are generally well correlated along the Pacific coast of North America and with SLH anomalies in the tropical Pacific, consistent with the strong El Niño association discussed earlier.

Tides

Tidal changes of ocean water level are caused by the interaction of gravitational forces between the moon, sun, and earth. Other astronomical bodies such as the planets also generate gravitational forces at the earth, but these forces are very small and have no practical effects on the tides. Because of the forces involved, the respective orbital patterns of the moon, sun and earth, and the earth's rotation, tidal fluctuations occur at frequencies around one and two cycles per day. This means that one or two high tides and one or two low tides, respectively, occur in each tidal day, which is 24-hours 50-min long.

The tide range is the elevation difference between consecutive high and low tides. On this coast, important tide range fluctuations occur at intervals of twice per month, twice per year, every 4.4 years, and every 18.6 years. The 18.6-year variations are related to a cycle of the lunar node (where the orbit of the moon crosses the ecliptic) and represents the longest periodicity of practical interest when evaluating tidal highs and lows.

In many locations, the tide provides the largest component of sea level variability on every time scale except those associated with ice ages at thousands of years. Furthermore, the tide is one of the few geophysical phenomena that can be accurately predicted. The relative astronomical motions between the earth and moon, and earth and sun are complex and the tidal forces upon the waters of the earth reflect this complexity. Although complicated, the tide generating forces at the surface of the earth are basically a function of time and latitude. However, the actual tidal response is affected

_

¹⁰ Lower pressure over a region gives a more negative NPI, which is associated with more storminess across the North Pacific basin, so the negative is used to be consistent with the sign conventions of the other indices.

by geography, especially along the coasts where water depth and the shape of the continental edges are very important. This means that the tide patterns and characteristics on the Pacific coast of San Diego, CA are expected to be quite different from those (for example) at the Atlantic coast of Charleston, SC, even though both places are at essentially the same latitude. For these reasons, the tide generating forces can be predicted, but the actual tidal amplitudes cannot be predicted without tide measurements at a given location.

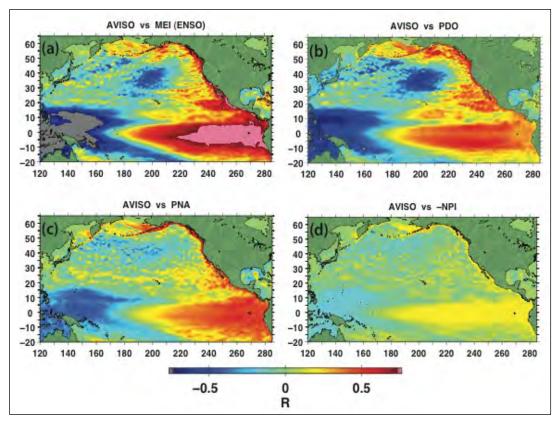


Figure 2-57. Correlations of satellite altimetry sea level height monthly anomalies (AVISO¹¹) with (a) the multivariate ENSO index (MEI), (b) the Pacific decadal oscillation (PDO), (c) the Pacific-North America (PNA) index, and (d) the North Pacific index (see text).

Waves

Both the generation of waves by wind over the ocean and their propagation through the islands and across the continental shelf to the beach are complex physical processes. Nevertheless, these phenomena are now relatively well understood. For practical purposes, our limited ability to forecast future ocean winds is the sole limiting factor in simulating future wave conditions just outside the surfzone at these two military installations.

Ocean surface gravity waves are generated by the transfer of energy from winds to the sea surface producing a wave field that is characterized by its height (or energy), length (or frequency, or period between crests), and direction of propagation. Since there is always a mixture of wave heights,

_

¹¹ "Archiving, Validation and Interpretation of Satellite Oceanographic" data - AVISO distributes satellite altimetry data from Topex/Poseidon, Jason-1, ERS-1 and ERS-2, and EnviSat, and Doris precise orbit determination and positioning products.

lengths, and directions in any given wave field, wave characteristics must be specified as statistical quantities. This statistical description is commonly presented in terms of average quantities including wave parameters such as "significant wave height" denoted as H_s, which is defined as the average of the highest one-third of the waves in a given wave field, its peak frequency or period, and its mean wave direction at the peak period. However, to simulate the generation and evolution of waves using state-of-the-art models, the wave field is defined more precisely as a two-dimensional wave spectrum, which represents the distribution of wave energy as a function of frequency and direction.

Ocean wave characteristics depend on the strength of the generating wind field (wind speed), the size of the area the wind is blowing over (fetch), and how long the wind blows (duration). Big storms with strong winds that blow over large ocean areas for several days therefore generate high waves with long periods. Ocean surface gravity waves are dispersive. That is, waves with longer period (or length) propagate faster when they are in water that is deep relative to their wavelength.

Ocean swell are defined as waves that are no longer in their source fetch, or "generation" area. Swell propagate along great circle paths until they reach the offshore waters of a (sometimes very distant) coastline, with longer wave periods arrive first, as demonstrated by Munk *et al.* (1963). Contrastingly, ocean "seas" are defined as waves that are still in their source fetch area and are actively increasing in energy or maintaining their fully developed state owing to the continuing transfer of energy from the local winds. The height of short period seas is limited by wave breaking or white-capping, and they do not propagate great distances owing to the dissipation of their rapid orbital motions into the background turbulence of the upper ocean.

The distinction between sea and swell is blurry, particularly when winter or tropical storms make landfall. However, these "seas versus swell" distinctions are primarily for descriptive purposes, and do not affect the accuracy of wave model simulations if the models include the appropriate wave generation and propagation physics.

Offshore Wave Sources

Incoming waves along the southern California coast fall into four main categories as illustrated in Figure 2-58 (USACE, 1988a):

- North Pacific (extra-tropical) swell
- Southern hemisphere swell
- Tropical storm swell
- Seas generated locally by coastal marine layer dynamics or arriving storms

In the winter (November-March) and spring, the wave climate is dominated by North Pacific swell generated remotely by extra-tropical storms that begin as low pressure systems off Asia, and then develop into Pacific Ocean storms of various sizes and intensities depending in part on the following:

- Position of jet stream
- Degree to which lower latitude tropical moisture is entrained
- Ocean sea surface temperatures along the storm's path

North Pacific sea surface temperatures are largely described by the North Pacific Decadal Oscillation (PDO) of warm/cool sea surface temperatures between the NE and NW Pacific at midlatitudes, and the El Niño-La Niña Southern Oscillation (ENSO) of cool and warm in the eastern

North Pacific. As a result, both interannual and interdecadal variations in the southern California winter wave climate can be conceptually tied to the combined influence of multi-decadal PDO and multi-year ENSO ocean warming and cooling events (Graham, 2003).

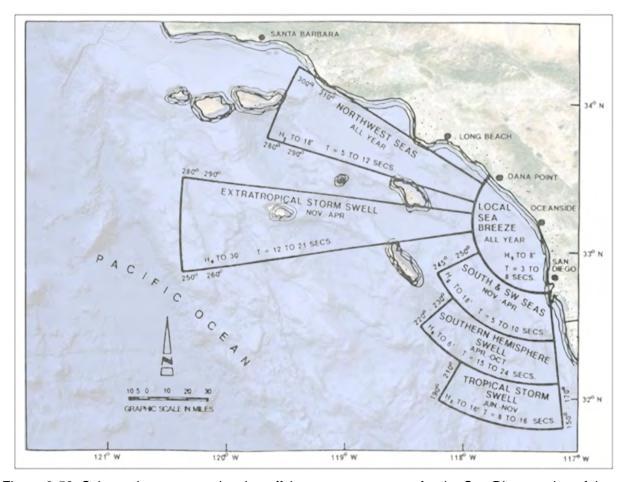


Figure 2-58. Schematic summary showing offshore wave exposure for the San Diego region of the Southern California Bight (overlay adapted from USACE, 1988a; image data: Google, SIO, NOAA, U.S. Navy, NGA, GEBCO, Landsat, LDEO-Columbia, NSF).

In summer and fall, the southern California wave climate is dominated by long period swell arriving from Southern Hemisphere storms (where it is winter and spring). The Southern Ocean extends in a continuous band around Antarctica and west-to-east propagating storms are not limited in their fetch or duration by continental land masses. As a result, the southern ocean continually generates pulses of long-period waves that propagate northeastward across the ocean basins. Unlike North Pacific storms, Southern Ocean storms occur throughout the year and are a background component of the southern California wave climate in the winter and spring.

While the southern California wave climate is dominated by swell arrivals from open-ocean storms, steeper, shorter-period waves generated more locally are also important components to the overall wave climate.

Local waves fall broadly into three categories:

• Wind swell, which are NW seas with 5-12 s period generated primarily off Point Conception and in the Southern California Bight's (SCB) outer waters;

- Prefrontal seas from the south that occur when winter low pressure systems pass through southern California; and
- Sea breeze waves, which are daily local waves of less than 8 s period that occur year-round near the coast owing to the sea breeze generated by differential heating and cooling of land relative to the coastal ocean.

The presence and size of wind swells and sea breeze waves are primarily controlled by coastal marine layer dynamics in the SCB. When high pressure dominates over southern California, the coastal marine layer boundary between cool moist ocean air and warm dry land air is offshore of Catalina and San Clemente islands, and strong NW winds are present off the central California coast south past Point Conception, with a weak cyclonic recirculation eastward into the SCB and then northward into the Los Angeles basin area. This is known as the "Catalina Eddy" (Maas and Albright, 1989).

These conditions result in weak local wind swell in the SCB, but daily sea breeze waves near the coast can be quite significant. Alternatively, when inland high pressure breaks down, the marine layer boundary moves inland with brisk NW winds in the outer waters of the SCB, and wind swell is more prevalent with little or no sea breeze activity. When very strong inland high pressure develops in the fall, it can force very strong offshore-directed "Santa Ana" winds, particularly downward through coastal canyons. Santa Ana conditions typically lead to benign local waves at the mainland shoreline, but potentially dangerous and rapidly developing short, steep, westward-propagating waves in the outer waters, and on the eastern shores of the offshore islands.

Finally, during the summer and fall, southern California can be impacted by waves from Pacific Ocean tropical storms and hurricanes that develop off Central America. Tropical hurricanes commonly develop at low latitudes off the west coast of Mexico during the months of July-October. They first move west and then curve north and northeast before dissipating in the colder waters off Baja California. The swell waves generated by these events usually do not exceed 2 m in height by the time they reach southern California. However, on rare occasions the offshore waters are warm enough to sustain a hurricane much farther north than normal (Smith, 1986; Chenoweth and Landsea, 2004). This happened in September 1939, when a hurricane passed directly over southern California and the resulting waves caused widespread destruction, especially on south-facing beaches.

In summary, the SCB wave climate is a blend of remotely generated long period swell, more locally generated mid-period wind swell and prefrontal seas, and even more local short period sea breeze-generated waves. Extreme wave events are most commonly associated with large winter storms and high prefrontal seas from the south, followed by large swells from the west.

In September and October, large hurricane or tropical storm waves from the south and perhaps followed by the actual landfall of the storm system in southern California, have historically been rare. However, such a scenario potentially poses the greatest marine weather exposure to south-facing military base infrastructure, such as is found at NBC-North Island. Due to their rarity, it is not possible to calculate a return period, or a statistical probability associated with such an event.

Wave Propagation, Shoaling, Refraction and Sheltering

When ocean waves reach the continental shelf a new set of processes affect their propagation and determine their ultimate impact on the shoreline. In southern California the main effects involve the coastal orientation, blocking or shadowing by the offshore islands, and refraction by the complicated under-water bathymetry (Arthur, 1951).

The southern California coast make distinct breaks in direction at Points Arguello and Conception, where it changes from generally north-south to generally east-west. It then gently curves toward a more north-south orientation approaching San Diego thus forming the SCB. This configuration greatly decreases the exposure of southern California to waves from the North Pacific Ocean. Island sheltering is also very important, and simply means that where waves reach the outer coasts of the islands wave energy is dissipated creating a shadow zone of lower wave height in their lee.

Waves that pass between the islands refract and shoal over the shallow depths around the islands and the mainland continental shelf (Pawka, 1983). Refraction is the change in wave propagation direction in water depths less than the deep water wavelength, leading to the convergence and/or divergence of wave energy at the coast. Shoaling is the increase in wave height owing only to changes in local water depth.

An individual wave's circular orbital motion extends surprisingly far down into the water column as it travels at a constant speed in water depths greater than or equal to its deep-water wavelength. As the wave propagates into progressively shallower water across the continental shelf, the ocean bottom boundary constrains the wave motion in the vertical, which is sometimes described as the wave "feeling" the bottom. This forces the wave orbital motion to become increasingly elongated in the horizontal, decreasing the wave speed and length, while the period between wave crests passing a fixed point remains constant. Variations in water depth along a wave crest results in variable wave speeds and the bending or refraction of the crest like light passing through a convex or concave lens (Munk and Traylor, 1947). In addition, as the wave slows in shallow water, its wave height increases or shoals in order to conserve the flux of energy (energy passing a point per unit time) towards the shoreline.

Refraction can increase or decrease near-shore wave heights relative to deep water, depending on the near-shore location and surrounding bathymetry. Shoaling increases near-shore wave heights, relative to offshore, and depends only on depth. The two phenomena can be treated independently and refraction and shoaling coefficients can be combined to estimate the overall near-shore wave heights along the coast (Longuet-Higgins, 1957; O'Reilly and Guza, 1991; O'Reilly *et al.*, 1993; O'Reilly, 1993).

Wave sheltering, refraction, and shoaling contribute in varying degrees to the wave climate at southern California beaches. Near-shore wave conditions are highly sensitive to the direction and period of offshore waves, and the directional "windows" open to deep-ocean waves vary alongshore. Consequently, on any given day, waves can vary strongly alongshore with regions of high and low waves separated by only a few km. This sensitivity can in turn lead to significant changes in alongshore location of the potential impact of future offshore wave climate change scenarios. For example, a northward shift in wave directions could decrease energy at most beaches, while increasing it at most others.

2.3.2 Beach Processes

Beaches form from whatever loose sedimentary material is deposited at the shoreline. Southern California beaches exist in a delicate balance controlled by the local sand budget, which encompasses sand supply, transport, and loss, the wave climate, and the rate of MSLR. On long time scales of

decades and centuries the rate of MSLR determines the shoreline position. When MSLR is low and the sand supply large, the shoreline advances and the beach widens. As the rate of MSLR increases or the rate of sand supply decreases, the shoreline retreats until the sea cliff or other backshore environment is undermined and also retreats or becomes flooded (Masters and Aiello, 2007). On short time scales of days to years, and most noticeably on seasonal scales, the wave climate largely determines the shape and width of the beach.

It must be emphasized that MSL changes themselves do not cause beach erosion or accretion – on this coast, only waves transporting sand do. However, MSL provides the background water level that enables waves and wave-driven run-up to reach farther up the beach and move sand offshore, or not. The balance between long-term shoreline retreat and cliff or dune retreat determines whether or not a beach exists along almost all of southern California.

Littoral Cells

Section 2.2 of this report outlines how headlands along the California coast naturally divide it into a series of compartments called littoral cells, as shown in Figure 2-23. Sand contributions from rivers, cliffs, and anthropogenic sources in varying proportions provide each littoral cell with sand. This sand is moved cross-shore and alongshore, on average toward the east or south, by wave action. Recent work by O'Reilly at Scripps Institution of Oceanography suggests that near-shore topography alters wave patterns to create littoral sub-cells, only a few kilometers long, with boundaries often located at lagoon mouths. Inman and Masters (1991) also used a sub-cell approach, but based on physiographic barriers, in analyzing the sediment budget of the San Diego area littoral cells. These include the Oceanside cell, the northern half of which comprises the coast of MCBCP, and the Silver Strand cell, almost all of which is part of or used by NBC.

Sand is funneled offshore through submarine canyons at the southern, down-coast end of each major littoral cell, or by wave action, including wave-induced rip currents, in each smaller sub-cell. Sand is also lost offshore during large or unusually persistent wave events. Because of the structure of the southern California coast with its more-or-less short and isolated littoral cells and sub-cells, the sand budget of a particular beach is largely localized. In other words, if sand shortages, surpluses, or interruptions to transport occur from place-to-place or time-to-time, the beach width effects are relatively isolated, spreading at most a few tens of kilometers.

Most beaches in north San Diego County, including MCBCP, consist of a thin veneer of sand over a rocky, low-tide terrace. Most beaches in the southern part of San Diego, including NBC, are low-lying, with a relatively thick sand layer. In both regions, naturally supplied sand is derived either from upland erosion or from relic deposits offshore. Upland-derived material arrives at the coast through the ephemeral rivers or from gullies and the cliff faces as result of terrace erosion. In southern California a substantial amount of beach sand has been supplied by human activity, particularly bay and wetland dredging, offshore borrowing, and as by-products of coastal construction projects (Herron, 1980; Flick, 1993; Flick and Ewing, 2009; Flick *et al.*, 2010).

Wave-Driven Sand Transport

Normal wave action pushes the sand landward over the terrace and piles it up in a berm against the base of the sea cliff, sea wall, or other back beach structure. This sand layer varies in thickness from zero to several meters, depending on location, season and other factors. Figure 2-59A shows an oblique conceptual view of a typical section of California coast, while Figure 2-59B provides a typical cross section that illustrates these concepts. Waves provide nearly all of the energy input that drives beach processes in southern California. In particular, waves provide the energy that moves sand on beaches.

Sand moves both on-offshore and long-shore. The magnitude and direction of sand transport changes with wave height, period, and incoming direction. Figure 2-59B illustrates typical changes in the beach profile from summer (stippled) to winter (broken line) conditions. Essentially, the higher, more energetic waves of winter strip sand off the subaerial beach and move it lower down on the profile. This reduces the width of the beach berm, the flat section of the upper beach profile, while also often forming one or more offshore sand bar features. This beach profile, of lower overall slope, is more efficient at dissipating incoming wave energy.

Gentler wave action in summer pushes the sand back up the slope, making it steeper. With sufficient sand supply, the berm may not completely disappear in winter thus shielding the cliff base from wave erosion at all but the highest tides and coinciding high wave conditions. On the other hand, in particularly active winters waves may strip all the sand off the wave-cut platform and expose the cliff base.

Bruun Rule

The berm height in summer is determined by the maximum height that wave uprush can push sand. As MSL rises, the waves can build progressively higher berm and associated profile elevations during the summer. Meanwhile, during the winter the same higher water levels allow wave action to undermine the cliffs or dunes causing coastal retreat. The net effect over centuries and millennia is to raise the beach profile and the berm while the entire profile moves landward. This geometric concept was first proposed and quantified by Bruun (1962) and quickly became known as the "Bruun Rule." It was refined and modified, by him and others, and also criticized by many ever since (*e.g.*, Dean *et al.*, 2002; Pilkey and Cooper, 2004; Cowell *et al.*, 2006). The Bruun Rule is illustrated in Figure 2-60, and can be written mathematically as

Equation 2-1

$$R = SL / (h + B)$$
,

where "R" is the horizontal beach retreat of a sandy coast under a MSLR of "S," and "L" is the cross-shore width of the active profile, "h" is the depth below MSL of closure (where sediment transport due to wave action stops), and "B" is the berm height. This equation balances the amount of sand R (h + B) yielded by horizontal retreat with that needed for the vertical rise, SL. This formulation implies that the rate of shoreline retreat (dR/dt) is directly proportional to the rate of sea level rise (dS/dt). Another consequence is that

Equation 2-2

$$R = S / \tan \beta$$
,

where "β" is the foreshore slope, or for very long-term coastal retreat, the slope of the shore platform.

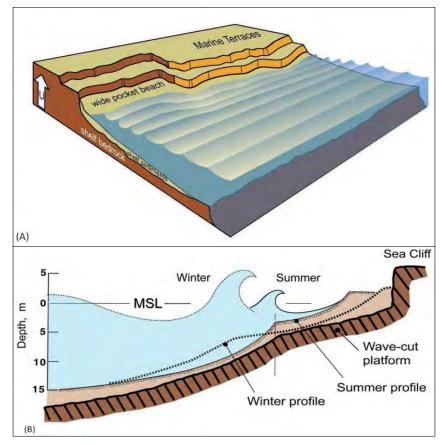


Figure 2-59. Oblique conceptual view of a typical California cliff-backed beach (upper A). Cross-section illustrating wave-cut platform (terrace), sea cliff, and typical effects of winter and summer waves on beach width (lower B) (courtesy of D.L. Inman, Scripps Institution of Oceanography, University of California, San Diego).

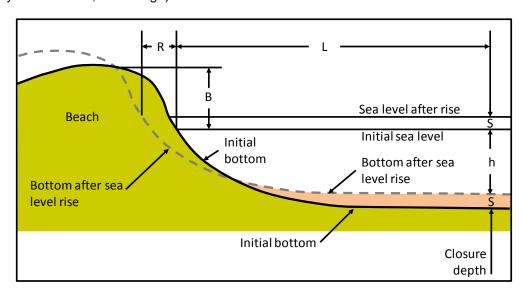


Figure 2-60. Illustration (adapted from Gutierrez *et al.*, 2009) showing the basic parameters used in the Bruun Rule (see text).

The response of the beach to sea level rise as proposed by Bruun (1962) is plausible on very long time scales of centuries to millennia during which MSLR rise dwarfs all other effects. However, the relationship of beach response to MSLR on shorter time scales of years to decades is much more difficult to convincingly demonstrate (Zhang *et al.* 2004), mainly owing to the large variations in beach width due to other variables, mainly beach sand supply, and wave variability. Observed shoreline variations at MCBCP and NBC will be related to waves and other factors at these locations, to the extent possible, during the first half of the second-year effort in this study. During the latter half of the second year effort these relationships will be used to create possible shoreline change scenarios from the future MSLR and wave scenarios, which were developed in the first study year and are presented in this report.

Littoral Sand Budgets

Sand budgets are always uncertain simply because the rates of sand movement over time cannot readily be measured – in other words, there is no "sand flux meter." For example, there are no reliable measurements of cross-shore sand movement to or from deep water, or of long-term down-canyon sand losses. The elements of a sand budget must therefore be pieced together from indirect evidence, such as river sand yield estimates, inferred sand accumulation rates at the ends of littoral cells or sub-cells, or observed long-term changes in beach width¹². These measurements are always intermittent and inaccurate when they even exist. The sand budgets based on them are therefore also inaccurate.

Sand fluxes may also be calculated from the long-shore and cross-shore wave driving forces. In this approach, accurate sand movement estimates depend first upon the relationships between cross-shore and along shore sand transport rates and the wave characteristics, and second on having accurate long-term information about the waves. However, the theoretical relationships quantifying sand transport rates and waves are highly uncertain, especially when it comes to on-offshore transport. Systematic coastal wave measurements and modeling is at most 10 years old, so the input wave data to reconstruct reliable past sand budgets does not exist. The lack of data and unreliable cross-shore wave-driven sand transport relationships makes estimates of on- offshore sand transport undependable.

Beach sand budgets for the northern-half of the Oceanside littoral cell (MCBCP) and the Silver Strand cell (NBC) were developed by Inman and Masters (1991) as part of the U.S. Army Corps of Engineers *Coast of California Storm and Tidal Waves Study*. This work incorporated earlier work, including Everts (1987, 1990). The summaries relevant to the modern sediment budgets of MCBCP and NBC are included below. Together with the shoreline and cliff and gully erosion histories presented in following sections, these provide a rough guide concerning what kinds and magnitudes of future coastal change might be expected.

Table 2-2 provides a key for the variable names that are used in Figure 2-61 and Figure 2-62, which respectively present the sand budget summaries for the Oceanside and Silver Strand littoral cells. Each figure presents a summary sediment budget for each sub-call (three in the Oceanside cell, Figure 2-61; four in the Silver Strand littoral cell, Figure 2-62), for three different past settings.

_

¹² The construction of sand budgets involves balancing the long-term "average" rates of input and output of sand in a "control volume." Cross-shore, this is usually the active part of the beach, from the berm down along the beach face to the depth of closure, usually defined as the deepest depth that wave-driven sand movement normally takes place. Alongshore control volume limits can be chosen to coincide with physiographic boundaries, much like littoral cells or sub-cells are defined, and for the same purposes.

The first setting corresponds to the "natural" condition (from 1900–1938 in the Oceanside cell; 1905–1936 in the Silver Strand cell), before dams artificially reduced the rate of sand supply to the coast. The second setting corresponds to a period of "uniform" wave climate, which extended roughly from 1950 or 1960–1978 (see Figure 2-55 and related discussion above). There are strong indications of a "regime shift" in the late 1970s when the relatively benign storm and wave conditions that prevailed from the mid-1940s changed to a more variable climate with more big wave events, such as those of 1978–1979, 1979–1980, and 1982–1983 that was mentioned above (Hare and Mantua, 2000).

Oceanside Littoral Cell - MCBCP

The coastline of MCBCP spans the "Central" portion of the Oceanside cell delineated on the map at the right edge of Figure 2-61 (San Mateo Point to Oceanside Harbor). The sand budget analysis suggests that from 19601978 this segment suffered a net deficit of sand supply of about 65,000 m³/yr, which lead to a loss of beach width of about 7 cm/yr. Note that this deficit would have been greater if not for the $Q_a = 50,000 \text{ m}^3/\text{yr}$ of artificial supply from the construction of SONGS described in Section 2.2.2. River supply amounted to an estimated $Q_r = 20,000 \text{ m}^3/\text{yr}$, which was dwarfed by cliff and gully erosion contributions at an estimated rate of $Q_b = 280,000 \text{ m}^3/\text{yr}$. However, wave-driven offshore transport was estimated to be 350,000 m³/yr. Wave-driven long-shore transport from the northern sub-cell, which contains San Juan Creek, provided an estimated $Q_1 = 145,000 \text{ m}^3/\text{yr}$ to the MCBCP coastline. However, long-shore transport to the south was even greater amounting to 210,000 m³/yr. Taken together, this produced the sand budget deficit at MCBCP.

After the regime shift of the late 1970s the sediment budget of MCBCP improved, mainly because wave-driven losses along shore are estimated to have decreased by about 75%, while offshore losses disappeared altogether. Long-shore sand supply rates and cliff erosion contributions both decreased by one-half or more from 1983 to the time of the analysis in 1990. But the net budget was in surplus by about 150,000 m³/yr over this time, and would have led to an increase in beach width of about 40 cm/yr.

Silver Strand Littoral Cell - NBC

The Silver Strand littoral cell sand budget shown in Figure 2-62 was analyzed in four segments over three time periods. The northern-most area is the "Zuniga" sub-cell, which went into a severe 620,000 m³/yr sand deficit after Zuniga Jetty was completed in 1904. The jetty initially prevented sand from re-circulating to the beach from Zuniga Shoals offshore, while at the same time allowing sand to aspirate into the entrance to San Diego Bay, from which it was transported offshore by tidal currents. This deficit accounts for the severe beach erosion in Coronado up until large amounts of artificial sand were provided by the dredging in San Diego Bay after World War II discussed in Section 2.2.2. This filled the sub-cell and prevented further losses. Since about 1950 the Zuniga sub-cell has been in balance, and the shoreline stable.

The next sub-cell to the south is denoted "Strand" in Figure 2-62, and extends from the Hotel Del Coronado to SSTC-South (see Figure 2-38). Its sand budget was essentially in balance under natural conditions, but went into a massive surplus from $Q_a = 630,000 \text{ m}^3/\text{yr}$ in the 1950–1978 time span owing to the sand produced by harbor dredging and discussed previously. This caused an average beach width increase of 3.75 m/yr. Currently Silver Strand is in a small, 30,000 m³/yr net sand deficit, presumably bringing with it the estimated 21 cm/yr shoreline erosion rate. Aside from a sharp decrease in anthropogenic sand supply, the deficit seems mainly related to the 130,000 m³/yr of wave-driven sand transport to the Zuniga sub-cell in the north, while waves only bring about 50,000 m³/yr from the south.

The southern-most sub-cell of concern to this discussion of NBC is the "Delta" reach, which extends from the SSTC-South to the International border. In pre-dam conditions, this sub-cell was in sand balance and stable as 75% of the sand produced by the Tijuana River was moved north, and 25% was moved south by the waves. Since about 1950 the Delta sub-cell has been in a net deficit owing mainly to a decrease in river sand supply, which was reduced from $Q_r = 200,000 \; \text{m}^3/\text{yr}$ to $50,000 \; \text{m}^3/\text{yr}$. Net shoreline erosion related to this sand budget deficit was estimated to be 47 cm/yr.

As discussed in Section 2.2.2 unless additional sand nourishment is provided to the Silver Strand littoral cell, continued decreases in beach width are to be expected. An increase in future MSLR rate will only accelerate beach losses without additional sand supply.

Table 2-2. Table Key to variables used in Figures 3-23 and 3-24.

Variable	Description and (Units) Volume transport rate of sandy material (m³/m/yr) q' = height of shoreline flux-surface (m) and volume-equivalent factor for shoreline change (m³/m)						
q							
z							
Q	$q'*\ell = total sand transport rate into or out of a cell (m3/yr)$						
l	Length of control cell						
Subscripts	Description						
1	Flux into cell (+)						
2	Flux out of cell (-)						
a	Artificial nourishment, bypassing, dredging, etc. (+/-)						
b	Blufflands erosion (+); includes sea cliff, gullies, coastal terrace, slumps, etc., as distinct from rivers						
f	Shoreline flux-volume into cell (+) by shoreline erosion, or deposition out of cell (-) by shoreline accretion, in accordance with movement of shoreline flux-surface, $\delta X/\delta t * Z * \ell = Q_f$						
ı	Inlet material carried in or out by inlet flow (+/-)						
l	Longshore transport of sand in and near the surfzone, versus n						
n	Nearshore transport along the coast, outside the surfzone						
О	On/offshore transport at the base of the shorerise (+/-)						
ow	Overwash (-)						
r	River yield to the coast (+)						
S	Lost to submarine canyons (-)						
w	Windblown sand removed from the beach (-)						

2.3.3 Historical Shoreline Position

The coastal sections of MCBCP and NBC have undergone significant natural and anthropogenic changes over the past century. While most of MCBCP, including the coastline, remains relatively natural, the construction and operation of SONGS have introduced major anthropogenic changes (Flick *et al.*, 2010). The Coronado and Silver Strand coastline is one of the most heavily modified in all of southern California (Flick, 1993; Flick, 2005, and references therein). Some details of these changes have been discussed in Section 2.2 and above. Here we focus on the available beach profile

measurements at MCBCP and NBC. Profile data were found from 1950–1989 at MCBCP and 1950–2009 at NBC.

A total of 265 profiles are available on 13 range lines. The earliest measurements are sparse in time and space. Most unfortunately, some profile start-locations changed over time on some ranges making it difficult to register profiles and reliably track shoreline position changes. Further attempts to register earlier with later data will continue in year-two of the present effort. Profiles were recovered from the U.S. Corps of Engineers, which gathered data for many decades as part of their interest in shoreline-change monitoring and beach nourishment and restoration. Since 2001 the San Diego Association of Governments (SANDAG) has been sponsoring twice-yearly regional profile measurements, but these are confined to the area between Oceanside (south of MCBCP) to Imperial Beach (at the southern end of Silver Strand), and so do not contain any data from MCBCP, but do include NBC. Shoreline change information is also available from the Southern California Beach Processes Study (SCBPS)¹³, which collects LiDAR data twice per year and monthly or more frequent GPS-based beach topography surveys.

Range line start locations are usually primary survey benchmarks that consist of permanent monuments, usually brass plaques engraved with the designated name and/or number that are fixed either in the ground with long rods set in concrete, or to slabs or other horizontal surfaces with epoxy. Secondary starting points farther seaward are also sometimes used, especially in places where the primary benchmark is not conveniently accessible from the beach (*e.g.*, high on a bluff), or when the back beach is unusually wide. Once set, the vertical and horizontal benchmark locations are determined using standard survey techniques, now usually GPS-based. Profile surveys consisting of location and elevation measurements are then made using a benchmark as a starting point and oriented in fixed directions as perpendicular as possible to the local shoreline orientation. GPS and fathometer-equipped boats or jet skis are now used to measure the under-water portions of profiles.

Benchmark location information was re-constructed for this study from various sources, including original benchmark and survey records available at Scripps Institution of Oceanography, reports presenting results of studies at SONGS (*e.g.*, Elwany and Flick, 2000; Flick *et al.*, 2010), U.S. Army Corps of Engineers information developed during the Coast of California Storm and Tidal Waves Study (*e.g.*, USACE, 1986; Moffatt & Nichol, 1987), and data from SANDAG.¹⁴

Benchmark names refer to the designations that were assigned in the 1980's USACE studies using letters to indicate regions ("PN" for Pendleton, "SO" for San Onofre, "SS" for Silver Strand), and numbers giving approximate shoreline distances in 100's of meters from the international border and measuring north. Thus, benchmark "SS0090" is located on Silver Strand approximately 90 * 100 = 9,000 m (9 km) north of the U.S.Mexico border, and so on.

¹³ http://cdip.ucsd.edu/SCBPS/

¹⁴ http://www.sandag.org/programs/environment/shoreline_management/pubs/beach_profile_data.zip

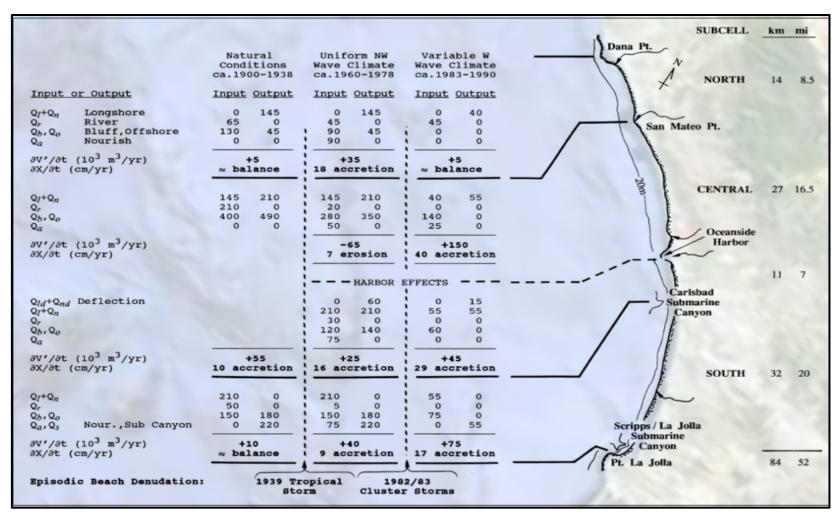


Figure 2-61. Summary of the sediment budget of the Oceanside littoral cell (overlay adapted from Inman and Masters 1991; image data: Google, SIO, NOAA, U.S. Navy, NGA, GEBCO, Landsat, LDEO-Columbia, NSF). MCBCP occupies the North and Central sub-cells (see text).

	Conditions ca.1905-1936	Wave Climate ca.1950-1978	Wave Climate ca.1983-1990		North Island Coronad	50 +
Input or Output	Input Output	Input Output	Input Output		Coronad	1 22
$egin{array}{lll} Q_l + Q_n & & & & & & & & & \\ Q_r, Q_i & & & & & & & & & \\ Q_{on}, Q_w & & & & & & & & \\ Q_a & & & & & & & & \\ \end{array}$	130 0 0 750 0 0 0 0	130 0 0 130 0 0 0 0	130 0 0 130 0 0	SUBCELL	km mi	T Same
∂V'/∂t (10 ³ m³/yr) Zuñiga Shoal	-620 erosion	0 balance	0 balance	ZUNIGA	4.3 2.6	San Diego Bay
$Q_l + Q_n$ (north) Q_r, Q_i Q_{on}, Q_w Q_a	150 130 0 0 0 20 0 0	50 130 0 0 0 20 630 0	50 130 0 0 50 20 20 0	STRAND	10.1 6.3	olego Bay Miss
∂V'/∂t (10 ³ m ³ /yr) ∂X/∂t (cm/yr)	balance	+530 375 accretion	-30 21 erosion			1
$Q_l + Q_n$ (north) $Q_l + Q_n$ (south) $Q_r + Q_i$ $Q_o + Q_w$ Q_a	0 150 0 50 200 0 0 0	0 50 0 150 50 0 100 0	0 50 0 50 50 0 0 0	DELTA	7.6 4.7	Imper Beac Tiju
∂V'/∂t (10 ³ m ³ /yr) ∂X/∂t (cm/yr)	0 balance	-50 47 erosion	-50 47 erosion			Riv
$Q_l + Q_n$ (south) Q_r, Q_i Q_{on}, Q_w Q_b Bluff	50 50 0 0 0 0 0 0	150 150 0 0 0 0 0 0	50 75 0 0 0 0 10 0	PLAYA DE TIJUANA	4.5 2.8	MEXI
θV'/θt (10 ³ m ³ /yr) θX/θt (cm/yr)	m ³ /yr) 0 balance		-15 24 erosion			

Figure 2-62. Summary of the sediment budget of the Silver Strand littoral cell (overlay adapted from Inman and Masters 1991; image data: Google, USGS, SIO, NOAA, U.S. Navy, NGA, GEBCO, LDEO-Columbia, NSF). NBC occupies most of this cell (see text).

The SCBPS twice-yearly LiDAR surveys describe the cliff and gully changes at MCBCP and may be suitable to derive "profile" cross sections that mimic beach profile data where these are not available due to access restrictions at MCBCP. This has not yet been undertaken, but will be included in next year's effort in this project. The LiDAR data contain 15 twice-yearly over-flights between May 2002 and March 2009, potentially providing an important increase in profile data coverage at MCBCP. Full analysis of the LiDAR beach topography data at both MCBCP and NBC is also possible, but beyond the scope of this effort.

The original units of measurement were feet relative to MLLW.¹⁵ However, all profile data was adjusted to metric units relative to North American Vertical Datum of 1988 (NAVD88). Shoreline position¹⁶ was calculated by determining the distance from the starting point of the profile to the elevation of the National Geodetic Vertical Datum (NGVD) contour using linear interpolation between the two adjacent survey points. NGVD was used since it is a fixed geodetic datum that is close to MSL at both MCBCP and NBC. This information was utilized to calibrate both process and physics-based shoreline change models.

Marine Corps Base Camp Pendleton

A total of 104 beach profiles spanning 1950 to 1989 are available on eight range lines, as shown in Figure 2-63. Table 2-3 gives the details of the available profile data at MCBCP¹⁷.

Figure 2-64 to Figure 2-79 show plots of all profile data at MCBCP that were found for this study and the shoreline position history derived from them.

Figure 2-64 and Figure 2-65 show data from Range SO1530, which is located at San Onofre State Beach near the northern end of Camp Pendleton. This is north of SONGS. Data are available from 1983 to 1989. Note that the shoreline position steadily retreats from over 100 m to about 50 m over this time interval. This decrease is attributable to completion of construction of the SONGS in early 1985. At that time, the second of two sheet pile structures called "laydown pads" were removed. These pads were used for construction equipment and staging areas between 1964 and 1984. Over this time period the beach at SONGS was artificially widened by the addition of sand and the presence of the laydown pads, especially in the state park north of the plant. When the pads were finally removed, this beach returned to its pre-construction width (see Flick *et al.*, 2010).

Range SO1470 is located about 3 km south of SO1530 as well as south of SONGS. The data from Range SO1470 is shown in Figure 2-66. Figure 2-67 suggests that the shoreline position remained unchanged from 1984–1986, and advanced about 25 m from 1986–1988, presumably as a result of previously trapped sand moving south past the Units 2 and 3 laydown pad area after it was removed. Range PN1340 (Figure 2-68 and Figure 2-69) shows a similar history, but with the shoreline position remaining unchanged until about 1988, and then advancing about 15 to 20 m by 1989. A similar pattern

_

 $^{^{15}}$ Early profile data were tabulated relative to MLLW (1960–1978), while later data were relative to MLLW (1983–2001).

¹⁶ Note: "Shoreline position" is used in this discussion rather than the more descriptive term "beach width." Beach width is usually defined as the distance from a given contour elevation (such as MSL) to either the back of the beach berm or dune field, or the base of the cliff. If the survey start point is not located at these places, "beach width" is inconsistent, and "shoreline position" (relative to the benchmark) is more accurate. Either way, observed changes can be thought of as changes in beach width.

¹⁷ Note that the location of benchmark PN1280 is uncertain, since no survey data could be found for it. The approximate location shown in Table 4-1 was determined from the benchmark description information referenced to Google Earth, and is estimated to be accurate to about 5 m.

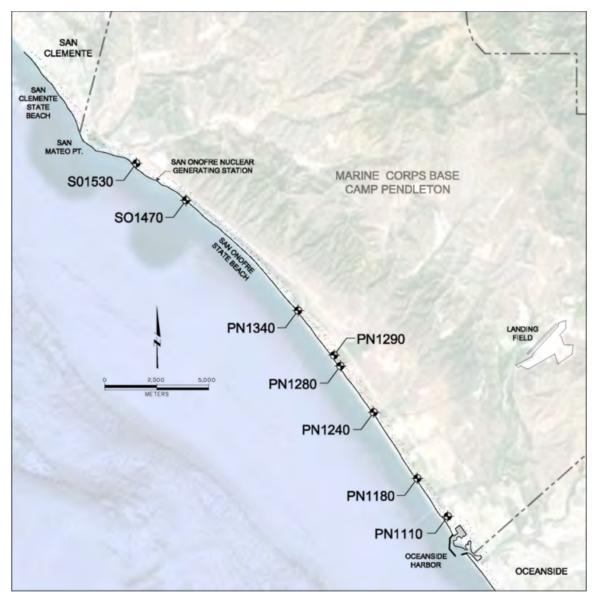


Figure 2-63. Schematic map of MCBCP shoreline shows locations and designations of available historical beach profile data. See Table 4-1 for profile range information (image data: Google, SIO, NOAA, U.S. Navy, NGA, GEBCO, DigitalGlobe, CSUMB, SFML, CA-OPC).

is repeated at Range PN1290 (Figure 2-70 and Figure 2-71), but with a smaller advance of only about 12 m observed from 1988-1989.

The close-by Range PN1280 (Figure 2-72 and Figure 2-73) indicates essentially the same behavior as PN1290 during the time of data coverage overlap, 1984–1989. But, PN1280 has a longer history reaching back to 1972. The range shows a net decrease in beach width of about 20 m from 1972–1981, followed by an increase of about 25 m by 1982. The shoreline position stayed relatively constant fluctuating only about 10 m until 1989.

Range PN1240 (Figure 2-74 and Figure 2-75) is located just north of the MCBCP LCAC facility, and has one of the two longest profile histories at MCBCP, with data from 1950–1989.

Table 2-3. MCBCP beach profile range information.

Date Range Earliest Profile	Data	Earliest Latest	No. of Profiles	Benchmark Elevation		Orientation		Northing	Easting	Latitude	Longitude
	Earliest			NAVD88		degrees		CA Zone 0406 (NAD27)		conversion http:// noaa.nos.gov	
	Tronic			ft	m	mag	true N	ft	ft	degrees	degrees
SO1530	1983 Nov	1989 Dec	10	19.92	6.07	225	239	442,900.00	1,597,300.00	33.376952	117.569122
SO1470	1983 Dec	1989 Dec	9	24.25	7.39	225	239	437,000.00	1,605,300.00	33.361014	117.542680
PN1340	1984 Jan	1989 Dec	10	18.54	5.65	225	239	420,009.93	1,622,398.95	33.314892	117.486025
PN1290	1984 Jan	1989 Dec	9	16.80	5.12	225	239	412,247.00	1,628,244.64	33.293747	117.466595
PN1280	1972 Jan	1989 Dec	11	14.61	4.45	225	239	410,350.07	1,629,568.87	33.288576	117.462190
PN1240	1950 Oct	1989 Dec	15	14.64	4.46	225	239	402,762.36	1,634,865.77	33.267891	117.444574
PN1180	1972 Jan	1989 Dec	13	14.25	4.34	225	239	392,545.46	1,641,624.23	33.240024	117.422089
PN1110	1950 Oct	1989 Dec	27	14.02	4.27	225	239	386,301.87	1,646,356.70	33.223010	117.406386

(Note Columns are (respectively) the range identification; the first and last dates profiles are available; the number of profiles between these dates; the starting-point benchmark elevation in (the original) ft and m; orientation of the profile in magnetic and true directions looking seaward from the start point; the North and East Lambert Coordinates; and the latitude and longitude.)

The close-by Range PN1280 (Figure 2-72 and Figure 2-73) indicates essentially the same behavior as PN1290 during the time of data coverage overlap, 1984–1989. But, PN1280 has a longer history reaching back to 1972. The range shows a net decrease in beach width of about 20 m from 1972–1981, followed by an increase of about 25 m by 1982. The shoreline position stayed relatively constant fluctuating only about 10 m until 1989.

Range PN1240 (Figure 2-74 and Figure 2-75) is located just north of the MCBCP LCAC facility, and has one of the two longest profile histories at MCBCP, with data from 1950–1989.

Unfortunately, only the data from 1984–1989 can be confirmed to have the same origin, since the starting point elevations from earlier profiles are different – some are 0.4 m higher, and some are lower by as much as 0.55 m. Since no obvious way to reconcile the starting points of the earlier with the later data has yet been found, there is uncertainty in the shoreline position history derived at this location. Further research and analysis will be conducted in the second year of this study to try to reconcile the profile origins of this obviously valuable data set. Disregarding the pre-1984 data for now, there was an 18 m widening of the beach at PN 1240 from 1984–1989.

Figure 2-76 and Figure 2-77 show the profile and shoreline position data from Range PN1180. Similar differences in starting elevations exist here as were found at PN1240. Therefore, shoreline position data from 1972–1982 relative to post-1984 is uncertain. Interestingly, this range shows much larger short-term changes in beach width ranging up to 35 to 40 m from 1986–1989. The proximity of Range PN1180 to the northern edge of the Santa Margarita River mouth suggests that it plays a role in the beach width at this location.

The SCBPS carries out the aforementioned twice-yearly LiDAR over-flight surveys as well as a series of conventional GPS-based ground surveys using beach buggies and jet skis. Figure 2-78 shows a map of the MCBCP study section located south of the LCAC facility and north of the Del Mar Boat basin. Figure 2-79 shows shoreline position data from a range line about 0.5 km south of the LCAC facility and about 1 km north of Range PN1180 derived from the SCBPS surveys covering January 2007–July 2010. The seasonal fluctuations are about 20-40 m and comparable to those observed at Range PN1180 (Figure 2-77). Actual horizontal registration of the shoreline position data from the recent SCBPS surveys and the historical surveys should be possible.

Figure 2-80 shows profile data from Range PN 1110 located near the southern end of Camp Pendleton, just north of the Del mar Boat Basin and Oceanside Harbor. This range also has a long history, with data spanning from 1950–1989, just like Range PN1240, but with nearly twice as many surveys. Four surveys exist from the 1950s. Additional early surveys are from the 1960s through 1982. Unfortunately, again, profiles taken prior to 1984 show a considerable range of starting elevations that make estimation of shoreline position uncertain. However, at this range there exist a sufficient number of profiles to attempt an adjustment that is described in the following.

Note that the early surveys (1950–1982) are plotted in black in Figure 2-80, while the profiles taken starting in 1983 are plotted in green. Inspection of the profile plot suggests that the later (green) profiles had an origin farther landward, and so appear to show features like the berm crest and the shoreline position farther seaward than they actually are. Figure 2-81 shows the raw shoreline position history derived from the profiles in Figure 2-80 before adjustment. Note the sudden upward (positive) jump in shoreline position (i.e., widening) between the July 1982 and June 1983 surveys. It is virtually certain that this apparent increase in beach width between these two dates is not correct, since the El Niño storms of winter 1982–1983 caused massive erosion and loss of beach width almost everywhere. In an attempt to resolve this discrepancy, the later shoreline positions (1983–1989) were adjusted downward by 102.5 m, which make the mean shoreline positions of the early and later data equal.

This adjustment results in the shoreline position time history shown in Figure 2-82. This approach is supported by the fact that the earlier data from 1950–1982 suggest that there was very little net change in shoreline position over these three decades (noting the uncertainty associated with the apparently moving survey origin).

Likewise, the later data from 1983–1989 also suggest little net change following recovery from winter 1982–1983. The composite adjusted shoreline position plot suggests that there was a 40-m decrease in beach width during the winter of 1982–1983 prior to the 50-m decrease in winter 1986–1987. Additional corroborating evidence to support this adjustment will be sought and evaluated as this study proceeds.

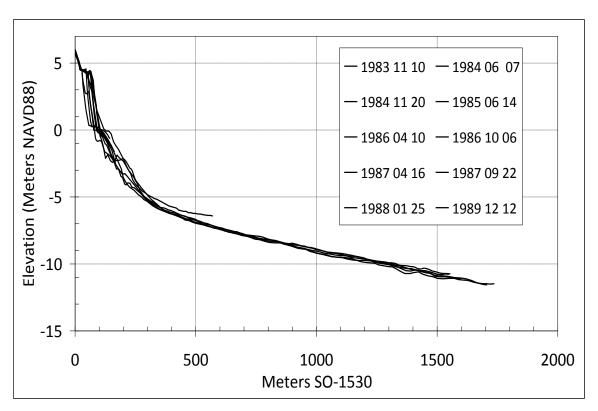


Figure 2-64. Beach profiles from MCBCP Range SO1530 (see text).

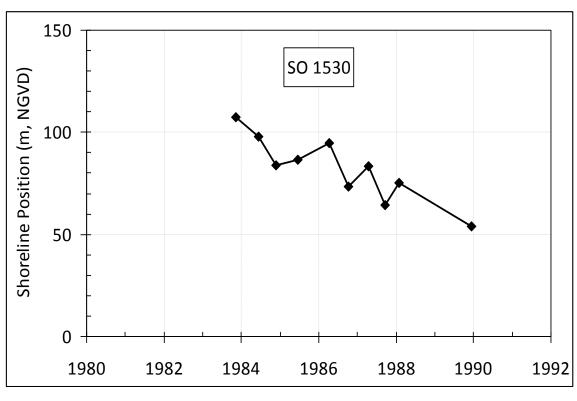


Figure 2-65. Shoreline position history for 1983–1989 at MCBCP Range SO1530.

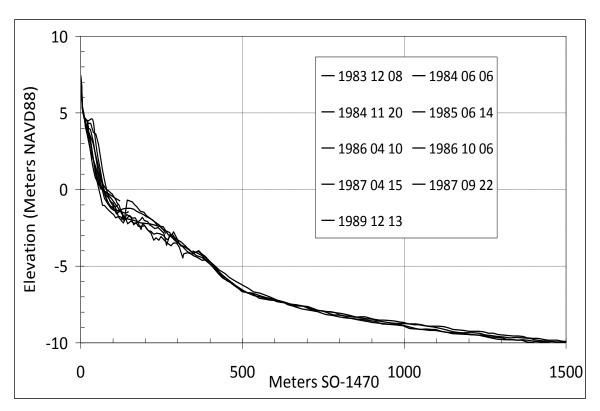


Figure 2-66. Beach profiles from MCBCP Range SO1470.

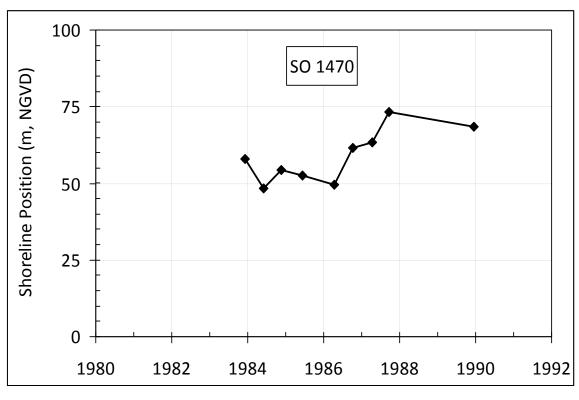


Figure 2-67. Shoreline position history for 1983–1989 at MCBCP Range SO1470.

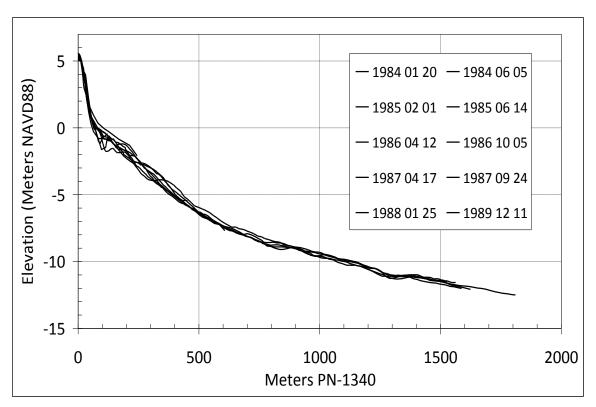


Figure 2-68. Beach profiles from MCBCP Range PN1340.

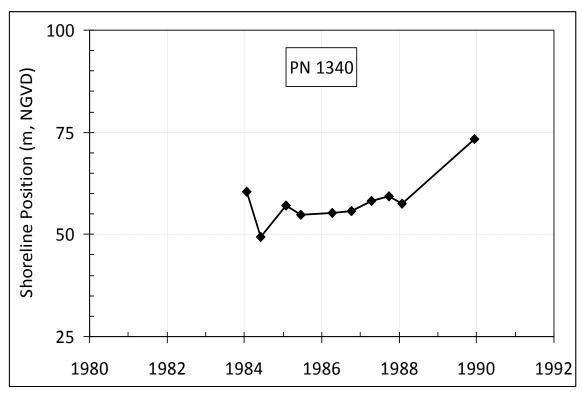


Figure 2-69. Shoreline position history for 1984–1989 at MCBCP Range PN1340.

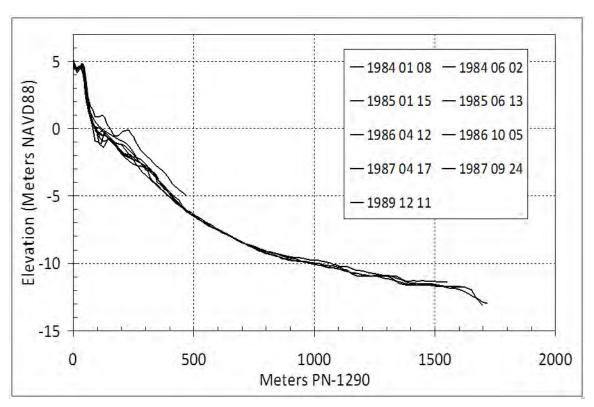


Figure 2-70. Beach profiles from MCBCP Range PN1290.

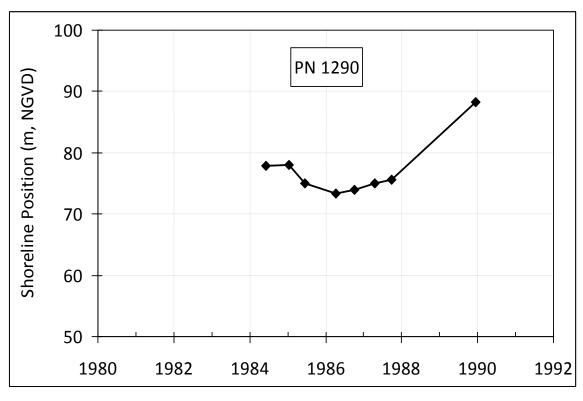


Figure 2-71. Shoreline position history for 1984–1989 at MCBCP Range PN1290.

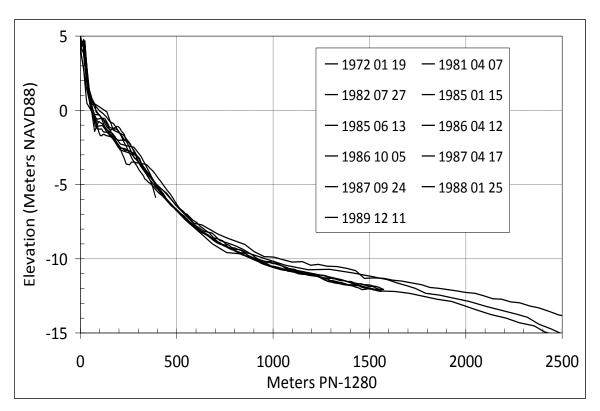


Figure 2-72. Beach profiles from MCBCP Range PN1280.

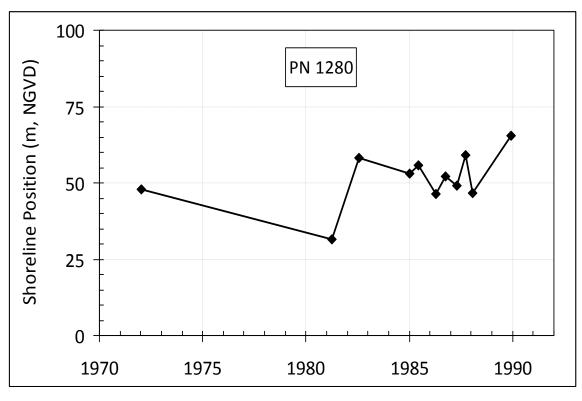


Figure 2-73. Shoreline position history for 1972–1989 at MCBCP Range PN1280.

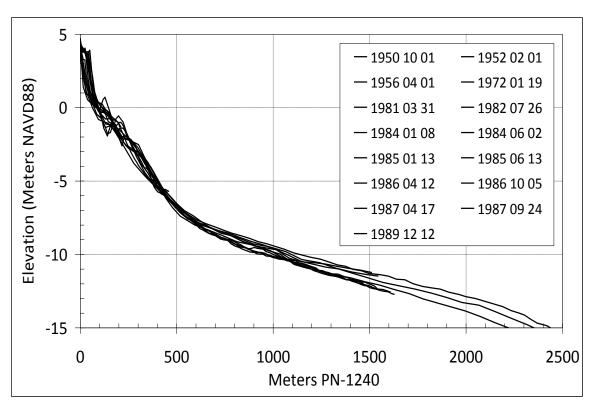


Figure 2-74. Beach profiles from MCBCP Range PN1240.

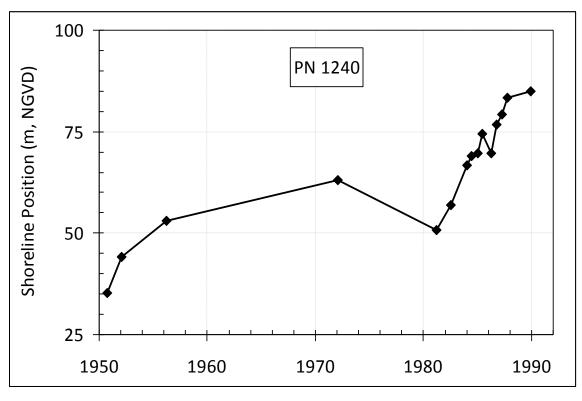


Figure 2-75. Shoreline position history for 1972–1989 at MCBCP Range PN1240.

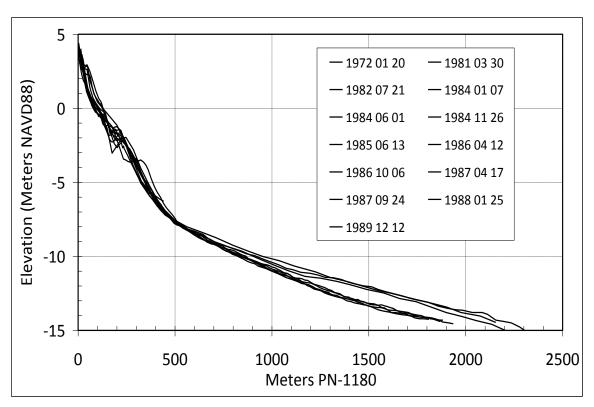


Figure 2-76. Beach profiles from MCBCP Range PN1180.

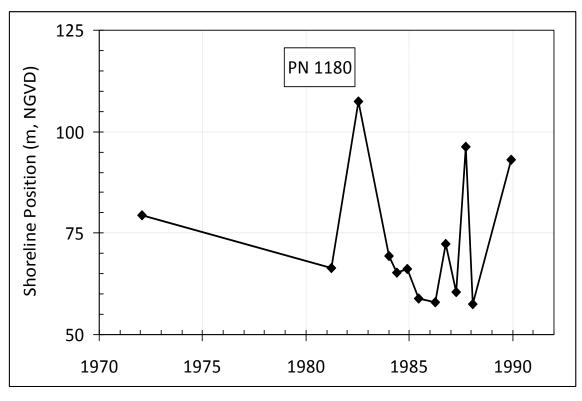


Figure 2-77. Shoreline position history for 1972–1989 at MCBCP Range PN1180.



Figure 2-78. Google Earth image shows location of SCBPS beach surveys near Range PN1180, between LCAC facility and Del Mar Boat Basin (image data: Google, Digital Globe).

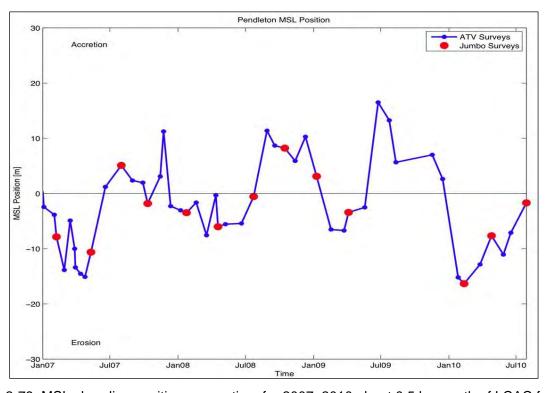


Figure 2-79. MSL shoreline position versus time for 2007–2010 about 0.5 km south of LCAC facility.

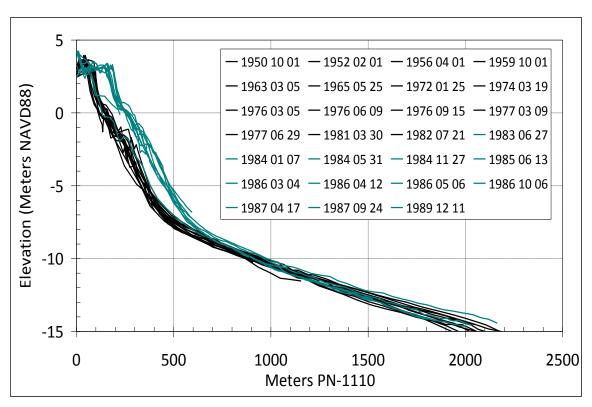


Figure 2-80. Beach profile data from MCBCP Range PN1110.

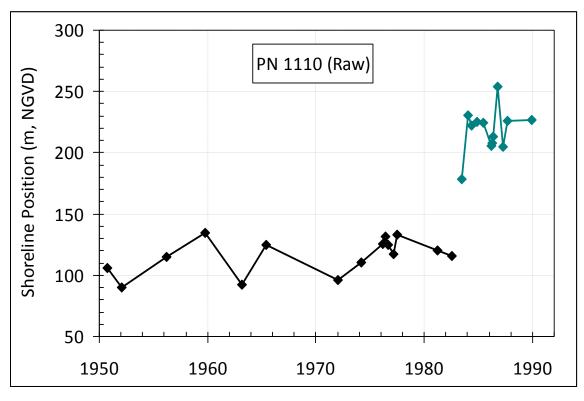


Figure 2-81. Unadjusted shoreline position history 1950–1989 at MCBCP Range PN1110.

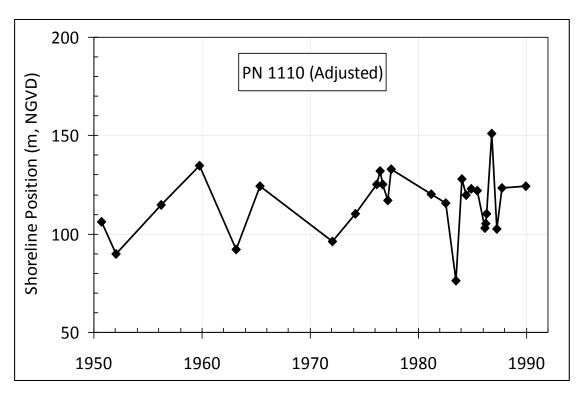


Figure 2-82. Adjusted shoreline position history 1950–1989 at MCBCP Range PN1110 (see text).

Naval Base Coronado

In all, 161 beach profiles spanning the years from 1962 to 2009 are available on five range lines whose range names and starting locations are shown in Figure 2-83. Table 2-4 gives the details of the available profile data at NBC. Figure 2-84 to Figure 2-95 show plots of all profile data at NBC that were found for this study and the shoreline position histories derived from them.

Figure 2-84 and Figure 2-85 show data from Range SS0160 situated on the southwest-facing portion of Coronado, near North Island. This is the closest range line to North Island where data were found and profiles are available from 1983–2009. Range SS0160 also shows changes in profile start elevations of about 0.34 m between the earlier (1983–1998) and later profiles (1999–2009). Fortunately, the earlier and later profile sets are self-consistent, that is, all the starting elevations are respectively equal in each group. Again, no clear way suggested itself to reconcile the earlier and later data, so the derived shoreline positions, shown in Figure 2-85, should be considered separately until the matter can be considered further and perhaps resolved. Positions from 1983–1998 are plotted in black and those from 1999–2009 in green.

 18 Access to the beach at North Island is restricted and difficult to obtain.

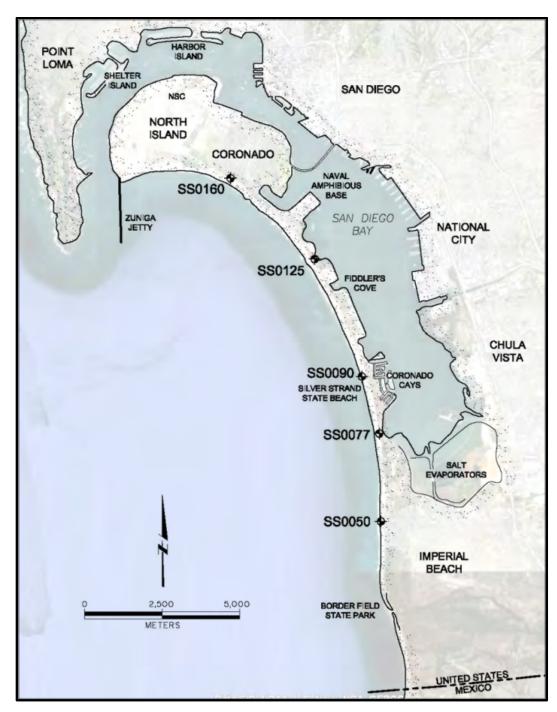


Figure 2-83. Schematic map of Silver Strand and Coronado shows locations of available historical beach profile data.NBC, including the Naval Amphibious Base, is located at North Island and along Coronado and Silver Strand. Profile range information in Table 4-2 (image data: Google, SIO, NOAA, U.S. Navy, NGA, GEBCO, LDEO-Columbia, NSF).

This location is exposed to southern wave attack and shows a slight (~ 10 m) increase in maximum shoreline position from about 235 m to about 245 m from 1983–1998. Note that these earlier seasonal shoreline position fluctuations are apparently much larger than those indicated in later years (1999–2009). This is most likely attributable to the fact that the early-year profile date were taken earlier in each winter season, usually between January and April, while the later-year "winter" surveys were

not conducted until May. It is known that beaches in southern California recover very quickly after winter storm events narrow them, and that May is usually too late to reliably capture the minimum seasonal beach width. Seasonal beach width fluctuations (1983–1998) range from 35 to 50 m at Range SS0160. Shoreline position data from 1999–2009 suggests that the shoreline is stable.

Date Range Earliest Profile				Benchmark Elevation		Orientation		Northing	Easting	Latitude	Longitude
	Date Latest Profile	No. of Profiles	NAVD88		degrees		CA Zone 0406 (NAD83)		conversion http:// noaa.nos.gov		
			ft	m	mag	true N	ft	ft	deg.deg	deg.deg	
SS0160	1983 Oct	2009 Oct	38	18.22	5.55	195	209	1,829,962.0	6,274,127.1	32.684051	117.184539
SS0125	1984 Jan	1989 Nov	13	15.82	4.82	230	244	unknown	unknown	32.660284	117.155543
SS0090	1983 Oct	2009 Oct	37	13.56	4.13	250	264	1,808,804.9	6,288,013.6	32.626238	117.138825
SS0077	1983 Oct	2009 Oct	35	14.34	4.37	245	259	1,802,713.2	6,289,788.6	32.609538	117.132892
SS0050	1954 Mar	2009 Oct	38	13.69	4.17	250	264	1,793,115.6	6,289,795.9	32.583161	117.132605

Table 2-4. NBC beach profile range information.

Figure 2-86 shows the limited profile data available from Range SS0125, which is located at Boat Lane 5 (U.S. Navy 2010) at the Naval Amphibious Base beach. An interesting feature is the large depression in the profile from 500 to 900 m offshore that appears between the August 1985 and December 1985 surveys¹⁹. This is almost certainly the borrow pit from which about 840,000 m³ sand was extracted and placed on Imperial Beach as part of a beach re-nourishment project²⁰. Figure 2-87 gives the shoreline positions derived from the profile data at Range SS0125.

Range SS0090 is located at Silver Strand State Beach between Boat Lanes 10 and 11. Profile information is available from 1983–2009 with a gap from 1989–1996, but with no changes in the profile starting elevations. Profile and shoreline position data are shown in Figure 2-88 and Figure 2-89. Figure 2-89 suggests that this shoreline is stable as well, with little or no change in maximum beach width from 1983–1998, and a modest 15-m increase from 1999–2009.

Range SS0077 is also located on Silver Strand State Beach and just north of Boat Lane 11. The beach profile and shoreline position data are shown in Figure 2-90 and Figure 2-91. Profiles are also available from 1983–2009 with a similar gap from 1989–1997 and consistent starting elevations. The shoreline position history suggests a small decrease in maximum beach width of about 15 m between the period from 1983–1987 and 1999 (with an anomalous width in 1989, green curve, Figure 2-90). A slow recovery of about 10 m followed from 1997–2009.

Range SS0050 is located at the northern border of Imperial Beach adjacent to SSTC-South and Boat Lane 14. It has the longest history of available beach profiles at NBC, with data spanning from March 1954 to October 2009 in three distinct sets. Unfortunately, the profiles in Set 1 taken from 1954–1975 (Figure 2-92, green curves) clearly have a different origin than those in Set 2 taken from 1978–1987 (Figure 2-92, black curves). The likely explanation is that the earlier profile measurements were started farther landward than the later ones, thus making it appear that the beach was wider. Set 3, the latest measurements, shown in Figure 2-93 are from 2001–2009 and are

-

¹⁹ Earlier profiles are plotted in green (1984–1985), w hile later ones are black (1985–1989).

²⁰ http://www.surfrider.org/stateofthebeach/05-sr/state.asp?zone=wc&state=ca&cat=bf

reasonably well registered with Set 2, albeit with different starting elevations again making interpretation of shoreline position uncertain. Figure 2-94 shows the unadjusted shoreline positions derived from the profile data plotted in Figure 2-92 and Figure 2-93.

Inspection of Figure 2-92 suggests that the shift between profile Sets 1 and 2 can be reconciled by assuming that the dune crest, which appears in all the early (1954–1975, green) profiles at an average position of 86 m from the origin, and in the 1978–1979 profiles at 23 m, did not move. Shifting the earlier profiles landward by 63 m results in a much better registration of Sets 1 and 2. Note also that the deeper sections of the profiles become more convincingly aligned with this adjustment.

Adjustment of the shoreline positions by this amount results in the time history shown in Figure 2-95. The data suggest that there was a steady decrease in maximum beach width from about 25 to 30 m from 1954–1987, with a partial recovery of 10 to 15 m from 2001–2009. This is consistent with data from Range SS0090, the location with the second-longest profile history. Corroboration of the assumption that the dune did not shift between 1975 and 1978–1979 is important, and may be possible from aerial photographs. This is being pursued because of the importance and value of this long-term shoreline position history.

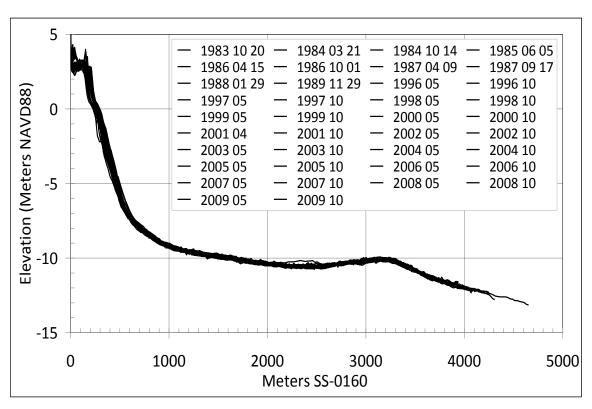


Figure 2-84. Beach profile data from NBC Range SS0160.

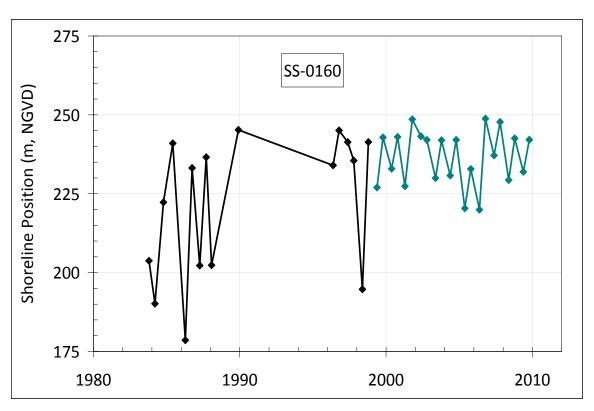


Figure 2-85. Shoreline position history from 1983–2009 at NBC Range SS0160.

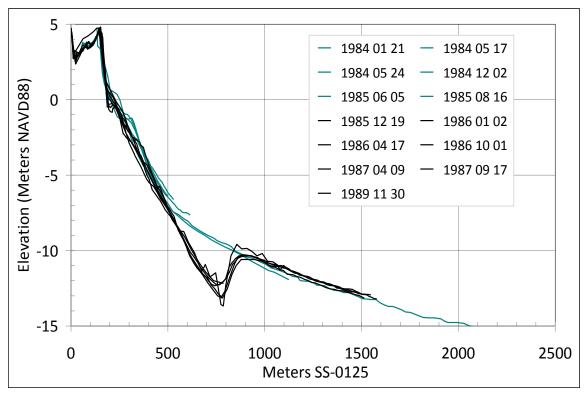


Figure 2-86. Beach profile data from NBC Range SS0125. Note the sand borrow pit from 500 to 900 m offshore (see text).

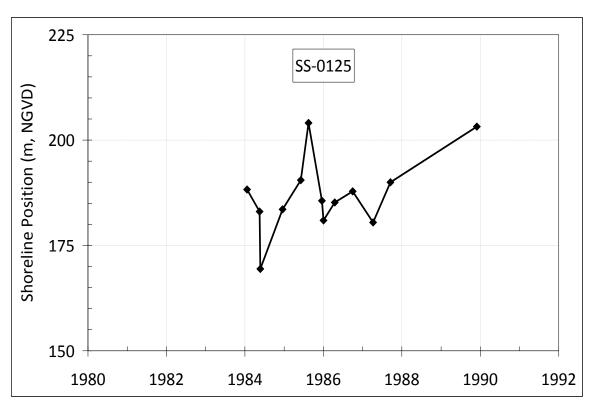


Figure 2-87. Shoreline position history from 1984–1989 at NBC Range SS0125.

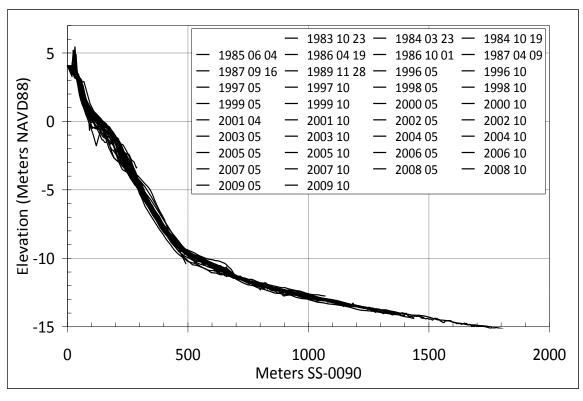


Figure 2-88. Beach profile data from NBC Range SS0090.

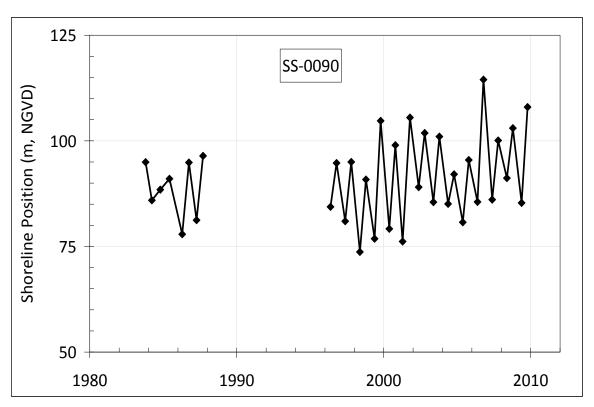


Figure 2-89. Shoreline position history from 1983–2009 at NBC Range SS0090.

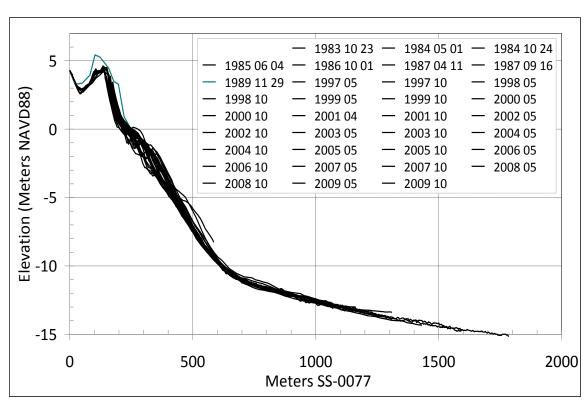


Figure 2-90. Beach profile data from NBC Range SS0077.

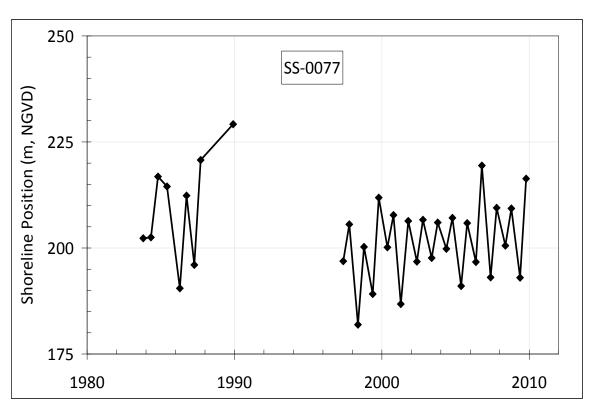


Figure 2-91. Shoreline position history from 1983–2009 at NBC Range SS0077.

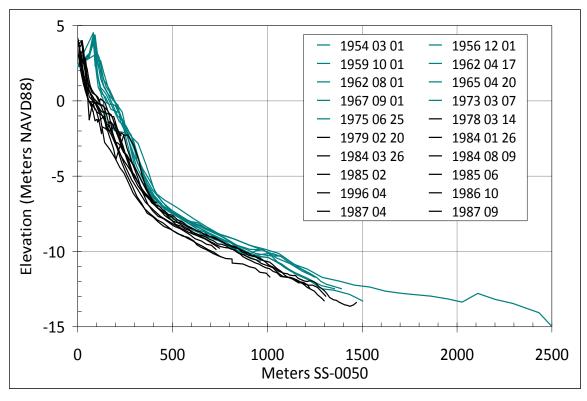


Figure 2-92. Early 1954–1987 beach profile data from NBC Range SS0050 (see text).

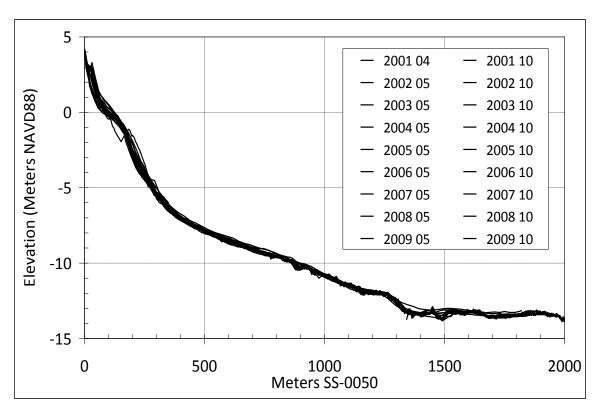


Figure 2-93. Later 2001–2009 beach profile data from NBC Range SS0050 (see text).

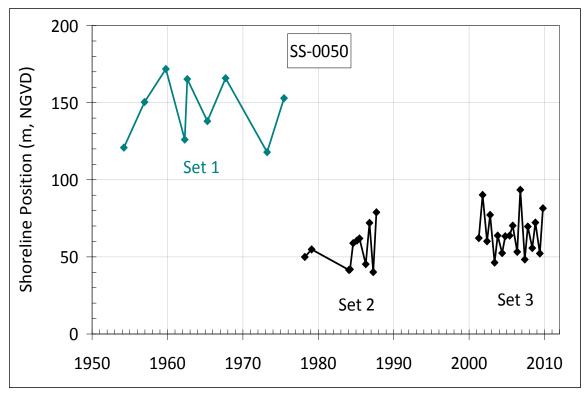


Figure 2-94. Unadjusted shoreline position from 1954–2009 at NBC Range SS0050 (see text).

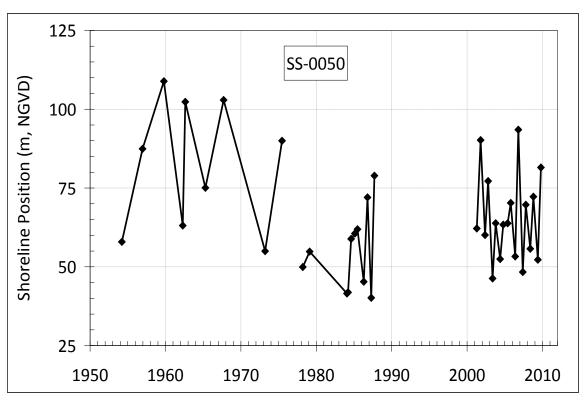


Figure 2-95. Adjusted shoreline position from 1954-2009 at NBC Range SS0050 (see text).

2.3.4 Historical Cliff Erosion and Gullying

The Camp Pendleton coast, north of the Santa Margarita River, consists of an uplifted marine terrace that rises in elevation from south to north along the coast. Erosion of the terrace through marine and subaerial processes resulted in coastal cliffs, gullies, and ravines (see also Section 2.2.1). The coastal cliffs extend along the seaward edge of the terrace, but are interrupted where gullies intercept the coastline and cause abrupt changes in cliff height (Figure 2-96). Cliff composition mapping is based on conflicting previous studies and limited site access, and therefore is only approximate.

Las Pulgas Canyon (Figure 2-96) effectively divides the cliffs into a northern and southern section. The northern segment extends 5.4 km south from the border with San Onofre State Beach, while the southern one reaches another 7 km south to the Santa Margarita River. On average, cliffs heights (27 m) in the northern section are twice as high as in the southern section (13 m). The geologic conditions, such as resistance to erosion, vary alongshore at a range of scales, and contribute to the alongshore variation of erosion rates.

Cliff Composition

The cliffs are generally composed of two geologic units: A lower unit of lithified Miocene or Pliocene mudstone, shale, sandstone, and siltstone; and an upper unit of unlithified Pleistocene terrace deposits. The contact between the upper and lower units is unconformable and decreases in elevation towards the south. Previous geologic maps and studies (Berggreen, 1979; Ehlig, 1977; Flick, 1994; Kennedy, 2001; Kennedy and Tan, 2008; Tan 2001) are inconsistent in their interpretation of the geology in the coastal region, where the lower unit has been mapped as both the San Mateo Formation and as sandy facies of the Monterey Formation.

Here, the lower unit was delineated into regions based on the sample sand content (Young *et al.*, 2010a) and labeled as geologic Units A and B (Figure 2-96), where Unit A contains significantly more sand compared to Unit B. However, this designation is based on relatively few samples because of limited access to Camp Pendleton, and additional data will be required to more accurately map the cliff composition.

The lower-unit Miocene-age Monterey Formation contains various amounts of sandstone, siltstones, claystones, and shales. Geologic conditions of the Monterey Formation shale layers including a SW-dip, impermeability, and low friction slide plane contribute to cliff instability and deep seated land sliding. Numerous relic coastal deep seated landslides are present in the region including one in MCBCP (Figure 2-97). The age, dynamics, and stability of these slides are unknown. However, Kuhn and Shepard (1991) described a new slide initiated by the heavy rains in 1978 that extended 215 m alongshore and 100 m inland. Young *et al.* (2009) describe two slides exhibiting recent movement in the San Onofre cliffs.

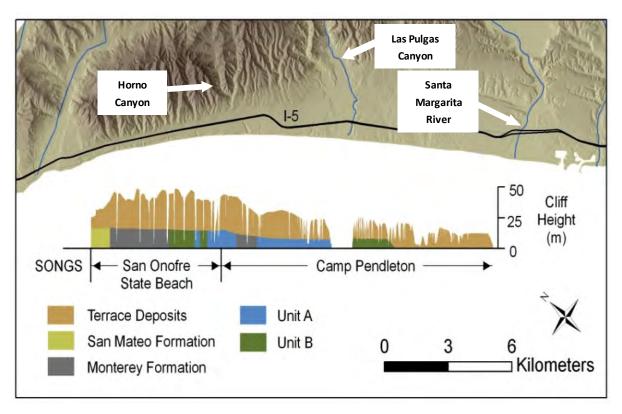


Figure 2-96. Schematic map showing coastal cliff setting and general composition, and place names (adapted from Young et al., 2014).

Anthropogenic Terrace Changes

Although the MCBCP coastal region is relatively undeveloped compared with other southern California coastal areas, Hwy 101 and I5 have affected the local coastal processes. Hwy 101 and I5, constructed in the 1910s, and 1960s, respectively, radically altered the natural drainage patterns by culverts that concentrated runoff. According to Kuhn and Shepard (1991), these drainage changes caused erosion and collapse of Hwy 101 at Horno Canyon in 1978; the erosion of a massive new canyon, including 140 m of landward retreat between 1968 and 1980; and 230 m of retreat in Dead Dog Canyon from 1932 to 1980 (Figure 2-97). Figure 2-97 and Figure 2-98 illustrate the problems related to MCBCP vehicle movement as gully erosion and landslides continue west of Hwy 101 and I5.

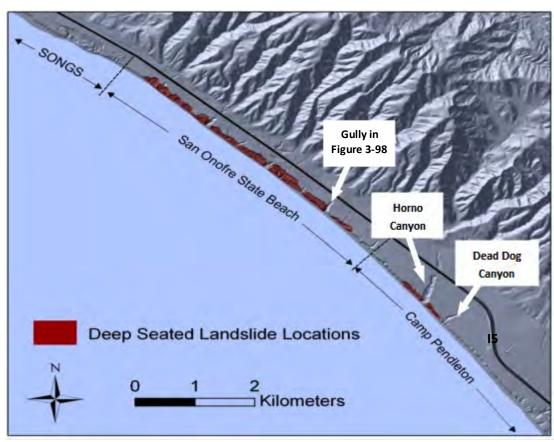


Figure 2-97. Map shows extent of relic and active deep-seated landslides south of SONGS. Note that coastal drainages under I5 develop into gullies through the terrace to the west.

Previous Erosion and Retreat Studies

Previous studies (USACE, 1988b; USACE, 1990; Everts, 1991; Runyan and Griggs, 2003; Young and Ashford, 2006; Hapke and Reid, 2007; and Young *et al.*, 2009) have estimated the mean cliff retreat and gully erosion rates ranging from about 1.5 to 19 cm/yr, and 1.5 to 24 m³/m/yr normalized alongshore, respectively (Figure 2-99). It is difficult to directly compare these studies because they use different quality sources, time periods, extents, and methods. For example, when estimating gully erosion, Young and Ashford (2006) examined a 6-year dry period with limited inland extent, while USACE (1988b) examined a 79-year period with several major anthropogenic-induced erosion events and a much larger inland extent.

Cliff retreat and gully erosion can occur very rapidly and the reported mean rates do not capture the episodicity and magnitude of large events. For example, Kuhn and Shepard (1991) describe several rapid retreat events in excess of 30 m, including 70 m of retreat from a single storm. Retreat rates can vary widely alongshore and local retreat rates are often several times larger than mean rates. In the MCBCP cliff section Hapke and Reid (2007) measured a maximum local retreat rate of 131 cm/yr, over six times the average.



Figure 2-98. Photo of large, deep gully at San Onofre State Beach area of MCBCP (see Figure 2-97 for location; California Coastal Records Project Image 200407227, October 2004; Copyright (C) 2002–2014 Kenneth & Gabrielle Adelman, California Coastal Records Project, www.Californiacoastline.org).

Although previous studies vary widely in their estimated rates, most agree that over the last century, cliff retreat generally increased towards the north (Figure 2-99). They also stress the importance of subaerial processes for this particular cliff section (Kuhn and Shepard 1991, USACE 1988b, USACE 1990, and Young *et al.* 2009). Historical events including severe gully erosion, deep seated land sliding, damage to infrastructure, and cliff erosion have all been linked to heavy rainfall. Although marine processes are certainly important, no studies could be found that document historical damage from wave action at MCBCP, potentially because of limited access and/or the presence of a protective beach.

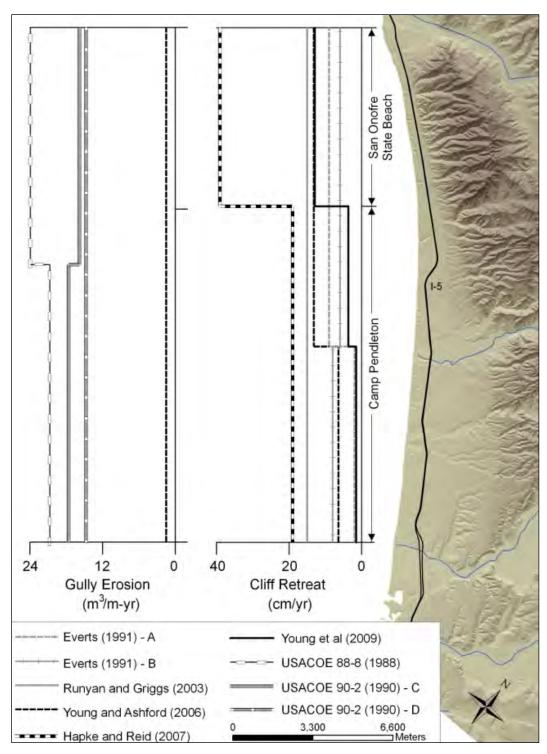


Figure 2-99. Estimates of cliff retreat and gully erosion from previous studies normalized alongshore. A - Everts (1991) with rates adapted from USACE (1988b). B - Everts (1991) with modeled toe retreat rates for 1954–1988. C - USACE (1990) adapted from USACE (1988b) including some cliff erosion. D - USACE (1990) adapted from USACE (1988b) and excludes cliff erosion and fine sediments.

3. MATERIALS AND METHODS

In this section, the methods developed and applied in this project are described. Because much of the project focused on methods development, these descriptions represent an important aspect of the work that we carried out. The methods development focused on four key areas in the context of sea level rise influences on military installations in the southwestern U.S. These included sea level rise projection methods, methods for delineation of the coastal system including both the terrain and the infrastructure, methods for evaluating the physical response of the system to sea level rise, and methods for the assessment of vulnerability.

3.1 SEA LEVEL RISE PROJECTIONS

Sea level rise projections developed for this study are presented in this section. These projections span the century from 2000–2100. Water level scenarios used in this study are a superposition of four components (Figure 3-1), which include:

- MSLR scenarios with increases of 0.5, 1.0, 1.5, and 2.0 m by 2100 relative to 2000;
- Hourly astronomical tide heights;
- Non-tide residual (NTR) water level variability from global circulation models enhanced with El Niño-related sea level fluctuations specific to the southwestern US; and
- Wave-driven run-up on beaches.

In the present study, the MSLR scenarios were specified by SERDP in order to provide a common background set of projections across a number of projects focused on different parts of the U.S. The non-tide residual (NTR) water level fluctuations, largely comprised of storm surges and oceanographic changes, were derived from the A2 and B1 GHG emission scenarios outputs from National Center for Atmospheric Research (NCAR) Community Climate System Model Version 3 (CCSM3) model runs. Interannual fluctuation enhancements related to El Niño specifically for California followed Cayan *et al.* (2008a, 2008b, 2009). Tide heights for 2000-2100 were predicted using published constituents for La Jolla, CA, and were deemed applicable to the study region. Finally, run-up on beaches was projected from future local wave conditions derived from the A2 scenario and applying the method of Stockdon *et al.* (2006). The approximate amplitudes of these four components of the projected sea level are shown schematically as a function of time from "today" (taken as 2000 in this study) to 2100 in Figure 3-2.

We note that this method of constructing total future sea level projections is not entirely self-consistent. For example, each GCM run was based on a specified GHG emissions scenario (along with other assumptions) and produces its own set of outputs, including projections of temperature and MSL. Imposing MSLR curves a priori and then adding only the fluctuating parts of sea level from the GCM output was therefore not self-consistent. Nevertheless, because no other practical alternative exists to construct projections, this was the approach followed.

It should also be noted that the existing GCM MSL outputs seem themselves to be inconsistent with their own temperature projections (i.e., too small) and therefore unreliable. This first lead Rahmstorf (2007) to fashion MSLR scenarios directly from the GCM temperature projections, a GCM output parameter considered to be reasonably robust. This approach, which is now widely applied (Cayan *et al.*, 2008a, 2008b, 2009; OPC, 2010), supports the method used in the present study.

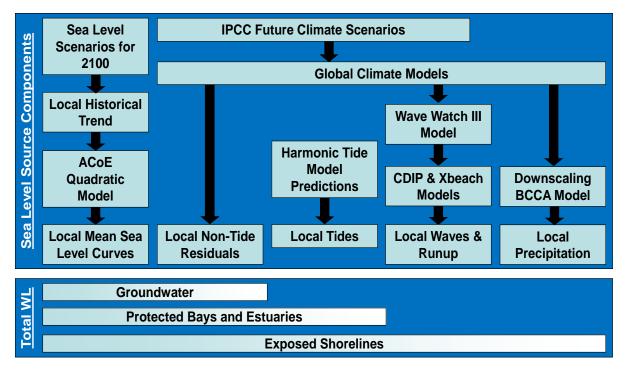


Figure 3-1. Flow chart of sea level rise projection components.

3.1.1 Mean Sea Level

Four global future MSL elevation-endpoint scenarios of 0.5, 1.0, 1.5, and 2.0 m rise between 2000 and 2100 were specified by SERDP for use in this study and several other associated studies. These scenarios were assumed to have quadratic trajectories following NRC (1987) and USACE (2009, 2011). This implies an initial rate of rise and a constant acceleration.

The curves used in the present study are shown in Figure 3-3 plotted as elevations relative to NAVD88²². They were named NRC I, NRCides

II, NRC III, and SERDP 2.0 respectively defining the four specified MSLR scenarios. The nomenclature of the first three follows that of the USACE. The name of the fourth, added for this study, reflects its MSLR from 2000–2100 and origin at SERDP. These MSLR curves used 2000 as the start year instead of 1986 that NRC and USACE specify. In practice, this merely changed the curve shapes slightly but left the 2100 endpoints the same. To account for different base years, and because MSL fluctuates from year to year, smoothly melding past observations with future MSLR projections with a specific start year presents some subtle problems addressed by Flick *et al.* (2013).

²¹ USACE relying on NRC (1987) considered three scenarios: 0.5, 1.0, and 1.5 m MSLR between 1986 and 2100.

-

²² NAVD88 datum lies 0.778 m below MSL (1991–2009) at La Jolla (see Section 3.3.2, Tables 3-3 and 3-4 for datum values, and Flick *et al.* (2013) for step-by-step adjustment procedure).

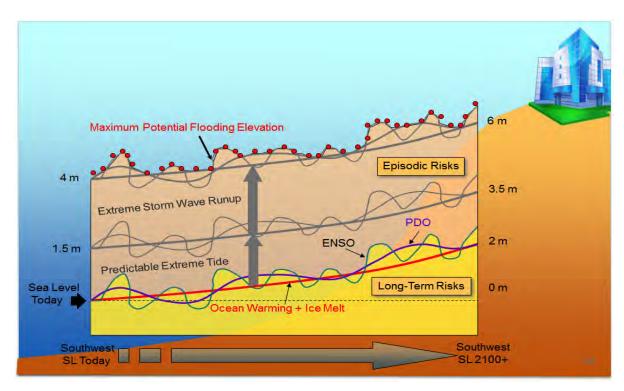


Figure 3-2. Schematic of approximate amplitudes of MSLR, tides, non-tide residual (NTR) variations, and wave-driven run-up during 21st century.

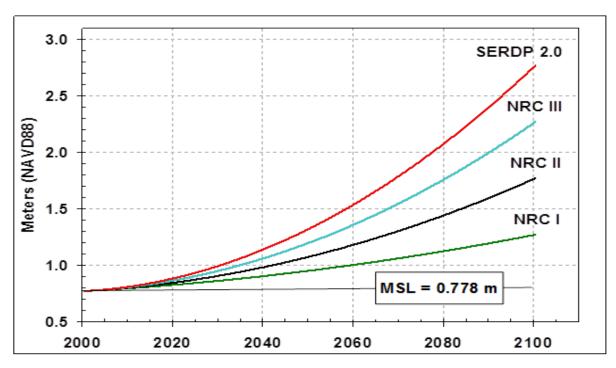


Figure 3-3. MSLR curves considered in this study plotted relative to NAVD88.

Most, if not all of the published projected future MSLR curves are "concave-up" with increasing rates of rise over time. Assuming a constant acceleration of MSL implies a quadratic MSL curve, the simplest concave-upward form. An initial rate of rise in a given starting base year together with either an endpoint value of sea level at any future year, or a specified constant increase of the rate of rise (acceleration) completely define the quadratic sea level curve coefficients. How these MSLR curves are selected can have ramifications for the outcomes of vulnerability assessments. It must be emphasized that the projected outcomes are predicated on these MSLR curves, which have unknown, or at least highly uncertain, probabilities of occurrence.²³ This is probably the single biggest obstacle to more quantitative assessments.

Although the NRC (1987) study could now be considered "old science," MSLR curves based on it (and including the new "SERDP 2.0" 2-m-by-2100 curve) exceed the range of (now generally-considered under-estimated) MSLR projections in the IPCC (2001) Third Assessment and Report (TAR) and the IPCC (2007a) Fourth Assessment Report (AR4), which range from 0.09-0.88 m and 0.18-0.59 m, respectively.²⁴

In addition, the present four scenarios span the 0.60-1.46 m range in Cayan *et al.* (2008a, 2009), as well as the 0.5- to 1.4-m range in Rahmstorf (2007), the estimates of Vermeer and Rahmstorf (2010) of 0.81 to 1.79 m, and coincide with the 0.5 to 2.0 m of Nicholls *et al.* (2011). They also nearly cover the (5 to 95 percentile) range of Grinsted *et al.* (2009), which is 0.3 to 2.15 m. In contrast, new work by Houston (2013) argues that confidence levels for 0.18, 0.48, and 0.82 m MSLR from 1990–2100 respectively are 5, 50, and 95%, which is substantially lower than Grinsted *et al.* (2009), but with mid- and upper-ranges within the span herein considered.

The differences between published projections underscore the large uncertainties associated with MSLR projections. They also underscore the astuteness of simply choosing these four plausible and illustrative future scenarios without the distraction of attempting to overly motivate or justify their selection.

The aforementioned NRC (1987) - USACE (2009, 2011) approach leads to a set of MSL curves represented by the quadratic relationship:

Equation 3-1

$$MSL-MSL_0 = a (Y-Y_0) + b (Y-Y_0)^2$$
,

where MSL and MSL $_0$ respectively represent mean sea level at future year Y relative to a given "starting" mean sea level at year Y_0 , while "a" is the initial rate of sea level rise and "b" is (half) the rate of annual increase, i.e., the acceleration. The units of "a" are L/T while the units of "b" are L/T where L represents length and T is time in whatever units of measure are being used.

Taking $Y_0 = 2000$ as the initial reference year and considering sea level rise relative to it (in meters), then $MSL_0 = 0$. In this way we can simplify Equation 4-1 to

Equation 3-2

$$MSLR = a \Delta Y + b (\Delta Y)^2,$$

_

²³ More generally, the continuum of possible future MSLR trajectories has an unknown probability distribution.

²⁴ Note that the AR4 model MSLR range "excludes future rapid dynamical changes in ice flow," which therefore makes the upper limit almost certainly too low, likely substantially so.

where $\Delta Y = (Y - 2000)$, represents the number of years after 2000, and MSLR is the sea level rise relative to 2000. To completely define any given quadratic scenario curve, either both the initial rate "a" and the constant acceleration term "b" must be specified, or one of these and the "endpoint" or MSLR value must be given.

In this study, we selected the initial MSLR rate for base year 2000 as 0.0028 m/yr, which was the global value derived from satellite data as shown in Figure 2-52. We then calculated the respective acceleration constants to give the specified endpoints. Table 3-1 shows the coefficients "a" and "b" as a function of the specified year-2100 endpoint values of MSLR.

Scenario	2100 Sea	Level (m)	а	b	
Designation	NAVD88	MSLR from 2000	(m/yr)	(m²/yr)	
NRC I	1.27	0.5	2.80 x 10 ⁻³	2.20 x 10 ⁻⁵	
NRC II	1.77	1.0	2.80 x 10 ⁻³	7.20 x 10 ⁻⁵	
NRC III	2.27	1.5	2.80 x 10 ⁻³	1.22 x 10 ⁻⁴	
SERDP 2.0	2.77	2.0	2.80 x 10 ⁻³	1.72 x 10 ⁻⁴	

Table 3-1. Quadratic sea level rise formula coefficients.

3.1.2 Tides

Methodologies adopted for the prediction and incorporation of tides into the sea level projections are described below. The analysis included specification of tidal datums, prediction of future tidal elevations, and a description of the important patterns of water level related to tidal variability.

Tidal Datums

A tidal datum is a vertical sea level reference elevation based on a long-term average value of a particular phase of the tide. MLLW, Mean Sea Level (MSL), and Mean High Water (MHW) are examples of tidal datums. Fixed land-based geodetic elevation datums are cross-referenced to tidal datum elevations using leveling data. Because the typical scale of coastal tide variation is hundreds of kilometers, the characteristics of the tide at MCBCP and the ocean-side of NBC were assumed to be well represented by the tide at La Jolla, CA. Continuous tide measurements began there (Scripps Pier) in 1924. Tide conditions inside San Diego Bay, which are significantly different, must be considered for bayside developments at NBC, including those at the Amphibious Base and carrier berthing facilities. These are best characterized by the downtown San Diego tide station located on Navy Pier and in continuous operation since 1906.

Each tidal datum is an average over a specific 19-year epoch, currently defined as the years 1983-2001, and called the National Tidal Datum Epoch (NTDE). Note that the center-year of NTDE is 1992. The 19-year value is the nearest whole number of years spanning the 18.6 year lunar node cycle. It is also presumably a sufficiently long time to average out meteorological and oceanographic variability unrelated to the tides. For example, MLLW is defined as the average of the single lowest water level reading each day in the NTDE, while MHW is the corresponding average of both of the two high waters observed each day. Finally, MSL is the arithmetic average of all water level readings obtained during the epoch. The highest and lowest observed values are from the entire tide gauge

records (1924–present at La Jolla and 1906–present at San Diego). Note that all tidal datums, including MSL, are "floating" reference elevations subject to change as MSL rises or falls.

For the purposes of the present study, the start-year for sea level projections was 2000. For this reason, 19-year tidal datum averages were calculated for the 1991–2009 epoch, which has 2000 as its center-year. This simplified calculations needed to relate past sea level observations and fixed, land-based geodetic reference elevations (*e.g.* NAVD88) to the projected scenarios of future MSLR with 2000 as the start-year that were used in the present study (Flick *et al.*, 2013). Table 3-2 summarizes the tidal datum values and extreme observed water levels (and dates) for the 1983–2001 NTDE at the La Jolla (No. 941 to 0230) the San Diego (No. 941 to 0170) tide gauges as calculated by the National Ocean Service (NOS, a part of NOAA) relative to NAVD88 (Columns 2 and 4) and MLLW (Columns 3 and 5), ordinarily the reference for tide tables and navigation charts.

Table 3-3 gives the equivalent information for the 1991–2009 epoch. Table 3-2 and Table 3-3 also contain entries for NAVD88 and NGVD, which are fixed, land-based datum reference elevations. Note that the mean tide ranges (MHW-MLW) at La Jolla and San Diego bay are respectively about 1.1 and 1.2 m, a difference of about 10%. The diurnal ranges (MHHW-MLLW) are approximately 1.6 and 1.7 m, respectively.

Tide Predictions

Hourly tide predictions for La Jolla and San Diego Bay were prepared for 2000–2100 using a FORTRAN computer program prepared by Professor Walter Munk and long used at Scripps Institution of oceanography. The latest available tidal constituent (non-zero) amplitudes and phases from the National Ocean Service at NOAA were used. These are presented in Table 3-4.

Tide Patterns

Tides along the California coast are "mixed," with diurnal (once-per-day) constituents almost as large as the semidiurnal (twice-per-day) constituents. There are almost always two each (respectively unequal) high tides and low tides per tidal day. The diurnal components arise from the enhanced response of this part of the Pacific Ocean to the forcing associated with the declination of the moon and sun. The highest tide ranges occur in winter and summer when the declination of the sun is largest. Relatively smaller tide ranges occur in spring and autumn. Figure 3-4 shows a typical set of seasonal tide curves that illustrate these characteristics.

Flick (2000) demonstrated that in southern California, the higher-high tide always occurs in the morning (loosely defined as midnight to noon) during the winter, and in the afternoon (noon to midnight) during the summer, as shown in Figure 3-5. Winter peak highs tend to cluster in the morning around 08:00 with summer highs in the evening at about 20:00; summer lows tend to occur around 03:00, with winter lows at about 15:00. This pattern has consequences for winter storm preparedness. If the first warning of possibly damaging waves comes on the evening news, then damage avoidance, such as sand-bagging or window-covering must be carried out at night in anticipation of the early-morning high tide.

Two episodes of higher (and corresponding lower) tides occur each month. They are referred to as "spring" tides (regardless of season) and last for a few days around the time of new or full moon. The periods in between (waxing and waning half-moons) have lower tide ranges and are called "neap" tides. The twice-monthly spring tides that occur during the summer and winter are generally higher than those in spring and autumn, owing to the declination of the sun and the resulting increased diurnal contributions.

Table 3-2. Tidal datum relationships (1983–2001).

1983-2001 (NTDE)		La Jolla 941-0230			San Diego 941-0170	
m		NAVD88	MLLW		NAVD88	MLLW
Highest	11 Jan 2005	2.28	2.34	27 Jan 1983	2.35	2.48
MHHW		1.57	1.62		1.61	1.74
MHW		1.34	1.40		1.39	1.52
MSL		0.77	0.83		0.76	0.90
NGVD		0.64	0.70		0.63	0.77
MLW		0.22	0.28		0.15	0.29
NAVD88		0.00	0.06		0.00	0.13
MLLW		-0.06	0.00		0.13	0.00
Lowest	17 Dec 1933	-0.93	-0.87	17 Dec 1937	-1.07	-0.94

Table 3-3. Tidal datum relationships (1991–2009).

1991-2009 (This Study)		La Jolla 941-0230			San Diego 941-0170	
т		NAVD88	MLLW		NAVD88	MLLW
Highest	11 Jan 2005	2.28	2.33	27 Jan 1983	2.35	2.48
MHHW		1.57	1.62		1.62	1.75
MHW		1.35	1.40		1.39	1.52
MSL		0.78	0.83		0.77	0.90
NGVD		0.64	0.69		0.63	0.76
MLW		0.22	0.27		0.16	0.28
NAVD88		0.00	0.05		0.00	0.13
MLLW		-0.05	0.00		-0.13	0.00
Lowest	17 Dec 1933	-0.93	-0.88	17 Dec 1937	-1.07	0.95

Figure 3-6 shows the patterns of variability of the peak predicted high tides at La Jolla from 2000–2050. Zetler and Flick (1985a, 1985b) showed that along the west coast the lunar perigee and node cycles (respectively) produce peak high tides every 4.42 and 18.6 years. The highest winter and summer high tides are about 0.15 m higher during the peaks of these cycles than they are during years in between. Their study revealed that the 4.42-year cycle lead to unusually high maximum tides during the El Niño winter of 1982–83, specifically in late January 1983. These peak tides were an important contributory cause of the extensive coastal flooding and erosion that occurred at that time.

The 4.42-year cycle has been attributed by Cartwright (1974) to the precession of the longitude of the lunar perigee relative to the node (both ascending and descending), a phenomenon that has an 8.85-year period. This 8.85-year cycle produces a noticeable tide range perturbation at half the period on the California coast. The second important pattern of extreme high tides is the 18.61-year lunar node regression cycle. Together, the 4.42- and 18.6-year cycles produce clear variations in the peak high and low tide patterns, as well as the tide range.

3.1.3 Sea Level Fluctuations

Coastal non-tide sea level fluctuations (non-tide residuals) were obtained using the methodology of Cayan *et al.* (2008a), which incorporated time-varying GCM-generated parameters that included winds, sea level pressure (SLP), and Niño 3.4-region²⁵ SST. Although the amplitudes of non-tide fluctuations were relatively small compared with tidal variability and wave run-up from large storm waves (discussed below), the non-tide contribution to sea level can become important when the sum of other factors contributing to total sea level approaches critical levels, particularly during concurrent high-energy wave activity.

Probability density functions (PDFs) of the non-tide fluctuations over November–March winter periods (Figure 3-7) indicated that this model generated non-tide levels that were similar to those observed historically. Only the Centre National de Recherches Météorologique (CNRM) model (green curves) gave projections whose distribution mean was significantly different form the observations, *i.e.*, fell outside the 1-sigma bounds of the observations.

Table 3-4. Tide prediction constituents.

Co	nstituent	La Jo	olla	San Diego Bay		
No.	Name	Amplitude (m)	Phase (° local)	Amplitude (m)	Phase (º local)	
1	M2	0.580	338.7	0.556	271.3	
2	S2	0.137	338.4	0.229	260.2	
3	N2	0.123	317.3	0.130	256.2	
4	K1	0.368	106.1	0.347	87.6	
5	M4	0.023	38.2			
6	01	0.230	98.5	0.220	80.8	
7	M6			0.004	85.7	
8	MK3	0.019	136.7			
10	MN4	0.009	19.9			
11	NU2	0.026	320.1	0.025	260.6	
13	MU2	0.007	237.1	0.016	229.2	
14	2N2	0.014	295.2	0.016	234.3	
15	001	0.011	131.9	0.011	111.9	
16	LAM2	0.006	341.8	0.003	253.1	
17	S1	0.007	164.8	0.004	218.8	
18	M1	0.011	128.5	0.013	104.4	
19	J1	0.019	119.1	0.020	95.9	
21	SSA	0.039	286.2			
22	SA	0.038	221.0	0.069	178.9	
25	RHO	0.009	94.5	0.009	76.5	
26	Q1	0.040	96.0	0.041	77.5	
27	T2	0.009	316.9	0.014	247.6	
28	R2	0.001	338.3	0.002	259.7	
29	2Q1	0.004	105.1	0.004	79.2	
30	P1	0.116	103.6	0.109	85.8	
32	M3	0.005	38.9	0.003	358.2	
33	L2	0.016	349.5	0.015	267.7	
34	2MK3	0.014	113.2			
35	K2	0.040	329.2	0.067	253.6	
37	MS4	0.010	42.4	-		

_

²⁵ The Niño 3.4 region lies between 120°W-170°W and 5°S-5°N in the equatorial central Pacific Ocean. Surface water warming in this region is a defining characteristic of El Niño events.

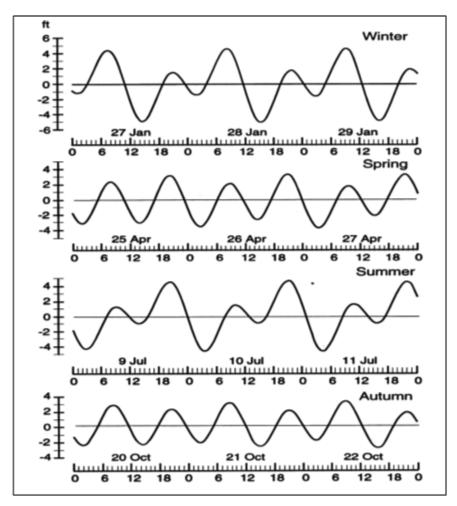


Figure 3-4. Typical seasonal tide curves in the San Diego region (see text)(adapted from Flick and Sterrett, 1984).

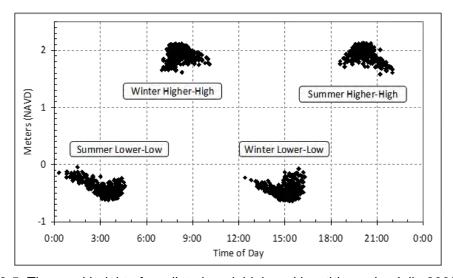


Figure 3-5. Time and height of predicted peak high and low tides at La Jolla 2000–2050.

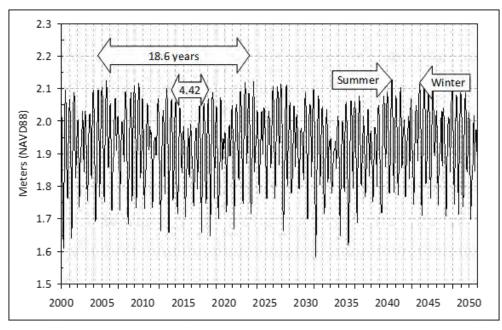


Figure 3-6. Monthly maximum tide predictions at La Jolla 2000–2050 illustrating the important periodicities.

The 98th percentile winter (November–March) non-tide projections for all A2 scenarios (Figure 3-8) had slightly downward trends, consistent with a northward shift in storm track that is generally expected by the climate change community (*e.g.*, Karl *et al.*, 2008). Note that the B1 amplitudes were not significantly different, but there was a slight upward trend for the CCSM3 model. The difference in trends is consistent with a smaller impact on storm track under the lower B1 GHG emission scenario – that is, a smaller climate change effect.

The range of variability in Figure 3-8 was reasonably consistent for the NOAA Geophysical Fluid Dynamics Laboratory (GFDL) and NCAR climate models, but was somewhat larger than the observations. The difference in the range between model projections and historic observations was more striking when comparing the incidence of model extremes (Figure 3-9) with observations (Figure 3-10). The incidence of GFDL and NCAR model-derived non-tide projection levels for both A2 and B1 GHG scenarios generally exceeded the observations at SIO, while the CNRM model gave incidence estimates of non-tide projections that were consistently less than the observations.

However, the range of variability for the GFDL and NCAR models (Figure 3-8) was similar to the observations until about 2010. This suggests that either the incidence of extreme non-tide fluctuations will increase substantially, or the non-tide model needs adjustment, or the GCMs are not producing accurate projections. Both the GFDL and NCAR A2 models suggested a downward trend in non-tide extreme incidence towards the end of the 21st century, while no clear pattern emerged for their respective B1 projections. Given that the non-tide residuals were a relatively small contribution to local sea level, the CCSM3 model results were comparable to the historical observations, and that the residuals for different emission scenarios were of the same order, we chose to use the CCSM3 A2 results to develop the non-tide fluctuation component of our sea level rise scenarios.

3.1.4 Waves

Future military installation wave climate projections were required as inputs for wave run-up and shoreline change projections. Most critically, wave projections were needed to estimate future trends in near-shore wave climate parameters including height and period, and the probability of

exceedance of critical thresholds. Future trends in wave height or period can potentially amplify or lessen the impacts of sea level rise by increasing or decreasing the maximum run-up elevations.

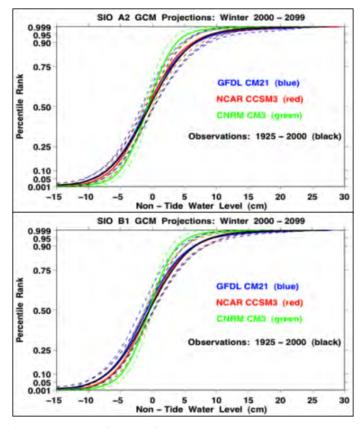


Figure 3-7. Mean (solid) and 1-sigma (dashed) non-tide water level probability density function for A2 (upper) and B1 (lower) from three climate models and observations.

Because of the complicated offshore bathymetry and the islands in the SCB, wave sheltering, refraction, and shoaling result in equally complex increases or decreases in wave heights relative to deep water outside the Bight. For example, Figure 3-11 shows the modeled results of these processes in the SCB for an energetic winter North Pacific extra-tropical swell arriving from the west. Further, it is not unusual to have two or three separate swell wave trains present at the same time in the SCB, in addition to any local seas.

Wave sheltering, refraction, and shoaling contribute in varying degrees to the wave climate at southern California beaches. Near-shore wave conditions are highly sensitive to the direction and period of offshore waves, and the directional "windows" open to deep-ocean waves vary along shore. Consequently, on any given day, waves can vary strongly alongshore with regions of high and low waves separated by only a few km. This sensitivity can in turn lead to significant changes in alongshore location of the potential impact of future offshore wave climate change scenarios. For example, a northward shift in wave directions could decrease energy at most beaches, while increasing it at most others.

Wave exposure for any given coastal location relative to deep-water wave height and period conditions can be summarized using exposure diagrams such as those in Figure 3-12 and Figure 3-13 calculated according to the methods of O'Reilly (1991, 1993) and O'Reilly and Guza (1991). These provide the ratio of local to deep water height as a function of period and deep-water approach

direction for locations at (respectively) Marine Corps Base Camp Pendleton and Naval Base Coronado. While almost all northerly-approaching waves are blocked, amplification of offshore heights by factors of 1.5 to 3.0 is possible for narrow windows at both near-shore locations.

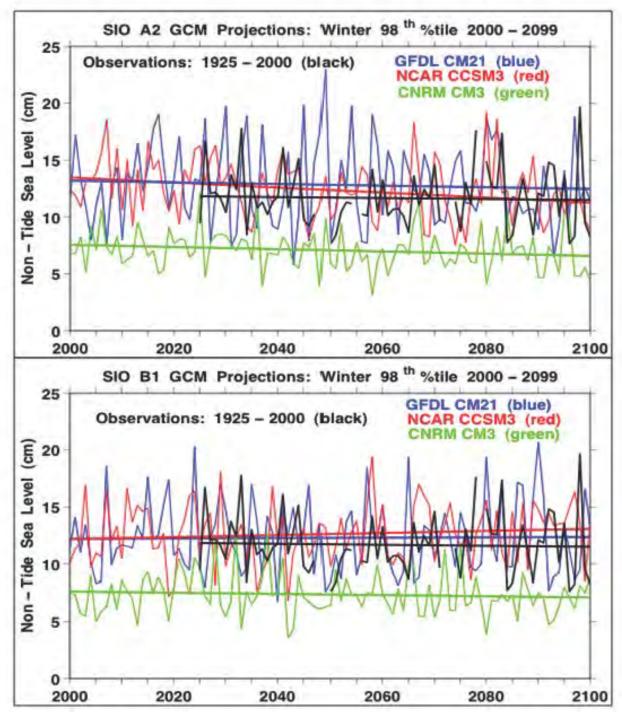


Figure 3-8. Extreme (98th percentile) non-tide fluctuations for A2 (upper) and B1 (lower), and tide gauge observations at La Jolla, CA (SIO) (offset 100 years). Only the CNRM A2 trend (upper, green) is statistically significant from zero at 95% confidence level.

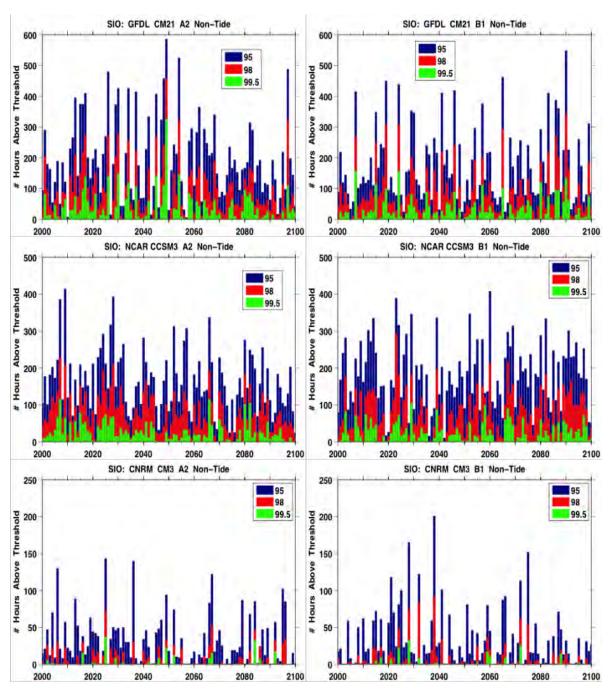


Figure 3-9. Hours non-tide projections during winter (November-March) exceed 95th (9.3 cm), 98th (12.2 cm), and 99.5th (16.4 cm) percentile thresholds. A2 scenario (left), B1 (right).

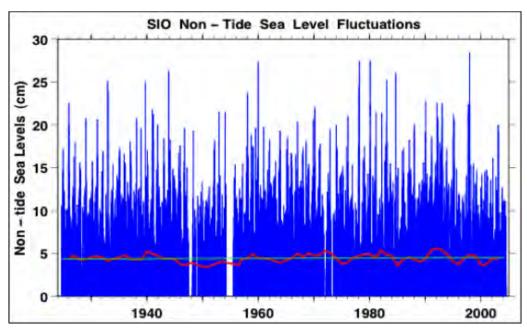


Figure 3-10. Positive non-tide sea level fluctuations relative to MSL with 3-year running mean (red) and least squares trend (green) superimposed.

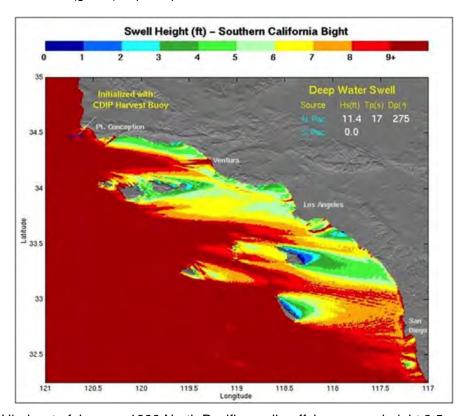


Figure 3-11. Hindcast of January 1998 North Pacific swell - offshore wave height 3.5 m (11.4 ft). Island shadows appear as areas with lower wave height (yellow-green) in lee of islands. Red areas along coast are locations with strong refractive focusing from underwater escarpments, relic sediment fans off river mouths, and submarine canyons (courtesy of the Coastal Data Information Program http://cdip.ucsd.edu).

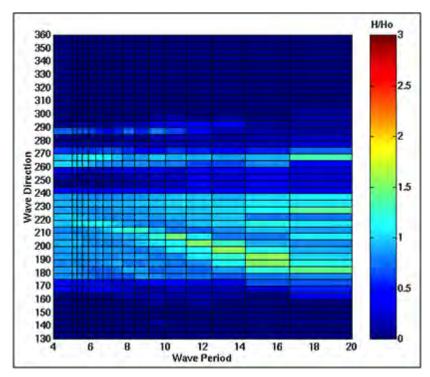


Figure 3-12. Wave exposure at central MCBCP (Range PN1290). Colors show ratio of near-shore wave height (H) to deep water (Ho) as a function of offshore direction and period.

Assessment of the vulnerability associated with future wave climate on the southwest US coastline is challenging and must be viewed as qualitative. Shoreline changes resulting from the action of historic and present-day waves are poorly understood, and quantitative, site-specific relationships between wave measurements and shoreline change have only recently been developed (Yates *et al.*, 2009). This is primarily because wave and shoreline measurements suited to this task have been collected for only about 25 years, and mostly during a warm phase of the PDO. Additionally, high quality hindcast wave fields with sufficient spatial resolution to be useful in reconstructing historical extreme wave conditions, extend back to only about 1960. The likelihood of a repeat of the 1939 Hurricane that made landfall in southern California is also unknown, even in a stable climate. Pacific Ocean wave hindcasting remains an active field of research. The variation of the southwest U.S. wave climate includes interannual and decadal components, as well as strong seasonality. There is considerable uncertainty in estimating the probability of exceedance statistics for large wave heights at base locations for next winter, let alone for the next century.

An important finding of this study of wave climate was that our ability to estimate long-term *trends* in near-shore wave parameters may significantly outpace our ability to quantify even short-term wave impacts. For example, most GCM scenarios indicated a northward migration of the mean jet stream latitude over the North Pacific. This leads to a northward shift in the mean offshore wave direction and a *decrease* in mean winter wave heights at MCBCP and NBC owing to island sheltering and the resulting change in wave exposure.

An important finding of this study of wave climate was that our ability to estimate long-term *trends* in near-shore wave parameters may significantly outpace our ability to quantify even short-term wave impacts. For example, most GCM scenarios indicated a northward migration of the mean

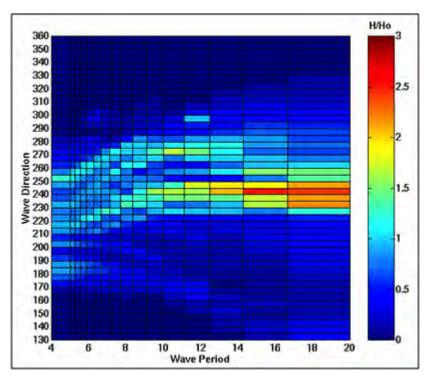


Figure 3-13. Same as Figure 4-11 for Coronado City Beach (Range SS0160) representative of west-facing Coronado portion of NBC.

jet stream latitude over the North Pacific. This leads to a northward shift in the mean offshore wave direction and a *decrease* in mean winter wave heights at MCBCP and NBC owing to island sheltering and the resulting change in wave exposure.

Wave climate assessment for this project used a three stage process:

- Forecast offshore wave conditions (as frequency-directional spectra) based on GCM-output wind fields over the Pacific Ocean;
- Transform the offshore wave spectra to near-shore wave parameters at multiple locations at each military installation; and
- Interpret any long-term trends in the near-shore wave parameters in the context of both known natural variability in the waves, and sensitivity of the results to modeling errors.

This assessment framework will ultimately allow for an ensemble of GCM wind-driven wave scenarios to be considered. The current project methodology focused on demonstrating the use of a single GCM scenario that was currently available to develop the wave climate analysis and make an initial assessment of what aspects of the changing Pacific Ocean wave climate were likely to be most critical to forecasting future installation wave vulnerability.

A long-term goal of the wave assessment framework would potentially be to bypass the need to run deterministic wave model scenarios every time there is new GCM scenario. Instead, the goal would be to use an initial ensemble of GCM scenarios and wave model runs to link changes in the modeled near-shore wave climate to commonly used metrics in assessing and comparing different GCM scenarios directly. For example, changes in the mean jet stream location, or the strength and frequency of PDO and ENSO cycles should be related to expected wave climate changes. This approach would maximize the utility of the framework in assessing both short-term and long-term

wave impacts. Viewed in the context of climate change projections, wave assessment could conceptually be correlated with five climate variables that are found in or derived from GCM scenarios:

- Mean jet stream location over the North Pacific;
- Interdecadal oscillations in the PDO index;
- Interannual oscillations in the ENSO index;
- Persistence of high pressure over the southwestern U.S.;
- Autumn surface water temperatures off northern Mexico.

The first three variables impact winter storm waves, the fourth impacts local wind swell and sea breeze dynamics, and the last determines the potential for hurricane landfall in southern California.

Wave Projections

For the purposes of illustrating our methodology, near-shore wave projections were developed using a well-documented 100-year (2000-2099) GCM and offshore wave model data set created for the California 2008 Climate Change Impact Assessment report (Messner *et al.* 2008) and used in a California state-funded assessment of sea level rise effects in northern California (Revell *et al.*, 2009). The GCM is the CCSM3, run with the A2 (moderately high) greenhouse gas emission scenario. The CCSM3 model is known to produce a reasonable representation of seasonal precipitation, the variability of annual precipitation, and El Niño/Southern Oscillation when run for historic periods and when compared to known conditions (Cayan *et al.* 2008b).

Wavewatch III wind-wave model simulations (Tolman, 2002) were performed using the CCSM3 output Pacific Ocean wind fields produced by Dr. N.E. Graham at Scripps Institution of Oceanography for the Messner et al. (2008) report. For 2000–2099, only the five winter months (November-March) were modeled and output provided at 3-hour time steps. Since this work was completed for the present study, at least eight more WW III runs scenario have been completed for several different model runs base on the A2 and B1 scenarios. These runs can be used according to the methods developed in this study to improve and update the assessments in the future, especially to quantify the uncertainties.

Systematic biases in the CCSM3 wind fields were removed by comparison of the wave model spectra output to offshore buoy measurements in California for the 2000–2007 time period (Graham, personal communication). The resulting 100 years of projected two-dimensional (amplitude versus frequency and direction) wave spectra for a deep water location southwest of Point Conception (34° N, 121° W) were used as the initial conditions for estimating near-shore wave conditions at MCBCP and NBC.

Prior to transforming the offshore wave spectra to near-shore locations in the vicinity of MCBCP and NBC, the 100-year projection was analyzed for long-term trends in wave heights and directions (Figure 3-14) as well as wave height exceedance statistics (Figure 3-15). While the mean annual winter wave height of 2 m showed a very slight 10-cm downward trend over the next century, the maximum annual winter wave height showed a marked drop of 1 m (upper panel, Figure 3-14). At the same time, the offshore wave arrival direction band with the greatest total wave energy (summed

⁻

²⁶ The A2 emissions scenario represents a differentiated world in which economic growth is uneven and the <u>income</u> gap remains large between now-industrialized and developing parts of the world; people, ideas, and capital are less mobile so that technology diffuses more slowly (IPCC, 2007).

over the winter months) shifted 5° northward. These trends are consistent with a northward migration of the jet stream owing to climate change.

Similar downward trends were found when defining the severity of the winter wave climate by the hours different wave height thresholds are exceeded (Figure 3-15). All of these results were consistent with the GCM results indicating a northward shift in the jet stream that leads to a northward shift in the mean winter storm tracks and fewer extreme storms reaching southern California. It is interesting to note that for a mid-latitude region like southern California that has a relatively mild climate and only episodic storminess, the mean winter wave height (Figure 3-14, upper panel, blue line) is a poor indicator of long-term changes in the more severe wave conditions associated with flooding and shoreline erosion.

Detailed wave predictions were made along the shorelines of MCBCP and NBC by transforming offshore wave spectra to the near-shore using a spectral refraction model (Longuet-Higgins 1957, LeMehaute and Wang 1982, and many others). The spectral refraction model includes wave shoaling in shallow water and wave blocking by islands and headlands. The model is linear and therefore wave transformation matrices (wave energy transformation coefficients as a function of wave period and offshore direction) can be pre-computed for each coastal site and subsequently used to transform wave hindcasts, buoy observations, or wave projections to the near-shore in a computationally efficient manner. The wave transformation model is applicable to any coastline with a narrow continental shelf where bottom dissipation of wave energy can be neglected (most U.S. Pacific coastlines) if suitable bathymetry data exists.

The wave transformation model was validated at MCBCP and NBC using near-shore wave buoy measurements available from the Scripps Institution of Oceanography Coastal Data Information Program (CDIP, http://cdip.ucsd.edu). The resulting comparisons (Figure 3-16 and Figure 3-17) show excellent agreement demonstrating that the coastal model is capturing the important wave transformation physics in the region.

Figure 3-16 shows buoy observation-driven model predictions for December 2009 at MCBCP compared to observations from the Camp Pendleton near-shore buoy located in 20-m depth offshore of the Santa Margarita River. The model (green lines) was initialized with buoy observations of swell outside the islands and local seas offshore of Oceanside, CA. The model predictions of significant wave height (top panel), peak wave period (middle panel), and the mean direction at the peak period (bottom panel) all agree with the shallow water buoy measurements (blue lines), particularly for the two large wave events that occurred that month.

A similar validation test at NBC, also for December 2009 and with equally good agreement, is shown in Figure 3-17. This utilized the Imperial Beach Buoy located in 20-m water depth offshore of Imperial Beach Pier south of NBC. The model for NBC was initialized with buoy observations of swell outside the islands and local seas offshore of Point Loma. Similar agreement at MCBCP and NBC was found for radiation stress estimates.

Near-shore Wave Projections – MCBCP

Results of statistical analysis of the MCBCP wave climate using a 10-year buoy-driven hindcast are shown in Figure 3-18. The higher maximum annual maxima on the southern half of the base over the last decade is consistent with the most extreme base events being associated with infrequent storms from more westerly direction. The alongshore variability of extreme wave conditions, represented by the variation in the annual maximum wave heights at the alongshore hindcasts sites, shows much more spatial structure and mirrors conditions during a large swell event from 270° rather than the more common peak direction of 295°. However, note that the mean annual maxima over the last

decade (black asterisks, Figure 3-18) are relatively homogeneous across the base as well. The only alongshore wave height long-term statistic that shows significant alongshore variability is the height of the most extreme events.

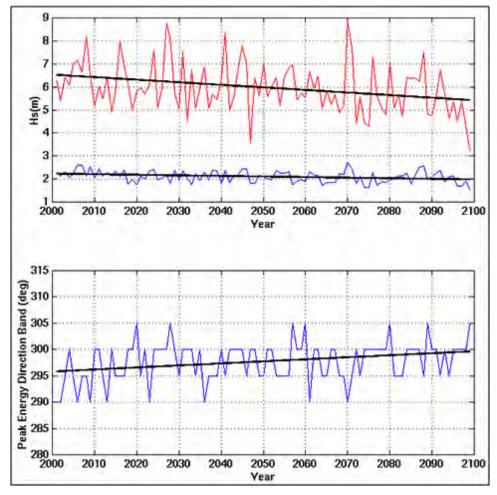


Figure 3-14. Wave height and direction for CCSM3-A2 scenario winter wave conditions in deep water SW of Pt. Conception, CA for 2000–2099.Black lines are least square fit trends. The mean annual significant wave height (blue, upper panel) trends down only slightly, while maximum annual winter wave height (red, upper panel) trends downward by approximately 1 m over coming century. Incoming peak wave directions trend northward (lower panel).

The alongshore homogeneity of the mean wave height and mean maximum annual wave height has implications for future MCBCP shoreline evolution. Barring any future GCM scenarios that produce extremely large increases in the size and/or frequency and/or southward direction shifts of storm events (the CCSM3-A2 scenario predicts none of these), this finding suggests that any alongshore variability in MCBCP shoreline change owing to waves has been and will continue to be dominated by extreme events, rather than any underlying alongshore trend in mean wave conditions.

The alongshore homogeneity of the mean wave height and mean maximum annual wave height has implications for future MCBCP shoreline evolution. Barring any future GCM scenarios that produce extremely large increases in the size and/or frequency and/or southward direction shifts of

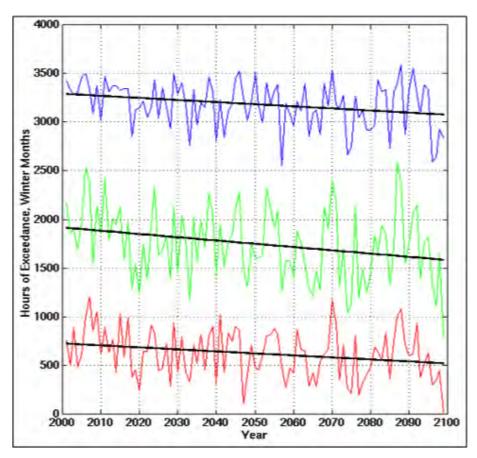


Figure 3-15. Wave height exceedance trends for the CCSM3-A2 scenario winter wave conditions in deep water SW of Pt. Conception, CA from 2000–2099. Black lines are least square fit trends. Annual hours of exceedance for three significant wave height thresholds: 1 m (blue), 2 m (green), and 3 m (red). Downward trends are projected for coming century.

storm events (the CCSM3-A2 scenario predicts none of these), this finding suggests that any alongshore variability in MCBCP shoreline change owing to waves has been and will continue to be dominated by extreme events, rather than any underlying alongshore trend in mean wave conditions.

GCM-derived 100-year near-shore projections of significant wave height at the eight beach profile survey ranges at MCBCP were reduced to the same long-term mean and extremal wave height statistics calculated from the 10-year hindcast (Figure 3-19). Although there are some clear differences in the wave height statistics at each range shown in Figure 3-19 as compared to those in Figure 3-18 (marked by the vertical dashed lines and labels in the plot), they are consistent with the known bias in the GCM-derived transformations described above.

Note that the average GCM-derived wave heights (Figure 3-19) are approximately 0.5 m lower than the buoy-derived averages (green bars, Figure 3-18 and Figure 3-19), consistent with the neglect of local seas in the GCM. In addition, the minimum annual maxima (lower red bars) in the GCM-derived projections are also lower than the 10-year hindcast by approximately 1 m. Stated a different way, the GCM is projecting one or more future winters with extremely mild waves in the next 100 years, much lower than the minimum annual maxima predicted by the (very high skill) hindcast of the last 10 years. This bias is a result of the combination of factors, including the missing local seas already discussed, compounded by the plausible CCSM3-A2 GCM scenario projection of

decreasing maximum wave heights offshore over the next century owing to a northward migrating jet stream.

As expected, the maximum annual maxima in the 100-year projections are significantly higher than in the 10-year hindcasts. This is consistent with the fact that the longer the model prediction time window, the more likely it is to encounter a larger maximum wave event. Finally, the mean annual maxima (black asterisks) in the GCM projection are surprisingly similar to those in the 10-year hindcast (approximately 3 m). This result is unexpected, given the downward trend in the offshore annual maxima, but is confirmed by close inspection of the 100-year projection series at the individual MCBCP profile sites in combination with their wave exposure diagrams.

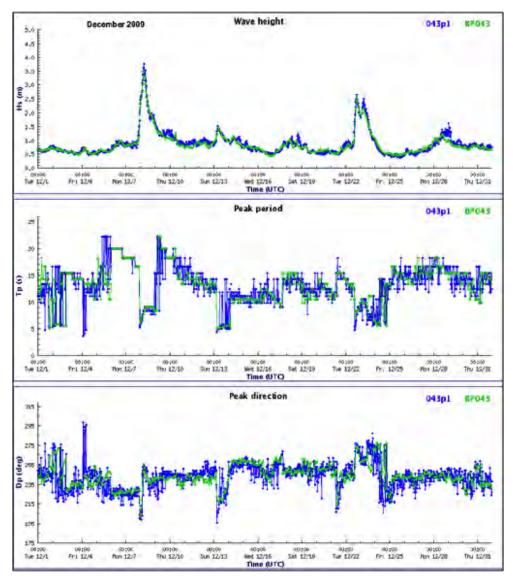


Figure 3-16. Model (green) and observed (blue) wave height (upper), peak period (middle), and peak direction (lower) at MCBCP during December 2009.

To understand the differing GCM-derived extreme annual wave height trends between the offshore waters and the MCBCP shoreline, we examined range PN1290 in the middle of the MCBCP shoreline. The corresponding wave exposure diagram is shown in Figure 3-12. The 100-year time

series of annual mean and maximum wave heights at PN1290 is shown in Figure 3-20. Unlike the offshore wave height maxima, the PN1290 maxima do not have a downward trend over the next century. The CCSM3-A2 GCM-based wave prediction scenario, when transformed through the islands to Range PN1290, predicts that the winter wave climate will become milder on average at this site over the next century. However, the severity of the extreme wave events will remain approximately the same in both height and duration.

In summary, owing primarily to Santa Catalina Island sheltering, the more severe wave conditions along the MCBCP shoreline are dominated by swell events from the west. West swells occur more frequently during the warm phase of ENSO, and show little long-term change in height or duration at MCBCP in the 100-year CCSM3-A2 GCM-derived wave climate projections for the base. Contrastingly, more typical winter storm wave conditions are dominated by swell events from the WNW. These swells are influenced more by the mean location of the jet stream and the larger scale Pacific Ocean weather patterns. The overall duration of typical winter storm waves trends downward at MCBCP in the GCM-derived wave climate projections.

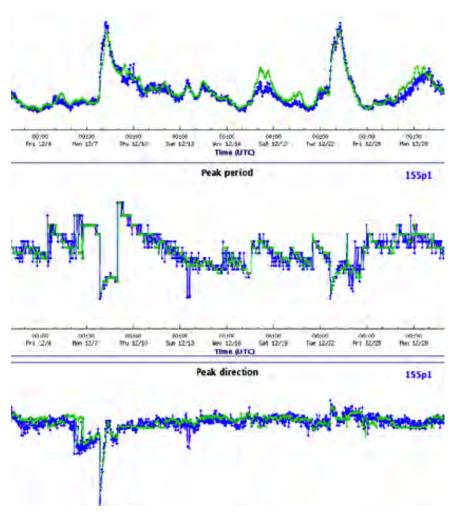


Figure 3-17. Model (green) and data (blue) comparisons of wave height (upper), peak period (middle), and peak direction at NBC during December 2009.

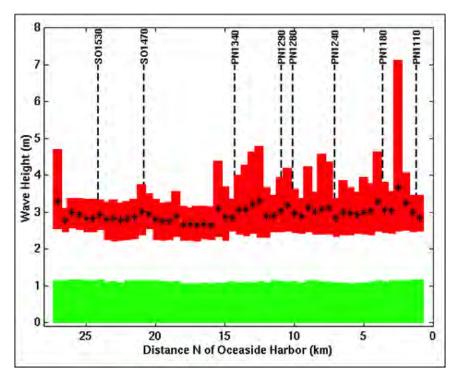


Figure 3-18. Same as Figure 5-17. Mean (green) and extreme (red and asterisks) alongshore wave height statistics for a 10-year (January 2000–December 2009) wave hindcast spanning MCBCP.

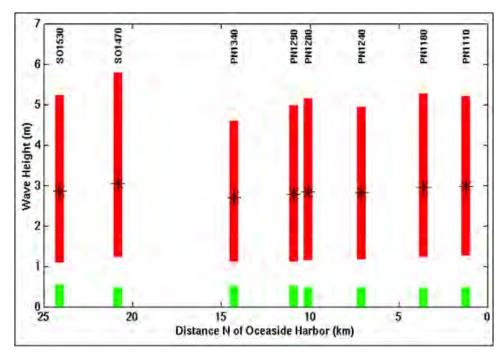


Figure 3-19. Same as Figure 5-21. Mean and extreme along shore wave height statistics for 100-year CCSM3-A2 GCM-derived near-shore wave height projection at MCBCP beach profile ranges. Green bars show mean significant wave height, black asterisks show means of annual wave height maxima, and red bars give range of annual maximum wave height.

٠

Near-shore Wave Projections - NBC

Longer-term mean and extreme wave statistics for the NBC shoreline based on the full 10-year buoy-driven hindcast are shown in Figure 3-21. These statistics show considerably more alongshore variation than seen at MCBCP. While the alongshore mean wave heights only show modest differences, it is notable in the context of how little variability was evident at MCBCP. The mean annual wave height maxima show significantly larger differences in the alongshore compared to MCBCP, while the alongshore variation in the most extreme waves is similar to MCBCP. The spatial pattern of maximum annual maxima from the border to the San Diego Bay entrance is consistent with the most extreme NBC winter wave events occurring with storms from more westerly directions.

One albeit speculative interpretation of the differences illustrated in Figure 3-18 (MCBCP) and Figure 3-21 (NBC) is that MCBCP is a more "mature" or stable coastline (i.e., single orientation to the WSW and backed by cliffs) that has come into balance with the wave climate for all but the most episodic and extreme wave events. In contrast, the Coronado-Silver Strand coastline of NBC is a more dynamic, hook-shaped barrier spit that remains out of balance with the alongshore wave climate.

GCM-derived 100-year near-shore projections of significant wave height at the five beach profile survey ranges at NBC were reduced to the same long-term mean and extremal wave height statistics calculated from the 10-year hindcast (Figure 3-22). As was the case in comparing the 10-year wave data-derived hindcasts and 100-year GCM-derived projections at MCBCP the similarities and differences in the resulting wave climate statistics at NBC (Figure 3-18 and Figure 3-22) are consistent with the inherent differences between the hindcast and projection methods and time spans. Like MCBCP, the similar alongshore variation in maximum wave height statistics in the projection support its use in examining long-term NBC severe wave climate variability.

Again, for comparison of the offshore trend with the NBC shoreline, we examined the conditions at NBC Range SS0160 located at North Island (exposure diagram shown in Figure 3-13). The 100-year annual wave climate statistics time series for Range SS0160 are shown in Figure 3-23. Like MCBCP, the 100-year GCM-derived projection for SS0160 shows little trend in annual maximum wave height (red line, upper panel, Figure 3-23). However, it did indicate a clear downward trend in wave height exceedance rate (not shown) that is consistent with the offshore wave height exceedance trends displayed in Figure 3-15, but not seen at the MCBCP sites. The downward trend in exceedance rate suggests that NBC variability mirrors the long-term winter wave variability found offshore more directly than MCBCP.

Wave-Driven Run-up

Run-up is the height of the maximum excursion of water on a beach and is a crucial factor in causing beach erosion and coastal flooding. Run-up is determined by two different wave-driven dynamical processes: the time-averaged set-up, and fluctuating swash excursions. Set-up is a shoreward sloping increase in average water level that results from the conversion of mean momentum flux or "radiation pressure" of waves into a pressure gradient as they dissipate their energy by breaking in the surf zone. Swash excursions can be decomposed into two period bands: that of the incident waves, usually in the 6-20 second range and that of the infragravity waves, commonly from 20 to 200 seconds and associated with breaking wave "sets."

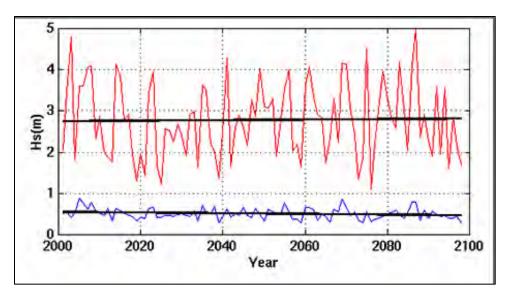


Figure 3-20. Same as Figure 5-22. Annual GCM-derived near-shore wave statistics for MCBCP Range PN1290 including annual significant wave height mean (blue) and maximum (red).

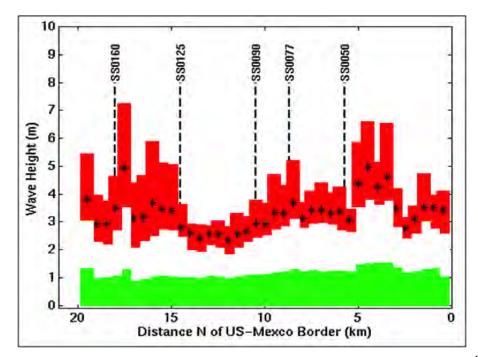


Figure 3-21. Same as Figure 5-20. Mean (green) and extreme (red and asterisks) along/shore wave height statistics for a 10-year (January 2000 to December 2009) wave hindcast at NBC.

Stockdon *et al.* (2006) summarized the theory and data available to guide modeling of run-up on natural beaches. Wave set-up and swash were modeled separately and the results combined to provide best available estimates of the 98th-percentile extreme swash for a wide variety of incoming and beach configuration conditions. As expected, it was found that mean set-up and both incident and infragravity wave swash excursion depended strongly on incoming wave amplitude and period. However, only the set-up and incident swash showed any dependence on the beach slope, while the infragravity swash was statistically independent of beach slope.

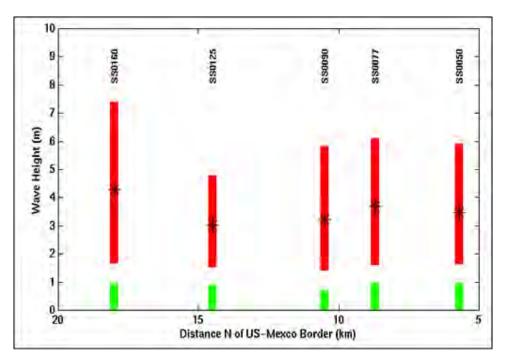


Figure 3-22. Same as Figure 5-26. Mean and extreme alongshore wave height statistics for 100-year CCSM3-A2 GCM-derived near-shore wave height projection at NBC beach profile ranges. Green bars show mean significant wave height, black asterisks show means of annual wave height maxima, and red bars give range of annual maximum wave height.

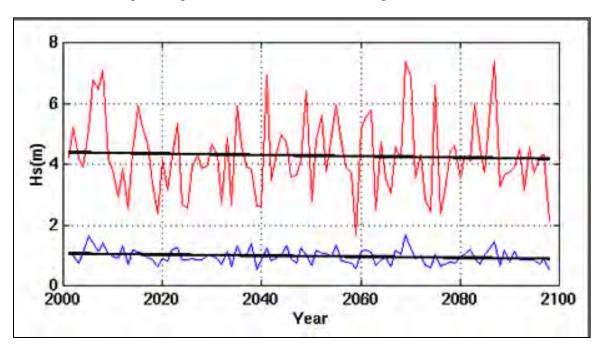


Figure 3-23. Same as Figure 5-27. Annual GCM-derived near-shore wave statistics for NBC Range SS0160 including annual significant wave height mean (blue) and maximum (red).

This is important since infragravity swash usually represents the single largest component of runup excursion on medium and high energy dissipative beaches. It is straightforward to parameterize the incoming wave conditions. But, it is more difficult to pick a characteristic "beach slope" since it changes with location on concave beaches, which get steeper toward shore, as well as with season since winter profiles tend to be flatter than those in summer. Beaches in the study area, especially during large wave storms, tend to be dissipative. This potentially simplifies the application of Stockdon *et al.* (2006) to projecting the extreme run-up conditions in the study area by neglecting the beach slope.

Empirical Run-up Estimates

Run-up calculations were made using the 100-year CCSM3 A2 scenario wave forecasts above using the beach slope-independent formulation of Stockdon *et al.* (2006), which is their Equation 18:

Equation 3-3

$$R_2 = 0.043(H_0xL_0)^{1/2}$$

where R_2 is the 2% run-up exceedance (same as 98^{th} percentile), H_0 and L_0 respectively denote the local deep-water wave height and length, in which $L_0 = gT^2/(2\pi)$ and where the acceleration of gravity $g = 9.81 \text{ m/sec}^2$.

The winter (November-March) run-up 98th percentile exceedance for MCBCP Range SO1470 is shown in Figure 3-24. Peak run-up varied from about 1.4-2.3 m, which was the same or larger than the 1.6 m diurnal tide range along the open coast. By way of comparison and for a measure of the uncertainty involved in the run-up calculations, Figure 3-25 shows the 98th percentile exceedance of run-up from the same wave inputs, but using the full beach slope-dependent formulation in Stockdon *et al.* (2006, their Equation 19), and three slopes, 1:10, 1:20, and 1:50. Higher beach slopes generally produced higher run-up for equal incoming wave conditions. Extreme run-up projections varied by a factor of about 50% with peak values of about 2 m at the flattest slope (1:50) and about 3.5 m at the steepest slope (1:10). Actual foreshore and beach face slopes vary over this range at MCBCP and NBC.

Figure 3-26 and Figure 3-27 respectively show the same information for NBC Range SS0160 located at Coronado City Beach. Run-up from both formulations at these example ranges was higher at NBC than it was at MCBCP owing to greater sheltering of MCBCP from west and northwest approaching waves by Santa Catalina Island. Peak values neglecting beach slope varied from about 1.7-2.7 m, with a variation of approximately 2.5 to 4.5 m for the range of beach slopes shown.

Numerical Run-up Modeling

Along with the empirical run-up estimates, we also conducted extensive development and application of the numerical run-up model XBEACH (Roelvink *et al.*, 2009). XBeach models near-shore processes with a focus on natural coastal response during time-varying storm and hurricane conditions, including dune erosion, overwash and breaching. The XBeach model simulates propagation of short wave and non-stationary shallow water waves in the near-shore zones and on the beach. In particular, it is designed to simulate non-linear run-up on the beach by solving time-dependent wave equations, including the wave refraction with variation of wave action in x, y, time and over the directional space (Figure 3-28), thus it can be used to simulate the propagation and dissipation of wave groups. In addition, the model considers full wave-current interaction in the short wave propagation. Roelvink (1993) wave dissipation model is implemented for use in the non-stationary wave energy balance (in other words, when the wave energy varies on the wave group timescale).

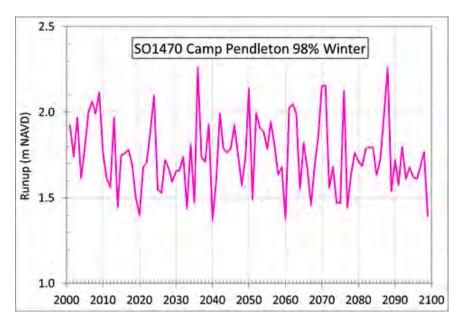


Figure 3-24. Extreme (98th percentile) run-up projection at MCBCP Range SO1470 for winters (Nov-Mar) 2000–2100 using the A2 CCSM3 scenario and the slope independent formulation of Stockdon *et al.* (2006).

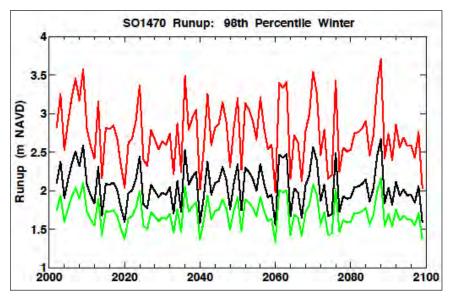


Figure 3-25. Same as Figure 3-24 but using the slope-dependent run-up formulation of Stockdon *et al.* (2006) for beach slopes of 1:10 (red), 1:20 (black), and 1:50 (green).

Initial testing was carried out with the model on simple, uniform-slope beach geometries using a range of beach slopes and wave forcing conditions. Beach slopes ranged from 0.02 to 0.1, and wave conditions spanning significant wave heights of 2 m up to 10 m and wave periods ranging from about 4 to 19 seconds. Tests were conducted using both discrete wave frequencies and Joint North Sea Wave Project (JONSWAP) wave spectra characterized by the peak wave-frequency and significant wave height. The results of these tests were compared to the empirical formulation of Stockdon et al. (2006) to get a sense of how the XBeach model run-up simulations compared to estimates based on field observations. Results for the JONSWAP-based simulations are shown in Figure 3-29 in comparison to Stockdon et al. (2006) estimates using both the slope dependent and slope independent

formulas. In general, the XBeach results showed reasonable agreement with Stockdon. XBeach results were comparable to the slope independent Stockdon estimates over the range of test conditions, but generally indicated lower run-up than the slope dependent estimates. The test results provided confidence that XBeach could provide comparable run-up estimates to field-based methods, while allowing for profile-specific analysis and the ability to accommodate overtopping for the flooding analysis.

To support the flooding analysis for this project, we focused on the application of XBeach to provide a more refined estimate of local wave run-up that accounted for the localized beach profile and wave conditions at each coastal MOP station along the installation shore. With this focus, we applied several simplifying conditions. The model was applied individually at each profile, rather than over the whole domain simultaneously. The beach profiles were fixed and no morphological change was evaluated over the short durations of the runs used to generate the run-up statistics. While wave forcing functions for XBeach can utilize a range of formats, including statistical wave spectra which can be either time invariant or time varying, for this study, we used the time-invariant JONSWAP wave spectrum defined by wave amplitude and frequency. Waves were imposed and prescribed as boundary conditions at the deep ocean model boundary, and propagate toward the beach (Figure 3-28).

Simulations were carried out for the target mean sea level rise conditions combined with a range of five projected statistical wave and total water level rise conditions (week, month, year, decade, and century return periods). The sea level rise scenarios included the baseline condition and projected sea level rises of 0.5m, 1m, 1.5m and 2m between 2000 and 2100. The run-up simulations were performed using the MOP profile locations at 100 m intervals along the shoreline of both installations. The profiles were derived from the baseline elevation model described in Section 3.2.1. The profiles were assumed to retain the same shape relative to mean sea level for future sea level conditions, but be shifted vertically and inland in accordance with the long-term response modeling described in Section 3.3.1 and 3.3.2. Wave forcing and total water levels for the simulations were derived from the scenarios described above in Section 3.1.

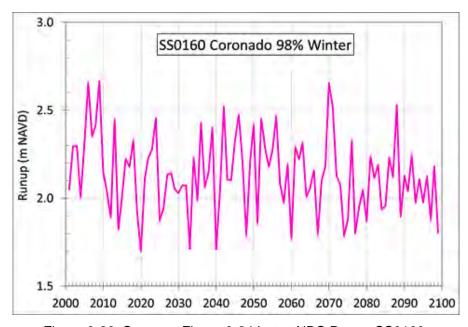


Figure 3-26. Same as Figure 3-24 but at NBC Range SS0160.

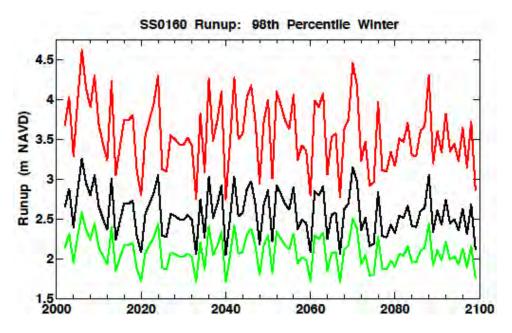


Figure 3-27. Same as Figure 3-25 for NBC Range SS0160.

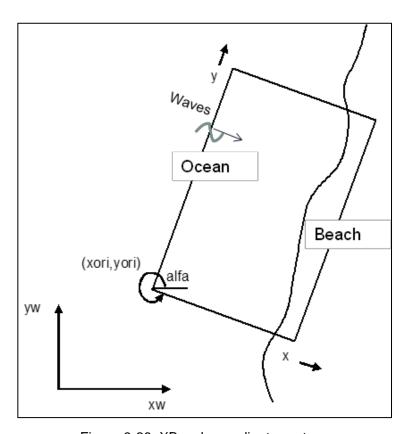


Figure 3-28. XBeach coordinate system.

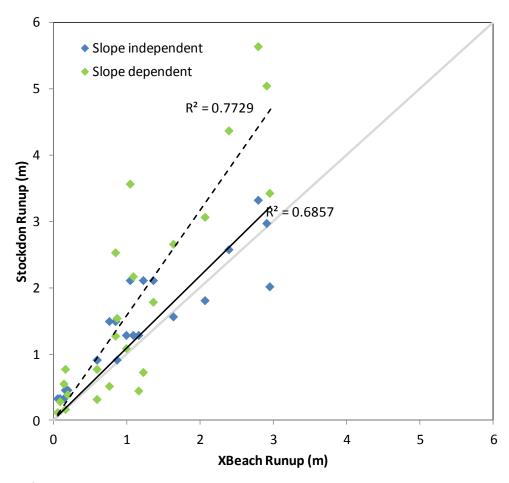


Figure 3-29. Comparison of constant-slope run-up testing results from XBeach and the slope dependent and independent estimates from Stockdon *et al.*, 2006.

Based on these forcing scenarios, the XBeach model was used to simulate wave run-up at the 185 MOP profile locations for NBC and 267 MOP profiles at MCBCP. Simulated wave run-ups were then incorporated with other water level constituents to construct spatially-varying total water level scenarios for the two installations. These scenarios formed the basis for all subsequent inundation and flooding analysis. Because of the spatially varying nature of the profiles and wave forcing, individual XBeach simulations were performed for each of the 185 (NBC) and 267 (MCBCP) beach profiles, and to each of the five wave scenarios. A total of 2260 model simulations were conducted with each simulation lasting 4.33 hours to provide sufficient output to develop statistical estimates of run-up.

Figure 3-30 shows an example beach profile at MOP station 970 at MCBCP for the yearly returnperiod wave condition. The baseline profile from the elevation model (solid pink line) was referenced to NAVD88. For XBeach modeling purposes, this was adjusted with reference to Mean Sea Level (MSL), tide, and NTR constituents to establish the underlying water level over which the wave runup was simulated. Figure 3-31 shows time series of water surface elevation on the beach profile at MOP station 970 at MCBCP under the forcing of weekly, yearly, and decadal waves, respectively. These three figures are shown as they are representative of most of the model results. As wave forcing increased from week to decade and century, wave height and run-up reached higher and further landward.

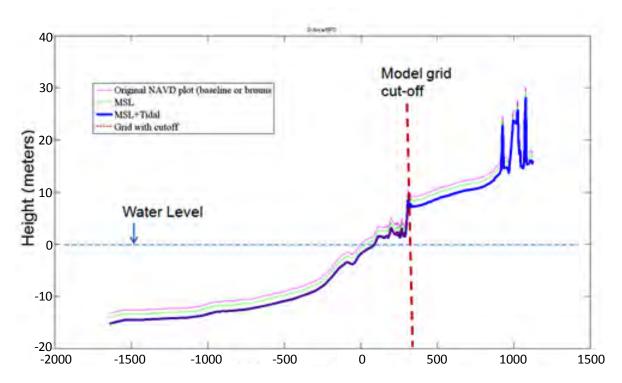


Figure 3-30. Beach profile at MOP station 970 at MCBCP with reference to NAVD88, and adjustments for underlying MSL, Tide, and Non-Tidal Residuals for yearly waves.

Results from the full profile analysis with XBeach were also compared with the slope-independent empirical relationship from Stockdon *et al.* (2006). The methods showed reasonable agreement over the range of conditions at both installations (Figure 3-32 and Figure 3-33). In general, the XBeach run-up estimates were slightly lower than Stockdon for smaller wave conditions (week to month return period), comparable for the mid-range waves (year to decade return period), and somewhat higher than Stockdon for the more extreme 100-year return period conditions. The relationship seems consistent with the notion that higher slopes at the higher elevations of the beach could explain the differences in the two methods. To evaluate this, we calculated the slope required under each return period wave condition to bring the data sets into agreement as $\beta = (0.043R_{xbeach})/(0.73R_{stock})$, where β is the required beach slope, R_{xbeach} is the run-up from the XBeach simulation, and R_{stock} is the run-up from the slope independent Stockdon *et al.* (2006) formula.

The results (Figure 3-34) showed that plausible values were obtained for the beach slope, and that these values do increase with increasing wave attack as hypothesized above. The differences in runup from the two methods could also be explained by the different basis for the two approaches, Stockdon et al. (2006) being based on field data, and the XBeach results being based on a theoretical model in which simplifying assumptions may have limited our ability to reproduce conditions that are equivalent to the field. For example, the XBeach simulations assumed normally incident waves (zero directional spread) while the Stockdon results are for natural waves (finite directional spread). Bowers (1992) showed that "even a relatively narrow RMS spread of 22.5° in short crested (e.g., finite directional spread) incoming waves will almost halve the long (infragravity) wave height associated with long crested unidirectional (e.g., zero spread) waves." In any case, there is still much to investigate in the application of these approaches to sea level rise impacts, but the reasonable agreement provides sufficient confidence to apply the results in the current study.

3.2 DELINEATION OF THE COASTAL SYSTEM

Coastal delineation is the process of acquiring, transforming and inter-calibrating the diverse set of multi-source raster and vector data needed to produce a self-consistent, high-resolution coastal terrain, bathymetry and engineered-infrastructure model (Zhang, 2010; Titus and Richman, 2001; Poulter and Halpin, 2008). The development of a high-quality terrain and bathymetry basemap is essential to all parts of this project. To effectively assess the vulnerabilities to engineered infrastructure it is necessary to have high-resolution data with sufficient horizontal and vertical control. The projected changes in sea-level are measured in meters so that vertical errors that are large fractions of a meter contribute significantly to uncertainties in any subsequent analyses. To minimize these errors it is critical to have a sound vertical datum with the ability to locally correct it to engineering-quality resolution (i.e., accuracy and precision).

Our project convention was to reference all surveys to the same vertical datum, NAVD88, and horizontal datum, North American Datum 1983 (NAD83). Because the integrated basemap has multi-source component data with variable accuracy and precision in addition to differences in datums, the first step was to establish what the datum errors are in each source and then transform each one individually and synthesize a fused, self-consistent dataset that can be progressively improved as better data are made available. The challenge for this project was to produce the best-possible basemap at the 2-meter (horizontal) and sub-meter (vertical) range in order to be meaningful in the context of projections of a few meters of sea level rise with additional water-level forcing by weather and tides. These scales of measurement are ultimately needed for engineering evaluation of impacts to structures and natural resources from rising sea-level including contributions from tides and storms imposed on eustatic changes.

The overall approach to delineating the coastal system was to construct geospatial models of the terrestrial and marine topography using the best-available data sources into geospatial basemaps. They are basemaps in the sense that are the underlying data layer for all subsequent analyses; not because they describe military bases. On top of these basemaps we superimposed other datasets to produce new models of the location of interest, Naval Base Coronado (NBC) or Marine Corps Base Camp Pendleton (MCBCP) for a given sea-level rise scenario as defined in Section 3.1. NBC and MCBCP were modeled individually to limit the spatial extents of each basemap. All spatial models were constructed using the NAVD88 vertical and NAD83 horizontal datums at 2-meter resolution to maximize the utility of the approximately 1-meter Coastal LiDAR data at a manageable data volume. The models for NBC are approximately 250 megabytes (MB) and approximately 700 MB for MCBCP as stored in NetCDF format.

To optimally delineate the coastal system, we decomposed each setting into terrestrial, littoral and bathymetric domains. The terrestrial domain was modeled using a combination of LiDAR from the US Army Corps of Engineers and Scripps Institution of Oceanography (SIO) with gaps filled in using USGS data (Barnard and Hoover, 2010). We refer to the SIO LiDAR as *coastal LiDAR* to differentiate it since it has been extensively field-controlled during data acquisition and post-processing by the SIO Coastal Studies Group (personal communication with Prof. Robert Guza, SIO Coastal Studies Group). The littoral domain was modeled using a new method developed for this project based on beach profiles collected by various organizations since 1950. The bathymetric domain was modeled using a combination of data from the USGS (Barnard and Hoover, 2010) and the U.S. Navy ²⁷. The general workflow for the construction of the elevation models is shown in Figure 3-35.

2

²⁷ Courtesy of M. Perdue and B. Chadwick

To optimally delineate the coastal system, we decomposed each setting into terrestrial, littoral and bathymetric domains. The terrestrial domain was modeled using a combination of LiDAR from the U.S. Army Corps of Engineers and Scripps Institution of Oceanography (SIO) with gaps filled in using USGS data (Barnard and Hoover, 2010). We refer to the SIO LiDAR as *coastal LiDAR* to differentiate it since it has been extensively field-controlled during data acquisition and post-processing by the SIO Coastal Studies Group (perssonal communication with Prof. Robert Guza, SIO Coastal Studies Group). The littoral domain was modeled using a new method developed for this project based on beach profiles collected by various organizations since 1950. The bathymetric domain was modeled using a combination of data from the USGS (Barnard and Hoover, 2010) and the U.S. Navy ²⁸. The general workflow for the construction of the elevation models is shown in Figure 3-35.

3.2.1 Terrain Data and Methods

A wide range of data sources were reviewed in order to select those used in this study. The data sources were chosen with preference given to those of highest horizontal and vertical resolution but also to the degree of confidence with which their quality can be determined with respect to vertical and horizontal control. Software was written to convert the source data from their native format and reference frame to enable validation and quality control as well as to produce a standardized set of basemap products. The programming was done in Bash, Perl, MATLAB[®], R, SAS, GMT, MB-System, Qgis, GRASS and Fledermaus. Data products were produced using community-standard, interoperable formats as shapefiles, NetCDF, and American Standard Code for Information Interchange (ASCII) text files. The data sources were blended using the MB-system tool (Caress and Chayes, 1995). The data sources are listed in Table 3-5 and Table 3-6, respectively. Table 3-7 and Table 3-8 show the initial biases in the USGS and USACE LiDAR data that were used to calibrate these data sets to the previously ground-truthed SIO coastal data. Figure 3-36 shows an example of the fusing process for the USACE LiDAR with the SIO coastal LiDAR for MCBCP, and Figure 3-37 shows the coverage from the USGS data. The primary data gap for the purposes of this work was the lack of good high-resolution topographic data for the littoral zone.

Littoral-zone modeling was accomplished using the approach illustrated in Figure 3-38. We employed transect lines, referred to as MOP (Coastal Data Information Program (CDIP) MOnitoring and Prediction System) lines²⁹ arranged orthogonally alongshore in the offshore direction. These were used to interpolate the fiducial transects as shown in Figure 3-38B, C. The resulting interpolated transects were then applied to the original transects to replace the littoral zone extents as shown in Figure 3-38B. Once this was done the new, improved profiles were used to construct a new littoral zone model using a near-neighbor algorithm. This surface was then resampled, cleaned of NaNs and anomalous edge values and combined into the final geophysical model used in the subsequent segmented beach modeling and flood modeling.

MOP transect end-points were used to generate transects with 1000 m (NBC) and 800 m (MCBCP) seaward extents at each end and the resulting set of transects to sample the base model and recover the NAVD88 elevation at the (Easting, Northing) locations. These were used to compute distance along transect relative to horizontal zero defined by a selected elevation within that LiDAR data that maximized the back-beach extent into the littoral zone. These were then combined into a set of files (one per MOP station) containing (Easting, Northing, Longitude, Latitude, Elevation, Distance) used to compute spline functions at observed locations for selected observational dates

²⁸ Courtesy of M. Perdue and B. Chadwick

²⁹ Courtesy of W. O'Reilly, http://cdip.ucsd.edu/documents/index/product_docs/mops/mop_intro.html

chosen to best reflect the seasonal erosion occurring during the winter. The spline functions were used to create a high-density (3500 points) along-transect and use these locations to interpolate elevations at these locations from the spline function. The back-beach and off-shore limits define a section of the basemodel to be replaced with an interpolated profile based on the high-density locations. The interpolated observational profiles were censored at the defined cutoff and attach its landward end to the back-beach cutoff to avoid spurious values being blended with the truncated LiDAR. The substituted profile was scaled to meet the first landward point on the censored off-shore profile and along-track distances were offset to the point such that d=0 where z=0 where landward positions are negative and seaward positions are positive.

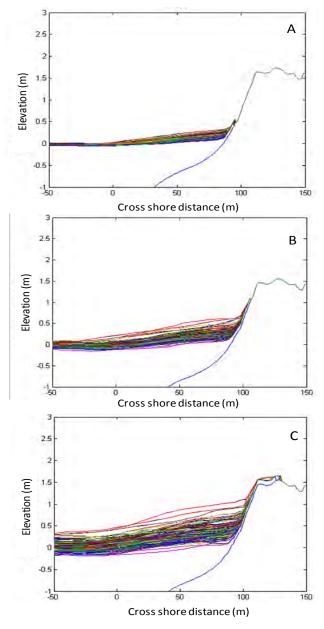


Figure 3-31. An example of XBeach simulated water surface elevations on MCBCP breach profile (MOP 970) for the week (A), year (B), and decade (C) return period wave and total water level conditions.

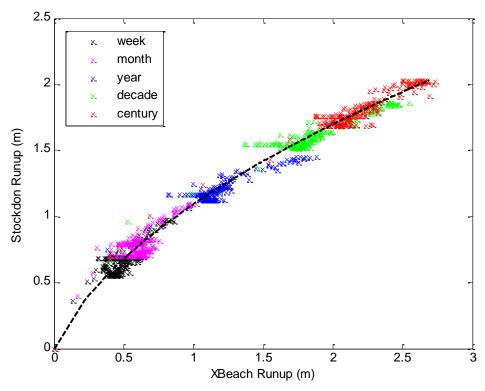


Figure 3-32. Comparison of run-up from Stockdon *et al.* (2006) versus the XBeach results at NBC. The dashed line is a polynomial best fit.

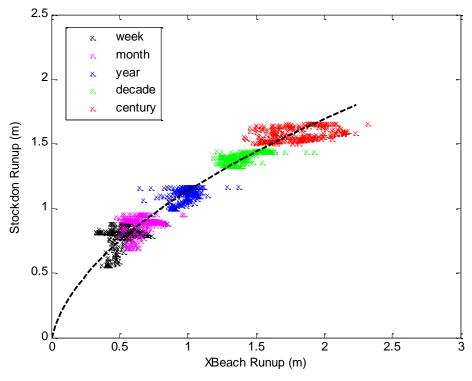


Figure 3-33. Comparison of run-up from Stockdon *et al.* (2006) versus the XBeach results at MCBCP. The dashed line is a polynomial best fit.

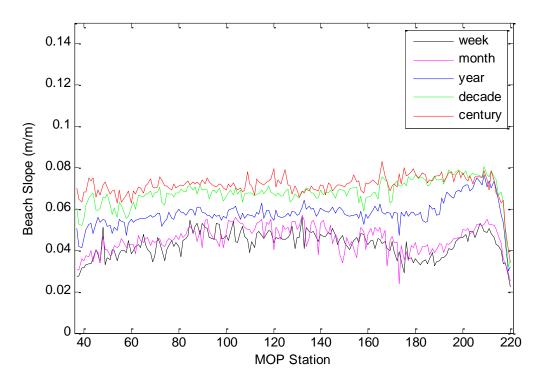


Figure 3-34. Best-fit beach slopes for concurrence between the XBeach simulated run-up values and the Stockdon *et al.* (2006) slope dependent run-up estimates.

A georeferenced version of these transects was used to write out a new set of files for (Easting, Northing, Elevation, Distance) with the name of the MOP transect as part of the filename but not in the file itself as a field so the data can be combined into a dataset for computing a surface. All data and software was converted to UTM11N in order to work with distances resulting in an integrated basemap in UTM11N with USACE LiDAR and SIO Coastal LiDAR data for the terrestrial portion including a portion of the inter-tidal zone. The littoral-zone models were used for a complementary portion of the inter-tidal zone and sub-tidal zone extending into the offshore surf zone and beyond. While this approach was adequate to illustrate the use of the coastal response models employed in this project, it was not optimal, and improved data sets and a better understanding of the variability of this dynamic near shore zone should be a future priority.

3.2.2 Installation Data and Methods

Installation data to support this project was provided by the Naval Facilities Engineering Command (NAVFAC) and Marine Corps Base Camp Pendleton. The receptor-level (consistent with the "screening level" of the framework) and component-level assessment (consistent with the "detailed level" of the framework) methodologies described here utilized facility information extracted from the existing GIS and Internet Facility Real Estate Data Store (INFADS) software currently used by NAVFAC and MCBCP. The following is a brief discussion of the data types acquired.

Geographic Information System Data

Local and regional NAVFAC personnel provided ArcGIS data for NBC and MCBCP. These data included shapefiles for facility information, maps, building data and infrastructure data. The shapefiles consisted of vector data for many types of assets including: buildings, roads, parking areas, waterfront structures, natural resources, and other facilities. Each shapefile had attribute data

assigned to the individual feature by the installation personnel. Attribute data included aspects of the asset such as: facility name, date built, type, facility number, size, location, usage description and various other data pertinent to the structure as determined by facility planners. The accuracy of the shapefiles and attribute data varied by installation and receptor type. The shapefiles received did not include elevation data, MDI, replacement cost, or condition index, because these values, except for elevation data, are maintained in an online database (see INFADS below).

Geographic Information System Data

Local and regional NAVFAC personnel provided ArcGIS data for NBC and MCBCP. These data included shapefiles for facility information, maps, building data and infrastructure data. The shapefiles consisted of vector data for many types of assets including: buildings, roads, parking areas, waterfront structures, natural resources, and other facilities. Each shapefile had attribute data assigned to the individual feature by the installation personnel. Attribute data included aspects of the asset such as: facility name, date built, type, facility number, size, location, usage description and various other data pertinent to the structure as determined by facility planners. The accuracy of the shapefiles and attribute data varied by installation and receptor type. The shapefiles received did not include elevation data, MDI, replacement cost, or condition index, because these values, except for elevation data, are maintained in an online database (see INFADS below).

INFADS Data

The Internet Facility Real Estate Data Store (INFADS) is used by facility planners to manage the real estate database. Current facility information is added to the data base periodically by the facility planners and includes: estimated replacement cost, MDI and facility condition index (CI). For this study, the existing facility data (MDI and replacement value) from the INFADS system were used to provide a uniform method of determining the relative importance of each facility and the cost impact of SLR. For this approach to be effective, it is important that the Navy continue to update the facility replacement values and MDIs to provide the best data set for future sea level rise assessments.

Facility Replacement Value

Three methods of determining facility replacement value were used including INFADS, DoD Facility Pricing Guide, and rough order of magnitude (ROM) values as summarized below.

INFADS System

The INFADS system includes an estimated facility replacement value which is "present worth" value. The INFADS facility replacement values have historically proven to be approximately 50% below actual, however for this study to be integrated with other planning documents used by the Navy it was beneficial to use the replacement values from INFADS. For some assets in the database, a replacement value was not included. For these assets, an alternative method was chosen based on the asset type, which included the average unit cost for similar assets, the DoD Facility Pricing Guide, or ROM cost estimate.

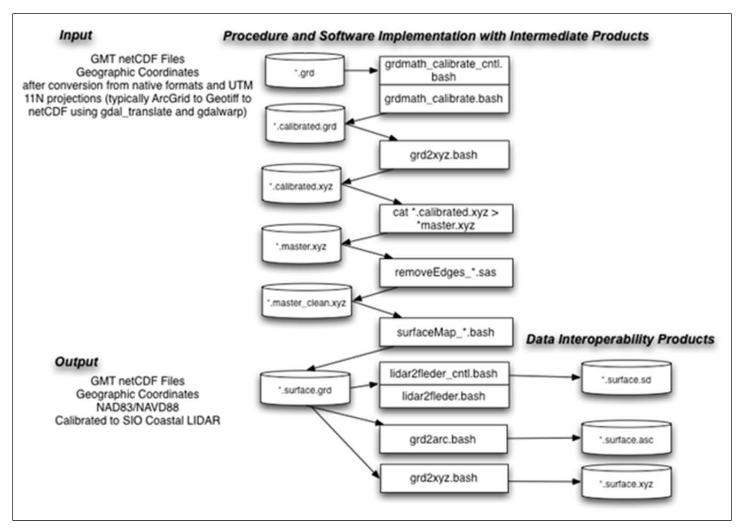


Figure 3-35. Overall data processing workflow for producing calibrated, interoperable data products from source data.

Table 3-5. Input datasets for Naval Base Coronado and surrounding area of San Diego Bay as shown in Figure 3-37. Dataset names reflect the sequence of processing that has been applied to produce the data layer.

Domain	Dataset Name		
Bathymetry SD Bay	sdbay_bathy_GC.1m.nozeroes_nans.xyz		
Littoral Model (constructed from fiducial transects) w/ Erosion Included in Profiles	NBC_BeachProfiles_GC_nearneighbor_filtered_resampled_clean_masked.xyz		
Bathymetry Ocean	OceanBathymetry.GC.NAVD88.1m.clean.masked.xyz		
LIDAR Coastal (water removed)	SIO_Coastal_LIDARcoastalLIDAR_NBC_noOffshoreLIDAR.xyz		
Regional BathyTopo	USGS_Socal_Seamless_GC_NAVD88.sd01.NBC.1m.bathy.clean.xyz		
LIDAR (water removed)	ACOE_LIDAR_GC_XYZACOE_san_ysidro_tile1_noOffshoreLIDAR.xyz		
LIDAR (water removed)	ACOE_LIDAR_GC_XYZACOE_san_ysidro_tile6_noOffshoreLIDAR.xyz		
LIDAR (water removed)	ACOE_LIDAR_GC_XYZACOE_SD_master_noOffshoreLIDAR.xyz		
Global BathyTopo	BathyTopo BathyTopoNBC.BathyTopo.GC.xyz		

Table 3-6. Input datasets for Marine Corps Base Camp Pendleton as shown in Figure 3-36.

Domain	Dataset Name		
Infrastructure Modifications	MCBCP_I5_Cutout_GC_masked_replace.xyz		
Erosion Model (e.g., 2.0m SLR superimposed on Littoral Model)	MCBCP_DefNeg15_replace20_1m.txt		
Littoral Model	MCBCP_BeachProfiles_GC_{Baseline}_nearneighbor_filtered_resampled_clean_masked.x		
LIDAR (water removed)	CoastalLIDAR_SIO_master_GC_20120412_masked.xyz		
LIDAR (water removed)	MCBCP_ACOE_LIDAR_master_GC_clean_masked.xyz		
Global BathyTopo	MCBCP.BathyTopo.GC.xyz		

Table 3-7. Comparison of coastal calibration points at specified locations within the SIO March coastal LiDAR with data from the USGS Seamless, High-resolution dataset for Southern Califo (Barnard and Hoover, 2010).

Calibration Point Selected Along the Coast Using Google Earth	Longitude	Latitude	SIO LIDAR Elevation March 2006 Dataset (median meters, scale factor 100000)	Delta (meters)	USGS Seamle Hi-Resolutio (95th Percent meters)
BM010_SanClementePier_01	-117.622367	33.41833	N/A	N/A	N/A
BM010_SanClementePier_02	-117.621228	33.418965	N/A	N/A	N/A
BM100	-117.456675	33.285718	26.9731	0.0731	26.90
BM200	-117.434015	33.26001	19.0981	0.2521	18.846
BM300 OceansidePier 01	-117.387512	33.192397	9.6789	0.3999	9.27900
BM300 OceansidePier 02	-117.385187	33.193786	8.6276	4.0876	4.54000
BM400	-117.300752	33.054753	25.193	0.67976	24.51324
BM500	-117.260445	32.934302	7.5203	0.3903	7.13
BM600_SIOPier_01	-117.25636	32.866792	9.8829	2.577266	7.305634
BM600 SIOPier 02	-117.255326	32.866498	9.6823	0.05557	9.62673
BM700	-117.244418	32.667457	10.7351	0.1779	10.5572
BM800	-117.218369	32.68917	N/A	N/A	3.74
BM900_ImperialBeachPier_01	-117.135423	32.579568	9.0182	13.71186	-4.69366
BM900_ImperialBeachPier_02	-117.132839	32.579549	5.42740	2.81387	2.61353
MEAN of values < 1.0				0.28980	

Table 3-8. Comparison of coastal calibration points at specified locations within the SIO Marc coastal LiDAR with data from the USACE 2002 LiDAR.

rni

Calibration Point Selected Along the	SIO LIDAR Elevation March 2006 Dataset De				ACOE LIDAR 2002 Dataset Ita (95th percentile, meters, scale factor 100			
Coast Using Google Earth	Longitude	Latitude	(median meters, scale factor 100000)	(meters)	CPEN DelMar001	CPEN DelMar002	SD001	SDC
BM010_SanClementePier_01	-117.622367	33.41833	N/A	N/A	N/A	N/A	N/A	N/
BM010_SanClementePier_02	-117.621228	33.418965	N/A	N/A	N/A	N/A	N/A	N/
BM100	-117.456675	33.285718	26.9731	35.54413	N/A	-8.57103	N/A	N/
BM200	-117.434015	33.26001	19.0981	35.388	-16.2899	N/A	N/A	N/
BM300_OceansidePier_01	-117.387512	33.192397	9.6789	34.9601	-25.2812	N/A	N/A	N/
BM300 OceansidePier 02	-117,385187	33.193786	8.6276	35.5798	-26.9522	N/A	N/A	N/
BM400	-117.300752	33.054753	25.193	N/A	N/A	N/A	N/A	N/
BM500	-117.260445	32.934302	7.5203	N/A	N/A	N/A	N/A	N/
BM600 SIOPier 01	-117.25636	32.866792	9.8829	N/A	N/A	N/A	N/A	N/
BM600 SIOPier 02	-117.255326	32.866498	9.6823	N/A	N/A	N/A	N/A	N/
BM700	-117.244418	32.667457	10.7351	N/A	N/A	N/A	N/A	N/
BM800	-117.218369	32.68917	N/A	N/A	N/A	N/A	N/A	N/
BM900 ImperialBeachPier_01	-117.135423	32.579568	9.0182	N/A	N/A	N/A	N/A	N/
BM900 ImperialBeachPier 02	-117.132839	32.579549	5.42740	N/A	N/A	N/A	N/A	N/
MEAN				35.368008				

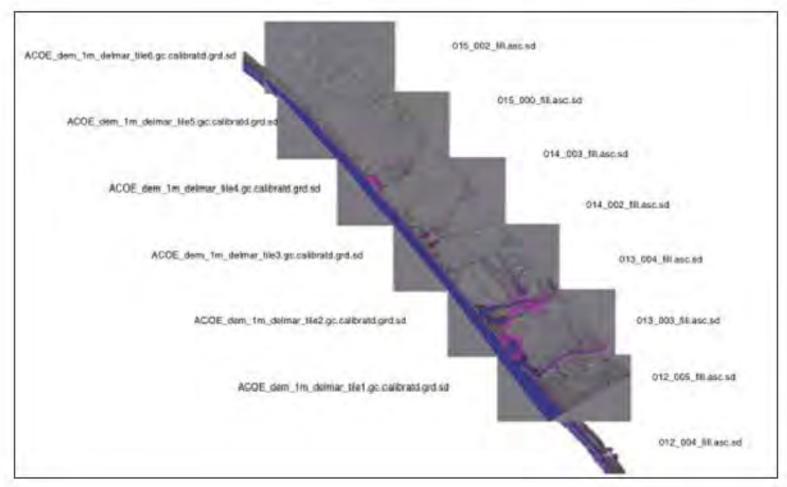


Figure 3-36. Tile index for fused USACE LiDAR (calibrated) with SIO coastal LiDAR for Camp Pendleton locale.

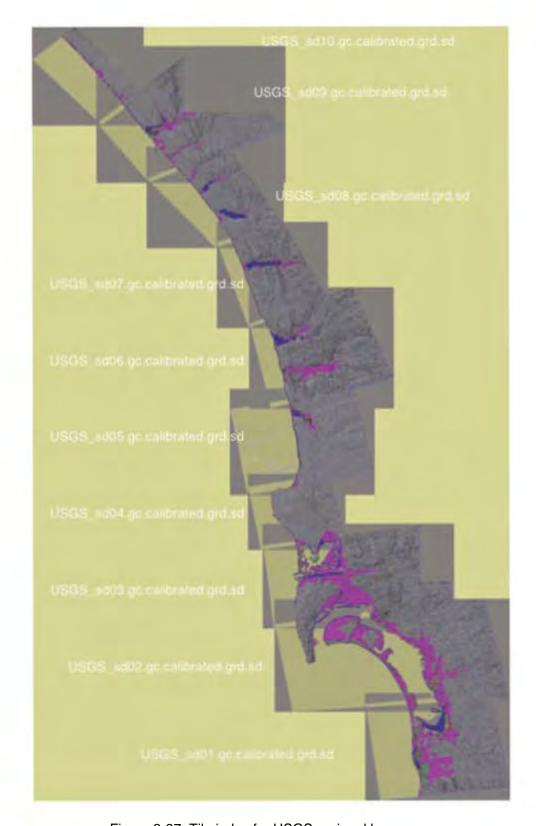


Figure 3-37. Tile index for USGS regional basemap.

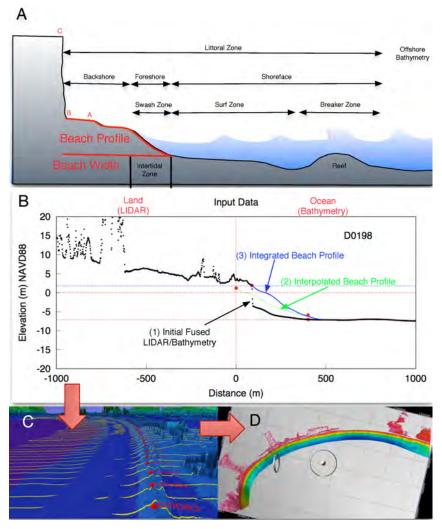


Figure 3-38Èlllustration of littoral-zone modeling using field-measures beach profiles as fiducial transects in combination with MOP lines.

UFC 3-701-09 DoD Facility Pricing Guide

Unified Facilities Criteria (UFC) documents provide planning, design, construction, sustainment, restoration, and modernization criteria, and apply to the Military Departments, the Defense Agencies, and the DoD Field Activities. The DoD Facilities Pricing Guide supports a spectrum of facility planning, investment, and analysis needs. The basic method provided by the DoD Facility Pricing Guide was a facility quantity (square footage basis) multiplied by unit cost (\$/ft²) that was adjusted for location, historical records, planning and design, supervision inspection and overhead, and contingency (NAVFAC, 2011) – reference the equation below:

Plant Replacement Value = Facility Quantity x Replacement Unit Cost x Area Cost Factor x Historical

Records Adjustment x Planning and Design Factor x Supervision Inspection and Overhead Factor x

Contingency factor

ROM Construction Cost Estimate

If the structure did not have a replacement cost included in the INFADS System, or fall within categories of the DoD Facility Pricing Guide, then a ROM value was assigned to the facility. Rough order of magnitude cost estimates were based on experience relative to previous projects with a similar facility size and usage.

Mission Dependency Index

The MDI is an operational risk management measure that links facilities to mission. This is accomplished by associating specific facilities and evaluating their relationship to the Command's mission readiness in terms of *interruptability*, *relocatability*, *and replaceability*. When combined with other metrics, such as facility condition and performance, MDI provides the Commander Naval Installations Command (CNIC) with a powerful facilities management decision tool. CNIC has adopted the MDI as a readiness metric for distinguishing mission critical facilities from non-mission critical facilities. MDI can be used for multiple purposes including prioritization of shore facility sustainment; restoration and modernization; or identification and evaluation of physical security and vulnerability issues from a mission perspective. MDI is quantified as a number between 0 and 100, with 100 representing highest risk severity or impact to mission.

Risk Severity Categories

Risk severity as it relates to facility support is illustrated in Figure 3-39. Mission Readiness becomes increasingly at-risk based on two factors:

- 1. Functional Need: As the need to use a particular facility becomes increasingly imperative, Mission Readiness becomes more at-risk.
- 2. Ease of Replacement: Relocating operations from one site to another is always challenging. Mission Readiness becomes increasingly at-risk as the difficulty of relocating increases.

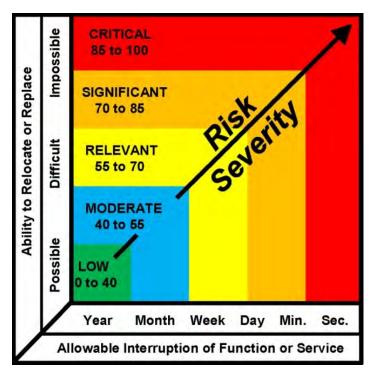


Figure 3-39. Mission Dependency Index rating system used by NAVFAC ESC.

Waterfront Facilities Inspection Reports

The Naval Facilities Engineering Service Center (NAVFAC ESC) has maintained a Waterfront Facility Inspection (WFI) program that was initiated in the early 1980s. Information for most Navy waterfront facilities in the U.S. and abroad exists in the form of a WFI Report which is typically updated on a 6-year basis. The WFI report contains facility descriptions; photographs, facility numbers, condition assessments, structural plans, and sections of the structural system (including fendering); and an asset inventory database. For an initial receptor-level assessment, these reports are helpful for gaining a better understanding of the waterfront structures in the GIS and INFADS databases. In order to conduct a component-level assessment, these reports (or similar sources of information) are necessary to determine operational limits and impacts of SLR on the facilities.

Condition Index

For waterfront structures, the Condition Index is determined from routine structural condition assessments. A Condition Index is assigned to each structure to allow facility planners a tool to prioritize repairs between installations and facilities worldwide. The condition assessment rating varies from "Good" to "Critical" as shown in Figure 3-40. The condition index is a useful metric for weighing the impact of SLR on a facility relative to age, replacement cost, and costs associated with adaption to accommodate SLR.

The Condition Index is used for waterfront structures. Research has not identified a similar U.S. Navy metric for civil infrastructure, buildings, and coastal structures. The degradation rate and potential impacts of deterioration typically identified with waterfront structures are more rapid than civil infrastructure, buildings, and coastal structures due to the harsh exposure of the marine atmosphere.

Assessment Rating	Equivalent CI Rating	Description of Condition
"Good"	90	No problems or only minor problems noted. Structural elements may show some very minor deterioration, but no significant reduction in structural capacity.
"Satisfactory"	75	Minor to moderate defects or deterioration observed, but no overstressing observed, but no significant reduction in structural capacity.
"Fair"	60	All primary structural elements are sound; but minor to moderate defects or deterioration observed. Localized areas of moderate to advanced deterioration may be present, but do not significantly reduce the structural capacity.
"Poor"	45	Advanced deterioration or overstressing observed on widespread portions of the structure. Some reducion in structural capacity.
"Serious"	30	Advanced deterioration, overstressing or breakage may have significantly affected the load bearing capacity of primary structural components. Local failures are possible.
"Critical"	15	Very advanced deterioration, overstressing or breakage has resulted in localized failure(s) of primary structural components. More widespread failures are possible or likely to occur.

Figure 3-40. Condition Index ratings used by NAVFAC ESC for waterfront structures.

Record Drawings

The local Public Works Officer may have access to Record Drawings ("as-built"), or recent facility repair or upgrade drawings in electronic format. Record drawings will contain the information necessary to conduct a component-level assessment.

3.2.3 Receptor Categories

For purposes of our framework, we adapted previous coastal infrastructure category definitions to align with general categories more commonly used by planners, engineers and facilities personnel at military installations. These receptor categories included:

- Training and Testing Lands
- Buildings
- Waterfront Structures
- Coastal Structures
- Civil Infrastructure
- Military and Civilian Personnel
- Protective Buffers and Natural Resources

Within our study, we focused on the first five (italics) of these categories to align with both project directives and the expertise areas of our team. These categories served as fundamental generalized receptors that spanned a reasonable cross section of the potential endpoints of interest for coastal military installations. We evaluated the potential vulnerabilities of these receptors from sea level rise on a site-specific basis, but taking a fairly broad, screening level approach to maintain sufficient breadth to gauge the overall impact to the installation.

Receptor category characteristics were quantified based on the data described above in Section 3.2.2. In general, the geospatial description and associated metadata for each category were compiled into shapefiles for each category at each installation. These shapefiles were compiled in an Arcview GIS® project for visual display and analysis. They were also linked to a series of MATLAB® analysis scripts that were developed to evaluate the assessment metrics for each receptor category. Site specific descriptions of the receptor categories compiled for NBC and MCBCP are provided in Section 3.4.

Training and Testing Lands

The training and testing lands category at NBC and MCBCP focused on sensitive, exposed shoreline training beaches. These areas support training for a wide range of military commands, using a variety of personnel, vessels, vehicles, equipment, and aircraft to meet their military readiness requirements. These areas are particularly sensitive to exposure pathways including erosion, inundation and flooding. Figure 3-41 shows a cross-section of a typical training beach at NBC. The beach area backs up onto the dunes and the highway and thus has limited ability to accommodate retreat. Figure 3-42 shows typical training patterns for SSTC. Many of these training operations require significant footprints on the beach. At MCBCP, amphibious training also requires accessible beach widths. The majority of amphibious assault training activities at MCBCP occur at Red Beach (Figure 3-43) with additional training at Gold, Green, White, and Blue Beaches. On the basis of these training requirements, methodologies were developed to extract key metrics from the beach training area shapefiles as a function of sea level rise. These included the average remaining beach width, and the average remaining surface are for each training lane. Results of this analysis are presented in Section 4.2.2.

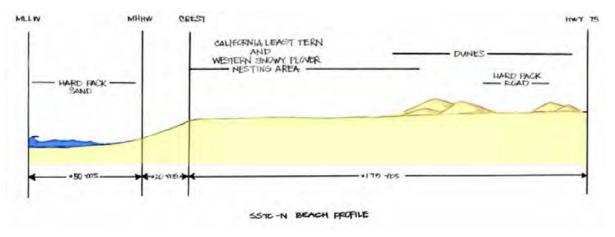


Figure 3-41. Typical beach training area profile at NBC (adapted from U.S. Navy, 2010).

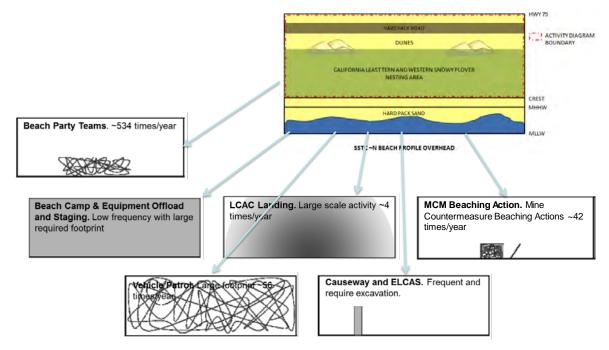


Figure 3-42. Typical training patterns for beach training areas at NBC.Rectangles indicate the approximate area of the beach zone in a training lane, and lines and shading indicate training traffic patterns (adapted from U.S. Navy, 2010).



Figure 3-43. Amphibious training at MCBCP Red Beach (courtesy of Marine Corps Base Camp Pendleton, http://www.pendleton.marines.mil).

Buildings

The building category at NBC and MCBCP included a range of buildings that support operations and missions of the installations. This spanned buildings for housing, logistics, training, testing, operations, storage and security. These receptors are susceptible to sea level rise sources through all major pathways including inundation, flooding, erosion and seawater intrusion. Of particular interest are building structures that are already to the high tide line, and the relationship of building foundation and finish floor elevation to projected sea level elevations. For NBC, the majority of the building receptors were located at North Island Naval Air Station and the Naval Amphibious Base. In particular, some of the buildings at NAB are situated particularly close to the shoreline on the exposed beach areas (Figure 3-44). At MCBCP, buildings are predominantly in the Del Mar area of the base near the recreational beach and the harbor (Figure 3-45). Building shapefiles and associated metadata were compiled for each installation. Impacts to these receptors were then characterized for erosion, inundation and flooding, using metrics related to the replacement cost of the structure as described in Section 3.4. Results for the analysis are described in Section 4.2.2.



Figure 3-44. Naval Amphibious Base Coronado buildings (image data: Google).



Figure 3-45. Buildings concentrated in the Del Mar area of MCBCP (image data: Google).

Waterfront Structures

This category included a range of structures at NBC and MCBCP that support waterfront operations and missions. This category encompasses structures such as piers, wharves, quay walls, floating docks and graving docks. These receptors are susceptible to sea level rise sources through all major pathways including inundation, flooding, erosion and seawater intrusion. Of particular interest for waterfront structures are vulnerabilities associated with overtopping, sea levels that obstruct mooring and berthing, loss of function for dockside utilities, and increased physical loading from water uplift or current forces in relation to the structural capacity. Waterfront structures at NBC are concentrated along the protected shorelines of San Diego Bay and include a number of piers and wharf areas (Figure 3-46). Waterfront structures at MCBCP are limited to small boat facilities in the Del Mar Basin. Shapefiles were compiled for waterfront structures using the data sources described in Section 3.4.2, and deck elevations were extracted from Record Drawings and WFI Reports and compared with the digital elevation model. Analysis focused on the incremental impacts to piers with elevated water levels, for which structure-specific response characteristics were developed. Results for this analysis are presented in Section 4.2.2.



Figure 3-46. Waterfront structures at NBC including the Carrier Wharves (far left) and the Ammunition Pier (far right) (red arrows). Shore protection coastal structures can also be seen along the bay shoreline (yellow arrows) (image data: Google).

Coastal Structures

This category includes a range of coastal structures at NBC and MCBCP whose primary purpose is to protect the shoreline and thus sustain operations and missions of the installation. This category encompasses structures such as jetties, groins and revetments which are used to protect the shoreline and dredged improvements. These receptors are susceptible to sea level rise sources particularly through inundation, flooding, and erosion. Of particular interest for coastal structures are vulnerabilities associated with changes in currents, wave climate and water levels that may influence the functionality and performance of coastal structures under various sea level rise scenarios. At NBC, coastal structure receptors are concentrated along the protected San Diego Bay shoreline (Figure 3-46), while at MCBCP the primary coastal structures are located at the Del Mar Basin. In general, existing GIS data for this receptor class was lacking, and these structures were digitized from high-resolution photographic imagery, and then elevations were extracted from the digital elevation model. Coastal structure analysis results are presented in Section 4.2.2

Civil Infrastructure

This receptor category describes a broad category of built infrastructure at NBC and MCBCP that is critical to the day-to-day operations and mission of the installation. The category includes receptors ranging from critical utility infrastructure such as buried utilities, fuel transfer/supply, transportation corridors, and storm water conveyance systems. These receptors are susceptible to sea level rise sources through all major pathways including inundation, flooding, erosion and seawater intrusion. Because of the breadth and complexity of this category, we focused our analysis on a subset of elements that exemplify the potential impacts from sea level rise. These included transportation infrastructure, storm water conveyance systems, airfield surfaces, and recreational areas. These data were compiled into receptor-specific shapefiles using the data sources described in Section 3.4.2.

3.2.4 Integrated Terrain and Infrastructure Model

Analysis of the receptor categories described above relied on the integration of the receptor data with the terrain data to create an integrated model. The integration consisted essentially of an overlay of the shapefiles onto the three dimensional terrain such that elevations for the infrastructure could be extracted to evaluate interactions with erosion, inundation and flooding areas. The procedure utilized three primary inputs including the receptor GIS layers described above, the baseline elevation model, and the modified coastal surfaces developed from the long-term beach and cliff modeling results (Figure 3-47). The new terrain models and the infrastructure layers were integrated through both Arcview for general display purposes, and through specialized MATLAB® tools that were developed for the analytical aspects of the project. These tools fell into two categories for (1) use in erosion analysis, and (2) use in inundation and flooding analysis. Results from the integration process are shown in Section 3.2.3.

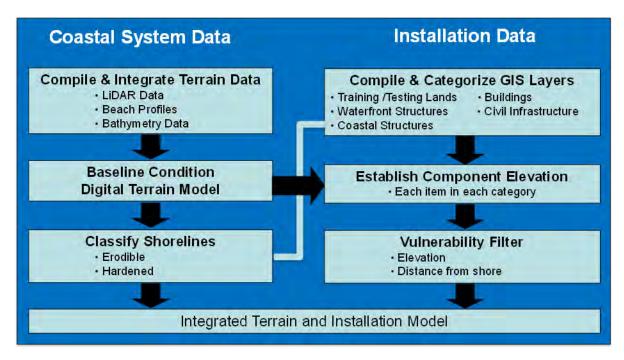


Figure 3-47. Methodology for integration of the terrain and infrastructure data.

3.3 PHYSICAL RESPONSE TO SEA LEVEL RISE

Physical response pathways represent the process or mechanism by which sea level rise sources act on receptors to cause impact. Pathways of action for sea level rise generally include inundation, flooding, erosion and seawater intrusion. Often, a given pathway may be governed by the combined action of multiple sources and may influence a range of potential receptors. A solid conceptual understanding of these pathways is critical to establishing a meaningful vulnerability assessment, as well as to formulating response and adaptation strategies. Primary pathways for this study are grouped by exposure under categories for exposed shorelines, protected shorelines and groundwater (Figure 3-48).

Exposed shorelines are generally those which are not protected from wave action. From the perspective of sea level, these shorelines are generally subject to the full spectrum of sea level source functions including changes in mean sea level, tides, storm surge, waves and non-tide processes. The interaction of these water level stressors combine to influence the response of the exposed shorelines primarily through pathways including erosion, inundation and flooding (Figure 3-48). For the purposes of this project, we separate the exposed shoreline long-term response into two categories including beach systems, and cliff/beach systems, which are generally representative of much of the southwest U.S., and specifically representative of NBC and MCBCP respectively. Development of methods for these two systems is described below. In addition, we have developed a methodology to estimate short-term response for the beach portion of the exposed shorelines. This methodology allows seasonal and short term storm response changes in the shoreline position to be superimposed on the longer term response to changing sea level.

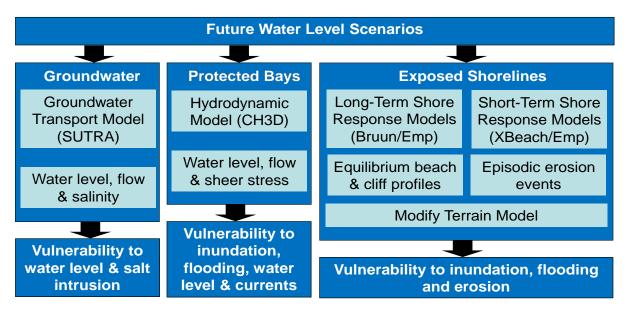


Figure 3-48. Pathway response modeling approach.

Protected shorelines are represented by areas with minimal wave exposure. These areas tend to be subject to mean sea level rise, tides, storm surges and other non-tide fluctuations, but not wave impact or run-up. For the southwest U.S., tides are the dominant driver of sea level variability for protected shorelines, and it is generally the interaction of tides with increasing mean sea level that combines to induce impacts through key pathways including inundation and flooding (Figure 3-48). Because protected shorelines are often represented by harbor areas, changes in sea level can also act directly (independent of inundation and flooding) on waterfront structures such as piers and wharfs since these structures are generally designed to function within a finite range of sea level' Increasing mean sea level can also act within these protected areas to influence tidal currents and associated bottom shear stress and thus sediment deposition and transport patterns. For this project, evaluation of protected shoreline areas focused on the San Diego Bay region adjacent to NBC which supports a broad range of critical infrastructure for the installation.

Coastal aquifers can be sensitive to the effects of sea level rise on seawater intrusion. Because the flow rate of groundwater within these systems is strongly damped by the soil matrix, high-frequency fluctuations in sea level are generally absent except very near the shoreline. For this effort, assessment of seawater intrusion focused on the Santa Margarita River Basin at MCBCP. MCBCP's water supply is produced primarily from aquifers that are recharged by percolation from overlying rivers and streams, and Santa Margarita River wells provide about 65% of the total water consumed on the Base. We utilized a density-dependent groundwater-flow and solute-transport model, combined with a range of historical data to explore the influence of seawater intrusion under the target range of sea level rise scenarios. The simulation utilized monthly mean sea levels as a forcing function, combined with a range of potential future groundwater pumping conditions. The simulation time frame extended from water year (WY) 1950 to 2100 and the assessment of the effects of a sea level rise extended from WY 2000 to 2100.

3.3.1 Exposed Beach Shoreline Erosion – Long-Term Response

Coastal recession caused by sea level rise is often estimated using the Bruun rule (Bruun 1962) concepts of equilibrium profile and sediment conservation, originally designed for low lying sandy coasts. The original Bruun rule method assumes a fixed active beach profile during coastal recession,

homogeneous coastal material, and no external sediment sources or sinks. Although commonly applied (i.e., Zhang et al., 2004), the Bruun rule assumptions are often ignored or not satisfied, prompting much criticism (i.e. Cooper and Pilkey, 2004; Pilkey and Cooper, 2004). Coastal settings rarely (if ever) satisfy the original Bruun rule assumptions, leading to the use of modifications including heterogeneous coastal material, external sediment sources and sinks, and variable inland topography (Dean and Maurmeyer, 1983; Hands, 1983; Dean, 1991; Bray and Hooke, 1997; Wolinsky and Murray, 2009). Alternatively, Revell et al. (2011) developed a downscaled model that predicts shoreline retreat at 500-m intervals based on total maximum water levels, which are assumed to be proportional to shoreline retreat, however, no sand budget balance was utilized. Here, we build upon the Bruun rule modifications, recent equilibrium modeling (Wolinsky and Murray, 2009; Ashton, Walken, and Dickson, 2011), and established coastal concepts to provide estimates of retreat based on coastal system sediment balance and process based relationships for coasts where sediment balance is important.

Methods development for exposed beach systems focused on a Cross-Shore Profile Equilibrium Model (CSPEM) to simulate long-term shoreline response related to sea level rise at NBC and the areas of MCBCP without cliffs. In addition, we evaluated short-term response of the beaches to variability in wave climate, through the use of an equilibrium model (YGOR model, Yates *et al.* 2009) that was superimposed on the long-term response. Thus the erosion pathway was evaluated as a function of the combined long- and short-term responses. Inundation and flooding for exposed beaches were evaluated by creating new elevation models that represented the simulated long-term shoreline response at certain time snapshots corresponding to the specified sea level conditions. At these snapshots, spatially-varying hydraulic connectivity analysis was performed to assess potential inundation and flood footprints. In this case, inundation was defined based on events with short return periods (days – months) while flooding was defined as events with longer return periods (year – century).

The long-term exposed beach response model relied on cross-shore profile equilibrium theory and the highly correlated and seasonal nature of wave- and rain-induced shoreline erosion and near-shore sand deposition events in a summer—dry climate. It was assumed (and supported by historical observations) that at the end of the mild summer—dry season (September—October) a near-shore portion of a sandy beach's cross-shore profile always returns to the same fixed, fully accreted equilibrium shape, relative to the mean water level (MWL), but the cross-shore location of this profile segment varies depending on the MWL elevation and local near-shore sand supply. The fixed shape of this fully accreted profile (PFA) is a function of the near-shore sand size distribution and the average summer—dry season wave climate, both of which were assumed to vary more slowly on long time scales than changes in MWL and the local sand supply. On inter-annual time scales, the PFA migrates in the vertical and cross-shore directions as a combined function of 1) changes in MWL and 2) winter-wet season changes in the cross-shore volume of sand available to build the PFA at the beginning of the next summer—dry wave season.

The Fully Accreted Equilibrium Profile

The PFA (shown schematically in Figure 3-49) is a fixed shape in the vertical (z) and cross-shore (x) directions, and its position within the overall cross-shore profile, z(x), was defined relative to the intersection of P_{FA} with the MWL shoreline location (x_0, z_0) at the end of the summer–dry season.

Equation 3-4

$$z(x) = z_O + P_{FA}(x - x_O - b)$$
; for $x = (x_O - b) \rightarrow (x_O + s)$

It was assumed that summer–dry season waves in combination with higher tides could only accrete sand up to a local maximum elevation, $z_o + h$ (e.g. something close to the MHHW elevation). It was also assumed that there is a minimum elevation (max depth), z_o -d, below which there is no net shoreward transport of sand by the mean summer–dry season wave climate (e.g. shallower than the depth of closure).

The shoreward extent of the P_{FA} , x_o - b, was then defined by the cross shore location of the farthest seaward crossing of the elevation z_o + h. The seaward extent, x_o + s, was defined by the first crossing of the elevation z_o - d in the offshore direction.

The portion of the cross-shore profile landward of the P_{FA} ($x < x_o - b$) was defined as the land profile, and seaward of the P_{FA} ($x > x_o + s$) the shelf profile (Figure 3-49). The land and shelf profile segments do not have fixed shapes and evolve over time with the changing shoreline.

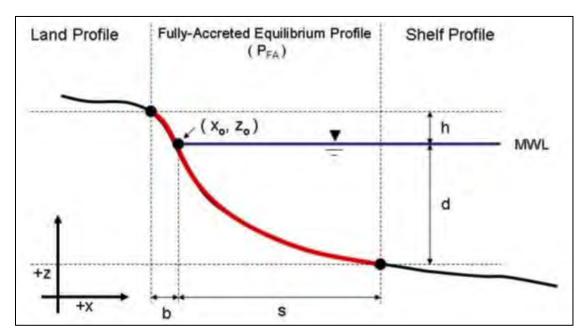


Figure 3-49. Schematic of the fully accreted summer. dry equilibrium profile.

The MWL-referenced, vertical and horizontal limits of the P_{FA} (h,d,b,s) are fixed parameters that were derived from a best fit to a beach's late summer—dry season profile surveys. Once surveys have established the horizontal and vertical elevation limits of a specific beach's P_{FA} , long-term changes in the annual P_{FA} shoreline elevation and cross-shore location were estimated using different scenarios of combined sea level rise and sand volume availability.

Shoreline Migration and Mass Conservation

The "near-shore volume" V (m^3/m of shoreline) was also defined relative to the P_{FA} reference frame (Figure 3-50),

Equation 3-5

$$V = \int_{x_o-b}^{x_o+s} [z(x)-(z_o-d)]dx$$

This near-shore volume can be calculated at any time throughout the year (e.g., at the beginning of the summer—dry season in the spring), but the PFA reference frame shoreline location (x_o, z_o) used in the calculation is only shifted at the end of each summer—dry season. At the end of each summer—dry season, when the PFA has been rebuilt by the summer waves at a cross-shore location and elevation consistent with the MWL and available near-shore sand supply, the sand volume within the (newly shifted) PFA reference frame will equal the constant $V_{\rm FA}$.

Equation 3-6

$$V_{FA} = \int_{x_o - b}^{x_o + s} [P_{FA}(x - x_o - b) - (z_o - d)] dx$$

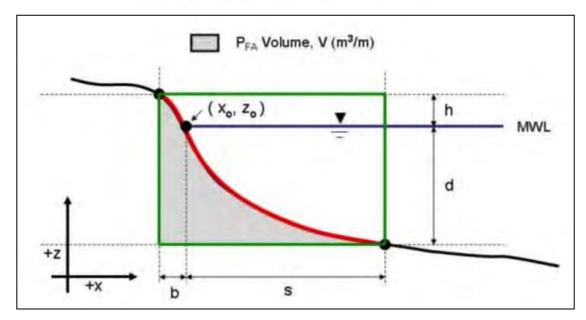


Figure 3-50. The near-shore sand volume is calculated relative to the PFA reference frame (green box).

Vertical and Horizontal Migration of the Annual, Fully-Accreted Profile

Two variables cause the P_{FA} to form at a new location at the end of the summer–dry season each year.

- A change in the near-shore volume, V, owing to a change in the profile z(x) within the PFA reference frame (set at the end of the previous summer–dry season). This causes the local P_{FA} reference frame (green square, Figure 3-50) to migrate *horizontally* during the subsequent summer–dry season until V calculated with a new cross-shore shoreline position, $x_o + \Delta x_o$, equals V_{FA} .
- A change in the summer–dry season MWL (e.g., sea level rise). This results in a change in the MWL shoreline location, both horizontally and vertically, with an identical shift in the PFA reference frame. The two-dimensional shift in the PFA reference frame with a changing MWL generally leads to a change in V, requiring an additional horizontal $x_0 + \Delta x_0$, reference frame "correction", as described above, until V once again equals V_{FA} .

In addition to P_{FA} reference frame volume changes owing to a rising or falling annual MWL, annual volume changes "within the green zone" in Figure 3-50 can occur owing to sediment transport processes, e.g.

- A net alongshore littoral transport gain or loss.
- A net aeolian transport gain or loss through the shoreward P_{FA} boundary.
- A cliff or terrace erosion gain through the shoreward P_{FA} boundary.
- A net cross-shore transport loss through the seaward P_{FA} boundary.

By definition, there can be no net loss through the shoreward P_{FA} boundary, or net gain through the seaward P_{FA} boundary, owing to shoreward wave transport.

Cross-Shore Profile Equilibrium Model

Given a cross-shore profile at the end of the summer–dry season with a defined near-shore profile segment that is in its fully accreted equilibrium state, V_{FA} can be calculated using Equation 36.

The annual horizontal migration of the PFA shoreline location (xo,zo) owing to changes in the MWL (Δzo), and/or observed or projected changes in z(x) that change the near-shore sand volume by ΔV , can then be estimated by iteratively solving to find the cross-shore shoreline change, Δxo , that results in V = VFA.

Equation 3-7

$$V = \int_{x_o + \Delta x_o - b}^{x_o + \Delta x_o + s} [z(x) - (z_o + \Delta z - d)] dx$$

In the case of a projected (vs. observed) change in near-shore sand volume owing to sediment transport processes, the exact form of z(x), within the $x_0 - b < x < x_0 + s$ boundaries that results in ΔV does not have to be specified. Instead, Equation 3-5 and Equation 36 can be used to include ΔV explicitly relative to P_{FA} ,

Equation 3-8

$$V = \int_{x_o + \Delta x_o - b}^{x_o + \Delta x_o + s} [z(x) - (z_o + \Delta z - d)] dx + \Delta V$$

where

Equation 3-9

$$z(x) = P_{FA}(x - x_o - b)$$
; for $x_o - b < x < x_o + s$

which can then be solved for the value of Δx_0 that will make $V = V_{FA}$ when P_{FA} forms as part of z(x) at the end of the subsequent summer–dry season.

To implement the CSPEM model, Equation 3-8 was solved iteratively for Δx_o by brute force using simple downhill minimization methods. The general scheme for the implementation is shown in Figure 3-51. The primary inputs to the model included the initial end of the summer–dry season cross-shore transect profile, a statistical representation of the wave climate or total water level absent

sea level rise, the sea level rise, and the external sand budget. The model then determined the active profile region, shifted it vertically in accordance with sea level rise, and iteratively marched the profile landward until mass balance was achieved. A new profile was then developed by re-inserting the active profile into the fixed inshore and offshore portions of the cross-shore transect using piecewise polynomial interpolation to smooth the connection areas.

We also investigated, but have not implemented, a more efficient solution method using predictor-corrector methods based on the known first-order relationships between P_{FA} reference frame volume changes and changes in x_o and z_o . In this approach, the horizontal translation of the reference frame with a change in V, can be estimated to first-order as a function of the P_{FA} constants h, and d.

Equation 3-10

$$\Delta x_o = \frac{\Delta V}{h+d}$$

and the horizontal reference frame translation owing purely to a change in the MWL (Δz_o) can be estimated to first-order as a function of PFA constants b, s, h, and d,

Equation 3-11

$$\Delta x_o = \frac{(b+s)}{(h+d)} \Delta z_o$$

where (b+s)/(h+d) is the mean slope of P_{FA} . Equation 3-10 is the exact solution for shoreline migration with sea level rise, if the land profile shoreward of P_{FA} has a slope equal to the P_{FA} mean slope (Figure 3-52). In this pathologic case, P_{FA} reference frame volume is conserved as the frame shifts with a sea level rise or fall.

Active Profile

The upper and lower boundaries for the end of summer–dry season beach profiles were estimated as the 10-year return-period total water level and the closure depth associated with the 10-year return-period significant wave height, respectively. The 10-year return-period total water was estimated from a 100-year (2000–2100) trajectory of future sea level constituents using extreme probability statistics for tide, non-tide residual (NTR, i.e., storm surge and other sea level enhancements such as El Niño, but excluding wave run-up) and wave run-up, and monthly extreme value analysis (Chadwick *et al.*, 2011). The closure depth was estimated from the method of Hallermeier (1978, 1981) using the 10-year return-period significant wave height (H_s) and associated wave period (T_p) from the same 100-year sea level projections.

While the extent of the active profile by this definition exceeds the range of influence for the typical summer wave climate, conceptually, the 10-year return period was chosen to represent a moderately high total water level condition that occurred frequently enough to be influential over the modeled time period of interest (100 years). Conditions corresponding to other appropriate return periods can be modeled, or a number of randomly sequenced conditions could be constructed to more realistically mimic nature. The choice of the 10-year return period total water level scenario for the upper limit, and the 10-year return period H_s for the closure depth was sufficient to illustrate the methodology. In any case, additional research on defining the most appropriate limits would be useful since the choice has implications for the estimation of future beach widths and erosion rates.

The upper and lower active beach profile boundaries were estimated as the 10-year total water level and closure depth, respectively. The 10-year total water was estimated using joint probability statistics for tide, non-tide residual (NTR, i.e. storm surge and other sea level enhancements such as El Niño, but excluding wave run-up) and wave run-up, and monthly extreme value analysis. The closure depth was estimated using significant wave height (H_s) and peak period (T_p) projections and the method of Hallermeier (1978; 1981).

Future Sea Level Scenarios

The future sea level scenarios describe in Section 3.1 were used to drive the CSPEM model.

Transect Profiles

Cross-shore transects, defined at 100 m intervals alongshore correspond to the CDIP MOP System locations (http://cdip.ucsd.edu/documents/index/product_docs/mops/mop_intro.html). Initial transect profiles were extracted from a digital basemap constructed from Army Corp of Engineers LiDAR data, bathymetry from the U.S. Geological Survey, and beach profile measured at eight monitoring transects. Water surface returns were removed from the LiDAR data and data gaps were interpolated using the measured beach profiles to provide a seamless bathymetric-topographic basemap.

Beach, cliff, and cliff top portions of the profile were manually interpreted and digitized from the extracted profiles. The initial cliff base location was estimated by extending the average cliff slope to current mean sea level. Average cliff slope was calculated for each transect between the manually selected cliff top and beach-cliff intersection.

External Sand Deficit and Supply Scenarios

In addition to a zero external sand deficit scenario, an additional sand deficit/supply scenario was established according to the historical sand budget analysis at NBC undertaken by Inman and Masters (1991) and described above. The external sand deficit was estimated as the beach change sand deficit minus the anthropogenic input. Normalized alongshore, the early (1950-1978) and late (1983–1990) period annual deficits were comparable, ranging from about 6.6 m³/m/yr at the south end of the cell, to 0 m³/m/yr at the north end (Zuniga Jetty). These two external deficit scenarios provide a possible range of future sand budgets and were run for each MSLR scenario.

Testing the Summer EDry Fully Accreted Profile Hypothesis

Sea level rise has been small over the ~ 30 years of measured beach profiles (Bromirski *et al.* 2011), so it is not possible to validate this aspect of shoreline change model. Nevertheless, if the FPA is a reasonable description of true summer—dry season beach behavior, a near-shore section of a beach's September—October profiles should exhibit a ~ fixed fully accreted equilibrium shape relative to the MWL. The profile should return to approximately the same shape and volume relative to the shoreline location at the end of each dry season, within the bounds of expected profile measurement uncertainties, regardless of changes in the absolute shoreline location or total cross shore sand volume.

More specifically, fixed z limits should be able to be chosen where the resulting inverse mean slope, $\Delta x/\Delta z$, remains ~ constant in the end-of-dry-season profiles over many years. Some historical survey locations (e.g., Del Mar) have exhibited significant changes in end-of-dry-season shoreline location in recent decades, while others have not. These observed differences should be consistent with, and explained by, the local sand volume term in Equation 3-8.

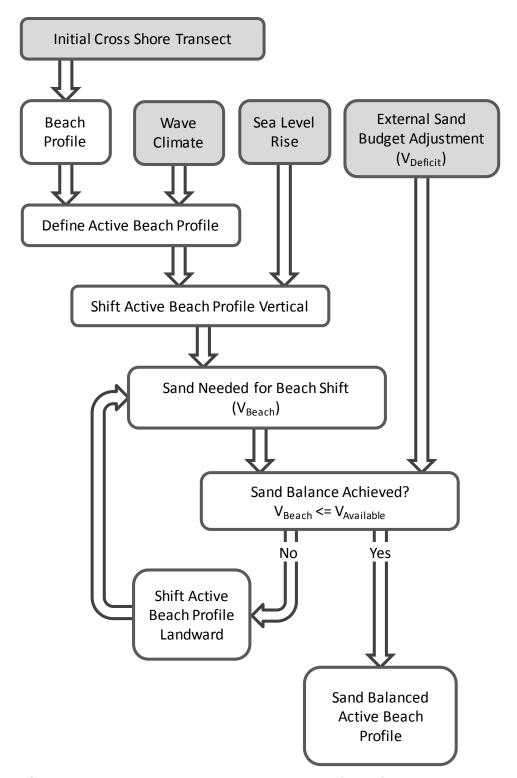


Figure 3-51. Schematic flow chart of the implementation of the Cross-Shore Profile Equilibrium Model.

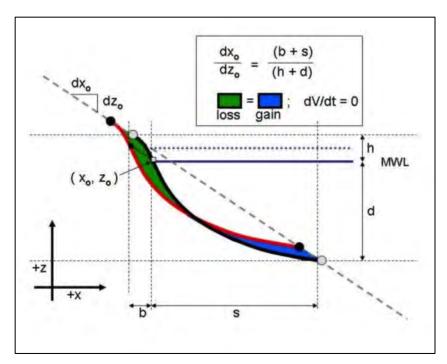


Figure 3-52. The theoretical volume conserving shoreline migration path with sea level rise is along the mean slope of the fully accreted equilibrium profile.

General Implications for Shoreline Evolution with Sea Level Rise and Sand Supply Loss

The relationships derived from the CSPEM model provide insight into expected response of Southwest U.S. exposed beach shorelines. For example, using typical cross shore beach profiles in San Diego County (Equation 3-10) $\Delta x/\Delta z \sim 1000$ m/10 m ~ 100 , a 100% sandy shoreline profile would migrate ~ 10 m landward for every 0.1m in mean sea level rise. For similar (Equation 3-9) $1/(h+d) \sim 1/10$ m ~ 0.1 , a 100% sandy shoreline profile would migrate ~ 10 -m landward for every $100\text{m}^3/\text{m}$ of near-shore sand volume loss owing to reduced sand supply from streams or bluffs, or offshore transport beyond z=-d during extreme storms. Shorelines with steeper equilibrium profiles (e.g. coarser sand sizes) have smaller $\Delta x/\Delta z$ ratios and will migrate more slowly with sea level rise (Equation 3-10). Shorelines with larger tide ranges (larger h), finer sediments (larger d), and/or more energetic summer beach building swells (larger d), have smaller values of 1/(h+d), and will migrate more slowly for a given change in nearshore sand volume (Equation 3-9).

Long-Term Beach Retreat

Using the CSPEM methodology and the constraints described above, we evaluated the long-term beach system response and developed erosion footprints for the beach system at NBC. The method was also used at the beach areas at MCBCP that were not backed by cliffs. The results spanned the target range of sea level rise as well as variations in the external sand deficit and supply. Sensitivity was evaluated for modeling assumptions, in particular assumptions regarding the extent of the active beach profile. Erosion footprints were developed for snapshots along the 2 m SLR curve that correspond to sea level increases of 0.5, 1.0, 1.5, and 2.0 m, and timeframes of 2046, 2069, 2087, and 2100. These cases are referred to as the "first occurrence" conditions because they represent the earliest time that these sea level values would occur based on the assumed range of sea levels used in the study. Example runs are shown in Figure 3-53 showing the comparison of beach retreat along the 2m sea level rise trajectory for conditions with and without sand budget deficits. The footprints were developed using the sand deficit estimates from Inman and Masters (1991) as the most conservative

assumption. The footprint for each condition is represented by a polygon which spans alongshore the entire active shoreline of NBC, and spans cross shore between the baseline (year 2000) shoreline position and the shoreline position for the snapshot time of interest. Results for the beach system response, and the resulting erosion footprints are presented Section 4.3.1.

3.3.2 Exposed Cliff/Beach Shoreline Erosion – Long-Term Response

Methods development for exposed cliff/beach systems focused on a unique Conditionally Decoupled Profile Model (CDPM) to simulate long-term shoreline response related to sea level rise at MCBCP. In addition, we evaluated short-term response of the beaches to variability in wave climate, through the use of an equilibrium model (YGOR model) that was superimposed on the long-term response. Thus the erosion pathway was evaluated as a function of the combined long- and short-term responses. Inundation and flooding were evaluated by creating new elevation models that represented the simulated long-term shoreline response at certain time snapshots corresponding to the specified sea level conditions. At these snapshots, spatially-varying hydraulic connectivity analysis was performed to assess potential inundation and flood footprints. In this case, inundation was defined based on events with short return periods (days – months) while flooding was defined as events with longer return periods (year – century).

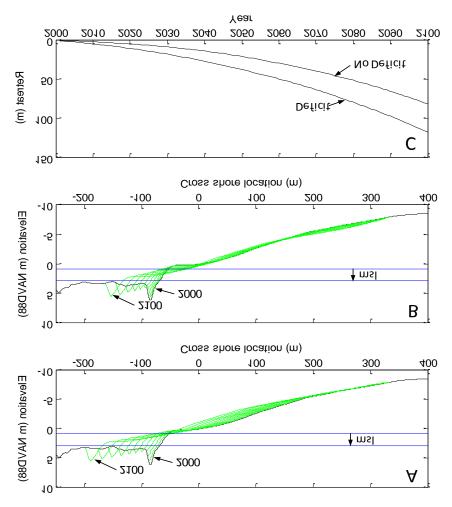


Figure 3-53. Example of beach profile adjustments and (a and b), and beach retreat (c) for a 100-year simulation with 2-m MSLR.Profiles in (a) include the sand budget deficit, while profiles in (b) assume zero deficit and retreat driven only by sea level rise.

Previous Cliff Models

Coastal recession associated with MSLR is often estimated using the Bruun Rule (Bruun 1962), which applied concepts of equilibrium profile and volume conservation originally designed for low-lying, sandy coasts. The original Bruun (1962) method assumed a fixed active beach profile during coastal recession, homogeneous coastal material, and no external sand sources or sinks. Although widely applied (*i.e.*, Zhang *et al.*, 2004), the underlying assumptions are often neglected or not satisfied, prompting much, somewhat misdirected, criticism (*i.e.*, Dubois, 1992; Cooper and Pilkey, 2004; Woodruffe and Murray-Wallace, 2012).

Cliffed coasts rarely (if ever) satisfy the original Bruun rule assumptions, leading to the use of modifications including heterogeneous coastal material, external sand sources and sinks, and variable inland topography (Dean and Maurmeyer, 1983; Hands, 1983; Dean, 1991; Bray and Hooke, 1997; Wolinsky and Murray, 2009). The combined modifications can be represented by Equation 3-12, which is illustrated in Figure 3-54.

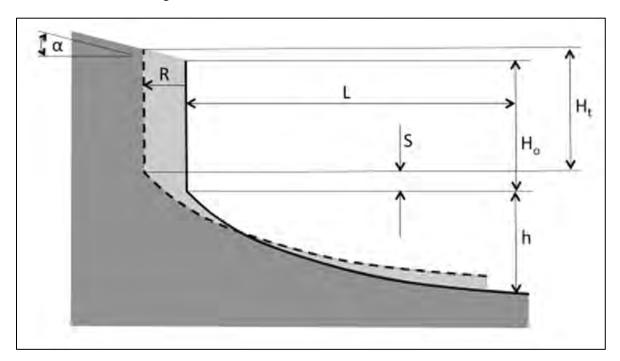


Figure 3-54. General geometric parameters of sand balance models.

Equation 3-12

$$R = \frac{SL - G}{P(\overline{H} + h)},$$

where R represents cliff retreat, S is the amount of MSLR, L is the length of active profile, G denotes the external sand surplus or deficit volume per unit length of coast, P is the fraction of coarse sand in the eroding cliff, \overline{H} is the average cliff height over the retreat distance, and h represents the closure depth.

For constant cliff-top inland slope α (positive for increasing inland elevation):

Equation 3-13

$$\overline{H} = H_o + \frac{R \tan \alpha - S}{2},$$

where H_o represents the initial cliff-edge height.

For constant non-zero inland slopes, the average cliff height (\overline{H}) is dependent on the retreat distance. Combining Equation 3-12 and Equation 3-13 yields a quadratic solution for the cliff retreat (Equation 3-14).

Equation 3-14

$$R = \frac{H_o - \frac{S}{2} + h + \sqrt{\left(H_o - \frac{S}{2} + h\right)^2 + 2\tan\alpha\left(\frac{SL - G}{P}\right)}}{\tan\alpha}$$

If the inland slope is zero, then \overline{H} is independent of retreat distance and combining Equation 3-12 and Equation 3-13 yields Equation 3-15.

Equation 3-15

$$R = \frac{SL - G}{P\left(H_o + \frac{S}{2} + h\right)}.$$

Other simple methods for estimating cliff retreat include historical extrapolation (National Research Council, 1987; Leatherman, 1990), a simplified Sunamura (1988) shore platform geometric model for cliffs without a dissipative beach (Bray and Hooke, 1997), and a simplified numerical model (SCAPE) equation for low sand-volume beaches (Walkden and Dickson, 2008). These models follow the general geometrical form of Equation 3-16 (Ashton, Walkden, and Dickson, 2011), where the exponent

m = 0 for no response (*i.e.*, retreat independent of MSLR); m = 1 for basic historical extrapolation, Bruun Rule or modified Bruun Rule models, and Sunamara's simplified platform model (Bray and Hooke, 1997); and 0 < m < 1 for simplified SCAPE (m = 0.5, Walkden and Dickson, 2008), and Sunamura's (1988) original platform model (Ashton, Walkden, and Dickson, 2011).

Equation 3-16

$$R_2 = R_1 \left(\frac{S_s}{S_1} \right)^m,$$

where *R1*, *R2* represent past and future cliff retreat, and *S1*, *S2* are past and future MSLR, respectively. Bray and Hooke (1997), Dickson *et al.* (2007), Dar and Dar (2009), and Brooks and Spencer (2012) provide applications and comparisons of these and other models.

Here, we build upon the Bruun Rule modifications, recent equilibrium profile cliff modeling (Wolinsky and Murray, 2009; Ashton, Walkden, and Dickson, 2011), and established rock coast

homogeneous coastal material, and no external sediment sources or sinks. Although commonly applied (i.e., Zhang et al., 2004), the Bruun rule assumptions are often ignored or not satisfied, prompting much criticism (i.e. Cooper and Pilkey, 2004; Pilkey and Cooper, 2004). Coastal settings rarely (if ever) satisfy the original Bruun rule assumptions, leading to the use of modifications including heterogeneous coastal material, external sediment sources and sinks, and variable inland topography (Dean and Maurmeyer, 1983; Hands, 1983; Dean, 1991; Bray and Hooke, 1997; Wolinsky and Murray, 2009). Alternatively, Revell et al. (2011) developed a downscaled model that predicts shoreline retreat at 500-m intervals based on total maximum water levels, which are assumed to be proportional to shoreline retreat, however, no sand budget balance was utilized. Here, we build upon the Bruun rule modifications, recent equilibrium modeling (Wolinsky and Murray, 2009; Ashton, Walkden, and Dickson, 2011), and established coastal concepts to provide estimates of retreat based on coastal system sediment balance and process based relationships for coasts where sedimentbalance is important.

Methods development for exposed beach systems focused on a Cross-Shore Profile Equilibrium Model (CSPEM) to simulate long-term shoreline response related to sea level rise at NBC and the areas of MCBCP without cliffs. In addition, we evaluated short-term response of the beaches to variability in wave climate, through the use of an equilibrium model (YGOR model, Yates *et al.* 2009) that was superimposed on the long-term response. Thus the erosion pathway was evaluated as a function of the combined long- and short-term responses. Inundation and flooding for exposed beaches were evaluated by creating new elevation models that represented the simulated long-term shoreline response at certain time snapshots corresponding to the specified sea level conditions. At these snapshots, spatially-varying hydraulic connectivity analysis was performed to assess potential inundation and flood footprints. In this case, inundation was defined based on events with short return periods (days – months) while flooding was defined as events with longer return periods (year – century).

The long-term exposed beach response model relied on cross-shore profile equilibrium theory and the highly correlated and seasonal nature of wave- and rain-induced shoreline erosion and near-shore sand deposition events in a summer—dry climate. It was assumed (and supported by historical observations) that at the end of the mild summer—dry season (September—October) a near-shore portion of a sandy beach's cross-shore profile always returns to the same fixed, fully accreted equilibrium shape, relative to the mean water level (MWL), but the cross-shore location of this profile segment varies depending on the MWL elevation and local near-shore sand supply. The fixed shape of this fully accreted profile (PFA) is a function of the near-shore sand size distribution and the average summer—dry season wave climate, both of which were assumed to vary more slowly on long time scales than changes in MWL and the local sand supply. On inter-annual time scales, the PFA migrates in the vertical and cross-shore directions as a combined function of 1) changes in MWL and 2) winter-wet season changes in the cross-shore volume of sand available to build the PFA at the beginning of the next summer—dry wave season.

The Fully Accreted Equilibrium Profile

The PFA (shown schematically in Figure 3-49) is a fixed shape in the vertical (z) and cross-shore (x) directions, and its position within the overall cross-shore profile, z(x), was defined relative to the intersection of P_{FA} with the MWL shoreline location (x_0, z_0) at the end of the summer–dry season.

Equation 3-4

$$z(x) = z_O + P_{EA}(x - x_O - b)$$
; for $x = (x_O - b) \rightarrow (x_O + s)$

Conceptually, the 10-year return period was chosen to represent a moderately high total water level condition that occurred frequently enough to be influential over the modeled time period of interest (100 years). Conditions corresponding to other appropriate return periods can be modeled, or a number of randomly sequenced conditions could be constructed to more realistically mimic nature. The choice of the 10-year return period total water level scenario for the upper limit, and the 10-year return period H_s for the closure depth is sufficient to illustrate the methodology. In any case, additional research on defining the most appropriate limits would be useful since the choice has implications for the estimation of future beach widths and erosion rates.

The upper and lower active beach profile boundaries were estimated as the 10-year total water level and closure depth, respectively. The 10-year total water was estimated using joint probability statistics for tide, non-tide residual (NTR, i.e., storm surge and other sea level enhancements such as El Niño, but excluding wave run-up) and wave run-up, and monthly extreme value analysis. The closure depth was estimated using significant wave height (H_s) and peak period (T_p) projections and the method of Hallermeier (1978, 1981).

Choosing the 10-year return period total water level scenario was somewhat arbitrary but does lay (logarithmically) half-way between the annual and century return periods. It is also sufficient to illustrate the methodology, which was the primary purpose of the SERDP-funded project. Conditions corresponding to other appropriate return periods can be modeled, or a number of randomly sequenced conditions could be constructed to more realistically mimic nature.

Beach and Cliff Profile Adjustments

Partially decoupling the active beach and cliff profiles allows the beach and cliff to retreat at different initial rates. Typical profile adjustments (Figure 3-57a) illustrate that the initial beach landward shifts can obtain beach profile sand balance without marine-driven cliff erosion, which is qualitatively realistic. During this time, the back-beach buffer width decreases and only subaerial processes cause cliff erosion (Figure 3-57b), which occurs on the exposed cliff face, the terrace surface and from gullying (Figure 3-57a). Only when the beach buffer width is reduced to zero do waves begin to erode the cliff base. For simplicity, all the overlying material is assumed to fail at once, thus generally maintaining the initial cliff face profile. In the CDPM, wave-driven cliff retreat occurs at the same rate as the beach retreat, the two being re-coupled during that time. Similar to other modified Bruun Rule models, the cliff base-back beach intersection notch shifts vertically by the MSLR.

Subaerial Erosion

Subaerial gully and cliff erosion processes were assessed using a coastal section within MCBCP that was not exposed to MSLR or wave action from at least 2002–2009. Sea level has not risen along much of the eastern Pacific Rim and all of southern California since about 1980 when changes in large-scale wind stress patterns began to offset global MSLR (Bromirski *et al.*, 2011, 2012). Total water level run-up analysis (Young *et al.*, 2009) and a review of oblique photos from the California Coastal Records Project (http://www.californiacoastline.org/) show no evidence of wave-induced cliff erosion, beach change at the cliff base, or indications of cliff-wave impact for this time period.

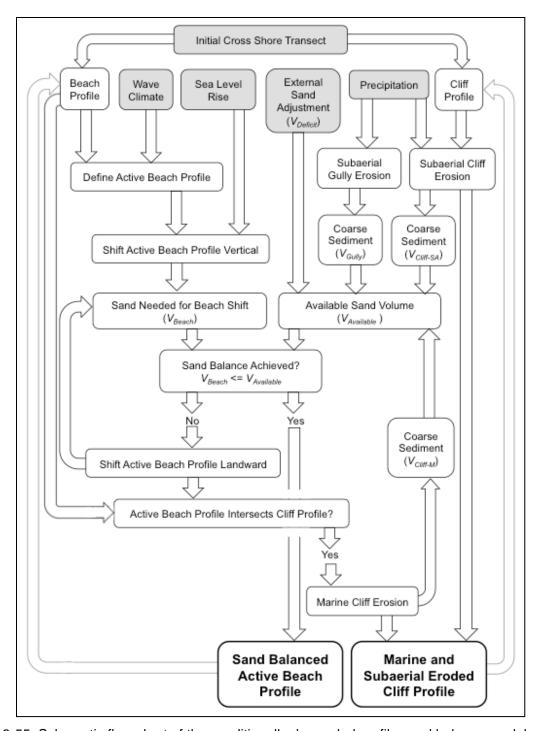


Figure 3-55. Schematic flow chart of the conditionally decoupled profile sand balance model.

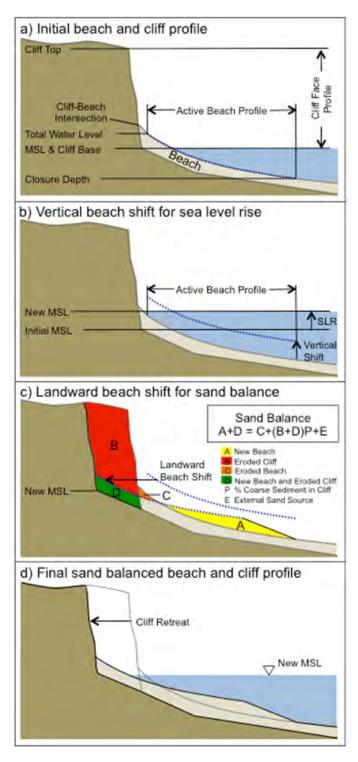


Figure 3-56. Model profile adjustments considering sea level rise. (a) Initial profile and active beach bounded by total water level and closure depth. The active beach profile shifts (b) vertically equal to the amount of sea level rise and (c) landward to obtain (d) sand balance.

Some back-beach topography changes did occur where talus was deposited on the beach at the cliff base, or where gullies intersected the cliff line and washed out onto the beach. However, these changes are not wave related, and it appears a relatively wide and elevated beach prevented waves from reaching the cliffs during that period. For these reasons, the only sediments contributed to the beach over this interval were derived from subaerial cliff face or terrace erosion, which was mainly in the form of gullying. A time series of seasonal LiDAR data available during this time permits change detection, estimation of subaerial eroded volumes, and derivation of a process-based relationship driven by local precipitation. The amount of subaerial sediment supply to the beach was adjusted for coarse sand content of the source material (Young *et al.*, 2010b).

Topographic Change Detection

Airborne LiDAR data collected each spring and fall from May 2002 through March 2009 through the Southern California Beach Processes Study (http://cdip.ucsd.edu/SCBPS/) were utilized for topographic change detection. SCBPS used an Optech Inc. Airborne Laser Terrain Mapper 1225 that made approximately four passes at an altitude of 300-1100 m during each survey. Typical survey swath extent varied from the near-shore and beach area to 250- to 500-m inland.

LiDAR data were processed into 0.5-m resolution digital elevation models using the second of two LiDAR returns (the last return is the most representative of the ground surface) and a modified "natural neighbors" technique, which removes over-vertical features and maintains vertical cliff edges and complex topography (Young *et al.*, 2011). The large majority of the cliffs lack the material strength required to maintain over-vertical features. However, localized areas of sea caves and notches may temporarily exist.

A time series of topographic change for 14 time intervals from May 2002-September 2008 were obtained by differencing successive digital elevation maps to create digital change grids, shows erosion (negative changes) and accretion (positive changes) at talus deposits (Figure 3-58). The net change (sum of positive and negative changes) is the material volume removed. The digital change grids were filtered and edited to remove noise and erroneous data.

Cliff and Gully Delineation

Coastal cliff and gully erosion result from different processes and were demarcated for analysis. Coastal cliffs fronted by beaches are potentially exposed to wave action, whereas gullies and coastal canyons are generally not exposed to wave action and erode through subaerial processes. At some locations, the boundary between cliffs and gullies is ambiguous and was delineated with respect to potential wave induced erosion and the existing topography.

Erosion and Precipitation Relationship

Subaerial gully and cliff erosion occurred seasonally with larger amounts of erosion during the winter intervals corresponding to elevated amounts of precipitation. Total eroded gully volumes were doubled to account for the area of coastal gullies not adequately covered by the LiDAR data. Both subaerial gully and cliff erosion totals were averaged alongshore and correlated with observed cumulative interval rainfall to establish precipitation-driven subaerial relationships (Figure 3-59). The model was run using Bias-Correction and Constructed Analogs (BCCA) downscaled daily rainfall (Figure 3-60) for the NCAR CCSM3 A2 scenario (Maurer *et al.*, 2010).

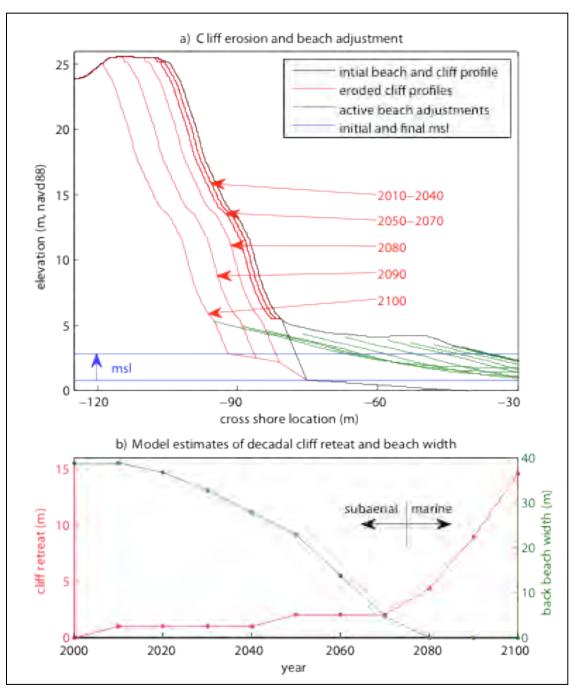


Figure 3-57. Example of decadal (a) active beach and cliff profile adjustments and (b) cliff retreat and back beach width for a 100-year simulation with 2-m MSLR.In this example, initial cliff erosion is exclusively subaerial and then becomes marine-dominated toward the end of the simulation.

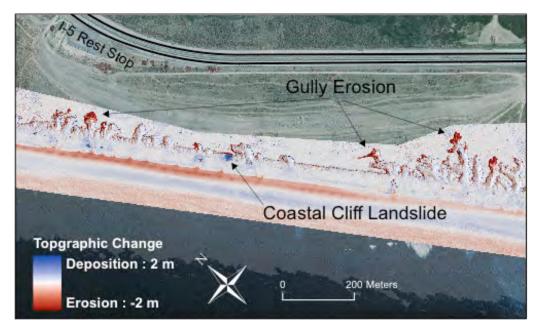


Figure 3-58. Cliff and gully airborne LiDAR change detection, May 2002–March 2009, southern MCBCP.

Future Sea Level Scenarios

The future sea level scenarios describe in Section 3.1 were used to drive the CDPM model.

Transect Profiles

Cross-shore transects, defined at 100 m intervals alongshore correspond to the CDIP MOP system locations (http://cdip.ucsd.edu/documents/index/product_docs/mops/mop_intro.html). Initial transect profiles were extracted from a digital basemap constructed from Army Corp of Engineers LiDAR data, bathymetry from the U.S. Geological Survey, and beach profile measured at eight monitoring transects. Water surface returns were removed from the LiDAR data and data gaps were interpolated using the measured beach profiles to provide a seamless bathymetric-topographic basemap.

Beach, cliff, and cliff top portions of the profile were manually interpreted and digitized from the extracted profiles. The initial cliff base location was estimated by extending the average cliff slope to current mean sea level. Average cliff slope was calculated for each transect between the manually selected cliff top and beach-cliff intersection.

External Sand Deficit and Supply Scenarios

In addition to a zero external sand deficit scenario, two additional sand deficit/supply scenarios were established according to the historical sand budget analysis at MCBCP undertaken by Inman and Masters (1991) and described above. The external sand deficit was estimated as the beach change sand deficit minus the anthropogenic input, and cliff/gully sand yield. Normalized alongshore, in the early (1960–1978) and late (1983-1990) periods, the annual deficit was 15 and -0.37 m³/m/yr, respectively. These three external deficit/supply scenarios provide a possible range of future sand budgets and were run for each MSLR scenario.

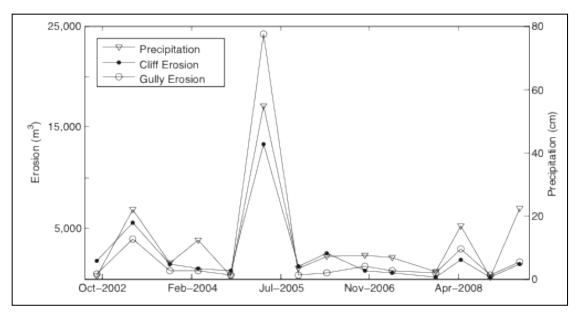


Figure 3-59. Subaerial eroded cliff and gully sand volumes and interval precipitation, southern MCBCP.

Long-Term Cliff/Beach Retreat

Using the CDPM methodology and the constraints described above, we evaluated the long-term cliff/beach system response and developed erosion footprints for the cliff/beach system at MCBCP. The results spanned the target range of sea level rise as well as variations in the external sand deficit and supply. Sensitivity was evaluated for modeling assumptions, in particular assumptions regarding the extent of the active beach profile. Erosion footprints were developed for snapshots along the 2 m SLR curve that correspond to sea level increases of 0.5, 1.0, 1.5, and 2.0 m, and timeframes of 2046, 2069, 2087, and 2100. These cases are referred to as the "first occurrence" conditions because they represent the earliest time that these sea level values would occur based on the assumed range of sea levels used in the study. The footprints were developed using the 15 m³/m/yr sand deficit as the most conservative assumption. The footprint for each condition is represented by a polygon which spans alongshore the entire active shoreline of MCBCP, and spans cross shore between the baseline (year 2000) shoreline position and the shoreline position for the snapshot time of interest. Results for the cliff/beach system response, and the resulting erosion footprints are presented in Section 4.3.1.

3.3.3 Exposed Beach Erosion - Short-Term Response

Short-term changes in shoreline position, or beach width, are those driven directly by wave forces that move sand mainly in the cross-shore direction. These are most pronounced on the time scale of wave storms (*i.e.*, a few days to several weeks), and with seasonal changes in wave energy. In the present study we adopted the equilibrium model published by Yates *et al.* (2009), which we refer to as "YGOR" after the authors. It was developed using data from Torrey Pines Beach in San Diego, California, and applied at MCBCP and San Onofre, among others. It is therefore deemed suitable for wave conditions at MCBCP and NBC.

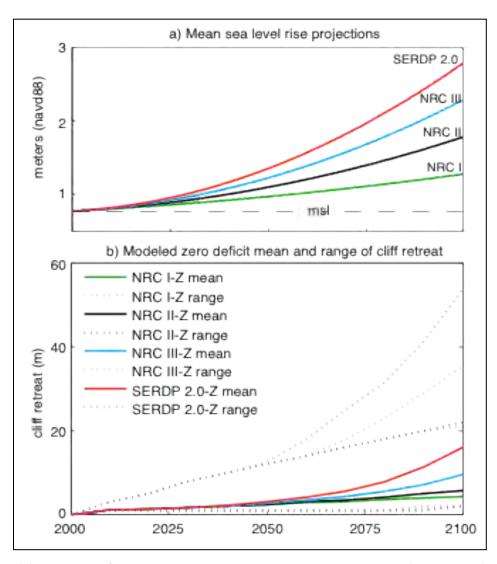


Figure 3-60. (a) The four MSLR curves considered in this study and current (1983–2001) MSL elevation. (b) Modeled mean and range of cliff retreat versus time for the zero deficit and four MSLR scenarios.

The model is based on the concept that any beach will reach an equilibrium configuration with respect to shoreline position and profile shape that depends on the wave conditions and other factors such as sand availability and grain size (Dean, 1977; Larson and Kraus, 1989; Inman *et al.*, 1993; Dean, 1991; Dubois, 1990; Kriebel and Dean, 1993; and Miller and Dean, 2004). This hypothesis has two parts: first, that a beach subject to steady wave conditions will evolve to and remain at a unique equilibrium configuration, and second, that the rate of change is proportional to both the wave energy and the wave energy dis-equilibrium. This implies that a beach wider than its equilibrium width will erode faster than the same beach narrower than equilibrium, even for the same wave energy. The sole condition addressed in the YGOR model is shoreline position (at MSL elevation) relative to the equilibrium. In essence, the model exploits the observation-based expectation that a beach will retreat (advance) faster as the wave energy increases (decreases) and also faster (slower) if it is initially wider (narrower) than its equilibrium width.

Defining the wave energy as $E=(\frac{1}{4}\,H_S)^2$ where H_S is the significant wave height and assuming that an equilibrium shoreline position S exists for any equilibrium energy E_Q such that $E_Q=aS+b$, where a and b are constants to be determined. If the departure of wave energy from equilibrium is defined as $\Delta E=E-E_Q$, then $\Delta E>0$ if the waves are larger than equilibrium (erosion) and $\Delta E<0$ if they are smaller (accretion). YGOR further assumes that the rate of change in shoreline position $dS/dt=C^\pm E^{1/2}\Delta E$, where C^+ and C^- are constants that apply if $\Delta E<0$ or $\Delta E>0$, respectively. This assumption is based on the general ideas outlined above, and some trials using different wave energy formulations by Yates et~al.~(2009). It is important to realize that essentially no physics underlies the formulation. Nevertheless, with this formulation the shoreline position S at any time can then be computed iteratively from the position S_0 at an earlier time using $S=S_0+\Delta S$, where $\Delta S=\int C^\pm E^{1/2}\Delta E~dt$ is based only on the given function of wave energy integrated over the interval.

Yates *et al.* (2009) utilized five-years of hourly near-shore wave measurements and weekly or monthly shoreline position surveys at Torrey Pines Beach to develop and calibrate the model. They found that calibration could be successful with as little as two years of monthly observations or with five years of ideally-timed semi-annual observations. More critical were the continuity of wave observations (or reconstructions), which must resolve individual storms in their erosion phases and during the subsequent recovery. Yates *et al.* (2009) used the first two years of the Torrey Pines Beach observations to "train" the model by determining the four free parameter coefficients (a, b, C^+ , and C^-) using complicated "simulated annealing" (Barth and Wunsch, 1990) and "surrogate management framework" (Booker *et al.*, 1999; Marsden *et al.*, 2004) methods. RMS fits were typically about 3 m. Yates *et al.* (2009) tabulated the range of values of the free parameters for various beaches. They then compared the model "predictions" to the observations for the remaining three years of their data set with surprisingly good results and RMS fits ranging up to about 5 m.

Nevertheless, YGOR model shortcomings are numerous. The most serious is that it is purely empirical with no actual physical basis underlying either the assumed relationship between wave energy and shoreline change, or the apparent relationship between the four constants and beach slope and sand grain size.

In its present form, the model also seems to overestimate the erosion from large wave storms. Part of the problem here is that the formulation was developed without the benefit of beach change data documenting peak erosion conditions during truly severe storm events such as those of the 1982-1983 El Niño winter. Furthermore, some crucial physical constraints and variables are neglected in the model, including: the presence of any underlying bedrock shore platform, which would limit the short-term "beach" erosion once all the overlying sand is gone; long-term erosion (accretion) of shoreline position due to sand shortages (surpluses), and; wave-driven, topographic, or structure-induced gradients in longshore sand transport rate where divergence (convergence) causes erosion (accretion). Research efforts are currently underway to address these shortcomings.

In the present study, we did not implement the free parameter computation methods, but instead started with the Yates *et al.* (2009) parameter values and adjusted them *ad hoc* to fit our six-hour interval wave hindcasts to the available beach width observations. A sample of results is shown in Figure 3-61 for Coronado City Beach (Range SS0160) where the RMS difference between model and observations is about 8 m over the nearly 30-year period from 1983–2010. Much of the model-data difference arises from the later (2003–2010) downward trend in shoreline position likely as a result of sand supply shortages not modeled by YGOR. Errors also arise from the aforementioned tendency to overestimate erosion from large wave events, as illustrated during 1986–1987 and 1997–1998 in Figure 3-61. As indicated, no beach measurements are available from the 1982–1983

winter during which visual observations and anecdotal evidence suggested that beach retreat was severe (NAS 1984). Even when data from severe winters exists, the timing of beach measurements rarely if ever coincides with the maximum erosion simply because of the difficulty of measuring beach condition during a storm. Both the model and anecdotal evidence suggests that beach width recovery is rapid once storm wave energy decreases. The post-storm measurements then occur while the beach is building rapidly, as suggested by the data shown in Figure 3-61 from the 1986–1987 and 1997–1998 events.

All in all, the results were deemed satisfactory, first of all because of the acceptable fit, and second perhaps more importantly, by the fact that the model remained stable over the 30-year calculation that comprised 43,832 six-hour iterations. The YGOR model had never before been run for this long (although five years of one-hour data produces the same number of iterations).

Success in modeling the moderately long observed shoreline changes using hindcast wave data led to confidence in being able to model short-term change driven by the 100-year, six-hour interval wave projections available for this study. The results are plotted in Figure 3-62, which contains five illustrative shoreline change (beach width) projections (upper), and a wave energy projection (lower) for 2000–2100. The uppermost (pink) line shows short-term beach width change from wave forcing alone using the YGOR model as outlined above. The green, black, turquoise, and red curves respectively indicate the sum of the short-term fluctuations and simplified estimates of sea level rise-driven shoreline retreat for the 0.5-, 1.0-, 1.5-, and 2.0-m MSLR by 2100 scenarios specified in this project.

As an example of the method, MSLR beach change projections were calculated from a simplified version of the Bruun Rule (1962), which can be reduced to $R = MSLR/\tan \beta$, where β is the overall beach slope. The curves in Figure 3-62 are based on an assumed slope of 0.025 (40:1), which result in total beach losses of 20, 40, 60, and 80 m for the 0.5, 1.0, 1.5, and 2.0 m by 2100 MSLR scenarios, respectively. These preliminary calculations were meant to be illustrative while actual assessments of erosion footprints were addresses using the integration of this short-term method with the long-term CSPEM and CDPM models described above, and those results are presented in Section 4.3.1.

3.3.4 Exposed Shorelines - Modification of Terrain Models

Elevation models for future sea level scenarios were developed based on results from the long-term shoreline response models described above. These models were constructed by creating new shallow water, beach and cliff surfaces from the modified profiles generated at each coastal MOP station. These surfaces were then inserted into the baseline elevation model to create elevation models representing the future scenarios. A new model was constructed for each target sea level condition (0.5, 1.0, 1.5, and 2.0 m). To illustrate the methodology we utilized the "first occurrence" of these conditions along the 2.0-m sea level rise curve which corresponded to time snapshots for the years 2046, 2069, 2087, and 2100, respectively see Figure 3-63).

3.3.5 Exposed Shorelines – Inundation and Flooding

New methods were developed for the evaluation of inundation and flooding along exposed shorelines that incorporated changes to the underlying elevation model due to erosion, spatially varying total water level exposures, and requirements for complete hydraulic connectivity. The shoreline change modeling described above for beach systems and cliff/beach systems was utilized to develop new shoreline profiles along the coast of both installations for the range of future sea level scenarios. These profiles were then interpolated and masked to create a new shoreline surface for each scenario that was inserted into the original elevation model to create a new elevation model for the future scenario as described above in Section 3.2.1. Total water levels at each coastal station

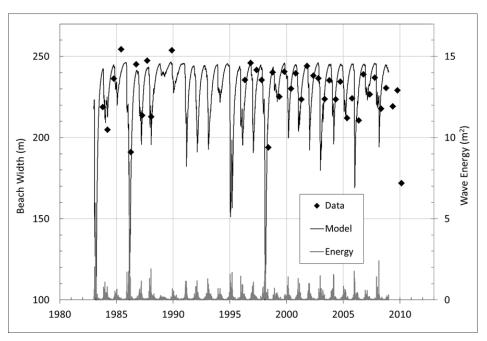


Figure 3-61. Beach width (shoreline position) comparison for the YGOR model and beach data (top, left scale), and wave energy derived from hindcasts (bottom, right scale) at Coronado City Beach, Range SS0160.

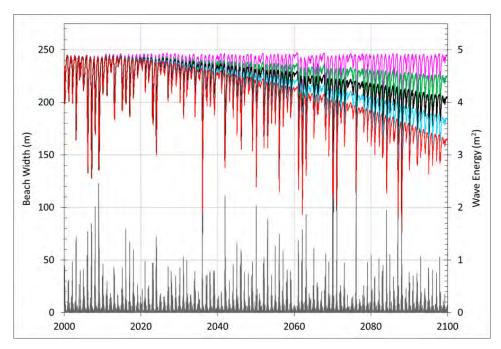


Figure 3-62. Projected future short-term wave driven beach change (upper, pink), and wave plus MSLR-driven beach retreat for the specified scenarios (upper, green, black, turquoise, red), and projected wave energy (lower, grey).

associated with a range of different return periods were then applied to using a hydraulic connectivity algorithm to simulate inundation and flooding. A method was developed using a sliding window of adjustable longshore scale to allow for a reasonable degree of lateral flooding along the upland topography.

Inundation and Flooding Scenarios

Inundation and flooding were examined across a continuum of total water levels defined through combined variations in sea level rise and return period total water level events. These scenarios spanned five sea level rise conditions from 0 to 2 m, and five return periods (week, month, year, decade, century) for a total of 25 scenarios at each MOP station for each installation. The development of these scenarios is detailed in Section 3.1, and the results are presented in Section 4.1. In the context of this project, we defined inundation as a process that leads to the frequent (weekmonth return) exposure of coastal areas to wetting, while flooding was considered to represent infrequent to rare events with long return periods (year—century). While the distinction is academic from the standpoint of how our methodology was applied, it had implications for interpreting the impacts to the installations since both the magnitude and frequency of the events can be important in terms of effects to infrastructure and operations.

Shoreline Segmentation

The shoreline change analysis and scenario development methods described above provide a relatively high-resolution definition of future shoreline conditions and water levels. The results are aligned onto MOP stations with a long-shore spacing of about 100 m. If the water levels associated with these scenarios are applied with hydraulic connectivity analysis to individual MOP-bounded segments, the resulting flood maps take on an un-natural segmented characteristic based on the MOP segment boundaries which limit lateral movement of water. If this constraint is completely relaxed, then the entire study area takes on the water level of the highest segment.

To provide a balance between maintaining a degree of spatial variation in the total water levels, and allowing for lateral connectivity between segments, we experimented with a range of folding scales for segment connectivity. The folding scale was increased until the choppiness between segments was no longer detectable visually, and the area of the wetted footprint approached a stable value. For NBC the final folding scale utilized 29 segments, while at MCBCP the final scale was 35 segments. While still somewhat qualitative, this method produced results that did appear to balance the factors described above, and seems to be an improvement over previous methods that either apply a single water level over the entire domain, or only within a localized segment.

Hydraulic Connectivity Analysis

Using the folding scale described above, inundation and flooding were simulated using standard hydraulic connectivity analysis with flood-fill algorithms. The seed location for the analysis was defined within the bounding ocean area of the central segment. The fill was constrained laterally to within the central segment and segments within +/- the folding scale on each side. For NBC, the fill for the exposed shorelines was further constrained by a mask file that excluded connectivity within San Diego Bay. The purpose of this mask was to prevent the bay from "filling" to the water level of the exposed shorelines which would result in unexposed shorelines within the bay being subjected to exposed shoreline total water level scenarios. The two-dimensional flood-fill was carried out with an 8-connected neighborhood connectivity for each grid cell in the elevation model. The resulting raster maps defined the water level in all hydraulically connected areas of the installation for each total water level scenario. Results for the application of this methodology are shown in Section 4.3.1.

To provide a balance between maintaining a degree of spatial variation in the total water levels, and allowing for lateral connectivity between segments, we experimented with a range of folding scales for segment connectivity. The folding scale was increased until the choppiness between segments was no longer detectable visually, and the area of the wetted footprint approached a stable value. For NBC the final folding scale utilized 29 segments, while at MCBCP the final scale was 35

segments. While still somewhat qualitative, this method produced results that did appear to balance the factors described above, and seems to be an improvement over previous methods that either apply a single water level over the entire domain, or only within a localized segment.

3.3.6 Protected Bays

Methods were developed to assess the response to sea level rise of protected bay areas such as the San Diego Bay facing portions of NBC. The methods included approaches to define water levels in these areas that can influence the operability of waterfront structures, methods to evaluate inundation and flooding that could occur from high tides interacting with sea level rise, and methods to evaluate changes in currents and associated bottom shear that could influence the transport and deposition rates of sediment.

Water Levels

Water levels in the protected areas of San Diego Bay were developed following the same methodologies described in Section 3.1 for exposed shorelines, but in the absence of wave run-up. Thus sea level rise variability was limited to tidal variations, and the non-tide residuals. The return period of water level extremes at NBC were computed from the water level time series using the extreme value method of order statistics (Makkonen 2011). The resulting scenarios are presented in Section 4.1.2 and the impacts related to the exposure along these protected shorelines are presented in Section 4.3.2.

Inundation and Flooding

Inundation and flooding analysis for the protected bay areas of NBC were evaluated using similar methods to those described above for the exposed shorelines. Total water level scenarios were developed for the same range of return periods (week – century), but excluding the wave run-up contribution. These water levels are thus dominated by tidal variations. This simplifies the analysis for the protected shoreline areas because there is essentially no spatial variation in the exposure throughout San Diego Bay. So for the protected areas, the shoreline segmentation reduces to a single segment for application of the hydraulic connectivity. Similarly to the exposed shorelines, the fill for the protected shorelines was constrained by a mask file that excluded connectivity within the ocean side of NBC. The purpose of this mask was to prevent the ocean from "filling" to the water level of the protected shorelines which would result in ocean shorelines being subjected to bay total water level scenarios. The two-dimensional flood-fill was carried out with an 8-connected neighborhood connectivity for each grid cell in the elevation model. The resulting raster maps defined the water level in all hydraulically connected areas of the installation for each total water level scenario. Results for the application of this methodology are shown in Section 4.

Changes in Currents and Bottom Shear

Due to the dominant influence of tidal action from the Pacific Ocean, and the lack of significant freshwater inflows during most of the year, currents, mixing, and bottom shear in San Diego Bay is well represented in a two dimensional (2-D) model construct. Over the last decade, in collaboration with the U.S. Geological Survey (USGS), we have developed, calibrated and validated a two-dimensional hydrodynamic and transport model, TRIM (Tidal Residues Inter-tidal Mudflat; Figure 3-64), for San Diego Bay. The model has been calibrated and validated for current day conditions using both measured and historical tide and current data (Wang *et al.*, 1998), measured at multiple locations throughout the Bay. The TRIM model has been used to support a number hydrodynamic, fate and transport studies, including changes to hydrodynamics from dredging, sediment transport from ship resuspension and creek outflows, and the transport and fate of a range of chemical contaminants for San Diego Bay (Chadwick *et al.*, 2008).

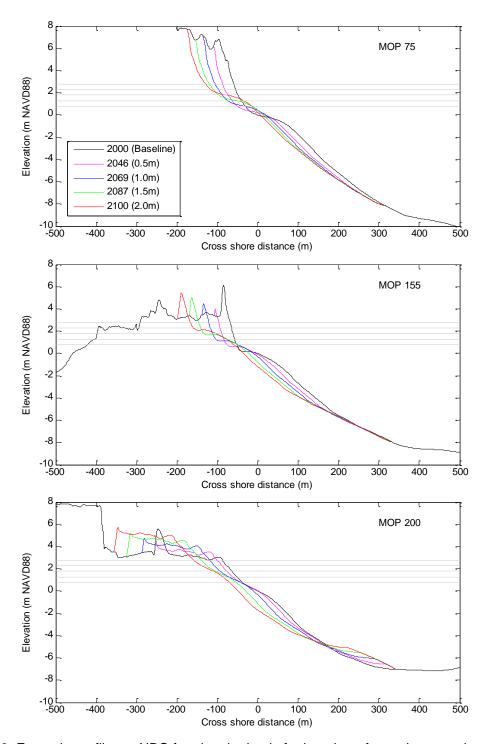


Figure 3-63. Example profiles at NBC forming the basis for beach surfaces that were inserted into the baseline elevation model to create the future elevation models.

Here, we explored the potential influence of changing sea level on the hydrodynamic response of the bay to tidal forcing. The TRIM model was used to simulate and compare magnitudes of currents and bottom shear stresses in San Diego Bay among the five scenarios: existing condition, and the four scenarios with the projected sea level rises of 0.5, 1, 1.5, and 2 m.

Hydrodynamic Modeling

TRIM model is a 2-D dynamic model with the model grid covering the entire San Diego Bay and part of the Pacific Ocean with boundaries outside the mouth (Figure 3-64). The TRIM model solves the depth-averaged shallow-water equations with several assumptions, including the hydrostatic (shallow water) approximation, the Boussinesq approximation, and incompressibility. It is also assumed that velocity and density are nearly constant over the water column. However, horizontal density gradients are treated explicitly in the momentum equations. Bottom shear stress is approximated using a Manning-Chezy formulation with Manning's n coefficient assigned as a function of water depth. The TRIM model has been previously applied to study hydrodynamics in estuaries on the west coast, including San Francisco Bay (Gartner, 1990; Cheng *et al.*, 1993), and San Diego Bay (Wang et. al., 1998).

The San Diego Bay model grid covers an area of 20 km (W-E) by 15.4 km (S-N). The western and southern open ocean boundaries are located about 5 km west and 7 km south of Point Loma, respectively (Figure 3-64). The computational mesh has 30,800 grid nodes at equal spacing of 100 m in both x (east) and y (north) directions. A six-minute time step is chosen for time integration. Water surface elevation and water velocity are set to zero as the initial conditions. The model is allowed to spin up from quiescent initial condition for two days before any model results are saved for analysis.

The San Diego Bay model grid covers an area of 20 km (W-E) by 15.4 km (S-N). The western and southern open ocean boundaries are located about 5 km west and 7 km south of Point Loma, respectively (Figure 3-64). The computational mesh has 30,800 grid nodes at equal spacing of 100 m in both x (east) and y (north) directions. A six-minute time step is chosen for time integration. Water surface elevation and water velocity are set to zero as the initial conditions. The model is allowed to spin up from quiescent initial condition for two days before any model results are saved for analysis.

The model grid was developed using high-resolution bathymetry from the same digital elevation model developed for the baseline condition for the NBC domain. A total of five model scenarios were conducted: the baseline condition, and the four scenarios with the projected sea level rises of 0.5, 1, 1.5, and 2 m. No other water level constituents (waves, storm surge, etc.) were considered in these simulations because they were run for extended periods with a focus on identifying general changes in currents and bottom shear stress associated with the deeper water depths related to sea level rise, not to evaluate extreme events. Simulated currents were compared at four selected locations that are important for operations at NBC including Bravo Pier (Station 1), Turning Basin (Station 2), Glorietta Bay (Station 3) and In-Bay Silver Strand (Station 4) (Figure 3-65). Simulated currents and bottom shear stress were estimated and are presented in the results Section 4.3.2.

3.3.7 Seawater Intrusion

The goal of the pathway assessment for groundwater was to estimate the effect of a potential SLR on seawater intrusion and water-level rise in the Coastal Santa Margarita River basin (Figure 3-66). The seawater intrusion was a concern because the U.S. Environmental Protection Agency (US EPA) National Secondary Drinking Water Standards (SMCL) recommends that the chloride concentration of drinking water be less than 250 mg/L (U.S. EPA, 2013a). SUTRA (Voss and Provost, 2002), a two-dimensional (x-z), density-dependent groundwater-flow and solute-transport model, was used to simulate seawater intrusion that may result from a SLR. The SUTRA model was selected because it is a well-accepted model, provided the capability to simulate the important processes relevant to the exposure pathway of interest, and could be configured and implemented within the limited resources and data constraints of the project. The simulation time frame was from water year (WY) 1950 to 2100 and the assessment of the effects of a SLR was from WY 2000 to 2100. A water year starts in October and ends in the following September. This document refers to observation and extraction

wells by a 3 to 4 character short name to make images and tables easier to read. For example well 011S005W09J001S is referred to as 09J1 or 9J1.

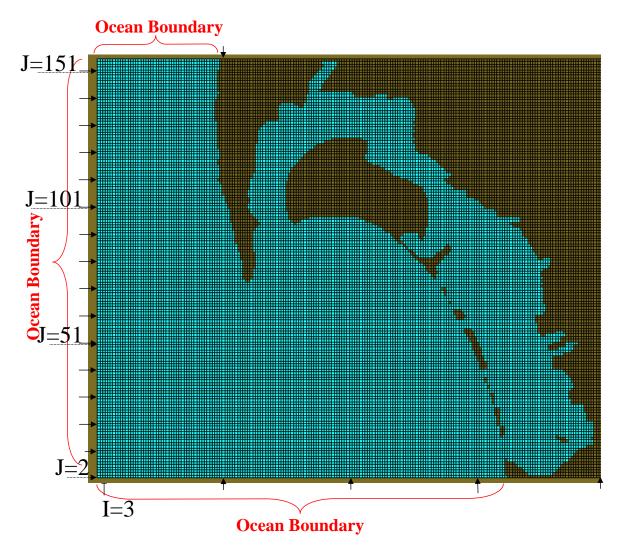


Figure 3-64. Hydrodynamic TRIM model grid for San Diego Bay.

Table 4-9 lists all wells that are referenced in this report and their corresponding short names.



Figure 3-65. Selected station for model output analysis (image data: Google, SIO, NOAA, U.S. Navy, NGA, GEBCO).



Figure 3-66. Figure showing study area, cross-section trace, location of wells used for cross section, and offshore bathymetry, Santa Margarita River Basin, CA (image data: Google, Digital Globe).

Hydrogeology

The primary source of data on lithology and bottom of alluvium for the hydrogeologic cross-section was a cross-section along the Santa Margarita River developed by Worts and Boss (1954, plate 4). The cross-section of Worts and Boss (1954) included approximately 30 well and test hole logs along the study reach. Additional driller's logs were used to supplement the Worts and Boss (1954) cross-section. Supplemental sources of driller's logs included: additional logs published in appendix 2 of Worts and Boss (1954), archives of the USGS San Diego office, available drillers' logs from the California Department of Water Resources, and logs of supply wells (or other well logs that penetrate the entire thickness of the alluvium) for Camp Pendleton in the Ysidora, Chappo, and Upper subbasins. The stratigraphic units in the SMR basin include Eocene to Miocene rocks and Quaternary alluvial deposits. Eocene to Miocene rocks of the San Onofre Breccia and La Jolla Formation make up the basement rocks underlying the basin. The Quaternary alluvial deposits overlie the basement.

Worts and Boss (1954) reported that the Quaternary alluvial deposits are the primary water-bearing formation in the SMR basin. It was assumed that the basement did not contribute water to the aquifer system. Worts and Boss (1954) defined two parts of the Quaternary alluvial deposits: the upper and lower members, which were termed the upper and lower aquifers in this report. The upper aquifer system ranges in thickness from about 20 to 34 m and is fine-grained made up of clays and silts (Worts and Boss, 1954). The lower aquifer system ranges in thickness from about 15 to 70 m and is coarse grained made up of gravels and sands (Worts and Boss, 1954).

Seawater Intrusion Conceptual Model

The conceptual model is presented in Figure 3-67. The bathymetry was based on work by Osborne *et al.* (1983, plate XIV-D). From the Pacific Ocean moving upstream, there are three subbasins of interest: the Ysidora, Chappo, and Upper subbasins. The length of the hydrogeologic cross-section from the coastline to the inland Upper subbasin is approximately 14.25 km. The inland boundary of the hydrogeologic cross-section is located upstream Camp Pendleton supply wells in the Upper subbasin. Extending the hydrogeologic cross-section into the Chappo and Upper subbasins permitted consideration of the effects of hydraulic gradients and groundwater management in these subbasins on seawater intrusion further downgradient. The cross-section extended from the coastline approximately 5.8 km offshore to the 80 m bathymetric contour. The seafloor geometry of the conceptual model is indicative of the approximate limits of the offshore ancestral Santa Margarita River (Figure 3-67 and Figure 3-68).

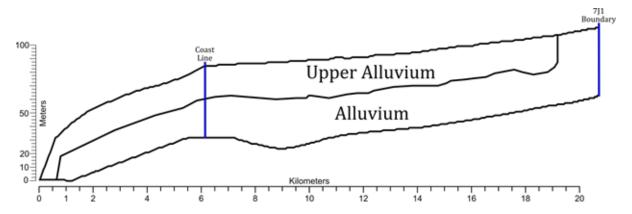


Figure 3-67. Lithologic geometry for conceptual model, Santa Margarita River Basin used in SUTRA with an inland freshwater boundary condition located at well 010S005W07J001S (7J1).

Table 3-9. Relationship with USGS well name with this documents short name.

Well Name	Short Name
011S005W09J001S	9J1
011S005W10B001S	10B1
011S005W02N004S	2N4
011S005W02F001S	2F1
011S005W02D003S	2D3
011S005W02A001S	2A1
010S005W35K005S	35K5
010S005W35K001S	35K1
010S005W26F001S	26F1
010S005W26C001S	26C1
010S005W24N001S	24N1
010S005W23K001S	23K1
010S005W23G001S	23G1
010S005W23J001S	23J1
010S005W23G002S	23G2
010S005W14R001S	14R1
010S005W13R002S	13R2
010S004W18M004S	18M4
010S004W18L001S	18L1
010S004W18E003S	18E3
010S004W07R002S	7R2
010S004W07J001S	731



Figure 3-68. 10-meter bathymetry contour lines (blue lines).

A SUTRA-based groundwater-flow and solute-transport model was developed on the basis of the conceptual model (Figure 3-67). Figure 3-67 is a 1 to 50 vertical exaggeration of the groundwater system simulated using SUTRA. An irregular finite-element grid was used with three different nominal element sizes that are presented in Figure 3-69. The white area of was set to a nominal element size of 5 by 100 m, the red region was set to 2 by 40 m and remaining blue region was 1 by 5 m. The refined areas in Figure 3-69 were added to improve the stability of the hydrostatic inland boundary condition. The final resulting finite-element grid is presented in Figure 3-70.

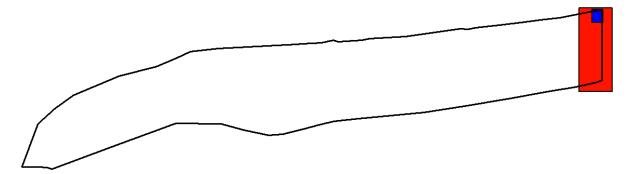


Figure 3-69. Sutra Model Element size refinement scheme. The white area has a nominal size of 5 x 100 m, red a nominal size of 2 x 40 m, and blue a nominal size of 1 x 20 m.

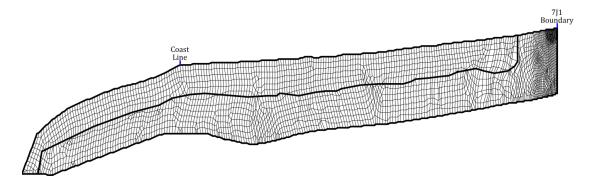


Figure 3-70. SUTRA finite element layout used in the model simulation.

There were two time-varying hydrostatic boundary conditions that were located at the seafloor and the vertical inland boundary (Figure 3-71). The seawater and freshwater densities used for the seafloor and inland boundary were 1,024 and 1,000 kg/m³, respectively. The inland freshwater boundary condition followed the historical trend from 1950 to 2000 at well 010S005W07J001S (7J1). These data were collected from the USGS National Water Information System (NWIS) database and provided by Khan (Khalique Khan, MCBCP, personal communication, 2011) (Figure 3-72).

Previous versions of SUTRA required modification of the source code to incorporate time-dependent boundary conditions. In addition, SUTRA did not allow a boundary condition to vary spatially. For example, as sea level rises, the ocean boundary will move farther inland. A new feature added to SUTRA was the ability to specify a time- and spatially-varying boundary conditions through an additional input file called the ".bcs" file. A FORTRAN preprocessor was written to construct the ".bcs" file from historical water levels and specified SLR scenarios.

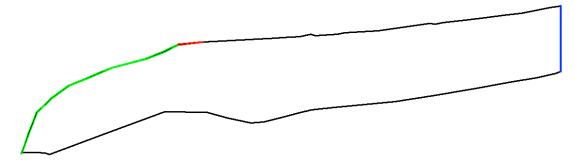


Figure 3-71. Defined hydrostatic pressure regions in the model. The blue line represents the inland freshwater boundary that follows observed head measurements at 010S005W07J001S (7J1). The green line is the specified pressure boundary that represents the overlying ocean. The red line represents specified pressure nodes that may be submerged by the ocean due to sea level rise.

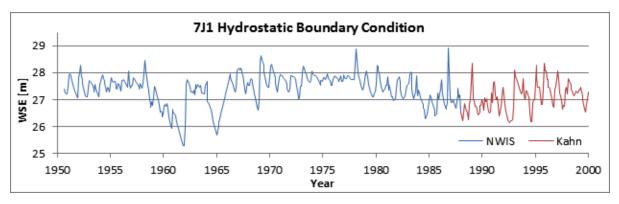


Figure 3-72. Hydrostatic freshwater inland boundary condition based on historical records from well 7J1.

Pumping data were provided by MCBCP for 14 extraction wells from WY 1961 to 2000 (Figure 3-73). The pumping data from WY 1961 were used in to simulated WY 1950 to 1960 conditions. Conversely the pumping data from WY 2000 were used to simulate WY 2001 to 2100 conditions. For example the pumping schedule for WY 2013 used the monthly pumpage recorded for water year 2000. Figure 3-74 is a bar graph of the total monthly pumpage used for WY 1961 and 2000.

The width of the aquifer can impact the water availability for extraction wells. The model was divided into two regions of uniform width that are based on an average width of the basin determined using a GIS. Observation sites with historical records obtained from the NWIS database were incorporated into the model for its calibration. The location of each of the observation wells, pumping wells and width regions are presented in Figure 3-75.

Precipitation data and discharge information for the Santa Margarita River were not directly included in the model. The model was a two-dimensional slice of a confined aquifer; therefore, the rainfall and river information was indirectly included through the inland boundary condition. If the SMR was included as a boundary condition it would have over specified the model.

Model Calibration

The model was run in a three-step process: (1) a steady-state simulation to simulate a preliminary pressure distribution, (2) a 10,000-year transient simulation to estimate the steady-state pressure and concentration distribution using the initial pressure distribution from step 1 as an initial condition, and (3) a transient simulation from water year 1950 to 2100. The historical matching only occurred between water years 1950 and 2000.

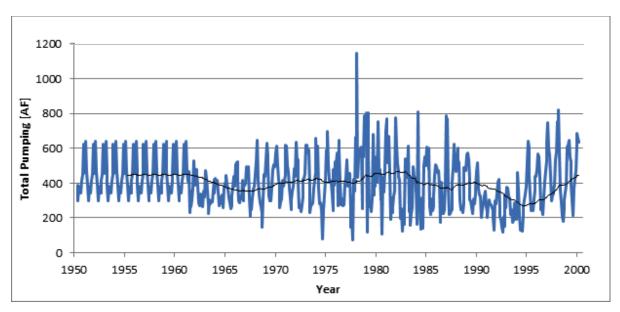


Figure 3-73. Total monthly pumpage for all wells in the SMR model in acre-ft (blue line) with a 5-year moving average (black line).*Note that pumping for WY 1950 to 1959 is a repeat of the pumping values reported for WY 1961.

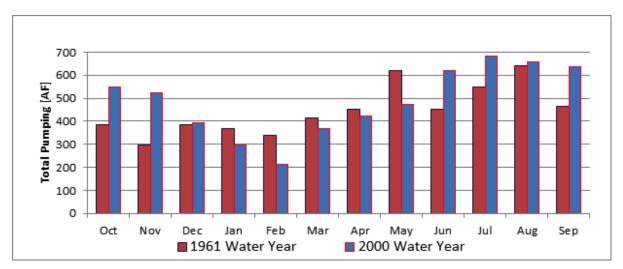


Figure 3-74. Total pumping in acre-ft during water years 1961 and 2000 of wells located in the model.

Hydraulic properties of the alluvial sediments were assembled from the USGS NWIS database, Worts and Boss (1954), California Department of Water Resources (1956), Roff (1998), and other publications. The key hydraulic properties of density-dependent groundwater flow and solute transport are permeability, porosity, and dispersivity. Permeability is a measure of the degree to which pore spaces (water bearing locations in the soil) are interconnected and the size of the interconnections. It can be viewed as a measurement of how easily groundwater can flow through the soils. Porosity is the percentage of soil void volume compared to the total volume of the soils and controls the groundwater velocity. Dispersivity is an empirical factor that affects the spreading of a solute front, here seawater intrusion, during groundwater transport. Estimates of permeability, dispersivity, and porosity were based on published data and qualitative matching to historical records. Published data, including drillers' logs and borehole resistivity logs, indicate that the upper

alluvium has a lower permeability and dispersivity than the alluvium. Table 4-10 lists the final properties that produced the best match to historical records.

The given set of parameters in Table 3-10 resulted in a good match to observed hydrographs and breakthrough curves. Figure 3-77 through Figure 3-81 are hydrographs that compare the simulated hydraulic head with the observed water levels at selected wells. The simulated hydraulic heads matched the observed seasonal trends and captured the recovery (increasing water level) that was present from WY 1960 to 1980 (Figure 3-77 through Figure 3-81). The simulated results did not match the observed water levels in early time (WY 1950) and from WY 1979 to 1981. The observed water levels in WY 1950 were much lower than the simulated hydraulic heads at wells 9J1, 10B1, 2N4, and 35K5 (Figure 3-77 through Figure 3-80) indicating that the assumed pumping (WY 1960) was probably lower than what occurred in reality. The simulated drawdown was greater than the observed in WY 1979 to 81 in all the simulated hydrographs (Figure 3-77 through Figure 3-81). During this time there may have been an unknown or unreported water source that was not included in the model. This additional water may have come from heavier rainfall or better infiltration from the SMR as was indicated by the extreme events during this time period (Figure 3-76). However, this time period also had the largest total pumping for the entire simulation time frame (Figure 3-73).

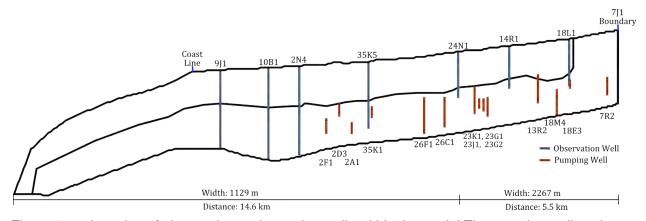


Figure 3-75. Location of observation and pumping wells within the model. The pumping wells only show the screening interval of the well. The short names of each well are provided either above or below each location.

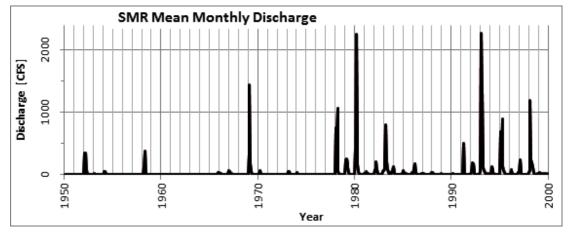


Figure 3-76. Mean monthly discharge from the Santa Margarita River from USGS Gauge 11046000 at Ysidora.

The given set of parameters in Table 3-10 resulted in a good match to observed hydrographs and breakthrough curves. Figure 3-77 through Figure 3-81 are hydrographs that compare the simulated hydraulic head with the observed water levels at selected wells. The simulated hydraulic heads matched the observed seasonal trends and captured the recovery (increasing water level) that was present from WY 1960 to 1980 (Figure 3-77 through Figure 3-81). The simulated results did not match the observed water levels in early time (WY 1950) and from WY 1979 to 1981. The observed water levels in WY 1950 were much lower than the simulated hydraulic heads at wells 9J1, 10B1, 2N4, and 35K5 (Figure 3-77 through Figure 3-80) indicating that the assumed pumping (WY 1960) was probably lower than what occurred in reality. The simulated drawdown was greater than the observed in WY 1979 to 81 in all the simulated hydrographs (Figure 3-77 through Figure 3-81). During this time there may have been an unknown or unreported water source that was not included in the model. This additional water may have come from heavier rainfall or better infiltration from the SMR as was indicated by the extreme events during this time period (Figure 3-76). However, this time period also had the largest total pumping for the entire simulation time frame (Figure 3-73).

The response of the simulated breakthrough curves were slower than the observed trends, but the general trend and concentrations were reasonable. Figure 3-82 through Figure 3-85 present the simulated and observed chloride levels for selected observation wells located near the coast. The simulated chloride concentrations for well 9J1 had the worst fit by only capturing the first and last observed value (Figure 3-82). As stated above, the pumpage used to simulate this time period was probably too low, as indicated by the hydrographs. If the pumpage was much greater than assumed, this may have resulted in much greater seawater intrusion and chloride concentrations as indicated by the relatively high observed chloride concentrations in early time (Figure 3-82).

The response of the simulated breakthrough curves were slower than the observed trends, but the general trend and concentrations were reasonable. Figure 3-82 through Figure 3-85 present the simulated and observed chloride levels for selected observation wells located near the coast. The simulated chloride concentrations for well 9J1 had the worst fit by only capturing the first and last observed value (Figure 3-82). As stated above, the pumpage used to simulate this time period was probably too low, as indicated by the hydrographs. If the pumpage was much greater than assumed, this may have resulted in much greater seawater intrusion and chloride concentrations as indicated by the relatively high observed chloride concentrations in early time (Figure 3-82).

The simulated breakthrough curves for wells 10B and 2N4 (Figure 3-83 and Figure 3-84) captured the majority of the observation points and showed a general increasing trend due to increased pumpage from 1970 to 1990, as indicated by the 5-year moving average in Figure 3-73. The simulated chloride concentration at well 35K5, Figure 3-85, was lower than the observed; however, but both were less than the U.S. EPA SMCL of 250 mg/L. The generally higher levels of variability in the chloride observations compared to the modeled chloride concentrations likely resulted from a combination of the uncertainty in the pumping rates (especially in the early times), lack of information on variability in the pumping rates, and the fact that the observations were single point measurements rather than average conditions which would have been more comparable to the model outputs. Figure 3-86 and Figure 3-87 compare the observed and simulated chloride concentration profile during 1962 and 1965. These two years had common observations for all the observation wells with chloride data. The figures show the rapid reduction in chloride concentration the further away from the ocean/coastline. The chloride concentration reduced as distance was increased from the coastline.

Table 3-10. Soil properties used in the SMR SUTRA model.

	Upper	Lower	Units
Property	Alluvium	Alluvium	Units
Porosity	0.4	0.22	
Horizontal Permeability	3.596E-12	8.990E-11	m ²
Vertical Permeability	1.798E-12	4.495E-11	m ²
Calculated Horizontal Hydraulic	3	76	
Conductivity	3	70	m/d
Calculated Vertical Hydraulic	1.5	38	
Conductivity	1.5	30	m/d
Horizontal Longitudinal	750	1500	
Dispersivity	730	1300	m
Horizontal Transverse Dispersivity	50	500	m
Vertical Longitudinal Dispersivity	250	50	m
Vertical Transverse Dispersivity	50	50	m

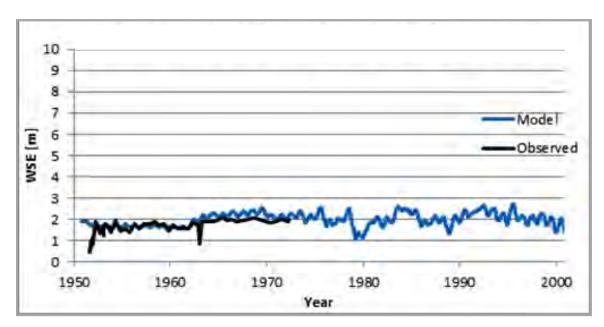


Figure 3-77. 11S005W09J001S (9J1) observed and simulated hydrograph from 1950 to 2000.

The response of the simulated breakthrough curves were slower than the observed trends, but the general trend and concentrations were reasonable. Figure 3-82 through Figure 3-85 present the simulated and observed chloride levels for selected observation wells located near the coast. The simulated chloride concentrations for well 9J1 had the worst fit by only capturing the first and last observed value (Figure 3-82). As stated above, the pumpage used to simulate this time period was probably too low, as indicated by the hydrographs. If the pumpage was much greater than assumed, this may have resulted in much greater seawater intrusion and chloride concentrations as indicated by the relatively high observed chloride concentrations in early time (Figure 3-82).

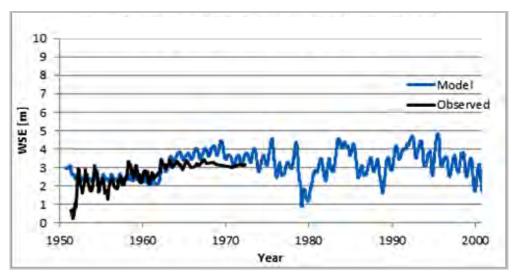


Figure 3-78. 11S005W10B001S (10B1) observed and simulated hydrograph from 1950 to 2000.

The simulated breakthrough curves for wells 10B and 2N4 (Figure 3-83 and Figure 3-84) captured the majority of the observation points and showed a general increasing trend due to increased pumpage from 1970 to 1990, as indicated by the 5-year moving average in Figure 3-73. The simulated chloride concentration at well 35K5, Figure 3-85, was lower than the observed; however, but both were less than the U.S. EPA SMCL of 250 mg/L. The generally higher levels of variability in the chloride observations compared to the modeled chloride concentrations likely resulted from a combination of the uncertainty in the pumping rates (especially in the early times), lack of information on variability in the pumping rates, and the fact that the observations were single point measurements rather than average conditions which would have been more comparable to the model outputs. Figure 3-86 and Figure 3-87 compare the observed and simulated chloride concentration profile during 1962 and 1965. These two years had common observations for all the observation wells with chloride data. The figures show the rapid reduction in chloride concentration the further away from the ocean/coastline. The chloride concentration reduced as distance was increased from the coastline.

Sensitivity Analysis

Two sensitivity analyses were performed using the groundwater flow and solute-transport model. The first assumed that the entire aquifer system was homogeneous. The second assumed that the aquifer properties were reversed, i.e., the upper aquifer was more permeable than the lower.

Model Testing: Homogeneous Case

A homogenous test case was used to evaluate the sensitivity of the model to the effect of the low-permeability upper alluvium layer on the SMR basin. The homogeneous case was exactly the same as the calibrated model, except that all the properties used to describe the lower alluvium layer were applied to the upper alluvium. The homogenous case increased the simulated hydrographs and the seawater intrusion (Figure 3-88 through Figure 3-91). The reason for these increases compared to the calibrated model was that, for the calibrated model case, the upper alluvium acted as a cap that enhanced the outflow of groundwater in the deep aquifer and thus retarded inflow from the ocean into the SMR basin. With this constraint relaxed (homogenous case), the water surface elevations increased well above observed levels indicating the calibrated model conditions provided a better representation of the system.

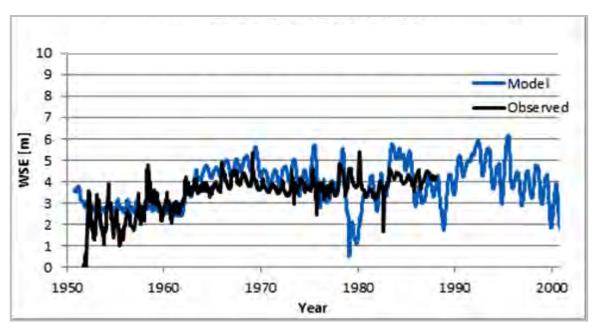


Figure 3-79. 11S005W02N004S (2N4) observed and simulated hydrograph from 1950 to 2000.

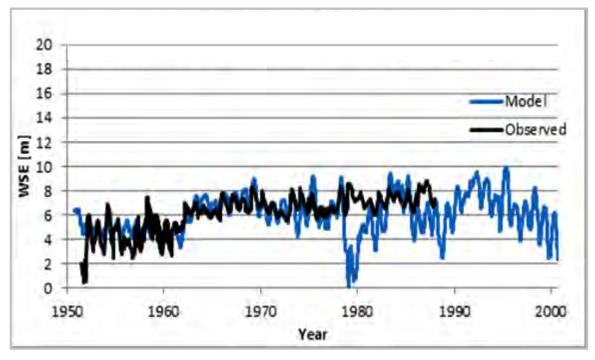


Figure 3-80. 10S005W35K005S (35K5) observed and simulated hydrograph from 1950 to 2000.

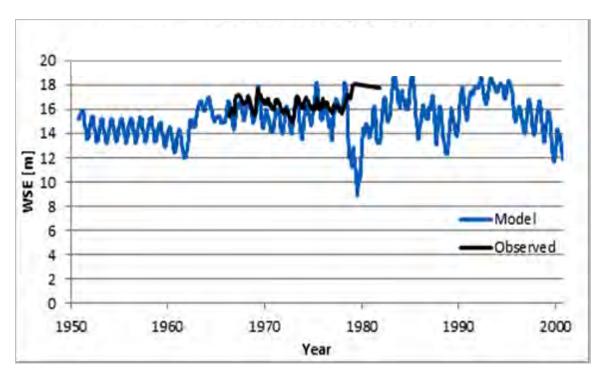


Figure 3-81. 10S005W14R001S (14R1) observed and simulated hydrograph from 1950 to 2000.

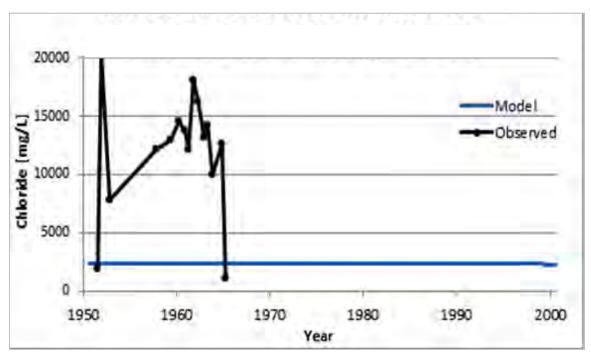


Figure 3-82. 11S005W09J001S (9J1) observed and simulated breakthrough curves from 1950 to 2000.

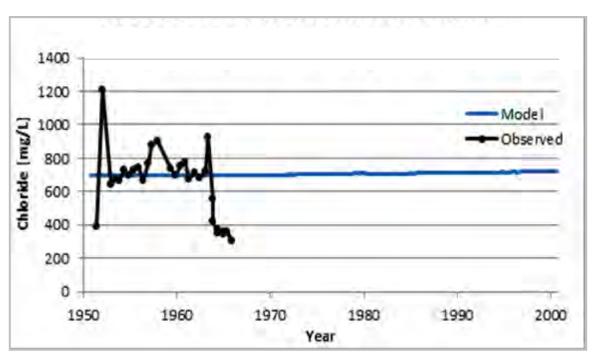


Figure 3-83. 11S005W10B001S (10B1) observed and simulated breakthrough curves from 1950 to 2000.

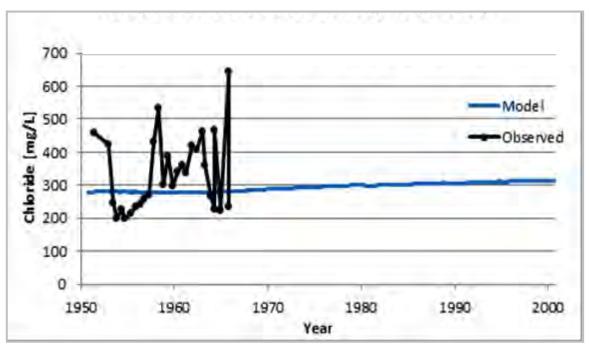


Figure 3-84. 11S005W02N004S (2N4) observed and simulated breakthrough curves from 1950 to 2000.

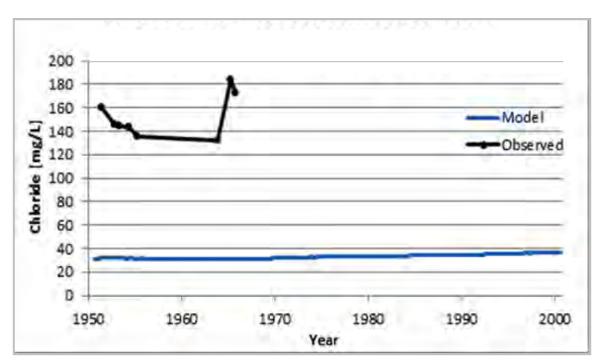


Figure 3-85. 10S005W35K005S (35K5) observed and simulated breakthrough curves from 1950 to 2000.

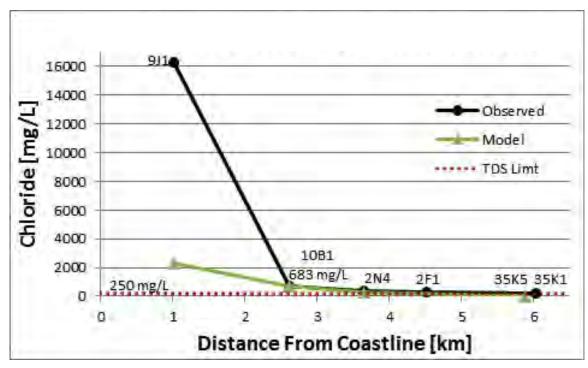


Figure 3-86. Observed and simulated chloride levels in 1962 for selected wells arranged by distance from the coastline.

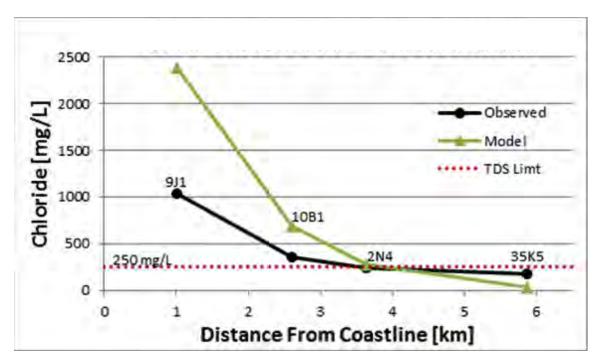


Figure 3-87. Observed and simulated chloride levels in 1965 for selected wells arranged by distance from the coastline.

Model Testing: Homogeneous Case

A homogenous test case was used to evaluate the sensitivity of the model to the effect of the low-permeability upper alluvium layer on the SMR basin. The homogeneous case was exactly the same as the calibrated model, except that all the properties used to describe the lower alluvium layer were applied to the upper alluvium. The homogenous case increased the simulated hydrographs and the seawater intrusion (Figure 3-88 through Figure 3-91). The reason for these increases compared to the calibrated model was that, for the calibrated model case, the upper alluvium acted as a cap that enhanced the outflow of groundwater in the deep aquifer and thus retarded inflow from the ocean into the SMR basin. With this constraint relaxed (homogenous case), the water surface elevations increased well above observed levels indicating the calibrated model conditions provided a better representation of the system.

Model Testing: Reversed Properties Case

To evaluate the sensitivity of the model to having a lower permeability upper alluvium, a reversed property test case was constructed. This "flipped" all the calibrated model's properties by applying the properties of the lower aquifer to the upper and properties of the upper aquifer to the lower. Reversing the aquifer properties caused a significant drop in the simulated hydraulic heads (Figure 3-92 and Figure 3-93), because all of the pumping occurs in the upper aquifer, which now has a very low permeability. Since the upper aquifer now had a higher permeability, it allowed easier communication between the ocean boundary and the aquifer. The combination of these two effects resulted in a significant increase in seawater intrusion in the system after pumping began in WY 1950 (Figure 3-94 and Figure 3-95). The runaway of the chloride levels under this scenario, and the significant drop in water surface elevations compared to the available observations both indicated that the calibrated model paramterization provided a better representation of the system.

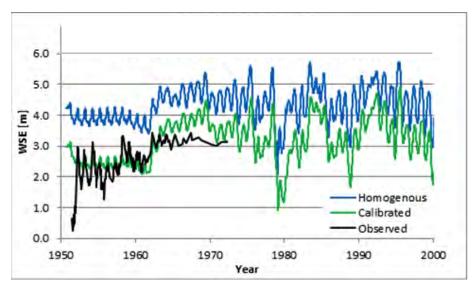


Figure 3-88. Comparison of the 11S005W10B001S (10B1) hydrograph produced by a homogeneous system that has the properties of the alluvium layer with the original calibrated model and observations.

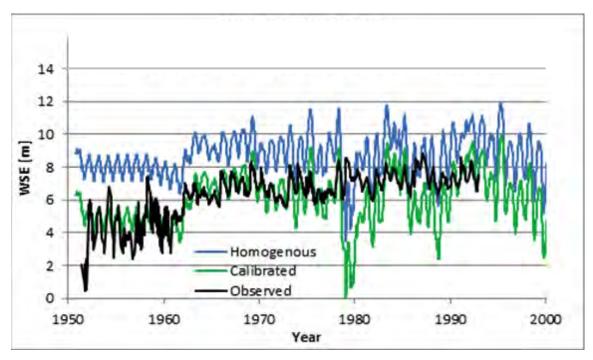


Figure 3-89. Comparison of the 10S005W35K005S (35K5) hydrograph produced by a homogeneous system that has the properties of the alluvium layer with the original calibrated model and observations.

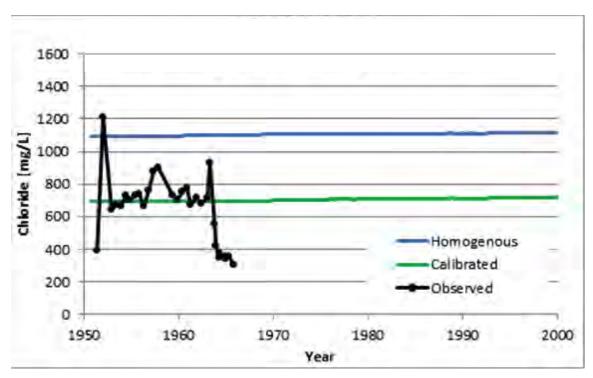


Figure 3-90. Comparison of the 11S005W10B001S (10B1) breakthrough curve produced by a homogeneous system that has the properties of the alluvium layer with the original calibrated model and observations.

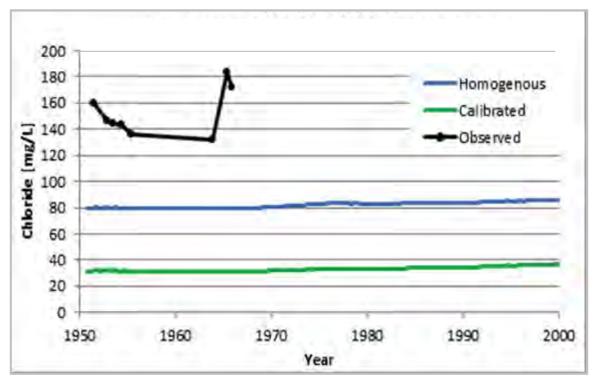


Figure 3-91. Comparison of the 10S005W35K005S (35K5) breakthrough curve produced by a homogeneous system that has the properties of the alluvium layer with the original calibrated model and observations.

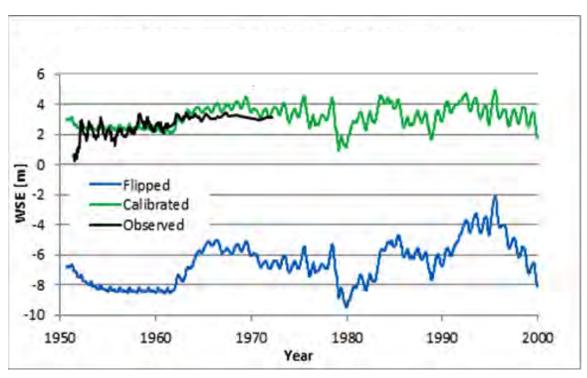


Figure 3-92. Comparison of the 11S005W10B001S (10B1) hydrograph produced by a reversed system with the original calibrated model and observations.

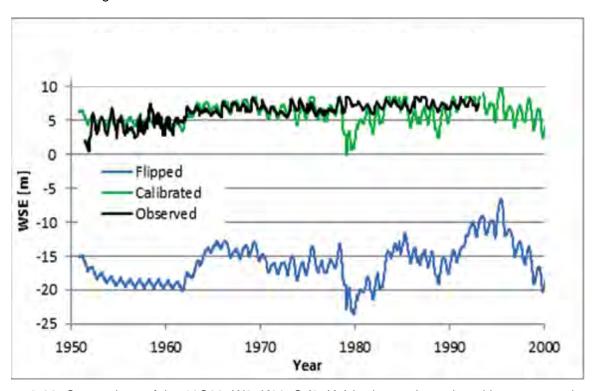


Figure 3-93. Comparison of the 10S005W35K005S (35K5) hydrograph produced by a reversed system with the original calibrated model and observations.

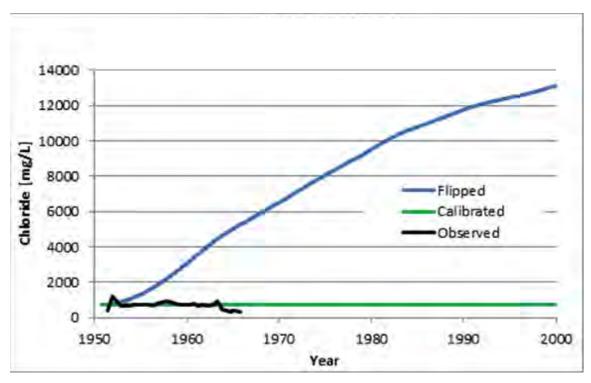


Figure 3-94. Comparison of the 11S005W10B001S (10B1) breakthrough produced by a reversed system with the original calibrated model and observations.

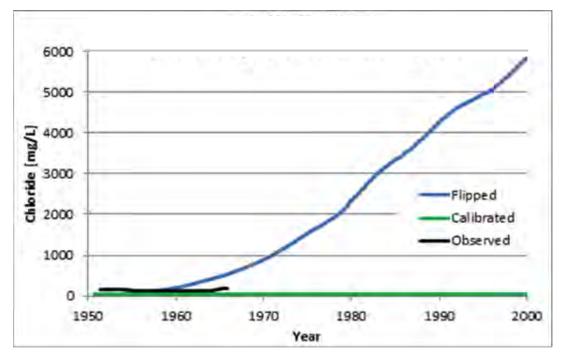


Figure 3-95. Comparison of the 10S005W35K005S (35K5) breakthrough produced by a reversed system with the original calibrated model and observations.

Sea-Level Rise Scenarios

Based on the model development, calibration and validation described above, five SLR scenarios for the time period of 2000 to 2100 were evaluated using three different inland boundary conditions. The five SLR scenarios assumed no SLR (base case) and four potential SLRs as shown in Figure 3-96. The ocean boundary was held constant at 0.78 m (the average elevation of the coastline) from 1950 to 2000 then the SLR scenarios were imposed from 2000 to 2100. The inland boundary followed the 1950 to 2000 historical water levels and from 2000 to 2100 it was set to a constant value equal to the average historical water level, lower 5%, and upper 95%, for well 7J1, which were 27.3 m, 26.26 m, and 28.06 m, respectively. Only hydrographs and breakthrough curves using the average boundary condition are presented in this section. Appendix A8 contains all images using the lower 5% and upper 95% boundary conditions. Results for the seawater intrusion modeling for these scenarios are presented in Section 4.3.3.

3.4 METHOD FOR ASSESSMENT OF VULNERABILITY

Methods for the assessment of vulnerability were explored under both receptor category and receptor component levels of analysis. The methodologies differ primarily in breadth and depth, with the receptor-level assessment retaining to the degree possible the full breadth of the installation, but at a relatively shallow level of detail and analysis, and the component-level method focusing on more specific receptors but at a finer level of detail.

3.4.1 Receptor-Level Vulnerability Assessment Methods

The receptor-level assessment methodology integrates sea level rise scenarios with operational and damage impact metrics. For long-term planning it is necessary to determine the critical sea level elevations which would: (1) impact the day-to-day operations of the infrastructure and/or (2) make the infrastructure vulnerable to a design storm event. For the receptor-level assessment, it is necessary to streamline the analysis to get an overall view of an installation to determine the breadth of vulnerable facilities and potential impacts to operations.

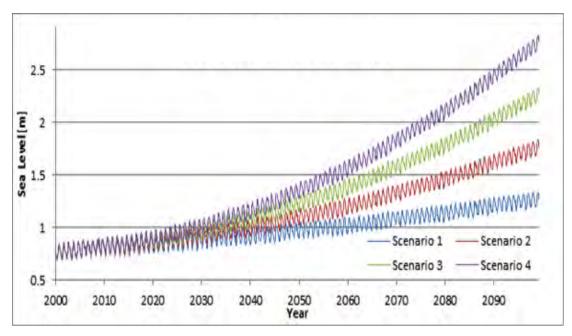


Figure 3-96. Four scenarios for mean sea level rise including tidal variability.

Overview of the Receptor-Level Assessment Methodology

The methodology developed for the receptor-level assessment of the impacts of SLR on the built infrastructure is outlined below. The methodology encompassed the breadth of the data compilation, modeling, and analysis methods described in previous sections. This included installation and exposure specific sea level rise source scenarios, pathway-specific physical response of the coastal system, and the characteristics sensitivities and response functions for the installation receptors (Figure 3-97). The receptor-level assessment process depends on the quality of the elevation models and GIS database, and it may also be affected by the size and complexity of the DoD installation. Following is a discussion of each component of the screen level assessment method including the exposure scenarios, response pathways, receptors assessed, and the minimum asset information necessary to conduct the receptor-level assessment using this methodology.

Sea Level Rise Scenarios and Exposure Pathways

For the receptor-level assessment, total water levels were determined for NBC and MCBCP for a range of combined mean sea level conditions and return period events including: week, month, year, decade, and century as shown in Section 4.1. The total water level statistics were developed for three conditions including:

- NBC and MCBCP Exposed Shoreline: Locations exposed to ocean waves have a higher total water level that includes a wave run-up component that increases for each return period event.
- NBC Protected Shoreline: Locations that are protected from ocean waves, such as inside of San Diego Bay, do not have a wave component and are governed by tides with a non-tide component. Boat wakes and wind driven waves were not included in the total water levels for San Diego Bay.

In the receptor-level assessment, these sea level scenarios were evaluated for three key exposure pathways at each installation including erosion, inundation, and flooding, as applicable. Receptor-specific methodologies for the receptor-level impact assessment are described below.

Training and Testing Lands

Training and testing lands are a category of receptors that encompass the coastal land areas that support training and testing missions. In many instances, testing and training require a broad range of coastal terrain and conditions. This category can span many different land forms such as beaches, bays, estuaries, rivers, barrier islands, wetlands, bluffs and lagoons. These areas support many types of training and testing missions, including amphibious assault training, coastal components of maneuver corridors, amphibious landing beaches, airfields, and beach and bay training areas. For this analysis, we focused on the training beaches on the wave-exposed shorelines, and the potential impacts to these areas from erosion, inundation and flooding associated with sea level rise.

Required Asset Information

For training and testing lands, the receptor-level analysis requires an accurate description of the spatial extent and boundaries of the training area. While both installations provided general shapefiles describing the location of training areas, the spatial delineation in these products was generally insufficient to characterize the beach portion of the training area that was vulnerable to sea level rise. For example, at NBC, the training shapes generally included the offshore boat lanes that are already underwater and thus are not vulnerable, and the landward boundary of the training area also needed refinement to match the contour of the highway that backs the beach training areas. Knowledge of the training activities, frequency, duration, and spatial extent were also important in developing metrics of impact for this receptor class.

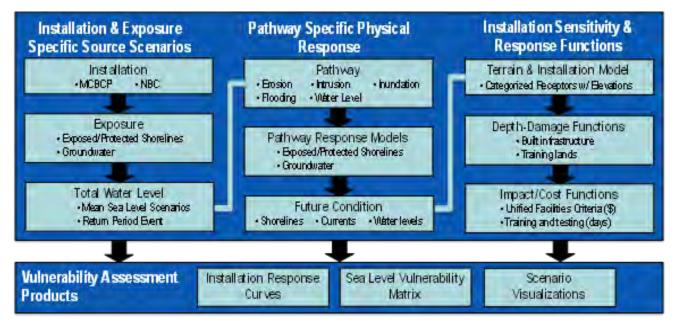


Figure 3-97. Overview of the receptor-level assessment methodology.

Impact Metrics

From this underlying information, we developed response metrics for the training areas that included the following:

- Baseline training area (m²) and beach width (m)
- Training area remaining (m² or % of baseline)
- Training beach width remaining (m or % of baseline)
- Damage cost (replenishment \$ to maintain baseline)

Baseline Training Area and Width. The baseline training area was extracted from the individual training area shapefiles by loading the files into MATLAB® and evaluating with the "polyarea" function. The baseline training beach width was determined by measuring the length of each training area in the GIS, and dividing the length into the area.

Training Area Remaining. For the erosion pathway, the training area remaining was determined by intersection of the original training area shapefile with the corresponding erosion footprint polygon using the MATLAB "polybool" function, and then subtracting this area from the original area. For the inundation and flooding pathways, the training are remaining was determined by determining the number of flooded grid cells within the training footprint using the MATLAB "inpolygon" function, multiplying by the square of the grid spacing for the flood model, and then subtracting this area from the original area.

Training Beach Width Remaining. The training beach width remaining was calculated by dividing the training area remaining calculated above by the training area length from the GIS.

Damage Cost. Training areas and testing lands do not have a replacement cost that is tabulated like other infrastructure categories maintained in INFADS. Instead, the replacement cost of training areas and testing lands were estimated as the cost to maintain the baseline conditions via sand replenishment along the exposed shorelines of the installations. Because the beaches at both

installations are generally already subject to sand budget deficits, replenishment costs were estimated for both the existing deficit component, and the replenishment required to accommodate sea level rise. This analysis was not meant to represent an adaptation measure, but rather to provide a rough estimate of the value of the training area using the same metric (cost) as was used for most other receptor categories. The volume of sand required to achieve a net-zero retreat of the shoreline was determined using the CSPEM model by adjusting the sand budget until the no retreat condition was obtained.

Functional Elevations. Functional elevations and depth-damage relationships were not developed or utilized for the training and testing lands in favor of the more relevant metrics described above.

Buildings

This category includes a range of buildings that support the operations and missions of the installation. This includes buildings for housing, logistics, training, testing, operations, and security. These receptors are susceptible to sea level rise sources through all major pathways including inundation, flooding, erosion and seawater intrusion. Of particular interest are building structures that are already close to the high tide line and at a low elevation relative to mean sea level. Buildings located adjacent to the shore may be exposed to ocean waves, boat wakes, erosion, flooding or inundation. Buildings located away from the shoreline may be flooded from intrusion of water through the storm water conveyance system during high tide elevations or from inadequate drainage during a rain.

Required Asset Information

The receptor-level analysis requires an accurate description of the spatial extent, area and boundaries of the buildings, and an estimate of the building floor elevation. Measures of the building value (replacement cost) and the operational value (MDI) for each structure were also used in the receptor-level assessment.

Impact Metrics

From this underlying information, we developed response metrics for the buildings that included the following:

- Tiered functional elevations (m NAVD88)
- Baseline building replacement value (\$)
- Baseline building area (m²)
- Quantity of impacted buildings
- Damage cost (\$)
- Mission Dependency Index of impacted buildings

Functional Elevations. Due to the screening-level nature of the assessment, the large number of buildings at each installation, and the non-traditional nature of many of the buildings, depth-damage curves for assessment of inundation and flooding impacts were not applied in the receptor-level assessment. The floor elevation was used to determine if the building was subject to inundation or flooding, and in combination with the water level, to determine the magnitude of the damage. Based on analysis of INFADS and GIS data supplied by NAVFAC for NBC and MCBCP, the building floor elevations were not included in the database. Therefore, elevations around the perimeter of each building were extracted from the baseline elevation model by applying the MATLAB* "bufferm2" function to the building shapefile. The finish floor elevation was assumed to be 0.3 m (1 ft) above the lowest point on the perimeter. The operational impacts

and damage from inundation and flooding were estimated based on the maximum exterior flood depth. Three inundation/flood depth ranges were used to quantify impacts, see Table 3-11.

Table 3-11. Inundation/flood depth ranges, scenarios, and operational impacts to buildings. Actual damage and impacts will depend on building structure type and usage.

Critical Elevation	Exterior Flood Depth (m)	Flood Scenario	Operational Impacts
Exterior Grade	D < 0.3	The areas surrounding the building are flooded. No damage to the building is expected.	Access to the building may be temporarily limited, but still remains operational.
Minor Flooding	0.3 < D < 1.0	The flood water has reached the first (lowest) floor of the building and is less than 0.6 m deep. Minor damage to the interior finishes, flooring and contents is expected.	Temporary closure for cleaning and minor/moderate repairs are required.
Major Flooding	D > 1.0	The flood level is greater than 0.6 m inside the building. Damage to the interior finishes, flooring, structure, electrical system and interior contents is expected.	The building is non- operational for an extended period of time for cleaning and major repairs.

For the erosion pathway, functional elevations were not used. Instead the conservative assumption was made that the building damage was assumed to be 100% if any portion of the building fell within the erosion footprint.

Baseline Building Replacement Value. The baseline building replacement values were compiled in accordance with the methodology described in Section 3.2.2. This approach combined information from INFADS, DoD Facility Pricing Guide and ROM analysis to provide estimated replacement costs for each building in the database. These data provided a basis for the assessment of sea level rise impacts for individual structures, as well as a sense of the aggregate value of the building receptor category for the installation. An average unit replacement cost (\$/SF) was calculated for the buildings at each installation. This unit cost was multiplied by the building footprint area to calculate the replacement value of buildings in the database that were missing replacement values.

Baseline Building Footprint Area. Building areas were derived from the database provided by NAVFAC. These areas were used to estimate replacement values for buildings that did not have a replacement value assigned in the database.

Quantity of Impacted Buildings. For inundation and flooding, the quantity of impacted buildings was determined by summing all of the buildings with any portion of their perimeter areas within the inundation/flooding footprint. For the erosion pathway, the quantity of impacted buildings was determined by summing all of the buildings with any portion of the building within the erosion footprint.

Damage Cost. The maximum perimeter depth was determined by applying the MATLAB "bufferm2" function to the building shapefile and finding the maximum water depth from the flood model that fell within the building perimeter. The minimum and average water depths were also extracted.

Three inundation/flood depth ranges were used to categorize operational and damage impacts to the buildings, see Table 3-11. For the receptor-level assessment, the full replacement value of the

buildings that are vulnerable to inundation or flooding was used to compare the total value of vulnerable buildings within each water depth range. A tiered damage percentage level was not used for the buildings because of the wide range of structure types within the installation, and insufficient attribute information was provided to assign damage levels for the receptor-level assessment. The operational impacts caused by the temporary relocation of equipment, personnel, and operations while flood repairs are executed is a significant portion of the inundation/flood impacts.

For the erosion pathway, functional elevations were not used, but the building damage was assumed to be 100% of the replacement cost if any portion of the building fell within the erosion footprint.

Mission Dependency Index of Impacted Buildings. The Mission Dependency Index is defined in Section 3.2.2. For NBC, MDI values were pulled from the INFADS database. The INFADS data for Marine Corps Base Camp Pendleton did not include MDI values. For purposes of this study, we assigned an approximate MDI value for the buildings at MCBCP. For example, with buildings it was necessary to distinguish between housing areas and infrastructure that is housed in buildings that provide electrical power supply, potable water, medical services, and security or training operations. The buildings were assigned approximate MDI values based on their usage description provided in the INFADS database. These approximate MDI values were distinguished from the Navy generated values in the GIS database by adding the data under a separate heading. The attributes that were used to assign an approximate MDI value included Structure Type, Structure Name, Structure Use, and Narrative. The objects were grouped into the MDI categories based on the relative importance for both day-to-day operations and necessity during a natural disaster. The groupings are summarized in Table 3-12.

For inundation and flooding, impacted buildings were identified as all of the buildings with any portion of their perimeter areas within the inundation/flooding footprint, and the MDI values for these buildings were compiled. For the erosion pathway, impacted buildings were identified as all of the buildings with any portion of the building within the erosion footprint and the MDIs were similarly compiled.

Waterfront Structures

This category includes a range of structures that support waterfront operations and missions of the installation. This category encompasses structures such as piers, wharves, and floating docks. The facility type and function is important to understand for the analysis of impact of sea level rise on operations. Waterfront structures such as piers and wharves are either used in support of home port berths or as a port-of-call. The homeport facility is one to which a ship is permanently assigned and offers all requisite services required by the vessel, including the full complement of utility services. In contrast, a port-of-call facility would be any port where a ship stops while under-way, including calls at fueling facilities, ammunition piers, supply piers, or short-term repair facilities.

Required Asset Information

Waterfront structures are susceptible to sea level rise sources through all major pathways including inundation, flooding, erosion and seawater intrusion. However, for the installations studied here, the primary exposure for waterfront structures is via inundation and flooding along protected shoreline areas. The receptor-level analysis requires an accurate description of the spatial extent, area and boundaries of the waterfront structures and an estimate of the deck and infrastructure elevations. Measures of the structure value (replacement cost) and the operational value (MDI) for each structure were also used in the receptor-level assessment.

Table 3-12. MDI groupings associated with building usage descriptions.

MDI Category	Approximate MDI	Building Usage Description
Critical	85 to 100	Fire house, Hospital, Magazine, Power generating facility, San Onofre Nuclear Generating Station (SONGS), and Water plant.
Significant	70 to 85	Heat cool plant, Industrial waste plant, Medical center, Radio facility, Utility related, Waste water plant.
Relevant	55 to 70	Law enforcement, Jail or prison, Office, Security, Marine Corps Tactical Systems Support Activity (MCTSSA), Combat town, Warehouse.
Moderate	40 to 55	Community Center, Mechanical Unit
Low	1 to 40	Canopy, Carport, Church, Dwelling, Residential Housing, Garage, Memorial, Commercial stores, post office, School, Storage Shed.

Required Asset Information

Waterfront structures are susceptible to sea level rise sources through all major pathways including inundation, flooding, erosion and seawater intrusion. However, for the installations studied here, the primary exposure for waterfront structures is via inundation and flooding along protected shoreline areas. The receptor-level analysis requires an accurate description of the spatial extent, area and boundaries of the waterfront structures and an estimate of the deck and infrastructure elevations. Measures of the structure value (replacement cost) and the operational value (MDI) for each structure were also used in the receptor-level assessment.

Impact Metrics

From this underlying information, we developed response metrics for the waterfront structures that included the following:

- Functional elevations (m NAVD88)
- Baseline structure replacement value (\$)
- Quantity of impacted structures
- Damage cost (\$ or %)
- Mission Dependency Index of impacted structures

Functional Elevations. For the receptor-level assessment, the specific vulnerabilities of each structure were simplified and approximated based on the deck elevation. Fixed waterfront structures were assumed to fail operationally when the water level rose to within 0.75 m of the deck elevation. This is consistent with findings of our more detailed analysis of these structures that indicates failure of subsystems such as fender systems and utility systems in this range. These facilities are designed to remain fully operational for the full tidal range and environmental conditions expected over the design life of the structure. The substructure (piles) and superstructure (beams and deck) are unlikely to fail if the water level reaches the deck elevation because the structure is designed for significant mooring, berthing, seismic, wind and current loads. However, the fender systems and utility services may be impacted by SLR as the water level approaches this threshold. For the receptor-level, the overtopping elevation was the threshold used to quantify damage impacts. The full replacement cost of the structure was used for the assessment methodology because of the relationship between the design life of the structure, the remaining service life, and the costs of repair or replacement. At this point, the structure requires replacement because the cost of upgrades would exceed the cost of

replacement. The facility replacement cost was used for waterfront structures because of the limited service life and increased rate of deterioration caused by higher water levels will likely warrant facility replacement for all waterfront structures that are overtopped.

Baseline Structure Replacement Value. The baseline waterfront structure replacement values were compiled in accordance with the methodology described in Section 3.2.2. This approach combined information from INFADS, UFC, and ROM analysis to provide estimated replacement costs for each waterfront structure in the database. These data provided a basis for the assessment of sea level rise impacts for individual structures, as well as a sense of the aggregate value of the waterfront structure receptor category for the installation.

Quantity of Impacted Structures. For inundation and flooding, the quantity of operationally impacted assets was determined by summing all of the structures for which the functional elevation was exceeded under a given scenario. Similarly, the quantity of waterfront structures subject to damage was determined by summing up all of the structures for which the water level exceeded the deck elevation.

Damage Cost. Damage costs were estimated assuming 100% of the replacement cost for any structure for which the water level exceeded the deck elevation.

Mission Dependency Index of Impacted Structures. For Navy-owned waterfront structures, the MDI value was obtained from the INFADS database. At MCBCP, the waterfront structures did not include MDI values. MDI values were estimated and added to a separate column of the GIS database to facilitate assessment of the waterfront infrastructure at MCBCP. For inundation and flooding, impacted items were identified as all of the structures for which the water level exceeded the functional operational elevation, and the MDI values for these structures were compiled.

Coastal Structures

Coastal structure receptors include engineered shoreline protective structures that support waterfront operations and missions of the installation. The category includes structures such as: revetments, jetties and bulkheads/seawalls. These receptors are susceptible to sea level rise through means of inundation and/or wave overtopping.

Required Asset Information

Coastal structures are susceptible to sea level rise sources through all major pathways, including inundation, flooding, erosion, and seawater intrusion. Of interest for coastal structures are vulnerabilities associated with overtopping and damage to structural components due to increased water levels. The receptor-level analysis requires an accurate description of the spatial extent, area and boundaries of the coastal structures and an estimate of the overtopping elevation. Measures of the structure value (replacement cost) for each structure was also used in the receptor-level assessment.

Impact Metrics

From this underlying information, we developed response metrics for the coastal structures that included the following:

- Functional elevations (m NAVD88)
- Baseline structure replacement value (\$)
- Quantity of impacted structures
- Length of impacted structure
- Damage cost (\$ or %)

Functional Elevations. For the receptor-level assessment, the specific vulnerabilities of each structure were simplified and approximated. Coastal structures were assumed to fail operationally when the water level rose to within 0.33 m of the top of structure elevation. This elevation provides operational buffer for boat wakes, wind waves and other fluctuations that might occur in the protected areas where most of these structures are found. For the receptor-level, the overtopping elevation was the threshold used to quantify damage impacts.

Baseline Structure Replacement Value. The baseline coastal structure replacement values were compiled using the ROM analysis to provide estimated replacement costs for each coastal structure in the database. These data provided a basis for the assessment of sea level rise impacts for individual structures, as well as a sense of the aggregate value of the coastal structure receptor category for the installation.

Quantity of Impacted Structures. For inundation and flooding, the quantity of operationally impacted items was determined by summing all of the structures for which the functional elevation was exceeded under a given scenario. Similarly, the quantity of waterfront structures subject to damage was determined by summing up all of the structures for which the water level exceeded the top of structure elevation.

Damage Cost. Damage costs were estimated assuming 100% of the replacement cost for any structure for which the water level exceeded the top of structure elevation. This is conservative for rock revetments because of their adaptive capacity. Rough estimates suggest that actual damage from overtopping would be on the order of 30 to 50% of the replacement value, but these costs do not include assets that depend on the performance of the structure for protection.

Mission Dependency Index. Coastal structures are not assigned MDI values in INFADS, however, by nature the structures serve to protect landward areas that are mission critical. Therefore, in order to assess the MDI of the coastal structure, the MDI of the landward facilities should be considered.

Civil Infrastructure

This receptor category describes a broad category of built infrastructure that is critical to the day-to-day operations and mission of the installation. The category includes receptors ranging from critical utility infrastructure such as buried utilities, fuel transfer/supply, transportation corridors, and storm water conveyance systems. The breadth of this category was beyond the scope of the project to address fully, so we focused on a limited subset of receptors that represent the general characteristics of the category, and for which sufficient information was available from the installations to perform a meaningful analysis. These subcategories included storm water conveyance systems, roadways, airfields, and recreation areas.

Required Asset Information

Civil infrastructure is susceptible to sea level rise sources through all major pathways including inundation, flooding, erosion and seawater intrusion. For the installations studied here, and the subcategories of receptors considered, we focused on the primary exposure pathways via erosion, inundation and flooding along both the exposed and protected shoreline areas. The receptor-level analysis requires an accurate description of the spatial extent, area and boundaries of the infrastructure elements and the associated elevation data. Measures of the structure value (replacement cost) was also used in the receptor-level assessment.

Impact Metrics

From this underlying information, we developed response metrics for the civil assets that included the following:

- Functional elevations (m NAVD88)
- Baseline infrastructure replacement value (\$)
- Baseline infrastructure area (m²) or length (m)
- Quantity of impacted infrastructure elements
- Area (m² or %) or length (m or %) of infrastructure impacted
- Damage cost (\$)

Functional Elevations. For civil infrastructure, functional elevations were developed to assess inundation and flooding based on the subcategory of the receptor class. For each subcategory, the element was assumed to be operationally impacted if the invert (lowest) elevation within the element area was below water level.

For the erosion pathway, functional elevations were not used. Instead the conservative assumption was made that the element damage was assumed to be 100% if any portion of the asset fell within the erosion footprint.

Baseline Structure Replacement Value. The baseline infrastructure replacement values were compiled using the ROM analysis to provide estimated replacement costs for each civil asset in the database. For roadways and airfields, the area was multiplied by the estimated ROM replacement value to calculate a total replacement value for each asset. For storm water conveyance systems, the length and quantity of storm drain inlets was used to estimate replacement value of each asset. The recreation areas were not assigned a replacement value, instead, the area was used as the metric to quantify impacts. These data provided a basis for the assessment of sea level rise impacts for individual elements, as well as a sense of the aggregate value of the civil infrastructure receptor category for the installation.

Quantity of Impacted Infrastructure Elements. For inundation and flooding, the quantity of operationally impacted items was determined by summing all of the elements for which the functional elevation was exceeded under a given scenario. Similarly the quantity of elements subject to damage was determined by summing up all of the structures for which the water level exceeded the invert elevation. These determinations were generally made using the MATLAB® "inpolygon" function to determine the overlap between the flood model and the infrastructure, and the associated water depths of the flooded elements. For erosion, the quantity of impacted elements was determined by summing up all of the elements for which any portion fell within the erosion footprint as determined using the MATLAB® "polybool" function.

Area/Length of Infrastructure Impacted. For inundation and flooding, the area or length of impacted items was determined using the MATLAB® "inpolygon" function to determine the overlap between the flood model and the infrastructure, and the associated water depths of the flooded elements. For erosion, the area or length of impacted elements was determined using the MATLAB® "polybool" function to evaluate the overlap between the infrastructure element and the erosion footprint.

Damage Cost. Damage costs for erosion, inundation and flooding were estimated assuming unit areas replacement cost for the portion (area or length) of each element that was impacted.

3.4.2 Component-Level Vulnerability Assessment Methods

The component-level assessment generally focused on refinement of the assumptions, methods, and data used during the receptor-level assessment to provide a more quantitative analysis and reduce uncertainties. In the context of sea level rise, component-level assessment may require moving from the use of limited available data to extensive data collection. It may also require the application of more sophisticated models, extending beyond simple inundation analysis to include, for example, more rigorous shoreline evolution modeling, dynamic flood modeling and mapping, and two or three dimensional groundwater intrusion modeling. The component-level assessment may also adopt more rigorous methods for projecting socioeconomic conditions. Here we focus on methodological considerations for the component-level assessment in the context of the evaluation of vulnerability for the designated receptors. Key considerations are summarized below by receptor class with an emphasis on operational impacts. The general approach is shown in Figure 3-98 which incorporates refinement of the existing receptor condition, classification of common sub-categories of receptors, development of operational limits for those categories, and a refined assessment of vulnerability at this higher level of detail based on specified exposure scenarios. While a facilitywide component-level assessment was beyond the scope of this effort, example applications from the two installations are described in Section 4.4.3.

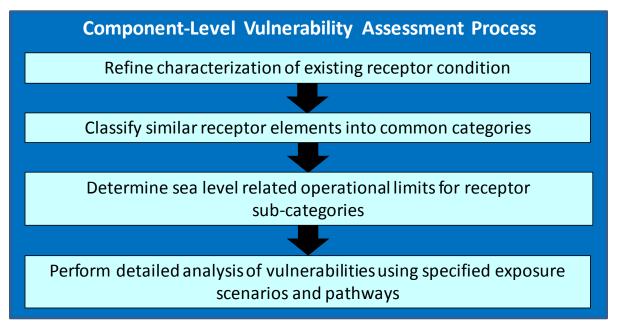


Figure 3-98. General process approach for the component-level vulnerability assessment approach.

Training Areas and Testing Lands

Training and testing lands at naval installations typically include a range of onshore and offshore zones that are designated to support the requirements of the resident command. The methodology for the component-level assessment of Training and Testing Lands focuses on beach training areas, and builds on the receptor-level assessment methodology but incorporates additional detail with respect to both the physical characteristics of the training areas as well as the operational requirements for the training. The methods provide a basis to determine the future physical characteristics of the training areas and how changes in beach area and width may affect specific training activities.

Existing Training Area Conditions

While naval training areas include areas on both land and in the water, this analysis focuses on the landside training areas and in particular the beach training areas which are generally the most sensitive areas to sea level rise. The receptor-level assessment analyzed the change in physical characteristics of the training areas such as beach width remaining and beach training area. For the component-level assessment, the future shoreline position analysis considers the interaction of sea level rise with operational requirements, physical configurations and constraints, existing shoreline protective structures, and habitat protection requirements. The goal is to provide sufficient information to allow planning personnel to assess whether or not a specific training activity is limited. Physical components of the beach training areas are segmented into zones based on the elevation relative to the tidal range (Figure 3-99).

- Tidal Zone: beach width between MLLW and MHHW tide lines.
- Dune Zone: beach width between the MHHW tide line and the berm.
- Back Beach Zone: beach width between the berm and the Navy property line or hardened structure.

Local knowledge of the existing conditions and seasonal variability in beach characteristics is necessary to quantify minimum and maximum physical characteristics of the baseline conditions. A history and broad understanding of the area complements the analysis. To formalize the compilation of this information, we developed an Existing Conditions Checklist (see Figure 3-100) that defines key training area features that are important to the evaluation of impacts from sea level rise.

Based on the characteristics developed above for the existing conditions, sub-categories of training areas for a given installation are developed that reflect similarities with respect to expected operational response to sea level rise. For example, dune-backed beaches used for special warfare training may have similar physical and operational characteristics which may be distinctive from cliff-backed beaches that are used for amphibious landing training. The purpose of this is so that operational limits can be developed that are applicable to a reasonable range of similar areas rather than developing response characteristics for every aspect of every training area.

Operational Limits

While command personnel may have a list of training activities, the minimum or maximum required characteristics of the training areas are not commonly defined and may be difficult for command personnel to articulate. To refine the assessment of the operational impacts of SLR on the beach training areas, the following information is necessary to determine the operational impacts:

- Are beach training operations scheduled with consideration of: high and low tide, surf and swell conditions, wind or weather?
- Would a reduction in beach width from the existing width impact training operations?
- Are training activities located at the installation based on beach width?
- Are there any training activities that require a minimum beach width?
 - o What is the minimum overall beach width?
 - o Minimum width within tidal zone?
 - o Minimum width above high water line?
 - o What frequency of return period event would make the training area non-operational (daily, weekly, monthly, or yearly)?

- How many personnel are involved in each training activity?
- What other factors may be used to determine if SLR will have an impact on beach training activities?

Assessment of Vulnerability

The criteria used to determine when a training area is considered non-operational is subjective because of the wide variety of training areas and training activities. Each training area category may have different operational requirements. One aspect of the assessment of training areas, is the need for the military to be prepared for a variety of physical settings and conditions. A change in the physical characteristics may not cause a loss of the training area. The following criteria were used to define the vulnerability of beach training areas.

Beach is non-operational for training

- Beach width is reduced to zero or to a width insufficient for training on a regular basis.
- The regularly recurring high water level reaches or approaches a hardened structure, seawall, property line, cliff or other defined boundary to such a degree that it prevents training.

Beach training area is partially operational

- Beach width is reduced to zero or to a width insufficient for training on an occasional basis.
- Occasional high water levels reaches or approaches a hardened structure, seawall, property line, cliff or other defined boundary to such a degree that it prevents training.
- Or, regular or occasional high water levels are such that certain aspects of training can no longer be conducted.

Beach training area is fully operational

• Sufficient beach width remains that training is not restricted beyond the baseline condition.

In addition, training activities conducted at coastal naval installations often include mitigation measures to protect marine mammals, sea turtles, birds, eelgrass, and overall water quality. At NBC, the protection of these areas is described in the *Silver Strand Training Complex (SSTC) Consistency Determination* (Department of the Navy). For example, due to the seasonal variability in the location and quantity of least tern and snowy plover nests at NBC, there may be at least portions of the year (nesting seasons) when it is not practical to include these protected areas in the analysis of usable beach training width. Thus operational limits should also consider the classification of beach zones with respect to potential bird nesting areas or other habitat restrictions which may interact with increasing sea level to further impact the operational use of beach training areas.

Buildings

Below is a summary of the additional information necessary to conduct a component-level assessment of buildings; a discussion of vulnerabilities specific to buildings; and an outline process for conducting a component-level assessment. The component-level assessment for the building receptor category focuses on the vulnerability of specific buildings to sea level rise related damage and operational impacts. Buildings identified during the receptor-level assessment as being vulnerable to sea level rise, particularly those with a high replacement value and/or mission dependency index would be good candidates for further analysis in the component-level assessment.



Figure 3-99. Beach Training Area, MCBCP. A view looking north at the beach zones from the bluff.

Existing Conditions - Check List Applicable Information from the Screening Level Assessment ☑ Facility Number ☑ Training Area Name ☑ Beach Training Area Shapefile Spatial Area and Beach Width Physical Delineation ☑ Tidal, Dune and Back Beach Zones ☑ Area, Width and Elevation Range of Each Zone ☑ Elevation range of each beach zone ☑ Beach Width Limits (cliff, road, or coastal structure) Other Coastal Structures that Affect Beach Changes (groins or artificial reefs) Operational Function & Requirements ☑ Types of Training Conducted ☑ Spatial and Temporal Requirements by Training Type ☑ Beach Width and Area Constraints on Training ☑ Tide, Weather and Ocean Condition Constraints on Training Extent of Personnel and Equipment Involved in Training Other Operational Considerations **Habitat Considerations** Restrictions in Place for Habitat Protection ☑ Spatial and Temporal Extent of these Restrictions ☑ Habitat Requirements for these Species

Figure 3-100. Existing conditions checklist for the component-level assessment of training areas.

Facility Existing Conditions

The information necessary to perform a detailed assessment of the impact of SLR on building infrastructure is listed below. It is anticipated that this information will be collected from field investigations and review of Record Drawings. The local Public Works Officer may have access to record Drawings, or more recent facility repair or upgrade drawings. Base facility operations personnel may maintain additional databases that have useful information relating to buildings and contents. If not available, field investigations may be required. To formalize the compilation of this information, we developed an Existing Conditions Checklist (see Figure 3-101) that defines key building features that are important to the evaluation of impacts from sea level rise.

Common Element Classification

Based on the characteristics developed above for the existing conditions, sub-categories of buildings for a given installation are developed that reflect similarities with respect to expected operational response to sea level rise. For example, operation and training buildings that support similar mission areas, have similar structures, contents and utility infrastructure would be assigned to a common sub-category. The purpose of this is so that operational limits can be developed that are applicable to a reasonable range of similar structures rather than developing response characteristics for every aspect of every structure.

Operational Limits

The extent of vulnerability to SLR is a function of the building type, floor elevation and proximity to the shoreline. Buildings located adjacent to the shore may be exposed to ocean waves or boat wakes once the water level has exceeded the elevation of the protective structure, i.e. beach, revetment, sand dunes, etc. Buildings located farther away from the shoreline may be flooded from intrusion of water through the storm water drainage systems or because of inadequate drainage during a rain event.

The operational limits of a building are determined from evaluation of the location, building type, usage, and appurtenances. The factors to be considered in association with a typical building structure include: functional floor elevations; foundations; accessibility; interior finishes; and building contents. A brief description of each of the building systems and the associated vulnerabilities follows.

Functional Floor Elevation. There are several critical elevations of building structures that impact the operational and damage impacts of SLR. The critical elevations include: first floor elevation, basement or below grade asset elevation, and exterior grade. The operational capability of the building will be impacted if the area outside of the building is inundated and personnel cannot access the building. If the water level reaches the first floor elevation, then the inside of the building, including, interior finishes and contents will be damaged. The degree of damage depends on the water depth and exposure to waves or floating debris.

Building Foundations. Two types of foundations are common for buildings in coastal areas: deep foundations and shallow foundations. Deep foundations are used for structures resisting lateral loads or when the soil near the surface has inadequate load bearing capacity. Deep foundations typically include pile caps and/or grade beams supported by piling or drilled caissons. For buildings sites located on competent soils, shallow foundations are the most common foundation type and include spread footings, strip footings (grade beams), or mat foundations. Sea level rise could impact the shallow foundations of buildings because of the increased elevation of the water table causing a reduction in allowable bearing capacity and an increased potential for settlement.

The bottom of a building shallow foundation is typically located between 0.6-m and 1.2-m (2-ft and 4-ft) below lowest adjacent grade. A shallow foundation is designed to transfer the loads to the soil without overstress. Overstressing the soil typically results in excessive settlement which can cause damage to the structure.

The bearing capacity of a shallow foundation is reduced if the groundwater table is within 1.5 times the footing width below the bottom of the footing. Figure 3-102 shows three water table scenarios for calculating load bearing capacity and settlement for shallow foundations. For the three scenarios shown, (a) would have the lowest bearing capacity; (c) would have the highest bearing capacity.

Existing Conditions - Check List					
Applicable Information from the Screening Level Assessment					
☑ Facility name					
☑ Building Number					
☑ Mission Dependency Index (MDI)					
☑ Replacement value (INFADS, UFC, or Engineer's estimate)					
Functional Elevations					
✓ Interior floor elevations					
☑ Below grade asset elevations (basement, trenches, vaults, etc.)					
☑ Exterior grade elevation					
Building Characteristics					
☐ Building structural system and foundation type					
☑ Age of Structure					
☑ Condition of the Structure					
☑ Interior finishes					
☑ Interior contents					
☐ Type and configuration of building utilities					
Operational Type & Function					
☑ Family Housing					
☑ Supply					
☑ Maintenance & Production					
☐ Troop Housing & Mess Facilities					
☑ Administrative					
Operation & Training					
☑ Community Facilities					
Research, Development, Test & Evaluation					
☑ Hospital & Medical					
☑ Utility & Ground Improvements					

Figure 3-101. Existing conditions checklist for the component-level assessment of buildings.

At Naval Base Coronado, two scenarios exist for groundwater elevation as a function of sea level and proximity to the ocean or bay. For soils close to the ocean or bay, the groundwater level will rise and fall with the tidal cycle. The groundwater will lag behind the open water level as the two levels "communicate" through the soil or retaining structure (seawall, bulkhead, revetment, etc.). For locations farther (0.25 miles) from the ocean or bay, the ground water elevation attenuates to mean sea level (MSL). After a rain event, water infiltrates into the ground and a mound effect occurs as the water attenuates to mean sea level. The difference in elevation between the bay or ocean, the groundwater mound elevation, and the permeability of the soil determines the rate of infiltration and attenuation (Todd, 1959) For design purposes, geotechnical engineers typically assume a mound effect of one meter above mean sea level for the design of building foundations, buried utility pipes, and buried tanks.

Sea level rise will cause the ground water table to rise. A rise in MSL will change the design criteria for buoyant forces, and load bearing capacity of shallow foundations for buildings. For cohesionless soils, such as sand, the bearing capacity might be reduced by up to one-half when the soil below the foundation is completely saturated. Building foundations are typically designed with a significant allowable load safety factor to account for variability in site conditions. The reduction in bearing capacity caused by saturated soils would reduce the factor safety, but distress is unlikely for standard loading conditions. A significant seismic event may result in excessive settlement and damage to the structure.

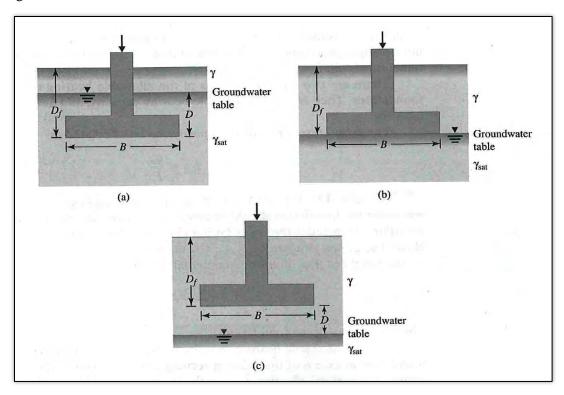


Figure 3-102. The groundwater table location influences the bearing capacity and settlement of shallow foundations. (a) The groundwater table is above bottom of the footing; (b) the groundwater table is at the bottom of the footing; (c) the groundwater table is below the bottom of the footing. (Das, 2002).

Access to Buildings. The elevation of parking lots and walkways adjacent to a building will determine if access to the building will be impacted by SLR. These areas will be affected at a lower SLR elevation than the first floor of the building. In general, water depths greater than 3-in. will limit pedestrian access to building structures. Paved areas are typically sloped to provide storm water runoff and prevent water accumulation greater than 1-in. (2.5-cm).

The increase in water table and ocean water levels will reduce the efficiency of storm water drainage systems. For the San Diego region which averages approximately 10-in. of rainfall per year, this may not be of great concern. However, for areas with more rainfall, the efficiency of storm water drainage systems should be assessed for a higher ground water table and ocean water level.

Interior Finishes of Buildings. A variety of structural systems and building interior finishes are used at Installations. Each structural system and interior finish has a different susceptibility to damage from flooding. Sometimes the structure is used for the interior finish, for example concrete or concrete block walls. A list of typical building interior finishes and susceptibility to flood damage is shown below.

Interior Contents of Buildings. Building contents will most likely be damaged when inundation occurs. For non-military installation flood assessments, the estimated value of the contents of buildings may be approximated as a percentage of the total replacement cost of the building. A variety of depth-damage functions are used for estimating flood losses to buildings and their contents by the Federal Emergency Management Agency (FEMA) and USACE Institute for Water Resources.

Interior Finish	Susceptibility
Concrete	Low
Concrete Masonry Units	Low
Brick Masonry Units	Low
Metal studs and corrugated sheathing	Low
Drywall (Gypsum board)	High
Plywood or Oriented Strand Board (OSB)	High

Table 3-13. Building interior finishes and susceptibility to SLR damage.

Buildings typically have alternating current (AC) electrical outlets within 18-in. (0.5-m) of the floor. If a building is flooded, the building interior finishes and electrical system would require repair or replacement.

Interior Contents of Buildings. Building contents will most likely be damaged when inundation occurs. For non-military installation flood assessments, the estimated value of the contents of buildings may be approximated as a percentage of the total replacement cost of the building. A variety of depth-damage functions are used for estimating flood losses to buildings and their contents by the Federal Emergency Management Agency (FEMA) and USACE Institute for Water Resources.

Department of Defense Installations contain a variety of building types with specialized military uses. For military buildings which contain specialized equipment, tools, and machinery the FEMA approach is not recommended. At MCBCP, there is a housing area adjacent to Del Mar Boat Basin

that may be vulnerable to inundation. For these residential structures, it is appropriate to apply the associated depth-damage functions provided by FEMA.

Assessment of Vulnerability

Assessment of the impact of SLR includes both short and long return period scenarios. These impacts include both damage to the facility and potential loss of operational functionality. In general, damage to buildings will relate to the flood depth and duration, as well as the type of building, its construction methods, finish type and interior contents. Operational impacts may begin to occur at lower flood depths in relation to loss of access, or impacts to building subsystems such as electrical vaults and communications systems, and then increase at higher water depths if the building is significantly damaged and its operational function is lost for a significant period of time. If the building is of non-standard construction, or if knowledge of these lower water depth operations is important, then development of component-level operational limits may be warranted. From a duration standpoint, if a facility can remain operational for short return period events, but is not operational for the 10-year or 100-year storm event, then a more detailed analysis of the facility type and usage is necessary to determine the operational impacts. The facility type and mission dependency (MDI rating) will determine if a facility can have operations limited by tides and storm events, or must remain fully operational at all times.

Damage and Operational Impacts. Assessment of operational impacts and damage to buildings at the component-level requires the development of response curves that delineate the impacts to the building as a function of water elevation. For standard buildings with low MDI values, standard damage response curves from FEMA or other sources may be used, and damage can be estimated based on comparison of estimated total water levels for a given scenario to the response function for the building. For non-standard buildings or for high MDI buildings where knowledge of potential impact to operations is critical, the development of more detailed response functions is required to better resolve the potential impact of different water elevations. These response functions can then incorporate in increasing spectrum of impacts relating to access, intrusion through storm drains, impacts to foundation components, impacts to related subsystems, and impacts to specialized contents, as well as significant damage to the building structure itself. Response functions developed at this level can then be related to both the magnitude and frequency of the SLR scenario of interest.

High MDI Value Facilities. Based on a review of the MDI criteria, we subjectively established an MDI rating of 55 as the cutoff above which designates facilities that must remain fully operational at all times and tidal cycles with maximum interruption of service of a day or less. For these facilities, each incremental SLR high water scenario is evaluated in comparison to the maximum operational water levels for the component. When the monthly return-period total water level exceeds the operational limits, the structures are considered non-operational. In this case, it is assumed that the structures will require replacement or upgrades to accommodate the higher water levels and the costs associated with these requirements are derived from the checklist information described above.

Low MDI Value Facilities. High MDI ratings are reserved for facilities that must remain operational at all times. Buildings with an MDI rating of 55 or lower is indicative of facilities with operations that may be occasionally interrupted in the future by tidal or other high-water related fluctuations. The monthly return-period total water level may cause conditions leading to operational losses for short intervals during the peak tide. The number of days or months per year that the structure is non-operational can be estimated. This assumes that the structure can be operational at lower water levels and can still support operations. Facility Managers and Operations personnel will need to use tide and other predictions to determine the specific days in the month that are likely to have a high water

level exceeding the operational limits of the building and will coordinate operations around these high water events.

Tidal Cycle and Return Period. If a facility can remain partially operational, then variations in tidal cycles or total water level return period can be used to estimate the time periods and durations that the facility is non-operational. For example, the maximum monthly tides for the next 100-years without sea level rise vary from 1.94-m to 2.45-m inside of San Diego Bay. If water level dependent operations are allowable, then the prediction of water levels used to estimate operational loss is critical for an accurate assessment. There are various approaches to predict these water levels for protected harbor areas including the use of monthly or daily maximum tidal conditions. Here, to be consistent with the approach used for the exposed shorelines, we focused on the use of total water level scenarios with sea level rise for the week, month, year, decade and century return periods. These were then compared to the maximum operational water level for the sub-category to determine the return period and sea level rise combinations for which the facility is non-operational. Component-level assessment vulnerability assessment examples for buildings are presented in Section 4..4.3.

Waterfront Structures

Waterfront structures at naval bases typically include piers, wharves, quaywalls, floating docks, boat ramps and other specialized facilities. This methodology was developed primarily for the assessment of the impact of SLR on piers and wharves, but is conceptually applicable to the full range of waterfront structures. Key background information regarding the general configuration of naval waterfront structures was developed based on the Unified Facility Criteria (UFC) design manual *UFC 4-152-01 Design: Piers and Wharves* (NAVFAC, 2005).

Facility Existing Conditions

The information necessary to perform a detailed assessment of the impact of SLR on a waterfront structure is listed below. Much of the necessary information can be obtained from the previously described NAVFAC documents. Information for virtually every Navy waterfront facility in the U.S. and abroad exists in the form of a WFI Report which is typically updated on a six-year basis. The WFI report typically contains structural and utility plans and sections; photographs; facility description; asset inventory; and a condition assessment for each part of the waterfront structure. The local Public Works Officer may have access to As-Built (Record) Drawings, or more recent facility repair or upgrade drawings in electronic format. To formalize the compilation of this information, we developed an Existing Conditions Checklist (see Figure 3-103) that defines key infrastructure features that are important to the evaluation of impacts from sea level rise.

Common Element Classification

Based on the characteristics developed above for the existing conditions, sub-categories of waterfront structures for a given installation are developed that reflect similarities with respect to expected operational response to sea level rise. For example, pier structures that support similar ship classes, have similar structures, fender systems and utility infrastructure would be assigned to a common sub-category. The purpose of this is so that operational limits can be developed that are applicable to a reasonable range of similar structures rather than developing response characteristics for every aspect of every structure.

Operational Limits

For long-term planning, it is necessary to determine the critical sea level elevations at which sea level rise would limit operations. The maximum operational water level of a structure or subcategory of structures is determined from evaluation of the checklist elements described above in the context of the operational requirements of the structure including: deck elevation (overtopping); load

capacity; vessel mooring and berthing; and utility services. A brief description of each of the systems and the associated operational limitations follows.

Deck Elevation (Overtopping). Waterfront structures used for the mooring of vessels are designed based on guidance from the Unified Facilities Criteria (UFC) 4-152-01, Design: Piers & Wharves (NAVFAC, 2005). The document recommends locating the deck elevation as close as possible to the grade of the adjacent land for smooth access of mobile cranes, service vehicles, personnel vehicles, and railroad. Other considerations for establishing the deck elevation include:

- Overtopping The tendency for the facility to become inundated from a body of water as a result of tide waves, wake, seiche, river-rise, or any other significant change of water level (sea level rise).
- Vessel type Marine structures are designed to service a specific range of vessels. The deck elevation is located to support embarkation and disembarkation. The deck elevation is also located to facilitate the loading of cargo, ordnance and other supplies. The deck is typically lower for smaller vessels, and higher for large vessels.
- Utilities Most facilities provide utility services for both general use and/or vessel support.
 These services have varying sensitivity to water level depending on the type of service,
 material composition, location (above/below deck) on the facility, and the method of
 attachment.
- Tidal cycle –Tidal ranges vary based on geographical location. The deck elevation is located to accommodate the tidal variations of the particular site.
- Wave height This forcing function can vary substantially. Factors influencing potential wave height include: location (in-bay or open-ocean facility); fetch; bathymetry; and boat wake.

When a waterfront structure is vulnerable to overtopping, it may also be subjected to uplift pressures on the underside of the deck. Once the potential water elevation nears the deck elevation, the structure may be further jeopardized by wave or wake-generated forces.

Vessel Mooring and Berthing. The primary purpose of many Naval waterfront structures is for the mooring of vessels. The fender system is the interface between the ship and the shore facility. During the berthing of a ship, the fender system is meant to act as a buffer in absorbing or dissipating the impact energy of the ship without causing permanent damage to the ship or the shore facility. Once the ship is successfully berthed and moored to the shore facility, the fender system continues to provide the interface between ship and shore and transmits energy from the environmental loads (wind, waves, and current) to the structure. For submarine and other low-profile vessels, the fender system also provides a physical barrier to prevent the vessel from going underneath the pier at low tide. There are a variety of fender systems used at Naval installations to support the fleet (UFC 4-152-01, Design: Piers & Wharves (NAVFAC, 2005); Figure 3-104).

Fender systems using floating foam-filled fenders are the predominant system used by the Navy in the San Diego Region and are vulnerable to sea level rise. Existing fender systems are designed to operate through the full tidal range. During mooring and berthing operations, the foam-filled fenders are designed to compress up to 60% of their diameter as shown in Figure 3-106. The top of fender pile elevation is established to provide backing for the compressed fender at high tide (Figure 3-107).

A rise in sea level combined with a high tide could cause the floating elements to "roll-over" the top of the fender piles and deck. The water elevation at which the fender system becomes susceptible to "roll-over" may be well below the top-of-deck elevation, see Figure 3-105. This type of failure could allow the vessel to impact the pier causing damage to the structure, to the ship hull and/or personnel.

For a component-level assessment, a maximum operational water level can be determined from analysis of the fender system elements, vessel types, and mooring conditions. The critical elevation for a floating foam filled fender system is a function of the fender size and elevation of the top of fender pile – see Figure 3-108.

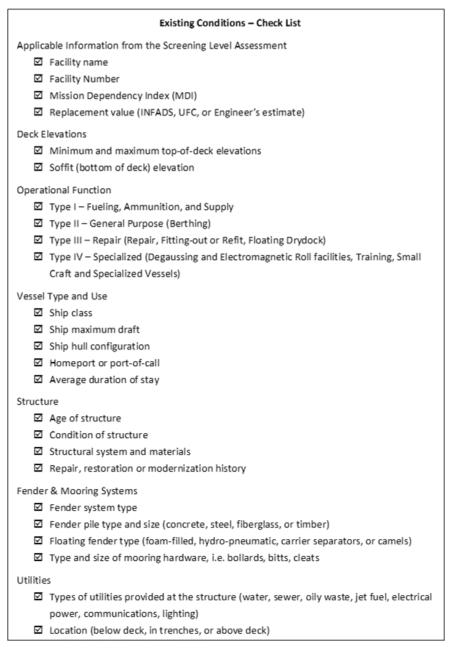


Figure 3-103. Existing conditions checklist for the component-level assessment of waterfront structures.



Figure 3-104. Typical pier fender system with floating fenders and concrete reaction piles at a close spacing for bearing.

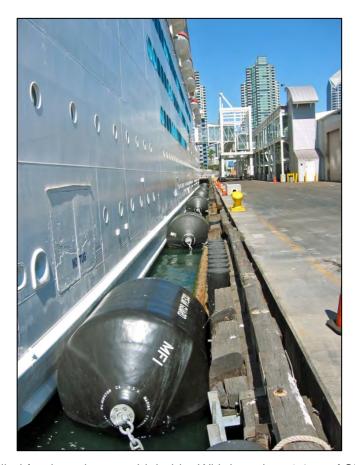


Figure 3-105. Foam filled fenders shown at high tide. With less than 1.0 m of SLR, "roll-over" could occur.

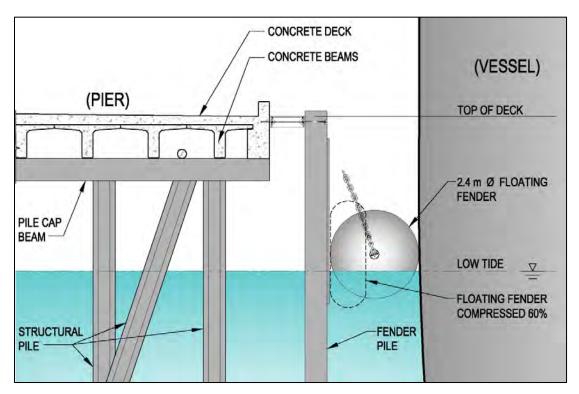


Figure 3-106. Partial pier section showing a floating fender system at low tide. The compressed fender (dashed) is fully supported by the fender piles.

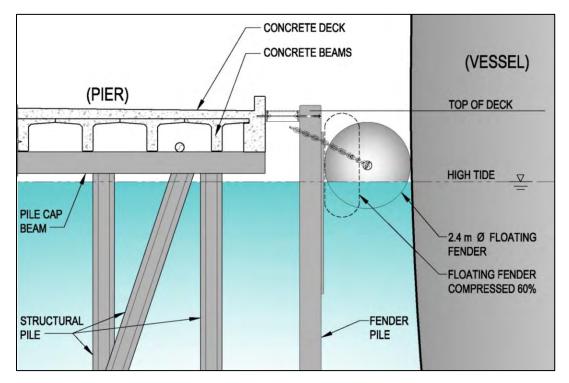


Figure 3-107. Partial pier section showing a floating fender system at high tide. The top of the fender system is below the top of the fender pile. The compressed fender (dashed) is fully supported by the fender piles.

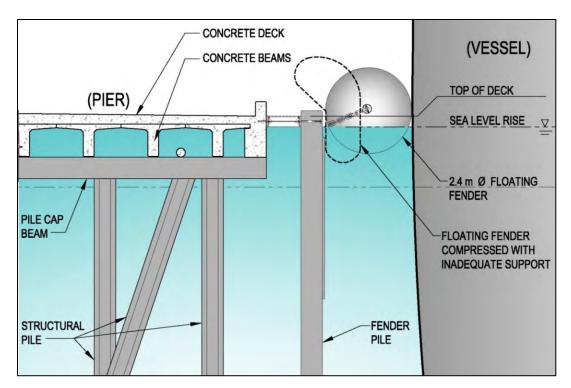


Figure 3-108. Partial pier section showing a floating fender system subjected to SLR. The fender is at the critical elevation where it becomes susceptible to "roll-over".

Utility Services. Utilities common to waterfront structures include electrical power, communications, water, sewer, oily waste, steam and compressed air. Less common utilities include fuels and pure water. If sea level rise causes piping located below deck (originally above water) to be submerged, then the pipes and hangers would have additional wave and current loading. If the pipes were not designed for submerged conditions and the hangers were not designed for wave and current loading, then damage will result. Utility lines that are submerged in the tidal cycle may also catch kelp and other floating debris that cause additional loading on the support brackets – See Figure 3-109 and Figure 3-110.

Some facilities have utility trenches that are integral to the deck structure and are accessed from the top of the deck. Utility trenches protect the pipes from wave and current loading and are common for modern piers and wharves.

Service Life. This study evaluates the effects of 0.5-, 1.0-, 1.5-, and 2.0-m sea level rise on military infrastructure as extrapolated over a 100-year period. Aside from the direct effects of SLR on infrastructure, a secondary effect is the reduction of the service life of structures constructed on or adjacent to harbor or ocean waterfronts. "Service life" is defined as "That period of time over which only minimal routine maintenance is performed on a structure. Service life is exceeded when major repairs, rehabilitation or modernization become necessary for the structure to remain functional. The return-on-investment for repairs of this magnitude usually exceeds the capital improvement cost for demolition and replacement of the facility."

Under normal conditions, the service-life of a reinforced concrete structure in a marine environment operating in the Southern California Region is considered to be on-the-order of 50 years. The overwhelming majority of the facilities in the Navy's inventory are constructed of reinforced concrete. The structures located at Naval Base Coronado and Marine Corps Base Camp Pendleton were constructed between the early 1940s and 2003, with the average age of the facilities

being approximately 40 years old. It is highly probable that most of the structures will be replaced sometime within the 100-year-span considered in this document. Sea level rise will certainly be considered as a factor in establishing the functional deck elevation of the replacement structures, which will be required to remain operational for both the short and long-term.

For example, the existing fuel pier at Naval Base Point Loma (Fleet Industrial Supply Center Fuel Pier 180) was constructed in 1908 with a significant addition in 1941. This facility is scheduled for replacement under a project identified as "P-151 Fuel Pier Replacement." This project is currently being designed and construction is scheduled to be completed in 2016. The new structure is being designed for a 75-year service life. The deck elevation for the new structure has been set 305 mm (12-inch) higher than the previous structure to account for future sea level rise.

However, exposure from sea level rise may accelerate aging of these structures, and reduce the expected service life. As steel corrodes, it undergoes a volumetric expansion, swelling to more than nine times the original volume. Since the steel is restrained by the surrounding concrete, an outward pressure is exerted on the concrete. This outward pressure is inherently a tensile force, and as concrete is relatively weak in this mode of loading; cracks and eventually spalling of the concrete occurs (Figure 3-111). The loss of cover over the bar leads to increased rate of corrosion, and loss of cross-sectional area of the bar.

The corrosion mechanism described above is based on the ingress of chlorides (salt) through the concrete and into the reinforcing steel. The degree of chloride contamination has a direct relationship to the potential for concrete damage as a result of corrosion of the reinforcing steel. As sea level rises, the concrete structure – particularly the sides and under side of the deck - are increasingly exposed to the alternate wetting of seawater and drying, leading to a more rapid build-up of chlorides.



Figure 3-109. Pier with utility pipes located below deck in the tidal zone.he pipes are submerged during high tides and collect kelp and other debris.



Figure 3-110. Pier with water pipe located below deck. The pipe and hangers may not be designed for wave and current loading.

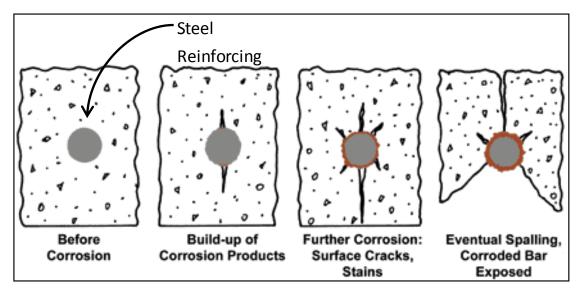


Figure 3-111. Process of steel corrosion-related concrete damage (adapted from American Galvanizers Association, http://archive.galvanizeit.org/about-hot-dip-galvanizing/how-long-does-hdg-last/in-concrete).

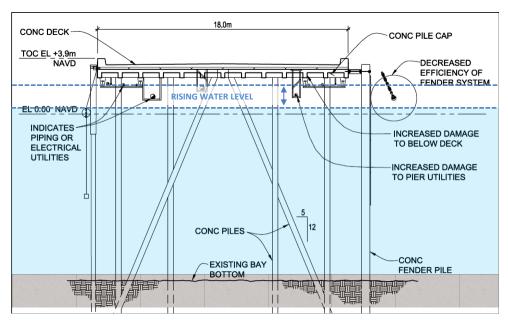


Figure 3-112. Effects of sea level rise on a typical pier.

Assessment of Vulnerability

Assessment of the impact of SLR includes both short and long return period scenarios. If a facility can remain operational for short return period events, but is not operational for the 10-year or 100-year storm event, then a more detailed analysis of the facility type and usage is necessary to determine the operational impacts. The facility type (fueling, ammunition, cargo/supply or repair) and mission dependency (MDI rating) will determine if a facility can have operations limited by tides and storm events, or must remain fully operational at all times.



Figure 3-113. Waterfront structure that has excessive deterioration from chloride contamination and corrosion of the reinforcing steel (courtesy of Blaylock Willis and Associates).

High MDI Value Facilities. Based upon a review of the MDI criteria, we subjectively established an MDI rating of 55 as the cutoff above which designates facilities that must remain fully operational at all times and tidal cycles with maximum interruption of service of a day or less. For these facilities, each incremental SLR high water scenario is evaluated in comparison to the maximum operational water levels for the receptor sub-category. When the monthly return-period total water level exceeds the operational limits, the structures are considered non-operational. In this case, it is assumed that the structures will require replacement or upgrades to accommodate the higher total water levels and the costs associated with these requirements are derived from the checklist information described above.

Low MDI Value Facilities. High MDI ratings are reserved for facilities that must remain operational at all times. Waterfront facilities with an MDI rating of 55 or lower is indicative of facilities with operations that may be occasionally interrupted in the future by tidal or other high-water related fluctuations. The monthly return-period total water level may cause conditions leading to operational losses for short intervals during the peak tide. The number of days or months per year that the structure is non-operational can be estimated. This assumes that the structure can be operational at lower water levels and can still support operations. Facility Managers and Port Operations personnel will need to use tide and other predictions to determine the specific days in the month that are likely to have a high water level exceeding the operational limits of the waterfront structure and will coordinate operations around these high water events.

Tidal Cycle and Return Period Discussion. If a facility can remain partially operational, then variations in tidal cycles or total water level return period can be used to estimate the time periods and durations that the facility is non-operational. For example, the maximum monthly tides for the next 100-years *without* sea level rise vary from 1.94-m to 2.45-m inside of San Diego Bay.

This requires evaluation of the facility type and corresponding usage with respect to the frequency of the high water level scenario. A fuel or ammunition pier may need as few as three to five consecutive days for operations; accordingly, it could be possible to work around periods of highest tide. However, a pier used for homeporting or repair may require one month to six months of consecutive time without a high tide exceeding the operational limits of the structure.

If water level dependent operations are allowable, then the prediction of water levels used to estimate operational loss is critical for an accurate assessment. There are various approaches to predict these water levels for protected harbor areas including the use of monthly or daily maximum tidal conditions. Here, to be consistent with the approach used for the exposed shorelines, we focused on the use of total water level scenarios with sea level rise for the week, month, year, decade and century return periods. These were then compare to the maximum operational water level for the subcategory to determine the return period and sea level rise combinations for which the facility is non-operational. Component-level assessment vulnerability assessment examples for waterfront structures are presented in Section 4.4.3.

Coastal Structures

Coastal structures at naval bases typically include a range of structures whose primary purpose is to protect the shoreline from erosion and thus sustain operations and missions of the installation. This category encompasses structures such as jetties, groins and revetments which are used to protect the shoreline and dredged improvements. The methodologies presented below identify common types of additional information and steps that are necessary to conduct a component-level assessment and characterize vulnerabilities specific to coastal structures.

Facility Existing Conditions

The existing conditions for coastal structures are typically documented in construction Record Drawings. The detailed analysis of coastal infrastructure requires the expertise of a coastal engineer with experience in the design of such structures. The information contained in the Record Drawings is necessary to analyze any of the systems described below. The local Public Works Officer or the USACE may have access to Record Drawings, or more recent facility repair or upgrade drawings. Defining the existing conditions may include determination of: rock sizes, slope, wall tiebacks, subgrade type, geotextile fabrics, etc. If Record Drawings are not available, then field surveys and investigations may be necessary to determine the existing conditions. To formalize the compilation of this information, we developed an Existing Conditions Checklist (see Figure 3-114) that defines key infrastructure features that are important to the evaluation of impacts from sea level rise.

Common Element Classification

Based on the characteristics developed above for the existing conditions, sub-categories of coastal structures for a given installation are developed that reflect similarities with respect to expected operational response to sea level rise. For example, revetment structures installed on similar shoreline exposures and protect similar infrastructure would be assigned to a common sub-category. The purpose of this is so that operational limits can be developed that are applicable to a reasonable range of similar structures rather than developing response characteristics for every aspect of every structure.

Operational Limits

The coastal structures provide coastal storm damage and flooding protection to buildings, waterfront structures, and training areas. Accordingly, coastal structures can be critical to the operations of an installation. The coastal infrastructure has vulnerabilities to SLR based on the type, elevation and location of the structure. Coastal infrastructure located within a bay or harbor is generally less vulnerable since it is generally exposed to much lesser waves as compared to structures exposed to ocean waves (Figure 3-115). However, this logic assumes that the coastal structures have been adequately designed for existing conditions. Coastal structures are designed to protect critical landward infrastructure. For example, a coastal structure that protects a training facility may allow episodic flooding while a structure that protects critical buildings could not. Therefore, the vulnerability of the landward protected structure should be considered in combination with the vulnerability of the coastal structure itself. The operational limits of coastal infrastructure are determined from evaluation of the location, type, function, and elevation. Brief descriptions of each type of coastal infrastructure are as follows.

Revetment. Revetments are onshore, engineered structures designed for the principal function of protecting the shoreline from erosion. Revetments are rubble-mound structures and slope seaward at varying degrees contingent on function, which act to dissipate wave energy. Revetments are generally not designed to be overtopped as wave overtopping will damage structures in the lee of a revetment. Revetment stone size and placement types vary dependent on the wave environment they are being designed for. Hand placed, large stones are typical along ocean wave exposed shorelines. Smaller stone such as rubble rip-rap is commonly used on low-wave energy, bay shorelines. An example of a typical rubble-mound revetment structure is shown in Figure 3-116.

Seawall. Seawalls have the principal function of preventing or alleviating overtopping or flooding of the land. Seawalls include rubble-mound sloping structures (sometimes armored with concrete armor units), vertical face structures such as massive gravity concrete walls, tied walls using steel or concrete piling, and stone-filled cribwork to sloping structures with typical surfaces being reinforced concrete slabs (U.S. Army Corps of Engineers, 2006).

Bulkhead. Bulkheads are primarily intended to retain land along a waterway. While bulkheads can protect against relatively small wave attack and they can be used in combination with a rubble mound seawall, they seldom used as solely as shore protection. Bulkheads are generally designed to withstand waves less than three feet. This design consideration limits these structures to areas of relatively mild wave conditions, such as bays and harbors. A typical bulkhead design is shown is Figure 3-117.

Jetty. Jetties are engineered structures designed to stabilize and provide protection to vessels transiting a navigation entrance channel to a harbor and/or bay. Jetty designs vary, but are generally rubble-mound structures. A typical jetty configuration is shown in Figure 3-118.

Vulnerabilities on these coastal structures due to SLR vary; however, can be generalized into the following categories:

Increased Loading. Increased water levels fronting the structure result in greater wave forces on the structure, which may result in damage or failure. This is a product of an increase in the depth-limited breaking wave height. Simplistically, the height of a wave is limited in shallow waters by wave breaking. For a given water depth, there is a limit to the largest wave that can break in that depth. If the water level increases with SLR then the limiting breaking wave height will be larger. This potentially increases the exposure for the existing coastal structures. The depth-limited maximum wave height (H_{max}) can be expressed as:

Equation 3-17

$$H_{max} \approx (0.8 \text{ to } 1.0) \times d$$

where d is the water depth. A larger wave may cause damage to a coastal structure leading to failure or reduced design life.

Increased Overtopping. SLR results in increases in the baseline from which storm events will be added. Thus, the probability and frequency of overtopping of coastal structures could be expected to increase as water levels increase. Overtopping can lead to scour or erosion of areas landward of the structure, which could lead to the instability of coastal structures.

Decreased Function. For structures such as jetties, the intended function could be compromised as water levels increase. Jetties serve to provide safe navigation to harbors. Increases in water levels could cause damage to the structure or allow larger waves to impact navigating vessels in an entrance channel.

Assessment of Vulnerability

Assessment of the impact of SLR includes both short and long return period scenarios. If the coastal structure can remain operational for short return period events, but is non-operational (i.e., fails/overtopped or is damaged) during the 10-year or 100-year storm event, then a more detailed analysis of the structure and its specific function is necessary to determine the operational impacts. The structure type and mission dependency (MDI rating) of the facilities it protects will determine if the structure can be non-operational during these storm events, or if it must remain fully operational at all times. If the protected facilities will be damaged by inundation or flooding because the coastal structure is inadequate, then upgrades to the coastal structure will be required.

Coastal structures protecting these facilities may not need to be replaced or upgraded; however, this is contingent on the acceptable non-operational duration of each of these specific facilities. If water level dependent operations are allowable, then the prediction of water levels used to estimate operational loss is critical for an accurate assessment. Here, to be consistent with the approach used for the exposed shorelines, we focused on the use of total water level scenarios with sea level rise for

the week, month, year, decade and century return periods. These were then compared to the maximum operational water level for the sub-category to determine the return period and sea level rise combinations for which the facility is non-operational. Coastal infrastructure vulnerability is discussed per structure type below, and component-level assessment examples for coastal structures are presented in Section 4.4.3.

	Existing Conditions – Check List
Applica	able Information from the Screening Level Assessment
\square	Facility name
\square	Structure location and type
\square	Replacement value (INFADS, UFC, or Engineer's estimate)
	Coastal Structure Shapefile
Operat	ional Characteristics
. 🗹	Operational function
	Infrastructure and/or assets protected by the structure
	Mission Dependency Index (MDI) of protected infrastructure
	are Characteristics and Condition - Revetments
☑	Crest detail (i.e. elevation and width)
	Stone detail (size, layers, core, approximate weight, placement type)
	Seaward and landward structure slope
\square	Porosity
\square	Toe elevation
	Structure condition
Structi	re Characteristics and Condition - Seawalls/Bulkheads
\square	Tip of wall elevation
\square	Tieback presence
$\overline{\mathbf{v}}$	Wall type (reinforced concrete, sheetpile)
\square	Rip-rap to e protection
	Hinterland type (i.e. earthen, asphalt)
\square	Structure condition (i.e. signs of failure or damage, erosion of hinterland)
Structi	re Characteristics and Condition - Jetties
\square	Crest detail (i.e. elevation and width)
\square	Structure head detail (i.e. rock size)
	Stone detail (size, layers, core, approximate weight, placement type)
	Structure porosity
-	Rock slope (head and trunk)
1	Toe elevation
	Structure condition (i.e. percent damage)

Figure 3-114. Existing conditions checklist for the component-level assessment of coastal structures.



Figure 3-115. Wave breaking on the rubble-mound structure at Oceanside Harbor (California Coastal Records Project Image 8921042; Copyright (C) 2002. 2014 Kenneth & Gabrielle Adelman, California Coastal Records Project, www.Californiacoastline.org).

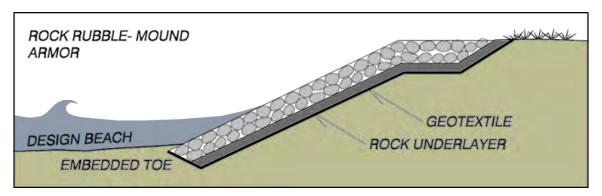


Figure 3-116. Typical rubble-mound revetment section (adapted from USACE, 2006).

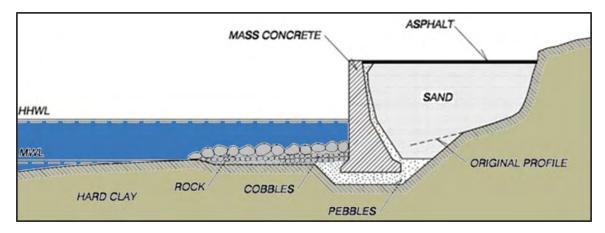


Figure 3-117. Typical Seawall or Bulkhead Section (adapted from USACE, 2006).

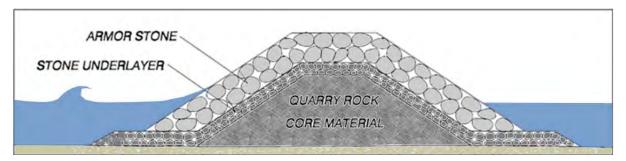


Figure 3-118. Typical rubble-mound jetty section (ædapted from USACE, 2006).

Revetment Vulnerabilities. A revetment is susceptible to sea level rise from increases in the depth-limited breaking wave height approaching the structure as well as scour of the hinterland if (1) this area is erodible, and (2) overtopping of the structure occurs frequently. These two processes could result in increased damage or failure of the structure.

Seawall Vulnerabilities. Seawalls are vulnerable to SLR from increased wave overtopping. More frequent overtopping can result in scour of the hinterland, which can ultimately lead to structure damage.

Bulkhead Vulnerabilities. Bulkheads are vulnerable to wave impact and overtopping damage that will be exacerbated by SLR.

Jetty Vulnerabilities. Jetties are particularly vulnerable at the head (seaward most end) of the structure where the largest waves impact the structure and because of way that incident wave strike the head. Changes in SLR could have an impact on the depth-limited breaking wave height approaching the structure. Increased water levels could result in changes in wave interactions within these structures and/or increases in the shoaling of navigation channels.

Civil Infrastructure

Civil Infrastructure includes transportation corridors, and utility infrastructure such as buried utilities, fuel transfer/supply, and storm water conveyance systems. Outlined below is a summary of the additional information necessary to conduct a component-level assessment of a civil infrastructure; a discussion of vulnerabilities specific to civil infrastructure; and an outline process for conducting a component-level assessment.

Facility Existing Conditions

The original construction for civil infrastructure is documented in construction Record Drawings. The detailed analysis of civil infrastructure requires the expertise of a civil engineer with experience in the design of roadways, storm water systems and utility systems. The information contained in the Record Drawings is necessary to analyze any of the systems described above. The local Public Works Officer may have access to Record Drawings, or more recent facility repair or upgrade drawings.

The details of existing conditions may include: pipe invert elevations, lengths, and diameters; grading plan of the area; and vault details. If Record Drawings are not available, then field surveys and investigations may be necessary to determine the details of existing conditions. A checklist of existing condition information is listed in Figure 3-119. To perform a component-level assessment of the impact of SLR on civil infrastructure, the user should obtain as much of the listed information as possible.

Common Element Classification

Based on the characteristics developed above for the existing conditions, sub-categories of civil infrastructure for a given installation are developed that reflect similarities with respect to expected operational response to sea level rise. For example, transportation systems constructed of similar materials, supporting similar access requirements, and subject to similar exposure conditions would be assigned to a common sub-category. The purpose of this is so that operational limits can be developed that are applicable to a reasonable range of similar structures rather than developing response characteristics for every aspect of every structure.

Operational Limits

The civil infrastructure at an installation provides access (transportation corridors) and utility service to buildings, waterfront structures, training areas, and is critical to the operations of the installation. The civil infrastructure of an installation is vulnerable to SLR based on the type, elevation and proximity to the shoreline. Civil infrastructure located adjacent to the shore may be exposed to ocean waves or boat wakes once the existing/original design water level has been exceeded. Such structures include revetments, seawalls, or natural barriers like cliffs or sand dunes. Civil infrastructure located away from the shoreline may be flooded from intrusion of water through the storm water drainage system during high tides because increased sea levels will reduce the ability of the storm water system to drain.

Infrastructure assets are often interrelated and failure of one may cause impacts to others. For example, as sea level rise impedes the storm water drainage system, the impeded system will cause flooding on the roadways and building parking areas during a significant rain. If standing water accumulates over a sewer or electrical vault lid, then water will leak in and flood the vault. Vault covers that are closed may use joint seal; however, water will still likely penetrate. For a component-level assessment, it is necessary to analyze each SLR scenario with and without a range of rainfall events including the corresponding return period rain event.

The operational limits of civil infrastructure are determined from evaluation of the overall system, location, type, usage, and appurtenances. A brief description of some of the more common types of civil infrastructure and the associated vulnerabilities follows.

Storm Water Conveyance Systems. Storm water management systems typically include storm drains and a variety of other construction features to manage the volume, flow and quality of runoff during rain events. Storm water runoff from impervious surfaces, such as roadways and parking areas, is routed to detention ponds or swales and ultimately routed through underground piping to discharge into the bay or the ocean. Storm water pipes are typically gravity fed and have minimal slope to accommodate the low lying elevations and the long distances the pipes have to run. Modern storm water pipes are typically comprised of reinforced concrete pipe with compression joints between pipe sections. A storm water pipe is vulnerable to SLR from intrusion of water from the bay or ocean, as well as reduced flow rates when the differential head between the system entrance and exit is reduced. The reduction in capacity owing to SLR will likely cause flooding depending on drainage system design/resiliency. Flooding from impaired storm water drainage can impact transportation corridors; gravity sewer systems; electrical vaults; building access; and flooding in low-lying areas located away from the shoreline.

Transportation Corridors. A roadway is typically designed with a transverse slope of approximately 2% from the high point at the centerline to the edges to eliminate ponding. If a roadway has poor drainage and standing water after a rain event, then the water could cause damage to the subgrade and deterioration of the road surface. Many areas of NBC are comprised of loosely-consolidated dredge material placed by hydraulic methods as part of bay dredging. This is typical of

many Naval installations. If accelerated sea level occurs, an investigation of the potential for additional settlement should be undertaken.

	Existing Conditions - Check List
Applica	ble Information from the Screening Level Assessment
\square	Facility name
\square	System type, elevation, proximity to shoreline, shapefile
\square	Replacement value (INFADS, UFC, or Engineer's estimate)
Operat	ional Characteristics
\square	Operational function and relevance
\square	Infrastructure and/or assets supported/protected by the system
	Mission Dependency Index (MDI) of supported/protected infrastructure
Infrastr	ucture Characteristics and Condition – Stormwater System
\square	Component elevations
\square	Pipe sizes, materials, slopes and design capacity
\square	Drainage area and volumes
	System condition
Infrastr	ucture Characteristics and Condition – Sewer System
20.0	Gravity or pressurized
	Pump locations and type
	Pipe sizes and materials
223	Component elevations
	System condition (i.e. seals, pipe condition)
	ructure Characteristics and Condition – Power and Communications
	Cable types and voltage levels Above or below ground
	Vault contents, materials, seals and waterproofing
	Component elevations
	System condition (i.e. vault seals, underground cables and splices)
	ucture Characteristics and Condition – Transportation and Airfield
	Surface and subsurface materials
$\overline{\mathbf{v}}$	Drainage and slope
\square	Surface and subsurface condition (i.e. wear, potholes, erosion)
Infrastr	ructure Characteristics and Condition – Potable Water Systems
	Component elevations
	Pipe sizes and materials
	Location and types of above/below ground components
	System condition (i.e. pipe corrosion, leaks)
	Surface and subsurface condition (i.e. wear, potholes, erosion)

Figure 3-119. Existing conditions checklist for the component-level assessment of civil infrastructure.

A roadway structural section is comprised of a compacted gravel and soil subgrade with either asphaltic concrete or cementations concrete surface. The damage mechanism for water on or adjacent to a roadway starts with erosion and deterioration at the roadway edges or cracked areas. As the surface or edges erode, the foundation subgrade materials will be exposed and further erode.

An asphaltic concrete roadway will break apart and crack causing potholes and settlement. A cementations concrete roadway will settle and break in larger sections when the subgrade becomes saturated and erodes. If a roadway is inundated or flooded and exposed to small waves and over wash, the rate of erosion and deterioration will be faster than standing water because of the erosive forces of the moving water.

Airfields. Airfields are typically comprised of an approximately 12-in. thick reinforced concrete slab to support the high wheel loads from aircraft. Airfields will have will have vulnerabilities similar to Transportation Corridors, including settling and drainage concerns.

Sewer Systems. Sewer systems infrastructure includes gravity mains, force mains, pump stations, holding tanks, and metering stations. Sewer systems can be divided into two types: gravity flow system or pressurized pump system. For gravity sewer systems the pipe is less than half full and acts as an open channel. The pipe is typically comprised of large diameter reinforced concrete pipe (RCP) or vitrified clay pipe (VCP). The joints between RCP or VCP sections are sealed with a compression joint; however, minor leaking is common. If the water table rises above the bottom of the pipe, then groundwater will leak through the joints and decrease the capacity of the pipe for sewer waste water. If the pipe continues to fill with ground water, and becomes greater than 90% full, the velocity will decrease and may back-up and overflow at manholes. The increased conveyance volume, which includes groundwater, may exceed the capacity of the water treatment facility.

Pressure sewer systems use sealed pipes, such as cast iron, and the waste is pumped between lift stations. The wet well at a lift station could fail if groundwater or storm water runoff enters the wet well. The additional water could cause a failure because the pump cannot keep up with the increased demand of groundwater, storm water and sewage.

Potable Water Systems. Potable water infrastructure includes pressurized water mains, pressure-reducing valves, and meter vaults. Below ground potable water systems typically use sealed pipes such as cast iron or high-density polyethylene. Cast iron fresh water pipes are typically not sensitive to SLR related damage because the pipes have sealed joints and the self-weight balances the buoyant forces. However, HDPE pipes are lighter weight and could shift when the water table rises above the pipe and a buoyancy force is added, coupled with the reduced strength of soil upon saturation. Above ground components of the system including hydrants, valves, service access, and meters could be exposed to inundation.

Electrical Systems. Electrical systems can be categorized into power and communication systems. Power systems are further categorized as high voltage, medium voltage, and low voltage distribution systems. Communication systems consist of telephone and data/communication systems. Electrical distribution systems may be located above ground, as in overhead distribution or transmission lines, or be routed below ground using cables in conduits, in duct banks, or directly buried in ground. Below ground cable installations in conduits or duct banks normally includes a series of manholes and vaults that are placed along duct bank runs to aid in pulling long cable.

Cables in these manholes are typically rated for continuous submersion and wet application, and use splices and equipment connections that are also rated for continuous submersion. Sealed/Insulated electrical lines are not vulnerable to SLR related damage except at switch panels,

vaults or other below ground connection points. Continuous submersion of below ground connection points causes additional stress on the connections and may require increased maintenance.

Electrical Vaults. Electrical vaults are used to house switching equipment, connection panels, transformers, capacitors, and other electrical equipment. The type of equipment and susceptibility to flooding varies at each vault. Some vaults can remain operational when full of water (see Figure 3-120) and other vaults cannot. Older vaults have equipment that may have exposed wire connections – (see Figure 3-121) and could be susceptible to damage from inundation and flooding.

Below grade electrical vaults are designed to prevent groundwater intrusion and storm water runoff from entering the vault. The vault covers are precast concrete or steel and typically have joint seal to prevent rain water from entering. These joint seals require maintenance and covers can leak over time allowing water to enter the vault. If the street or sidewalk that contains the vault cover is inundated as a result of failure of the storm water drainage system, then the quantity of water leaking through the vault cover would increase.

Buried vaults typically include a french drain through the floor or have a sump and pump to remove water from the vault. A vault with a french drain would be susceptible to inundation if the water table rises above the floor of the vault with sea level rise. Constant flooding inside the vault introduces potential failure in the electrical system if not regularly maintained. If the vault has a sealed floor, a rise in the ground water elevation would impose a buoyancy force on the floor of the vault. An increase in the elevation of the water table could cause flooding of vaults that were designed for a lower water table and lower buoyancy force.

Natural Gas Systems. Natural gas systems use steel pipe with sealed joints or HDPE sealed pipe. Natural gas pipe lines are typically not vulnerable to SLR related damage.

Oily Waste. Oily waste systems are used to dispose of ship bilge water and typically use steel pipe with sealed joints. The pipes are typically located in a concrete tunnel or are double walled to prevent a leak from contaminating the soil and groundwater. Oily waste pipe lines are not vulnerable to SLR related damage, however the double containment systems or tunnels could become inundated. Under this scenario, pipe leaks could transmit contaminants to the flooded containment.

Operational Limits

The coastal structures provide coastal storm damage and flooding protection to buildings, waterfront structures, and training areas. Accordingly, coastal structures can be critical to the operations of an installation. The coastal infrastructure has vulnerabilities to SLR based on the type, elevation and location of the structure. Coastal infrastructure located within a bay or harbor is generally less vulnerable since it is generally exposed to much lesser waves as compared to structures exposed to ocean waves (Figure 3-115). However, this logic assumes that the coastal structures have been adequately designed for existing conditions. Coastal structures are designed to protect critical landward infrastructure. For example, a coastal structure that protects a training facility may allow episodic flooding while a structure that protects critical buildings could not. Therefore, the vulnerability of the landward protected structure should be considered in combination with the vulnerability of the coastal structure itself. The operational limits of coastal infrastructure are determined from evaluation of the location, type, function, and elevation. Brief descriptions of each type of coastal infrastructure are as follows.

Revetment. Revetments are onshore, engineered structures designed for the principal function of protecting the shoreline from erosion. Revetments are rubble-mound structures and slope seaward at varying degrees contingent on function, which act to dissipate wave energy. Revetments are generally not designed to be overtopped as wave overtopping will damage structures in the lee of a revetment. Revetment stone size and placement types vary dependent on the wave environment they are being designed for. Hand placed, large stones are typical along ocean wave exposed shorelines. Smaller stone such as rubble rip-rap is commonly used on low-wave energy, bay shorelines. An example of a typical rubble-mound revetment structure is shown in Figure 3-116.

Seawall. Seawalls have the principal function of preventing or alleviating overtopping or flooding of the land. Seawalls include rubble-mound sloping structures (sometimes armored with concrete armor units), vertical face structures such as massive gravity concrete walls, tied walls using steel or concrete piling, and stone-filled cribwork to sloping structures with typical surfaces being reinforced concrete slabs (U.S. Army Corps of Engineers, 2006)

Bulkhead. Bulkheads are primarily intended to retain land along a waterway. While bulkheads can protect against relatively small wave attack and they can be used in combination with a rubble mound seawall, they seldom used as solely as shore protection. Bulkheads are generally designed to withstand waves less than three feet. This design consideration limits these structures to areas of relatively mild wave conditions, such as bays and harbors. A typical bulkhead design is shown is Figure 3-117.

Jetty. Jetties are engineered structures designed to stabilize and provide protection to vessels transiting a navigation entrance channel to a harbor and/or bay. Jetty designs vary, but are generally rubble-mound structures. A typical jetty configuration is shown in Figure 3-118.

Vulnerabilities on these coastal structures due to SLR vary; however, can be generalized into the following categories:

Increased Loading. Increased water levels fronting the structure result in greater wave forces on the structure, which may result in damage or failure. This is a product of an increase in the depth-limited breaking wave height. Simplistically, the height of a wave is limited in shallow waters by wave breaking. For a given water depth, there is a limit to the largest wave that can break in that depth. If the water level increases with SLR then the limiting breaking wave height will be larger. This potentially increases the exposure for the existing coastal structures. The depth-limited maximum wave height (H_{max}) can be expressed as:

Equation 3-18

$$H_{max} \approx (0.8 \text{ to } 1.0) x d$$

where d is the water depth. A larger wave may cause damage to a coastal structure leading to failure or reduced design life.

Steam. Steam pipes are typically steel with exterior insulation. The pipes are typically located in a concrete tunnel or have a fiberglass protective pipe over the insulation for protection from damage. At the aircraft carrier wharves at Naval Base Coronado (Berths Juliet, Kilo and Lima), a steam pipe is located on the outboard edge of the wharf. If the steam pipeline is inundated from SLR, it will cool the outside of the pipe causing increased condensation on the inside of the pipe and reduced efficiency. The outside of the pipe will also have an increased rate of corrosion and a reduced service life.



Figure 3-120. The photo shows a below-grade electrical vault partly full of water. A connection panel is visible above the water. The vault remains operational.

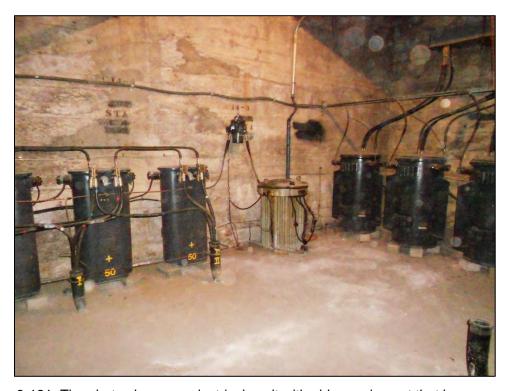


Figure 3-121. The photo shows an electrical vault with older equipment that has exposed connections and is susceptible to flood damage.

Buoyancy Effects on Buried Pipes. Buried pipes that are located below the water table have a buoyant force equal to the weight of water displaced by the pipe. The buoyant force is resisted by the weight of the pipe, its contents and the soil or concrete above the pipe. The buoyancy effect increases with an increase in pipe diameter. Larger pipes are more vulnerable to buoyancy because of a smaller weight to volume ratio. Buoyancy effects can be problematic if the pipe is empty, has minimum soil above, or the pipe is made of a lightweight material. Pipe materials may include: reinforced concrete, vitrified clay, corrugated metal, plastic and steel, see Table 3-14.

Table 3-14. Comparison of the uplift force on a 36-in. diameter pipe in various materials: reinforced concrete (RCP), corrugated metal (CMP), high-density polyethylene (HDPE), and polyvinyl chloride (PVC).

Pipe Material	Pipe Weight (lbs/ft)	Water Weight (lbs/ft)	Net Uplift Force (lbs/ft)
RCP	524	658	134
CMP	36	441	405
HDPE	18	554	536
PVC	54	486	432

For storm drain pipes that have an open end at the bay, buoyancy is not problematic because as the water table rises with the tide, the inside of the pipe is also filled with water. The net effect is zero additional force on the pipe. The only upward force would be the material lighter than water, such as plastic, that even full of water has minimal buoyancy. However, if a storm drain pipe does not have an open end at the bay or ocean, the buoyancy force can be substantial. See Table 3-15.

Table 3-15. Buoyancy force on reinforced concrete pipes per linear foot.

Pipe OD (in)	Pipe ID (in)	Area (in²)	Volume (in ³ /ft)	RCP Weight (lbs/ft)	Buoyant Force (lbs/ft)	Net Uplift Force of Empty Pipe (lbs/ft)
16	12	113.1	1,357.2	93	-87.1	5.9
19.5	15	176.7	2,120.6	127	-129.4	-2.4
23	18	254.5	3,053.6	168	-180.0	-12.0
26.5	21	346.4	4,156.3	214	-239.0	-25.0
30	24	452.4	5,428.7	264	-306.3	-42.3
33.5	27	572.6	6,870.7	322	-381.9	-59.9
37	30	706.9	8,482.3	384	-465.9	-81.9
44	36	1,017.9	12,214.5	524	-658.9	-134.9
51	42	1,385.4	16,625.3	686	-885.2	-199.2
58	48	1,809.6	21,714.7	867	-1,144.9	-277.9
65	54	2,290.2	27,482.6	1068	-1,437.9	-369.9
72	60	2,827.4	33,929.2	1295	-1,764.3	-469.3
86	72	4,071.5	48,858.0	1811	-2,517.1	-706.1

Assessment of Vulnerability

The civil infrastructure of an installation provides access (transportation corridors) and utility service to buildings, waterfront structures, training areas, and is critical to the operations of the installation. The assets and associated vulnerabilities are interrelated and failure of one may cause impacts to others. Failure of the storm water drainage system will cause flooding on the roadways and building parking areas. Therefore, it is necessary to analyze each SLR scenario with and without the corresponding return period rain event and combinations of the SLR scenario with a range of rainfall return period events. Before inundation or intrusion occurs, flooding will occur because of failure of the storm water drainage system.

Assessment of the impact of SLR includes both short and long return period scenarios. If a facility can remain operational for short return period events, but is not operational for the 10-year or 100-year storm event, then a more detailed analysis of the facility type and usage is necessary to determine the operational impacts.

Storm Water System Vulnerability. Storm water systems are designed to drain rain water from impervious surfaces and restrict standing water to a maximum of 1 inch to allow pedestrian access. The operational limits of a storm water system depend on the slopes of the pipes and the elevation head difference between the ocean, bay, or water table and the ground surface. The following are suggested definitions for various levels of operational readiness.

- Fully operational Storm water runoff drains through the system as designed. The elevation of the ocean, bay or water table does not reduce the efficiency of the system.
- Partially operational Storm water runoff drains through the system with reduced efficiency
 causing localized flooding at the trench drains and catch basins (low points) during heavy
 rain events. The elevation of the ocean, bay or water table has reduced the efficiency of the
 system.
- Non-Operational Storm water runoff does not drain through the system. The elevation of the ocean, bay or water table has caused the system to fail. Storm water accumulates at low areas causing flooding of roads, parking lots and low areas.

Transportation Corridor Vulnerability. Failure of the storm water drainage system may cause ponding and standing water on the roadways. The depth of water determines the impacts on the accessibility of the roadway and the rate of degradation. Suggested categories for operational readiness for a defense base, with civilian vehicles include:

- Fully operational Water on the roadway is less than 3-in. deep. The roadway remains open for moderate speed traffic.
- Partially operational Water on the roadway is between 3-in. and 6-in. deep. Vehicles may traverse the water at low speed. Excessive traffic congestion is caused by ponded water and poor drainage. The roadways have increased rate degradation causing potholes, and failure at the roadway edges.
- Non-Operational Water on the roadway is greater than 6-in. deep. The roadway may not allow vehicles with low clearance to traverse flooded areas. The roadways have an increased rate of degradation causing potholes, subgrade and surface failure at the roadway edges.

4. RESULTS AND DISCUSSION

Results for the key elements of the project are described below including sea level rise projections, delineation of the coastal system, physical responses to sea level rise, and the assessment of vulnerabilities related to these responses at the two installations. While the installations lie within the same region, they offer key contrasts in virtually every aspect of the research and analysis. Projected total water level scenarios at the two installations differ primarily as a function of differing wave exposures, the topography of the two installations is markedly different. The installation infrastructure, while having common elements is significantly different with respect to proximity to the coast, and the density of the development between the two installations. These differences are all reflected in the vulnerabilities that results from sea level rise at the two installations as described below.

4.1 SEA LEVEL RISE PROJECTIONS

Results for the development of sea level rise projections are presented below. Time series of total water level results are illustrated and used as the basis to specify specific future sea level scenarios for the installations at NBC and MCBCP.

4.1.1 Total Water Levels

As detailed in Section 3.1, total water levels used in this study comprise the superposition of four components (Figure 3-2), including four 2000 to 2100 MSLR scenarios; hourly tide heights; non-tide residual (NTR) water level variability, including El Niño-related fluctuations: and wave-driven runup on beaches. Figure 4-1 shows projections of future 98th-percentile extreme total water levels that are combinations of MSL for each MSLR curve (Figure 3-3), predicted tides, and the atmospherically-driven non-tide residual (NTR) sea level derived from the high-GHG CCSM3 A2 scenario, and El Niño fluctuations. Note that the endpoint elevations by year-2100 respectively reach about 1 m higher than MSLR alone owing mainly to the influence of the tide. These curves apply regionally, including throughout the Coronado and Camp Pendleton study areas. They do not include the run-up contribution, which differs from place to place. The MSLR curves are assumed to incorporate local vertical land motions, although for the areas of interest these rates are negligibly small (~ 0.1 to 0.2 mm/year) relative to projected changes in sea level (Louie, 1986; Gornitz, 1997; Kern et al., 1996; Sheldon, 1994). The high-GHG CCSM3 A2 scenario was selected for illustrative purposes of the methodology, and that other future scenarios could result in different NTR results.

The wave-driven run-up calculations used in this study are presented in Section 3.1, which details the Stockdon *et al.* (2006) methodology used and illustrates the uncertainty (about 50%) associated with the range of beach slopes plausibly used as input. As explained in Section 4, the decision was ultimately made to use the simplified version of the Stockdon *et al.* (2006) model, which neglects beach slope but is deemed appropriate for dissipative beaches. Run-up projections were developed for each of the 13 range lines where beach profile information was available (eight at MCBCP and five at NBC).

Time series of projected total water levels at each range were then constructed that are the sum of the three components that are the same at each range (*i.e.*, tide, NTR, and El Niño enhancements), and the run-up that respectively differs at each range. These time series are considered to describe the expected fluctuations of water level based on the future projections of tide, NTR, El Niño, and wave-driven run-up, but not including any future MSLR. In other words, the fluctuations and their statistics describe expected behavior for "current" MSL conditions, and in that sense represent "current" or "baseline" conditions even though they are projections of future conditions under one particular climate scenario.

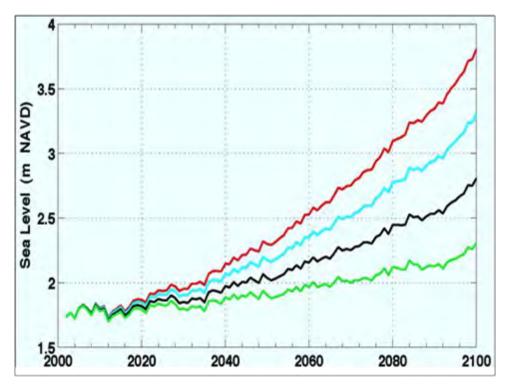


Figure 4-1. Winter 98-percentile combined total winter water level projections not including run-up.

4.1.2 Future Sea Level Scenarios

The return period of water level extremes at MCBCP and NBC were computed using the extreme value method of order statistics (Makkonen, 2011) based on the pioneering work of Gumbel (1958). Return periods were also computed using joint-probability convolution methods available in MATLAB, but these calculations were not completed until after the order statistic results were applied for the assessment portions of this project. Comparisons of results from the two methods are both encouraging and useful, in that they essentially agree and also provide a measure of the uncertainty in the return period estimates.

Time series of projected total water levels for 2000-2100 at each of the 13 ranges were constructed as described above. Monthly maximum values were extracted from these time series, and the results ordered from smallest to largest. This resulted in n = 1,200 monthly extreme values. The cumulative probability is $P_m = m/(n+1)$ where m is the rank of the mth ordered value, its return period (in months) is $R_m = 1/(1 - P_m)$, and m = 1, n.

Examples of the results are shown in Figure 4-2 for MCBCP Range PN1180, and in Figure 4-3 for NBC Range SS0160 at Coronado City Beach. Each graph gives the return period of maximum total sea level relative to MSL. In order to derive the change in return period for given MSLR, the respective MSLR value is added to this maximum total water level. As an example, the 10-year return value for total maximum water level at SS0160 under baseline conditions and relative to MSL is 2.92 m, which is equivalent to elevation 3.69 m relative to NAVD88. If MSLR = 0.5 m, then the 10-year return total water level will be 3.69 + 0.5 = 4.19 m (NAVD88). This illustrates the phenomenon often called "return-period creep" as specified return period elevations become progressively higher, or equivalently, as given maximum water levels become increasingly more frequent.

Return periods calculated using the joint probability method based on Tawn (1988), Tawn and Vassie (1989), and Tawn (1992) are also given in Figure 4-2 and Figure 4-3. In this approach, the probability distribution of the projected regional water level fluctuations (tide, NTR, and El Niño) of elevation a is $p_{WL}(a)$, and that of the runup at each of the 13 ranges at elevation b is $p_{RU}(b)$. The probability $p_{TOT}(s)$ of a total water level (tide, NTR, El Niño, and run-up) s is then given by the convolution $p_{TOT}(s) = \int p_{WL}(s-x)p_{RU}(x)dx$, which expresses the fact that a given total water level can be reached by any combination of water level and run-up that adds up to the given amount, and that the probability of that total elevation is the sum of the products of the probabilities of its constituents.

The cumulative probability distribution of any total water level S is $P_{TOT}(S) = \int_{l}^{S} p_{TOT}(x) dx$ where the integral is carried out from l, the lowest total water level to S. The return period of water level S is $R_{TOT}(S) = 1/(1 - P_{TOT}(S))$, which has the same form as the previous calculation based on order statistics. The primary difference between the methods is thus the manner in which the cumulative probability function is calculated.

Inspection of Figure 4-2 and Figure 4-3 indicates that the joint probability results for beach slopes of 0.04 and 0.02 bracket the order statistics result derived from the slope-independent run-up formula (Stockdon 2006) in the range of return periods from about 1-year to exceeding 100-years with a maximum differences of about 0.2 m (or about 10%) for any given return period. This leads to confidence in the methods while providing a measure of uncertainty.

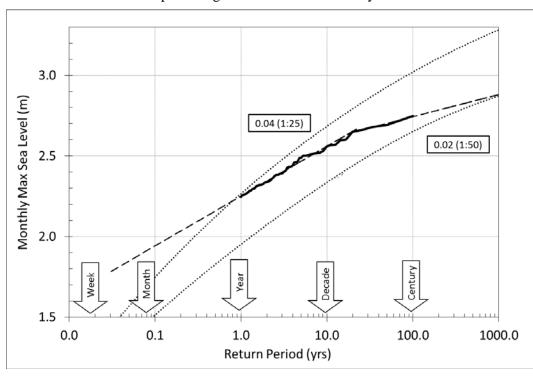


Figure 4-2. Return period from monthly extreme order statistics (dark curve) with two-slope fit (broken lines), and from joint probability convolution method with run-up beach slopes of 0.04 and 0.02 (upper and lower dotted curves, respectively) for MCBCP Range PN1180 with respect to the NAVD88 Datum.

Looking at the results conversely, a difference of 0.2 m in water level may imply a small or a large difference in return period owing to the logarithmic shape and slope of the curves, which flatten at

higher return periods. For example, at Coronado the difference between 2.1 m and 2.3 m total water elevation represents a difference of only about 6-mon to about 1-year in return period. On the other hand, the range from 3.0 m to 3.2 m total water level is equivalent to a return period range of about 20 years to about 100 years. This well illustrates the sensitivity and uncertainty of these results.

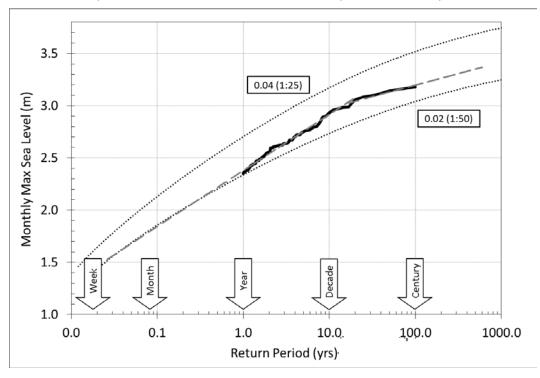


Figure 4-3. Same as Figure 4-2 for NBC Range SS0160 (Coronado City Beach).

The results were then interpolated to the 100-m spaced MOP lines within each base and averaged to produce results for MCBCP and NBC. These average return periods are shown in Table 4-1, which also gives results for NBC inside San Diego Bay. The bay is sheltered from waves and therefore excludes wave-driven run-up. San Diego Bay total water level return periods were based on projected bay tides (which have a range about 10% greater than open-ocean tides outside the bay), but use the same NTR and El Niño enhancements as the open-coast projections.

To further refine the water level scenarios, we also evaluated total water levels using the XBeach run-up results. To do this, we used the total water levels estimated using the Stockdon run-up to identify characteristic return period events within the time series that had total water levels consistent with a given return period. From this sub-population of total water level conditions, we calculated the average values of total water level, tide, NTR and significant wave height. We then used the Stockdon formula to calculate the wave period required to generate the required run-up for that average wave height that would satisfy the difference between the average total water level minus the tide and the NTR. This allowed us to determine wave heights and periods that were characteristic of our target range of return periods. These wave characteristics were then used to drive the XBeach model and generate run-up results at each MOP station for each installation. Combining these XBeach run-up results with the underlying tide, NTR and sea level rise components provided our final total water level scenarios that were used in the inundation and flooding analysis described in the following sections. The results are shown in Figure 4-4 for NBC and Figure 4-5 for MCBCP.

Table 4-1. Extreme water levels as a function of return period and MSLR.

Location/	Return	Baseline		Future MSLR (m)			
Condition	Period	(m NAVD88)	0.5 > 2045	1.0 > 2070	1.5 > 2085	2.0 > 2100	
ter	Week	2.5	3.0	3.5	4.0	4.5	
posed al Wa ional e)	Month	2.6	3.1	3.6	4.1	4.6	
MCBCP Exposed Shoreline Total Water Level (Regional Average)	Year	3.0	3.5	4.0	4.5	5.0	
VICB(relin Level	Decade	3.3	3.7	4.2	4.7	5.2	
Sho	Century	3.5	4.0	4.5	5.0	5.5	
lline ll e)	Week	2.2	2.7	3.2	3.7	4.2	
shore Leve	Month	2.5	3.0	3.5	4.0	4.5	
NBC Exposed Shoreline Total Water Level (Regional Average)	Year	3.0	3.5	4.0	4.5	5.0	
Expo otal V egion	Decade	3.5	4.0	4.5	5.0	5.5	
NBC T	Century	3.7	4.2	4.7	5.2	5.7	
ay ter	Week	2.0	2.5	3.0	3.5	4.0	
go Ba al Wa onal e)	Month	2.1	2.6	3.1	3.6	4.1	
NBC San Diego Bay Shoreline Total Water Level (Regional Average)	Year	2.2	2.7	3.2	3.7	4.2	
3C Sa reline evel	Decade	2.2	2.7	3.2	3.7	4.2	
Sho	Century	2.4	2.9	3.4	3.9	4.4	

Key	m (NGVD)
	2.0 < R < 3.0
	3.0 < R < 4.0
	4.0 < R < 5.0
	5.0 < R < 6.0

Table 4-2. Parameters for five wave scenarios (week, month, year, decade and century) at the six range stations of NBC.

NBC Average	Return	Tide	NTR	Hs	Тр
	Yrs	m	m	m	S
Week	0.019	0.83	0.00	0.82	13.02
Month	0.08	0.98	0.00	1.03	13.99
Year	1	1.06	0.01	2.13	14.84
Decade	10	1.06	0.05	3.67	15.56
Century	100	1.14	0.02	3.74	16.63
SS0182 Synthetic	Return	Tide	NTR	Hs	Тр
	Yrs	m	m	m	S
Week	0.019	0.83	0.00	1.95	13.02
Month	0.08	0.98	0.00	2.13	13.99
Year	1	1.06	0.01	3.31	14.84
Decade	10	1.06	0.05	4.97	15.56
Century	100	1.14	0.02	4.83	16.63
SS0160 Synthetic	Return	Tide	NTR	Hs	Тр
	Yrs	m	m	m	S
Week	0.019	0.83	0.00	0.80	13.02
Month	0.08	0.98	0.00	1.17	13.99
Year	1	1.06	0.01	2.68	14.84
Decade	10	1.06	0.05	4.65	15.56
Century	100	1.14	0.02	5.17	16.63
SS0125 Synthetic	Return	Tide	NTR	Hs	Тр
	Yrs	m	m	m	S
Week	0.019	0.83	0.00	0.62	13.02
Month	0.08	0.98	0.00	0.86	13.99
Year	1	1.06	0.01	1.98	14.84
Decade	10	1.06	0.05	3.46	15.56
Century	100	1.14	0.02	3.76	16.63

Table 5-2. (cont.)

SS0090 Synthetic	Return	Tide	NTR	Hs	Тр
	Yrs	m	m	m	S
Week	0.019	0.83	0.00	0.86	13.02
Month	0.08	0.98	0.00	1.03	13.99
Year	1	1.06	0.01	2.01	14.84
Decade	10	1.06	0.05	3.28	15.56
Century	100	1.14	0.02	3.55	16.63
SS0077 Synthetic	Return	Tide	NTR	Hs	Тр
	Yrs	m	m	m	S
Week	0.019	0.83	0.00	0.98	13.02
Month	0.08	0.98	0.00	1.21	13.99
Year	1	1.06	0.01	2.38	14.84
Decade	10	1.06	0.05	3.87	15.56
Century	100	1.14	0.02	4.33	16.63
SS0050 Synthetic	Return	Tide	NTR	Hs	Тр
	Yrs	m	*	m	S
Week	0.019	0.83	0.00	0.95	13.02
Month	0.08	0.98	0.00	1.12	13.99
Year	1	1.06	0.01	2.14	14.84
Decade	10	1.06	0.05	3.43	15.56
Century	100	1.14	0.02	3.87	16.63

Table 4-3. Parameters for five wave scenarios (week, month, year, decade and century) at the eight range stations of MCBCP.

MCB Average	Return	Tide	NTR	Hs	Тр
	Yrs	m	m	m	S
Week	0.019	0.93	0.001	0.92	14.57
Month	0.08	1.02	0.00	1.04	15.32
Year	1	1.10	0.01	1.47	16.54
Decade	10	1.09	0.02	2.32	16.61
Century	100	1.11	0.04	3.27	15.87
SO1530 Synthetic	Return	Tide	NTR	Hs	Тр
	Yrs	m	m	m	S
Week	0.019	0.93	0.001	0.92	14.57
Month	0.08	1.02	0.00	1.11	15.32
Year	1	1.10	0.01	1.54	16.54
Decade	10	1.09	0.02	2.45	16.61
Century	100	1.11	0.04	3.30	15.87
SO1470 Synthetic	Return	Tide	NTR	Hs	Тр
	Yrs	m	m	m	S
Week	0.019	0.93	0.001	0.92	14.57
Month	0.08	1.02	0.00	0.70	15.32
Year	1	1.10	0.01	1.25	16.54
Decade	10	1.09	0.02	2.29	16.61
Century	100	1.11	0.04	3.70	15.87
PN1340 Synthetic	Return	Tide	NTR	Hs	Тр
	Yrs	m	m	m	S
Week	0.019	0.93	0.001	0.92	14.57
Month	0.08	1.02	0.00	1.18	15.32
Year	1	1.10	0.01	1.48	16.54
Decade	10	1.09	0.02	2.21	16.61
Century	100	1.11	0.04	3.10	15.87
PN1290 Synthetic	Return	Tide	NTR	Hs	Тр
	Yrs	m	m	m	S
Week	0.019	0.93	0.001	0.92	14.57
Month	0.08	1.02	0.00	1.15	15.32
Year	1	1.10	0.01	1.60	16.54
Decade	10	1.09	0.02	2.55	16.61
Century	100	1.11	0.04	3.73	15.87

Table 4-3. (cont.)

PN1280 Synthetic	Return	Tide	NTR	Hs	Тр
•	Yrs	m	m	m	S
Week	0.019	0.93	0.001	0.92	14.57
Month	0.08	1.02	0.00	1.21	15.32
Year	1	1.10	0.01	1.56	16.54
Decade	10	1.09	0.02	2.37	16.61
Century	100	1.11	0.04	3.29	15.87
_					
PN1240 Synthetic	Return	Tide	NTR	Hs	Тр
	Yrs	m	m	m	S
Week	0.019	0.93	0.001	0.92	14.57
Month	0.08	1.02	0.00	1.19	15.32
Year	1	1.10	0.01	1.61	16.54
Decade	10	1.09	0.02	2.43	16.61
Century	100	1.11	0.04	3.15	15.87
PN1180 Synthetic	Return	Tide	NTR	Hs	Тр
	Yrs	m	m	m	S
Week	0.019	0.93	0.001	0.92	14.57
Month	0.08	1.02	0.00	1.22	15.32
Year	1	1.10	0.01	1.68	16.54
Decade	10	1.09	0.02	2.63	16.61
Century	100	1.11	0.04	3.46	15.87
PN1110 Synthetic	Return	Tide	NTR	Hs	Тр
	Yrs	m	m	m	S
Week	0.019	0.93	0.001	0.92	14.57
Month	0.08	1.02	0.00	1.35	15.32
Year	1	1.10	0.01	1.73	16.54
Decade	10	1.09	0.02	2.59	16.61
Century	100	1.11	0.04	3.78	15.87

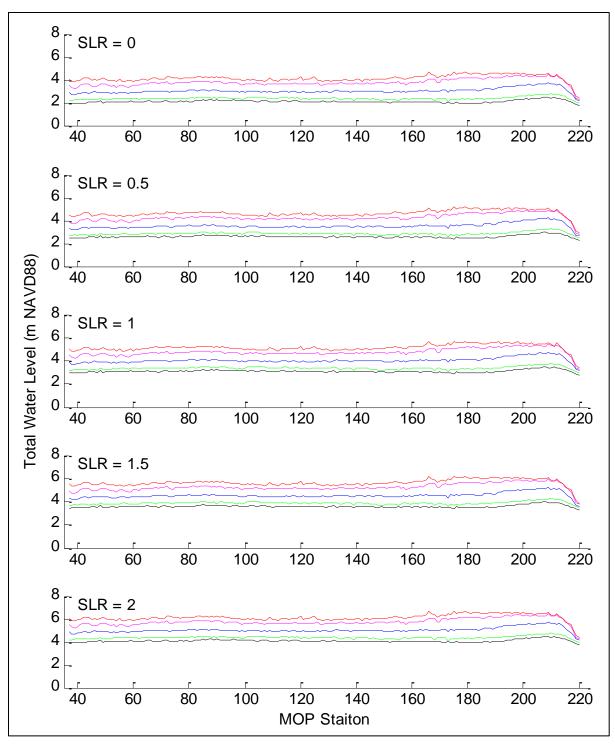


Figure 4-4. Total water level scenarios for NBC using the XBeach run-up results.Line colors are return periods as follows: black = week; green = month; blue = year; magenta = decade; red = century.

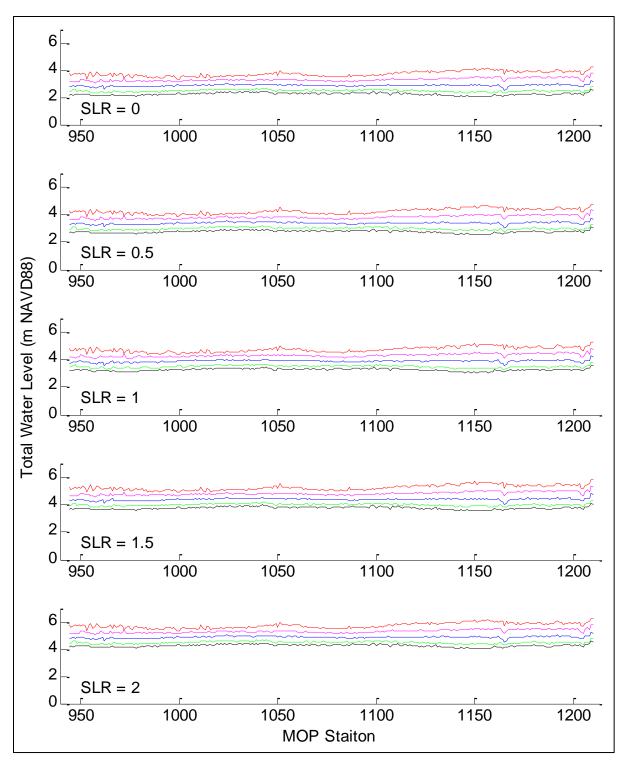


Figure 4-5. Total water level scenarios for MCBCP using the XBeach run-up results. Line colors are return periods as follows: black = week; green = month; blue = year; magenta = decade; red = century.

4.2 DELINEATION OF THE COASTAL SYSTEM

Results of the coastal system delineation process for NBC and MCBCP are describe below. The results illustrate the application of methods for the development of baseline terrain models, installation infrastructure models, and the integration of these into a full digital description of the coastal system.

4.2.1 Baseline Terrain Models

Baseline terrain models were compiled from the data sets described in Section 3.2.1. These terrain models are unique in that they are the first, regional, high-resolution Digital Elevation Models (DEMs) that incorporate available data for the near-shore littoral zone. Although the current models are based on interpolations of a limited amount of data in this zone, the incorporation of reasonable beach profiles through this process was fundamental to our ability to model the shoreline response.

The resulting baseline terrain models for NBC and MCBCP are shown in Figure 4-6 and Figure 4-7, respectively. The elevation models themselves are useful in visualizing the coastal terrain and quickly understanding the low relief areas that are likely to be sensitive to sea level rise. From this perspective, the contrast between the terrain at the two coastal installations is immediately apparent, with NBC poised almost entirely on low elevation areas surrounded on both sides by water, and MCBCP set in an area where the terrain rises rapidly near the coast, with lower lying areas concentrated near the lagoons and in the southern portions of the region.

The terrain model for NBC is characterized by relatively flat topography over much of the area. Low elevations are visible in the eastern portion of North Island, much of NAB and SSTC North, and the southern portion of SSTC South. Somewhat higher elevation regions are limited to the central portion of North Island, and the northern portion of SSTC South. On the ocean side of NBC, the beaches slope fairly uniformly offshore with the exception of the westernmost beaches off of North Island where the offshore topography is flatter as the sand accumulates along the Zuniga Jetty. On the San Diego Bay side, the areas along North Island are characterized by deep, dredged channels while much of the area along NAB and the Silver Strand are shallower flats with localized small boat channels.

The terrain model for MCBCP is characterized by steeper topography with cliffs along the ocean interspersed with lagoons and deep gullies. The terrain is generally lower and flatter to the south, and steeper and higher toward the north. The beaches are also wider to the south. The topography slopes offshore fairly uniformly along the coast of the installation. Man-made structures along the coast are limited to the harbor area at the south.

General characteristics of the terrain at the two installations are illustrated in the histogram shown in Figure 4-8 and the percentile elevations summarize in Table 4-4. These histograms summarize the elevations (excluding building areas) that are above current-day mean sea level. Because the terrain model for MCBCP only covers a portion of the inland extent of the installation, the histogram for MCBCP is not representative of the whole installation.

The terrain at NBC is largely restricted to elevations less than 10 m, and the majority of the installation is below 5 m. Over 60% of the installation is below the 5.7 m maximum elevation of our average scenarios in Table 4-1. In contrast, the vast majority (~98%) of the installation at MCBCP is well above the reach of the maximum scenario value of 5.5 m. While this contrast is skewed by the much larger inland extent of MCBCP compared to NBC, it does have ramifications for the relative ability of the two installations to adapt to sea level rise through managed retreat.



Figure 4-6. The baseline digital terrain model for NBC.Red outline show the primary areas of NBC that were evaluated in this study.

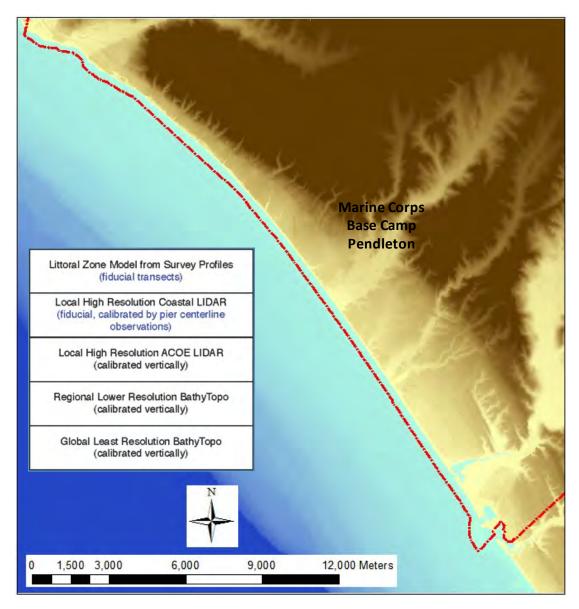


Figure 4-7. The baseline digital terrain model for MCBCP. The red outline shows the primary areas of MCBCP that were evaluated in this study.

4.2.2 Installation Infrastructure Models

Installation infrastructure GIS models were developed for key receptor categories at each installation as described in Section 3.2.2. The infrastructure models were limited to the areas within the property lines of each installation. While the installations are likely to have vulnerabilities that are related to infrastructure that lies outside the property lines, the scope of this project, and limitations on access to non-military stakeholders precluded a broader analysis. From a methodological perspective, we do highly recommend that the broader regional issues be included in any future operational analysis. Characteristics of the five key receptor category models compiled for the two installations are summarized below, and detailed shapefiles and receptor characteristics are included in Appendix A3.

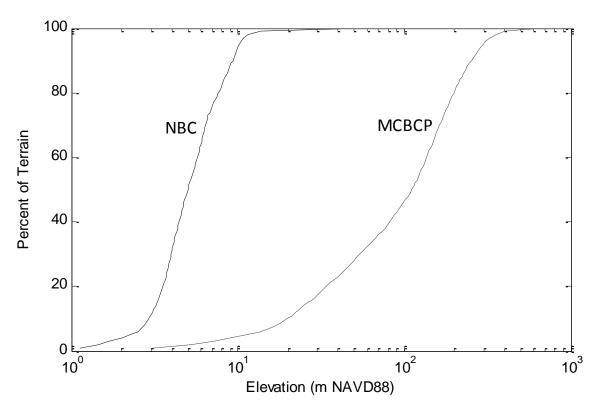


Figure 4-8. Cumulative histogram of the terrain model elevations at NBC and MCBCP.

Table 4-4. Cumulative histogram percentile bands for terrain model elevations at NBC and MCBCP. All values are in meters NAVD88.

Installation	Terrain Model Elevations Percentiles						
	5th	25th	50th	75th	95th		
NBC	2.3	3.8	5.0	6.9	10.2		
MCBCP	11.5	43.6	110.8	179.0	296.5		

Training and Testing Lands

The training and testing lands category at NBC and MCBCP focused on sensitive exposed shoreline training beaches. These areas support training for a wide range of military commands, using a variety of personnel, vessels, vehicles, equipment, and aircraft to meet their military readiness requirements. These areas are particularly sensitive to exposure pathways including erosion, inundation and flooding. Figure 4-9 shows the training area receptor category for NBC. These beach training areas are essentially fixed with respect to retreat because they already back up against the highway. The beach training areas at NBC are separated between the Silver Strand Training Complex components in the north and south (Figure 4-10). SSTC North consists of 10 zones and STTC South consists of four zones, all of which lie at the head of the corresponding ocean training lanes. Current day beach areas and beach widths for these training areas are summarized in Table 4-5. Areas ranged from a maximum of 84630 m² at Lane 3 to a minimum of 26444 m² at Lane 1, with a total area of 931330 m². Widths ranged from a maximum of 179 m at Lane 3 to a minimum of 51 m at Lane 1, with an average overall width of 142 m.

At MCBCP, amphibious training also requires accessible beach widths. The majority of amphibious assault training activity at MCBCP occurs at Section C Las Pulgas Beach (Red), with additional training at Section E Aliso Beach (White), Section G Margarita Beach (Blue), Amphibious Vehicle Training Area, Assault Amphibious Vehicle (AAV) Training Area, and Section A San Onofre Beach (Green). Figure 4-11 through Figure 4-13 show the training area receptor category for MCBCP, and Table 4-6 summarizes the current-day beach areas and beach widths for these training areas. Areas ranged from a maximum of 656723 m² at Blue Beach to a minimum of 281506 m² at Green Beach, with a total area of 2202696 m². Widths ranged from a maximum of 246 m at Blue Beach to a minimum of 63 m at San Onofre Beach, with an average overall width of 115 m. In contrast to NBC where the beach training areas are restricted from retreat by existing infrastructure, the beaches at MCBCP will naturally retreat (autonomously adapt) as the cliffs that back them erode. Thus the analysis of impacts to the beaches at MCBCP incorporated this retreat, redefining the beach areas and widths during each scenario to incorporate the new position of the back beach based on the cliff erosion condition for a given sea level rise scenario.

Beach Training Area Lane 4 Lane 5 Lane 1 Lane 2 Lane 3 Lane 6 Lane 7 Average Width (m) 51 143 179 172 162 163 144 142 Area (m²) 26444 68451 84630 79243 76247 74992 67961 66524 Lane 9 Lane 10 Lane 11 Lane 12 Lane 13 Lane 14 Lane 8 Total Width (m) 162 175 158 132 113 112 121 NA Area (m²) 73912 83809 71596 59929 55275 51388 57455 931330

Table 4-5. Beach training area characteristics at NBC.

Table 4-6. Beach training area characteristics at MCBCP.

		Beach Training Area						
	Blue	White	Red	Green	SO	Total	Average	
Width (m)	246	130	75	64	63	NA	115	
Area (m²)	656723	436124	388641	281506	439702	67961	2202696	

Buildings

The building receptor category at NBC and MCBCP included a range of buildings that support operations and missions of the installations. This spanned buildings for housing, logistics, training, testing, operations, storage and security. These receptors are susceptible to sea level rise sources through all major pathways including inundation, flooding, erosion and seawater intrusion.

The building receptor category for NBC is shown in Figure 4-14 through Figure 4-15 including a total of 1637 structures. The majority of these buildings were at elevations below 10 m (Figure 4-16). Key metrics for these buildings included footprint areas, replacement values and MDIs. Building footprints ranged in size from as small as 1.4 m² to 25839 m² with a total inventory area of 1205935 m². The replacement values ranged from a low off \$4.6K to a high of \$94.2M with a total across the installation of \$2511M. MDIs ranged from a low of 0 to a high of 100 with an average MDI of 27. The majority of the building receptors were located at North Island Naval Air Station and the Naval Amphibious Base. Figure 4-17 illustrates the building category characteristics for NBC.

The building receptor category for MCBCP is shown in Figure 4-18 through Figure 4-20 including a total of 6779 structures. Building elevations generally fell within the range of 10 to 100 m although a number of buildings were below 10 m in the range that could be sensitive to sea level rise (Figure 4-16). Key metrics for these buildings included footprint areas, replacement values and MDIs. Building footprints ranged in size from 2.0 m² to 242306 m² with a total inventory area of 22819235 m². The replacement values ranged from a low off \$124 to a high of \$257M with a total across the installation of \$7240M. MDIs ranged from a low of 0 to a high of 90 with an average MDI of 24. In contrast to NBC, the majority of the building inventory at MCBCP is located away from the water with the exception of the buildings in the Del Mar and San Onofre areas. Building characteristics for MCBCP are illustrated in Figure 4-21.

Waterfront Structures

This category included a range of structures at NBC and MCBCP that support waterfront operations and missions. This category encompassed structures such as piers, wharves, quay walls, floating docks and graving docks. The waterfront structures receptor category for NBC is shown in Figure 4-22 through Figure 4-24. Waterfront structures at NBC are concentrated along the protected shorelines of San Diego Bay and include a number of pier and wharf areas. There are over 40 structures located on NBC, and 80% are piers while the remaining 20% include landing craft ramps, fueling piers and one seaplane ramp. Structures in this category were characterized with respect to deck area, replacement value, and MDI. Structure deck footprints ranged in size from 20 m² to 22775 m² with a total inventory area of 85168 m². The replacement values ranged from a low off \$109K to a high of \$184M with a total across the installation of \$659M. MDIs ranged from a low of 0 to a high of 93, with an average MDI of 40.

Waterfront structures at MCBCP are shown in Figure 4-25 and are limited to small boat facilities in the Del Mar Basin including a total of roughly 8 structures. Structures in this category were characterized with respect to deck area, replacement value, and MDI. Structure deck footprints ranged in size from 584 m² to 6271 m² with a total inventory area of 50165 m². The replacement values ranged from a low of \$64K to a high of \$10.7M with a total across the installation of \$36.6M. MDIs ranged from a low of 0 to a high of 75 with an average MDI of 56.

Coastal Structures

This category includes a range of coastal structures at NBC and MCBCP whose primary purpose is to protect the shoreline and thus sustain operations and missions of the installation. This category encompasses structures such as jetties, groins and revetments which are used to protect the shoreline and dredged improvements.

Coastal structures at NBC are shown in Figure 4-26 through Figure 4-28. There are a total of 10 structures including rip rap, revetments and bulkheads, primarily lining the protected shoreline of NBC within San Diego Bay, but also including the large Zuniga Jetty that protects the entrance of San Diego Bay as well as portions of the ocean shoreline at NBC. The individual average elevations of these structures ranged from 3.5 to 5.0 m, they ranged in length from about 188 to 2264 m, and had replacement costs ranging from about \$2.2M to \$25M with a total inventory value of about \$107M.

Coastal structures at MCBCP are shown in Figure 4-29 through Figure 4-30. There are a total of 8 structures, primarily around the Del Mar basin. The individual average elevations of these structures ranged from 3.7 to 6.1 m they ranged in length from about 150 to 1560 m, and had replacement costs ranging from about \$2.9M to \$42M with a total inventory value of about \$92M. The SONGS facility is protected by a seawall with an approximate elevation of 19.2 m, with a length of 770 m, and an approximate replacement cost of \$23M.



Figure 4-9. Training area receptor category for NBC.

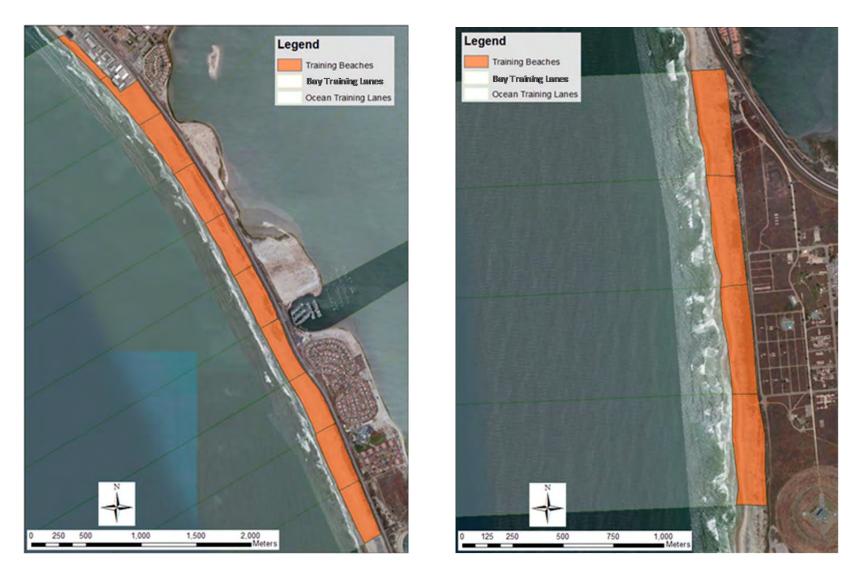


Figure 4-10. Detailed view of the training areas at SSTC North (left) and South (right).



Figure 4-11. Training area receptor category for MCBCP.



Figure 4-13. Detailed view of the training areas for Gold Beach (left), and San Onofre Beach (right).



Figure 4-13. Detailed view of the training areas for Gold Beach (left), and San Onofre Beach (right).



Figure 4-14. Building receptor category for NBC.



Figure 4-15. Detail view of the buildings at North Island (left) and NAB (right).



Figure 4-16. The Navy housing complex at Silver Strand.

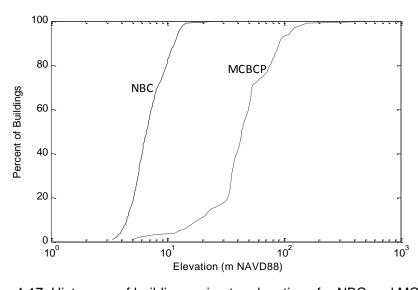


Figure 4-17. Histogram of building perimeter elevations for NBC and MCBCP.

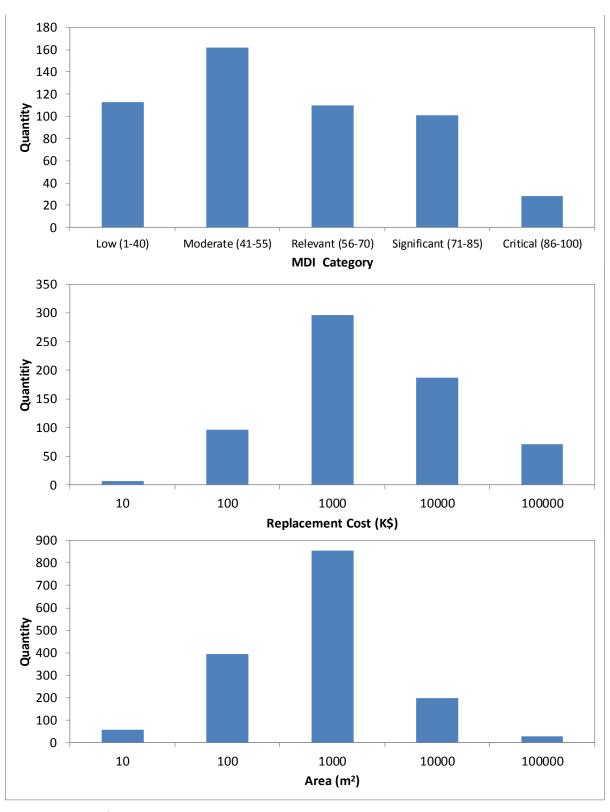


Figure 4-18. NBC building category characteristics including non-zero MDI, replacement cost and building area.



Figure 4-19. Building receptor category for MCBCP.



Figure 4-20. Detailed view of the buildings for southern (left) and central (right) MCBCP.



Figure 4-21. Detailed view of the buildings for northern MCBCP.

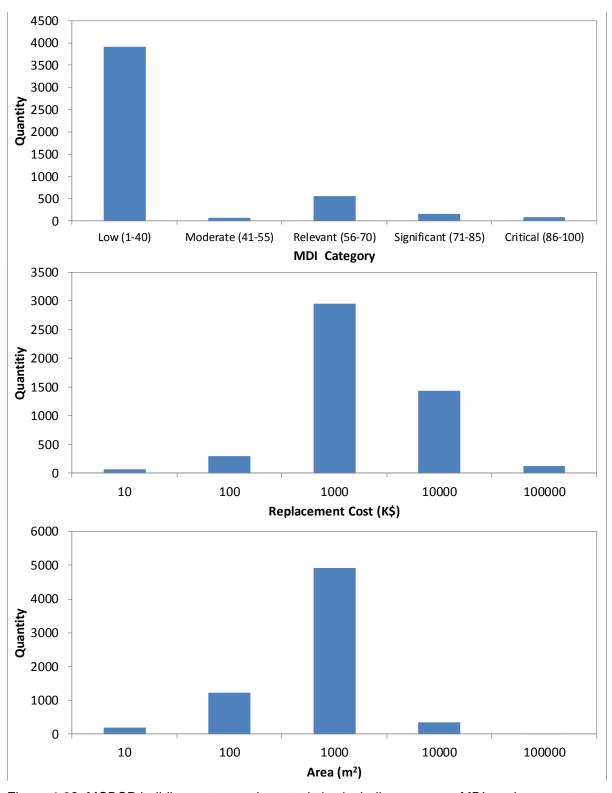


Figure 4-22. MCBCP building category characteristics including non-zero MDI, replacement cost and building area.



Figure 4-23. Waterfront structures receptor category for NBC.



Figure 4-24. Detail views of the waterfront structures at North Island.

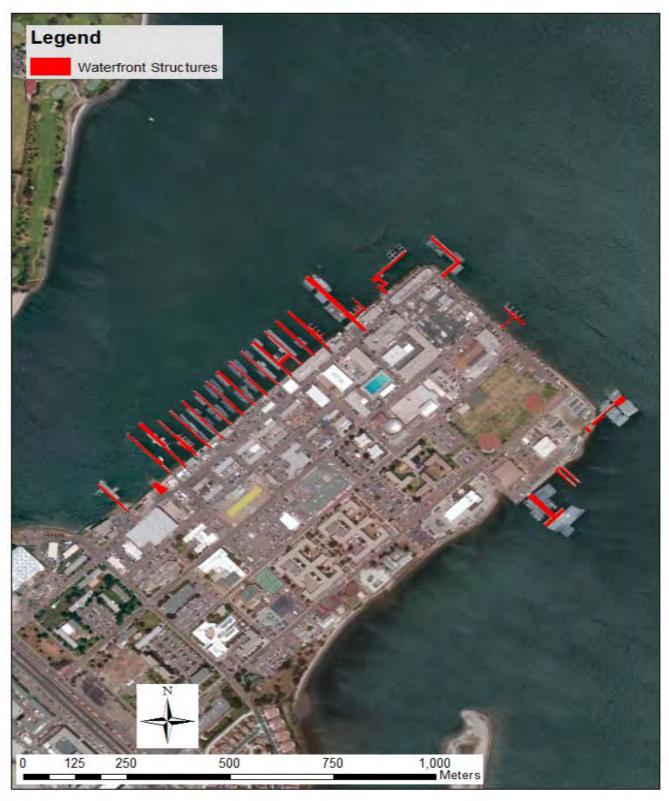


Figure 4-25. Detailed view of the waterfront structures at NAB.



Figure 4-26. Waterfront structure receptor category for MCBCP.

Coastal structures at MCBCP are shown in Figure 4-29 through Figure 4-30. There are a total of 8 structures, primarily around the Del Mar basin. The individual average elevations of these structures ranged from 3.7 to 6.1 m they ranged in length from about 150 to 1560 m, and had replacement costs ranging from about \$2.9M to \$42M with a total inventory value of about \$92M. The SONGS facility is protected by a seawall with an approximate elevation of 19.2 m, with a length of 770 m, and an approximate replacement cost of \$23M.

Civil Infrastructure

This receptor category describes a broad category of built infrastructure at NBC and MCBCP that is critical to the day-to-day operations and mission of the installation. The category includes receptors ranging from critical utility infrastructure such as buried utilities, fuel transfer/supply, transportation corridors, and storm water conveyance systems. These receptors are susceptible to sea level rise sources through all major pathways including inundation, flooding, erosion and seawater intrusion. Because of the breadth and complexity of this category, we focused our analysis on a subset of elements that exemplify the potential impacts from sea level rise. These included transportation infrastructure, storm water conveyance system, airfield surfaces, and recreational areas (Figure 4-31 through Figure 4-47). Components within this category at NBC included 1166 storm drain inlets and 94525 m of storm drain piping, 1996921 m² of airfields, 154189 m of roadways, and 529935 m² of recreational areas. Components within this category at MCBCP included 1756 storm drain inlets and 132785 m of storm drain piping, 131934 m² of airfields, 140456085 m of roadways, and 571760 m² of recreational areas.

4.2.3 Integrated Terrain and Infrastructure Models

The baseline terrain and infrastructure models were combined in Arcview to produce a complete, integrated model of the two installation study areas. These models represent the current day conditions at the installation, and form the basis for all subsequent analysis and products for evaluation of physical responses and vulnerabilities to sea level rise. The datasets underlying these integrated models are based on community standard, open-specification NCAR Network Common Data Form (NetCDF) files for the terrain models, and ESRI Shapefiles for the infrastructure data and are thus easily transportable to various platforms and applications.

Results for the NBC model are shown in Figure 4-48 through Figure 4-51. Figure 4-48 provides an overview of the extent of the terrain model and the installation infrastructure that spans much of the coast of southern San Diego County from Coronado to Imperial Beach. Components of the five infrastructure receptor categories were clustered in three areas including North Island Naval Air Station to the northwest, Naval Amphibious Base and Silver Strand Training Complex North at the north end of the Silver Strand, and Silver Strand Training Complex South near Imperial Beach. Much of the built infrastructure was concentrated in the northern areas, while the southern area was primarily used for training. Figure 4-49 through Figure 4-51 show more detailed views of these three areas.

Results for the MCBCP model are shown in Figure 4-52 through Figure 4-55. Figure 4-52 provides an overview of the extent of the terrain model and the installation infrastructure that spans the entire coastal area of northern San Diego County from Oceanside in the south to San Onofre in the north. The contrast between MCBCP and NBC is immediately striking in both the significantly large scale of the MCBCP installation, and the general lack of built coastal infrastructure near the immediate shoreline areas. Coastal built infrastructure at MCBCP was concentrated in the Del Mar area at the southern end of the base near Oceanside. Scattered structures and airfields were found along the cliffs further to the north, and there was a concentration of built infrastructure at the northern end of the base including the power plant at San Onofre, and the recreational area at

Crescent Beach. Key training beaches lined much of the southern shoreline of the base. Figure 4-53 through Figure 4-55 show detailed views of the integrated terrain and infrastructure in some of these key areas.

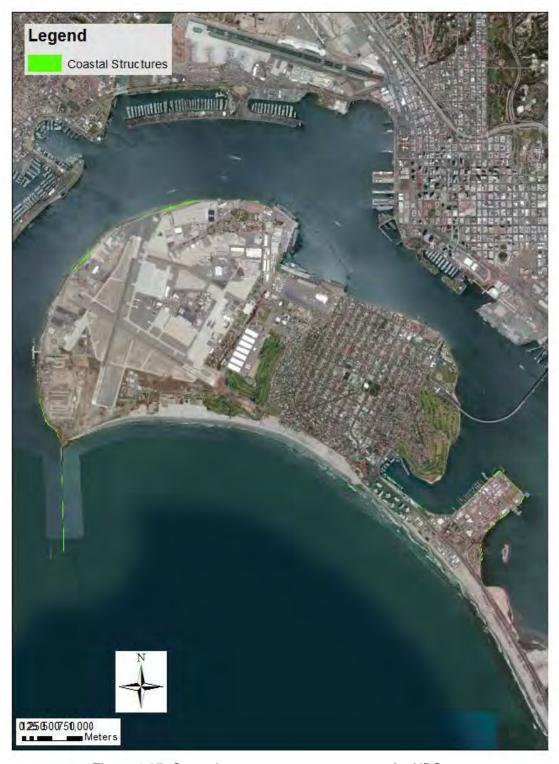


Figure 4-27. Coastal structure receptor category for NBC.





Figure 4-28. Detailed view of the coastal structures along North Island.

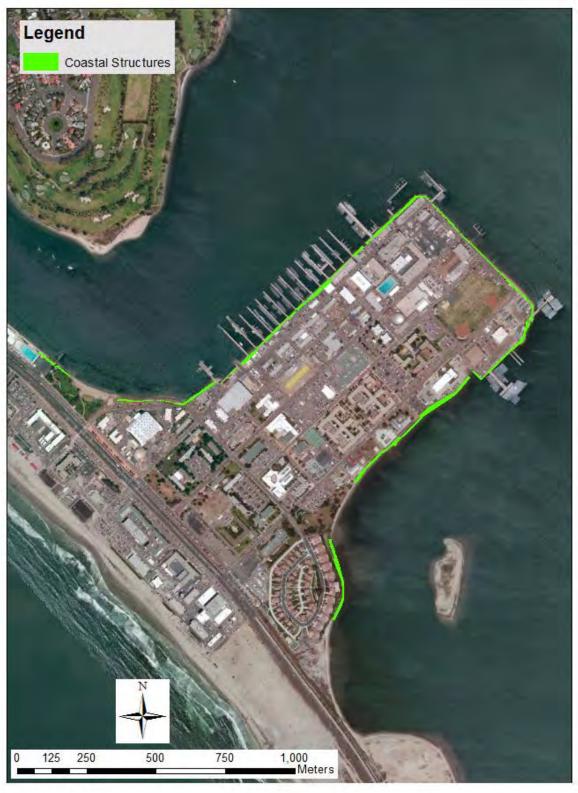


Figure 4-29. Detailed view of the coastal structures at NAB.

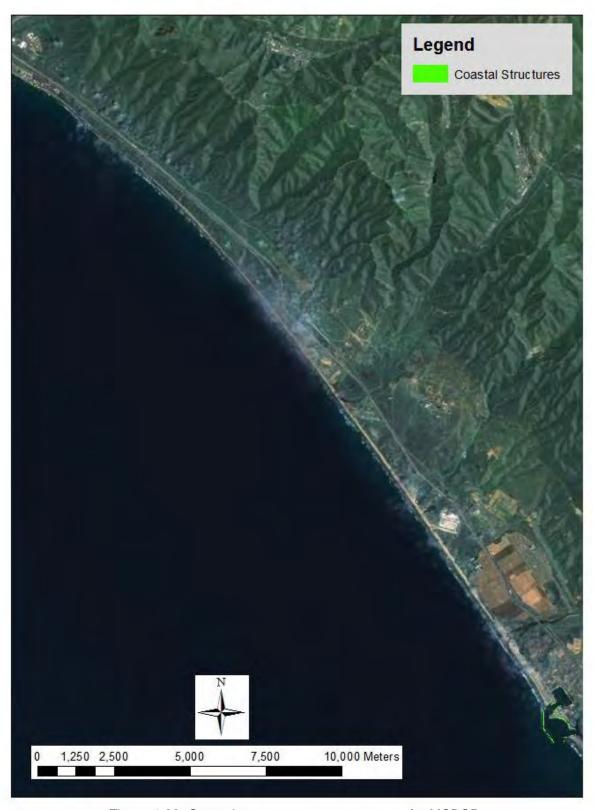


Figure 4-30. Coastal structure receptor category for MCBCP.



Figure 4-31. Detailed view of coastal structures at the Del Mar basin (left) and SONGS (right) areas of MCBCP.

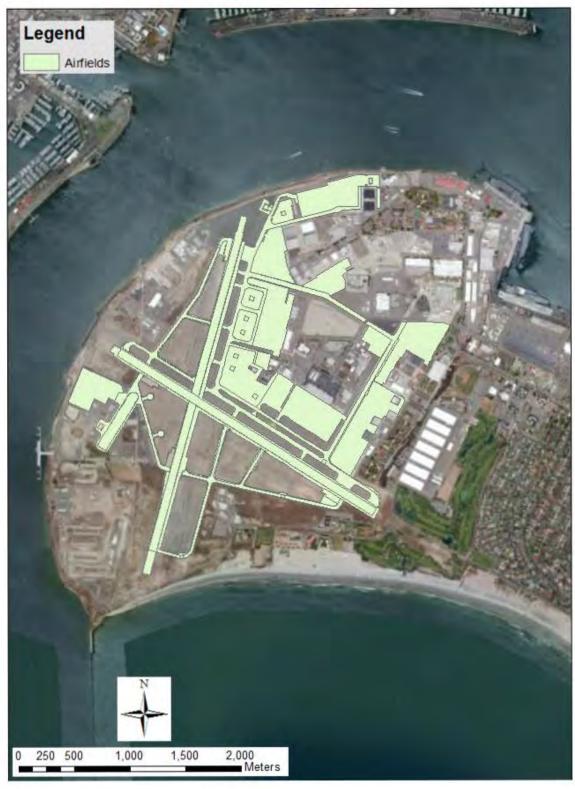


Figure 4-32. Civil infrastructure - airfields receptor category for NBC.



Figure 4-33. Civil infrastructure – airfields receptor category for MCBCP.

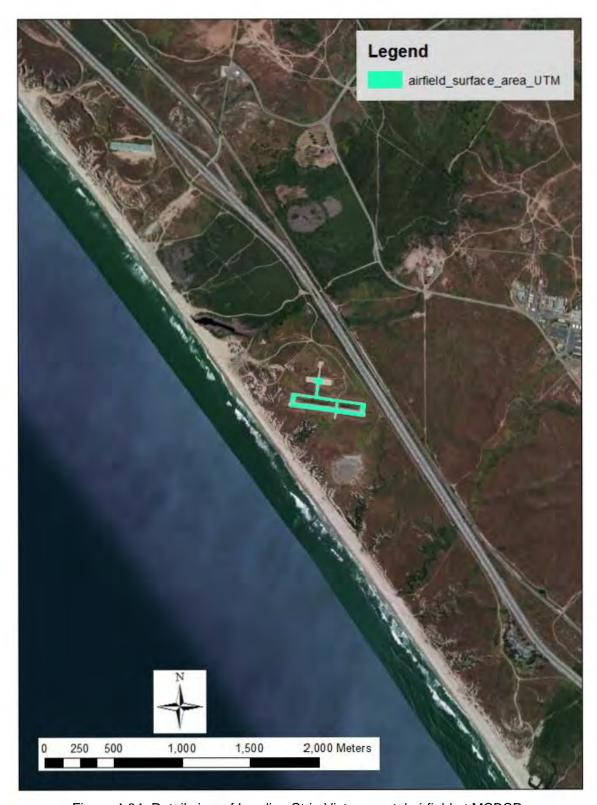


Figure 4-34. Detail view of Landing Strip Victor coastal airfield at MCBCP.

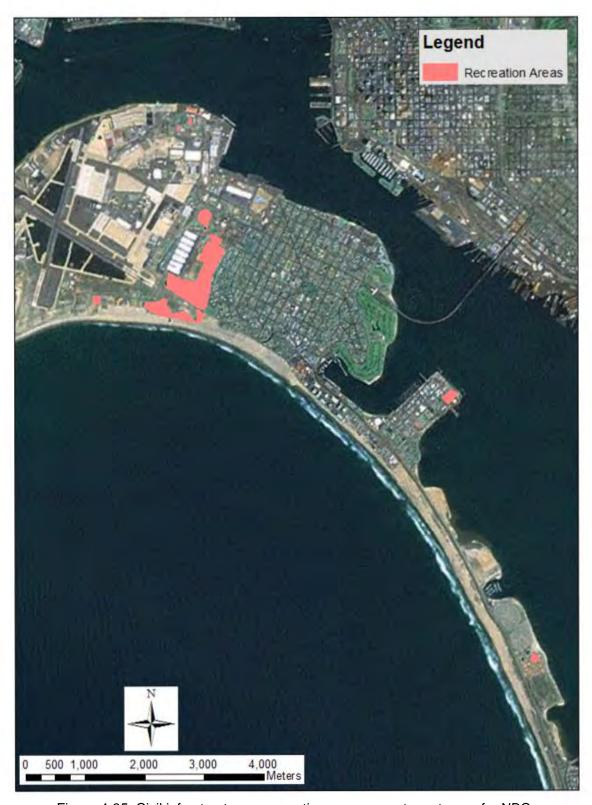


Figure 4-35. Civil infrastructure – recreation areas receptor category for NBC.



Figure 4-36. Detailed view of the recreation areas at North Island (left) and NAB and Silver Strand (right).



Figure 4-37. Civil infrastructure – recreation areas receptor category for MCBCP.



Figure 4-38. Civil infrastructure – recreation areas receptor category for MCBCP.



Figure 4-39. Civil infrastructure - roads receptor category for NBC.



Figure 4-40. Detailed view of the roadways at North Island (left) and NAB and Silver Strand North (right).



Figure 4-41. Detailed view of the roadways at Silver Strand South.



Figure 4-42. Civil infrastructure - roads receptor category for MCBCP.

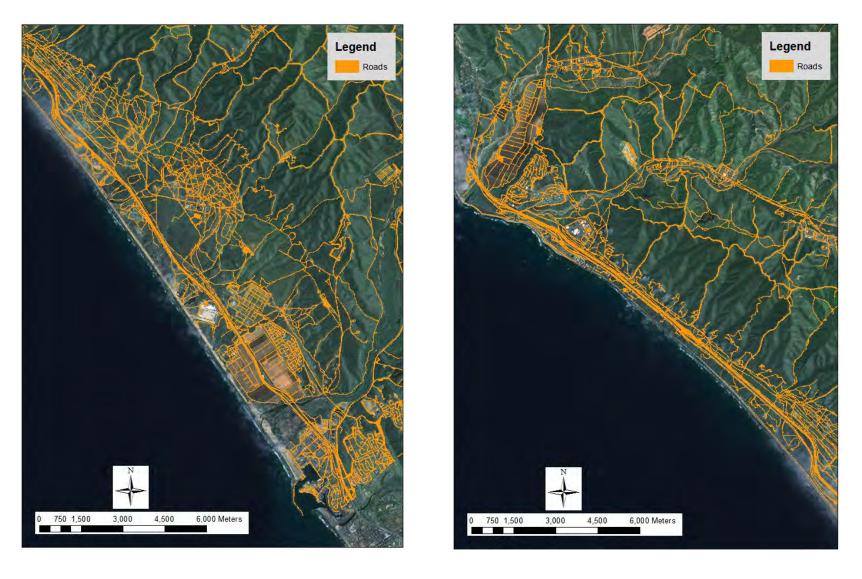


Figure 4-43. Detail view of the roads for the southern (left) and northern (right) areas of MCBCP.



Figure 4-44. Civil infrastructure – storm water system receptor category for NBC.



Figure 4-45. Detailed view of the storm water system at North Island (left) and NAB (right).

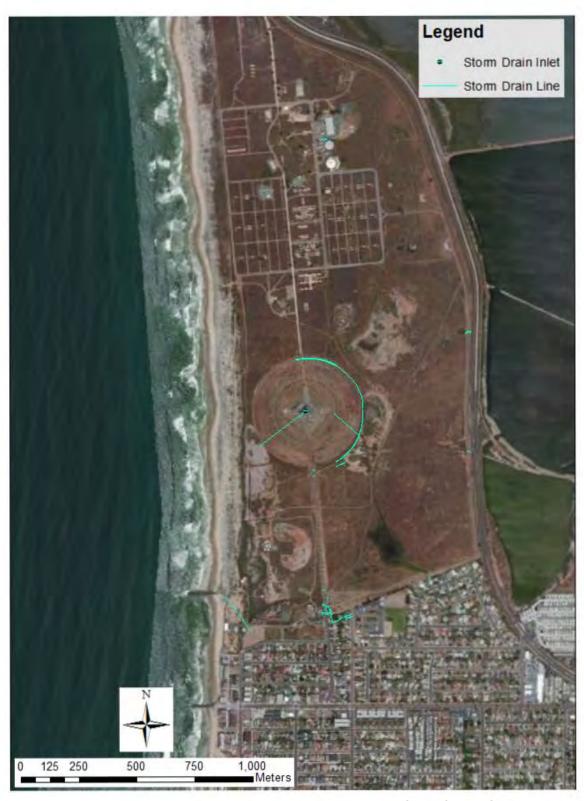


Figure 4-46. Detailed view of the storm water system at Silver Strand South.



Figure 4-47. Civil infrastructure – stormwater system receptor category for MCBCP.

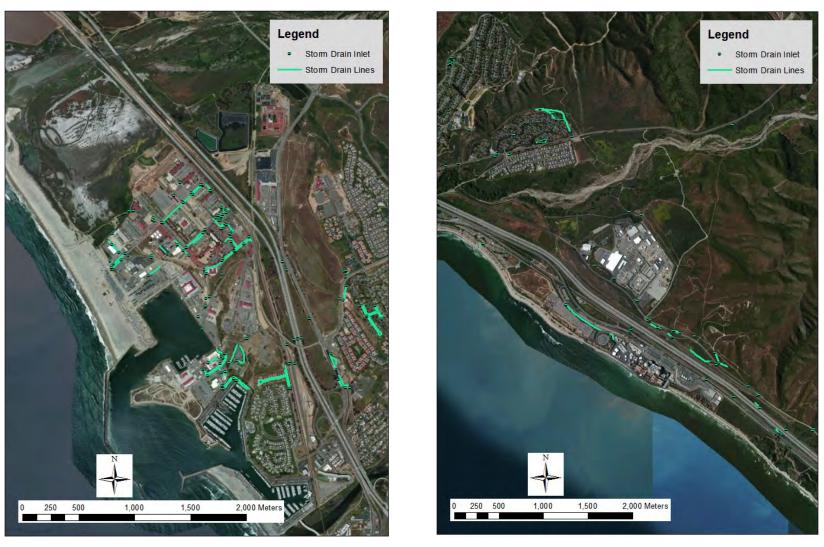


Figure 4-48. Detail view of the storm water system in the Del Mar (left) and SONGS (right) areas of MCBCP.



Figure 4-49. Integrated terrain and infrastructure model for NBC.

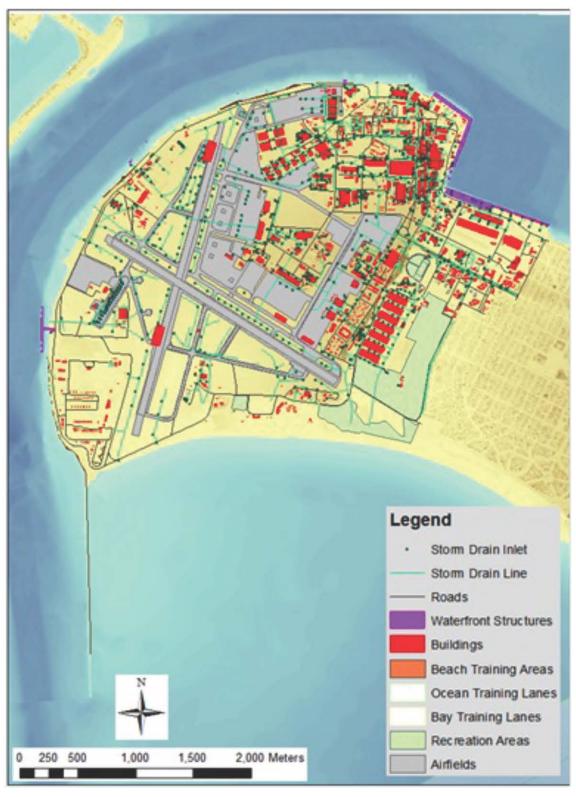


Figure 4-50. Detailed view of the integrated model for North Island Naval Air Station.



Figure 4-51. Detailed view of the integrated model for NAB/SSTC North (right).

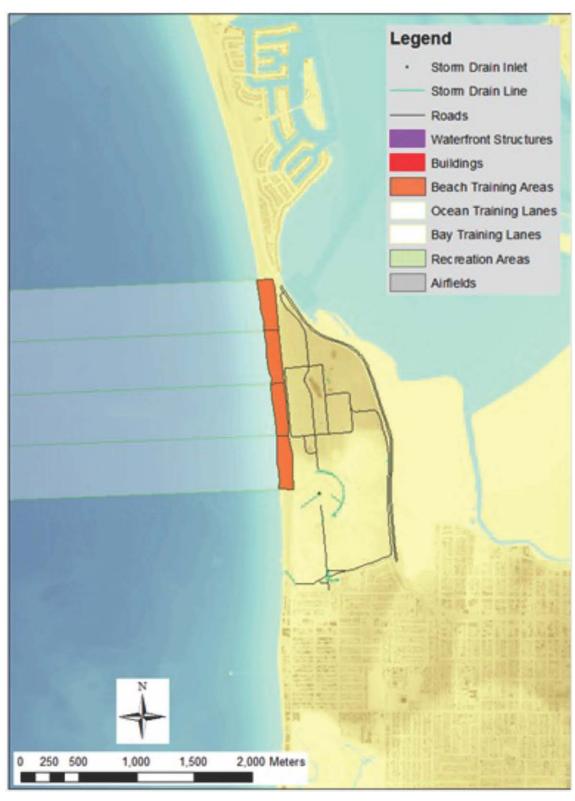


Figure 4-52. Detailed view of the integrated model at SSTC South.

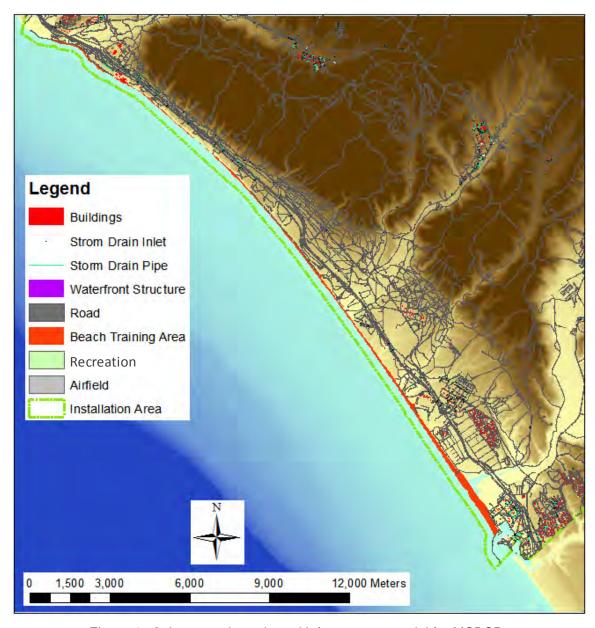


Figure 4-53. Integrated terrain and infrastructure model for MCBCP.

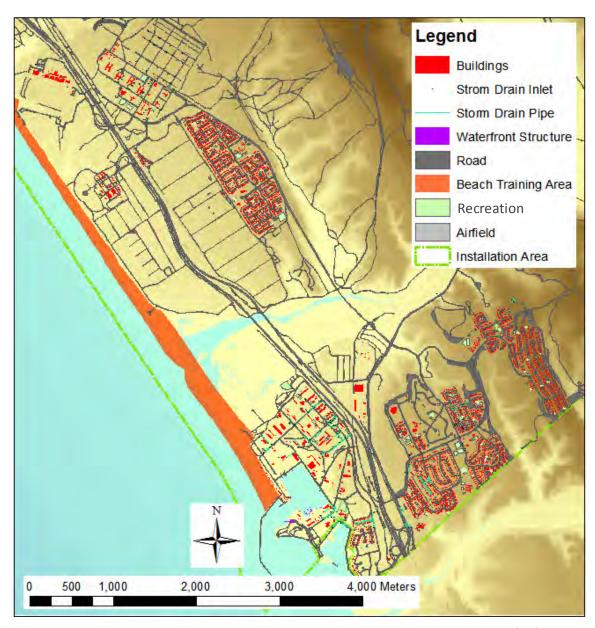


Figure 4-54. Detailed view of the integrated model for the Del Mar area of MCBCP.

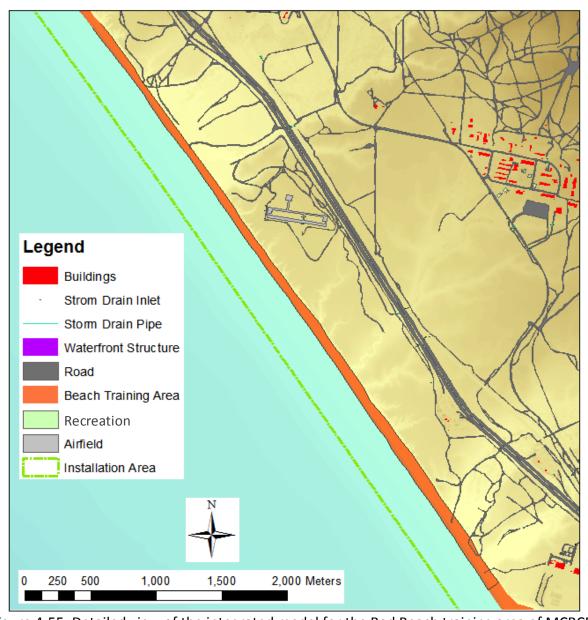


Figure 4-55. Detailed view of the integrated model for the Red Beach training area of MCBCP.

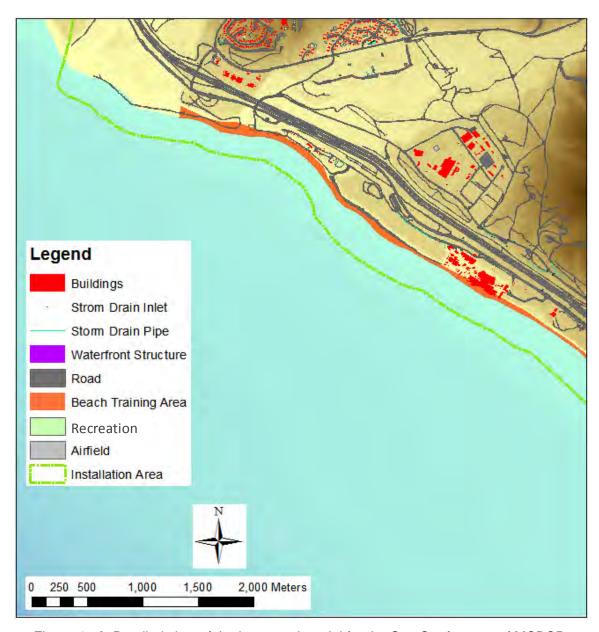


Figure 4-56. Detailed view of the integrated model for the San Onofre area of MCBCP.

4.3 PHYSICAL RESPONSE TO SEA LEVEL RISE

Pathways of physical response to sea level rise were quantified for exposed and protected shorelines at NBC, and for exposed shorelines and groundwater at MCBCP. Groundwater is not used for potable water at NBC, so we did not focus on this pathway, however it may still have important ramifications for impacts to underground infrastructure. Similarly, we did not focus on protected shorelines at MCBCP, however there are areas of the base such as the Del Mar basin and the Santa Margarita Lagoon where these conditions prevail.

The majority of our effort focused on the response along the exposed shorelines of the two installations. These results are presented based on pathway specific responses via erosion and inundation/flooding. The erosion results incorporate long-term response to sea level rise and sand budget deficits, as well as short-term response to variations in wave climate.

4.3.1 Exposed Shoreline Response

Exposed shoreline response was evaluated at the two installations using the models described in Section 3.3. Shoreline response is characterized in terms of key vulnerability pathways including erosion, inundation and flooding.

Erosion at NBC

Long-term erosion response at NBC was evaluated using the CSPEM model described in Section 3.3.1. This model incorporates the response of the beach system to sea level rise and sand budget deficits. Results for a two sand budget conditions were evaluated and presented below, with the final analysis focusing on the higher level deficit as a more conservative scenario.

Zero Deficit Scenario

Long-term beach retreat for the zero sand deficit condition increased linearly as a function of sea level rise (Figure 4-56). Scenario-mean beach retreat ranged from 21.3 m for 0.5 m of sea level rise, to 85.7 m for 2.0 m of sea level rise (Table 4-7) Maximum retreats ranged from 39.6 m to 156 m for the same scenarios. The effective average beach slope based on the linear relationship between retreat and sea level rise was about 42 m/m with a range from about 28 to 75 m/m based on the minimum and maximum retreat respectively.

Deficit Scenario

For NBC beach retreat, we focused on a sand deficit scenario that ranged from a high of about 6.5 m3/m/y for the southern portion of the study area to a low of 0 m3/m/y at the north end based on the estimates of Inman and Master, 1991. Including the existing sand deficit generally increased the retreat rate of the beach relative to the zero deficit scenario. Beach retreat for these conditions are shown in Figure 4-56. Including the effects of sea level rise and the sand budget deficit, scenariomean beach retreat ranged from 53.5 m for 0.5 m of sea level rise, to 121.2 m for 2.0 m of sea level rise, and maximum retreats ranged from 109.5 m to 226.1 m for the same scenarios. This represents an increase of 41 to 151% for the mean and 45 to 177% for the maximum relative to the zero deficit condition. Larger percent increases were associated with lower sea level rise scenarios as the sand budget deficit becomes the more dominant retreat driver under these conditions.

Alongshore distribution of beach retreat

The CSPEM model and other sand balance based models assume that the sand required to maintain the active profile in relation to sea level rise must be eroded from the back beach. Thus variations in the offshore shape of the profile result in different demand levels from the back beach, and variations in the back beach profile result in different source availability for the sand balance. These conditions vary alongshore in a way that causes variations in the retreat rate. In areas where the offshore profile is longer and flatter, more sand is required to maintain the profile. In areas where the back beach elevations are low, less sand is available to maintain the profile.

Figure 4-56 shows the alongshore variations in beach retreat at NBC for the zero deficit and Inman and Masters deficit conditions. For the zero deficit condition, retreat was generally higher in the northern and southern portions of the study area, and lower through the central region. This trend became more marked for the higher sea level rise scenarios. This large scale trend in the south was generally related to the lack of source material in the back beach once the coastal dunes have been eroded. In the north, the higher retreat was related more to the flatter and shallower offshore topography that requires more sand to maintain in the face of sea level rise. Through the central region, the offshore profiles are steeper and fairly uniform, and the back beach areas are generally higher at least up to the point where the erosion starts to exceed the width up to the highway. Finer scale variations were partly an artifact of the modeling approach, which did not include local beachwidth smoothing from alongshore sand transport.

For the Inman and Masters deficit condition, the retreat in the south and central portions of the study area were accentuated by the sand deficit, while the northern end was similar to the zero deficit case because the Inman and Masters values transition to zero in this area. The overall result was that, under moderate to high sea level rise conditions, retreat rates were highest in the south, and then fairly uniform over much of the rest of the study area. At lower sea level rise conditions, the retreat rates in the north were actually lower than in the central area because of the dominance of the sand budget term under low sea level rise scenarios.

Model assumptions

The primary assumptions underlying the CSPEM model were that the active profile shape was maintained from its current day configuration, the upper and lower limits of the active profile were governed by long-term processes on the time scale of a decade, and that the back beach material was 100% erodible sand that was available to replenish the offshore portions of the profile. The consistency of the profile shape was supported by the historical monitoring data at the fiducial transects (see Section 2.3.3. The assumptions regarding the extent of the active beach profile were subjective. Conceptually, the 10-year r return period was chosen to represent a moderately high total water level condition that occurred frequently enough to be influential over the modeled time period of interest (100 years). Additional research on defining the most appropriate limits would be useful since the choice has implications for the estimation of future beach widths and erosion rates. For NBC, the entire study area was primarily composed of sand, including the inland areas that would be subject to erosion, so the composition assumption is reasonable. The erosion does move into some areas that are paved or protected, so in these instances the erodability assumption would be invalid. However we were primarily interested in identifying areas that were vulnerable to erosion and from this perspective our assumption provided a conservative view of those vulnerabilities.

Model Sensitivity

Sensitivity analysis of the active profile boundaries was conducted at selected profiles using boundaries associated with week, month, year, decade and century return period conditions. The results showed relatively small differences in model outcomes over the range of conditions from week to year, with progressive increases in retreat associated with boundaries associated with decade and century return period conditions (Figure 4-57). Retreat for the decade condition generally exceeded the shorter return period conditions by about 15 to 20%. For the century condition, retreat increased over the shorter return period conditions by about 45 to 50%. These increases resulted from

two factors including a deeper extension of the offshore extent of the profile that encompasses flatter areas that require more sand for maintenance, and a higher back beach elevation that must also be maintained during retreat. Overall the model was not highly sensitive for assumed active profile ranges associated with 1- to 10-year return period conditions, and our choice of the 10-year return falls between the extremes of the outcomes from 1 week to 1 century.

Table 4-7. Beach retreat comparison for different sand deficit assumptions.

	Beach Retreat (m)						
SLR	Zero Deficit			Inman and Master 1991 Deficit			
	Average	Min	Max	Average	Min	Max	
0.5	21.3	15.9	39.6	53.5	24.4	109.5	
1.0	41.3	29.3	73.8	74.9	47.1	148.0	
1.5	62.7	43.0	109.6	97.6	69.1	184.8	
2.0	85.7	55.1	156.0	121.2	89.1	226.1	

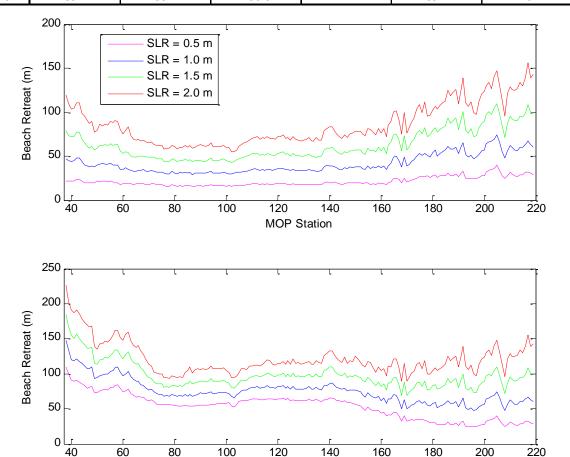


Figure 4-57. Alongshore variation in beach retreat at NBC for the zero sand deficit (above) and Inman and Masters 1991 sand deficit scenarios.

MOP Station

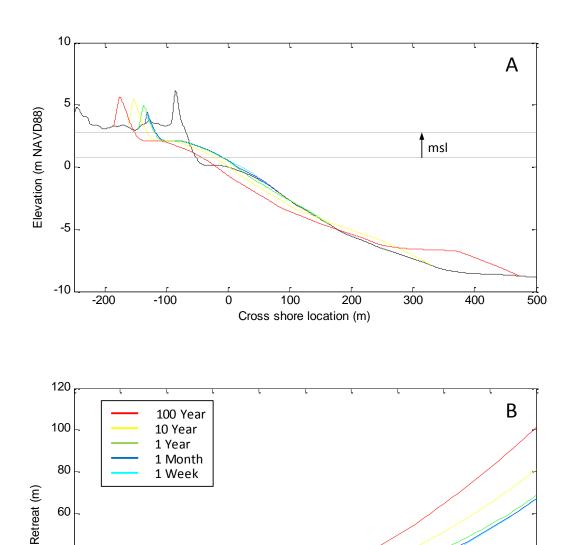


Figure 4-58. Comparison of retreat profiles for the year 2100 with no sand deficit at MOP station 155 for active profile boundaries defined by a range of return period conditions (above), and retreat curves for the corresponding conditions from 2000 – 2100.

Year

0 <u>L</u>

Short-Term Beach Response

Short-term beach response at MCBCP was examined using the YGOR model described in Section 3.3.3 at each of the fiducial transects. The return period statistics of shoreline position extremes were computed using the extreme value method of order statistics (Makkonen, 2011), and interpolated along the entire shoreline of the installation using a piecewise polynomial interpolation method. The resulting shoreline fluctuations for each return period were then superimposed on the long-term response results to construct shoreline positions for a range of sea level rise and return period conditions.

Erosion Footprints

Using the CSPEM methodology, we evaluated the long-term beach system response and developed erosion footprints for the beach system at NBC. Erosion footprints were developed for snapshots along the 2-m SLR curve that correspond to sea level increases of 0.5, 1.0, 1.5, and 2.0 m, and timeframes of 2046, 2069, 2087, and 2100. These cases are referred to as the "first occurrence" conditions because they represent the earliest time that these sea level values would occur based on the assumed range of sea levels used in the study. The footprints were developed using the sand deficit estimates from Inman and Masters (1991) as the most conservative assumption. The footprint for each condition was represented by a polygon which spans alongshore the entire active shoreline of NBC, and spans cross shore between the baseline (year 2000) shoreline position and the shoreline position for the snapshot time of interest. For each mean sea level condition, five overlapping polygons are shown that correspond to the overlay of the short-term beach response from the YGOR model simulations on the long-term mean shoreline retreat estimated from the CSPEM model. Results for the beach system response, and the resulting erosion footprints are presented in Figure 4-58 through Figure 4-69 for the baseline (SLR = 0 m), 1.0-m and 2.0-m sea level rise scenarios (note that the 0.5- and 1.5-m cases were also compiled in the GIS but are not shown here).

The erosion footprint areas reflect both the long- and short-term response of the shoreline to the combined effects of sea level rise, sand budget deficits and a range of wave conditions. In general, the erosion zones grew in response to higher sea levels, longer durations of sand budget deficits, and stronger wave climates. The baseline condition shown in Figure 4-58 through Figure 4-61 essentially represent only the effects of short-term wave response because the sea level rise is zero, as is the time duration associated with the sand budget deficit term. The spatial patterns of these eroded shorelines indicated higher erosion in the northern portions of the study area off of North Island where the wave energy is generally higher than the areas to the south. Under the baseline condition for the higher wave energy events, elements of the installation infrastructure that appeared to be vulnerable to erosion under current day conditions included roads and recreation areas in the North Island area, buildings and training areas in the NAB/SSTC North area, and the beach training areas at SSTC South.

For the 1.0-m SLR case (Figure 4-62 through Figure 4-65), the effects of sea level rise and the sand budget deficit were more apparent in the erosion patterns. The shoreline retreat was more uniform across the study area, though still somewhat more pronounced in the northern area in association with the higher wave energy. This case corresponded to a first occurrence year of 2069, so the influence of the sand budget deficit had sufficient time to contribute substantially to the long-term shoreline retreat. Close inspection of the detailed views in Figure 4-63 through Figure 4-65 show that for the smaller wave conditions (grey lines closest to the original shoreline), the shoreline retreat was comparable across the three installation areas, but grew wider in the north for the higher energy wave conditions in comparison to the areas in the south. Under the 1.0-m SLR condition, receptors that appeared to be vulnerable to erosion included buildings, roads, recreation areas and

storm water systems at North Island, buildings, training areas, and storm water systems at NAB/SSTC North, and training areas and roads at SSTC South.

For the 2.0-m SLR case (Figure 4-66 through Figure 4-69), the spatial pattern of retreat was similar to the 1.0-m case but more significant in magnitude. This case corresponded to a first occurrence year of 2100, so the influence of the sand budget deficit had the entire 100-year study period to contribute substantially to the long-term shoreline retreat. This was also the highest sea level rise condition studied, so it represented the worst case over the range of our scenarios. Under the combination of short- and long-term erosion patterns receptors that appeared to be vulnerable included buildings, roads, recreation areas, airfields and storm water systems at North Island, buildings, training areas, and storm water systems at NAB/SSTC North, and training areas and roads at SSTC South.

Erosion at MCBCP

Long-term erosion response at MCBCP was evaluated using the CDPM model described in Section 3.3.2. This model incorporated the coupled and decoupled response of the beach and cliff system to sea level rise and sand budget deficits. Results for a range of sand budgets were evaluated and presented below, with the final analysis focusing on the higher level deficit as a more conservative scenario.

Zero Deficit Scenario

The rate, alongshore mean distance, and range of cliff retreat increased with time and MSLR (Figure 4-70). By year 2100, alongshore scenario-mean cliff retreat ranged from 4 to 16 m. The maximum cliff retreat by 2100, and 10-year return interval, was 21, 22, 35, 54 m, and 0.3, 0.3, 0.7, 1.3 m/yr for the 0.5-, 1.0-, 1.5-, and 2.0-m MSLR by 2100 scenarios, respectively. The initial back beach buffer ranged from 1 to 183 m (mean, 40 m) with larger values toward the south and far north (Figure 4-71a). For all MSLR scenarios, the beach buffer prevented wave-driven erosion through 2100 at some locations and only subaerial processes caused erosion resulting in similar minimum 2100 retreat values of 2 m (Figure 4-71c). Although scattered, the sections with minimal back beach buffer (approximately 18 to 22 km north of Oceanside Harbor Figure 4-71a), experienced larger cliff retreat compared to other sections (Figure 4-71c). Retreat was highly variable over short distances from abrupt changes in beach buffer width and/or cliff height. This result is also partly an artifact of the modeling approach, which does not include local beach-width smoothing from alongshore sand transport.

Deficit and Surplus Scenarios

External sand deficit or surplus increased or decreased overall cliff retreat, respectively (Table 4-8). The surplus scenario (0.37 m³/m/yr) generally caused little change compared to the zero deficit scenario and reduced mean and maximum 2100 year retreat by 0 to 11%. Retreat distributions were also marginally different compared to the zero deficit scenario. In contrast, the deficit scenario (15 m³/m/yr) caused significant change in year 2100 retreat magnitude, increasing the mean 40-130%, and maximum two-six fold. Binned distributions (Figure 4-72) peaked around 50 to 80 m and were less skewed compared to the other scenarios. Increasing the sand deficit spread the distribution more evenly, similar to increasing MSLR.



Figure 4-59. Erosion footprint for the baseline (SLR = 0 m) scenario at NBC. The overall green shaded band spans the 100-year return period wave condition from the YGOR model, and the fine grey lines indicate the shorter return periods ranging from week to decade.

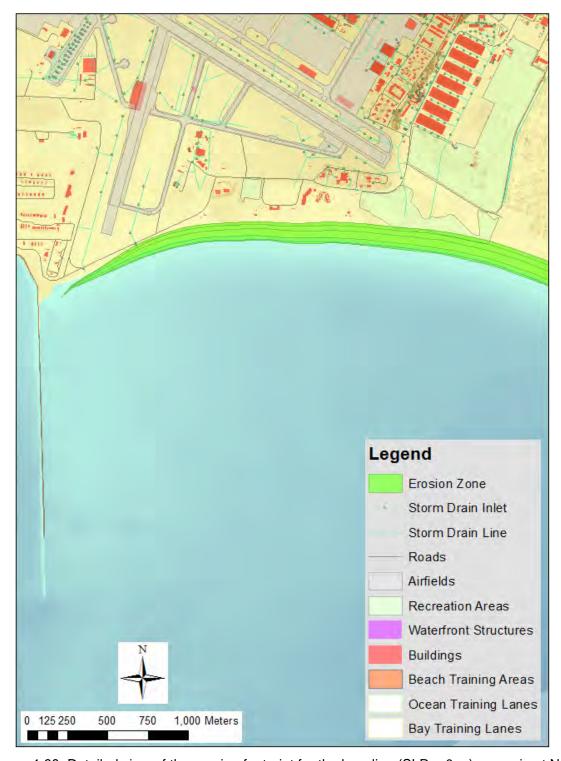


Figure 4-60. Detailed view of the erosion footprint for the baseline (SLR = 0 m) scenario at North Island. The overall green shaded band spans the 100-year return period wave condition from the YGOR model, and the fine grey lines indicate the shorter return periods ranging from week to decade.



Figure 4-61. Detailed view of the erosion footprint for the baseline (SLR = 0 m) scenario at NAB/SSTC North. The overall green shaded band spans the 100r year return period wave condition from the YGOR model, and the fine grey lines indicate the shorter return periods ranging from week to decade.

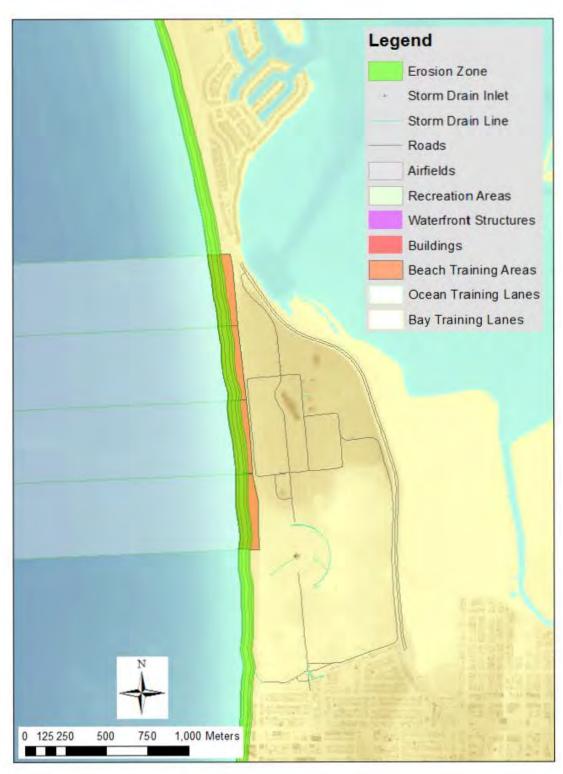


Figure 4-62. Detailed view of the erosion footprint for the baseline (SLR = 0 m) scenario at SSTC South. The overall green shaded band spans the 100-year return period wave condition from the YGOR model, and the fine grey lines indicate the shorter return periods ranging from week to decade.



Figure 4-63. Erosion footprint for the SLR = 1.0-m scenario at NBC. The overall green shaded band spans the 100-year return period wave condition from the YGOR model, and the fine grey lines indicate the shorter return periods ranging from week to decade.



Figure 4-64. Detailed view of the erosion footprint for the SLR = 1.0-m scenario at North Island. The overall green shaded band spans the 100-year return period wave condition from the YGOR model, and the fine grey lines indicate the shorter return periods ranging from week to decade.



Figure 4-65. Detailed view of the erosion footprint for the SLR = 1.0-m scenario at NAB/SSTC North. The overall green shaded band spans the 100-year return period wave condition from the YGOR model, and the fine grey lines indicate the shorter return periods ranging from week to decade.

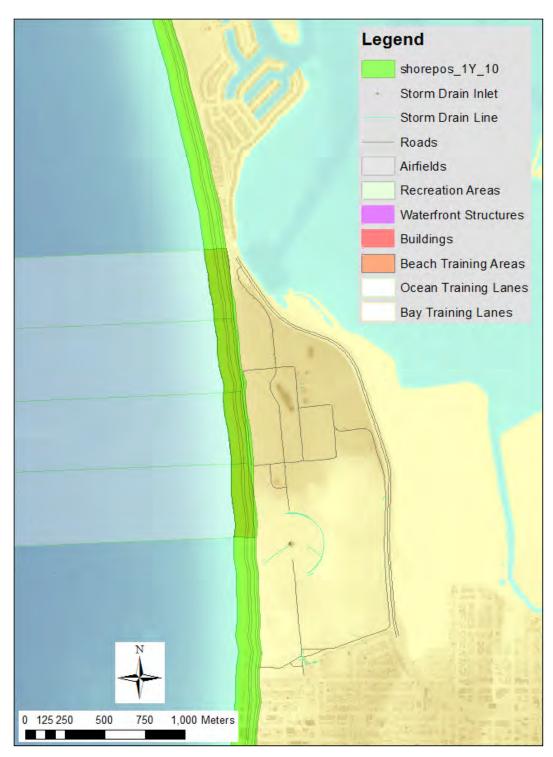


Figure 4-66. Detailed view of the erosion footprint for the SLR = 1.0-m scenario at SSTC South. The overall green shaded band spans the 100-year return period wave condition from the YGOR model, and the fine grey lines indicate the shorter return periods ranging from week to decade.



Figure 4-67. Erosion footprint for the SLR = 2.0-m scenario at NBC. The overall green shaded band spans the 100-year return period wave condition from the YGOR model, and the fine grey lines indicate the shorter return periods ranging from week to decade.



Figure 4-68. Detailed view of the erosion footprint for the SLR = 2.0-m scenario at North Island. The overall green shaded band spans the 100-year return period wave condition from the YGOR model, and the fine grey lines indicate the shorter return periods ranging from week to decade.



Figure 4-69. Detailed view of the erosion footprint for the SLR = 2.0-m scenario at NAB/SSTC North. The overall green shaded band spans the 100-year return period wave condition from the YGOR model, and the fine grey lines indicate the shorter return periods ranging from week to decade.



Figure 4-70. Detailed view of the erosion footprint for the SLR = 2.0-m scenario at SSTC South. The overall green shaded band spans the 100-year return period wave condition from the YGOR model, and the fine grey lines indicate the shorter return periods ranging from week to decade.

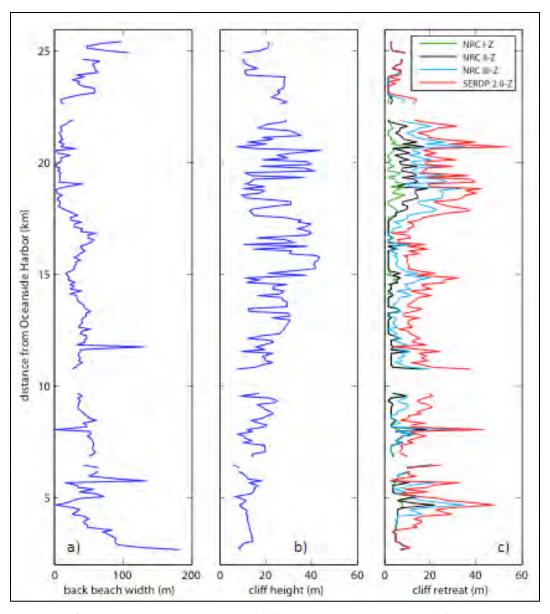


Figure 4-71. CDPM - Zero deficit scenario: (a) initial back beach width, (b) initial cliff height, and (c) end-point cliff retreat by year 2100 for the four MSLR scenarios.

Alongshore distribution of cliff retreat

CDPM and other sand balance based models indicate that cliff retreat increases with decreasing cliff height because taller cliffs provide more beach sand per unit of retreat (holding other variables equal). When alongshore cliff height changes abruptly (for example, from extensive gullying in MCBCP), the modeled cliff retreat also changes abruptly, resulting in large cliff line deviations in retreat over short distances and highly uneven and potentially unrealistic results. For coastlines lacking headlands and sand transport barriers (for instance, MCBCP) alongshore sand transport not included in the model will move eroded cliff sand to adjacent areas maintaining a relatively smooth shoreline, unlike the present results.

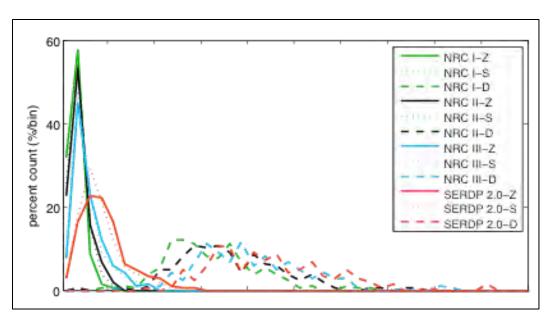


Figure 4-72. Comparison of modeled 100-year cliff retreat (n = 207) of 5-m bin width retreat distributions for MSLR scenarios and zero (Z), surplus (S), and deficit (D) scenarios.

Table 4-8. MCBCP 100-year cliff retreat projection summary.

Scenar	io	Min (m)	Mean (m)	Max (m)
NRC I-Z		2	4	21
NRC I-S	0.5 m	1	4	21
NRC I-D		7	62	131
NRC II-Z		2	6	22
NRC II-S	1.0 m	2	5	21
NRC II-D		7	70	148
NRC III-Z		2	9	35
NRC III-S	1.5 m	2	8	32
NRC III-D		21	79	163
SERDP 2.0-Z		2	16	54
SERDP 2.0-Z	2.0 m	2	15	50
SERDP 2.0-Z		37	87	179

Model assumptions

A primary assumption of sand balance models is that sand balance is attainable. For cliffs resistant to erosion, these models predict cliff retreat rates potentially exceeding the maximum possible. This is a significant problem where cliffs contain little or no coarse sand and models predict unrealistically large or infinite coastal retreat. Sand based models also fail when equilibrium is sand independent, for example at a rock coast devoid of sand. In this case, the models unrealistically predict no coastal retreat because no sand is needed to maintain equilibrium.

Most sand balance cliff retreat models assume an instant cliff response to sea level rise (if external sand supply is constant), ignoring the potential time lag caused by cliff erosion resistance. This assumption may hold for soft sandy cliffs and millennial time scales, but probably not for resistant cliffs and shorter time scales. CDPM modifications remove this assumption. By decoupling the beach and cliff profiles, the CDPM also decouples the instant response. An adequate beach buffer delays marine-driven cliff erosion and limits the instant response to the beach profile. While the buffer prevents marine cliff erosion, subaerial processes dominate and the cliff erosion is insensitive to sea level, temporarily resulting in a no-feedback system (Ashton, Walkden, Dickson, 2011). After complete buffer erosion, the beach and cliff profile become coupled again and the cliff-beach profile become an instant response system similar to previous models.

Previous sand balance models assume sufficient sand availability below the active beach profile to maintain sand balance. For cliffed coasts with thin beach cover, the active beach profile can potentially shift into the underlying shore platform when all overburden sand is removed; such as by a large wave storm event. This makes the assumption invalid if the substrate is erosion resistant or the underlying substrate is not 100% sand. The CDPM method permits active profile shifts to the shore platform and can accommodate substrates with partial sand content. If the active profile intersects an erodible platform, then the profile can maintain its overall equilibrium shape. However, if the platform is resistant, the profile shape must adjust according to the platform shape. In both cases CDPM, can still maintain sand balance, but indicates beach loss and platform exposure along at least part of the profile. Unfortunately, detailed subsurface platform profiles are not available for MCBCP or nearly all other sections of southern California coast. This represents an important deficiency that hinders better modeling of future shoreline and cliff changes from MSLR.

Model Sensitivity

Sensitivity analysis of the active profile boundaries showed relatively small differences in model outcomes for the typical values used (lower of -4 to -6 m and upper of 3 to 4 m, NAVD88, Figure 4-73). However, the present study only considered one possible method to estimate active profile boundaries and others could cause higher model sensitivity. Model sensitivity significantly increased at deeper closure depths where the offshore profile flattens out, and small changes of, say, 1 m resulted in double the cliff retreat. Changes of closure depth in flat portions of the profile substantially increased the sand volume needed to maintain sand balance due to MSLR. Other profile based models (*e.g.*, Bruun model) are similarly sensitivity to closure depth and often criticized because of this drawback.

Sand balance models only require achieving sand balance and ignore other factors that influence coastal change, such as deep-seated landslides found along MCBCP. Coastal deep-seated slide mechanics and their effects on the coastal system are complex, not well understood, and involve other factors beyond coastal sand balance. Inclusion of deep-seated landslides in the CDPM is beyond the current scope. However, marine driven erosion of the slide toe (estimated by sand balance) can instigate or permit continued landsliding, and future deep-seated landsliding should certainly be considered in areas with unfavorable geology.

Long-term Beach Retreat at MCBCP

Initial beach widths (Figure 4-71) exceeded the active profile cross-shore widths, providing a beach buffer against wave driven cliff erosion. During mean sea level rise the landward shifting of the active profile erodes the buffer until the active profile intersects the cliff and subaerial beach width (defined here as the width from the cliff base to the mean sea level beach intersection) is reduced (Figure 4-74). After the active profile intersects the cliff, subaerial beach width becomes constant (unless the beach width increases from external sediment input exceeding the volume need to maintain profile equilibrium) according to the equilibrium width defined by the active profile.

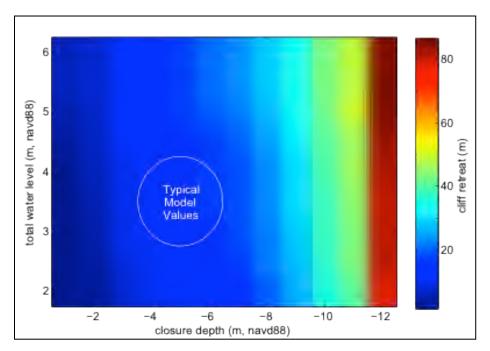


Figure 4-73. Typical model sensitivity and active profile boundaries used in the present study.

In all scenarios, beach widths were reduced more rapidly with increasing MSLR scenarios. However, the rate of reduction was more apparent in the zero deficit scenario compared to the negative 15 m³/m-yr scenario, where beach widths were reduced relatively rapidly to their constant equilibrium width. The rapid reduction and relatively similar time series of scenario beach changes highlights the importance and potential influence of external sediment deficit/supply.

Short-Term Beach Response

Short-term beach response at MCBCP was examined using the YGOR model described in Section 3.3.3 at each of the fiducial transects. The return period statistics of shoreline position extremes were computed using the extreme value method of order statistics (Makkonen, 2011), and interpolated along the entire shoreline of the installation using a piecewise polynomial interpolation method. The resulting shoreline fluctuations for each return period were then superimposed on the long-term response results to construct shoreline positions for a range of sea level rise and return period conditions.

In all scenarios, beach widths were reduced more rapidly with increasing MSLR scenarios. However, the rate of reduction was more apparent in the zero deficit scenario compared to the negative 15 m³/m-yr scenario, where beach widths were reduced relatively rapidly to their constant

equilibrium width. The rapid reduction and relatively similar time series of scenario beach changes highlights the importance and potential influence of external sediment deficit/supply.

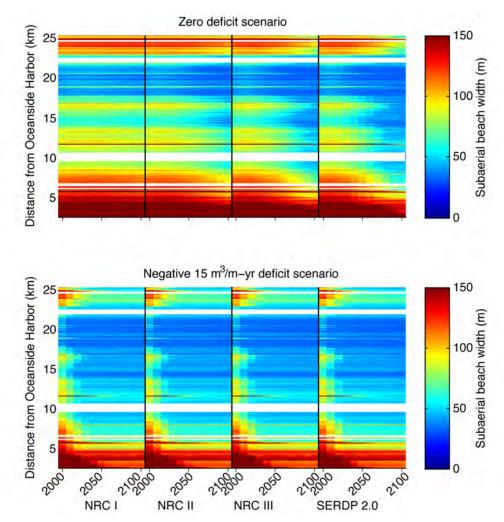


Figure 4-74. Time series of subaerial beach width change for (upper panel) the zero deficit and (lower panel) negative 15 m^3/m-yr deficit scenarios. Both upper and lower panels show 100-year color coded decadal beach widths for the four MSLR scenarios.

Erosion Footprints

Using the CDPM methodology, we evaluated the long-term beach/cliff system response and developed erosion footprints for the beach system at NBC. Erosion footprints were developed for snapshots along the 2-m SLR curve that correspond to sea level increases of 0.5, 1.0, 1.5, and 2.0 m, and timeframes of 2046, 2069, 2087, and 2100. These cases are referred to as the "first occurrence" conditions because they represent the earliest time that these sea level values would occur based on the assumed range of sea levels used in the study. The footprints were developed using the sand deficit estimates from Inman and Masters (1991) as the most conservative assumption. The footprint for each condition was represented by polygons for beach and cliff segments which spanned alongshore the entire active shoreline of MCBCP, and spanned cross shore between the baseline (year 2000) shoreline position and the shoreline position for the snapshot time of interest. For each mean sea level condition, five overlapping polygons of beach erosion are shown that correspond to the overlay of the short-term beach response from the YGOR model simulations on the long-term

mean shoreline retreat estimates from the CSPEM model. Results for the beach/cliff system response, and the resulting erosion footprints are presented in Figure 4-75 through Figure 4-86 for the baseline (SLR = 0 m), 1.0-m, and 2.0-m sea level rise scenarios (note that the 0.5- and 1.5-m cases were also compiled in the GIS but are not shown here).

The erosion footprints for the beach areas reflected both the long- and short-term response of the shoreline to the combined effects of sea level rise, sand budget deficits and a range of wave conditions. The erosion footprints for the cliffs reflected only the long-term response from the combination of subaerial processes and, in cases where the back beach buffer was sufficiently narrow, wave driven erosion. In general, the beach erosion zones grew in response to higher sea levels, longer durations of sand budget deficits, and stronger wave climates. The cliff erosion zones grew at the lower subaerial rate until sea level rise was sufficient to narrow the back beach, and then the rates accelerated in association with wave erosion.

The baseline condition shown in Figure 4-75 through Figure 4-78 essentially represent only the effects of short-term wave response on the beaches because the sea level rise is zero, as is the time duration associated with the sand budget deficit term and the subaerial cliff erosion term. The spatial patterns of these eroded shorelines were quite uniform throughout the study area, consistent with the fairly uniform wave energy climate. Under the baseline condition for the higher wave energy events, the primary receptor category that appeared to be vulnerable to erosion under current day conditions were the beach training areas particularly along the northern portions of the base where the beaches are already quite narrow.

For the 1.0-m SLR case (Figure 4-79 through Figure 4-82), the effects of sea level rise and the sand budget deficit were more apparent in the beach erosion patterns. The shoreline retreat was still fairly uniform across the study area, though still somewhat more pronounced in the southern area at Del Mar where there are no cliffs and limited sand supply from the back beach. This case corresponded to a first occurrence year of 2069, so the influence of the sand budget deficit had sufficient time to contribute substantially to the long-term shoreline retreat. Cliff erosion was apparent, and cliff erosion patterns were also fairly uniform across the study area though somewhat higher in the northern areas where wave erosion contributed more due to the narrow beaches. Under the 1.0-m SLR condition, receptors that appeared to be vulnerable included beach training areas, buildings, roads, and recreation areas.

For the 2.0-m SLR case (Figure 4-83 through Figure 4-86), the spatial pattern of retreat was similar to the 1.0 m case but more significant in magnitude. This case corresponded to a first occurrence year of 2100, so the influence of the sand budget deficit had the entire 100-year study period to contribute substantially to the long-term shoreline retreat. This was also the highest sea level rise condition studied, so it represented the worst case over the range of our scenarios. Beach erosion was more pronounced to the south. Cliff erosion was substantial, and fairly uniform across the study area. Under the combination of beach and cliff erosion patterns receptors that appeared to be vulnerable included buildings, roads, recreation areas, storm water systems, and beach training areas. Cliff erosion in this scenario reached the major interstate (I5) in the northern portion of the study area, and approached some of the airfields along the central portion of the installation.

Inundation and Flooding at NBC

Inundation and flooding along the exposed shorelines at NBC were assessed following the methodologies described in Section 3.3.5. Elevation models for future sea level scenarios were developed based on results from the long-term shoreline response models described above. A new model was constructed for each target sea level condition (0.5, 1.0, 1.5, and 2.0 m). To illustrate the methodology we utilized the "first occurrence" of these conditions along the 2.0-m sea level rise

curve which corresponded to time snapshots for the years 2046, 2069, 2087, and 2100, respectively. Inundation and flooding were examined for these elevation models across a continuum of total water levels defined through combined variations in sea level rise and return period total water level events. These scenarios spanned five sea level rise conditions from 0-2 m, and five return periods (week, month, year, decade, century) for a total of 25 scenarios at each MOP station for each installation. In the context of this project, we defined inundation as a process that leads to the frequent (week-month return) exposure of coastal areas to wetting, while flooding was considered to represent infrequent to rare events with long return periods (year-century). Due to the limitations of the flood mapping methodologies, the maps shown in the section should be interpreted as areas that are sensitive to inundation and flooding under these conditions, rather than strict predictions of inundation and flooding footprints.

Results of the inundation and flooding analysis for the baseline (SLR = 0 m), 1.0-m sea level rise, and 2.0-m sea level rise scenarios are shown in Figure 4-87 through Figure 4-89. The overall inundated/flooded area increased fairly linearly with increasing mean sea level. More rapid increases were projected for the yearly and decadal return periods in the transition from the baseline condition to a 0.5-m SLR (Figure 4-87). As a function of time, the inundated/flooded area showed some acceleration in the latter half of the century in conjunction with accelerating SLR. Estimated area sensitive to inundation (weekly return period) ranged from about 2 million m^2 for 0.5-m SLR, to 8 million m^2 for 2.0-m SLR, while estimated area sensitive to the 100-year return period flood event ranged from about 10 million m^2 to about 16 million m^2 .

For the baseline condition (SLR = 0 m), inundation as represented by the weekly return event was limited to the shoreline beach areas of the installation. There was no apparent vulnerability of any receptor category to inundation under current day conditions. For the 1-year return period condition, flooding was also limited to the beach areas with the exception of the installation areas at North Island where flood exposure extended inland up to about 500 m in some areas. Under the 100-year return period condition, more extensive flooding was projected including portions of all three regions of the installation. This exposure, even under current day conditions, reflects the low lying nature of the topography across much of NBC. Receptor categories that are potentially vulnerable to flooding under present day conditions include buildings, training areas, roads, airfields, recreation areas, and storm water systems.



Figure 4-75. Erosion footprint for the baseline (SLR = 0 m) scenario at MCBCP. The overall light green shaded band spans the 100-year return period wave condition from the YGOR model, and the fine grey lines indicate the shorter return periods ranging from week to decade.

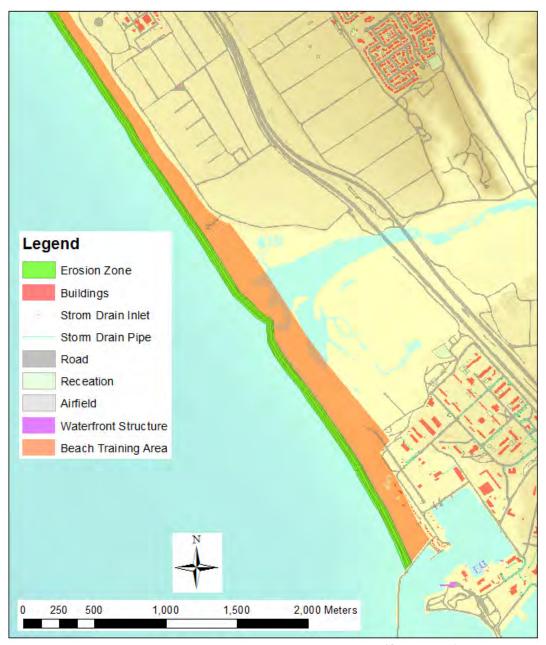


Figure 4-76. Detailed view of the erosion footprint for the baseline (SLR = 0 m) scenario at Del Mar. The overall light green shaded band spans the 100-year return period wave condition from the YGOR model, and the fine grey lines indicate the shorter return periods ranging from week to decade.

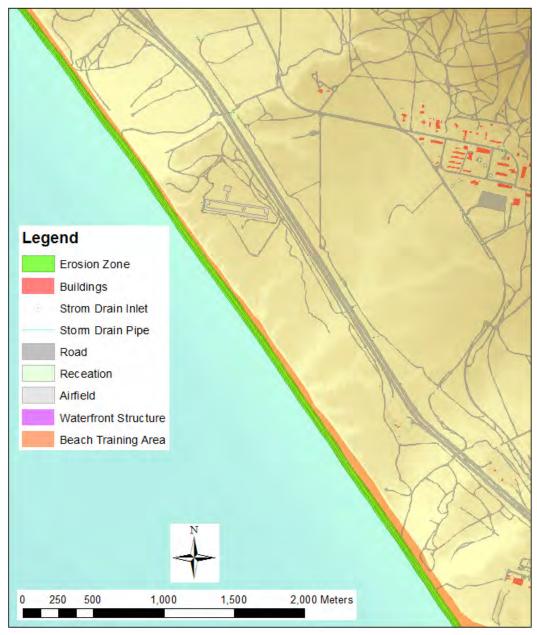


Figure 4-77. Detail view of the erosion footprint for the baseline (SLR = 0 m) scenario at Red Beach. The overall light green shaded band spans the 100-year return period wave condition from the YGOR model, and the fine grey lines indicate the shorter return periods ranging from week to decade.

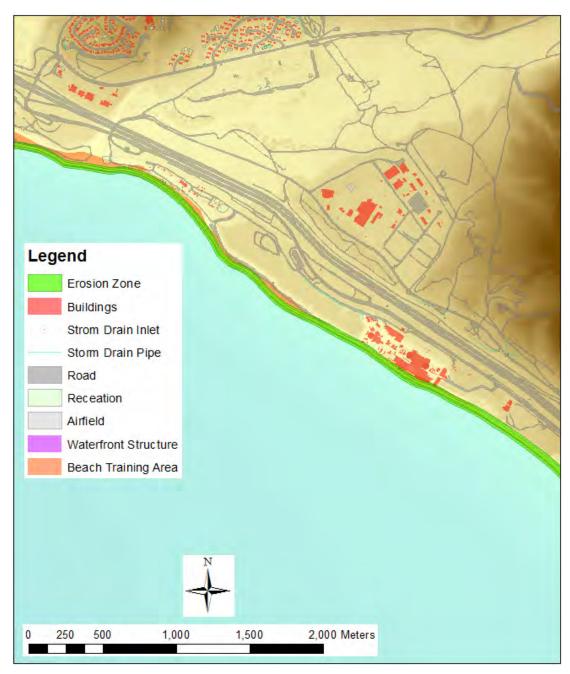


Figure 4-78. Detailed view of the erosion footprint for the baseline (SLR = 0 m) scenario at San Onofre. The overall light green shaded band spans the 100-year return period wave condition from the YGOR model, and the fine grey lines indicate the shorter return periods ranging from week to decade.



Figure 4-79. Erosion footprint for the SLR = 1.0-m scenario at MCBCP. The overall light green shaded band spans the 100-year return period wave condition from the YGOR model, and the fine grey lines indicate the shorter return periods ranging from week to decade. The dark green shaded band indicates the extent of cliff erosion.

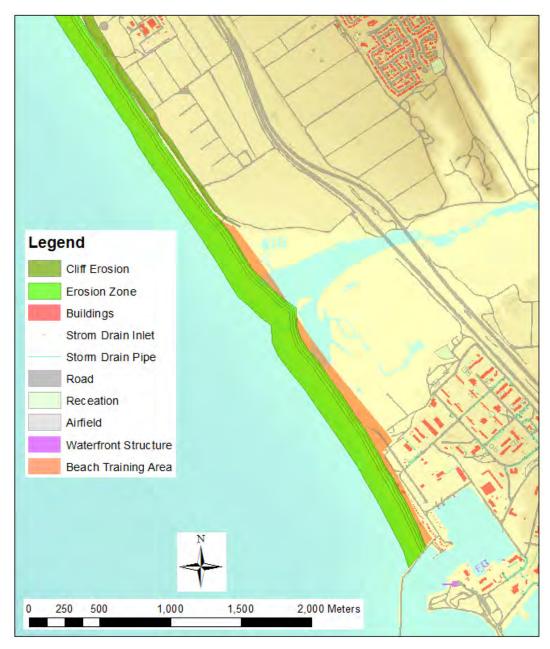


Figure 4-80. Detail view of the erosion footprint for the SLR = 1.0-m scenario at Del Mar. The overall light green shaded band spans the 100-year return period wave condition from the YGOR model, and the fine grey lines indicate the shorter return periods ranging from week to decade. The dark green shaded band indicates the extent of cliff erosion.

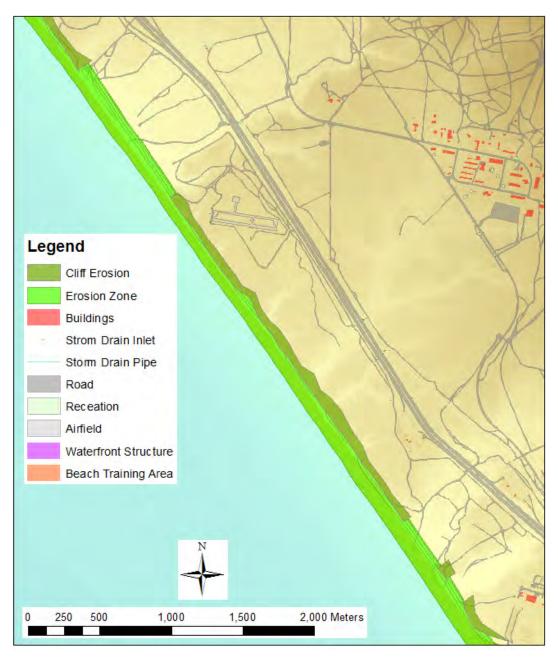


Figure 4-81. Detailed view of the erosion footprint for the SLR = 1.0-m scenario at Red Beach. The overall light green shaded band spans the 100-year return period wave condition from the YGOR model, and the fine grey lines indicate the shorter return periods ranging from week to decade. The dark green shaded band indicates the extent of cliff erosion.

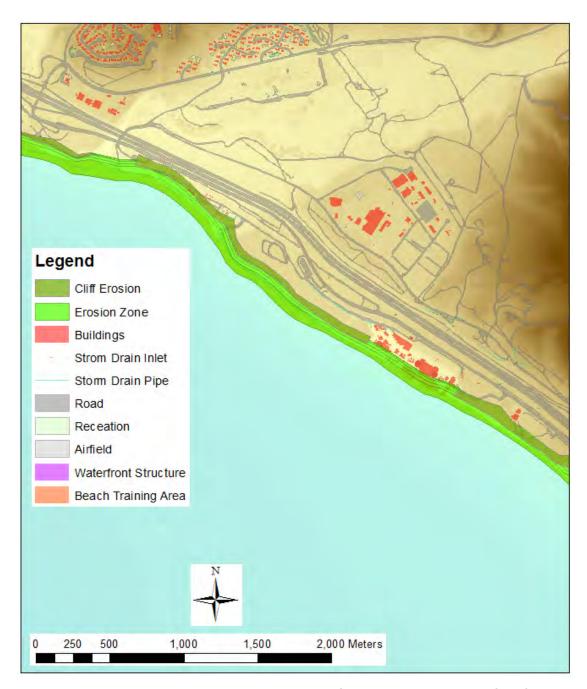


Figure 4-82. Detailed view of the erosion footprint for the SLR = 1.0-m scenario at San Onofre. The overall light green shaded band spans the 100-year return period wave condition from the YGOR model, and the fine grey lines indicate the shorter return periods ranging from week to decade. The dark green shaded band indicates the extent of cliff erosion.



Figure 4-83. Erosion footprint for the SLR = 2.0-m scenario at MCBCP. The overall light green shaded band spans the 100-year return period wave condition from the YGOR model, and the fine grey lines indicate the shorter return periods ranging from week to decade. The dark green shaded band indicates the extent of cliff erosion.

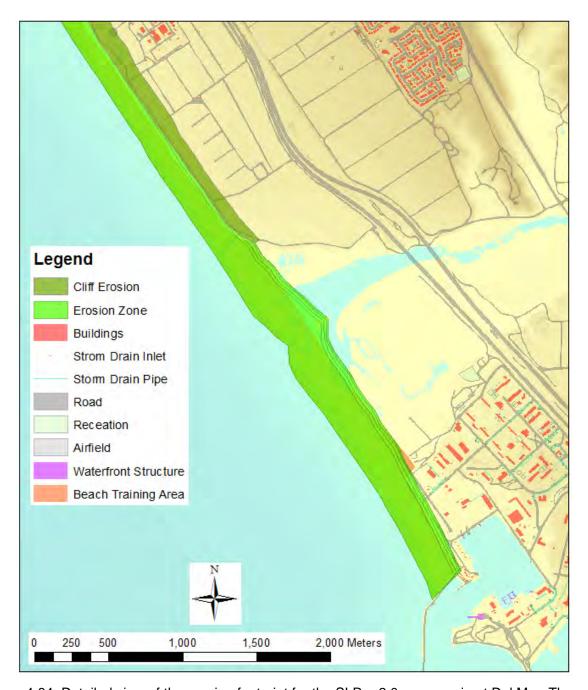


Figure 4-84. Detailed view of the erosion footprint for the SLR = 2.0-m scenario at Del Mar. The overall light green shaded band spans the 100-year return period wave condition from the YGOR model, and the fine grey lines indicate the shorter return periods ranging from week to decade. The dark green shaded band indicates the extent of cliff erosion.

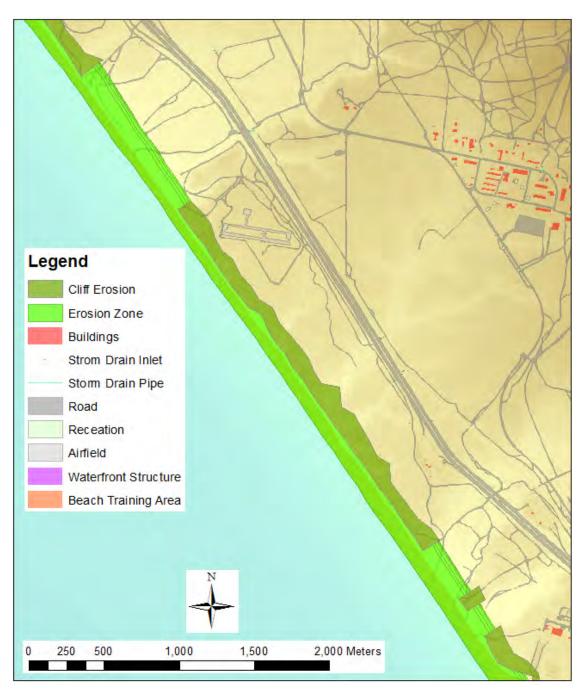


Figure 4-85. Detailed view of the erosion footprint for the SLR = 2.0-m scenario at Red Beach. The overall light green shaded band spans the 100-year return period wave condition from the YGOR model, and the fine grey lines indicate the shorter return periods ranging from week to decade. The dark green shaded band indicates the extent of cliff erosion.

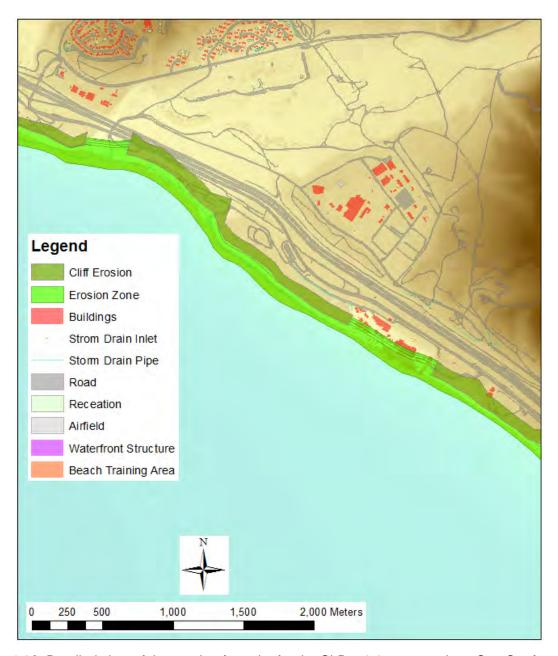


Figure 4-86. Detailed view of the erosion footprint for the SLR = 2.0-m scenario at San Onofre. The overall light green shaded band spans the 100-year return period wave condition from the YGOR model, and the fine grey lines indicate the shorter return periods ranging from week to decade. The dark green shaded band indicates the extent of cliff erosion.

For the 1.0-m sea level rise scenario (2069), inundation as represented by the weekly return event was more extensive particularly in the northern and southern areas of the installation. Inundation at North Island extended inland up to about 500 m in some areas, and as much as 100 m in the area of SSTC South. Receptor categories that are potentially vulnerable to inundation under the 1.0-m scenario included buildings, training areas, roads, airfields, recreation areas, and stormwater systems. For the 1-year return period condition, flooding was more extensive at all areas of the installation, extending inland 1500 to 2000 m at North Island and influencing built areas of NAB, and the Silver Strand Housing area. Under the 100-year return period condition, flooding was extensive, including significant areas of all three regions of the installation. Receptor categories that are potentially vulnerable to flooding under present day conditions include buildings, training areas, roads, airfields, recreation areas, and stormwater systems.

For the 2.0-m sea level rise scenario (2100), inundation as represented by the weekly return event was significant in all three areas of the installation. Inundation at North Island extended inland up 1500 to 2000 m in some areas, and as much as 2000 m in the area of SSTC South. Receptor that are potentially vulnerable to inundation under the 2.0-m scenario included all categories. For the 1-year return period condition, flooding was more extensive at all areas of the installation, spanning virtually all of NAB/SSTC North and major portions of North Island and SSTC South. Under the 100-year return period condition, flooding was dominant across the installation with only limited central regions of North Island and SSTC South directly unaffected. Receptors that are potentially vulnerable to flooding under the 2.0-m scenario include all categories.

Inundation and Flooding at MCBCP

Inundation and flooding along the exposed shorelines at MCBCP were assessed following the methodologies described in Section 3.3.5. Elevation models for future sea level scenarios were developed based on results from the long-term shoreline response models described above. A new model was constructed for each target sea level condition (0.5, 1.0, 1.5 and 2.0 m). To illustrate the methodology we utilized the "first occurrence" of the target conditions along the 2.0 m sea level rise curve which corresponded to time snapshots for the years 2046, 2069, 2087 and 2100, respectively. Inundation and flooding were examined for these elevation models across a continuum of total water levels defined through combined variations in sea level rise and return period total water level events. These scenarios spanned five sea level rise conditions from 0 to 2 m, and five return periods (week, month, year, decade, century) for a total of 25 scenarios at each MOP station for each installation. In the context of this project, we defined inundation as a process that leads to the frequent (week-month return) exposure of coastal areas to wetting, while flooding was considered to represent infrequent to rare events with long return periods (year-century). Due to the limitations of the flood mapping methodologies, the maps shown in the section should be interpreted as areas that are sensitive to inundation and flooding under these conditions, rather than strict predictions of inundation and flooding footprints.

Results of the inundation and flooding analysis for the baseline (SLR = 0 m), 1.0-m sea level rise, and 2.0-m sea level rise scenarios are shown in Figure 4-100 through Figure 4-112. The overall inundated/flooded area increased more rapidly up to 0.5-m SLR, then fairly linearly with increasing mean sea level up to 2.0 m (Figure 4-100). As a function of time, the inundated/flooded area showed some acceleration in the latter half of the century. Estimated area sensitive to inundation (weekly return period) ranged from about 4 million m² for 0.5-m SLR, to 7 million m² for 2.0-m SLR, while estimated area sensitive to the 100-year return period flood event ranged from about 6 million m² to about 9 million m².

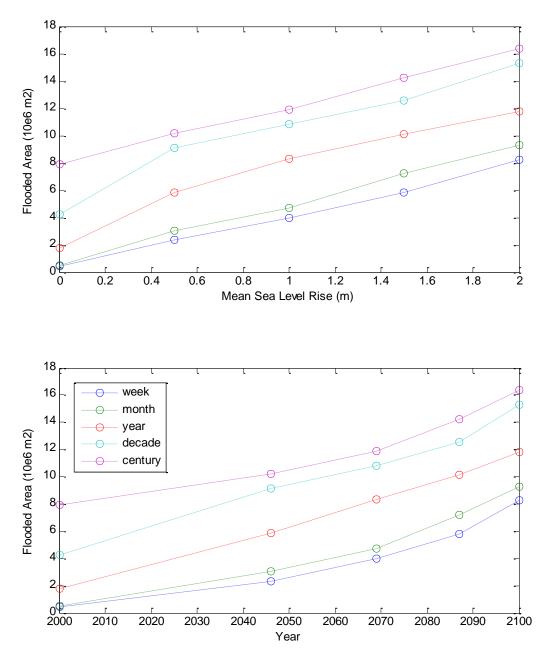


Figure 4-87. Estimated area vulnerable to inundation and flooding (cropped to NAVD88 = 0 m) for the 25 scenarios at NBC as a function of mean sea level rise (above) and time (below).



Figure 4-88. Inundation and flooding for the baseline (SLR = 0 m) scenario at NBC. The blue shaded zones represent week (dark blue), year (medium blue), and century (light blue) return periods.

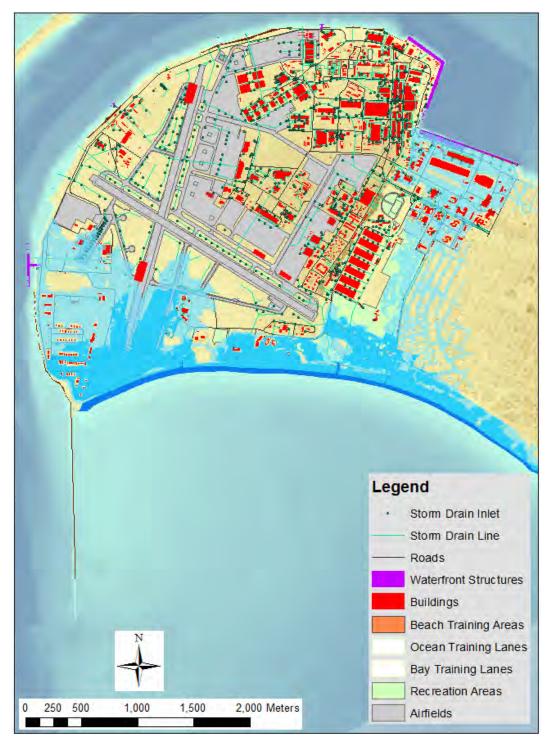


Figure 4-89. Detailed view of inundation and flooding for the baseline (SLR = 0 m) scenario at North Island. The blue shaded zones represent week (dark blue), year (medium blue), and century (light blue) return periods.



Figure 4-90. Detailed view of inundation and flooding for the baseline (SLR = 0 m) scenario at NAB/STTC North. The blue shaded zones represent week (dark blue), year (medium blue), and century (light blue) return periods.



Figure 4-91. Detailed view of inundation and flooding for the baseline (SLR = 0 m) scenario at STTC South. The blue shaded zones represent week (dark blue), year (medium blue), and century (light blue) return periods.



Figure 4-92. Inundation and flooding for the SLR,=1.0 m scenario at NBC. The blue shaded zones represent week (dark blue), year (medium blue), and century (light blue) return periods.

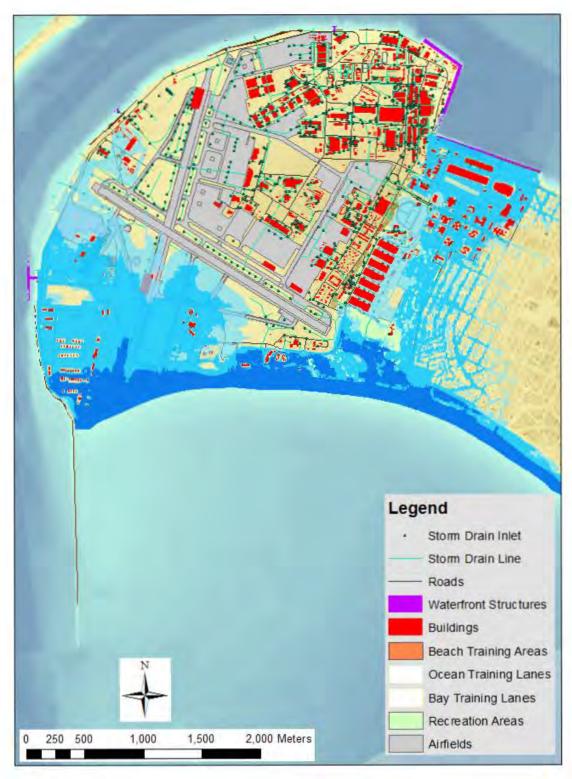


Figure 4-93. Detailed view of -and flooding for the SLR = 1.0-m scenario at North Island. The blue shaded zones represent week (dark blue), year (medium blue), and century (light blue) return periods.



Figure 4-94. Detailed view of inundation and flooding for the SLR = 1.0 m scenario at NAB/STTC North. The blue shaded zones represent week (dark blue), year (medium blue), and century (light blue) return periods.

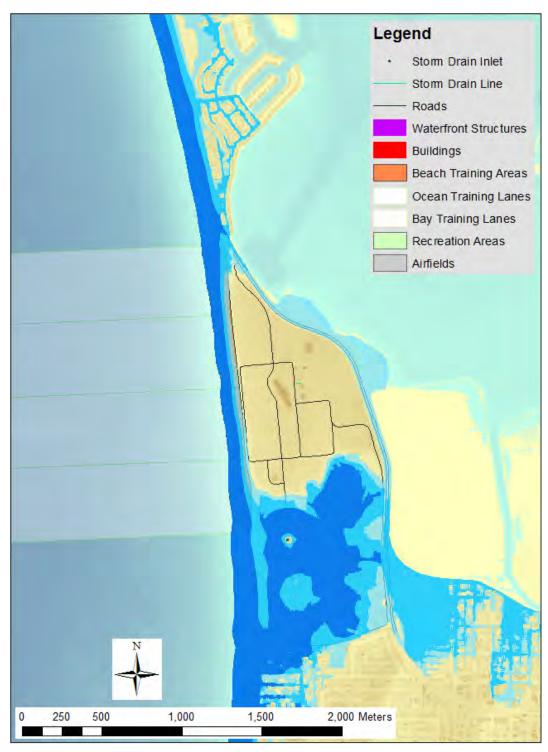


Figure 4-95. Detailed view of inundation and flooding for the SLR = 1.0-m scenario at STTC South. The blue shaded zones represent week (dark blue), year (medium blue), and century (light blue) return periods.



Figure 4-96. Inundation and flooding for the SLR = 2.0-m scenario at NBC. The blue shaded zones represent week (dark blue), year (medium blue), and century (light blue) return periods.

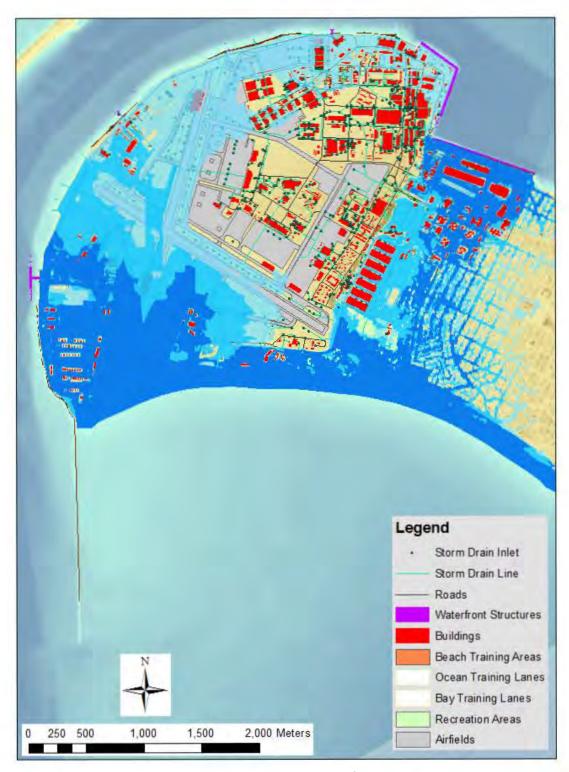


Figure 4-97. Detailed view of inundation and flooding for the SLR = 2.0-m scenario at North Island. The blue shaded zones represent week (dark blue), year (medium blue), and century (light blue) return periods.

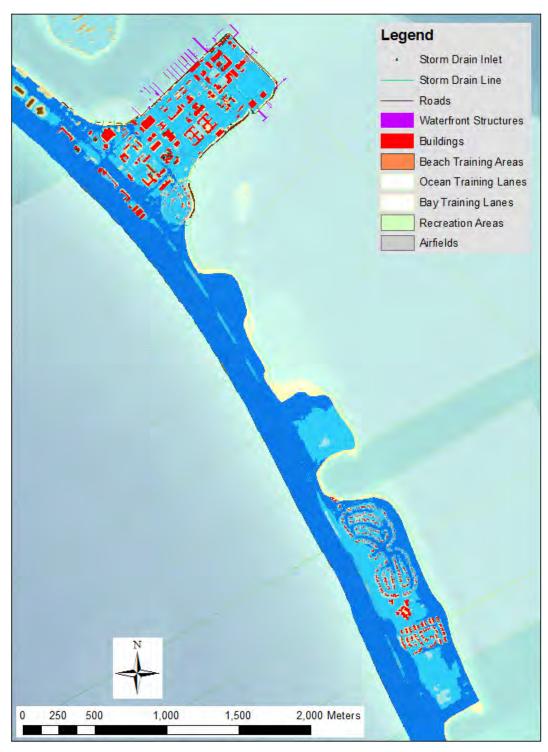


Figure 4-98. Detailed view of inundation and flooding for the SLR = 2.0-m scenario at NAB/STTC North. The blue shaded zones represent week (dark blue), year (medium blue), and century (light blue) return periods.



Figure 4-99. Detailed view of -and flooding for the SLR = 2.0-m scenario at STTC South.The blue shaded zones represent week (dark blue), year (medium blue), and century (light blue) return periods.

For the baseline condition (SLR = 0 m), inundation as represented by the weekly return event was limited to the shoreline beach areas of the installation. There was no apparent vulnerability of any receptor category to inundation under current day conditions. For the 1-year return period condition,

flooding was also limited to the beach areas with the exception of the inlet to Aliso Creek and some expanded wetting in the Santa Margarita Lagoon. Under the 100-year return period condition, more extensive flooding was projected in the largely undeveloped areas of Santa Margarita Lagoon, Aliso Creek, and Las Flores. Impact to receptors appeared to be limited to minor flooding around the small boat harbor at Del Mar, and substantial flooding of beach training areas. This limited exposure under current day conditions reflects the steeper topography of the installation, and the lack of significant development along the shoreline. Receptor categories that are potentially vulnerable to flooding (100 year) under current conditions include buildings, training areas, roads, recreation areas, and stormwater systems.

For the 1.0-m sea level rise scenario (2069), inundation as represented by the weekly return event was more extensive particularly in the Santa Margarita Lagoon and Del Mar Beach areas in the southern portion of the installation, and in the San Onofre Beach area to the north. The area of inundation was approximately equivalent to the area of flooding for the 100-year total water level with no sea level rise (Baseline - 100 years). Inundation along the southern beaches extended inland up to about 200 m in some areas, and as much as 150 m in the north. Receptor categories that are potentially vulnerable to inundation under the 1.0-m scenario included buildings, roads, recreation areas, stormwater systems, and particularly the beach training areas. For the 1-year return period condition, flooding was projected to be marginally more extensive in all areas of the installation, with the largest expansion of area in the south near Del Mar Beach and in the Santa Margarita Lagoon. Under the 100-year return period condition, flooding was extensive, extending farther upland along the Santa Margarita River and associated side basins, and including more significant areas of the Del Mar area. Receptor categories that are potentially vulnerable to flooding under present day conditions include buildings, training areas, roads, recreation areas, and stormwater systems.

For the 2.0-m sea level rise scenario (2100), inundation as represented by the weekly return event was more significant especially in the southern areas of the installation. Inundation was also expected upland into all of the coastal lagoons and inlets including Santa Margarita Lagoon, Aliso Creek, Las Flores, and San Mateo. The area of inundation for the 2.0-m sea level rise scenario was similar to the flooded area for the 1.0-m sea level rise scenario for the 100-year return period event. Receptors that are potentially vulnerable to inundation under the 2.0-m scenario included buildings, training areas, roads, recreation areas, and stormwater systems. For the 1-year return period condition, flooding was more marginally more extensive at all areas of the installation compared to inundation, with an increase of about 10% in flooded area. Under the 100-year return period condition, flooding was fairly extensive in the developed areas in the south at Del Mar and in the north at San Onofre. Receptors that are potentially vulnerable to flooding under the 2.0-m scenario include all categories except airfields.

4.3.2 Protected Bay Response

Water Levels

Water levels in the protected areas of San Diego Bay were developed as described in Section 3.3.6 with sea level rise variability limited to tidal variations, and the non-tide residuals. The return period of water level extremes at NBC were computed from the water level time series, and the resulting scenarios are shown in Table 4-1. The impacts related to the exposure along these protected shorelines are presented in Section 4.4.

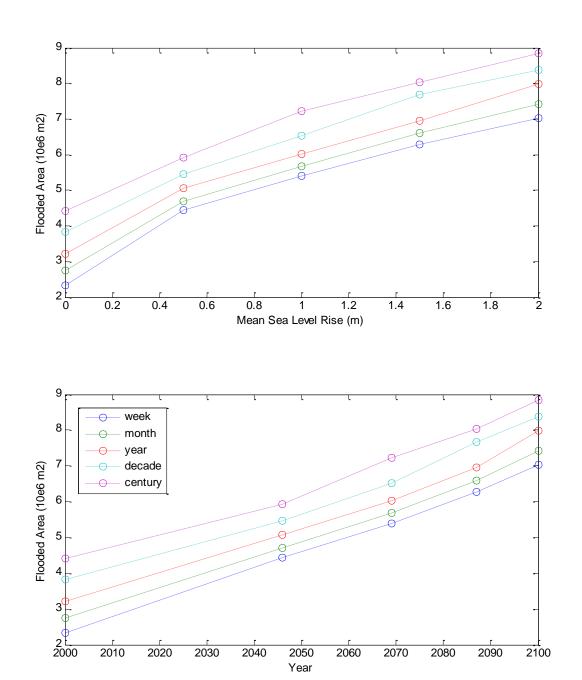


Figure 4-100. Estimated area vulnerable to inundation and flooding (cropped to NAVD88 = 0 m) for the 25 scenarios at MCBCP as a function of mean sea level rise (above) and time (below).

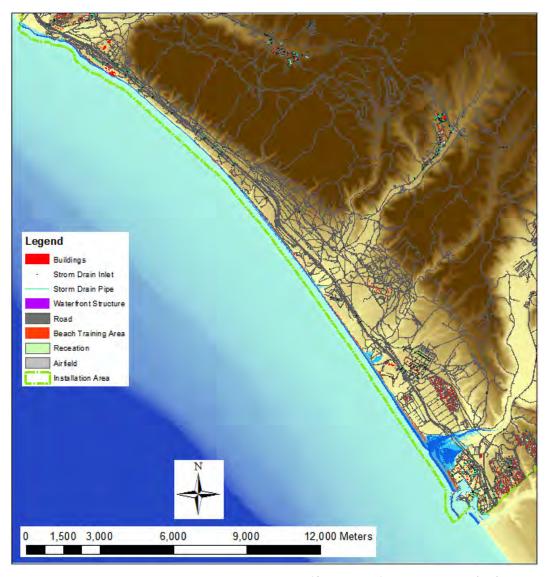


Figure 4-101. Inundation and flooding for the baseline (SLR = 0 m) scenario at MCBCP. The blue shaded zones represent week (dark blue), year (medium blue), and century (light blue) return periods.

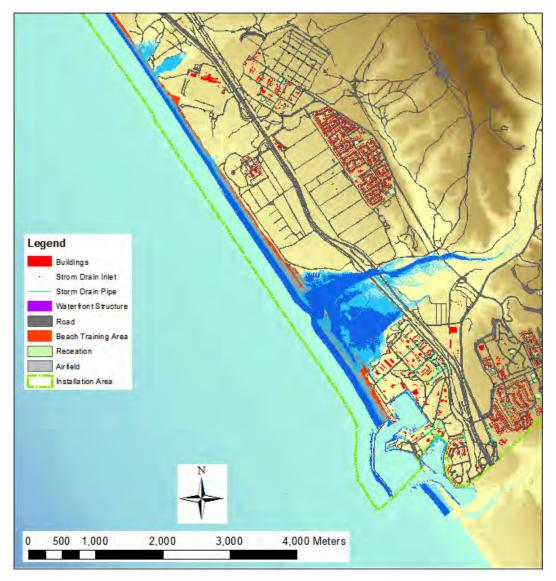


Figure 4-101. Detailed view of inundation and flooding for the baseline (SLR = 0 m) scenario at Del Mar. The blue shaded zones represent week (dark blue), year (medium blue), and century (light blue) return periods.

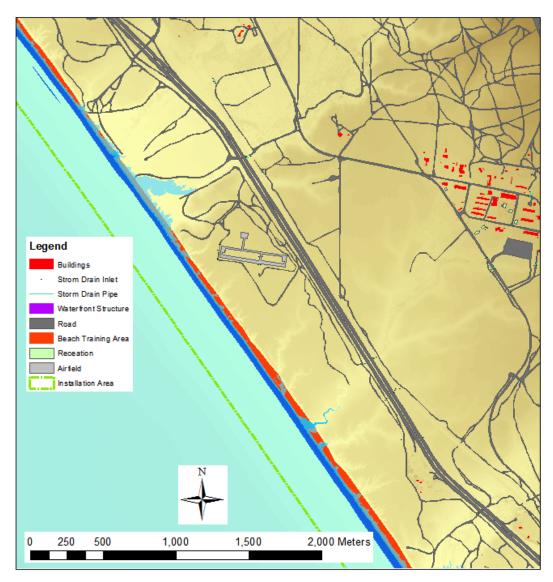


Figure 4-103. Detailed view of inundation and flooding for the baseline (SLR = 0 m) scenario at Red Beach. The blue shaded zones represent week (dark blue), year (medium blue), and century (light blue) return periods.

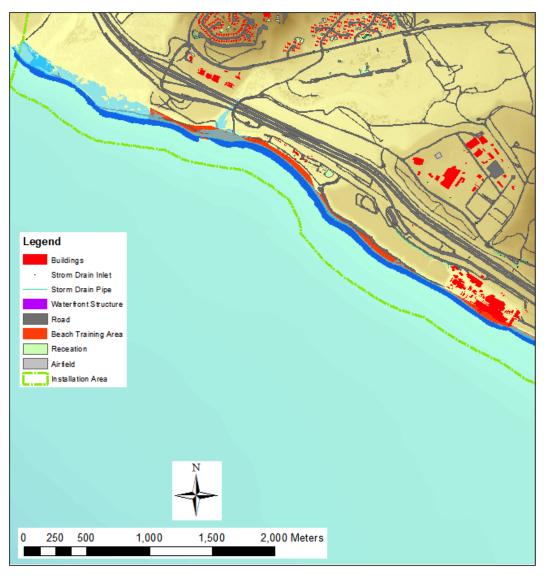


Figure 4-104. Detailed view of inundation and flooding for the baseline (SLR = 0 m) scenario at San Onofre. The blue shaded zones represent week (dark blue), year (medium blue), and century (light blue) return periods.

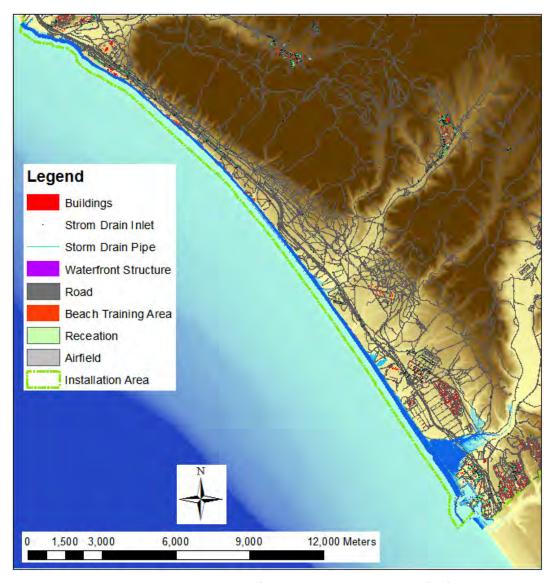


Figure 4-105. Inundation and flooding for the SLR = 1.0-m scenario at MCBCP. The blue shaded zones represent week (dark blue), year (medium blue), and century (light blue) return periods.

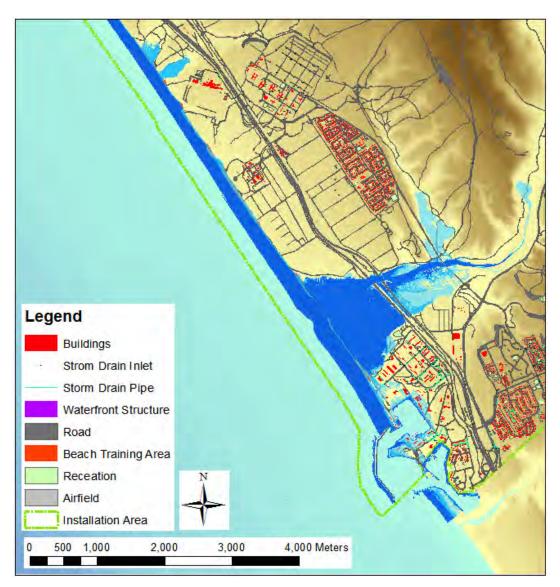


Figure 4-106. Detailed view of inundation and flooding for the SLR = 1.0-m scenario at Del Mar. The blue shaded zones represent week (dark blue), year (medium blue), and century (light blue) return periods.

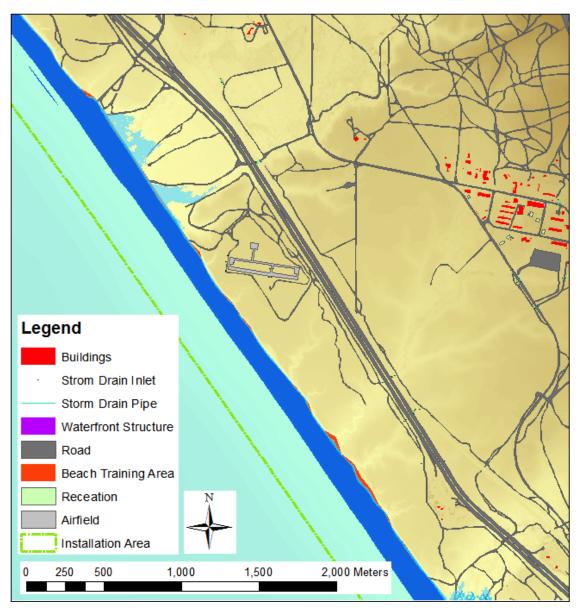


Figure 4-107. Detailed view of inundation and flooding for the SLR = 1.0-m scenario at Red Beach. The blue shaded zones represent week (dark blue), year (medium blue), and century (light blue) return periods.

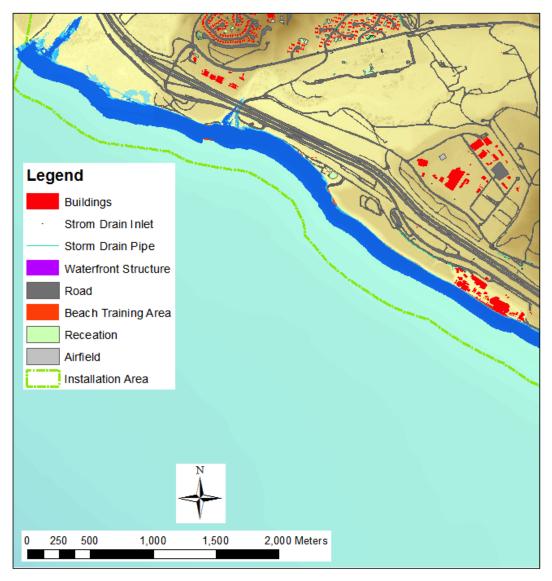


Figure 4-108. Detailed view of inundation and flooding for the SLR = 1.0-m scenario at San Onofre. The blue shaded zones represent week (dark blue), year (medium blue) and century (light blue) return periods.

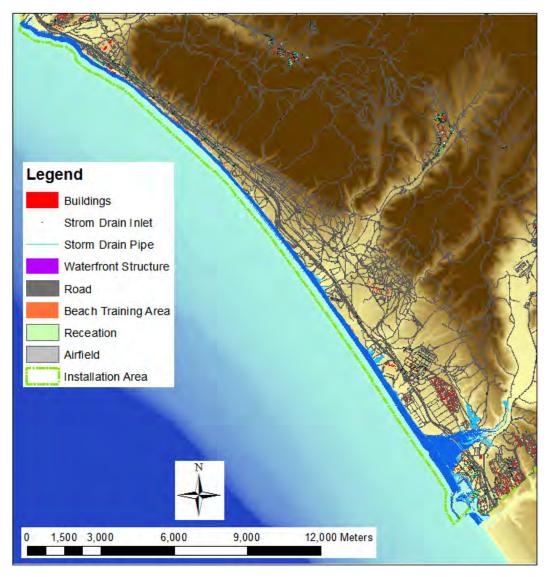


Figure 4-109. Inundation and flooding for the SLR = 2.0-m scenario at MCBCP. The blue shaded zones represent week (dark blue), year (medium blue), and century (light blue) return periods.

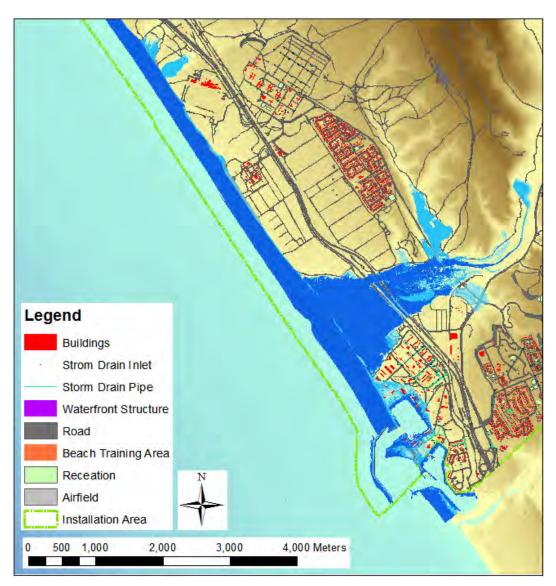


Figure 4-110. Detailed view of inundation and flooding for the SLR = 2.0 m scenario at Del Mar. The blue shaded zones represent week (dark blue), year (medium blue) and century (light blue) return periods.

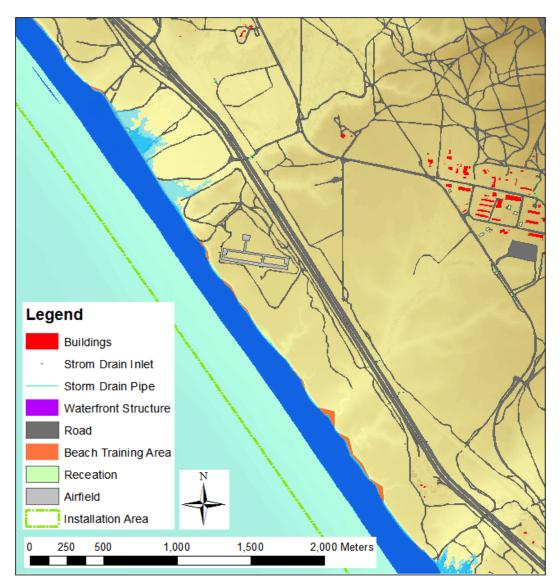


Figure 4-111. Detailed view of inundation and flooding for the SLR = 2.0 m scenario at Red Beach. The blue shaded zones represent week (dark blue), year (medium blue) and century (light blue) return periods.

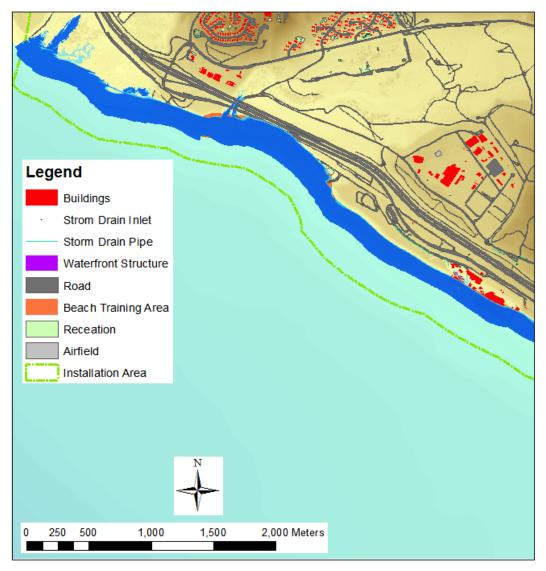


Figure 4-112. Detailed view of inundation and flooding for the SLR = 2.0-m scenario at San Onofre. The blue shaded zones represent week (dark blue), year (medium blue), and century (light blue) return periods.

Inundation and Flooding

Inundation and flooding along the protected shorelines at NBC were assessed following the methodologies described in Section 3.3.6. To illustrate the methodology we utilized the "first occurrence" of the target conditions along the 2.0-m sea level rise curve which corresponded to time snapshots for the years 2046, 2069, 2087, and 2100, respectively. Inundation and flooding were examined across a continuum of total water levels defined through combined variations in sea level rise and return period total water level events. These scenarios spanned five sea level rise conditions from 0to 2 m, and five return periods (week, month, year, decade, century) for a total of 25 scenarios at each MOP station. For the protected shoreline areas of NBC, there is no wave exposure and the variation among return period total water levels is limited (see Table 4-1). In the context of this project, we defined inundation as a process that leads to the frequent (week-month return) exposure of coastal areas to wetting, while flooding was considered to represent infrequent to rare events with long return periods (year-century). Results of the inundation and flooding analysis for the baseline (SLR = 0 m), 1.0-m sea level rise, and 2.0-m sea level rise scenarios are shown in Figure 4-113 through Figure 4-124.

For the baseline condition (SLR = 0 m), inundation as represented by the weekly return event was limited to the normally wetted bay shoreline areas of the installation (Figure 4-113 to Figure 4-116). There was no apparent vulnerability of any receptor category to inundation under current day conditions. The area of inundation on the bay side east of SSTC South is a wetland and saltworks area that is normally wet at high tide. Similarly for the 1 year and 100-year return period conditions, flooding was also limited to the bay shoreline areas and no significant incursion into the installation areas was present

For the 1.0-m sea level rise scenario (2069), inundation as represented by the weekly return event remained limited to the bay shoreline with the exception of some low lying areas at NAB and on the bay sides of SSTC North and SSTC South (Figure 4-117 to Figure 4-120). Receptor categories that are potentially vulnerable to inundation under the 1.0-m scenario included buildings, roads, and stormwater systems. For the 1- and 100-year return period conditions, flooding was marginally more extensive at NAB/SSTC North and SSTC South, but still essentially limited to the shoreline areas of North Island. Receptor categories that are potentially vulnerable to flooding under these bay-exposure flooding conditions include buildings, roads, and stormwater systems.

For the 2.0-m sea level rise scenario (2100), inundation as represented by the weekly return event was more significant in all three areas of the installation (Figure 4-121 to Figure 4-124). Inundation at North Island influenced areas extending inland up 1000 to 2000 m in some areas. Significant areas of NAB/SSTC North and SSTC South were also subject to inundation under this scenario. Receptors that are potentially vulnerable to inundation under the 2.0-m scenario included all categories. For the 1- and 100-year return period conditions, flooding patterns were similar to the inundation pattern but somewhat more extensive particularly at NAB and North Island. Receptors that are potentially vulnerable to flooding under the 2.0-m scenario include all categories.

Changes in Currents and Bottom Shear

The potential influence of changing sea level on the hydrodynamic response of San Diego Bay to tidal forcing was evaluated using the existing TRIM model. The analysis included simulations of complete spring-neap tidal cycles for five scenarios: existing condition, and the four scenarios with the projected sea level rises of 0.5, 1, 1.5, and 2 m. The model was used to simulate water surface elevations, water velocities, and bottom shear stress under these conditions.



Figure 4-113. Inundation and flooding for the baseline (SLR = 0 m) bay-exposure scenario at NBC. The blue shaded zones represent week (dark blue), year (medium blue), and century (light blue) return periods.

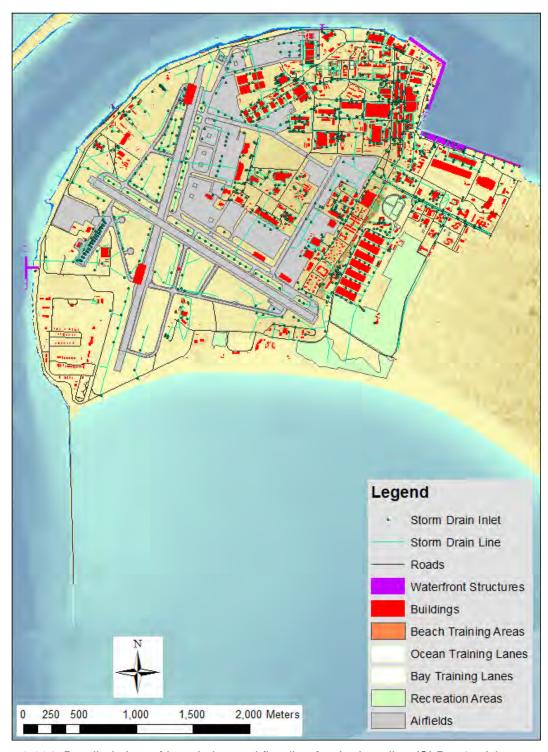


Figure 4-114. Detailed view of inundation and flooding for the baseline (SLR = 0 m) bay-exposure scenario at North Island. The blue shaded zones represent week (dark blue), year (medium blue), and century (light blue) return periods.



Figure 4-115. Detailed view of inundation and flooding for the baseline (SLR = 0 m) bay-exposure scenario at NAB/SSTC North. The blue shaded zones represent week (dark blue), year (medium blue) and century (light blue) return periods.



Figure 4-116. Detailed view of inundation and flooding for the baseline (SLR = 0 m) bay-exposure scenario at SSTC South. The blue shaded zones represent week (dark blue), year (medium blue), and century (light blue) return periods.



Figure 4-117. Inundation and flooding for the 1.0-m SLR bay-exposure scenario at NBC. The blue shaded zones represent week (dark blue), year (medium blue), and century (light blue) return periods.

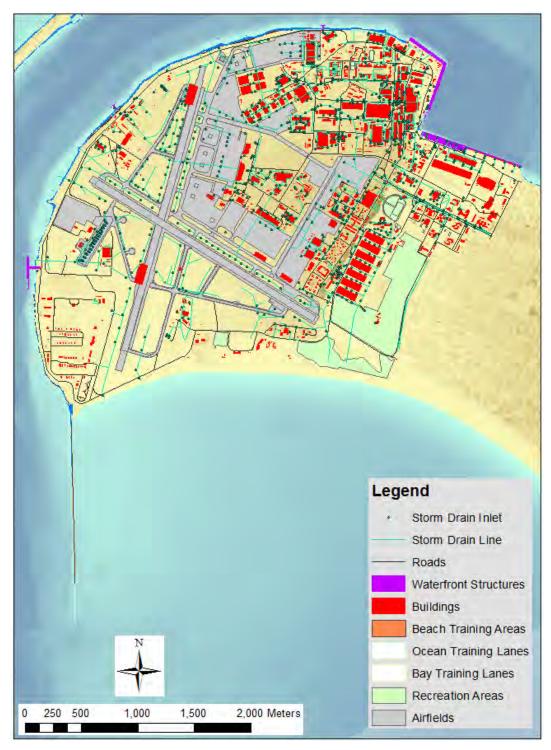


Figure 4-118 Detailed view of inundation and flooding for the 1.0-m SLR bay-exposure scenario at North Island. The blue shaded zones represent week (dark blue), year (medium blue), and century (light blue) return periods.



Figure 4-119. Detailed view of inundation and flooding for the 1.0-m SLR bay-exposure scenario at NAB/SSTC North. The blue shaded zones represent week (dark blue), year (medium blue), and century (light blue) return periods.



Figure 4-120. Detailed view of inundation and flooding for the 1.0-m SLR bay-exposure scenario at SSTC South. The blue shaded zones represent week (dark blue), year (medium blue), and century (light blue) return periods.



Figure 4-121. Inundation and flooding for the 2.0-m SLR bay-exposure scenario at NBC. The blue shaded zones represent week (dark blue), year (medium blue), and century (light blue) return periods.

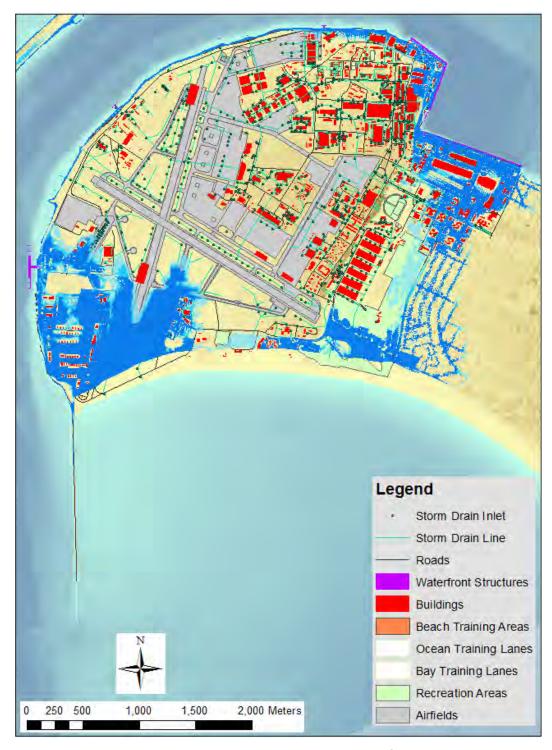


Figure 4-122. Detailed view of inundation and flooding for the 2.0-m SLR bay-exposure scenario at North Island. The blue shaded zones represent week (dark blue), year (medium blue), and century (light blue) return periods.



Figure 4-123. Detailed view of inundation and flooding for the 2.0-m SLR bay-exposure scenario at NAB/SSTC North. The blue shaded zones represent week (dark blue), year (medium blue), and century (light blue) return periods.



Figure 4-124. Detailed view of inundation and flooding for the 2.0-m SLR bay-exposure scenario at SSTC South. The blue shaded zones represent week (dark blue), year (medium blue), and century (light blue) return periods.

Simulated conditions were compared at four selected locations that are important for operations at NBC including Bravo Pier (Station 1), Turning Basin (Station 2), Glorietta Bay (Station 3) and In-Bay Silver Strand (Station 4) (see Figure 4-125). Figure 4-126 through Figure 4-130 show that current amplitudes fluctuate in both semi-diurnal (~ 12 hours) and spring/neap tidal cycles (~ 15 days). Overall, the currents are strongest at Bravo Pier (#1) with magnitude up to ~ 60 cm/sec during the spring tide. Currents at Glorietta Bay (#3) are the weakest with magnitude as low as 1 to 2 cm/sec during the spring tide. Currents can reach about 10 cm/sec during the spring tide at both the turning basin and Silver Strand.

Current amplitudes decreased with the sea level rise for all the stations, except for the turning basin (Station 2), where current amplitudes tended to increase in association with sea level rise during strong ebb flows, but otherwise be similar or lower during other phases of the tide. This general decrease in current speed is consistent with the increasing cross section area of the bay with sea level rise, but without a significant increase in the surface area of the bay that would increase the tidal prism. This is largely a function of the constructed shorelines that minimize the growth of the bay surface area with sea level rise. Localized departures from this general trend, as observed in the turning basin, may be expected due to changes in the local hydrodynamic balances and shifts in phases of the bay response to water elevations.

The decrease in current amplitude with sea level rise suggests that the effects of bottom shear will also be weaker compared to current day conditions. The corresponding bottom shear stresses simulated by the model at these stations are similar to the patterns of current amplitudes (Figure 4-131 through Figure 4-134). With increasing sea level rise, bottom shear stress generally decreased as a result of the reduced current speeds, except at Station 2 where bottom shear stress does not uniformly change with increasing water depth.

Broader mapping of changes in currents and bottom stress was carried out for the entire bay. This allowed a clearer visualization of the patterns of change related to sea level rise. Mapped results for differences between present day currents and bottom shear stress throughout the bay are shown in Figure 4-136 through Figure 4-139 for sea level rise conditions of 1.0 m and 2.0 m. For the 1.0-m SLR condition, currents were generally lower in the main channel areas and back-bay portions of the bay, comparable to present day in side embayments and near the shoreline, and higher in isolated areas to the east and west of the entrance channel. The maximum reduction in RMS current difference over the spring-neap cycle was about 5.1 cm/s (lower than present day) in the main entrance channel south of Bravo Pier, and the maximum increase was about 4 cm/s off the south end of Point Loma. For the 2.0-m SLR condition, currents differences followed a similar pattern as for the 1.0-m SLR case, but with larger differences and more extensive reductions in current speed throughout the bay. The maximum current difference over the spring-neap cycle was about 6.3 cm/s (lower than present day) in the main entrance channel south of Bravo Pier, and the maximum increase was about 5.7 cm/s off the south end of Point Loma.

Currents in the vicinity of key installation areas at NBC generally either decreased or stayed relatively unchanged compared to present day conditions. Along Bravo Pier and the northern shore of North Island, currents generally decreased slightly compared to present day conditions. Currents near the turning basin and the Carrier Piers were relatively unchanged, as was also the case for conditions in Glorietta Bay and in the bay training areas in the south bay.

Patterns of change for bottom shear stress from present day conditions followed similar patterns to the changes in currents with decreased shear stress in the main channel and some back-bay areas, and increased shear stress to the east and west of the main channel entrance. For the 1.0 m SLR condition, changes in shear stress over the spring-neap cycle ranged from a maximum decrease of 0.6

dyne/cm² in the entrance channel, to a maximum increase of about 0.9 dyne/cm² off the south end of Point Loma. For the 2.0-m SLR condition, bottom shear stress differences followed a similar pattern as for the 1.0-m SLR case, but with larger differences and more extensive reductions in shear along the main channel of the bay. The maximum decrease in shear over the spring-neap cycle was about 1.1 cm/s (lower than present day) in the main entrance channel south of Bravo Pier, and the maximum increase was about 1.5 cm/s off the south end of Point Loma.

Estimated changes in currents and bottom shear may have some implications for operations and sustainability at NBC. For example, lower current speeds may influence the processes for docking and undocking of vessels and the loadings on piers and other waterfront infrastructure. Lower currents may also reduce the flushing of areas of the bay, leading to potential increases in the retention time and concentrations of contaminants. Lower bottom shear stress my reduce bottom scour and increase the deposition rate of sediments in some areas. This increased deposition may be offset by the increase in sea level with respect to its impact on navigational depths. For example, typical current day sediment deposition rates in San Diego Bay range from about 0.5 to 2.0 cm/yr. Assuming reductions in shear moved this rate toward the higher end, then the deposition of sediment between 2000 and 2069 would be about 138 cm, compared to the first occurrence sea level rise of 100 cm estimated for 2069. This represents a net decrease in navigation depth of 38 cm. Without sea level rise and assuming a current day sedimentation rate of about 1.0 cm/yr, the net decrease in navigation depth by 2069 would be about 69 cm. Thus, even assuming a doubling of the deposition rate associated with sea level rise induced shear reduction, navigation depths would still be enhanced by sea level rise by 2069. While these are vastly simplified assumptions they provide a sense of some of the implications of sea level rise for changes in the hydrodynamics of San Diego Bay.

4.3.3 Groundwater Response

Sea-Level Rise Scenarios

Groundwater response of the SMR basin at MCBCP for the time period of water years 2000 to 2100 five SLR scenarios were evaluated using three different inland boundary conditions. The five SLR scenarios assume no SLR (base case) and four potential SLRs as shown in Figure 3-96. The ocean boundary was held constant at 0.78 m (the average elevation of the coastline) from water years 1950 to 2000, then the SLR scenarios were imposed from 2000 to 2100. The inland boundary followed the water years 1950 to 2000 historical water levels, and from water years 2000 to 2100, it was set to a constant value equal to the average historical water level, lower 5%, and upper 95%, for well 7J1, which are 27.3, 26.26, and 28.06 m, respectively. Only hydrographs and breakthrough curves using the average boundary condition are presented in this section. Appendix A8 contains all images using the lower 5% and upper 95% boundary conditions.

Base Case: No Sea Level Rise

Figure 4-140 through Figure 4-147 are the results from water years 2000 to 2100 with no sea level rise for the average inland boundary condition. They were used as the base case to assess the impact of SLR on the SMR basin. With no SLR, a constant inland boundary condition, and the same annual pumping schedule the simulated model begins to approach a new quasi-steady state condition. This quasi-steady state was reached quickly, about water year 2050, for the hydrographs, but was not reached for the breakthrough curves. The water levels were more responsive because of their dependence on the inland boundary condition, which was not impeded by the lower permeability upper alluvium. The water levels in the hydrographs fluctuated seasonally as a result of the changes in the repeated annual pumping schedule with the lowest levels during the summer months when

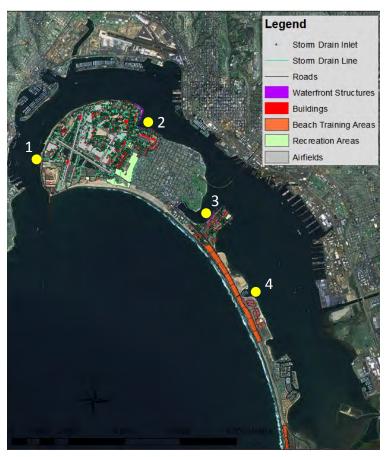


Figure 4-125. Station locations for the model simulations shown in Figure 4-12Î to Figure 4-13Í.

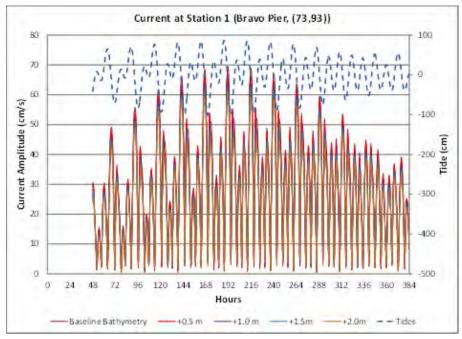


Figure 4-126. Simulated current amplitudes at Bravo Pier (#1) Afor the five sea level rise scenarios: baseline, 0.5, 1, 1.5, and 2 m for a spring-neap tide cycle.

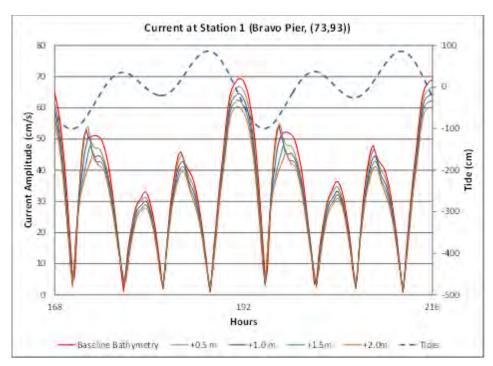


Figure 4-127. Simulated current amplitudes at Bravo Pier (#1) for the five sea level rise scenarios: baseline, 0.5, 1, 1.5, and 2 m for a 48-hour period.

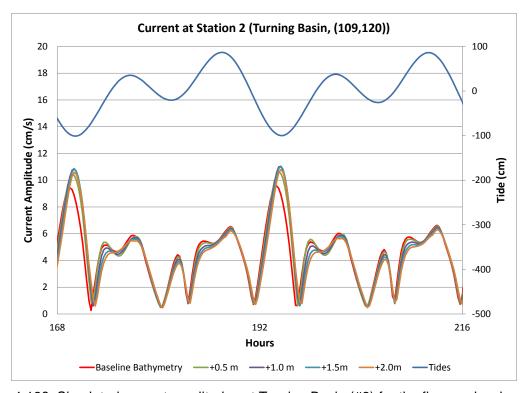


Figure 4-128. Simulated current amplitudes at Turning Basin (#2) for the five sea level rise scenarios: baseline, 0.5, 1, 1.5, and 2 m for a 48-hour period.

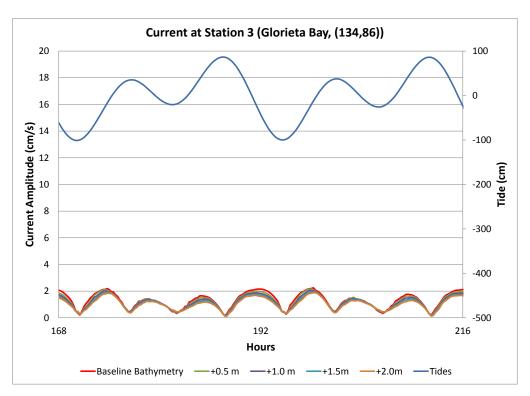


Figure 4-129. Simulated current amplitudes at Glorietta Bay (#3) for the five sea level rise scenarios: baseline, 0.5, 1m, 1.5, and 2 m for a 48-hour period.

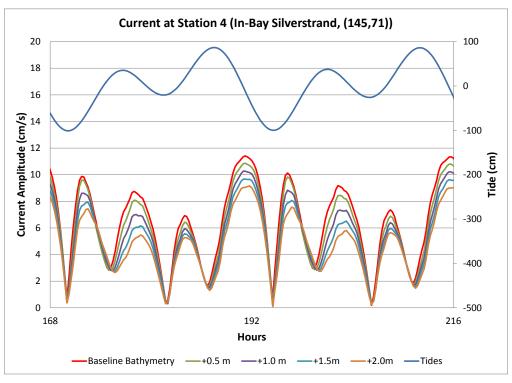


Figure 4-130. Simulated current amplitudes at Silver Strand (#4) for the five sea level rise scenarios: baseline, 0.5, 1, 1.5, and 2 m for a 48-hour period.

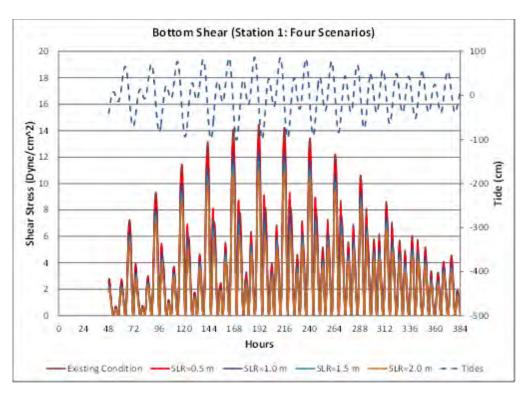


Figure 4-131. Simulated bottom shear stress at Bravo Pier (#1)for the five sea level rise scenarios: baseline, 0.5, 1, 1.5, and 2 m for a spring-neap tide cycle.

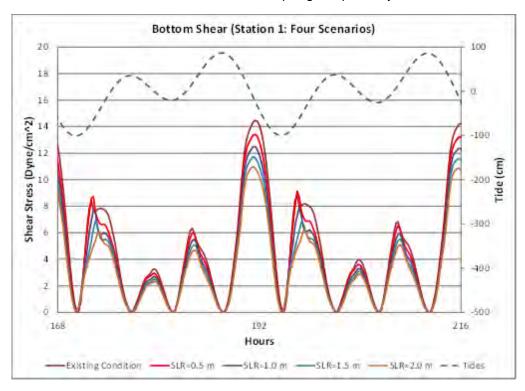


Figure 4-132. Simulated bottom shear stress at Bravo Pier (#1) for the five sea level rise scenarios: baseline, 0.5, 1, 1.5, and 2 m for a 48-hour period.

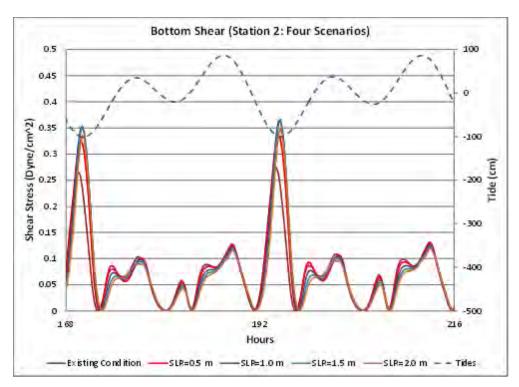


Figure 4-133. Simulated bottom shear stress at Turning Basin (#2) for the five sea level rise scenarios: baseline, 0.5, 1, 1.5, and 2 m for a 48-hour period.

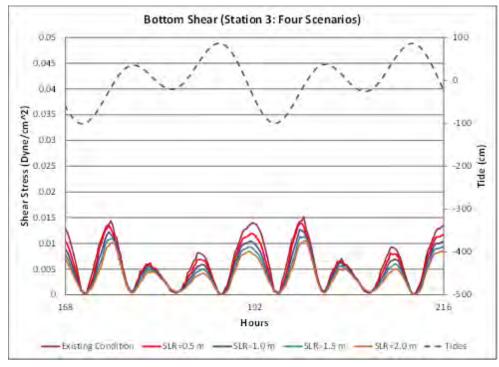


Figure 4-134. Simulated bottom shear stress at Glorietta Bay (#3) for the five sea level rise scenarios: baseline, 0.5, 1, 1.5, and 2 m for a 48-hour period.

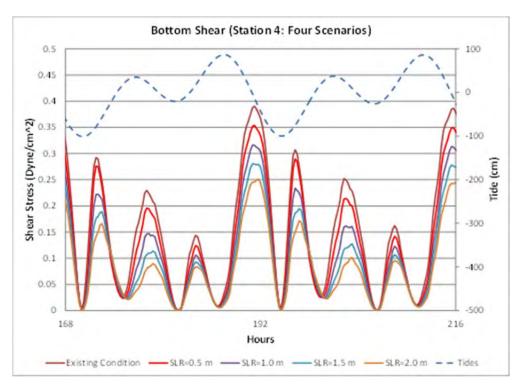


Figure 4-134. Simulated current amplitudes at Silver Strand (#4) for the five sea level rise scenarios: baseline, 0.5, 1, 1.5, and 2 m for a 48-hour period.

pumping was highest. The breakthrough curves had a slow response because the inflow from the ocean boundary condition was retarded by upper alluvium. Another factor that slowed the concentration was the positive slope of the basement of the alluvium layer (Figure 3-67), which caused the seawater to travel upgradient into the SMR basin. The zone of diffusion decreased from water years 2000 to 2100 and became more of a sharp interface as shown by the increase in chloride concentrations at wells 9J1 and 10B1 near the coast (Figure 4-144 and Figure 4-145) and a decrease in chloride concentrations at well 35K5 (Figure 4-147) from water years 2050 to 2100. Note that simulated chloride concentrations stayed above the SMCL at wells 9J1, 10B1, and 2N4 (Figure 4-144 and Figure 4-146). The observed narrow interface between the freshwater and seawater was also observed as shown in Figure 4-148.

Sea Level Rise Scenarios

The lower 5% and upper 95% inland boundary condition base cases had the same general trend as the average (Appendix A8). The lower 5% boundary condition resulted in lower water levels and consequently more seawater intrusion than base-case conditions. The upper 95% resulted in higher water levels and consequently less seawater intrusion than base-case conditions.

The four SLR scenarios are shown in Figure 3-96 and the resulting simulated hydrographs for selected wells are show in Figure 4-150 through Figure 4-153. The SLR increased the water levels at wells 9J1 and 10B1 (Figure 4-150 and Figure 4-151), which were closest to the coast and had less effect the farther inland the well was located, e.g., well 35K5 (Figure 4-153). Well 9J1 was influenced the greatest by the SLR because it was located closest to the ocean. From water year 2000 to 2100 the SLR created a damping effect that reduced the variability in water levels due to upstream pumping. This was most apparent in the Scenario 4 hydrograph (Figure 4-150), where the seasonal head fluctuations reduced during the SLR time period. The upper 95% and lower 5% inland boundary condition did not affect the hydrographs of the closest observation wells, 9J1, 10B1, 2N4,

and 35K5 (Appendix A8). This was due to their proximity to the increasing ocean boundary, which controlled their water levels compared to the distant inland boundary.

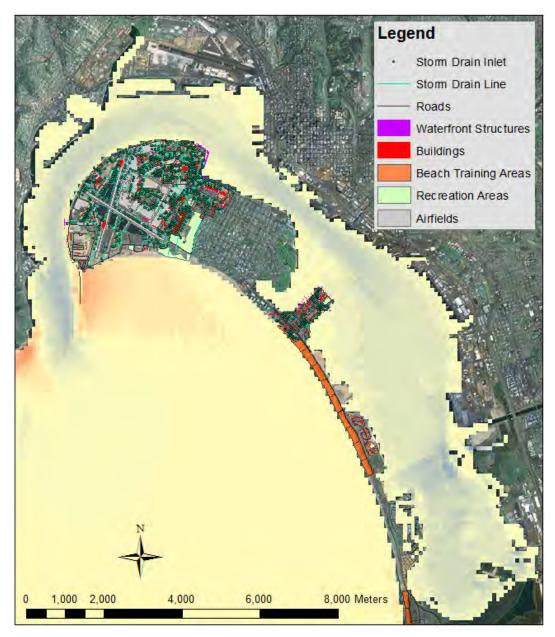


Figure 4-136. RMS velocity differences over a complete spring-neap tidal cycle with 1.0 m SLR at NBC.Blue indicates velocities lower than current day conditions (-) red indicates velocities higher than current day conditions (+), and yellow indicates little change. The range of the differences are from about -5.1 to 4 cm/s.

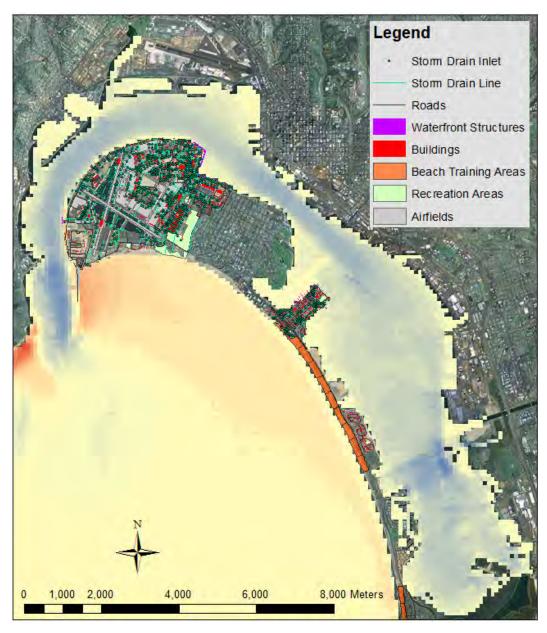


Figure 4-137. RMS velocity differences over a complete spring-neap tidal cycle with 2.0 m SLR at NBC.Blue indicates velocities lower than current day conditions (-) red indicates velocities higher than current day conditions (+), and yellow indicates little change. The range of the differences are from about -7.3 to 7.3 cm/s.

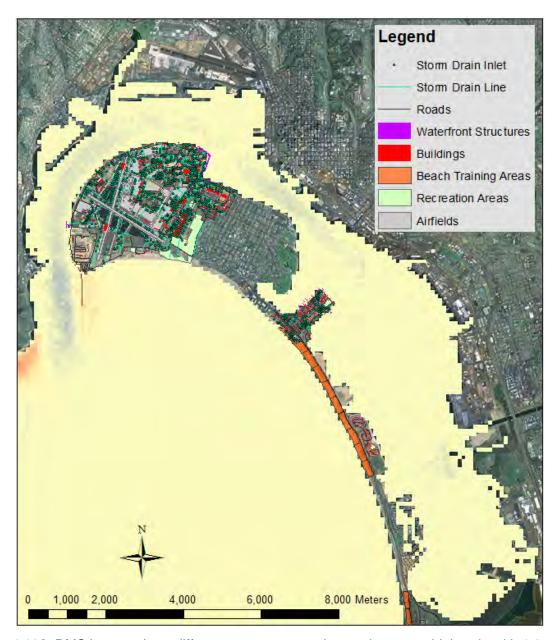


Figure 4-138. RMS bottom shear differences over a complete spring-neap tidal cycle with 1.0 m SLR at NBC.Blue indicates bottom shear lower than current day conditions (-) red indicates bottom shear higher than current day conditions (+), and yellow indicates little change. The range of the differences are from about -0.6 to 0.9 Dyne/cm².

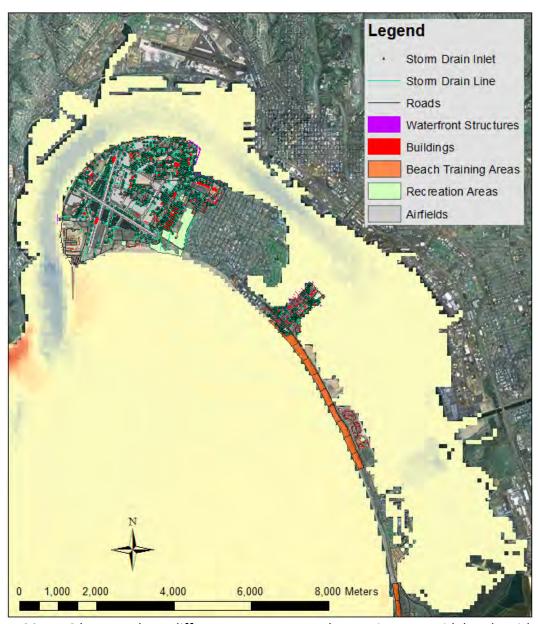


Figure 4-139. RMS bottom shear differences over a complete spring-neap tidal cycle with 2.0-m SLR at NBC.Blue indicates bottom shear lower than current day conditions (-) red indicates bottom shear higher than current day conditions (+), and yellow indicates little change. The range of the differences are from about -1.1 to 1.5 Dyne/cm².

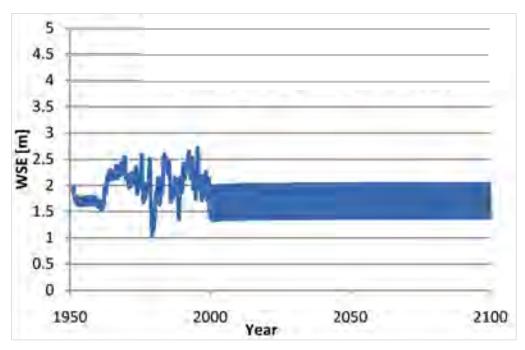


Figure 4-140. 11S005W09J001S (9J1) simulated hydrograph from 1950 to 2100 with no sea level rise. The sharp changes in the water levels occur from monthly changes in pumping. The same annual pump schedule is used from 2001 to 2100, causing the water levels to oscillate.

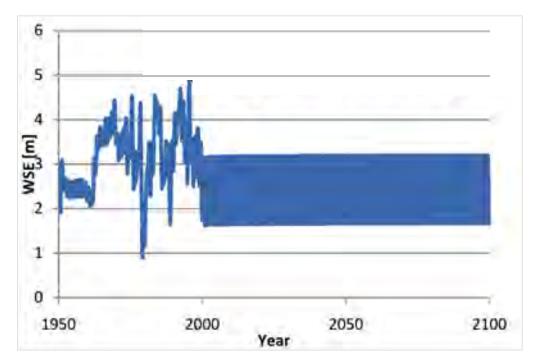


Figure 4-141. 10S005W35K005S (35K5) simulated hydrograph from 1950 to 2100 with no sea level rise.

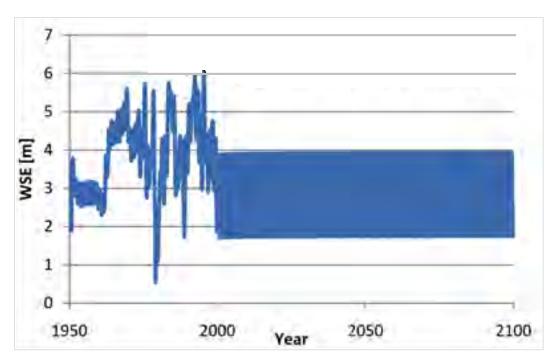


Figure 4-142. 11S005W02N004S (2N4) simulated hydrograph from 1950 to 2100 with no sea level rise.

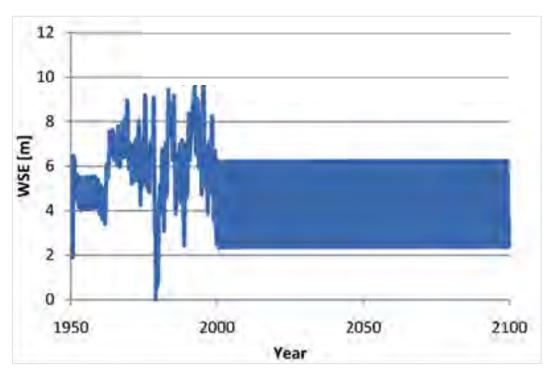


Figure 4-143. 11S005W10B001S (10B1) simulated hydrograph from 1950 to 2100 with no sea level rise.

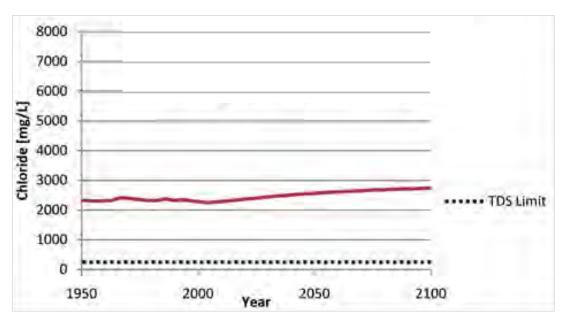


Figure 4-144. 11S005W09J001S (9J1) simulated breakthrough curve from 1950 to 2100 with no sea level rise.

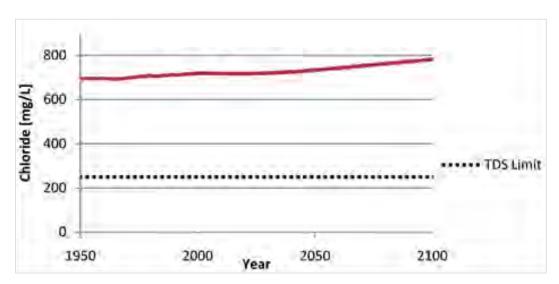


Figure 4-145. 11S005W10B001S (10B1) simulated breakthrough curve from 1950 to 2100 with no sea level rise.

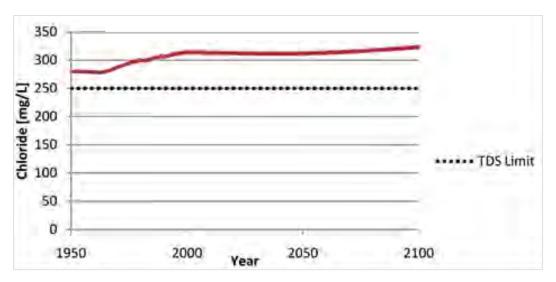


Figure 4-146. 11S005W02N004S (2N4) simulated breakthrough curve from 1950 to 2100 with no sea level rise.

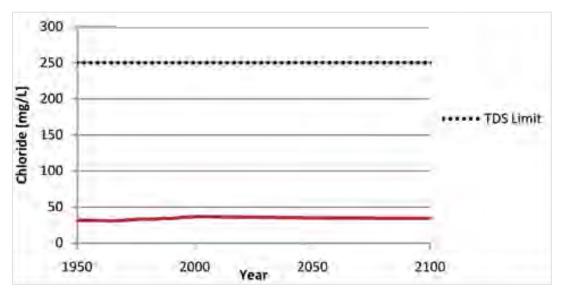


Figure 4-147. 10S005W35K005S (35K5) simulated breakthrough curve from 1950 to 2100 with no sea level rise.

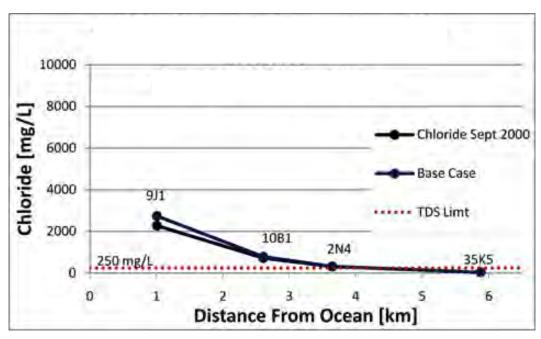


Figure 4-148. Final chloride of the base case at December 31, 2099, for selected wells arranged by distance from the coastline compared with the chloride at September 31, 2000.

The breakthrough curves for the two observation wells closest to the coast (9J1 and 10B1) showed an eventual point when chloride concentrations begin to increase rapidly (Figure 4-154 and Figure 4-155). For well 9J1 this occurred for Scenario 4 WY 2075, Scenario 3 in WY 2080, Scenario 2 in WY 2092, and was not apparent in Scenario 1. Chloride concentration at well 35K5 did not change as a result of SLR for any of the scenarios (Figure 4-157). The upper 95% and lower 5% inland boundary condition did effect the breakthrough curves where the 95% had a lower concentration and the 5% a higher concentration compared to the average boundary condition (Appendix A8). This result occurred because with lower inland water levels there was less freshwater available within the SMR basin.

The four scenarios influenced the location of high chloride concentrations making the SMR basin develop a sharper interface between the fresh and seawater. Figure 4-158 shows the spatial change between scenario 1 and 4 compared to the concentration prior to SLR. The closest observation well, 9J1, was influenced the greatest, while 35K5 had little change as result of SLR. Figure 4-159 shows the location of the 250 mg/L chloride-concentration contour for each SLR scenario. At the scale shown, the locations of the four contours were indistinguishable. Figure 4-160 compares Scenario 4 with the base case with no SLR at December 31, 2099, which was the end of the simulation time frame. The SLR from Scenario 4 influenced the location for concentrations around 10,000 mg/L, but did not change low concentrations around 250 mg/L.

Scenario 4 Inland Boundary Condition Analysis

Scenario 4 resulted in the greatest amount of seawater intrusion; therefore, it was used to test the sensitivity of changes in the inland boundary condition. Three additional simulations were performed by holding constant the inland boundary condition from water year 2000 to 2100 at 25 m, 22.5 m, and 20 m and compared to the results of the average boundary condition, 27.3 m. Figure 4-161 shows the simulated 250 mg/L chloride-concentration contour lines from each of the four different boundary conditions and the water table elevation. The results showed that the lower the inland boundary condition was, the more significant the seawater intrusion became. Lowering the boundary

condition by 7.3 m caused a shift in the 250 mg/L chloride-concentration contour inland by about 1.7 km causing the wells 2F1, 2D3, and 2A1 to no longer be lower than the U.S. EPA SMCL. Changes in the boundary condition did not affect the water table significantly other than shifting it up or down. Figure 4-161 is a 1:1 scale of Figure 4-161 with the water table removed.

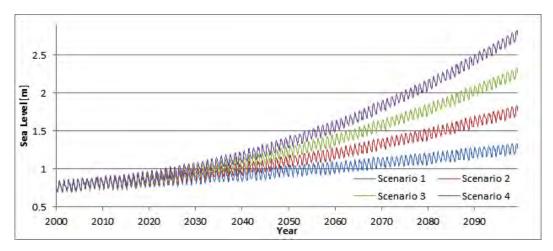


Figure 4-149. Four scenarios for mean sea level rise including tidal variability.

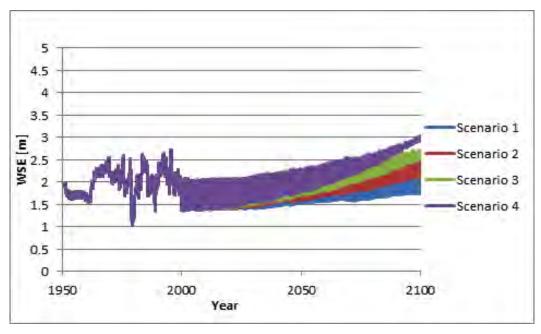


Figure 4-150. 11S005W09J001S (9J1) simulated Hydrograph during the sea level rise time frame 2000 to 2100 for the four scenarios.

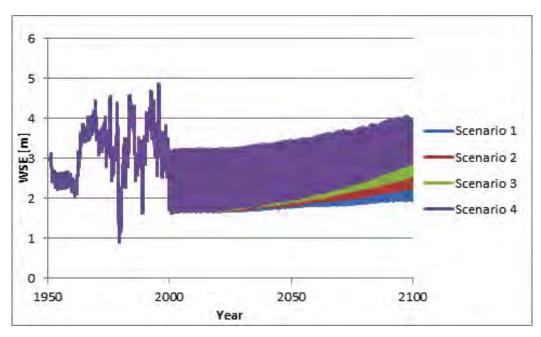


Figure 4-151. 11S005W10B001S (10B1) simulated hydrograph during the sea level rise time frame 2000 to 2100 for the four scenarios.

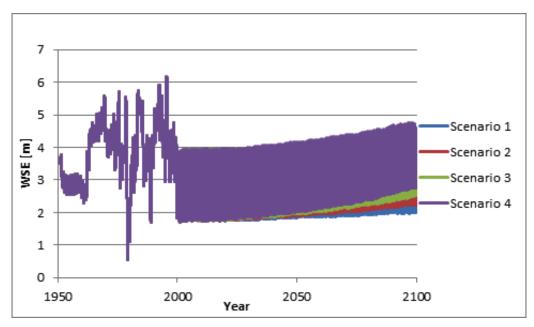


Figure 4-152. 11S005W02N004S (2N4) simulated hydrograph during the sea level rise time frame 2000 to 2100 for the four scenarios.

Pumpage Analysis

The volume of water extracted from a groundwater system can directly influence the level of seawater intrusion. As greater volumes of freshwater are extracted the more seawater intrudes upstream towards the wells. To evaluate the impact of pumping a comparison was made between different scaled increases of pumping with no SLR, Base Case Scenario, from water year 2000 to

2100 with the results of Scenario 4. The rates were scaled by 110%, 130%, and 150% of the WY 2000 pumping rates (i.e. a 10%, 30%, and 50% increase).

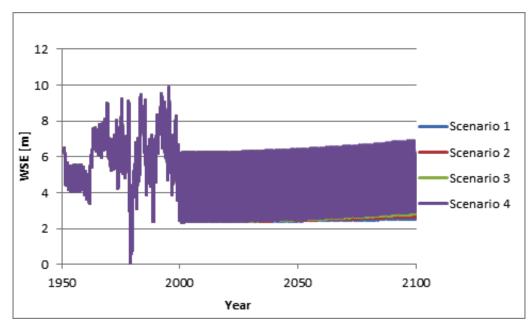


Figure 4-153. 10S005W35K005S (35K5) simulated hydrograph during the sea level rise time frame 2000 to 2100 for the four scenarios.

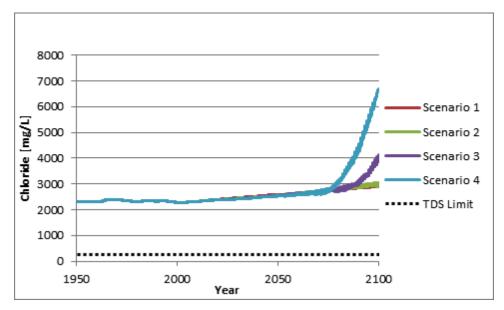


Figure 4-154. 11S005W09J001S (9J1) simulated breakthrough curves during the sea level rise time frame 2000 to 2100 for the four scenarios.

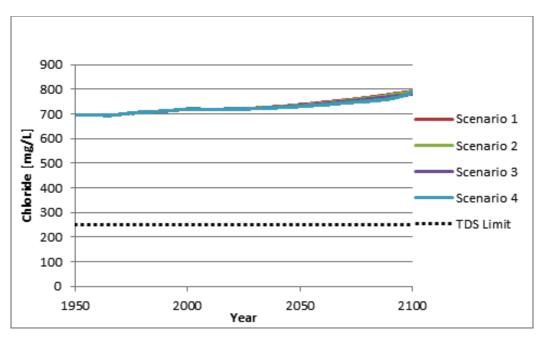


Figure 4-155. 11S005W10B001S (10B1) simulated breakthrough curves during the sea level rise time frame 2000 to 2100 for the four scenarios.

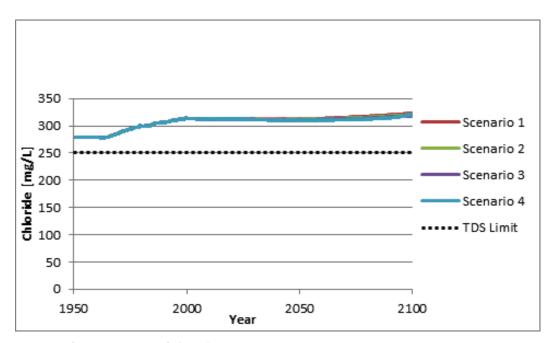


Figure 4-156. 11S005W02N004S (2N4) simulated breakthrough curves during the sea level rise time frame 2000 to 2100 for the four scenarios.

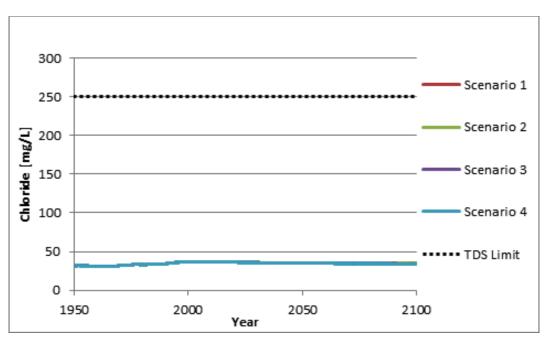


Figure 4-157. 10S005W35K005S (35K5) simulated Breakthrough curves during the sea level rise time frame 2000 to 2100 for the four scenarios.

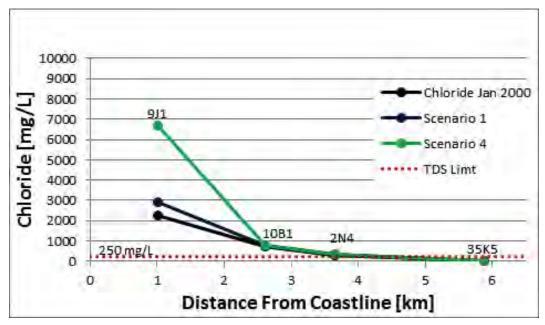


Figure 4-158. Final chloride for Scenario 1 and 4 for selected wells arranged by distance from the coastline compared with the observed values before sea level rise.

Figure 4-163 through Figure 4-166 present the simulated hydrographs for selected wells that result from different increases pumping. The notation for these figures is such that P110% refers to an increase of 10% in the pumping rate applied from water year 2000 to 2100. For all the hydrographs, the water level was the same from water year 1950 to 2000 because they follow the exact historical record. The water level from water year 1950 to 1980 is not presented in the figures to focus on the actual differences in the water levels, which occurred from water year 2000 to 2100. At water year 2000, when the increased pumping occurred, there was a decrease in the water level in response to the larger pumping rates. During the increased pumping from water year 2000 to 2100 there was a repeated sharp, cyclic change in the water levels that was the result of the monthly changes in pumping (see Figure 3-74 for non-scaled total pumping volumes). Other than the annual cyclic change in the water from water year 2000 to 2100 there was no overall shift in the water levels for each of the scaled pumping conditions. This was in contrast to Scenario 4, which had an increasing water level from the SLR at the closest observation wells.

The lower water levels from the increase in pumping caused higher chloride concentrations in the breakthrough curves. Figure 4-167 through Figure 4-170 show the break through curves for the closest four observation wells from 1980 to 2100. There was an immediate increase in the chloride levels in response to the increase in pumping. With the exception of the closest observation well, 9J1, a 10% increase in pumping produced a similar breakthrough curve to Scenario 4. Observation well 9J1 was the most sensitive to SLR because it is the closest (~ 1 km) to the coastline.

Figure 4-171 presents the location of the 250 mg/L chloride concentration contours for different pumping rates at the end of the simulation time. A 10% increase in pumping did not bring the contour significantly farther inland compared to Scenario 4. Increasing pumping by 25% caused well 2F1 to start extracting groundwater with chloride concentrations above the U.S. EPA SMCL. A 30% increase caused well 2D3 to exceed the SMCL and a 50% caused chloride concentrations in wells 2A1 and 35K1 to increase above the SMCL as well. With regards to the minimum drinking water standard (250 mg/L) a 10% increase in pumping would be roughly equivalent to the impact of the sea level rise of Scenario 4.

Scenario 4 Pumpage Analysis

To evaluate a worst-case situation that can occur the SLR of Scenario 4 (Figure 3-96) was combined with the lower 5% inland boundary condition, 26.26 m, and scaled increases of pumping from water year 2000 to 2100. The pumping rates during this time frame were scaled by 110%, 125%, and 150% of the reported rates from water year 2000. Figure 4-172 through Figure 4-175 present the simulated hydrographs that result from increasing pumping for selected wells located near the coast. The notation for these figures is such that P110% refers to an increase of 10% in the pumping rate applied from water year 2000 to 2100.

The simulated hydrograph for well 9J1 (Figure 4-172) indicated a large water level decline because of the increased pumping, but begins to recover as the sea level rises. The increasing sea level became a larger source of water into the system. The further away from the ocean, the less impact the SLR had on the hydrographs. For example, simulated water levels for well 35K5 (Figure 4-175) declined due to the increase in pumping, but had a smaller recovery from SLR compared to well 9J1 (Figure 4-172).

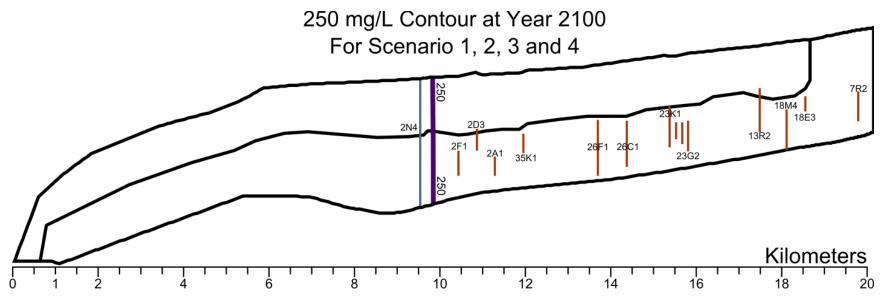


Figure 4-159. Location of the 250 mg/L Chloride contour at year 2100 For the four sea level rise scenarios with the average inland boundary condition. The contour lines are indistinguishable because the distance between the four lines is approximately 35 meters.

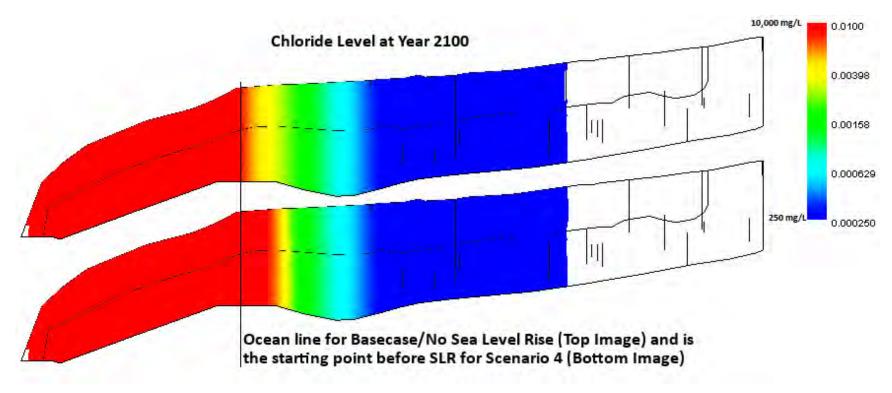


Figure 4-160. Comparison between Scenario 4 and the base case without sea level rise from 2000 to 2100.

The white area on the right of the image is freshwater with 0 mg/L chloride, the blue region has chloride levels between 0 and 250 mg/L, the red region contains concentrations greater than 10,000 mg/L and small white area on the bottom left of the figure contains chloride concentrations greater than 19,000 mg/L. The black vertical line is where the ocean line is located at the start of the sea level rise at year 2000.

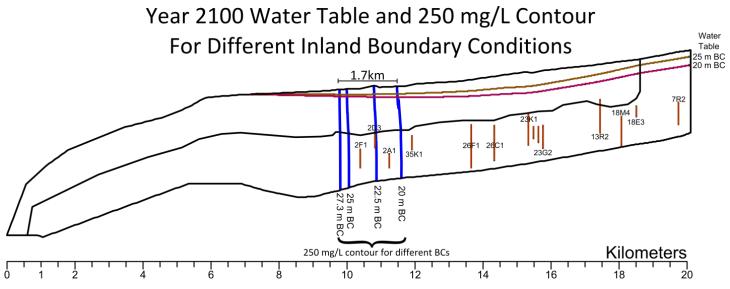
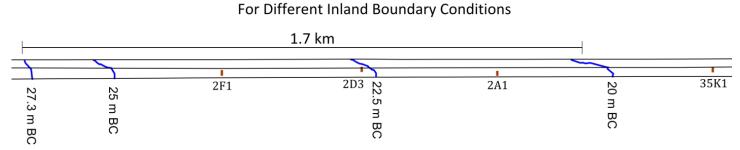


Figure 4-161. Location of the 250 mg/L Chloride contour line and water table at year 2100 for different 2000 to 2100 constant boundary conditions (BC) for Scenario 4. Note that this image has been scaled 1:50 in the vertical direction and that the 27.3 m BC is the average water level of 7J1.



Year 2100 Water Table and 250 mg/L Contour

Figure 4-162. This image is identical to Figure 4-161, except the water table has been removed and it is now a 1:1 scale to illustrate the density lens that is formed from the seawater intrusion.

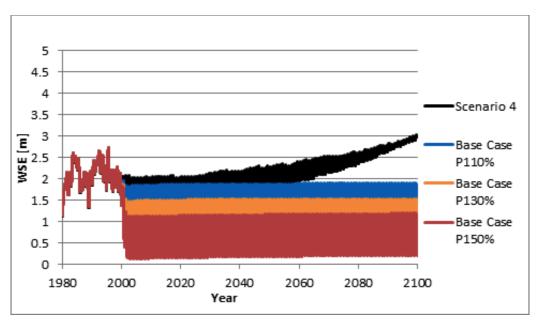


Figure 4-163. 11S005W09J001S (9J1) simulated hydrograph for different future pumping rates with no sea level rise compared with Scenario 4.P110% means that the pumping rate from WY 2000 is increased by 10% and then used from 2000 to 2100.

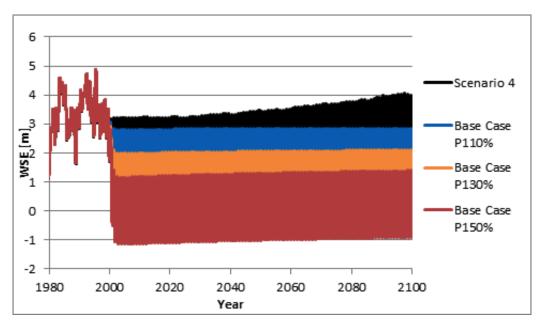


Figure 4-164. 11S005W10B001S (10B1) simulated hydrograph for different future pumping rates with no sea level rise compared with Scenario 4.P110% means that the pumping rate from WY 2000 is increased by 10% and then used from 2000 to 2100.

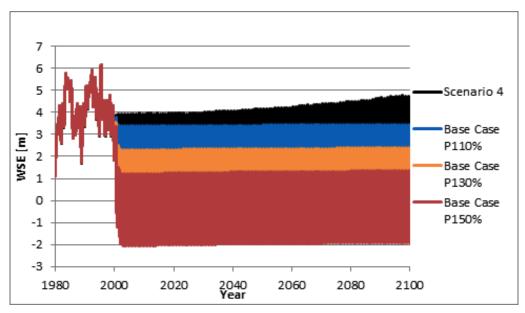


Figure 4-165. 11S005W02N004S (2N4) simulated hydrograph for different future pumping rates with no sea level rise compared with Scenario 4. P110% means that the pumping rate from WY 2000 is increased by 10% and then used from 2000 to 2100.

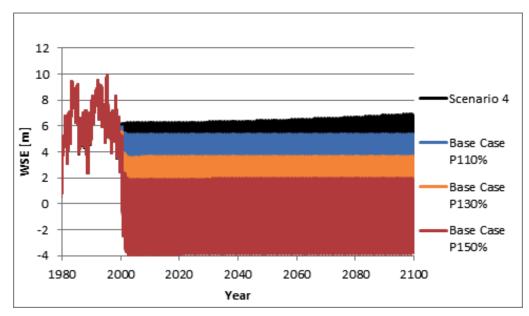


Figure 4-166. 10S005W35K005S (35K5) simulated hydrograph for different future pumping rates with no sea level rise compared with Scenario 4.P110% means that the pumping rate from WY 2000 is increased by 10% and then used from 2000 to 2100.

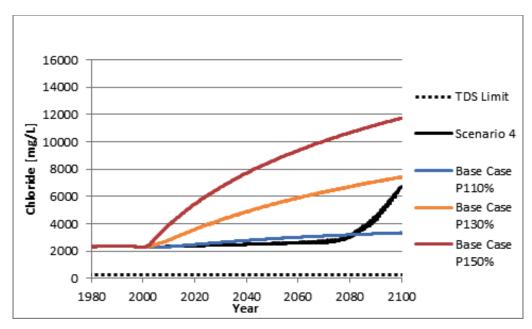


Figure 4-167. 11S005W09J001S (9J1) simulated breakthrough curve for different future pumping rates with no sea level rise compared with Scenario 4. P110% means that the pumping rate from WY 2000 is increased by 10% and then used from 2000 to 2100.

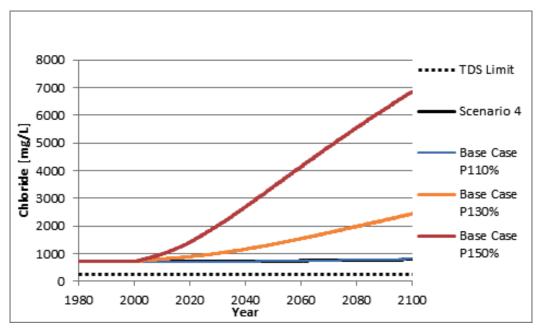


Figure 4-168. 11S005W10B001S (10B1) simulated breakthrough curve for different future pumping rates with no sea level rise compared with Scenario 4. P110% means that the pumping rate from WY 2000 is increased by 10% and then used from 2000 to 2100.

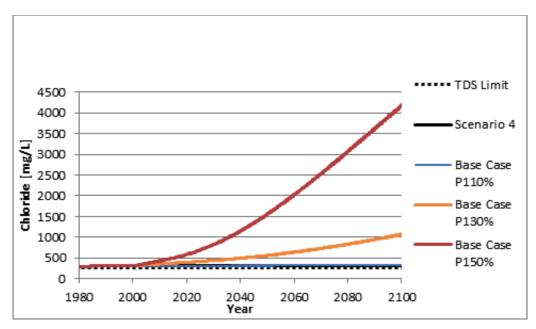


Figure 4-169. 11S005W02N004S (2N4) simulated breakthrough curve for different future pumping rates with no sea level rise compared with Scenario 4.P110% means that the pumping rate from WY 2000 is increased by 10% and then used from 2000 to 2100.

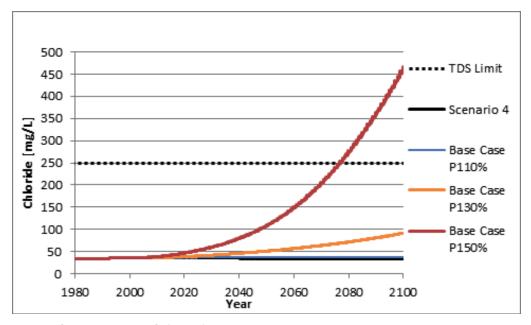


Figure 4-170. 10S005W35K005S (35K5) simulated breakthrough curve for different future pumping rates with no sea level rise compared with Scenario 4.P110% means that the pumping rate from WY 2000 is increased by 10% and then used from 2000 to 2100.

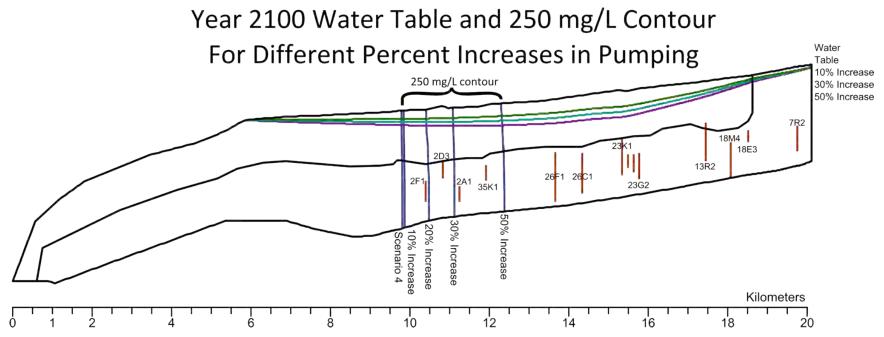


Figure 4-171. Location of the 250-mg/L chloride contour line and water table at year 2100 for different pumping rates from 2000 to 2100 with no sea level rise to Scenario 4.A 10% increase in pumping is equivalent to the sea level rise of Scenario 4.

The simulated chloride concentrations increased rapidly with the combination of increased pumping and SLR. The closer the well was located to the ocean the more dramatic the effect. Figure 4-176 through Figure 4-179 show how the breakthrough curves for Scenario 4 changed with different pumping rates. Increasing pumping had an exponential effect on the chloride concentration at the observation wells. For example at well 7J1 (Figure 4-176) a 10% increase in pumping resulted in a small change in the breakthrough curve compared to Scenario 4 while a 50% increase dramatically changed the chloride concentrations. Increased pumping also resulted in widening the zone of diffusion. For example, Figure 4-180 shows how the chloride concentration changed with distance from the coastline. A 50% increase in pumping produced a near linear reduction in chloride relative to the distance from the ocean compared to Scenario 4, which had an exponential reduction.

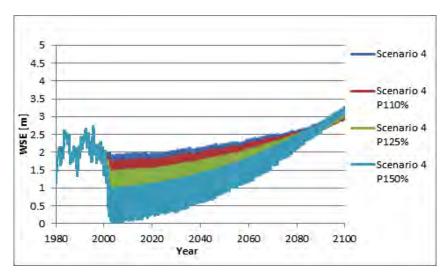


Figure 4-172. 11S005W09J001S (9J1) simulated hydrograph of Scenario 4 with scaled pumping. AP110% means that the pumping rate from WY 2000 is increased by 10% and then used from 2000 to 2100.

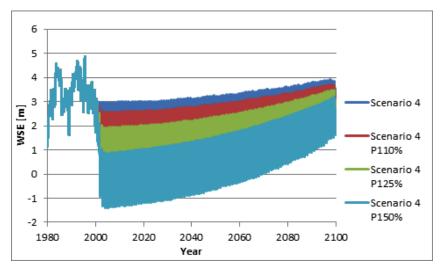


Figure 4-173. 11S005W10B001S (10B1) simulated hydrograph of Scenario 4 with scaled pumping.P110% means that the pumping rate from WY 2000 is increased by 10% and then used from 2000 to 2100.

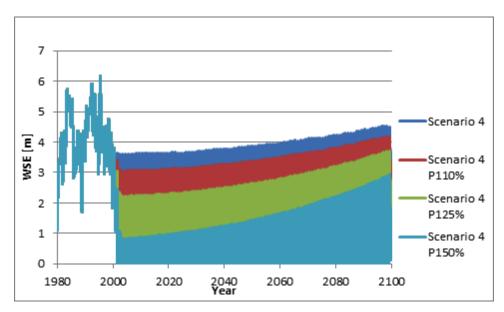


Figure 4-174. 11S005W02N004S (2N4) simulated hydrograph of Scenario 4 with scaled pumping.P110% means that the pumping rate from WY 2000 is increased by 10% and then used from 2000 to 2100.

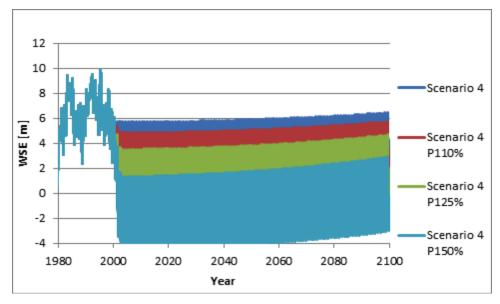


Figure 4-175. 10S005W35K005S (35K5) simulated hydrograph of Scenario 4 with scaled pumping.P110% means that the pumping rate from WY 2000 is increased by 10% and then used from 2000 to 2100.

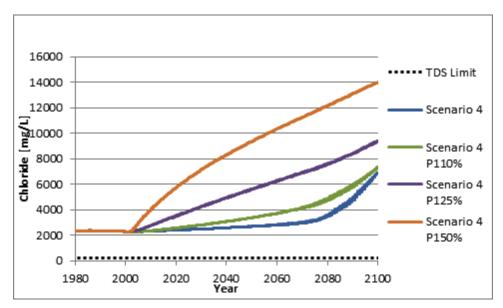


Figure 4-176. 11S005W09J001S (9J1) simulated breakthrough curve of Scenario 4 with scaled pumping. P110% means that the pumping rate from WY 2000 is increased by 10% and then used from 2000 to 2100.

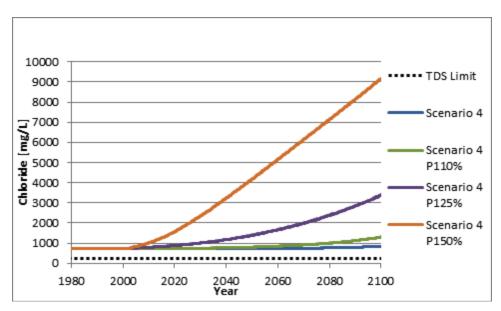


Figure 4-177. 11S005W10B001S (10B1) simulated breakthrough curve of Scenario 4 with scaled pumping.P110% means that the pumping rate from WY 2000 is increased by 10% and then used from 2000 to 2100.

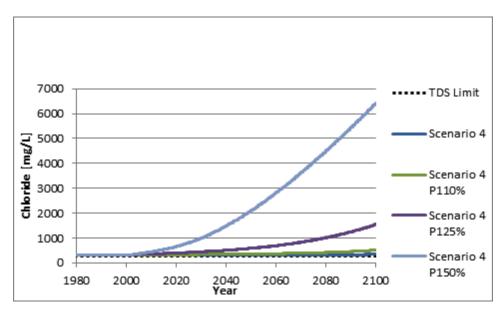


Figure 4-178. 11S005W02N004S (2N4) simulated breakthrough curve of Scenario 4 with scaled pumping.P110% means that the pumping rate from WY 2000 is increased by 10% and then used from 2000 to 2100.

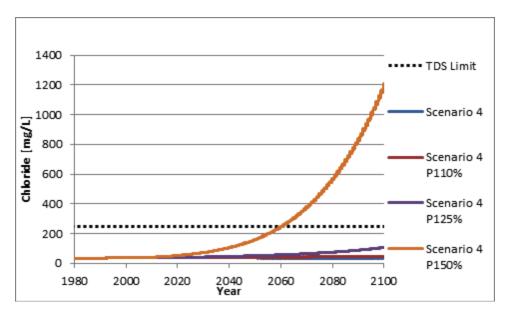


Figure 4-179. 10S005W35K005S (35K5) simulated breakthrough curve of Scenario 4 with scaled pumping.P110% means that the pumping rate from WY 2000 is increased by 10% and then used from 2000 to 2100.

Figure 4-181 shows the location of the 250 mg/L chloride-concentration contours for different pumping rates during Scenario 4 at the end of the simulation. The compounding effect of the increased pumping, the lower inland boundary condition, and the SLR from Scenario 4 caused a significant amount of seawater intrusion. A 10% increase in pumping under this situation had a similar impact to a 20% pumping increase with no SLR (Figure 4-171). The 250-mg/L contour from a 10% increase was only 20 m from well 2F1, which may cause it to start extracting groundwater with chloride concentrations above the U.S. EPA SMCL. A 25% increase caused chloride concentrations in wells 2F1, 2D3, and 2A1 to exceed the U.S. EPA SMCL. A 50% increase moved the 250 mg/L contour 7.3 km from the original coastline and caused the chloride concentrations in wells 2F1, 2D3, 2A1, and 35K1 to extract water above the U.S. EPA SMCL. The level of seawater intrusion was influenced strongly by a combination of the pumping rates, inland boundary condition, and SLR.

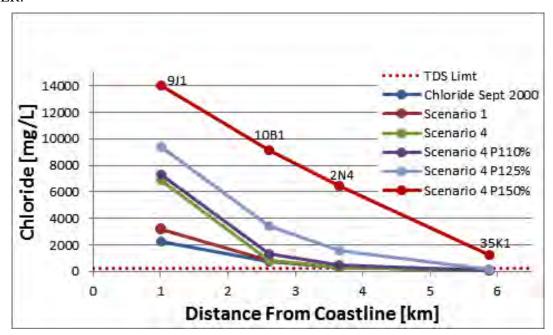


Figure 4-180. Final simulated chloride levels for different pumping schedules from 2000 to 2100 located at selected wells arranged by distance from the coastline.

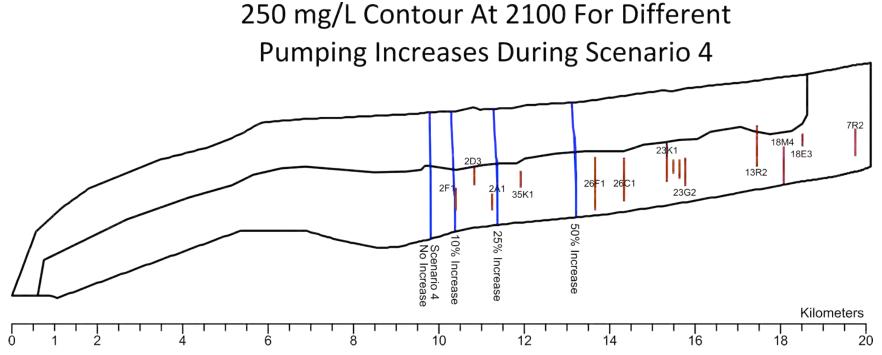


Figure 4-181. Location of the 250-mg/L chloride contour line at year 2100 for different scaled pumping rates of Scenario 4 from 2000 to 2100 with an inland boundary condition set to the 5% confidence (26.26 m). The compounding effects from the sea level rise, increases in pumping and a decrease in the inland boundary condition results in significant seawater intrusion.

4.4 APPLICATION TO THE ASSESSMENT OF VULNERABILITY

Sea level rise vulnerability at NBC and MCBCP was assessed through application of the methodologies described in the previous sections. The purpose of this analysis was not to perform an overall assessment of sea level rise vulnerability at these installations, but rather to test the physical response methodologies, illustrate their application, and evaluate approaches to adopt them within a generalized vulnerability framework such as the one described in Section 2.1. In the context of the framework, the methodologies were illustrated using two levels of analysis, Receptor Level and Component Level. The "Receptor Level" is an installation-level view in which general receptor category vulnerabilities to sea level rise were characterized in terms of key response metrics. The "Component Level" is a critical-component level view in which specific high-value or mission critical infrastructure elements are evaluated at a level of detail sufficient to characterize their response as a function of water level.

The results of the receptor-level assessment at each installation provided insight into the significant differences in sea level rise response and vulnerability that can be present at coastal installations that are in close geographic proximity. These differences were a function of multiple factors, including the topography, the degree of development at or near the coast, and the ability to accommodate coastal retreat. In the case of NBC, a higher degree of vulnerability stemmed from the low lying elevations, the concentration of built infrastructure near the shore, and the limited ability to allow for retreat in the face of sea level rise. In contrast, MCBCP has relatively steep topography, limited development along the coast, and cliffs to provide a natural buffering capacity through their erosion that will help to maintain the beach training areas.

The assessment results are described below, and organized at the analysis level (receptor-level or component-level), the installation level (NBC or MCBCP), the receptor level (buildings, training areas, etc.), and the exposure pathway level (erosion, inundation, flooding). The range of SLR scenarios analyzed provided upper and lower bound estimates of the types and ranges of responses and vulnerabilities that could be anticipated at installations in the southwest U.S.

4.4.1 Receptor-Level Assessment - Naval Base Coronado

At NBC, methods for the assessment of sea level rise vulnerability at NBC were evaluated under both receptor and component levels of analysis. The methodologies differ primarily in breadth and depth, with the receptor-level assessment retaining to the degree possible the full breadth of the installation, but at a relatively shallow level of detail and analysis, and the component-level method focusing on more specific receptors but at a finer level of detail. This section includes a brief overview of the metrics and vulnerability thresholds used to quantify the impacts of SLR for each receptor category. The analysis included the baseline conditions, four SLR scenarios, and five return period events. The analysis results quantified impacts to SLR in terms of replacement cost, quantity, area, and MDI value, as applicable. Following is a summary of the metrics and vulnerability thresholds for each receptor category.

Training Areas

The training areas at NBC include areas on both the exposed shoreline of Coronado and Silver Strand; and the protected shoreline inside of San Diego Bay. This analysis focused on the erosion and flooding pathway impacts on the beach training areas at Silver Strand. The beach training areas at SSTC-North and SSTC-South are defined by the adjacent boat training lanes (Figure 4-9).

The beach width remaining relative to Mean Sea Level was used to quantify the impacts of SLR to the beach training areas. The cost impact of SLR was estimated based on the volume of sand required (beach nourishment) to maintain the year 2000 beach widths. The beach training areas are vulnerable

to erosion and flooding for all SLR scenarios. The vulnerability threshold for the beach training areas was exceeded for the 1.0-m SLR scenario when the average beach width of all training lanes was reduced by 50% from the baseline condition. For this scenario, routine flooding during high tides reduced the beach width to zero in some areas.

Exposed Shoreline Erosion Pathway

The erosion pathway assessment determined the eroded and remaining beach width, and area above MSL for each SLR scenario. The beach width was defined as a metric that could be used by command personnel to determine impacts to beach training operations. The existing beach widths at NBC vary from 34- to 167-m wide for the baseline condition. The results of the analysis indicated that the average width of the beach training area decreased by approximately 30 m for each 0.5-m increment of SLR (Figure 4-182), although this rate also incorporated the effects of the sand budget imbalance.

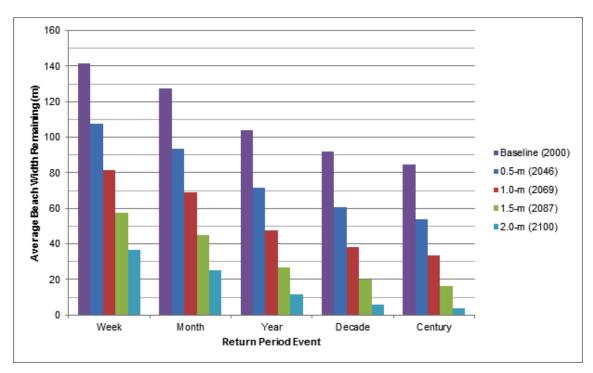


Figure 4-182. Erosion pathway assessment of beach width impacts to training lanes at NBC. The average beach width decreases by approximately 30 m for each SLR scenario.

The cost impacts of SLR-driven erosion on the beach training areas were estimated by determining the quantity of sand (beach nourishment) that would be required to maintain the baseline beach width. Historically, beach nourishment projects were not executed at a fixed frequency, and tended to be conducted on an as-needed basis. Based on the analysis conducted for this project, beach nourishment projects could be executed for the Silver Strand Littoral Cell at a 10-year interval with the sand volume required to maintain the existing beach width. The sand replenishment volume needed to keep pace with SLR and the sand deficit would increase from 1.0 million cubic meters in 2010 to 3.6 million cubic meters in 2100. The unit cost for a beach nourishment project depends on the total sand volume and dredge equipment mobilization costs. A unit cost of \$23.50 per cubic meter was used to estimate the cost of maintaining the existing beach width. The unit cost was based on a recent beach nourishment project in San Diego. See Figure 4-183 for a plot of a sand volume and replacement cost versus time for the Silver Strand Littoral Cell.

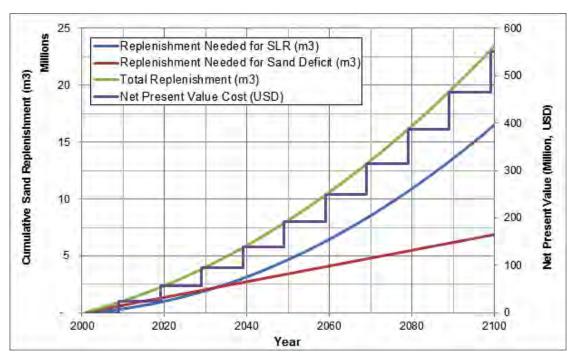


Figure 4-183. Silver Strand Littoral Cell beach nourishment. The sand replenishment volume required for both SLR and the sand deficit at NBC beaches. The associated costs are to maintain the existing baseline beach width.

Exposed Shoreline Inundation and Flooding Pathway

The beach training areas at NBC were analyzed for inundation and flooding impacts based on a spectrum (week – century) of return period total water level exposures over the eroded shoreline position for each SLR scenario. The water depths and flooded areas were calculated for all areas landward of the baseline shoreline position. The assessment results included the percentage flooded and water depth for each SLR scenario and return period event (Figure 4-184). The data provided a basis for understanding both the potential magnitude and frequency of inundation and flooding conditions that could inform command personnel on the future ability to sustain beach training activities. For example, the average percent of area inundated increased by about 85% between the baseline and 2.0-m SLR scenario. If the beach width becomes too narrow for training, then the flood data could also be used to plan for when beach nourishment is required to maintain training activities. While it is not uncommon for operations personnel to be unable to define the minimum beach width or area required for training activities, potential real-time scenarios require the military to accommodate a wide variety of beach conditions.

Buildings

The receptor-level assessment methodology was tested for buildings at NBC on an installation-wide basis for erosion and inundation/flooding for each SLR scenario. A sampling of the erosion and flood assessment results for NBC are discussed below.

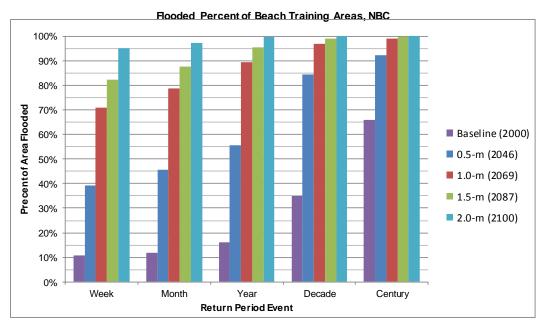


Figure 4-184. Inundation and flooding pathway assessment of beach area impacts to training areas at NBC.

The impacts of SLR to the buildings were quantified using replacement cost, area, MDI value, and exterior water depth. Buildings located near the exposed shoreline were vulnerable to erosion and flooding for all SLR scenarios. The buildings near the protected shorelines were vulnerable to flooding for the 1.5- and 2.0-m SLR scenarios. The exterior flood depths at buildings were used to assess the vulnerability to flood damage. For the exposed shoreline, a majority of the flooded buildings were vulnerable to damage with water depths greater than 1.0 m. The buildings that were near to the exposed shoreline were more vulnerable to erosion and flooding than buildings near the protected shoreline.

The building asset information used to make the assessment included elevation data, footprint area, replacement cost, and mission dependency index. Some buildings in the database did not include replacement costs. These buildings were assigned an estimated replacement cost based on the average unit replacement cost of the buildings within the erosion footprint for the 100-year return period event of the 2.0-m SLR scenario. The average unit replacement cost used was \$2,727 per sq. meter. The MDI value of a building may be used to determine if minor flooding can be tolerated on an infrequent basis.

Exposed Shoreline Erosion Pathway

Naval Base Coronado has buildings that are near the exposed shoreline and currently require a sand dike for protection from wave run up during large wave events coupled with high tides (Figure 4-185). The erosion pathway analysis determined the quantity (Figure 4-186) and replacement cost (Figure 4-187) of the buildings within the erosion footprint for each SLR scenario. If a building was located within the erosion footprint, then the full replacement cost of the building was used to quantify the impacts of that scenario. The erosion damage to buildings was sensitive to the return period event analyzed for each SLR scenario. For the 0.5-m scenario, the year, decade and century return period events had a similar total damage cost impact, with minimal impact for the month or week events. For the 1.0-m scenario, the month and year return periods were approximately \$35 million, whereas the decade and century events were approximately \$150 million.

Exposed Shoreline Inundation and Flooding Pathway

The inundation and flooding pathway assessment determined the maximum exterior flood depth at each building. Three flood depth ranges described in Section 3.4.1 were used for assessing the vulnerability of the buildings to different flood depths under the receptor-level methodology. The three flood depth ranges corresponded to increasing levels of damage and operational impacts. For example, the total number and replacement value of buildings in the highest depth range (> 1 m) are shown in Figure 4-188 and Figure 4-189, respectively. Inundation as represented by the weekly return period condition impacted a relatively small number of buildings with water depths of this magnitude, even under the 2.0-m SLR scenario where about 100 buildings were impacted with an estimated replacement value of about \$200 million. In contrast, less frequent flooding events impacted increasingly large number of buildings with the 2.0-m SLR 100-year return period event estimated to impact over 1,000 buildings with an estimated replacement cost of about \$2,500 million.

Protected Shoreline Inundation and Flooding Pathway

Model results indicated that inundation and flooding from the protected shoreline pathway at NBC was significantly more limited than for the exposed shorelines. Inundation impacts (based on the weekly return period condition) indicated the total number of buildings in the highest depth range (>1 m) ranged from zero for the baseline condition to 53 for the 2.0-m SLR scenario, with corresponding replacement values ranging from 0 to \$185M (Figure 4-190). Flooding impacts (based on the 100-year return period condition) increased fairly dramatically for SLR >1.5 m, with the total number of buildings in the highest depth range (>1 m) increasing from zero for the baseline to 21 for the 1.0-m SLR and then to 146 for the 2.0-m SLR scenario. Corresponding replacement values for flooding ranged from 0 to \$298M.



Figure 4-185. View looking north of the existing shoreline and sand dikes at the beachside improvements at NAB Coronado.

Building Quantity Impact Summary for SLR Related Beach Erosion Naval Base Coronado 70 60 **Quantity of Buildings** 40 ■ Baseline (2000) ■ 0.5-m (2046) ■ 1.0-m (2069) ■ 1.5-m (2087) 20 ■ 2.0-m (2100) 10 0 Week Month Year Decade Century

Figure 4-186. Erosion pathway analysis of buildings at the exposed shoreline of NBC. The quantity of buildings within the beach erosion footprint for each SLR scenario and return period event.

Return Period Event

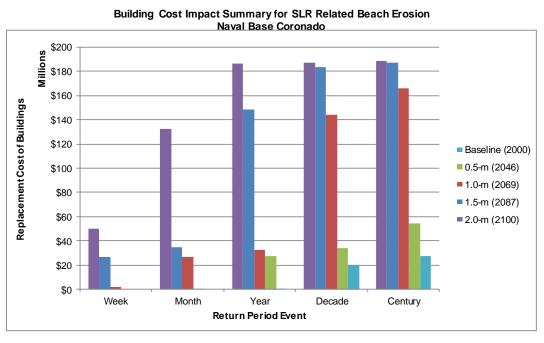


Figure 4-187. Total replacement cost of buildings within the beach erosion footprint at NBC.

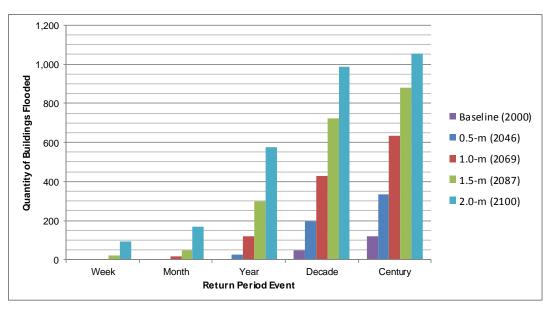


Figure 4-188. Inundation and flooding pathway analysis for buildings via the exposed shoreline of NBC showing the quantity of buildings within the inundation and flooding footprint with water depth exceeding 1 m for each SLR scenario and return period event.

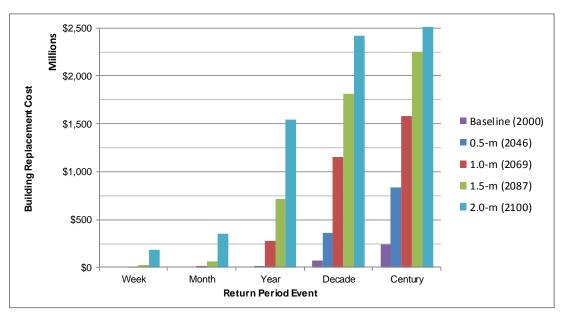


Figure 4-189. Total replacement cost of buildings within the exposed shoreline inundation/flooding footprint at NBC with water depth exceeding 1 m.

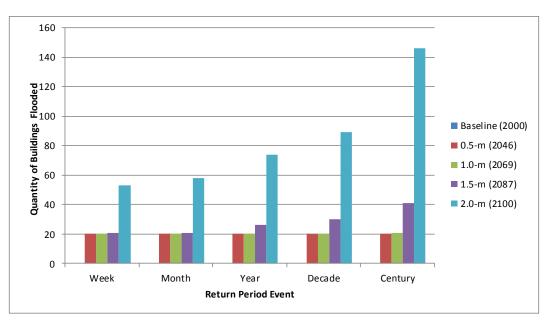


Figure 4-190. Inundation and flooding pathway analysis for buildings exposed via the protected shoreline of NBC showing the quantity of buildings within the inundation and flooding footprint with water depth exceeding 1 m for each SLR scenario and return period event.

Waterfront Structures

One of the missions of NBC is to support a variety of aircraft carriers, large and small craft and amphibious craft. This mission requires a large quantity of waterfront infrastructure at both NAB and NASNI. The receptor-level assessment included analysis of 43 waterfront structures including piers, wharves, floating docks, and boat ramps. The vulnerability of fixed elevation piers and wharves to SLR depends on the deck elevation, utility and fender systems. The impacts of SLR were quantified using replacement cost, area, and MDI values. Based on the range of conditions examined here, these structures were found to be vulnerable to operational impacts for SLR at or above the 0.5- to 1.0-m scenarios, and overtopping for SLR at or above the 1.5-m scenario via exposure primarily through the protected shorelines of San Diego Bay. The service life of waterfront structures is limited because of the aggressive marine environment; therefore, it may be important to consider the age of the structure in the vulnerability assessment.

The deck elevation of the piers and wharves vary from +3.22 to +4.14 m. For the receptor-level assessment, the typical method used to determine the deck elevation of a waterfront structure was to review construction record drawings and WFI Reports. These drawings and reports provided deck elevations for a majority of the structures. The DEM was used to confirm these elevations, where these data were available. The piers (perpendicular to shore) were typically not visible on the DEM. However, the CVN wharves (parallel to shore) at NASNI were included in the model. Elevations from the DEM were compared to the record drawings and found to be in good agreement (Table 4-9).

The receptor-level assessment of the waterfront structures determined the quantity and replacement cost of the facilities that would be overtopped, or have operational impacts for each SLR scenario and return period event. The fixed elevation piers and wharves were more vulnerable to SLR-related operational impacts, damage, and reduced service life than were floating docks and boat ramps. Therefore, the receptor-level assessment focused on these assets.

Table 4-9. Comparison of DEM and Construction Record Drawing Elevations at NBC

Facility	Construction Drawing Elevation (NAVD m)	DEM Elevation (NAVD m)	Delta (m)
Berth Juliet	4.0	3.97	0.03
Berth Kilo	3.96	3.98	0.02
Berth Lima	3.51	3.50	0.01
Carrier Quaywall	3.51	3.56	0.05

The receptor-level assessment of the waterfront structures determined the quantity and replacement cost of the facilities that would be overtopped, or have operational impacts for each SLR scenario and return period event. The fixed elevation piers and wharves were more vulnerable to SLR-related operational impacts, damage, and reduced service life than were floating docks and boat ramps. Therefore, the receptor-level assessment focused on these assets.

Protected Shoreline Inundation and Flooding Pathway

For the overtopping assessment, the deck elevation of the fixed-elevation piers and wharves was compared to the synthetic return period event total water level for each SLR scenario. When a structure was overtopped, it was assumed that it would require replacement. The results are presented in Figure 4-191 and Figure 4-192 in terms of quantity and replacement cost. For the 0.5-m SLR scenario, none of the structures were overtopped. For the 10- and 100-year return period events of the 1.0-m SLR scenario, approximately half of the piers were overtopped, with a total ROM replacement cost impact of \$345 million. For the 1.5- and 2.0-m SLR scenarios, almost all of the fixed elevation piers and wharves were overtopped at NBC, with a total ROM replacement cost impact of \$650 million.

For the operational impact assessment, the operational limit of the structure was compared to the synthetic return period event total water level (Figure 4-193). Refer to Section 3.4.1 for discussion of the functional elevations of waterfront structures. For the 0.5-m SLR scenario, approximately half of the structures had operational impacts. For the 1.0, 1.5, and 2.0-m scenarios, almost all of the fixed elevation piers and wharves had operational impacts on a frequent basis. In practice, the piers with operational limits below the overtopping elevation will require a more detailed assessment to determine if the investment required to upgrade the facility is warranted. The detailed assessment should consider the replacement cost, overtopping elevation, upgrade cost, year built, condition index, and remaining service life.

The floating docks at NBC are attached to a fixed-elevation pier, or anchored near the shore with access by a brow that transitions from the shore to the docks. Floating docks are designed to accommodate the current tidal range inside the bay; thus are generally able to accommodate some amount of SLR. The vulnerable items of a floating dock system are generally the guide piles that secure the dock in position and the brow. The maximum operational water level for a floating dock is a function of the bending capacity of the pile, the strength of the soil, and the elevation of the top of guide pile. At NBC, the top of guide piles are approximately +4.0 m. In the future, floating docks may require higher capacity guide piles or adjustments to the bro w connection details to accommodate SLR.

The boat ramps at NBC are typically configured with the top of slope elevation equal to the adjacent roadway elevation. The ramp is designed to accommodate the tidal range, and will generally have the ability to accommodate SLR. Boat ramps will not be damaged by flooding, but may have short-term operational impacts during high tides.

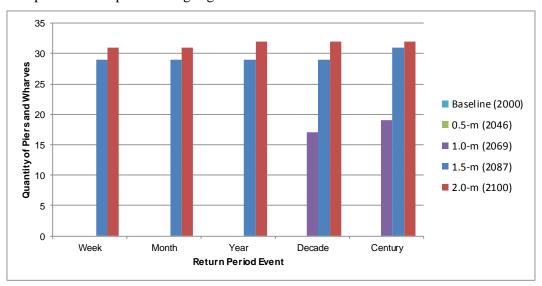


Figure 4-191. Receptor-level estimate of the quantity of piers and wharves overtopped at NBC. No impacts were projected for the baseline or 0.5-m SLR scenario.



Figure 4-192. Receptor-level estimate of the ROM replacement costs of Piers and wharves overtopped at NBC. No impacts were projected for the baseline or 0.5-m SLR scenario.

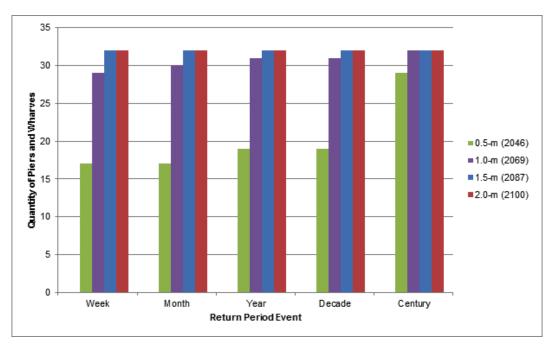


Figure 4-193. Receptor-level estimate of the quantity of piers and wharves with operational impacts at NBC. Operational impacts are expected for each SLR scenario except the baseline.

Coastal Structures

The coastal structures receptor category at Naval Base Coronado included bayside shoreline protection in the form of bulkheads, revetments, and rip-rap. These structures are primarily subject to inundation and flooding exposure along the protected shorelines of San Diego Bay. The DEM and record drawings were used to acquire critical functional and operational elevations for the receptor-level assessment of these coastal structures. When the DEM was used to obtain a structure's elevation, several cross sections would be evaluated and an average value was applied (Figure 4-194).

For a receptor-level assessment, if a coastal structure was overtopped for any SLR scenario during any return period event, it was considered as requiring replacement. A replacement value of each affected structure per unit length was derived based on design details of similar structures in the region. High-resolution aerial imagery was used to acquire the length of these structures when record drawings were unavailable. Applying full replacement value for revetments and rip-rap in this analysis is a conservative approach, as rock could be added to these structures at a lesser cost to increase protection. The shoreline length with rip-rap is non-engineered shore protection composed of miscellaneous concrete elements (chunks of concrete slabs, etc.), and is more vulnerable to erosion from boat wakes and wind-driven waves than an engineered rock revetment.

Protected Shoreline Inundation and Flooding Pathway

The protected shorelines with engineered coastal structures were estimated to have minimal impacts for the 0.5- and 1.0-m SLR Scenarios, but were overtopped for the 1.5- and 2.0-m SLR scenarios. The protected shorelines with non-engineered shore protection, such as rip-rap, will have increased erosion from boat wakes and wind driven waves for all SLR scenarios. Based on the receptor-level assessment of NAB and NASNI Coronado, no coastal structures were vulnerable in the baseline 0.5- and 1.0-m SLR scenarios (Figure 4-195). Therefore, no replacement costs were incurred. All structures were determined to be vulnerable and requiring replacement under the 2.0-m

SLR scenario. The total cost for replacement of all structures was estimated to be \$76 million. Note that the relatively flat impact response as a function of return period is explained by the uniformity of the total water levels for exposure along protected shorelines where the variability in sea level is primarily related to tides.

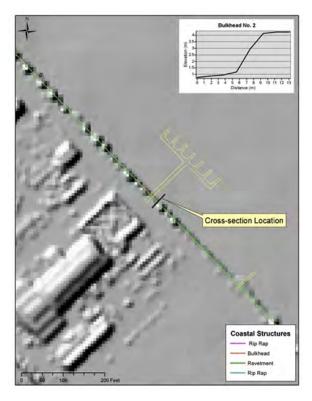


Figure 4-194. Example elevation extraction from the DEM.

Civil Infrastructure

Selected receptor subcategories of the civil infrastructure at NBC were analyzed to illustrate potential erosion, inundation, and flood impacts, including roads, airfields, storm water infrastructure, and recreation areas. For the erosion analysis, the area (or length) of the asset inside of the erosion footprint was tabulated for each scenario. For the inundation and flooding analysis, the wetted areas and water depths were determined for each asset. The metrics used to quantify the impacts of SLR to the civil infrastructure were the area eroded or flooded, replacement cost, and average water depth. Under the range of SLR conditions examined in the study, the roadways near exposed shorelines were shown to be vulnerable to erosion at or above the 1.0-m SLR scenario, and flooding for at or above the 1.5-m SLR scenario. The airfields were not within the erosion footprint, however, and were found to be vulnerable to flooding at or above the 1.0-m SLR scenario from both the exposed and protected shorelines. Low-lying portions of the storm water infrastructure were found to be vulnerable to reduced efficiency under all SLR scenarios, which could lead to increased flooding during rain events (although precipitation impacts were not examined in this study). At or above the 1.0-m SLR scenario, localized flooding was estimated to occur at low-lying storm drain inlets from intrusion of seawater back through the system and onto the installation. A summary of the analysis for each subcategory is provided below.

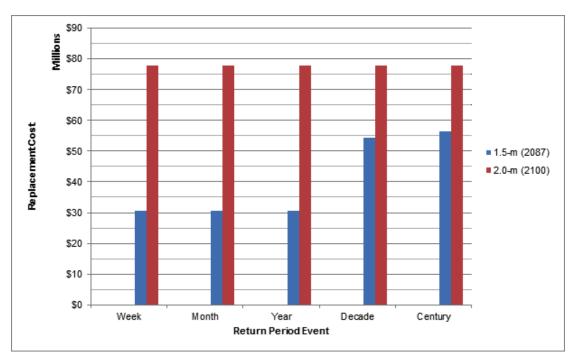


Figure 4-195. Receptor-level estimate of the ROM replacement cost of the bay-side coastal structures overtopped at NBC. No impacts were projected for the baseline, 0.5, or 1.0-m SLR scenarios.

Roads

At NBC the roads were defined in the GIS database provided by NAVFAC as a polyline along the centerline of the roadway. A typical two-lane road-width of 10 m was used to estimate the total roadway area and calculate the total replacement value of the impacted roadways. The estimated unit replacement cost of a typical two-lane roadway was \$67.27 per square meter, which includes replacement of the roadway base and asphalt paving. The cost assessment did not include the replacement of adjacent land area, the soil material beneath the roadway subgrade, environmental-related costs (permitting, mitigation, etc.). The volume of fill material lost below the roadway was determined as part of the beach erosion analysis.

Exposed Shoreline Erosion Pathway. The erosion assessment for the roadways at NBC calculated the total area and corresponding rough order of magnitude replacement cost of roadways within the erosion footprint for each SLR scenario (see Figure 4-196). For strong erosion events (100-year return period), coastal roadways along the exposed shorelines were subject to loss due to erosion, and the level of impact increased significantly with increasing SLR with the replacement cost for the baseline condition at about \$37K, increasing to a replacement cost of about \$3.6M for the 2.0-m SLR scenario.

Exposed Shoreline Inundation and Flooding Pathway. The inundation and flooding pathway assessment for NBC was conducted separately for the exposed and protected shorelines. The analysis determined the maximum water depth and the percentage of area subject to inundation or flooding for each roadway in the GIS database. Roadways with average water depths greater than 0.15 m were assumed to result in operational impacts to the installation. These flood scenarios and water depths did not consider the additional impacts of a rain event. At the exposed shoreline areas, flooding occurred for all SLR scenarios with maximum flood depths of 3.9 and 4.7 m for the 1.5- and 2.0-m SLR scenarios, respectively. For the exposed shoreline, the flood depths were calculated for all areas

landward of the baseline shoreline position, which included some areas inside of the erosion footprint. The length of flooded roadway was also calculated (see Figure 4-197). The estimated flood depths could also be used to estimate roadway damage and associated maintenance costs. The roadway maintenance costs will increase as the frequency and depth of flooding increases. Areas with routine flood depths greater than 0.3 m, and moving water, would likely be damaged by localized erosion, settlement, undermining, and potholes.

Protected Shoreline Inundation and Flooding Pathway. At the protected shoreline areas of NBC, roadway inundation occurred for the 1.5- and 2.0-m SLR scenarios only, while roadway flooding occurred for SLR of 1.0 m and above, with maximum flood depths for the 100-year return period conditions of 1.67 m for the 1.5-m SLR scenario and 2.17 m for the 2.0-m SLR scenario. The length of roadway subject to inundation ranged from about 10 km for the 1.5-m SLR scenario, to about 43 km for the 2.0-m SLR scenario (based on weekly return period condition), while the length of roadway subject to flooding ranged from about 1 km for the 1.0-m SLR scenario to about 70 km for the 2.0-m SLR scenario (see Figure 4-198).

Airfields

The receptor-level assessment of the airfields at NBC included runways, helicopter pads, and miscellaneous airfield pavement. The assessment included the erosion pathway for the exposed shoreline, and the flooding pathway for both the exposed and protected shorelines. The vulnerability of airfields to operational and damage impacts from flooding are similar to roadways.

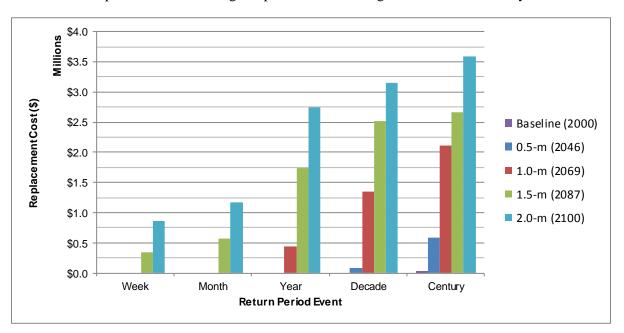


Figure 4-196. Roadway erosion at NBC showing the estimated roadway replacement cost for each SLR scenario for the erosion pathway.

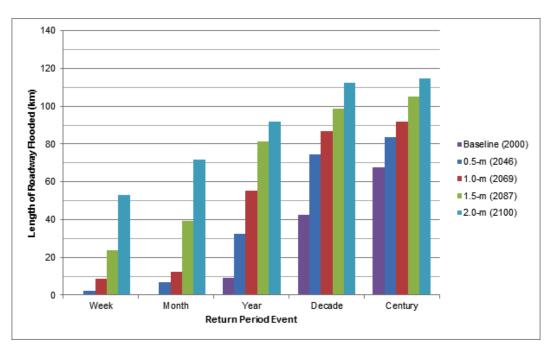


Figure 4-197. Roadway inundation and flooding at exposed shorelines of NBC. The length of roadway flooded increases for each return period event, with major flooding occurring for all SLR scenarios.

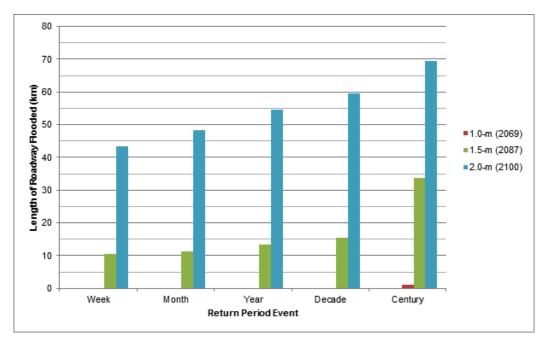


Figure 4-198. Roadway inundation and flooding at protected shorelines of NBC. The length of roadway flooded increases for each return period event for the 1.5- and 2.0-m scenarios. The roadways do not flood significantly for the 0.5- or 1.0-m scenarios.

Exposed Shoreline Erosion Pathway. The erosion pathway assessment determined that the airfields at NBC were not located within the erosion footprint. However, under the simulated erosion scenarios, the shoreline position moves closer to the airfields, offering less protection from wave runup and flooding.

Exposed Shoreline Inundation and Flooding Pathway. The inundation and flooding pathway at NBC could cause operational impacts and damage to the runways because of the percentage of the airfields flooded and the estimated water depths on the airfields. The exposed shoreline flood pathway assessment determined the total area flooded (Figure 4-199), the percentage of the airfields flooded, and maximum water depth for each SLR scenario. Airfield inundation was estimated to occur for SLR scenarios of 1.0 m and higher, while airfield flooding (100-year return) was projected under all SLR scenarios including the baseline scenario. The percentage of airfield subject to inundation (weekly return) ranged from about 0.2% for the 1.0-m SLR scenario to a high of about 6.2% for the 2.0-m SLR scenario. This corresponds to areas of inundation ranging from about 4500 m² to 132000 m², respectively. Airfield flooding percentages ranged from about 7.2% for the baseline scenario, to about 54.3% for the 2.0-m SLR scenario, with corresponding flooded areas for about 152000 m² to 1148000 m², respectively. The maximum water depth estimated for the airfields for the 100-year return period event ranged from 1.74 m for the 0.5-m scenario to 3.24 m for the 2.0-m scenario.

Protected Shoreline Inundation and Flooding Pathway. The protected shoreline inundation and flooding pathway assessment for airfields indicated that impacts was less severe relative to the exposed shoreline impacts, and that inundation and flooding occurred only under the 1.5- and 2.0-m SLR scenarios (Figure 4-200). The percentage of airfield area subject to inundation (weekly return period condition) ranged from 0.3% for the 1.5-m SLR scenario, to about 3.9% for the 2.0-m SLR scenario. The percentage of the airfield area subject to flooding (100-year return period condition) ranged from about 3% for the 1.5-m SLR scenario to about 6.1% for the 2.0-m SLR, corresponding to a range of about 64000 m² to 129000 m², respectively.

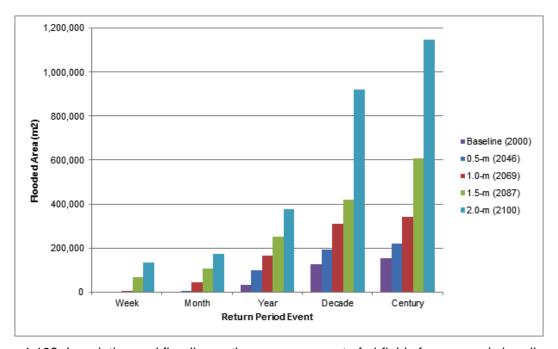


Figure 4-199. Inundation and flooding pathway assessment of airfields for exposed shorelines at NBC. The total flooded area increases for each SLR scenario and is approximately 10 times greater than for the protect shorelines.

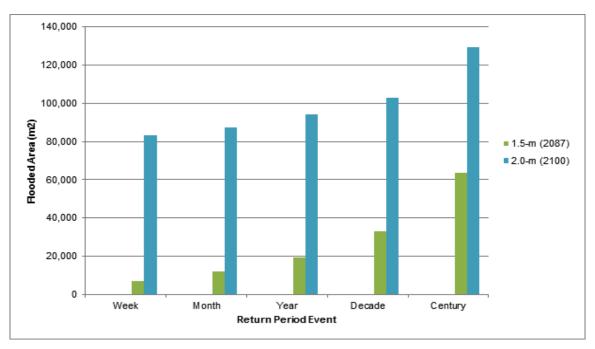


Figure 4-200. Inundation and flooding pathway assessment of airfields for protected shorelines at NBC. Minor flooding occurs for the 1.5- and 2.0-m SLR scenarios. No flooding occurs for the 0.5- or 1.0-m SLR scenarios.

Storm Water Infrastructure

The storm water conveyance system at NBC is critical to controlling storm water runoff during and after a rain event. The storm water system uses gravity flow with outlets to both San Diego Bay and the Pacific Ocean. NBC personnel indicated that the existing system performs poorly when a rain event coincides with a seasonal high tide.

Exposed Shoreline Erosion Pathway. The erosion pathway assessment of the storm water drainage system determined the length of underground drain pipe within the erosion footprint for each SLR scenario. The rough order of magnitude replacement cost of the storm drainage system was calculated for each SLR scenario. A unit replacement cost used for the system was estimated at \$922.74 per linear meter for a 0.6-m-diameter reinforced concrete pipe with inlets at 61 m on center. The erosion impacts to the storm water drainage system were a relatively small percentage of the total storm water drainage system at NBC (< 2% for the 2.0-m SLR and 100-year return period wave erosion condition). The length of pipe within the erosion footprint under the 100-year return period condition ranged from about 282 m for the baseline scenario, to a maximum of about 1648 m for the 2.0-m SLR scenario, with a corresponding range of replacement costs of about \$270K to \$1.5M (Figure 4-201).

Exposed Shoreline Inundation and Flooding Pathway. The inundation and flooding pathway assessment of the storm water drainage system estimated the water depth at each storm water drainage inlet. In general, the storm drain inlets are located at the low points of paved areas to collect water and thus may be subject to intrusion from elevated water levels, or to flooding from overtopping waves. A water depth of 0.3 m at the inlet was used as a threshold limit for operational impacts to the associated roads, buildings and parking areas that the storm water system drains. The total number of inlets identified within the GIS was 1166. Of these, the number subject to inundation (weekly return condition) ranged from zero for the baseline scenario, to 116 for the 2.0-m SLR scenario. For flooding (100-year return period condition), the number of inlets with water depths of

0.3 m or higher ranged from 143 for the baseline scenario, to a high of 533 for the 2.0-m SLR scenario, representing 12 to 46% of the total number of inlets, respectively (Figure 4-202).

Protected Shoreline Inundation and Flooding Pathway. The protected shoreline flood pathway assessment for the storm water conveyance system determined that flood impacts would be less severe than for the exposed shoreline. The number of storm drain inlets subject to inundation (weekly return condition) ranged from zero for the baseline scenario, to 96 for the 2.0-m SLR scenario. For flooding (100-year return period condition), the number of inlets with water depths of 0.3 m or higher ranged from zero for the baseline scenario, to a high of 160 for the 2.0-m SLR scenario, representing a maximum of 14% of the total number of inlets in the worst case.

Recreational Areas

The recreational areas included a number low-lying elements near the beach such as the golf course and ball fields. The assessment included the erosion pathway for the exposed shoreline, and the flooding pathway for both the exposed and protected shorelines. The recreational areas would likely be closed while flooded and may cause damage to grass covered areas from exposure to saltwater. The analysis determined the area impacted from erosion and flooding for each SLR scenario. A replacement value was not estimated for recreational areas.

Exposed Shoreline Erosion Pathway. The erosion pathway assessment determined the area of recreational spaces within the erosion footprint for each SLR scenario, as well as the fraction of the total recreational area that this represented. The results showed limited impacts to recreation areas with a maximum of about 11% of recreational areas impacted by 2.0 m of SLR combined with a 100-year return period erosion event (Figure 4-203).

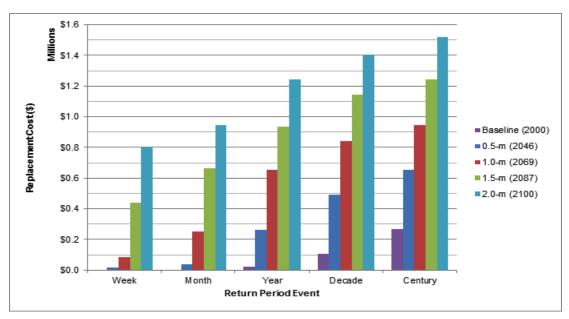


Figure 4-201. Exposed shoreline erosion pathway assessment of storm water conveyance system at NBC.

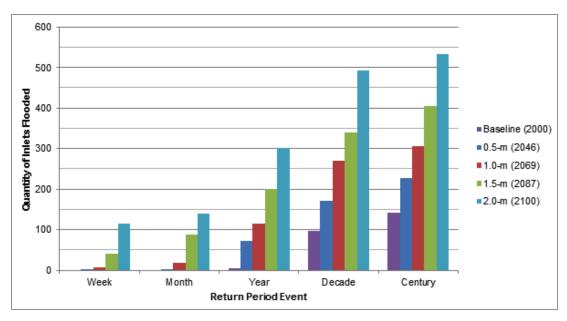


Figure 4-202. Inundation and flooding pathway assessment of stormwater drainage system at exposed shoreline of NBC. The quantity of stormwater inlets with flood depths greater than 0.3 m is shown.

Exposed Shoreline Inundation and Flooding Pathway. The exposed shoreline inundation and flooding pathway assessment of recreational areas also determined the area and percent of area impacted. For inundation (represented by the weekly return period), the impacted area was limited for the baseline and 0.5-SLR scenarios, but increased substantially to over 40% for the 2.0-SLR scenario (Figure 4-204). Flooding impacts for the 100-year return period exceeded 50% even for the baseline condition, and increased to over 90% for the 2.0 m SLR scenario. These percentages were driven largely by the golf course on North Island, which accounted for a significant portion of the overall recreational area.

Protected Shoreline Inundation and Flooding Pathway. The protected shoreline inundation and flooding pathway assessment showed much more limited impact (Figure 4-205). No significant impacts were projected for SLR scenarios of 1.0 m or less, and more widespread impacts were only shown for the 2.0-m SLR scenario where the impacted area ranged as high as about 32% for the 100-year return period event.

Receptor-Level Assessment Summary - Naval Base Coronado

As described above, sea level rise vulnerability of a range of NBC installation receptors was evaluated as a means of illustrating the application of the methodologies developed in this study. Vulnerability was evaluated as a function of receptor class for different exposure pathways and a range of potential future sea level rise scenarios. While the receptors evaluated here represent only a subset of those present at the installation, they do provide a representative cross-section of the infrastructure that could be vulnerable to sea level rise. Thus, a cumulative summary of the vulnerability provides a sense of which receptor classes tend to be more vulnerable, as well as the overall magnitude of the vulnerability across receptor classes.

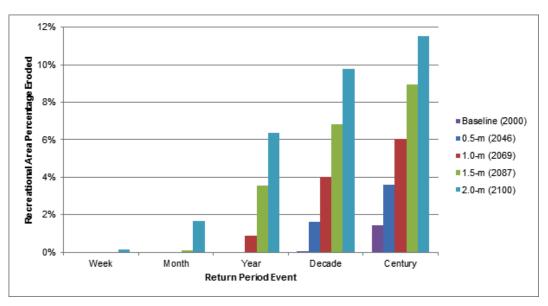


Figure 4-203. Erosion pathway assessment for recreational areas at NBC determined the percentage of recreational area within the erosion footprint.

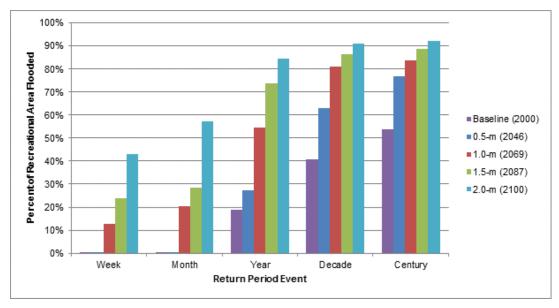


Figure 4-204. Exposed shoreline inundation and flooding pathway assessment for recreational areas of NBC determined the percentage of recreational area flooded.

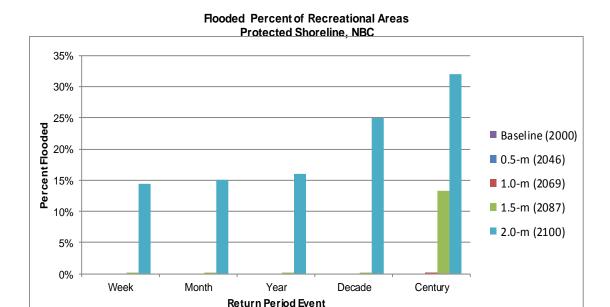


Figure 4-205. Protected shoreline inundation and flooding pathway assessment for recreational areas of NBC determined the percentage of recreational area flooded.

Erosion Pathway

The overall vulnerability of NBC receptors to sea level rise for the erosion pathway is summarized in Table 4-10 under the prescribed sea level rise conditions and the assumed sand budget deficit. The summary incorporated key receptors including training areas, buildings and civil infrastructure, and multiple metrics of response across the full range of both long-term sea level rise scenarios and short-term erosion events of various return periods. In general, the summary illustrates the increasing level of vulnerability to erosion as a function of increasing sea level, as well as the sensitivity of some receptors to short-term wave driven erosion events. For training areas, this translates into frequent (weekly return period) conditions with average beach widths reduced to about 82 m and a remaining area of about 53% of baseline for 1.0-m SLR (first occurrence by 2069), and further reductions to an average beach width of about 36 m and a remaining area of 23% of baseline for 2.0-m SLR (first occurrence by 2100). To preserve year 2000 beach widths, significant beach replenishment would be required with estimated costs in the range of \$250M to \$551M for the 1.0- and 2.0-m SLR scenarios, respectively, potentially the largest contribution to the overall erosion pathway vulnerability of the installation if retreat is not considered a viable option.

For buildings, weekly return period conditions resulted in erosion pathway vulnerability to about 13 structures for 1.0-m SLR 3 of which have an MDI >55 ("Relevant" classification or higher), and with an estimated replacement cost of about \$2M. This increased to about 23 structures and 6 with MDI >55 with an estimated replacement cost of \$50M for 2.0-m SLR. The building receptor class also contributed substantially to the overall erosion pathway vulnerability of the installation. For civil infrastructure, evaluation of roadways indicated limited vulnerability with replacement costs in the range of \$0M to \$1M for the 1.0- and 2.0-m SLR scenario, respectively. Overall vulnerability estimates for the receptors included in the erosion pathway analysis ranged from negligible for the baseline SLR scenario, to as high as ~ \$745M for the 2.0-m SLR scenario. This estimate is largely driven by "replacement cost" associated with beach replenishment, and it should be noted that if this replenishment were to take place then the other erosion impacts would be largely mitigated, so the total number should be viewed as a measure of summed vulnerability rather than a measure of the actual costs that might occur for a given scenario.

Exposed Shoreline Inundation and Flooding Pathway

Vulnerability of NBC receptors to sea level rise for the exposed shoreline inundation and flooding pathway is summarized in Table 4-11. The summary incorporated key receptors including training areas, buildings and civil infrastructure, and multiple metrics of response across the full range of both long-term sea level rise scenarios and short-term flooding events of various return periods. In general, the summary illustrates the increasing level of vulnerability to inundation and flooding as a function of increasing sea level and increasingly extreme short-term events flooding. The results reflect the relatively high sensitivity of NBC to inundation and flooding as a function of the generally low-lying nature of the installation, and the significant exposure along the open shoreline of the Pacific. For training areas, this translated into inundation impacts with average beach widths reduced to about 42 m and a remaining area of about 29% for 1.0-m SLR (first occurrence by 2069), and further reductions to an average beach width of only about 7 m and a remaining area of 5% for 2.0-m SLR (first occurrence by 2100). While infrequent flooding events can potentially be accommodated through scheduling, flooding impacts (100-year return period condition) are more significant with the entirety of the beach training areas being subject to flooding for SLR scenarios of about 1.0 m and above (first occurrence by 2069). Replacement costs for inundation and flooding of training areas were assumed to be equivalent to those estimated for the erosion pathway, because flooding events simply occur over top of the eroded shoreline, and the shoreline is generally expected to recover from storm-driven wave events naturally. The replacement costs simply provide a metric of the value of the asset value that is subject to operational limitations due to inundation and flooding.

For buildings, inundation (weekly return) resulted in vulnerability to about 31 structures for 1.0-m SLR 9 of which had an MDI >55 ("Relevant" classification or higher), and with an estimated replacement cost of about \$216M. This increased substantially to about 360 structures and 62 with MDI >55 with an estimated replacement cost of \$2010M for 2.0-m SLR. The building receptor class was especially vulnerable to flooding impacts (100-year return period) with about 881 potentially flooded structures for 1.0-m SLR 130 of which had an estimated MDI >55 ("Relevant" classification or higher), and with an estimated replacement cost of about \$2783M. This increased to about 1143 structures and 150 with MDI >55, with an estimated replacement cost of \$3013M for 2.0-m SLR. The building receptor class contributed substantially to the overall exposed shoreline inundation and flooding pathway vulnerability of the installation. For civil infrastructure, evaluation of roadways indicated vulnerability to inundation with about 9 km operationally impacted for the 1.0-m SLR scenario, increasing to about 53 km for the 2.0-m SLR scenario. This range increased substantially for flooding vulnerability (100-year event) with 92 km and 115 km impacted for the 1.0- and 2.0-m SLR scenarios, respectively. Airfields at NBC also were shown to contribute significantly to installation SLR vulnerability with flooded (100-year event) operationally impacted surface areas ranging from about 343000 m² for the 1.0-m SLR scenario to about 1148000 m² for the 2.0-m SLR scenario.

Overall vulnerability estimates for the summed replacement value metric of receptors included in the inundation and flooding pathway analysis ranged from negligible for the baseline SLR inundation scenario, to as high as ~ \$3752M for the 2.0-m SLR flooding scenario. This estimate was largely driven by vulnerability associated with building flooding, but with significant contributions from all other categories as well.

Protected Shoreline Inundation and Flooding Pathway

Overall vulnerability of NBC receptors to sea level rise for the protected shoreline inundation and flooding pathway is summarized in Table 4-12. The summary incorporated key receptors including buildings and civil infrastructure, and multiple metrics of response across the full range of both long-term sea level rise scenarios and short-term flooding events of various return periods. Training areas at NBC on the bayside are primarily in-water and do not have a significant shore or beach component so were not included in the analysis. In general, the summary illustrates the increasing level of vulnerability to inundation and flooding as a function of increasing sea level, with the variations in return period events being relatively small due to the lack of wave exposure on these protected shorelines. The results reflect the relatively high sensitivity of NBC to inundation and flooding as a function of the generally low-lying nature of the installation, and while the impacts along these protected shorelines are muted compared to the open shorelines of the Pacific, there are critical receptor categories including waterfront and shoreline structures that are unique to this environment.

For buildings, inundation (weekly return) resulted in vulnerability to about 22 structures for 1.0-m SLR none of which had an MDI >55 ("Relevant" classification or higher), and with an estimated replacement cost of about \$72M. This increased substantially to about 273 structures and 57 with MDI >55, with an estimated replacement cost of \$488M for 2.0-m SLR. Flooding impacts (100-year return period) were somewhat higher with about 26 potentially flooded structures for 1.0-m SLR only one of which had an estimated MDI >55 ("Relevant" classification or higher), and with an estimated replacement cost of about \$75M. This increased to about 584 structures and 81 with MDI >55, with an estimated replacement cost of \$1322M for 2.0-m SLR. The building receptor class contributed substantially to the overall protected shoreline inundation and flooding pathway vulnerability of the installation. For civil infrastructure, evaluation of roadways indicated no significant vulnerability to inundation for the 1.0-m SLR scenario, increasing to about 43 km for the 2.0-m SLR scenario. This range increased somewhat for flooding vulnerability (100-year event) with 1 and 70 km impacted for the 1.0- and 2.0-m SLR scenarios, respectively. Airfield vulnerability from protected shoreline inundation and flooding was projected to be limited to SLR scenarios of 1.5 m or higher. Airfield and storm drain vulnerabilities were estimated to be in the range of \$0M to \$10M based on the replacement cost of operationally impacted elements. Waterfront and coastal structures showed vulnerabilities in the range of 1.0 to 2.0 m of SLR, with the replacement costs of operationally impacted structures ranging as high as \$648M for waterfront structures and \$78M for coastal structures under the 2.0-m SLR scenario.

Overall vulnerability estimates for the summed replacement value metric of receptors included in the inundation and flooding pathway analysis ranged from negligible for the baseline SLR inundation scenario, to as high as ~ \$2113M for the 2.0- m SLR flooding scenario. This estimate was largely driven by vulnerability associated with buildings and water front structures, but with significant contributions from other categories as well.

Table 4-10. Receptor-level vulnerability assessment summary for Naval Base Coronado based on the exposed shoreline erosion pathway.

		Condition							Rece	eptor								√ €
.e	a)			Training			Buile	lings					Civil					wa) (\$№
ena	Occurance	ndi		ITallillig		Buildings				Ro	ads	Airf	ield	Storm	Rec	1	atn lue	
J Sc	cur			Metric			Metric						Metric				ľ	7 L S
Long-Term Scenario	First Oc	Short-Term	Remaining Width (m) Remaining Area (%) Replacemen t Value (\$M)		Number of Buildings	Building Area (m²) Replacemen t Value (\$M)		Building MDI > 55	Eroded Length (km)	Replacemen t Value (\$M)	Eroded Area (m²)	Replacemen t Value (\$M)	Eroded Length (m)	Replacemen t Value (\$M)	Eroded Area (m²)		Total Erosion Pathway Replacement Value (\$M)	
٤	2000	Week	142	97%	\$ -	0	0	\$ -	0	0.00	\$ -	0	\$ -	0	\$ -	0	\$	-
= 0.0 r		Month	128	86%	\$ -	0	0	\$ -	0	0.00	\$ -	0	\$ -	0	\$ -	0	\$	-
0		Year	104	67%	\$ -	3	157740	\$ 0	1	0.00	\$ -	0	\$ -	23	\$ 0.02	0	\$	0.1
SLR		Decade	92	59%	\$ -	14	195974	\$ 20	3	0.00	\$ -	0	\$ -	114	\$ 0.11	216	\$	20.4
		Century	85	53%	\$ -	17	339440	\$ 27	4	0.05	\$ 0	0	\$ -	292	\$ 0.27	9738	\$	27.5
Ε		Week	108	72%	\$ 140	0	0	\$ -	0	0.00	\$ -	0	\$ -	18	\$ 0.02	0	\$	139.9
0.5 1	2046	Month	94	61%	\$ 140	2	120	\$ 0	0	0.00	\$ -	0	\$ -	42	\$ 0.04	0	\$	139.9
II		Year	72	45%	\$ 140	15	167637	\$ 27	2	0.00	\$ -	0	\$ -	285	\$ 0.26	0	\$	167.3
SLR		Decade	61	38%	\$ 140	18	195760	\$ 34	3	0.14	\$ 0	0	\$ -	533	\$ 0.49	10992	\$	174.8
		Century	54	33%	\$ 140	25	340306	\$ 55	7	0.87	\$ 1	0	\$ -	711	\$ 0.66	24686	\$	195.9
Ε		Week	82	53%	\$ 250	13	8703	\$ 2	3	0.00	\$ -	0	\$ -	93	\$ 0.09	0	\$	252.0
1.0	99	Month	69	44%	\$ 250	16	166180	\$ 27	3	0.00	\$ -	0	\$ -	274	\$ 0.25	0	\$	276.9
II	2069	Year	48	29%	\$ 250	23	197096	\$ 33	6	0.66	\$ 0	0	\$ -	709	\$ 0.65	6057	\$	283.9
SLR		Decade	38	23%	\$ 250	38	860953	\$ 144	10	2.01	\$ 1	0	\$ -	912	\$ 0.84	27469	\$	396.1
		Century	34	20%	\$ 250	44	935679	\$ 166	13	3.13	\$ 2	0	\$ -	1024	\$ 0.94	41305	\$	418.7
٤		Week	58	37%	\$ 387	13	164611	\$ 27	3	0.51	\$ 0	0	\$ -	476	\$ 0.44	0	\$	414.3
1.5	37	Month	45	28%	\$ 387	22	196033	\$ 35	5	0.84	\$ 1	0	\$ -	718	\$ 0.66	621	\$	422.6
11	2087	Year	27	16%	\$ 387	42	877446	\$ 148	11	2.58	\$ 2	0	\$ -	1016	\$ 0.94	24493	\$	537.8
SLR		Decade	20	12%	\$ 387	53	1064362	\$ 183	16	3.75	\$ 3	0	\$ -	1241	\$ 1.15	46949	\$	573.9
		Century	16	10%	\$ 387	58	1077056	\$ 187	16	3.97	\$ 3	0	\$ -	1350	\$ 1.25	61394	\$	578.1
٤		Week	36	23%	\$ 551	23	319713	\$ 50	6	1.29	\$ 1	0	\$ -	872	\$ 0.80	1084	\$	602.8
2.0 m	00	Month	25	15%	\$ 551	34	812910	\$ 133	12	1.74	\$ 1	0	\$ -	1027	\$ 0.95	11317	\$	685.9
II.	2100	Year	11	7%	\$ 551	56	1075436	\$ 186	16	4.07	\$ 3	0	\$ -	1348	\$ 1.24	43580	\$	741.3
SLR		Decade	6	4%	\$ 551	56	1081583	\$ 187	16	4.69	\$ 3	0	\$ -	1525	\$ 1.41	66960	\$	743.0
		Century	4	2%	\$ 551	61	1084541	\$ 189	17	5.34	\$ 4	0	\$ -	1648	\$ 1.52	79072	\$	744.9

Table 4-11. Receptor-level vulnerability assessment summary for Naval Base Coronado based on the exposed shoreline inundation and flooding pathway.

										Receptor							, -
.9		ion		Training				Buildings					Civil				/νa) (\$Ν
ena	nce	ndit		Hallillig				bullulligs		Ro	ads	Air	ield	Storm	Drains	Rec	ath) ue (
Sce	nra	Ö		Metric				Metric					Metric			n Pi Val	
Long-Term Scenario	First Occurance	Short-Term Condition	Remaining Width (m)	Remaining Area (%)	Replacement	Value (\$M)	Number of Buildings Depth>0.3 m	Replacement Value (\$M)	Building MDI > 55	Inund/Flood Length (km)	Replacement Value (\$M)	Inund/Flood Area (m2)	Replacement Value (\$M)	Number of Inlets	Replacement Value (\$M)	Inund/Flood Area (m²)	Total Erosion Pathway Replacement Value (\$M)
Ε		Week	130	89%	\$	-	0	\$ -	0	0.00	\$ -	0	\$ -	0	\$ -	268	\$ -
0.0	0	Month	129	88%	\$	-	0	\$ -	0	0.00	\$ -	0	\$ -	0	\$ -	340	\$ -
= 0.0	2000	Year	123	84%	\$	-	18	\$ 198	9	9.09	\$	32252	\$ 2.17	12	\$ 0.68	107184	\$ 206.8
SLR		Decade	95	65%	\$	-	295	\$ 1,940	59	42.47	\$ 25	127548	\$ 8.58	140	\$ 7.88	232500	\$ 1,985.2
		Century	50	34%	\$	-	542	\$ 2,906	83	67.48	\$ 4.	152464	\$ 10.26	213	\$ 11.99	306524	\$ 2,973.2
Ε		Week	89	61%	\$	140	2	\$ 3	0	2.06	\$. 0	\$ -	4	\$ 0.23	352	\$ 144.2
0.5 r	2046	Month	79	54%	\$	140	7	\$ 133	6	6.91		304	\$ 0.02	6	\$ 0.34	404	\$ 277.9
H		Year	65	44%	\$	140	182	\$ 1,347	52	32.52	\$ 2	99592	\$ 6.70	105	\$ 5.91	155076	\$ 1,521.2
SLR	`	Decade	23	15%	\$	140	590	\$ 3,129	87	74.72	\$ 50	193832	\$ 13.04	252	\$ 14.18	360864	\$ 3,346.5
		Century	11	8%	\$	140	742	\$ 3,022	93	83.46	\$ 50	218924	\$ 14.73	293	\$ 16.49	440292	\$ 3,248.8
Ε		Week	42	29%	\$	250	31	\$ 216	9	8.90	•	4492	\$ 0.30	17	\$ 0.96	72920	\$ 473.2
1.0 r	6	Month	31	21%	\$	250	67	\$ 440	12	12.27	\$	42340	\$ 2.85	29	\$ 1.63	116188	\$ 702.8
Ш	2069	Year	15	11%	\$	250	405	\$ 2,218	61	55.13	\$ 3	167092	\$ 11.24	176	\$ 9.91	310960	\$ 2,526.4
SLR	`	Decade	5	3%	\$	250	794	\$ 2,911	93	86.87	\$ 5	308944	\$ 20.78	314	\$ 17.67	463804	\$ 3,258.1
•		Century	1	1%	\$	250	881	\$ 2,783	103	92.03	\$ 6	343064	\$ 23.08	339	\$ 19.08	479916	\$ 3,136.5
Ε		Week	26	18%	\$	387	118	\$ 728	21	23.64	\$ 1	67304	\$ 4.53	56	\$ 3.15	136980	\$ 1,138.7
1.5 n	7	Month	18	12%	\$	387	219	\$ 1,429	54	39.46	\$ 2	104724	\$ 7.04	124	\$ 6.98	161640	\$ 1,856.6
П	2087	Year	7	5%	\$	387	697	\$ 3,039	88	81.49	\$ 5	252348	\$ 16.98	290	\$ 16.32	421704	\$ 3,513.9
SLR	`	Decade	1	1%	\$	387	909	\$ 2,621	109	98.85	\$ 6	419160	\$ 28.20	397	\$ 22.35	493584	\$ 3,125.4
Ŭ,		Century	0	0%	\$	387	1014	\$ 2,805	125	104.96	\$ 7	606232	\$ 40.78	458	\$ 25.78	508396	\$ 3,329.1
Ε		Week	7	5%	\$	551	360	\$ 2,010	62	53.12	\$ 30	132076	\$ 8.88	155	\$ 8.72	246100	\$ 2,614.8
2.0 n	0	Month	4	3%	\$	551	557	\$ 2,912	77	71.59	\$ 48	172924	\$ 11.63	212	\$ 11.93	327808	\$ 3,535.5
H	2100	Year	0	0%	\$	551	858	\$ 2,784	103	92.08	\$ 63	376684	\$ 25.34	352	\$ 19.81	483788	\$ 3,441.9
SLR	`	Decade	0	0%	\$	551	1127	\$ 2,961	148	112.31	\$ 70	920052	\$ 61.89	555	\$ 31.24	521336	\$ 3,681.0
٥,		Century	0	0%	\$	551	1143	\$ 3,013	150	114.74	\$ 7	1148304	\$ 77.25	592	\$ 33.32	527620	\$ 3,751.9

Table 4-12. Receptor-level vulnerability assessment summary for Naval Base Coronado based on the protected shoreline inundation and flooding pathway.

				Buildings					Civil				Wate	rfront Stru	rtures	Coa	. =		
.e		ion				Ro	ads	Airf		Storm	Drains	Rec	wate		ctures		way (\$M		
ena	nce	ndit		Metric					Metric		1			Metric			ath ue (
Long-Term Scenario	First Occurance	Short-Term Condition	Number of Buildings Depth>0.3 m	Replacement Value (\$M)	Building MDI > 55	Inund/Flood Length (km)	Replacement Value (\$M)	Inund/Flood Area (m2)	Replacement Value (\$M)	Number of Inlets	Replacement Value (\$M)	Inund/Flood Area (m²)	Number of Structures Overtopped	Replacement Value (\$M)	Number of Operationally Impacted Structures	Overtopped Length (m)	Replacement Value (\$M)	Number of Operationally Impacted Structures	Total Erosion Pathway Replacement Value (\$M)
٤		Week	1	\$ 0	0	0.00	\$ -	0	\$ -	0	\$ -	0	0	0	0	0	0	0	\$ 0.1
= 0.0 m	00	Month	1	\$ 0	0	0.00	\$ -	0	\$ -	0	\$ -	0	0	0	0	0	0	0	\$ 0.1
=	2000	Year	1	\$ 0	0	0.00	\$ -	0	\$ -	0	\$ -	0	0	0	0	0	0	0	\$ 0.1
SLR		Decade	1	\$ 0	0	0.00	\$ -	0	\$ -	0	\$ -	0	0	0	0	0	0	0	\$ 0.1
		Century	1	\$ 0	0	0.00	\$ -	0	\$ -	0	\$ -	0	0	0	0	0	0	0	\$ 0.1
Ε	2046	Week	21	\$ 72	0	0.00	\$ -	0	\$ -	2	\$ 0.11	0	0	0	17	0	0	0	\$ 71.7
= 0.5 m		Month	21	\$ 72	0	0.00	\$ -	0	\$ -	2	\$ 0.11	0	0	0	17	0	0	0	\$ 71.7
=	20	Year	21	\$ 72	0	0.00	\$ -	0	\$ -	2	\$ 0.11	0	0	0	19	0	0	0	\$ 71.7
SLR		Decade	22	\$ 72	0	0.00	\$ -	0	\$ -	2	\$ 0.11	0	0	0	19	0	0	0	\$ 72.3
-		Century	22	\$ 72	0	0.00	\$ -	0	\$ -	2	\$ 0.11	0	0	0	29	0	0	0	\$ 72.3
Ε		Week	22	\$ 72	0	0.00	\$ -	0	\$ -	3	\$ 0.17	0	0	0	29	0	0	0	\$ 72.4
= 1.0 m	2069	Month	22	\$ 72	0	0.00	\$ -	0	\$ -	3	\$ 0.17	0	0	0	30	0	0	0	\$ 72.4
 	20	Year	22	\$ 72	0	0.00	\$ -	0	\$ -	3	\$ 0.17 \$ 0.23	0	0	0	31	0	0	0	\$ 72.4
SLR		Decade	22 26	\$ 72 \$ 75	0	0.00	\$ - \$ 1	0	\$ - \$ -	4	7 0.1.2	0 236	17	42 346	31	0	0	3	\$ 114.7 \$ 421.5
		Century		'	1	1.00	·	0		5	' '		19		32		0	4	
Ε		Week	58 66	\$ 111 \$ 133	11	10.37 11.24	\$ 7 \$ 8	6712 12092	\$ 0.45 \$ 0.81	34 39	\$ 1.91 \$ 2.20	560 632	29	383	32	1488	31	5 5	\$ 534.2 \$ 557.6
= 1.5 m	2087	Month	84	\$ 133 \$ 151	11 15	13.41	\$ 8 \$ 9	19140	\$ 1.29	48	\$ 2.20 \$ 2.70	672	29	383 383	32 32	1488	31	5	\$ 557.6 \$ 578.3
<u>۲</u>	20	Year Decade	107	\$ 151	20	15.41		32796	\$ 1.29	54	\$ 2.70	716	29	383	32	1488 2476	31 54	7	\$ 578.3
SLR			196	\$ 296	40	33.71	\$ 10 \$ 23	63644	\$ 4.28	92	\$ 5.18	76344	29 31	580	32	2664	5 4	7	\$ 964.9
-		Century	273	\$ 488	57	43.32		83024	\$ 5.59	126	\$ 7.09	82540	31	580	32	4019	-	7	\$ 1,188.0
E		Week Month	318	\$ 488	59	43.32	\$ 29 \$ 33	83024 87400	\$ 5.88	134	\$ 7.09	82540 85840	31	580	32	4019	78 78	7	\$ 1,188.0
= 2.0 m	2100	Year	386	\$ 795	70	54.62	\$ 33	94388	\$ 5.88	134	\$ 7.54	91252	32	648	32	4019	78 78	7	\$ 1,289.8
SLR =	21	Decade	447	\$ 1.027	70	59.50	\$ 40	102812	\$ 6.92	154	\$ 8.67	142532	32	648	32	4019	78	7	\$ 1,808.5
SL		Century	584	\$ 1,027	81	69.59	\$ 40	129480	\$ 8.71	190	\$ 10.69	183232	32	648	32	4019	78 78	7	\$ 1,808.5
Ц		century	J0 4	2,342 ب	OT	05.55	47 ب	123400	0./1	150	90.09 ج	103232	34	040	32	4013	70		ح.د۲۱۲

4.4.2 Receptor-Level Assessment - Marine Corps Base Camp Pendleton

Methods for the assessment of sea level rise vulnerability at MCBCP were evaluated primarily for the receptor-level of analysis. The analysis included the baseline conditions, four SLR scenarios, and five return period events. The analysis results quantified potential impacts from SLR in terms of replacement cost, quantity, area, and MDI value, as applicable. Following is a summary of the metrics and vulnerability thresholds for each receptor category.

Training Areas

The beach training areas at MCBCP evaluated here included areas on the exposed shoreline of the installation between the Del Mar area at the south and San Onofre at the north. The analysis focused on the erosion and inundation/flooding pathway impacts on the selected beach training areas including Gold Beach, Red Beach, White Beach, Blue Beach, and the San Onofre Beach. The beach width remaining relative to Mean Sea Level was used to quantify the impacts of SLR to the beach training areas. The analysis for MCBCP differs from NBC in that the training areas are generally backed by erodible cliffs, rather than by fixed infrastructure as is the case at NBC. Because the cliff erosion was also modeled, the landward boundary of the beach training area was allowed to retreat inland at the rate of retreat of the cliff base. Thus, the width of the training areas generally increased with time, and the beach width remaining was a function of the difference between retreat of the shoreline and the retreat of the cliff base. The exception to this was for the area of Blue Beach where the training beach is not backed by cliffs, and the back of the training beach was assumed to be fixed relative to existing infrastructure in the Del Mar area. Similarly to NBC, the erosion modeling included the existing sand budget deficit for the littoral cell. At MCBCP, this sand deficit is significant and contributes substantially to the erosion independent of whether or not there is erosion due to sea level rise.

Exposed Shoreline Erosion Pathway

Results for the analysis are shown in Figure 4-206 as the average beach width remaining for all training areas. The relatively large reduction in beach width between the baseline condition and the 0.5-m SLR condition reflected the 46 years of sand budget deficit combined with SLR impact, and the expected slow erosion of the cliffs (subaerial only) that occurred until the beach becomes narrow enough for wave attack on the cliff. As the beaches narrowed and the waves attacked the cliff on a regular basis (in accordance with the CDPM model), the cliff retreat accelerated, and the change in beach width decelerated, thus stabilizing to some degree the remaining width of the training beach. Using a comparable response threshold to the 50% reduction that was applied at NBC, Figure 4-206 indicates that, on average, impacts to training beaches would be expected for all SLR conditions at return periods of yearly or greater, for SLR of 1.0 m and greater for the monthly return period condition, and for SLR of 1.5 m and greater for the weekly return period condition.

However, the continued reduction in average beach width after 2046 was largely driven by the narrowing of the training area at Blue Beach under the assumption of a fixed back boundary for this training beach. The other training beaches all stabilized and variations after 2046 were generally small decreases that were regulated by spatial variations in the balance of the beach erosion and the cliff erosion (Figure 4-207). This also reflected the fact that these more northern training areas already had relatively narrow beaches.

The cost impacts of SLR-driven erosion on the beach training areas were estimated by determining the quantity of sand (beach nourishment) that would be required to maintain the baseline beach width. Historically, beach nourishment projects were not executed at a fixed frequency, and tended to be conducted on an as-needed basis. Based on the analysis conducted for this project, beach nourishment projects could be executed for the MCBCP portion of the Oceanside Littoral Cell at a

10-year interval with the sand volume required to maintain the existing beach width. The estimate included both the portion associated with sea level rise, and the portion associated with the estimated sand budget deficit. The sand replenishment volume needed to keep pace with SLR and the sand deficit increased from 4.4-million cm in 2010 to 58 million cm in 2100. Note that these volumes neglected the contribution of sand from cliff erosion since this input was assumed to be relatively small if the beach widths were maintained such that the cliffs were protected from wave attack. The unit cost for a beach nourishment project depends on the total sand volume and dredge equipment mobilization costs. A unit cost of \$23.50 per cubic meter was used to estimate the cost of maintaining the existing beach width. The unit cost was based on a recent beach nourishment project in San Diego. See Figure 4-208 for a plot of a sand volume and replacement cost versus time for the MABCP portion of the Oceanside Littoral Cell.

Exposed Shoreline Inundation and Flooding Pathway

The beach training areas at MCBCP were analyzed for inundation and flooding impacts based on a spectrum (week – century) of return period total water level exposures over the eroded shoreline position for each SLR scenario. The water depths and flooded areas were calculated for all areas landward of the baseline shoreline position. The assessment results indicated the percentage inundate/flooded, water depth, beach width and beach area for each SLR scenario and return period event. The data provide a basis for understanding both the potential magnitude and frequency of inundation and flooding conditions that could inform command personnel on the future ability to sustain beach training activities. The average beach width subject to inundation (weekly return) increased from about 43 m under the baseline scenario to a maximum of about 180 m under the 2.0-m SLR scenario (Figure 4-209). Note that these widths were measured from a common reference location of NAVD88 = 0 m. The beach width remaining narrowed substantially under inundation, especially between the baseline and 0.5-m SLR scenario, reducing from about 70 m on average, to about 24 m under the 0.5-m SLR scenario, then further to a width of only 16 m under the 2.0-m SLR scenario (Figure 4-210). The majority of this reduction occurred in the first half of the century as the back beach was eroded (up to about 0.5-m SLR), and then the cliff erosion rate accelerated under wave attack and the beach widths stabilized. This stability was also a function of the assumption that the back boundary of the training areas were allowed to retreat in concert with the location of the cliff base. Under flooding (100-year return period condition), the average beach width flooded increased from about 92 m for the baseline condition to a high of about 190 m for the 2.0-m SLR scenario. The beach width remaining under flooding was low in all cases, ranging from a high of about 21 m in the baseline scenario to a low of only 6 m in the 2.0-m SLR scenario.

Buildings

The receptor-level assessment methodology was applied for buildings at MCBCP on an installation-wide basis for erosion and inundation/flooding for each SLR scenario. Buildings along the coast of MCBCP were largely limited to areas in the south at Del Mar, and in the north near San Onofre (Figure 4-211). The impacts of SLR to the buildings were quantified using replacement cost, area, MDI value, and exterior water depth. Some buildings in the database did not include replacement costs. These buildings were assigned an estimated replacement cost based on the average unit replacement cost of the buildings within the erosion footprint for the 100-year return period event of the 2.0-m SLR scenario. The average unit replacement cost used was \$2,727 per sq. meter.

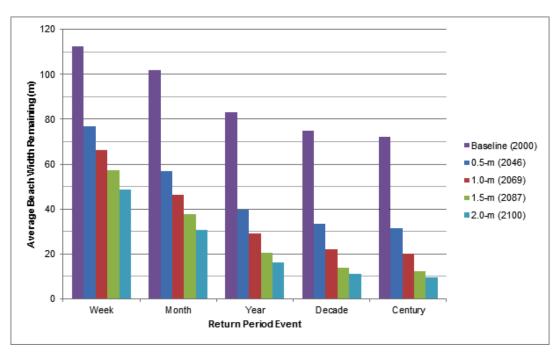


Figure 4-206. Erosion pathway assessment of average beach width impacts to training areas at MCBCP. The average beach width decreases by approximately 10 m for each SLR scenario.



Figure 4-207. Erosion pathway assessment of beach width impacts to individual beach training areas at MCBCP for the monthly return period condition.

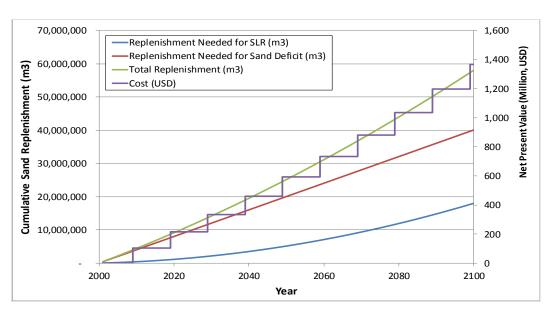


Figure 4-208. The sand replenishment volume required for both SLR and the sand deficit at MCBCP beaches. The associated costs are to maintain the existing baseline beach width.

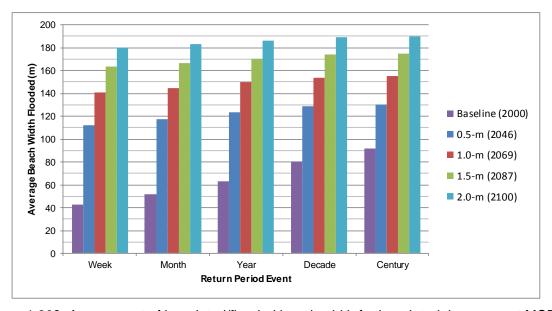


Figure 4-209. Assessment of inundated/flooded beach width for beach training areas at MCBCP.

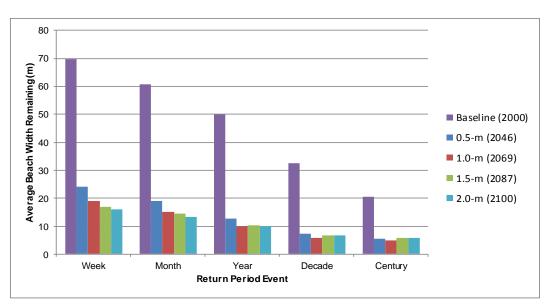


Figure 4-210. Inundation and flooding pathway assessment of beach width remaining for beach training areas at MCBCP.



Figure 4-211. View of the northern coastline of MCBCP showing buildings, transportation corridors and recreational areas potentially vulnerable to erosion under future SLR scenarios (from California Coastal Records Project Image 200803818, Copyright (C) 2002-2014 Kenneth & Gabrielle Adelman, California Coastal Records Project, www.Californiacoastline.org).

Exposed Shoreline Erosion Pathway

The erosion pathway analysis determined the quantity (Figure 4-212) and replacement cost Figure 4-213 and Figure 4-187) of the buildings within the erosion footprint for each SLR scenario. If a building was located within the erosion footprint, then the full replacement cost of the building was used to quantify the impacts of that scenario. As with the training areas, the results showed a relatively large increase in erosion impact to buildings between the baseline condition and the 0.5-m SLR condition that reflected the 46 years of sand budget deficit combined with SLR impact between 2000 and 2046.

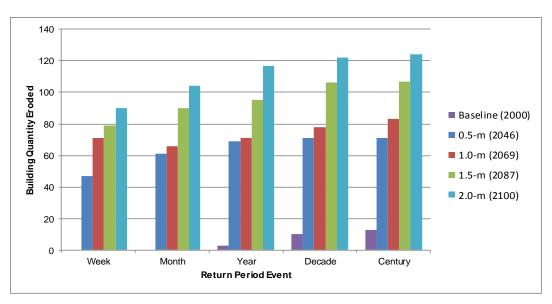


Figure 4-212. Erosion pathway analysis of buildings at the exposed shoreline of MCBCP. The quantity of buildings within the beach erosion footprint for each SLR scenario and return period event.

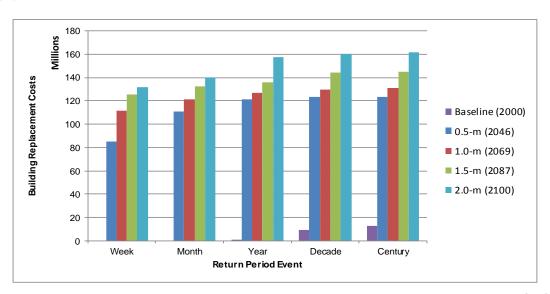


Figure 4-213 Total replacement cost of buildings within the beach erosion footprint at MCBCP.

The erosion damage to buildings was sensitive to both the return period event analyzed and the SLR scenario. For the 0.5-m SLR scenario, the number of buildings within the erosion footprint ranged from 47 under the weekly return period erosion event, to a high of 71 for the 100-year return period event. For 2.0 m of SLR, the number of buildings increased to 90 for the weekly return and 124 for the 100-year return, with corresponding replacement values ranging from about \$131M to \$162M.

Exposed Shoreline Inundation and Flooding Pathway

The inundation and flooding pathway assessment was based on the maximum exterior water depth at each building. The three flood depth ranges described in Section 3.4.1 were used for assessing the vulnerability of the buildings to different flood depths under the receptor-level methodology. The three flood depth ranges corresponded to increasing levels of damage and operational impacts. For example, the total number and replacement value of buildings in the highest depth range (> 1 m) are

shown in Figure 4-214 and Figure 4-215. Inundation as represented by the weekly return period condition impacted a very small number of buildings with water depths of this magnitude for the baseline condition, increasing to about 117 buildings with a replacement value of about \$158M under the 2.0-m SLR scenario. The buildings included in the baseline inundation footprint were generally anomalous and result as a function of the buffer zone used to calculate inundation and flood depths spanning into the small boat harbor area for buildings that were directly adjacent to the harbor. Less frequent flooding events impacted increasingly large number of buildings with the 2.0-m SLR 100-year return period event estimated to impact 191 buildings with an estimated replacement cost of about \$246M.

Waterfront Structures

Waterfront structures at MCBCP are limited to small craft support facilities in the Del Mar Boat Basin. The Del Mar Boat Basin provides a small craft harbor for barge landings, small craft moorings, recreational boats, and boat ramps. These facilities are protected from wave exposure by the harbor jetty, and the facilities are less vulnerable to sea level rise related impacts because they do not have a fixed fender system or significant utility services that are typically vulnerable to sea level rise related impacts at an elevation below the deck elevation.

Protected Shoreline Inundation and Flooding Pathway

Overall, the inundation and flood impacts for these structures is a function of the overtopping elevation. The boat ramps and barge landing platform at MCBCP are typically configured with the top of slope elevation equal to the adjacent roadway elevation. The ramp is designed to accommodate the tidal range, and will generally have the ability to accommodate SLR. Boat ramps will not be damaged by flooding, but may have short-term operational impacts during high tides.

The recreational floating dock at MCBCP is attached to a fixed-elevation quaywall with access by a brow that transitions from shore to the docks. Floating docks are designed to accommodate the current tidal range inside the harbor, thus are generally able to accommodate SLR. The vulnerable items of a floating dock system are the guide piles that secure the dock in position and the brow. The maximum operational water level for a floating dock is a function of the bending capacity of the pile, the strength of the soil, and the elevation of the top of guide pile. At MCBCP, the top of guide piles are approximately +4.0 m. In the future, floating docks may require higher capacity guide piles or adjustments to the brow connection details to accommodate SLR.

Coastal Structures

The coastal structures at MCBCP are primarily rock revetments and jetties at the Del Mar Boat Basin and a large seawall that protects SONGS. These structures are primarily subject to inundation and flooding exposure along the protected shorelines of the harbor. The DEM and record drawings were used to acquire critical functional and operational elevations for the screening level assessment of these coastal structures. When the DEM was used to obtain a structure's elevation, several cross sections would be evaluated and an average value was applied.

For the purposes the receptor-level assessment, if a coastal structure was overtopped for any SLR scenario during any return period event, it was considered as requiring replacement. A replacement value of each affected structure per unit length was derived based on design details of similar structures in the region. High-resolution aerial imagery was used to acquire the length of these structures when record drawings were unavailable. Applying full replacement value for revetments and jetties in this analysis is a conservative approach, as rock could be added to these structures at a lesser cost to increase protection.

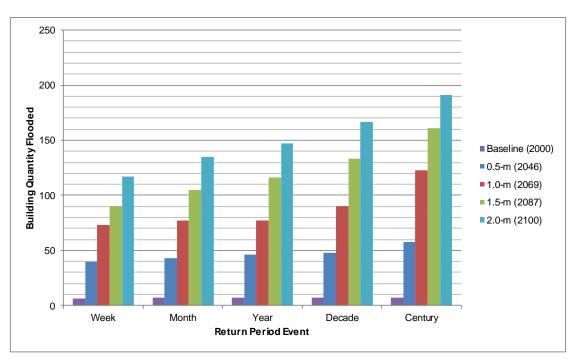


Figure 4-214. Inundation and flooding pathway analysis for buildings via the exposed shoreline of MCBCP showing the quantity of buildings within the inundation and flooding footprint with water depth exceeding 1 m for each SLR scenario and return period event.

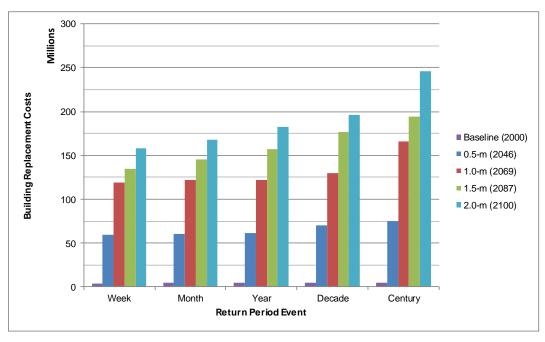


Figure 4-215. Total replacement cost of buildings within the exposed shoreline inundation/flooding footprint at MCBCP with water depth exceeding 1 m.

Exposed Shoreline Inundation and Flooding Pathway

The exposed shorelines with engineered coastal structures included the seawall at SONGS and the north and south jetties at Del Mar. The analysis indicated minimal impacts for the baseline and 0.5-m SLR scenarios, and increasing levels of impact for SLR scenarios of 1.0 m and above (Figure 4-216). These structures included only the south jetty and the south jetty head at Del Mar, while the north jetty at Del Mar and the seawall at SONGS were not projected to be overtopped under any of the SLR scenarios. Replacement costs associated with these impacts ranged from about \$14M to \$20M.

Protected Shoreline Inundation and Flooding Pathway

Within the harbor at Del Mar, there are a series of revetments that protect the shoreline. In general, these revetments are protected from wave exposure by the jetty, and so they were evaluated as protected shoreline structures, although in some areas near the harbor entrance they may receive some wave exposure. No overtopping of these structures was expected for SLR scenarios of 1.0 m or less. For the 1.5-m SLR scenario, overtopping was projected but only for the 100-year return period condition, while for the 2.0-m SLR scenario, overtopping was expected for all return period conditions (Figure 4-217). This overtopping was projected to be limited to the revetment inside the Del Mar Boat Basin with a replacement cost of about \$11M. Note that the relatively flat impact response as a function of return period is explained by the uniformity of the total water levels for exposure along protected shorelines where the variability in sea level is primarily related to tides.

Civil Infrastructure

Selected receptor subcategories of the civil infrastructure at MCBCP were analyzed to illustrate potential erosion, inundation and flood impacts including roads, airfields, storm water infrastructure, and recreation areas. For the erosion analysis, the area (or length) of the asset inside of the erosion footprint was tabulated for each scenario. For the inundation and flooding analysis, the wetted areas and water depths were determined for each asset. The metrics used to quantify the impacts of SLR to the civil infrastructure were the area eroded or flooded, replacement cost, and average water depth. Under the range of SLR conditions examined in the study, the roadways near exposed shorelines were shown to be vulnerable to erosion at or above the 0.5-m SLR scenario, and flooding for at or above the 1.5-m SLR scenario. The airfields were not within the erosion footprint, but were found to be vulnerable to flooding for all scenarios but progressively increasing with higher SLR scenarios. Minimal low-lying portions of the storm water infrastructure were found to be vulnerable to reduced efficiency under SLR scenarios of 0.5 m and higher, which could lead to localized increased flooding during rain events (although precipitation impacts were not examined in this study). A summary of the analysis for each subcategory is provided below.

Roads

At MCBCP the roads were defined in the GIS database provided by the installation as a polygon shapes from which eroded or inundated/flooded areas were calculated directly from the relevant footprints. The estimated unit replacement cost of a typical two-lane roadway was estimated at \$67.27 per square meter, which includes replacement of the roadway base and asphalt paving. The cost assessment did not include the replacement of adjacent land area, the soil material beneath the roadway subgrade, environmental-related costs (permitting, mitigation, etc.). The volume of fill material lost below the roadway was determined as part of the beach erosion analysis. For MCBCP, many of the roadways that fell within the impacted areas were graded dirt roads rather than paved, so the replacement cost estimate may be overly conservative. Also, because the proportion of roadways in the areas of protected shorelines was very small, no separate analysis for the protected shoreline areas was conducted.

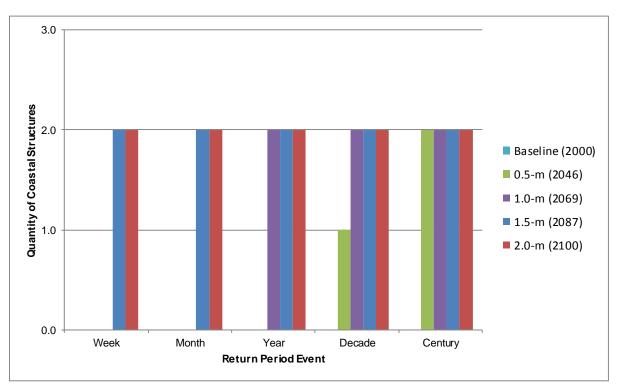


Figure 4-216. Receptor-level estimate of the number of coastal structures impacted by inundation and flooding along the exposed shorelines at MCBCP.

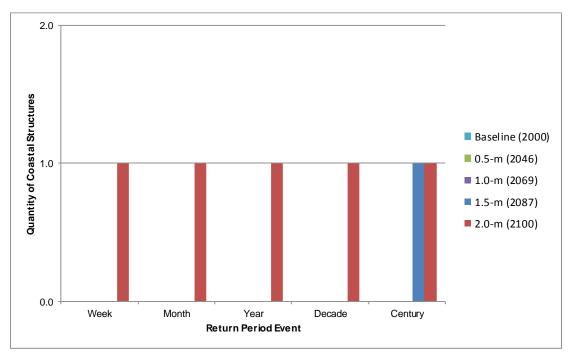


Figure 4-217. Receptor-level estimate of the number of coastal structures impacted by SLR along the protected shorelines at MCBCP.

Exposed Shoreline Erosion Pathway. The erosion assessment for the roadways at MCBCP calculated the total area and corresponding rough order of magnitude replacement cost of roadways within the erosion footprint for each SLR scenario. Roadway erosion was primarily a function of the SLR scenario, with very limited impacts expected for the baseline condition, but progressively higher impacts for higher sea levels (Figure 4-218). For the 100-year return period wave erosion event, the estimated area of roadway erosion ranged from a low of about 5000 m² for the baseline scenario, to a high of about 213000 m² for the 2.0-m SLR scenario. Corresponding replacement costs ranged from about \$333K to \$14.3M.

Exposed Shoreline Inundation and Flooding Pathway. For the exposed shoreline inundation and flooding pathway, roadways with average water depths greater than 0.15 m were assumed to result in operational impacts to the installation. These scenarios and water depths did not consider the additional impacts of a rain event. For inundation (weekly return period), the estimated length of impacted roadway ranged from about 0.7 km for the baseline scenario to a high of about 17.2 km for the 2.0-m SLR scenario. For flooding under the 100-year return period condition, the estimated length of flooded roadway increased from 5.8 km for the baseline scenario to about 28.7 km for the 2.0-m SLR scenario, with a corresponding range of replacement values ranging from about \$3.9M to \$19.3M. See Figure 4-219.

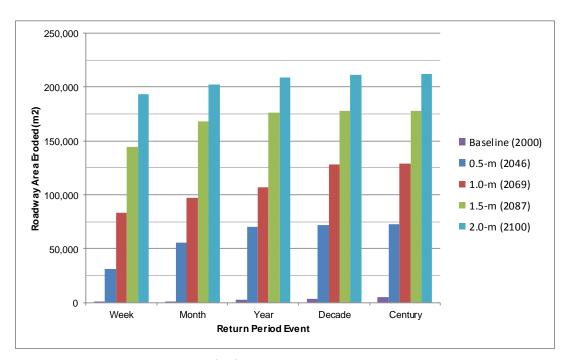


Figure 4-218. Roadway erosion at MCBCP showing the estimated roadway eroded area for each SLR scenario.

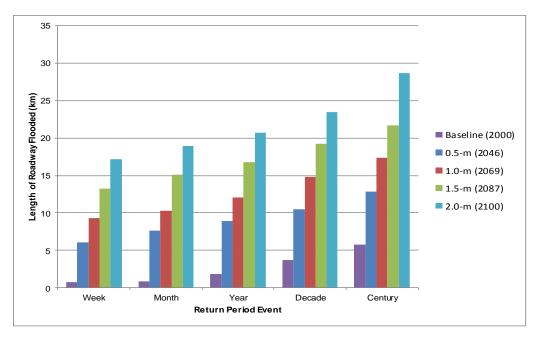


Figure 4-219. Roadway inundation and flooding at exposed shorelines of MCBCP.

Airfields

The receptor-level assessment of the airfields at MCBCP included runways, helicopter pads, and miscellaneous airfield pavement areas near the coast. The assessment included the erosion pathway for the exposed shoreline, and the inundation and flooding pathway for the exposed shorelines only. At MCBCP, the vulnerability of airfields to operational and damage impacts from flooding are distinct from roadways because most of the airfield areas are situated above the bluffs and thus are not readily exposed to sea level rise.

Exposed Shoreline Erosion Pathway. The erosion pathway assessment determined that the airfields at MCBCP were not located within the erosion footprint. However, under the expected erosion scenarios, the shoreline position moves closer to the airfields, offering less protection from future erosion and flooding events.

Exposed Shoreline Inundation and Flooding Pathway. The exposed shoreline inundation and flooding analysis for MCBCP indicated that there would be no inundation or flooding of airfields under any of the SLR scenarios evaluated

Storm Water Infrastructure

The storm water conveyance system at MCBCP controls storm water runoff during and after a rain event. The storm water system uses gravity flow with outlets to the Del Mar Basin and the Pacific Ocean. Storm water infrastructure along the coast of MCBCP is limited to relatively small systems in the Del Mar area and in the north near SONGS.

Exposed Shoreline Erosion Pathway. The erosion pathway assessment of the stormwater drainage system determined the length of underground drain pipe within the erosion footprint for each SLR scenario. The rough order of magnitude replacement cost of the storm drainage system was calculated for each SLR scenario. A unit replacement cost used for the system was estimated at \$922.74 per linear meter for a 0.6-m-diameter reinforced concrete pipe with inlets at 61 m on center. The erosion impacts to the storm water drainage system were very limited, ranging from no impacts under the baseline scenario, to a maximum of about 77 m of drain pipe within the erosion footprint

for the 100-year return period wave erosion combined with 2.0 m of SLR. The estimated replacement cost for this worst-case scenario was about \$71K. See Figure 4-220.

Exposed Shoreline Inundation and Flooding Pathway. The inundation and flooding pathway assessment of the storm water drainage system estimated the water depth at each storm water drainage inlet. In general, the storm drain inlets are located at the low points of paved areas to collect water and thus may be subject to intrusion from elevated water levels, or to flooding from overtopping waves. A water depth of 0.3 m at the inlet was used as a threshold limit for operational impacts to the associated roads, buildings, and parking areas that the storm water system drains. The total number of inlets identified within the GIS was 1765. Of these, the number subject to inundation (weekly return condition) was negligible, ranging from one for the baseline scenario to two for the 2.0-m SLR scenario. For flooding (100-year return period condition), the number of inlets with water depths of 0.3 m or higher ranged from two for the baseline scenario to a high of 19 for the 2.0-m SLR scenario, representing about 0.1 to 1.1% of the total number of inlets at MCBCP, respectively (Figure .4-202).

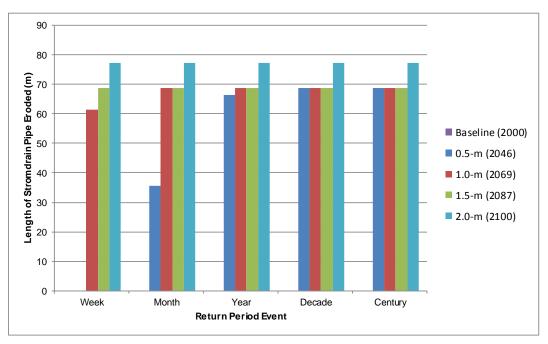


Figure 4-220. Exposed shoreline erosion pathway assessment of storm water conveyance system at MCBCP.

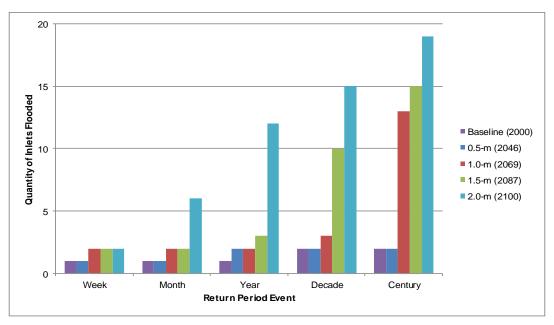


Figure 4-221. Inundation and flooding pathway assessment of stormwater drainage system at exposed shoreline of MCBCP. The quantity of stormwater inlets with flood depths greater than 0.3 m is shown.

Recreational Areas

The recreational areas included a number low-lying elements near the beach such as camping areas and ball fields. The assessment included the erosion pathway for the exposed shoreline, and the inundation and flooding pathway for the exposed shorelines. The recreational areas would likely be closed while flooded and may cause damage to grass covered areas from exposure to saltwater. The analysis determined the area impacted from erosion and flooding for each SLR scenario. A replacement value was not estimated for recreational areas.

Exposed Shoreline Erosion Pathway. The erosion pathway assessment determined the area of recreational spaces within the erosion footprint for each SLR scenario, as well as the fraction of the total recreational area that this represented. The results showed very limited impacts to recreation areas with a maximum of about 3400 m^2 (< 0.3%) of recreational areas impacted by 2.0-m of SLR combined with a 100-year return period erosion event (Figure 4-222).

Exposed Shoreline Inundation and Flooding Pathway. The exposed shoreline inundation and flooding pathway assessment of recreational areas also determined the area and percent of area impacted. For inundation (represented by the weekly return period), the impacted area was negligible for the baseline scenario (Figure 4-223), and increased to a maximum of about $3200 \text{ m}^2 (\sim 0.2\%)$ for the 2.0-SLR scenario. Flooding impacts for the 100-year return period were somewhat higher ranging from 2200 m^2 for the baseline scenario, to a high of about $4000 \text{ m}^2 (\sim 0.3\%)$ for the 2.0-m SLR scenario.

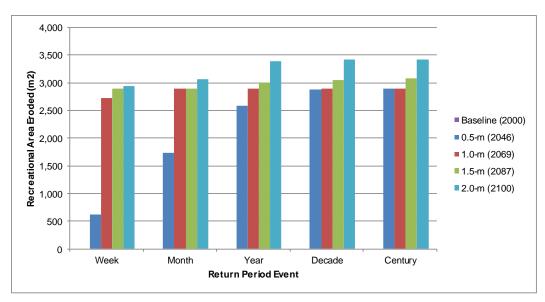


Figure 4-222. Erosion pathway assessment for recreational areas at MCBCP determined the percentage of recreational area within the erosion footprint.

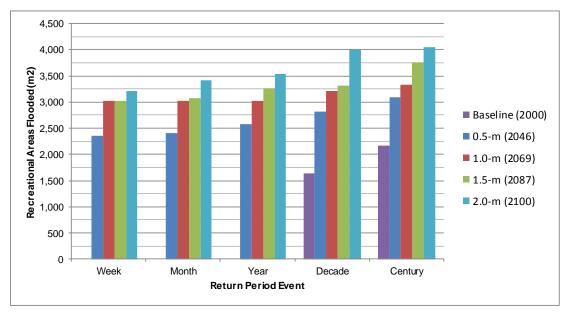


Figure 4-223. Exposed shoreline inundation and flooding pathway assessment for recreational areas of MCBCP determined the percentage of recreational area flooded.

Receptor-Level Vulnerability Assessment Summary - Marine Corps Base Camp Pendleton

As described above, sea level rise vulnerability of a range of MCBCP installation receptors was evaluated as a means of illustrating the application of the methodologies developed in this study. Vulnerability was evaluated as a function of receptor class for different exposure pathways and a range of potential future sea level rise scenarios. While the receptors evaluated here represent only a subset of those present at the installation, they do provide a representative cross-section of the infrastructure that could be vulnerable to sea level rise. Thus, a cumulative summary of the vulnerability provides a sense of which receptor classes tend to be more vulnerable, as well as the overall magnitude of the vulnerability across receptor classes.

Erosion Pathway

The overall vulnerability of MCBCP to sea level rise for the erosion pathway is summarized in Table 4-13 under the prescribed sea level rise conditions and the assumed sand budget deficit of 15 m³/m. The summary incorporated key receptors including training areas, buildings and civil infrastructure, and multiple metrics of response across the full range of both long-term sea level rise scenarios and short-term erosion events of various return periods. In general, the summary illustrates the increasing level of vulnerability to erosion as a function of increasing sea level, as well as the sensitivity of some receptors to short-term wave driven erosion events. For training areas, this translated into frequent (weekly return period) conditions with average beach widths reduced to about 66 m and a remaining area of about 41% of baseline for 1.0-m SLR (first occurrence by 2069), and further reductions to an average beach width of about 49 m and a remaining area of 27% of baseline for 2.0-m SLR (first occurrence by 2100). To preserve year 2000 beach widths, significant beach replenishment would be required with estimated costs in the range of \$732M to \$1366M for the 1.0- and 2.0-m SLR scenarios, respectively, potentially the largest contribution to the overall erosion pathway vulnerability of the installation if retreat is not considered a viable option.

For buildings, weekly return period conditions resulted in erosion pathway vulnerability to about 66 structures for 1.0-m SLR, 12 of which had an estimated MDI > 55 ("Relevant" classification or higher), and with an estimated replacement cost of about \$112M. This increased to about 90 structures and 14 with MDI > 55, with an estimated replacement cost of \$132M for 2.0-m SLR. The building receptor class also contributed substantially to the overall erosion pathway vulnerability of the installation. For civil infrastructure, roadways were the primary class of receptors evaluated here that indicated significant vulnerability with replacement costs in the range of \$56M to \$130M for the 1.0- and 2.0-m SLR scenario, respectively. Overall vulnerability estimates for the receptors included in the erosion pathway analysis ranged from less than \$1M for the baseline SLR scenario to as high as ~ \$1600M for the 2.0 m SLR scenario. This estimate was largely driven by "replacement cost" associated with beach replenishment, and it should be noted that if this replenishment were to take place then the other erosion impacts would be largely mitigated, so the total number should be viewed as a measure of summed vulnerability rather than a measure of the actual costs that might occur for a given scenario.

Exposed Shoreline Inundation and Flooding Pathway

Vulnerability of MCBCP receptors to sea level rise for the exposed shoreline inundation and flooding pathway is summarized in Table 4-14. The summary incorporated key receptors including training areas, buildings and civil infrastructure, coastal structures, and multiple metrics of response across the full range of both long-term sea level rise scenarios and short-term flooding events of various return periods. In general, the summary illustrates the increasing level of vulnerability to inundation and flooding as a function of increasing sea level and increasingly extreme short-term events flooding, but the results also reflect the relative resilience of MCBCP to inundation and flooding as a function of the generally steep nature of the installation topography, and the buffering effect of the coastal cliffs. Beach training areas were one of the most sensitive receptors to inundation and flooding, with inundation impacts reflected in reductions in average beach widths to about 24 m and a remaining area of about 17% for only 0.5-m SLR (first occurrence by 2046), and further reductions to an average beach width of only about 16 m and a remaining area of 10% for 2.0-m SLR (first occurrence by 2100). While infrequent flooding events can potentially be accommodated through scheduling, flooding impacts (100-year return period condition) were more significant with the nearly the entirety of the beach training areas (5% remaining) being subject to flooding for SLR scenarios of about 0.5 m and above (first occurrence by 2046). Replacement costs for inundation and flooding of training areas were assumed to be equivalent to those estimated for the erosion pathway,

because flooding events simply occur over top of the eroded shoreline, and the shoreline is generally expected to recover from storm driven wave events naturally. The replacement costs simply provide a metric of the value of the asset value that is subject to operational limitations due to inundation and flooding.

For buildings, inundation (weekly return) resulted in vulnerability to about 77 structures for 1.0-m SLR 11 of which had an estimated MDI > 55 ("Relevant" classification or higher), and with an estimated replacement cost of about \$122M. This roughly doubled to about 148 structures and 28 with an estimated MDI > 55, with an estimated replacement cost of \$183M for 2.0-m SLR. The building receptor class was more vulnerable to flooding impacts (100-year return period) with about 158 potentially flooded structures for 1.0-m SLR 30 of which had an estimated MDI >55 ("Relevant" classification or higher), and with an estimated replacement cost of about \$193M. This increased to about 200 structures and 35 with an estimated MDI >55, with an estimated replacement cost of \$250M for 2.0-m SLR. For civil infrastructure, evaluation of roadways indicated vulnerability to inundation with about 9 km operationally impacted for the 1.0-m SLR scenario, increasing to about 17 km for the 2.0 m SLR scenario. This range roughly doubled for flooding vulnerability (100-year event) with 17 and 29 km impacted for the 1.0- and 2.0-m SLR scenarios, respectively. Airfields at MCBCP were not projected to contribute significantly to installation SLR vulnerability for inundation or flooding.

Overall vulnerability estimates for the summed replacement value metric of receptors included in the inundation and flooding pathway analysis ranged from about \$4M for the baseline SLR inundation scenario, to as high as ~ \$1656M for the 2.0-m SLR flooding scenario. This estimate is largely driven by vulnerability associated with training areas, but with significant contributions from other categories as well.

Protected Shoreline Inundation and Flooding Pathway

The only receptor categories that were assessed for this pathway at MCBCP were the waterfront and coastal structures. The limited vulnerabilities for these receptors were described previously and were not included in the overall summaries. Also note that the seawater intrusion analysis was not incorporated in the summary, although some level of vulnerability was projected for extraction wells closer to the coast and particularly under the highest SLR scenario (2.0 m) and in combination with future increases in pumping rates.

4.4.3 Component-Level Assessment Examples

The component-level assessment methodologies described in Section 3.4.2 focus on refinement of the assumptions, methods, and data used during the receptor-level assessment to provide a more quantitative analysis and reduce uncertainties. Here we focused on methodological considerations for the component-level assessment in the context of the evaluation of vulnerability for the designated receptors, and especially for those receptors that have characteristics that are relatively unique to military installations. While a facility-wide component-level assessment was beyond the scope of this effort, example applications from the two installations are described below. The detailed assessment examples are provided to show how operational limits and impacts are determined for specific components of infrastructure within each receptor category. A majority of the examples are from NBC because detailed asset information was available from past construction projects.

Training Area Example

Beach training activities are a fundamental aspect of the mission at both NBC and MCBCP. Following the methodology described in Section 3.4.2, we combined the available data from the receptor-level analysis with more detailed data on specific beach training operations to illustrate the

application of the component-level assessment methodology for training areas. Detailed information on the training activities conducted at NBC were derived from the Silver Strand Training Complex (SSTC) Consistency Determination (Department of the Navy, 2011). This document was used to assess the impacts of increased training adjacent to sensitive habitats located at the beach and bay training areas at NBC. Included in the report are figures and tables that describe the location and type of training activities conducted at SSTC north and south. Below we illustrate the approach for the "Causeway Pier Insertion and Retraction" training activity at NBC.

Causeway Pier Insertion and Retraction

This training activity requires heavy equipment both landside and waterside. Causeway Section Powered/Warping Tug and Barge Ferrys make up the main building blocks for the modular causeway section and Elevated Causeway System (ELCAS) activities. The causeway sections are 24-ft by 80-ft platforms configured from compatible floating pontoons. Causeway sections are assembled to configure three subsystems: Floating Causeway, Roll On/Roll Off Discharge Facility (RRDF), and Causeway Ferry. The OUB (Offshore Petroleum Discharge System [OPDES] Utility Boat) to support ship to shore transfer of fluids.

Bulldozers dig notches in the beach in order to make an anchor point for the floating pier which is beached using a barge ferry. Pier sections are added end-to-end until the causeway extends out over the surf zone – see Figure 4-224. Training is conducted on both older causeway systems and on the newer, Improved Navy Lighterage System (INLS). The activity occurs at SSTC-N Boat and Beach Lanes 3 through 10 and Bravo Beach.

This training activity lasts approximately 5 days and occurs approximately 10 times per year. The minimum beach width required for this activity can be estimated based on the landside area necessary for the bulldozers to operate, and the turning area necessary for the vehicles to access the causeway. A staging area for the vehicles is also required on land. Based on the activity diagram shown in Figure 4-225, the required beach width for this activity was estimated to be about half of the current condition width or ~ 80 m.

Given the frequency and duration of the training activity, and the required beach width, the appropriate component-level analysis was conducted within the context of the 25 scenarios developed for the site. Based on the frequency of 10 training events per year, we assumed that training would be impacted by return periods of monthly frequency or less, and that events with return periods of one year or greater could be accommodated by schedule flexibility. Given the minimum requirement of ~ 80-m beach width, it is apparent from Figure 4-226 that this operational threshold is maintained under weekly and monthly return period events for SLR up to about 0.5 m. For SLR > 0.5 m, the operational beach width threshold would be impacted, and clearly even at SLR of 1.0 m the beach width is reduced to about 30 m under the monthly return period, which would be substantially lower than the requirement. The analysis was refined further by looking at the individual training lanes (Figure 4-227). This illustrated, for example, that while most of the training lanes at SSTC North remained operational up to and somewhat beyond 0.5 m of SLR, the training lanes at SSTC South were generally narrower to begin with and thus become narrower than the operational limit at SLR below 0.5 m. While these numbers are approximations, they illustrate the manner in which the command personnel that plan these training activity could utilize this approach to assess sustainability of specific beach training operations.

Table 4-13. Receptor-level vulnerability assessment summary for MCBCP based on the exposed shoreline erosion pathway.

									Rece	eptor							
		uo		Tuelalas			D!I.						Civil				ω W
Jari	Se	ditic		Training			Build	dings		Ro	ads	Airf	ield	Storm	Rec	hw e (\$	
Scer	First Occurance	Con		Metric			Me	tric		Metric							Pat /alu
Long-Term Scenario		Short-Term Condition	Remaining Width (m)	Remaining Area (%)	~ `		Building Area (m²)			Eroded Length (km)	Replacement Value (\$M)	Eroded Area (m²)	Replacement Value (\$M)	Eroded Length (m)	Replacement Value (\$M)	Eroded Area (m²)	Total Erosion Pathway Replacement Value (\$M)
ے	2000	Week	113	100%	\$ -	0	0	\$ -	0	0.03	\$ 0	0	\$ -	0	\$ -	0	\$ 0.2
= 0.0 m		Month	102	88%	\$ -	0	0	\$ -	0	0.03	\$ 0	0	\$ -	0	\$ -	0	\$ 0.2
0 =		Year	83	67%	\$ -	3	2112	\$ 1	1	0.23	\$ 2	0	\$ -	0	\$ -	0	\$ 2.4
SLR		Decade	75	59%	\$ -	10	30094	\$ 9	3	0.38	\$ 3	0	\$ -	0	\$ -	0	\$ 12.0
L°,		Century	72	56%	\$ -	13	30470	\$ 13	3	0.50	\$ 3	0	\$ -	0	\$ -	0	\$ 16.1
Е		Week	77	53%	\$ 459	47	32252	\$ 85	8	3.12	\$ 21	0	\$ -	0	\$ -	624	\$ 565.2
2	2046	Month	57	36%	\$ 459	61	33953	\$ 111	10	5.54	\$ 37	0	\$ -	36	\$ 0.03	1740	\$ 607.4
= 0.		Year	40	22%	\$ 459	69	37097	\$ 122	12	7.04	\$ 47	0	\$ -	66	\$ 0.06	2588	\$ 628.1
SLR		Decade	33	18%	\$ 459	71	41342	\$ 123	12	7.17	\$ 48	0	\$ -	69	\$ 0.06	2886	\$ 630.5
,		Century	32	17%	\$ 459	71	41342	\$ 123	12	7.24	\$ 49	0	\$ -	69	\$ 0.06	2895	\$ 631.0
_		Week	66	41%	\$ 732	66	36925	\$ 112	12	8.37	\$ 56	0	\$ -	61	\$ 0.06	2732	\$ 900.3
1.0 m	6	Month	47	26%	\$ 732	71	37600	\$ 122	12	9.72	\$ 65	0	\$ -	69	\$ 0.06	2895	\$ 919.4
= 1	2069	Year	29	15%	\$ 732	78	43938	\$ 127	13	10.71	\$ 72	0	\$ -	69	\$ 0.06	2895	\$ 931.1
SLR	,,	Decade	22	11%	\$ 732	83	48248	\$ 130	14	12.85	\$ 86	0	\$ -	69	\$ 0.06	2895	\$ 948.4
"		Century	20	10%	\$ 732	84	50005	\$ 131	14	12.89	\$ 87	0	\$ -	69	\$ 0.06	2895	\$ 949.8
		Week	57	33%	\$ 1,035	79	39810	\$ 125	12	14.47	\$ 97	0	\$ -	69	\$ 0.06	2895	\$ 1,257.5
1.5 m	7	Month	38	21%	\$ 1,035	90	50127	\$ 132	14	16.78	\$ 113	0	\$ -	69	\$ 0.06	2895	\$ 1,280.0
= 1	2087	Year	21	11%	\$ 1,035	95	54835	\$ 136	15	17.60	\$ 118	0	\$ -	69	\$ 0.06	3012	\$ 1,289.2
SLR	2	Decade	14	7%	\$ 1,035	106	58338	\$ 144	15	17.76	\$ 119	0	\$ -	69	\$ 0.06	3056	\$ 1,298.4
1 "		Century	12	6%	\$ 1,035	107	58349	\$ 145	15	17.79	\$ 120	0	\$ -	69	\$ 0.06	3085	\$ 1,299.6
		Week	49	27%	\$ 1,366	90	48769	\$ 132	14	19.33	\$ 130	0	\$ -	77	\$ 0.07	2938	\$ 1,627.8
2.0 m	0	Month	31	17%	\$ 1,366	104	53966	\$ 140	16	20.26	\$ 136	0	\$ -	77	\$ 0.07	3060	\$ 1,642.8
= 2.	2100	Year	16	9%	\$ 1,366	117	59523	\$ 157	18	20.87	\$ 140	0	\$ -	77	\$ 0.07	3396	\$ 1,663.9
SLR:	2	Decade	11	6%	\$ 1,366	122	60249	\$ 160	21	21.17	\$ 142	0	\$ -	77	\$ 0.07	3428	\$ 1,668.6
55		Century	10	5%	\$ 1,366	124	61164	\$ 162	21	21.25	\$ 143	0	\$ -	77	\$ 0.07	3428	\$ 1,671.1

Table 4-14. Receptor-level vulnerability assessment summary for MCBCP based on the exposed shoreline inundation and flooding pathway.

									Receptor										
				Training			Buildings					Civil				Cos	. =		
9.		ion		ITallillig					Ro	ads	Airf		Storm	Drains	Rec	Coa	Metric	uies	νay \$Ν
anaı	nce	ndit		Metric		Metric						Metric					ath ue (
Long-Term Scenario	First Occurance	Short-Term Condition	Remaining Width (m)	Remaining Area (%)	Replacement Value (\$M)	Number of Buildings Depth>0.3 m	Replacement Value (\$M)	Building MDI > 55	Inund/Flood Length (km)	Replacement Value (\$M)	Inund/Flood Area (m2)	Replacement Value (\$M)	Number of Inlets	Replacement Value (\$M)	Inund/Flood Area (m²)	Overtopped Length (m)	Replacement Value (\$M)	Number of Operationally Impacted Structures	Total Erosion Pathway Replacement Value (\$M)
Ε		Week	70	64%	\$ -	7	\$ 4	0	0.72	\$ 0	0	\$ -	1	\$ 0.06	0	0	0	0	\$ 4.8
SLR = 0.0 m	2000	Month	61	57%	\$ -	7	\$ 4	0	0.86	\$ 1	0	\$ -	1	\$ 0.06	0	0	0	0	\$ 4.8
= (20	Year	50	48%	\$ -	7	\$ 4	0	1.82	\$ 1	0	\$ -	1	\$ 0.06	0	0	0	0	\$ 5.5
SLF		Decade	32	34%	\$ -	7	\$ 4	0	3.73	\$ 3	0	\$ -	2	\$ 0.11	1632	0	0	0	\$ 6.8
-		Century	21	22%	\$ -	15	\$ 9	3	5.79	\$ 4	0	\$ -	2	\$ 0.11	2160	0	0	2	\$ 13.0
Ε		Week	24	17%	\$ 459	46	\$ 62	7	6.09	\$ 4	0	\$ -	1	\$ 0.06	2358	0	0	0	\$ 524.9
= 0.5	2046	Month	19	14%	\$ 459	48	\$ 70	7	7.62	\$ 5	0	\$ -	1	\$ 0.11	2406	0	0	0	\$ 534.2
<u>۳</u>	20	Year	13 7	10% 7%	\$ 459 \$ 459	50 59	\$ 70 \$ 76	8 9	8.95 10.50	\$ 6 \$ 7	0	\$ - \$ -	2	\$ 0.11 \$ 0.11	2574 2822	0 528	0 14	2	\$ 535.2 \$ 556.7
SLR		Decade	5	5%	\$ 459 \$ 459	81	\$ 76 \$ 96	14	12.89	\$ 7	0	\$ - \$ -	2	\$ 0.11	3094	724	20	2	\$ 583.7
		Century Week	19	13%	\$ 732	77	\$ 122	11	9.34	\$ 6	0	\$ - \$ -	2	\$ 0.34	3015	0	0		\$ 861.0
٤		Month	15	11%	\$ 732	90	\$ 130	15	10.24	\$ 7	0	\$ - \$ -	2	\$ 0.11	3015	0	0	2	\$ 868.9
= 1.0 m	2069	Year	10	8%	\$ 732	103	\$ 141	18	12.09	\$ 8	0	\$ -	2	\$ 0.11	3015	724	20	2	\$ 900.7
SLR =	2(Decade	6	6%	\$ 732	130	\$ 167	25	14.82	\$ 10	0	\$ -	3	\$ 0.11	3215	724	20	2	\$ 929.1
SI		Century	5	5%	\$ 732	158	\$ 193	30	17.33	\$ 12	0	\$ -	13	\$ 0.84	3323	724	20	2	\$ 957.0
		Week	17	11%	\$ 1,035	117	\$ 158	23	13.28	\$ 9	0	\$ -	2	\$ 0.11	3015	724	20	2	\$ 1,221.7
Ε.		Month	15	10%	\$ 1,035	132	\$ 176	26	15.13	\$ 10	0	\$ -	2	\$ 0.17	3071	724	20	2	\$ 1,240.6
= 1.5	2087	Year	10	8%	\$ 1,035	147	\$ 181	28	16.74	\$ 11	0	\$ -	3	\$ 0.34	3263	724	20	2	\$ 1,247.0
SLR =	2	Decade	7	6%	\$ 1,035	167	\$ 203	33	19.27	\$ 13	0	\$ -	10	\$ 0.84	3315	724	20	2	\$ 1,270.9
S		Century	6	5%	\$ 1,035	182	\$ 238	35	21.68	\$ 15	0	\$ -	15	\$ 0.96	3754	724	20	2	\$ 1,308.1
		Week	16	10%	\$ 1,366	148	\$ 183	28	17.18	\$ 12	0	\$ -	2	\$ 0.17	3219	724	20	2	\$ 1,580.4
0 m		Month	13	9%	\$ 1,366	166	\$ 196	32	18.91	\$ 13	0	\$ -	6	\$ 0.56	3423	724	20	2	\$ 1,594.5
= 2.	2100	Year	10	7%	\$ 1,366	178	\$ 209	33	20.73	\$ 14	0	\$ -	12	\$ 0.84	3542	724	20	2	\$ 1,609.4
SLR = 2.0 m	2	Decade	7	6%	\$ 1,366	192	\$ 244	35	23.49	\$ 16	0	\$ -	15	\$ 0.96	3990	724	20	2	\$ 1,646.8
03		Century	6	5%	\$ 1,366	200	\$ 250	35	28.72	\$ 19	0	\$ -	19	\$ 1.13	4045	724	20	2	\$ 1,656.2



Figure 4-224. Elevated Causeway System training activity. The causeway is anchored to shore, and extends beyond the surf zone (U.S. Navy photo by Mass Communication Specialist 2nd Class Bryan Niegel).

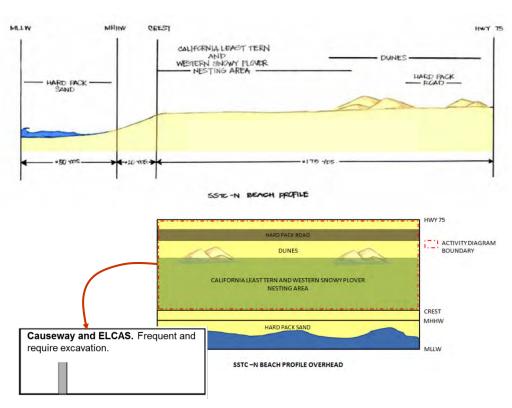


Figure 4-225. Estimated activity footprint for the elevated causeway training activity at STTC including typical beach profile (above), plan view of a training lane (middle), and activity footprint (bottom left) (adapted from U.S. Navy, 2010).

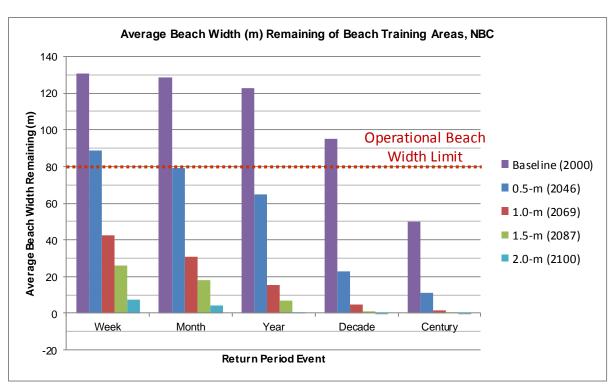


Figure 4-226. Average beach width remaining for all training areas at SSTC as a function of SLR and return period inundation and flooding events.

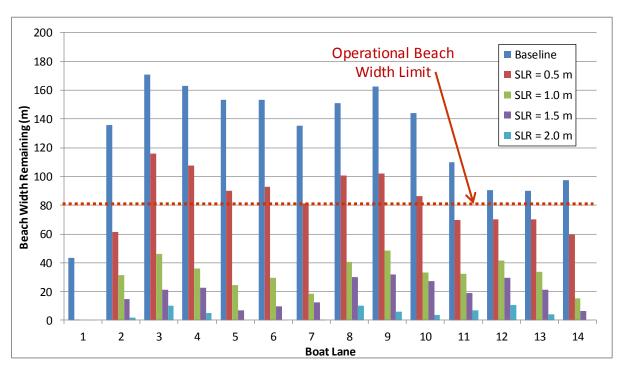


Figure 4-227. Beach width remaining by training lane at SSTC for the monthly return period flood event.

Building Examples

Buildings support a wide range of operations and missions of the installation including housing, logistics, training, testing, operations, and security. Buildings located adjacent to the shore may be exposed to ocean waves, boat wakes, erosion, flooding or inundation. Buildings located away from the shoreline may be flooded from intrusion of water through the storm water conveyance system during high tide elevations or from inadequate drainage during a rain. A general overview of the critical elevations and the corresponding impacts to operational capability of a building can be represented by a graph of water elevation versus operational capability. Buildings with common construction and function may have similar operational limits curves. Examples of the development of operational limits for two buildings at Naval Base Coronado are presented below. Comparison of these operational curves to estimated total water levels for a range of SLR scenarios then provides a basis for the more detailed component-level assessment.

CVN Warehouse at Berth Juliet at NAS Coronado

The CVN Warehouse located adjacent to Berth Juliet at NBC provides storage space to support CVN aircraft carriers moored at the facility (Figure 4-228 through Figure 4-230). The warehouse has roll-up doors and a loading dock ramp. The finish floor elevation of the warehouse is +3.92 m NAVD. The low end of the loading dock ramp is at +2.7 m. The exterior grade slopes away from the warehouse to a minimum grade elevation of +3.12 m at the storm water inlets. The inboard edge of the Berth Juliet wharf is +3.7 m.

The building is composed of a concrete slab-on-grade with concrete masonry unit walls to a height of 1.5 m above finish grade, and a steel frame above. The building is supported by shallow foundations that consist of spread footings for the columns and grade beams for the walls. The wall system and floor have a low vulnerability to flood damage. The building contains a small office and lounge area that has interior partitions that may be composed of metal studs with drywall and insulation. The drywall and insulation is vulnerable to flood damage. The building electrical system typically includes Alternating Current (AC) power, lighting, and telephone. The electrical outlets and points of connection are vulnerable to SLR damage. Other building utilities may include water and sewer, which are less vulnerable to SLR damage.

Based on the building characteristics described above, operational limits were developed for comparison to SLR scenarios. A component-level assessment of the building indicated that the building was vulnerable to SLR damage, limited access, intrusion and flooding under certain SLR scenarios. For the 0.5-m SLR scenario, the loading dock ramp flooded at a 2-month return period (Figure 4-231). With 1.0 m of SLR, the low areas near the building flooded from intrusion of water from San Diego Bay through the storm water drainage system (Figure 4-232). For the 1.5-m SLR scenario, the 100-year return period event water level reached the finish floor elevation of the warehouse (Figure 4-233). For the 2.0 m SLR scenario, the water level exceeded a depth of 0.3 m inside of the warehouse (Figure 4-234).



Figure 4-228. A portion of Berth Juliet at NAS Coronado is shown. The yellow outline indicates the CVN Warehouse (image: Google).

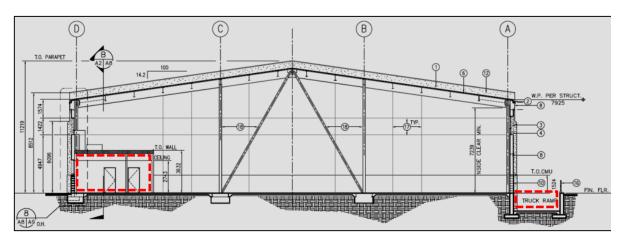


Figure 4-229. The CVN Warehouse at NBC showing a cross-section through the building. Note the truck ramp on the right and an office/lounge area on the left side of the figure.

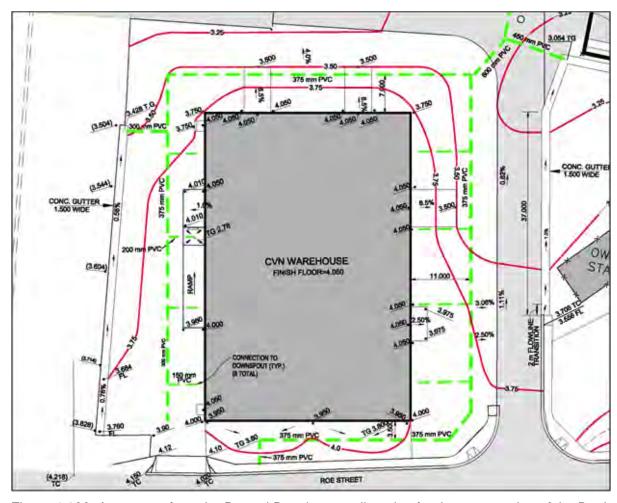


Figure 4-230. An excerpt from the Record Drawings grading plan for the construction of the Berth Juliet wharf, buildings and other improvements. The red lines indicate elevation contours in meters relative to MLLW. The green dashed lines indicate a below grade storm water drainage system.

Helicopter Training Facility at NAS Coronado

The helicopter training facility is located adjacent to Moffett Road on the north side of NAS Coronado (Figure 4-235). The building is used as a flight training complex with flight simulators and other antisubmarine weapons systems. The building also contains offices and classrooms to support the training activities.

The building is a braced-frame steel structure with building columns supported by conventional spread footings. The flight simulator equipment create powerful dynamic forces on the foundation as they imitate real aircraft movements. The poor-soil bearing capacity and high dynamic loads required the simulator equipment to have a pile foundation that is isolated from the building.

The grade elevation, floor elevation and vault floor elevations were estimated using the DEM and tools developed by the SERDP Project Team. Based on this analysis, the average grade elevation was +4.5 m. An architectural feature of this building was that some exterior areas berm up towards the building to lessen the height of the walls – see Figure 4-236. So, the typical assumptions for first floor elevation compared to grade elevation were not accurate. The first floor elevation was approximately 0.76 m below exterior grade for some areas, and equivalent to grade for other portions. The exterior grade elevation varied from +3.75 m to +4.5 m.

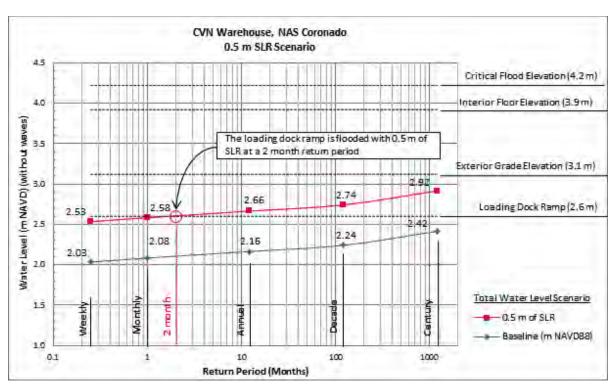


Figure 4-231. Operational limits for the CVN Warehouse, NBC in comparison to the 0.5-m SLR scenarios.

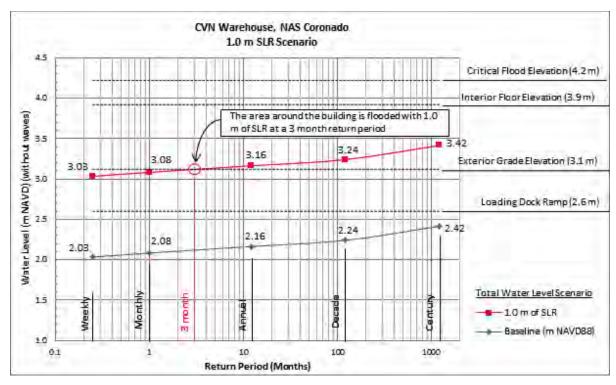


Figure 4-232. Operational limits for the CVN Warehouse, NBC in comparison to the 1.0-m SLR scenarios.

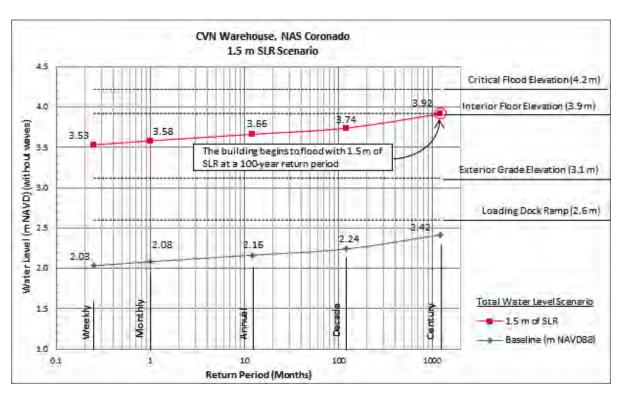


Figure 4-233. Operational limits for the CVN Warehouse, NBC in comparison to the 1.5 m SLR scenarios.

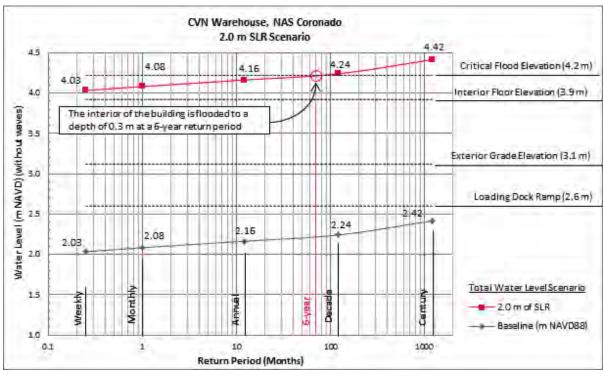


Figure 4-234. Operational limits for the CVN Warehouse, NBC in comparison to the 2.0 m SLR scenarios.

The building is located close to San Diego Bay. The existing seawall may be overtopped for future SLR scenarios (Figure 4-237 and Figure 4-238). If the seawall is overtopped, the building will be vulnerable to boat wakes and wind-driven waves or overtopping waters that have an approximate height of 0.5 m. Adjacent to the building is a below-grade electrical vault that contains a 69-kV substation. The electrical vault is vulnerable to flooding. The vault was designed for buoyant forces because of the close proximity to the bay and high water table. The floor of the electrical vault is approximately 2.3 m below grade, at an elevation of +2.2 m.

Based on the building characteristics described above, operational limits were developed for comparison to SLR scenarios. A component-level assessment of the building indicated that the building was vulnerable to SLR damage, limited access, intrusion, and flooding. For the 0.5-m SLR scenario, the below-grade electrical vault had increased buoyant forces, although damage was not expected (Figure 4-239). With 1.0 m of SLR, the electrical vault had further increased buoyant forces, and damage may occur (Figure 4-240). The storm water drainage system was projected to have reduced efficiency and localized flooding during a rain event. For the 1.5-m SLR scenario, the 25-year return period event water level reached the finish floor elevation of the warehouse (Figure 4-241). For the 2.0-m SLR scenario, the water level exceeded a depth of 0.3 m inside of the warehouse at a 2-month return period (Figure 4-242).



Figure 4-235. Naval Base Coronado looking north at the Helicopter Training Facility. The building is located approximately 70 ft from San Diego Bay.



Figure 4-236. Naval Base Coronado with the Helicopter Training Facility as seen from Moffett Road. The exterior surface (lawn) berms up towards the building to lessen the impact of the wall elevation. The interior finish floor is approximately 30-in. below adjacent exterior grade.

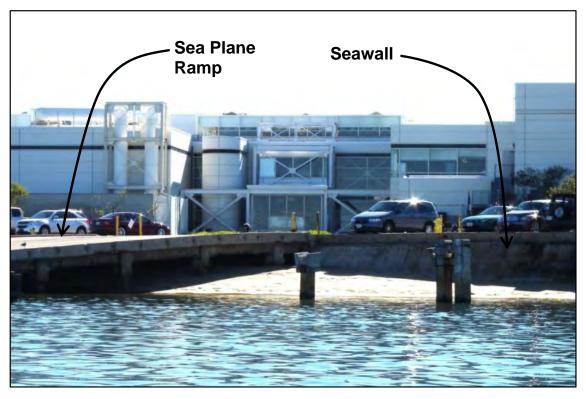


Figure 4-237. View from San Diego Bay looking south, the Helicopter Training Facility can be seen in the background. A concrete seawall provides shore protection.



Figure 4-238. View from San Diego Bay looking southeast at the seawall that protects Moffett Road and the Helicopter Training Facility.

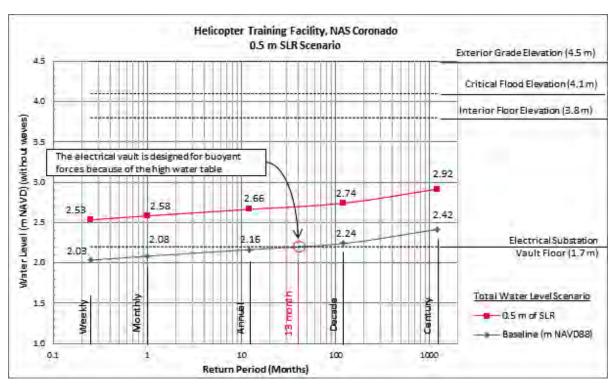


Figure 4-239. Operational limits for the Helicopter Training Facility, NBC in comparison to the 0.5-m SLR scenarios.

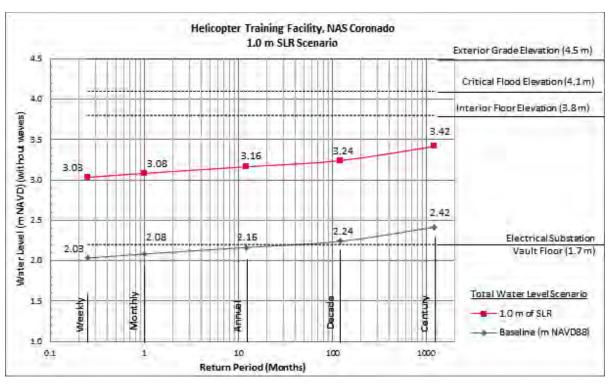


Figure 4-240. Operational limits for the Helicopter Training Facility, NBC in comparison to the 1.0-m SLR scenarios.

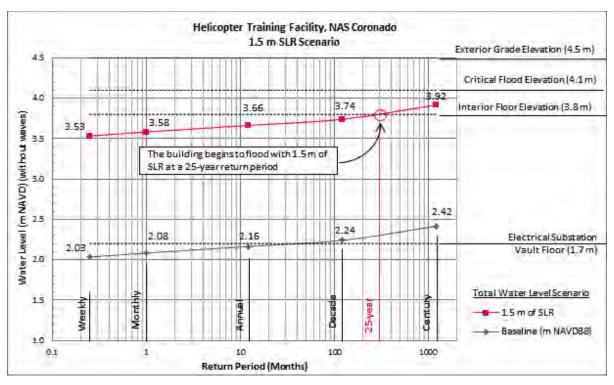


Figure 4-241. Operational limits for the Helicopter Training Facility, NBC in comparison to the 1.5-m SLR scenarios.

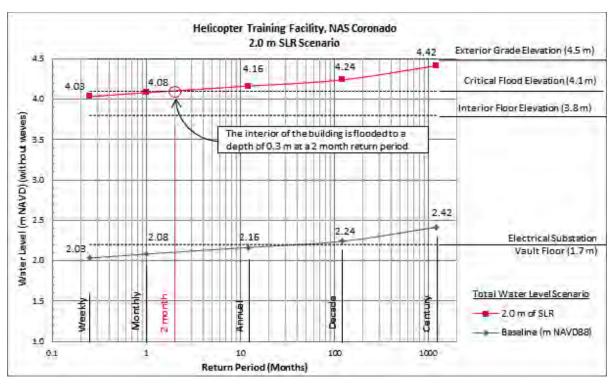


Figure 4-242. Operational limits for the Helicopter Training Facility, NBC in comparison to the 2.0-m SLR scenarios.

Waterfront Structures Examples

These structures support waterfront operations and missions of the installation and encompasses sub elements such as piers, wharves, and floating docks. Operationally, waterfront structures such as piers and wharves are either used in support of a home port where a ship is permanently assigned and offers all requisite services required by the vessel, or as a port-of-call facility that supports ship stops while under-way, including calls at fueling facilities, ammunition piers, supply piers, or short-term repair facilities. For the installations studied here, the primary exposure for waterfront structures is via inundation and flooding along protected shoreline areas. A general overview of the critical elevations and the corresponding impacts to operational capability of a waterfront structure can be represented by a graph of water elevation versus operational capability. Waterfront structures with common construction and function may have similar operational limits curves. Examples of the development of operational limits for three waterfront structures at Naval Base Coronado are presented below. Comparison of these operational curves to estimated total water levels for a range of SLR scenarios then provides a basis for the more detailed component-level assessment.

Pier Bravo - Ammunition Pier at NAS Coronado

Pier Bravo was built in 1976 and is a port-of-call facility used for transfer of ordnance on or off vessels. The facility is located on the north side of Naval Air Station (NAS) at Naval Base Coronado – see Figure 4-243. The deck elevation of Pier Bravo is at a higher elevation relative to other piers in San Diego Bay. A typical section through the pier with the major components indicated is shown in Figure 4-244.

Based on an analysis of the facility existing conditions, the vulnerabilities included the fender system and below deck utilities. The critical elevations of the pier are shown on the vulnerability assessment graphs for each SLR scenario. The floating foam-filled fenders were vulnerable to "roll-

over" when the high tide water level was greater than the critical elevation of the fender system (2.7 m) – see Figure 4-245. The fender system had limited operations and would require modifications to remain fully operational with 0.5 m of SLR (Figure 4-247).

The pier has fire suppression piping and electrical conduits that are supported below deck by hangers. The original design loads did not account for wave and current forces from being submerged. The additional wave and current loads could cause a failure of the fire suppression piping and electrical conduit systems (Figure 4-246). The electrical and plumbing systems had limited operations and would require modifications to remain fully operational with 1.0- and 1.5-m of SLR, respectively (Figure 4-248 and Figure 4-249). The service life of the structure would also be reduced when the pile caps began to be submerged during high tides. The increased exposure to chloride ion contamination in the concrete would hasten the concrete degradation process discussed in Section 3.4.2. Overtopping of the deck occurred for the 2.0-m SLR scenario with a return period of less than 1 year (Figure 4-250). Construction modifications could be made to the fender system, electrical utilities, and plumbing systems so that the pier could remain operational until the water level reaches the top of deck elevation.



Figure 4-243. Google Earth photo showing the configuration of Ammunition Pier Bravo at NBC (image: Google).

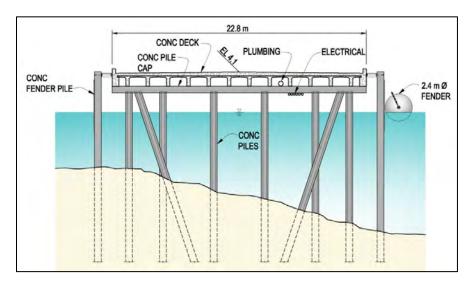


Figure 4-244. Typical section through Pier Bravo. The major components that are vulnerable to SLR are indicated.

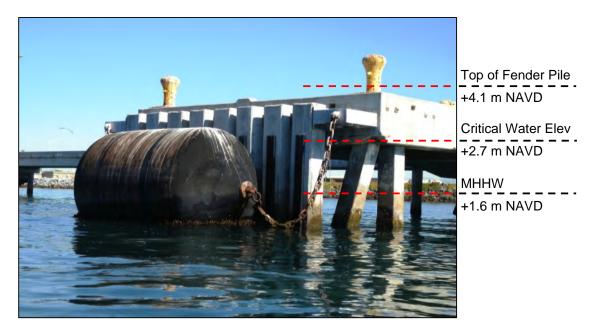


Figure 4-245. View of floating fender and concrete piles at Ammunition Pier Bravo, NBC. This system is vulnerable to "roll-over" with 0.5 m of SLR.



Figure 4-246. The fire suppression piping and electrical conduits at Ammunition Pier Bravo are located below the pier deck.

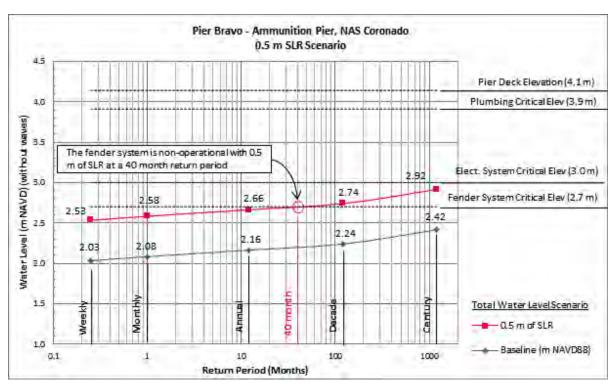


Figure 4-247. Operational limits for Ammunition Pier Bravo, NBC in comparison to the 0.5-m SLR scenarios.

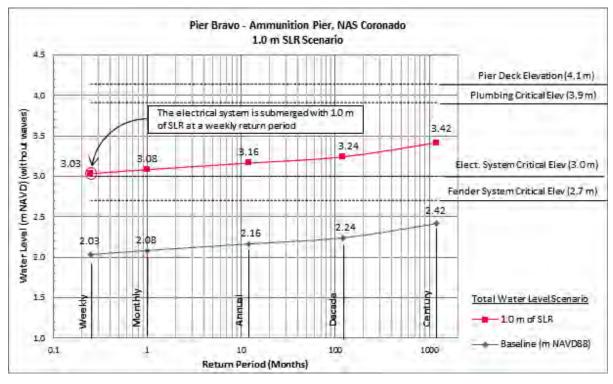


Figure 4-248. Operational limits for Ammunition Pier Bravo, NBC in comparison to the 1.0-m SLR scenarios.

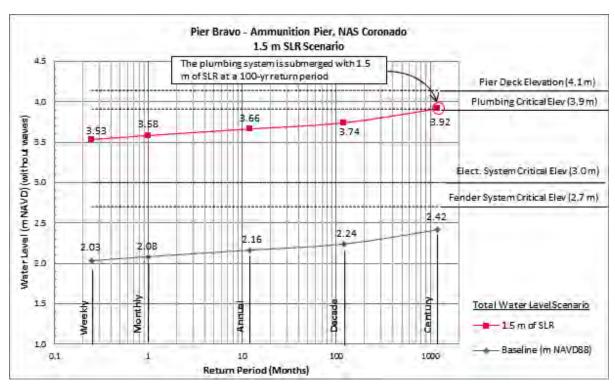


Figure 4-249. Operational limits for Ammunition Pier Bravo, NBC in comparison to the 1.5-m SLR scenarios.

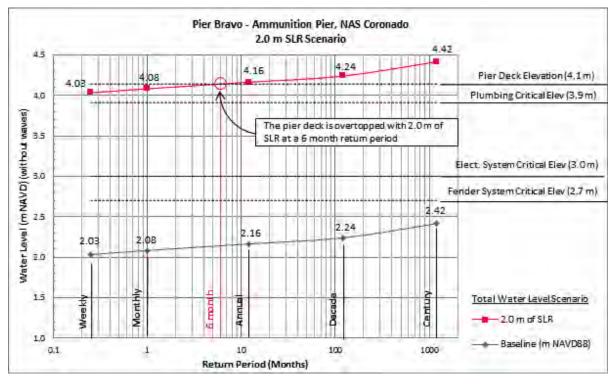


Figure 4-250. Operational limits for Ammunition Pier Bravo, NBC in comparison to the 2.0-m SLR scenarios.

Berths Juliet & Kilo - CVN Aircraft Carrier Wharves at NAS Coronado

Berths Juliet and Kilo were built in 2002 and 1998, respectively, and are used as homeport for aircraft carriers. The facilities are located on the northeast corner of NAS Coronado – see Figure 4-251. A typical section through the wharf with the major components that are vulnerable to SLR are indicated (Figure 4-252).

Steam and deionized water are required to support nuclear aircraft carriers. The deionized water system and the steam line are located on the face of the wharf and are sensitive to saltwater splash and submersion (Figure 4-253). Other utilities at the wharf include water, jet fuel, oily waste, fresh water, compressed air and waste water, which are all located inside a utility tunnel. For future SLR scenarios, when the water level exceeds the elevation of the tunnel floor, water will enter the tunnel at the expansion joints. No sealant was used at the joints. If this occurs, it will reduce the service life of the utility pipes, but will not limit the operations of the wharf.

The service life of the structure will also be reduced more rapidly as the height of the soffit above the water decreases. The increased exposure to chloride ion contamination in the concrete will hasten the concrete degradation process discussed in Section 3.4.2.

The fender system is comprised of concrete fender piles and two floating CVN separators. The separator provides the required standoff distance between the hull of the vessel, the elevator platforms and the wharf – see Figure 4-254. Future operations of the fender system will be limited by the elevation of the top of the fender piles.

Based on an analysis of the structure, fender system, and utilities, sea level rise first impacted the pier utility systems when the high tide water level combined with wind waves or boat wakes causes saltwater splash onto the steam and deionized water pipe systems with 0.5 m of SLR (Figure 4-255). For the 1.0 m-SLR scenario, the fender system would require modifications to remain operational (Figure 4-256).

The deck elevation of Berths Juliet and Kilo is at a lower elevation than Pier Bravo. Overtopping of the deck would occur for the 1.5 m SLR scenario with a 100-year return period event (Figure 4-257), and under weekly return period events for the 2.0 m SLR scenario (Figure 4-258). However, the elevation and exposed location of the steam and pure water utility systems would govern the operational limits of the facility at lower SLR scenarios.

Small Craft Piers No. 1 – 14 at NAB Coronado

The small craft piers at the Naval Amphibious Base (NAB) were built circa 1954. Originally designed for Patrol Torpedo boats, the facilities currently provide small craft berths to support various amphibious training and support activities – see Figure 4-259. The facilities are used for the following activities:

- Pier 1 is used by the Office of the Commander Naval Surface Fleet, Pacific and provides access to the admiral's barge.
- Pier 2 was configured to host the Shallow Water Mine Countermeasures Unit and will support mammal (dolphins) pens for special training (Figure 4-260).
- Piers 3 through 6 are used by the Expeditionary Warfare Training Group, Pacific and the Naval Special Warfare Center for small craft training.
- Piers 7 through 12 are used by Assault Craft Unit-1 for assault craft training.
- Pier 13 is used by the Commander Special Boat Squadron to support an oily waste pumping system and mooring of MK V, 85-ft SEAL delivery vessels.

• Pier 14 is used by the Commander Special Boat Squadron to moor MK V vessels and 11-m rubber inflatable boats.



Figure 4-251. An aircraft carrier moored at Berth Kilo, NBC.

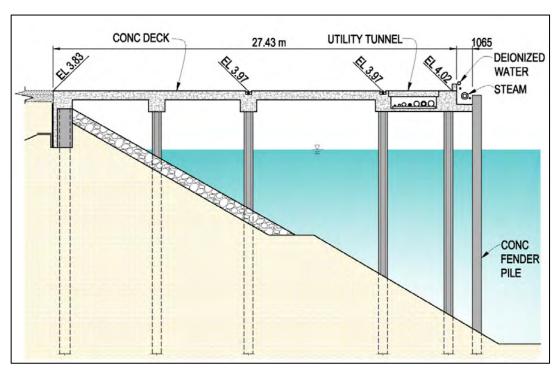


Figure 4-252. Typical section at berths Juliet and Kilo, NBC.The wharf has crane rails, a utility tunnel, and a fender system designed for aircraft carriers. Steam and deionized water are located outside of the utility tunnel, on the face of the wharf.

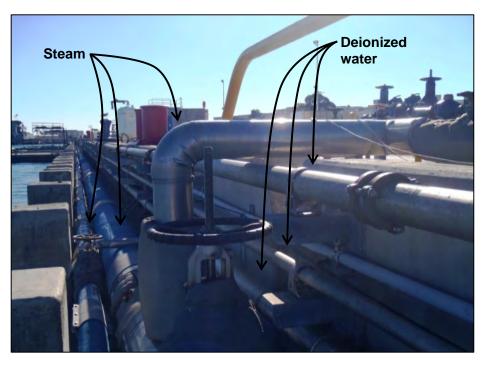


Figure 4-253. Steam and deionized water lines are located at the edge of the wharf at Carrier Wharf Berth Kilo, NBC. These utilities are not designed for saltwater submersion. The utility tunnel is located behind these utilities.



Figure 4-254. An aircraft carrier separator is a floating platform that provides clearance between the aircraft carrier and the wharf fender system, shown moored at Carrier Wharf Berth Kilo, NBC.

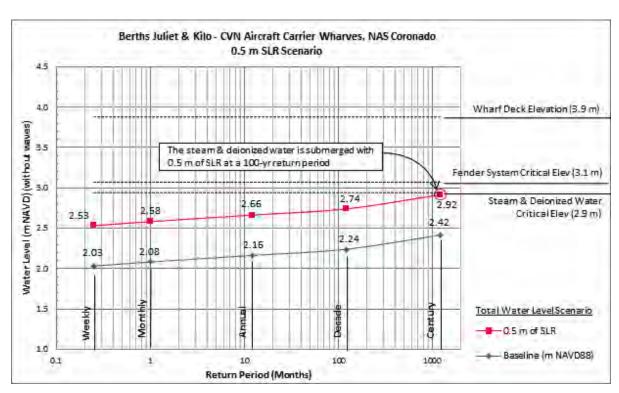


Figure 4-255. Operational limits for Berths Juliet and Kilo, NBC in comparison to the 0.5-m SLR scenarios.

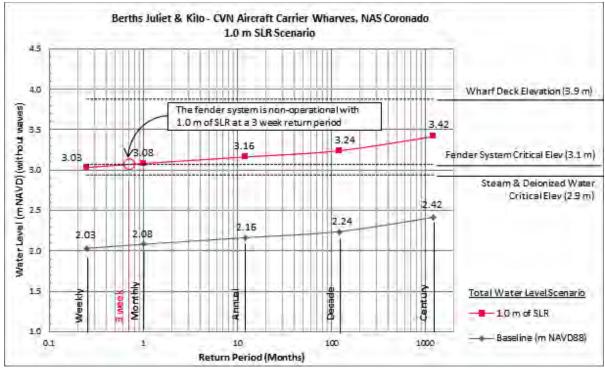


Figure 4-256. Operational limits for Berths Juliet and Kilo, NBC in comparison to the 1.0-m SLR scenarios.

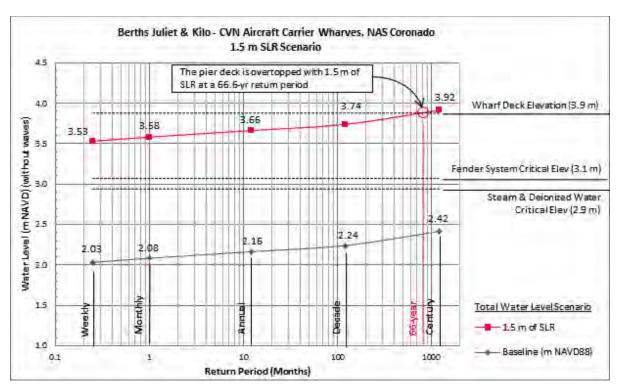


Figure 4-257. Operational limits for Berths Juliet and Kilo, NBC in comparison to the 1.5-m SLR scenarios.

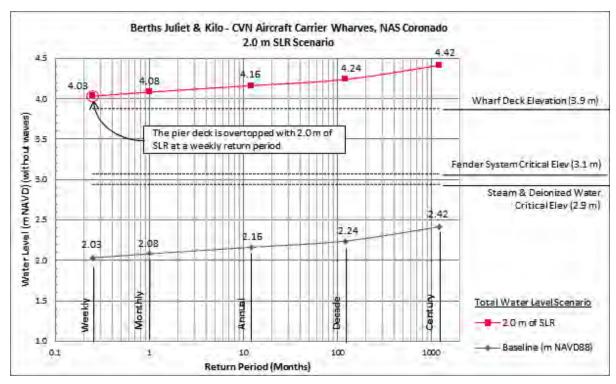


Figure 4-258. Operational limits for Berths Juliet and Kilo, NBC in comparison to the 2.0-m SLR scenarios.

The Small Craft Piers are 3.9 m wide and have minimal utility services, that may include compressed air, potable water, and low-voltage electrical power. The utility lines are housed in an above deck tunnel that is integral with the curb. The fender system is designed for small craft and consists of floating camels backed by fender piles. A floating camel distributes berthing loads to multiple fender piles. The pier deck elevation is set lower than Pier Bravo and Berths Juliet and Kilo to accommodate small craft (Figure 4-261).

Piers 1 to 14 are approximately 58 years old. The structures have exceeded their 50-year service life. When the pile caps and deck soffit begin to be submerged during high tides the increased exposure to chloride ion contamination in the concrete will hasten the concrete degradation process discussed in Section 3.4.2.

Based on an analysis of the structure, fender system, and utilities, 0.5 m of SLR would impact operations when the high tide water level causes the fender system to become non-functional. Inundation of the deck would also occur for the 0.5 m SLR scenario. Inundation of the deck is partially protected by a utility tunnel around the perimeter of the pier. The critical elevations of the wharf are shown on the vulnerability assessment graphs (Figure 4-262). The Small Craft Piers at NAB would be overtopped at a weekly return period for the 1.0-m SLR scenario (Figure 4-263).

Coastal Structures Examples

Coastal structure receptors include engineered shoreline protective structures that support waterfront operations and missions of the installation such as revetments, jetties and bulkheads/ seawalls. Of particular interest for coastal structures are vulnerabilities associated with overtopping and damage to structural components due to increased water levels. Examples of critical elevations that affect the function of coastal structures are provided in this section for typical systems at NBC. As mentioned previously, the vulnerability of these structures are generally of less relative importance than that of the infrastructure they serve to protect. Therefore, critical elevations discussed in this section are those that decrease the function of the structure, thereby increasing the vulnerability of landward infrastructure.

Pier Bravo Revetment

Pier Bravo Revetment is located on the north side of Naval Air Station (NAS) at Naval Base Coronado (Figure 4-264 and Figure 4-265). As-built information for the structure was not available so engineering detail was derived from high-resolution aerial imagery, the DEM, and engineering judgment. The structure is approximately 1,600 meters in length with a crest elevation of 4.0 m. The toe was estimated to at -0.6 m, which is consistent with engineering design for these types of structures in the region. A typical section through the revetment with the major components indicated is shown in Figure 4-266.

Based on an analysis of the structure's design, the revetment's functionality would be compromised in the future as a result of water levels overtopping the crest of the structure. As water levels increase, extreme events such as tides, floods, and waves would cause episodic overtopping of the structure at a decreasing return period. Wave-induced overtopping would occur as a result of ocean swell propagation, boat waves, and wind waves. Consideration of the sites wave exposure from boats, wind waves and ocean swell were incorporated for the component-level assessment analysis. Based on a recent wave analysis for another location in the bay, a typical wave height of 0.5 m was superimposed on the protected harbor total water level scenarios to accommodate this additional component that could be important in the context of these structures.



Figure 4-259. Naval Amphibious Base Coronado showing the location of the Small Craft Piers as indicated with a yellow line (image: Google).

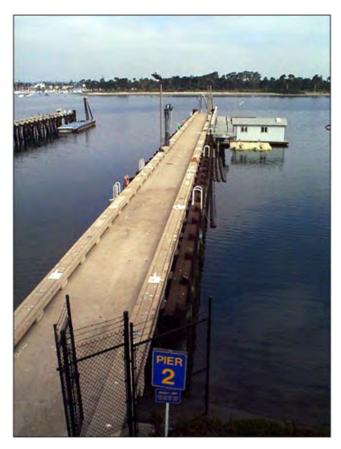


Figure 4-260. Small Craft Pier No.2, NAB Coronado. The pier is representative of 13 piers at NAB. The piers have fender systems for small craft, potable water service, and lighting.

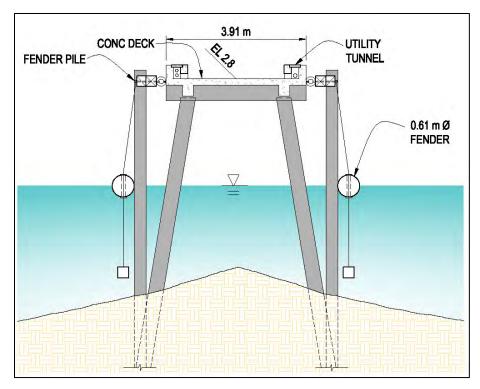


Figure 4-261. Typical section through Piers No. 1 through 14 at NAB, Coronado. The deck elevation is low to accommodate small craft berthing.

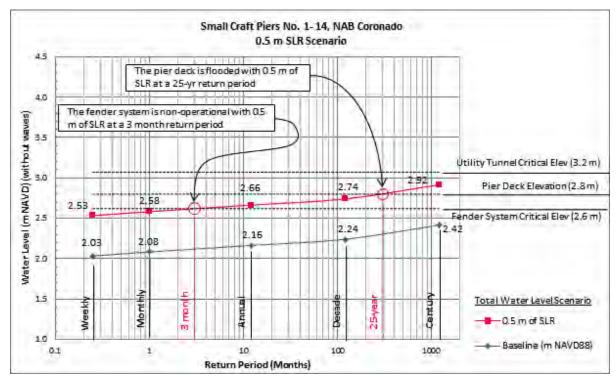


Figure 4-262. Operational limits for the small craft piers, NBC in comparison to the 0.5-m SLR scenarios.

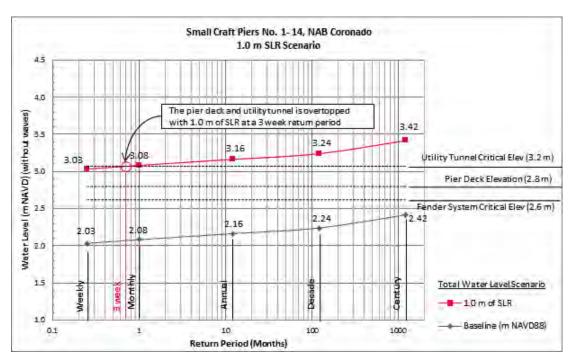


Figure 4-263. Operational limits for the small craft piers, NBC in comparison to the 1.0-m SLR scenarios.

The critical elevations of the revetment are shown on the vulnerability assessment graphs for each SLR scenario (Figure 4-267 through Figure 4-270). No overtopping of the crest of this structure was projected for the baseline, 0.5- or 1.0-m SLR scenarios. Wave-induced crest overtopping was possible for extreme wave events at the weekly return interval in the 1.5-m SLR scenario. The wave height needed to overtop the structure becomes less with time. Static water levels were projected to overtop the revetment in 2.0-m SLR scenarios with a weekly return period.



Figure 4-264. Google Earth photo showing the configuration of Pier Bravo and the Pier Bravo Revetment, NBC (image: Google).



Figure 4-265. Pier Bravo Revetment, NBC.

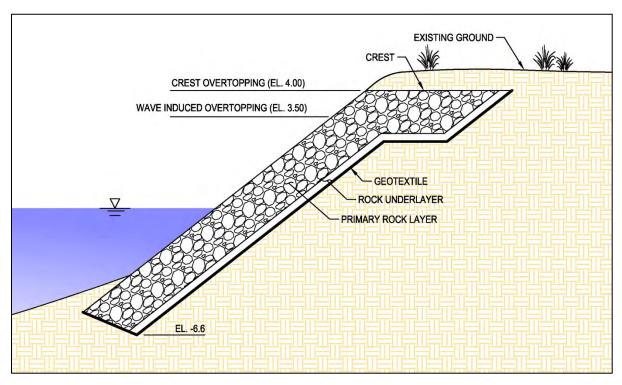


Figure 4-266. Typical cross section for the Pier Bravo Revetment. The major components that are vulnerable to SLR are indicated.

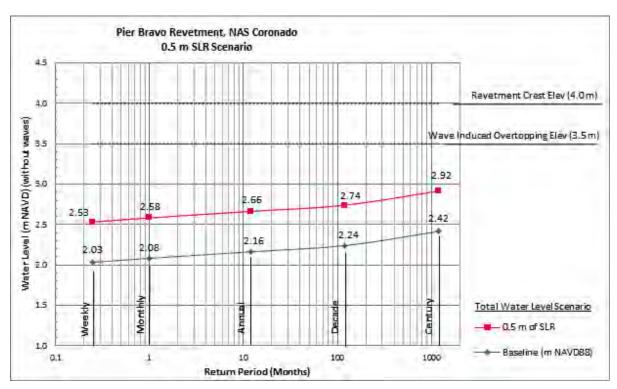


Figure 4-267. Operational limits for the Pier Bravo Revetment, NBC in comparison to the 0.5-m SLR scenarios.

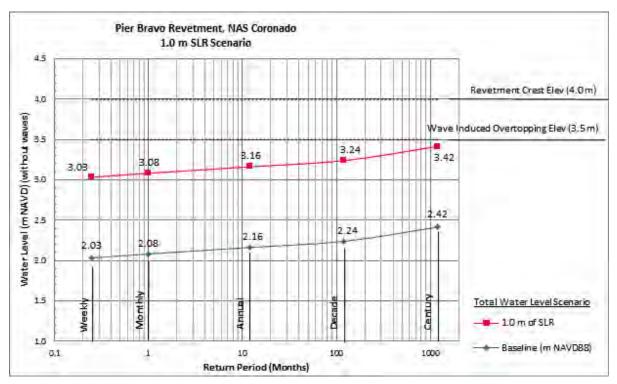


Figure 4-268. Operational limits for the Pier Bravo Revetment, NBC in comparison to the 1.0-m SLR scenarios.

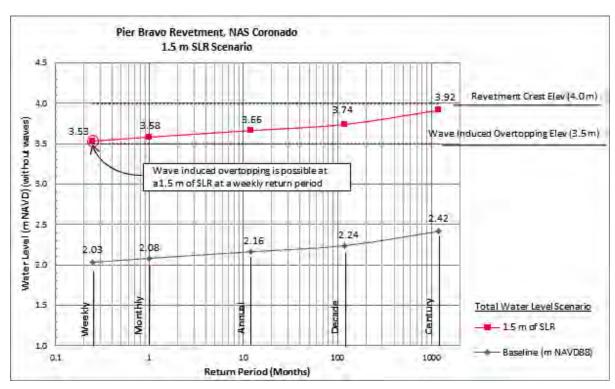


Figure 4-269. Operational limits for the Pier Bravo Revetment, NBC in comparison to the 1.5-m SLR scenarios.

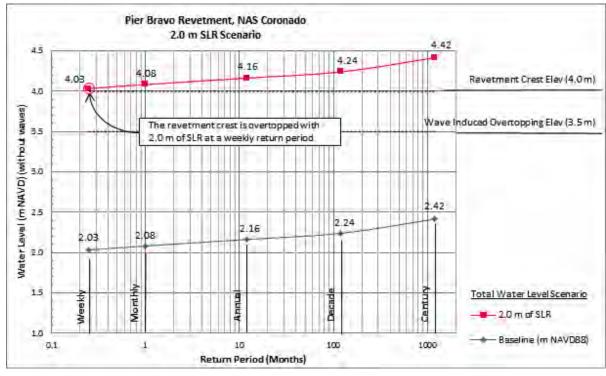


Figure 4-270. Operational limits for the Pier Bravo Revetment, NBC in comparison to the 2.0-m SLR scenarios.

Naval Amphibious Base Bulkhead

Bulkhead No. 2 is located on the east side of NAB Coronado (Figure 4-271). Based on the analysis of the structures design, the bulkhead's functionality would be compromised by future water levels that overtop the crest of the structure or that would increase the degradation of the walls tieback system through inundation or wetting/drying. It should be noted that inundation or wetting/drying may or may not affect the function of the tieback system contingent on the design. The most vulnerable designs would be those comprised of unprotected steel or a system located in aerated soil. These factors should be considered in the detailed assessment.

Critical elevations of these vulnerable components of the Bulkhead No.2 were extracted from available record drawings. The structure is approximately 1,600 meters in length with a crest elevation of 3.66 m and a tieback elevation of 2.35 m. A typical section of the bulkhead with vulnerable components specified is shown in Figure 4-272.

Critical elevation exceedances at various return intervals for the bulkhead example are shown for each SLR scenario in Figure 4-273 through Figure 4-276. No overtopping of the crest of this structure was projected for the baseline or 0.5-m SLR scenarios. Wave induced overtopping from high water events occurred at a 3.3-year return interval under the 1.0-m scenario. Static water levels were projected to overtop the crest at a 10-month return period under the 1.5-m SLR scenario. Higher water levels associated with wind waves or boat wakes (and less extreme waves with time) would also episodically overtop the structure under the 1.5 and 2.0 m SLR scenarios at the weekly return interval. Static water level overtopping was projected for the weekly return interval for the 2.0-m SLR scenario.

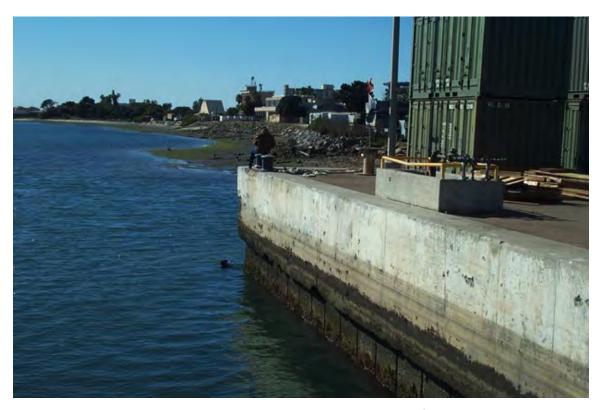


Figure 4-271. Typical concrete bulkhead at NAB Coronado.

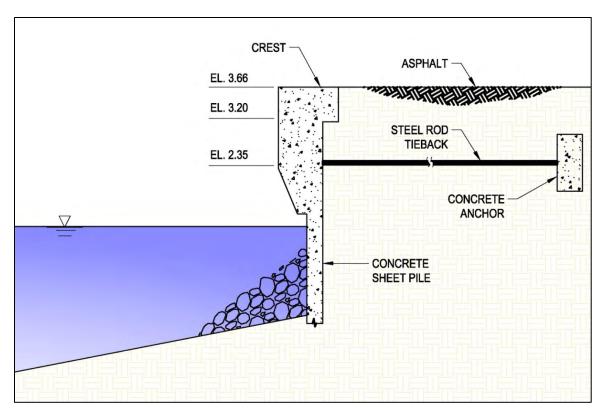


Figure 4-272. Bulkhead No.2 at NAB typical cross section. The major components that are vulnerable to SLR are indicated.

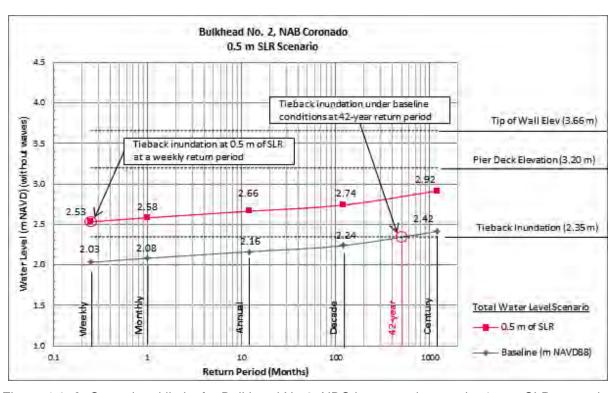


Figure 4-273. Operational limits for Bulkhead No.2, NBC in comparison to the 0.5-m SLR scenarios.

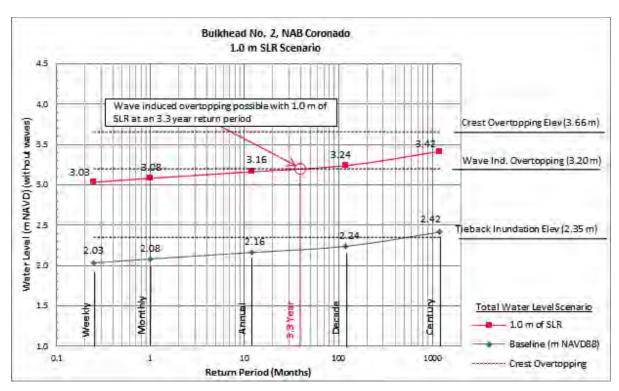


Figure 4-274. Operational limits for Bulkhead No.2, NBC in comparison to the 1.0-m SLR scenarios.

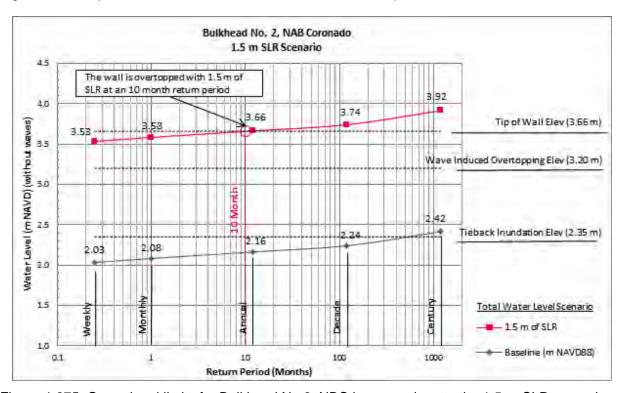


Figure 4-275. Operational limits for Bulkhead No.2, NBC in comparison to the 1.5-m SLR scenarios.

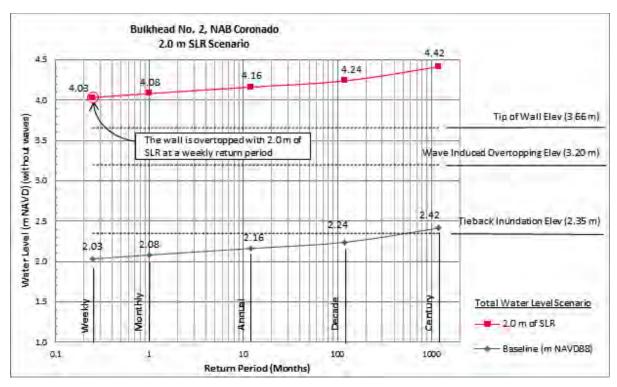


Figure 4-276. Operational limits for Bulkhead No.2, NBC in comparison to the 2.0-m SLR scenarios.

Civil Infrastructure Examples

Civil infrastructure describes a broad category of built infrastructure that is critical to the day-to-day operations and mission of the installation and includes sub-elements ranging from critical utility infrastructure such as buried utilities, fuel transfer/supply, transportation corridors, and storm water conveyance systems. The breadth of this category was beyond the scope of the project to address fully, so our receptor-level assessment focused on a limited subset of receptors including storm water conveyance systems, roadways, airfields, and recreation areas. Here we examine these systems in greater detail for a specific example within the Carrier Pier area at NBC with particular emphasis on the stormwater conveyance system.

Berth Lima and Quay Road at NBC

Quay Road is a major roadway for access along the waterfront of NBC. Berth Lima is an aircraft carrier wharf located adjacent to Quay Road. Storm water drains are provided along Quay Road and on the deck of Berth Lima to route storm water runoff to San Diego Bay – see Figure 4-277. A section through the storm drain pipe illustrates the roadway, wharf deck, and invert elevations with the baseline Mean Higher High Water (MHHW) level shown (Figure 4-278). It is common for storm drain profiles to show the vertical scale at ten times the horizontal scale.

Based on analysis of the existing topography and storm drain system functional elevations, SLR would impact operations by reducing the efficiency of the storm water drainage system, and later intrusion and flooding of the wharf deck and roadway (Figure 4-279). The invert elevation at the low end of the pipe at the bay was at 0.95 m NAVD88. It is common for storm drain pipes to have the low end invert elevation near mean sea level.

For storm drain systems, two scenarios should be analyzed, with and without a rain event. For the 0.5 m of SLR scenario, the efficiency of the storm water system would be reduced during rain events, which would increase the likelihood of flooding of Quay Road and Berth Lima (Figure 4-280). Without a rain event, when the San Diego Bay total water level was greater than the top-of-grate elevation at the catch basin of 2.93-m NAVD, water would flow from the bay and overflow onto the deck and onto Quay Road, i.e., intrusion. For the 1.0 m of SLR scenario with a 10-year return period event, the wharf deck and road would be flooded from intrusion (Figure 4-281). The critical flood level was assumed to be 12 in (0.3 m) of water on the deck or roadway.



Figure 4-277. Google Earth aerial view showing the configuration of Berth Lima and Quay Road, NBC. The dashed yellow line indicates the approximate location of the storm drain section shown in Figure 4-277 (image: Google).

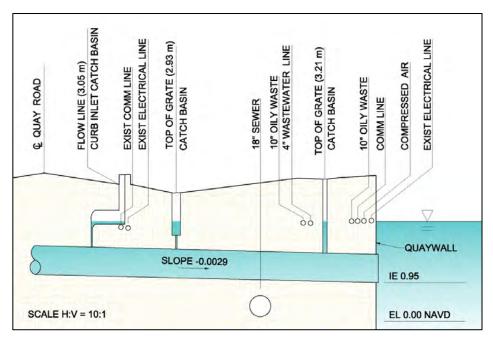


Figure 4-278. A section through Berth Lima between Quay Road and San Diego Bay showing the invert elevations (IE) of the storm water system.

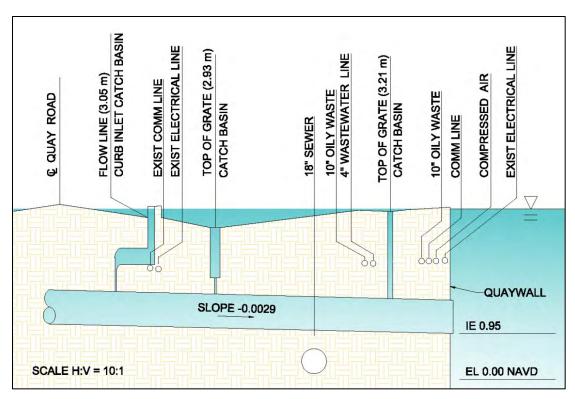


Figure 4-279. A section through Berth Lima between Quay Road and San Diego Bay showing the stormwater system with 1.0 m of SLR at a 10-year return period.

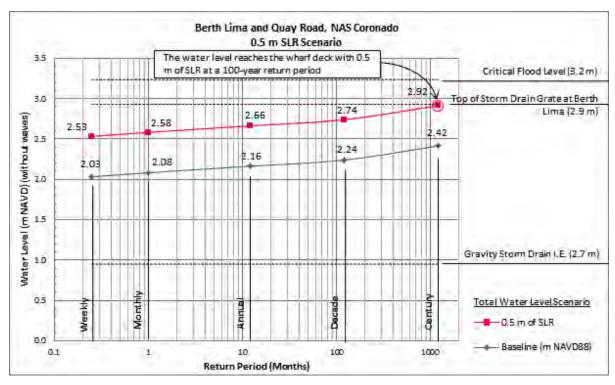


Figure 4-280. Operational limits for Berth Lima Storm Water System, NBC in comparison to the 0.5-m SLR scenarios.

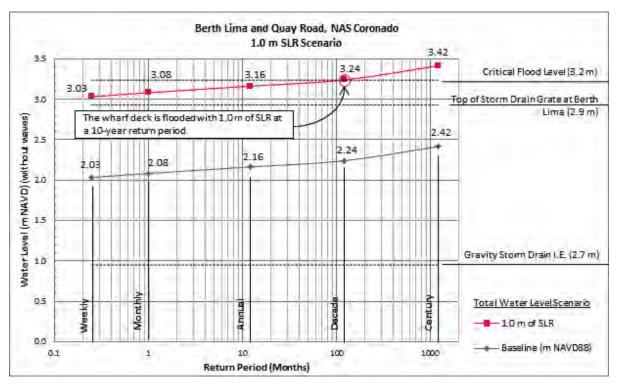


Figure 4-281. Operational limits for Berth Lima Storm Water System, NBC in comparison to the 1.0-m SLR scenarios.

Component-Level Assessment summary

In summary, these examples provide insight into the complexity of the systems involved in understanding sea level rise vulnerability at a coastal DoD installation. In general, the limited component-level analysis described above illustrates the important relationship between water level and operational response and damage for a range of key sub-elements of the receptor classes considered in this study. For receptors ranging from training areas, to buildings, waterfront structures and civil infrastructure, the operational impacts to these systems is often more gradual than catastrophic, and clearly developing an understanding of these response functions at the individual component level would require a significant level of effort. The purpose of these illustrated examples was not to provide that analysis, but rather to demonstrate that the combination of tools and methods developed under this project were capable of supporting that level of analysis.

5. CONCLUSIONS AND IMPLICATIONS FOR FUTURE RESEARCH

The objective of the project was to develop an analysis framework and methodologies to support the evaluation of regional military installation vulnerabilities and test them under prescribed scenarios of four SERDP-specified increases in local mean sea level (0.5, 1.0, 1.5, and 2.0 m) over the next century. Methodologies were developed to assess the potential scope and magnitude of impacts from physical effects of these sea level rise (SLR) scenarios, including flooding (wetting that occurs infrequently), inundation (wetting occurs regularly), erosion, seawater intrusion, and alteration of tidal flows.

Based on projected physical effects, strategies for assessing key installation vulnerabilities were evaluated for their ability to support future planning and recommendations for possible mitigation. Vulnerability assessment methodologies were structured around potential impacts to receptor categories that included buildings, civil infrastructure, training areas, and waterfront and coastal structures. The receptor-level assessment for the civil infrastructure category focused on a limited subset of receptors, including storm water conveyance systems, roadways, airfields, and recreation areas. The limited component-level analysis performed was meant to illustrate the important relationship between water level and operational response and damage for a range of key sub-elements of the receptor classes considered in this study. The project focused on conditions in the southwestern United States (U.S.) and utilized the key coastal military installations at Naval Base Coronado and Marine Corps Base Camp Pendleton to test the approach.

5.1 VULNERABILITY FRAMEWORK

A general review of existing frameworks was conducted to appraise the state of the science for vulnerability assessment, and to create a credible basis for a DoD-relevant framework that builds on the strategies already developed and utilized in other applications. Overall, we found that sea level rise vulnerability frameworks appear to be evolving from strategies to support large-scale, qualitative screening assessments for specific future conditions toward strategies that can be applied at regional and local scales to more quantitatively respond to specific vulnerability questions, evaluate a range of possible scenarios, and identify potential responses to vulnerability at the source, pathway, and receptor level.

The framework we developed reflects these trends and much of the project focused on methods development to support this framework. The description of these methods, along with examples of their application, thus represents an important aspect of the work that we carried out. The methods development focused on four key areas relevant to sea level rise influences on military installations in the southwestern U.S. These included sea level rise and sea level variability projection methods, methods for delineation of the coastal system including both the terrain and the infrastructure, methods for evaluating the physical response of the system to sea level rise, and methods for the assessment of vulnerability.

5.2 SEA LEVEL RISE PROJECTIONS

Sea level rise projection methods were successfully developed and applied for this study based on a superposition of four components including MSLR scenarios with increases of 0.5, 1.0, 1.5, and 2.0 m by 2100 relative to 2000; hourly astronomical tide heights; non-tide residual water level variability from general circulation models enhanced with El Niño-related sea level fluctuations specific to the southwestern U.S., and wave-driven run-up on beaches. The projections that are the product of this work represent state-of-the-science, complete 100-year time series for the period 2000 to 2100 that capture all of the key drivers of sea level variability in the southwest U.S., and they underpinned the formulation of specific exposure scenarios for this research effort. A key aspect of

the work is that the wave-driven run-up component of the projections was based on linkages between the GCM outputs and coastal wave models that incorporated spatial dependence along the entire shore of both of the installations.

Using these time series, we developed the desired robust regional scenarios based on water level extremes at MCBCP and NBC using extreme value methods. The results clearly illustrated the phenomenon often called "return-period creep" as specified return period elevations become progressively higher, or equivalently, as given maximum water levels become increasingly more frequent. These scenarios provided a matrix of future conditions that span both variations in potential future sea levels, as well as the frequency of their occurrence, and established a rigorous basis for the subsequent development and application of the physical response models used to assess pathways of impacts in sea level rise vulnerability assessment. As a limitation, we note that this method of superposition is not entirely self-consistent because it decouples the mean and fluctuating components of sea level in ways that may not be consistent with specific greenhouse gas emission scenarios.

5.3 COASTAL SYSTEM DELINEATION

Geospatial models of the terrestrial and marine topography were successfully constructed using the best-available data sources. We developed methods to optimally delineate the coastal system by decomposing each setting into terrestrial, littoral and bathymetric domains, constructing these submodels from targeted data sets, and them integrating them using a hierarchical re-gridding strategy. As part of this approach, the littoral domain was modeled using a new method developed for this project based on sparse beach profiles. The resulting elevation models showed the contrast between the terrain at the two coastal installations. NBC is poised almost entirely on low elevation terrain areas surrounded on both sides by water, while MCBCP is set in an area where the terrain rises rapidly near the coast, with lower lying areas concentrated near the lagoons and in the southern portions of the installation. Another unique aspect of the work was the development of methods to then accommodate future conditions by superimposing revised beach or beach/cliff elevation submodels into the changed domain of the basemodel using the results of the physical response models. These baseline and future conditions elevation models are a key product of our effort and formed the basis for detailed assessment of erosion and flooding footprints for a broad range of future sea level rise scenarios. Limitations of this approach are related to the fact that multiple data sets, collected at different times by different agencies, with varying methods and levels of resolution and accuracy, must be integrated to provide the desired coverage for the installation.

The infrastructure component of the system model was successfully compiled from installation data provided by the NAVFAC and MCBCP. Available data were cataloged to produce GIS layers and shapefiles for specific receptor categories defined within the source-pathway-receptor vulnerability framework, including testing and training areas, buildings, civil infrastructure, waterfront structures, and coastal structures. Metadata for components within these receptor categories including characteristics such as area, length, MDI, and replacement cost were cross-indexed from the INFADS database to provide quantitative metrics of impact. Analysis of these receptor categories relied on the integration of the receptor data with the terrain data to create an integrated model that consisted of an overlay of the shapefiles onto the three-dimensional terrain such that elevations for the infrastructure could be extracted to evaluate interactions with erosion, inundation and flooding areas. To meet our research objective for a three-dimensional GIS analysis capability, the new terrain models and the infrastructure layers were integrated through both Arcview for general display purposes, and through specialized MATLAB® tools that were developed for the three-dimensional analytical aspects of the project. The integration of high-resolution elevation models with infrastructure overlays and three dimensional analysis tools represents a significant

product of our effort. Primary limitations of this approach were related to the reliance on available data, gaps within these data sets, and changes to the infrastructure over time that may or may not be integrated into the data sets.

5.4 PHYSICAL RESPONSE OF THE SYSTEM

A key aspect of our research was the development of methods to account for physical response pathways that represent the process or mechanism by which sea level rise sources act on receptors to cause impact. To meet this objective, we developed methods based on available data and empirical and theoretical models to describe pathways of action, including inundation, flooding, erosion, and seawater intrusion. Primary pathways for this study were classified by exposure under categories for exposed shorelines, protected shorelines and groundwater. Methods were successfully developed and applied for each of these exposure pathways. To accomplish this for the exposed shoreline areas, we separated the exposed shoreline long-term response into two categories, including beach systems, and cliff/beach systems, which are generally representative of much of the southwest U.S., and specifically representative of NBC and MCBCP, respectively. In a novel aspect of the research, new modeling systems were developed that allowed the long-term topographic response of these beach and cliff/beach systems to sea level rise to be integrated with short-term storm wave response changes in the shoreline position.

New methods were developed for the evaluation of inundation and flooding along exposed shorelines that incorporated changes to the underlying elevation model due to erosion, spatially varying total water level exposures, and requirements for complete hydraulic connectivity. The shoreline change modeling described above for beach systems and cliff/beach systems was utilized to develop new shoreline elevation models along the coast of both installations for the range of future sea level scenarios. Total water levels associated with a range of different return periods at each coastal station were then applied using a hydraulic connectivity algorithm to simulate inundation and flooding. A method was developed using a sliding window of adjustable longshore scale to allow for a reasonable balance between the degree of lateral flooding along the upland topography and the maintenance of resolution for alongshore variations in total water level. Significant products from this analysis included raster inundation and flooding overlay maps for the complete matrix of sea level rise scenarios at each installation, which also served as a basis for further analysis of vulnerability to the specified receptor categories.

Similar methods and products were also developed to assess the response to sea level rise of protected bay areas such as the San Diego Bay facing portions of NBC. The methods included approaches to define water levels in these areas that can influence the operability of waterfront structures, methods to evaluate inundation and flooding that could occur from high tides interacting with sea level rise, and methods to evaluate changes in currents and associated bottom shear that could influence the transport and deposition rates of sediment.

Coastal aquifers can also be sensitive to the effects of sea level rise via the pathway of seawater intrusion. For this effort, method development focused on the assessment of groundwater in the Santa Margarita River Basin at MCBCP. MCBCP's water supply is produced primarily from underground aquifers that are recharged by percolation from overlying rivers and streams, and Santa Margarita River wells provide about 65% of the total water consumed on the base. We successful applied a density-dependent groundwater-flow and solute-transport model, combined with a range of historical data to explore the influence of seawater intrusion under the target range of sea level rise scenarios. The simulation utilized monthly mean sea levels as a forcing function, combined with a range of potential future groundwater pumping conditions over the period from 1950 to 2100. Significant products of this research included evaluations of the relative sensitivity of the system to changes in

future sea level, pumping rates, and combinations of these, and the resulting potential impacts to water quality and future extraction capacity.

5.5 ASSESSMENT OF VULNERABILITY

Sea level rise vulnerability at NBC and MCBCP was assessed through application of the methodologies described in the previous sections. The purpose of this analysis was not to perform an overall assessment of sea level rise vulnerability at these installations, but rather to test the physical response methodologies, illustrate their application, and evaluate approaches to adopt them within a generalized vulnerability framework such as the one described in this report. In the context of the framework, the methodologies were illustrated using two levels of analysis, receptor level and component level. The "Receptor-Level" is an installation-level view in which general receptor category vulnerabilities to sea level rise were characterized in terms of key response metrics. The "Component-Level" is a critical-component level view in which specific high-value or mission critical infrastructure elements are evaluated at a level of detail sufficient to characterize their response as a function of water level.

The receptor-level methodology encompassed the breadth of the data compilation, modeling, and analysis methods and included installation- and exposure-specific sea level rise source scenarios, pathway-specific physical response of the coastal system, and the characteristics sensitivities and operational thresholds for the installation receptors. Example products were developed for two primary coastal conditions, including (1) NBC and MCBCP exposed shorelines, and (2) NBC protected shorelines (with limited application for MCBCP). Based on the conceptual model from the framework, receptors were then evaluated for three key exposure pathways at each installation including erosion, inundation, and flooding, as applicable.

5.5.1 Naval Base Coronado

For NBC, the analysis illustrates the ability of these methods to resolve the increasing level of vulnerability of the installation to erosion as a function of increasing sea level, as well as the sensitivity of some receptors to short-term wave driven erosion events. For training areas, this translates into frequent (weekly return period) conditions with remaining area reduced to about 53% of baseline for 1.0-m SLR, and further reductions to a remaining area of about 23% of baseline for 2.0-m SLR. For buildings, these conditions result in erosion pathway vulnerability to about 13 structures for 1.0-m SLR 3 of which have an MDI >55, and this increases to about 23 structures and six with MDI >55 for the 2.0-m SLR scenario. Roadways, storm drain systems, and recreational areas were also found to be vulnerable to the erosion pathway along the exposed shoreline of NBC. Overall replacement value for vulnerable receptors included in the erosion pathway analysis ranged from negligible for the baseline SLR scenario to as high as ~ \$745M for the 2.0-m SLR scenario combined with a 100-year wave-driven erosion event. This estimate is largely driven by "replacement cost" associated with beach replenishment, and it should be noted that if this replenishment were to take place then the other erosion impacts would be largely mitigated, so the total number should be viewed as a measure of summed vulnerability rather than a measure of the actual costs that might occur for a given scenario.

Vulnerability of NBC receptors to sea level rise for the exposed shoreline inundation and flooding pathway also illustrates the increasing level of vulnerability to inundation and flooding as a function of increasing sea level and increasingly extreme short-term flooding events. The results reflect the relatively high sensitivity of NBC to inundation and flooding as a function of the generally low-lying nature of the installation, and the significant exposure along the open shoreline of the Pacific. For training areas, this translates into inundation impacts with average beach widths reduced to about 29% for 1.0-m SLR, and further reductions to a remaining area of 5% for 2.0-m SLR. While

infrequent flooding events can potentially be accommodated through scheduling, flooding impacts are more significant with the entirety of the beach training areas subject to flooding for SLR scenarios of about 1.0 m and above. The building receptor class at NBC is especially vulnerable to flooding impacts (100-year return period), with about 881 potentially flooded structures for 1.0-m SLR, 130 of which have an estimated MDI >55. This increases to about 1,143 structures and 150 with MDI >55 for 2.0-m SLR. Roadways, airfields, storm drain systems, and recreational areas all had significant levels of vulnerability to inundation and flooding as well. Overall replacement value for vulnerable receptors included in the inundation and flooding pathway analysis ranged from negligible for the baseline SLR inundation scenario to as high as ~ \$3752M for the 2.0-m SLR flooding scenario. This estimate is largely driven by vulnerability associated with building flooding, but with significant contributions from all other categories as well.

The analysis methods also show that while the exposure to sea level rise along the protected shorelines of NBC is limited by the lack of wave run-up, there is still relatively high vulnerability to inundation and flooding as a function of the generally low-lying nature of the installation, and while the impacts along these protected shorelines are muted compared to the open shorelines of the Pacific, there are critical receptor categories including waterfront and shoreline structures that are unique to this environment. For example, waterfront and coastal structures showed vulnerabilities in the range of 1.0 to 2.0 m of SLR, with the replacement value of operationally impacted structures ranging as high as \$648M for waterfront structures and \$78M for coastal structures under the 2.0 m SLR scenario.

For NBC, we also developed examples of the application of these methods at the component-level of assessment for elements of the training area, building, waterfront structures, coastal structures, and civil infrastructure receptor classes. For example, to illustrate the component-level assessment of training areas, we combined the available data from the receptor-level analysis with more detailed data on specific beach training operations for the "Causeway Pier Insertion and Retraction" training activity at NBC. The operational requirements for the training were estimated to include approximately 5 days that occur approximately 10 times per year, requiring a minimum beach width of about 80 m. Based on the physical response and exposure modeling we conducted, this operational threshold is maintained under weekly and monthly return period events for SLR up to about 0.5 m. For SLR > 0.5 m, the operational beach width threshold would be exceeded, and this operation would be considered to be vulnerable to sea level rise impacts under these conditions. The analysis was also carried to the level of individual training lanes for which it was illustrated that, while most of the training lanes at SSTC North remain operational up to and somewhat beyond 0.5 m of SLR, the training lanes at SSTC South are generally narrower to begin with, and thus become narrower than the operational limit at SLR even below 0.5 m. While these numbers are approximations, they illustrate the manner in which the command personnel that plan these training activities could utilize this approach to assess sustainability of specific beach training operations.

Similar examples were developed for sub-elements of the building, waterfront structures, coastal structures and civil infrastructure receptor classes. These examples provided insight into the complexity of the systems involved in understanding sea level rise vulnerability at a coastal DoD installation. In general, the limited component-level analysis was meant to illustrate the important relationship between water level and operational response and damage for a range of key sub-elements of the receptor classes considered in this study. For receptors ranging from training areas, to buildings, waterfront structures and civil infrastructure, the operational impacts to these systems was often more gradual than catastrophic, and clearly developing an understanding of these response functions at the individual component level would require a significant level of effort. The purpose of these illustrated examples was not to provide that analysis, but rather to demonstrate that the

combination of tools and methods developed under this project are capable of supporting that level of analysis.

5.5.2 Marine Corps Base Camp Pendleton

For MCBCP, the analysis also incorporated key receptors including training areas, buildings, and civil infrastructure, and multiple metrics of response across the full range of both long-term sea level rise scenarios and short-term erosion events of various return periods. The analysis for MCBCP differed from NBC in that the training areas are generally backed by erodible cliffs, and the landward boundary of the beach training area was allowed to retreat inland (autonomous adjustment) at the rate of retreat of the cliff base. Thus, the width of the training areas generally increased with time, and the beach width remaining was a function of the difference between retreat of the shoreline and the retreat of the cliff base. For training areas, this translated into frequent (weekly return period) conditions with remaining area reduced to about 41% of baseline for 1.0-m SLR, and further reductions to a remaining area of 27% of baseline for 2.0-m SLR. For buildings, the erosion pathway resulted in vulnerability to about 66 structures for 1.0-m SLR, 12 of which have an estimated MDI >55, increasing to about 90 structures and 14 with MDI >55 for 2.0-m SLR. Roadways were also found to be vulnerable to the erosion pathway along the exposed shoreline of MCBCP. Overall vulnerability estimates for the receptors included in the erosion pathway analysis ranged from less than \$1M for the baseline SLR scenario to as high as ~ \$1600M for the 2.0-m SLR scenario. As with NBC, this estimate is largely driven by "replacement cost" associated with beach replenishment.

Application of the methods to analysis of vulnerability of MCBCP receptors to sea level rise for the exposed shoreline inundation and flooding pathway included the full range of both long-term sea level rise scenarios and short-term flooding events of various return periods. While the analysis indicated an increasing level of vulnerability to inundation and flooding as a function of increasing sea level and increasingly extreme short-term events flooding, it also reflected the relative resilience of MCBCP to inundation and flooding as a function of the generally steep nature of the installation topography, and the buffering effect of the coastal cliffs. Beach training areas are one of the most sensitive receptors to inundation and flooding, with inundation impacts reflected in reductions in average beach widths to a remaining area of about 17% for only 0.5-m SLR, and further reductions to a remaining area of 10% for 2.0-m SLR. Flooding impacts (100-year return period condition) are more significant with nearly the entirety of the beach training areas (5% remaining) being subject to flooding for SLR scenarios of about 0.5-m and above. Because of the limited development along the shoreline, the building receptor class is far less vulnerable to flooding impacts at MCBCP compared to NBC (100-year return period), with about 158 potentially flooded structures for 1.0-m SLR, 30 of which have an estimated MDI >55, increasing to about 200 structures and 35 with an estimated MDI >55 for 2.0-m SLR. Roadways, storm drain systems, and recreational areas all had projected vulnerability to inundation and flooding as well. Overall replacement value for vulnerable receptors included in the inundation and flooding pathway analysis ranged from about \$4M for the baseline SLR inundation scenario to as high as ~ \$1656M for the 2.0 m SLR flooding scenario. This estimate is largely driven by vulnerability associated with training areas, but with significant contributions from other categories as well.

5.6 SUMMARY OF KEY ACCOMPLISHMENTS

To summarize, based on our objective to develop a robust analysis methodology that provides a reliable means to identify and plan for vulnerabilities under both currently projected sea level scenarios, and emerging scenarios in the future, our key accomplishments include:

- Demonstration of new methodologies for the development of southwest U.S. relevant sea level scenarios and return-period events and a capability to project these at 100-m increments along the shoreline
- Development and application of a range of "beyond the bathtub" pathway response models that link these sea level scenarios to potential impacts to coastal military installations
- Assessment and contrast of the response of two key southwest installations with an emphasis on military-specific receptors including beach training areas and waterfront infrastructure

5.7 REMAINING GAPS

The assessment of climate change vulnerability at DoD installations is highly challenging and complex, and much work remains to continue to improve our understanding of how these systems will respond, as well as how we can best prepare for and manage this response. Some key remaining gaps that we identified during the course of our effort included:

- Limitations related to the fact that multiple topographic data sets, collected at different times by different agencies, with varying methods and levels of resolution and accuracy must be integrated to provide the desired coverage for the installation.
- Limitations related to the reliance on available installation infrastructure data, gaps within these data sets, and changes to the infrastructure over time that may or may not be integrated into the data sets.
- Needed improvement of the methods that link projections of sea level variability with projections of mean sea level rise so that the resulting scenarios are self-consistent with respect to the underlying climate change conditions.
- Better quantification of uncertainty through improvements to allow for an ensemble of GCM wind-driven wave scenarios to be considered in driving wave model scenarios.
- Implementation of a wave assessment framework that would bypass the need to run deterministic wave model scenarios every time there is new GCM scenario by linking changes in the modeled near-shore wave climate to commonly used metrics such as mean jet stream location, the PDO index, the ENSO index, high pressure over the southwestern U.S., and autumn surface water temperatures off northern Mexico.
- A continued need for better data to more consistently define the topography and variability of topography of the coastal area in concert with wave data, and particularly the beach and surf zone, especially during and after storm events. Existing wave and shoreline measurements suited to this task have been collected for only about 25 years, and mostly during a warm phase of the PDO when SLR was limited on the West Coast. Regular and consistent monitoring are clearly critical to understanding the nature and trends of shoreline change, and these data were important to our ability to develop and calibrate models. Ideally these monitoring programs would be continued and expanded, especially as these assessments reveal the sensitive nature of our beach training areas. The timing of these monitoring events should be carefully considered to fully capture the range of the winter and summer excursions of shoreline position.
- A need to extend high-quality hindcast wave fields with sufficient spatial resolution to be useful in reconstructing historical extreme wave conditions, which currently extend back to only about 1960.
- Better understanding and parameterization of long-term shoreline response models with respect to the upland and seaward extents of the active profile definition.
- A need for better and more comprehensive monitoring of current day storm-driven flooding and damage along with better validation data sets for shoreline response models.

- A need for more rigorous analysis of flooding events that integrate detailed hydraulics and interaction of sea level rise with precipitation driven runoff.
- A need for improved groundwater-related record keeping, e.g., water-level, water-quality, and pumpage data.
- Installation specific issues that were raised at NBC included potential vulnerabilities at the Outlying Landing Facility south of the study area for the current project and the interaction of sea level rise with the Tijuana Estuary system, as well as potential erosional impacts at the south end of the airfield at the Naval Air Station were large erosion events have been observed historically.
- Installation specific issues that were raised at MCBCP included potential vulnerability of natural resources particularly in the lagoon and estuarine portions of the installation.

5.8 SUMMARY OF KEY PRODUCTS

As part of this research and development effort, a number of products were developed that advanced the research, and provided a testing ground for our methodologies. In addition, these products may serve future uses, particularly for the installations where the analysis was conducted, but also potentially as models for application to other areas with similar requirements and conditions. Some of these key products are summarized below.

- Regional sea level rise scenarios including mean and variability, and total water level estimates for a range of return periods (from week to century) at 100-m increments along the shoreline
- Seamless bathymetric/topographic digital elevation model for the current-day condition of the shoreline and the base areas
- A set of compete, seamless bathymetric/topographic digital elevation models for future sea level conditions of 0.5, 1.0, 1.5 and 2.0 m that reflect the expected changes to the shoreline
- A set of GIS map overlays that show the erosion footprints associated with 25 combinations of long-term sea level rise and short-term wave events
- A set of GIS map overlays that show the flooding footprints associated with 25 combinations
 of long-term sea level rise and short-term wave events for both exposed and protected
 shorelines
- GIS maps of changes in currents and bottom shear stress for future sea level conditions of 0.5, 1.0, 1.5 and 2.0 m
- Clean GIS layers for five categories of critical infrastructure including buildings, training areas, waterfront structures (e.g., piers), coastal structures (e.g., jetties), and civil infrastructure (roads, airfields, storm drains, recreation areas)
- Vulnerability analysis for assets within these five categories of infrastructure to higher water levels, erosion, inundation, and flooding based on category-specific metrics

REFERENCES

- Abbott, P. L. 1999. The Rise and Fall of San Diego. Sunbelt Publications, San Diego, CA..
- Adaptation Fund. 2013. "What is Adaptation?" https://www.adaptation-fund.org/about/adaptation, accessed 8/20/2013.
- Andrews, E. D., R. C. Antweiler, P. J. Neiman, and M. F. Ralph. 2004. "Influence of ENSO on Flood Frequency along the California Coast," *Journal of Climate 17.2*:337–348. Sciences Module, ProQuest. Web. 10 Nov 2009.
- Arthur, R. S. 1951. "The Effect of Islands on Surface Waves," SIO Waves Bulletin 6 (1):1–26.
- Ashton, A. D., M. J. Walkden, and M. E. Dickson. 2011. "Equilibrium Responses of Cliffed Coasts to Changes in the Rate of Sea Level Rise," *Marine Geology* 284(1):217–229.
- AVISO. 2010. http://www.aviso.oceanobs.com/.
- Barnard, P. L. and D. Hoover. 2010. "A Seamless, High-Resolution, Coastal Digital Elevation Model (DEM) for Southern California." http://pubs.usgs.gov/ds/487/.
- Basher, R. E. 1999. "Data Requirements for Developing Adaptations to Climate Variability and Change," *Mitigation and Adaptation Strategies for Global Change* 4(3): 227–237.
- Benioff, T., S. Guill, and J. Lee (Eds.). 1996. *Vulnerability and Adaptation Assessments: An International Guidebook*. Kluwer Academic Publishers, Dordrecht, The Netherlands.
- Berggreen, R. 1979. "Geology of the Proposed Camp Pendleton LNG Site, San Diego County, California." *Geologic Guide of San Onofre Nuclear Generating Station and Adjacent Regions of Southern California*, pp. 49–62, D. L. Fife, Ed. Publications Committee, Pacific Section AAPG, Thousand Oaks, CA.
- Bijlsma, L., C. N. Ehler, R.J.T. Klein, S. M. Kulshrestha, R. F. McLean, N. Mimura, R. J. Nicholls, L.A. Nurse, H. Pérez Nieto, E.Z. Stakhiv, R.K. Turner, and R.A. Warrick. 1996. "Coastal Zones and Small Islands." In *Climate Change 1995: Impacts, Adaptations, and Mitigation of Climate Change: Scientific-Technical Analyses. Contribution of Working Group II to the Second Assessment Report of the Intergovernmental Panel on Climate Change*, pp. 289–324, R. T. Watson, M. C. Zinyowera, and R. H. Moss, Eds. Cambridge University Press, Cambridge, UK and New York, NY.
- Booker, A. J., J. E. Dennis, P. D. Frank, D. B. Serani, V. Torczon, and M. W. Trosset. 1999. "A Rigorous Framework for Optimization of Expensive Functions by Surrogates," *Structural and Multidisciplinary Optimization* 17 (1):1–13.
- Bowers, E.C. 1992. "Low Frequency Waves in Intermediate water Depths." *Proceedings of the 23rd International Conference Coastal Engineering* (pp. 832–845). ASCE.
- Bray, M. J. and J. M. Hooke. 1997. "Prediction of Soft-cliff Retreat with Accelerating Sea-level Rise," *Journal of Coastal Research*:453–467.
- Bromirski, P. D., A. J. Miller, and R. E. Flick. 2012. "Understanding North Pacific Sea Level Trends, *Eos, Transactions American Geophysical Union (AGU) 93(27)*:249.
- Bromirski, P.D., A.J. Miller, R.E. Flick, and G. Auad. 2011. "Dynamical Suppression of Sea Level Rise Along the Pacific Coast of North America: Indications for Imminent Acceleration," Journal Geophysical Research C *116*:C07005.

- Bromirski, P. D., R. E. Flick, and D. R. Cayan. 2003. "Storminess Variability along the California Coast: 1858–2000," Journal of Climate 16(6):982–993.
- Brooks, S. M., T. Spencer, and S. Boreham. 2012. "Deriving Mechanisms and Thresholds for Cliff Retreat in Soft-rock Cliffs under Changing Climates: Rapidly Retreating Cliffs of the Suffolk Coast, UK," *Geomorphology* 153–154:48–60.
- Bruun, P. 1962. "Sea Level Rise as Cause of Shore Erosion," *Journal of Waterways and Harbors Division* 88:117–130. American Society of Civil Engineers.
- Burkett, V. R., D. B. Zilkoski, and D. A. Hart. 2003. "Sea-level Rise and Subsidence: Implications for Flooding in New Orleans." In *U.S. Geological Survey Subsidence Interest Group Conference, Proceedings of the Technical Meeting* (pp. 63–70. Keith R. Prince and Devin L. Galloway, Eds. 27–29 November ,Galveston, TX. U.S. Geological Survey, Water Resources Division Open File Report 03-308. http://pubs.usgs.gov/of/2003/ofr03-308/
- Burton, I., J. B. Smith, and S. Lenhart. 1998. "Adaptation to Climate Change: Theory and Assessment." *In Handbook on Methods for Climate Change Impact Assessment and Adaptation Strategies, Version 2.0* (Chapter 5). J.F. Feenstra, I. Burton, J.B. Smith, and R.S.J. Tol, Eds. United Nations Environment Assembly (UNEP)/National Institute of Public Health and the Environment (RIVM), Nairobi, Kenya, and Amsterdam, The Netherlands.
- Byrd, B. F. and S. Berryman. 2006. "Approaching Prehistory in the Future on MCB Camp Pendleton, Southern California." *Proceedings of Society for California Archaeology* 19:229–232.
- California Department of Water Resources. 1956. "Santa Margarita River Investigation." Bulletin No. 57. California Department of Water Resources, Sacramento, CA.
- Caress, D. W. and D. N. Chayes. 1995. "New Software for Processing Sidescan Data from Sidescan-Capable Multibeam Sonars." *Proceedings of Oceans '95 MTS:IEEE: Challenges in Our Changing Environment, Volume 2* (pp. 997–1000). 9–12 October, San Diego, CA. IEEE.
- Carter, T. R., M. L. Parry, H. Harasawa, and S. Nishioka. 1994. IPCC Technical Guidelines for Assessing Climate Change Impacts and Adaptations. University College London, London, UK.
- Cartwright, D. E. 1974. "Years of Peak Astronomical Tides," *Nature* 248:656–657.
- Cartwright, A. 2008. "Global Climate Change and Adaptation A Sea-Level Rise Risk Assessment. Phase Three: Final Report, A Sea-Level Rise Risk Assessment for the City of Cape Town." Prepared for the Environmental Resource Management Department, City of Cape Town. South Africa.
- Cayan D. R., E. P. Maurer, M. D. Dettinger, M. Tyree, and K. Hayhoe. 2008b. "Climate Change Scenarios for the California Region," *Climatic Change* 87(1):21–42.
- Cayan, D., M. Tyree, M. Dettinger, H. Hidalgo, T. Das, E. Maurer, P. Bromirski, N. Graham, and R. Flick. 2009. "Climate Change Scenarios and Sea Level Rise Estimates for the California 2009 Climate Change Scenarios Assessment." Publication #CEC-500-2009-014-F. California Climate Change Center.
- Cayan, D., P. Bromirski, K. Hayhoe, M. Tyree, M. Dettinger, and R. Flick. 2006. "Projecting Future Sea Level." CEC-500-2005-202-SF. California Climate Change Center. California Energy Commission, Public Interest Energy Research Program.

- Cayan, D. R., P. D. Bromirski, K. Hayhoe, M. Tyree, M. Dettinger, and R.E. Flick, 2008a. "Climate Change Projections of Sea Level Extremes along the California Coast," *Climatic Change* 87 (1):57–73.
- Center for Global Environmental Research. 1996. National Institute for Environmental Studies, Environment Agency of Japan.
- Center for Naval Analysis (CNA). 2010. "National Security and the Threat of Climate Change." Alexandria, VA. http://securityandclimate.cna.org/.
- Chadwick, D. B, R. Flick, J. Helly, T. Nishikawa, P.F. Wang, W. O'Reilly, R. Guza, P. Bromirski, A. Young, W. Crampton, B. Wild, and I. Canner, 2011. "A Framework for Sea Level Rise Vulnerability Assessment for Southwest U.S. Military Installations." *Proceedings Oceans* '11, Mar. Tech. Soc., Institute of Electrical and Electronic Engineers, pp. 110426–001.
- Chadwick, D.B., I. *Rivera*-Duarte, G. Rosen, P.F. Wang, R.C. Santore, A.C. Ryan, P.R. Paquin, S.D. Hafner, and W. Choi. 2008. "Demonstration of an Integrated Compliance Model for Predicting Copper Fate and Effects in DoD Harbors Environmental Security Technology Certification Program (ESTCP) Project ER-0523. "Technical Report 1973. SSC Pacific, San Diego, CA.
- Chelton, D. B. and R. E. Davis. 1982. "Monthly Mean Seal-level Variability along the West Coast of North America," *Journal of Physical Oceanography* 12:757–784.
- Cheng, R. T., V. Casulli, and J. W. Gartner. 1993. "Tidal, Residual, Intertidal Mudflat (TRIM) Model and Its Applications to San Francisco Bay, California," *Estuarine, Coastal, and Shelf Science* 36(3):235–280.
- Chenoweth, M. and C. Landsea. 2004. "The San Diego Hurricane of 2 October 1858," Bulletin of the American Metetorological Society *85(11)*:1689–1697.
- Church, J. A. and N. J. White. 2006. "A 20th Century Acceleration in Global Sea-Level Rise," *Geophysical Research Letters 33(1)*. L01602, doi:10.1029/2005GL024826.
- Commonwealth of Australia. 2006. "Climate Change Impacts & Risk Management: A Guide for Business and Government." Australian Greenhouse Office, Department of the Environment and Heritage.
- Cooper, J. A. G. and O. H. Pilkey. 2004. "Sea-level Rise and Shoreline Retreat: Time to Abandon the Bruun Rule," *Global and Planetary Change* 43(3):157–171.
- Cowell, P. J., B. G. Thom, R. A. Jones, C. H. Everts, and D. Simanovic. 2006. "Management of Uncertainty in Predicting Climate-Change Impacts on Beaches," *Journal of Coastal Research* 22(1):232–245.
- Cubash, U., G. A. Meehl, et al. 2001. "Projections of Future Climate Change. Chapter 9, IPCC Third Assessment Report of the Intergovernmental Panel on Climate Change." Cambridge University Press, Cambridge, UK, and New York, NY.
- Dar, I. A and M. A. Dar. 2009. "Prediction of Shoreline Recession using Geospatial Technology: A Case Study of Chennai Coast, Tamil Nadu, India," *Journal of Coastal Research*:1276–1286.
- Das, B. M. 2002. Principles of Geotechnical Engineering. Wadsworth Group, Pacific Grove, CA.
- Dean, R. G. 1991. "Equilibrium Beach Profiles: Characteristics and Applications," *Journal of Coastal Research*:53–84.

- Dean, R. G. and E. M. Maurmeyer. 1983. "Models for Beach Profile Response." In CRC *Handbook of Coastal Processes and Erosion*, pp. 151–165, CRC Press, Boco Raton, FL.
- Dean, R. G. 1977. "Equilibrium Beach Profiles: U.S. Atlantic and Gulf Coasts." Technical Report. 12, University of Delaware, Department of Civil Engineering, Newark, DE.
- Dean, R. G., D. L. Kriebel, and T. L. Walton. 2002. "Cross-shore Sediment Transport Processes." Chap. 3, Part III, In *Coastal Engineering Manual*, Chapter 3, Part III, EM 1110-2–1100. U.S. Army Corps of Engineers.
- Department of the Navy. 2011. "Silver Strand Training Complex Environmental Impact Statement." Naval Facilities Engineering Command Southwest, San Diego, CA.
- Department of the Navy. (n.d.). "Silver Strand Training Complex EIS." Retrieved 24 October 2012, from http://www.silverstrandtrainingcomplexeis.com/Documents/CCC-CZMA_20100526_CCD_Final.pdf
- Di Lorenzo, E., N. Schneider, K. M. Cobb, P.J.S. Franks, K. Chhak, A. J. Miller, J. C. McWilliams, S. J. Bograd, H. Arango, E. Curchitser, T. M. Powell, and P. Riviere. 2008. "North Pacific Gyre Oscillation Links Ocean Climate and Ecosystem Change," *Geophysical Research* Letters 35:L08607, doi:10.1029/2007GL032838.
- Dickson, M. E., M. J. Walkden, and J. W. Hall. (2007). Systemic Impacts of Climate Change on an Eroding Coastal Region over the Twenty-First Century," *Climatic Change* 84(2):141–166.
- Dolan, A. H. and I. J. Walker. 2006. "Understanding Vulnerability of Coastal Communities to Climate Change Related Risks," *Journal of Coastal Research* SI 39 (Proceedings of the 8th International Coastal Symposium, Itajaí, SC, Brazil):1316–1323.
- Dubois, R. N. 1992. "A Re-evaluation of Bruun's Rule and Supporting Evidence," *Journal of Coastal Research*:618–628.
- Dubois, R. N, 1990. "Barrier Beach Erosion and Rising Sea Level," Geology 18:1150-1152.
- Ehlig, P. L. 1977. "Geologic Report on the Area Adjacent to the San Onofre Nuclear Generating Station, Northwestern San Diego County, California." In *Neotectonics and Coastal Instability: Orange and Northern San Diego Counties, California*, pp. 113–132, M. R. Legg, G. G. Kuhn, and R. J. Shlemon, Eds.
- Elwany, H. and R. E. Flick. 2000. "San Onofre Nuclear Generating Station (SONGS), Unit 1 Deconstruction Marine Impacts Study, Phase I, Coastal Environments." Submitted to Southern California Edison, CE Ref. 2000–03, San Clemente, CA.
- Enfield, D. B. and J. S. Allen. 1980. "On the Structure and Dynamics of Monthly Mean Sea Level Anomalies along the Pacific Coast of North and South America," *Journal of Physical Oceanography* 10:557–578.
- Everts, C. H. 1987. "Silver Strand Littoral Cell, Preliminary Sediment Budget Report." Prepared by Moffatt & Nichol Engineers for U.S. Army Corps of Engineers, Los Angeles District, Coast of California Storm and Tidal Waves Study (CCSTWS) Report 87–3.
- Everts, C. H. 1990. "Sediment Budget Report, Oceanside Littoral Cell." Prepared by Moffatt & Nichol Engineers, for U.S. Army Corps of Engineers, Los Angeles District, Coast of California Storm and Tidal Waves Study (CCSTWS) Report 90–2.

- Everts, C. H. 1991. "Seacliff Retreat and Coarse Sediment Yields in Southern California," *Coastal Sediments '91: Proceedings of a Specialty Conference on Quantitative Approaches to Coastal Sediment Processes, Volume 1*, pp. 1586–1598, 25–27 June, Seattle, WA. American Society of Civil Engineers.
- Feenstra, J. F., I. Burton, J. B. Smith, and R.S.J. Tol, Eds. 1998. "Handbook on Methods for Climate Change Impact Assessment and Adaptation Strategies, Version 2.0." United Nations Environment Programme, Nairobi, and Institute for Environmental Studies, Vrije Universiteit, Amsterdam.
- FEMA. 1991. "Projected Impact of Relative Sea Level Rise on the National Flood Insurance Program (PDF)." October 1991.
- Fleming, J., C. Fulcher, R. Luettich, B. Estrade, G. D. Allen, and H. S. Winer. 2008. "A Real Time Storm Surge Forecasting System using ADCIRC," *Estuarine and Coastal Modeling X*: 373–392.
- Fleming, K., P. Johnston, D. Zwartz, Y. Yokoyama, K. Lambeck, and J. Chappell. 1998. "Refining the Eustatic Sea-level Curve since the Last Glacial Maximum using Far- and Intermediate-Field Sites," *Earth and Planetary Science Letters* 163(1-4):327–342.
- Fleming, K. M. 2000. "Glacial Rebound and Sea-level Change Constraints on the Greenland Ice Sheet." Australian National University. Ph.D. Thesis.
- Fletcher, C. H. 2009. "Sea Level by the End of the 21st Century: A Review," *Shore & Beach* 77(4):1–9.
- Flick, R. E. and A. Badan-Dangon. 1989, "Coastal Sea Levels during the January 1988 Storm off the Californias," *Shore & Beach 57(4)*:28–31.
- Flick, R. E. and D. R. Cayan. 1984. "Extreme Sea Levels on the Coast of California,." *Proceeding of the 19th International Conference on Coastal Engineering*, pp. 886–898, American Society of Civil Engineering.
- Flick, R. E. and L. C. Ewing, 2009. "Sand Volume Needs of Southern California Beaches as a Function of Future Sea Level Rise Rates, *Shore & Beach* 77(4):36–45.
- Flick, R. E. 1986, "A Review of Conditions Associated with High Sea Levels in Southern California," *Science of the Total Environment* 55:251–259.
- Flick, R. E. 1993. "The Myth and Reality of Southern California Beaches," *Shore & Beach 61(3)*:3–13.
- Flick, R. E. 1994. "Shoreline Erosion Assessment and Atlas of the San Diego Region." 2 vols. California Department of Boating and Waterways. Sacramento, CA.
- Flick, R. E. 1998. "Comparison of California Tides, Storm Surges, and Sea Level during the El Niño Winters of 1982–83 and 1997–98," *Shore & Beach 66(3):7–11*.
- Flick, R. E., 2000. "Time-of-day of Peak Tides in a Mixed-Tide Regime," *Shore & Beach* 68(4):15–17.
- Flick, R. E., 2005, "Dana Point to the International Border," Living with the Changing California Coast." Chap. 20, G. Griggs, K. Patch, and L. Savoy, Eds. University of California Press, Berkeley, CA.

- Flick, R. E., J. F. Murray and L. C. Ewing. 2003. "Trends in United States Tidal Datum Statistics and Tide Range," *Journal of Waterway, Port, Coastal and Ocean Engineering* 129(4):155–164, American Society of Civil Engineering.
- Flick, R. E., J. R. Wanetick, M. Hany S. Elwany, R.S. Grove, and B. W. Waldorf. 2010. "Beach Changes from Construction of San Onofre Nuclear Generating Station 1964-1989," *Shore & Beach* 78(4):12–25.
- Flick, R. E., K. Knuuti, and S. K. Gill. 2013. "Matching Mean Sea Level Rise Projections to Local Elevation Datums," *Journal of Waterway, Port, Coastal and Ocean Engineering* 139(2):142–146.
- Flick, R. E. and E. H. Sterrett. 1984. "The San Diego Shoreline." In Shoreline Erosion Assessment and Atlas of the San Diego Region, Volume I." Unpublished Report. California Department of Boating and Waterways, Sacramento, CA.
- Gartner, J. W. and R. N. Oltmann, 1990. "Comparison of Recording Current Meters in Shallow Waters of San Francisco Bay, California, 1990." U.S. Geological Survey Water Resources Investigation Report 90-4018.
- Gornitz, V. C. Rosenzweig and D. Hillel, 1997. "Effects of Anthropogenic Intervention in the Land Hydrologic Cycle on Global Sea Level Rise, *Global and Planetary Change 14*:147–161.
- Graham, N. E. 2003. "Variability in the Wave Climate of the North Pacific: Links to Inter-annual and Inter-decadal Variability." *Oceans 2003 Proceedings, Volume Five*, pp. 969–972, 22–26 September, San Diego, CA. San Diego Marine Technology Society.
- Greene, H. G. and M. P. Kennedy, 1978. "Geology of the Inner-Southern California Continental Margin, California Continental Margin Geologic Map Series." California Division of Mines and Geology and U.S. Geological Survey.
- Grinsted, A., J. C. Moore, and S. Jevrejeva. 2009. "Reconstructing Sea Level from Paleo and Projected Temperatures 200 to 2100 AD," *Climate Dynamics 34*:461–472.
- Gumbel, E. J. 1958. "Statistics of Extremes." Columbia University Press, New York, NY.
- Gutierrez, B. T., E. R. Thieler, and S. J. Williams. 2009. "Synthesis and Assessment Product 4.1." In *Coastal Elevations and Sensitivity to Sea-level Rise: A Focus on the Mid-Atlantic Region*, pp. 11–24, U.S. Environmental Protection Agency, Washington, DC.
- Hallermeier, R. J. 1981. "A Profile Zonation for Seasonal Sand Beaches from Wave Climate.," *Coastal Engineering* 4:253–277.
- Hallermeier, R. J. 1978. "Uses for a Calculated Limit Depth to Beach Erosio," *Proceedings of the 16th Coastal Engineering Conference*, Volume 1, pp. 1493–1512, 27 August to 3 September, Hamburg, Germany. American Society of Civil Engineers..
- Hammar-Klose, and Thieler, E.R., 2001. Coastal Vulnerability to Sea-Level Rise: A Preliminary Database for the U.S. Atlantic, Pacific, and Gulf of Mexico Coasts. U.S. Geological Survey, Digital Data Series DDS–68.
- Hands, E. B. 1983. "The Great Lakes as a Test Model for Profile Responses to Sea Level Changes." In *Handbook of Coastal Processes and Erosion*, pp. 176–189, P. D. Komar, Ed. C.R.C. Press, Boca Raton, FL.

- Hapke C. and D. Reid. 2007. "Cliff Erosion Rates for Southern California Generated at a 20 m Transect Spacing, 1928-1998." Open-File Report 2007-1112. U.S. Geological Survey, Coastal and Marine Geology Program, Santa Cruz, CA.
- Hapke, C. J., D. Reid, B. M. Richmond, P. Ruggiero, and J. List. 2006, "National Assessment of Shoreline Change: Part 3: Historical Shoreline Change and Associated Coastal Land Loss Along Sandy Shorelines of the California Coast." U.S. Geological Survey Open-file Report 2006-1219 (http://pubs.usgs.gov/of/2006/1219).
- Hare, S. R. and N. J Mantua. 2000. "Empirical Evidence for North Pacific Regime Shifts in 1977 and 1989," *Progress in Oceanography* 47(2-4):103–145.
- Hays, J. D., J. Imbrie, and N. J. Shackleton. 1976. "Variations in the Earth's Orbit: Pacemaker of the Ice Ages," *Science* 194(4270):1121–1132.
- Heberger, M., H. Cooley, P. Herrera, P. H. Gleick, and E. Moore. 2009. "The Impacts of Sea Level Rise on the California Coast." CEC-500-2009-024-F. California Climate Change Center.
- Herron, W. J. 1980. "Artificial Beaches in Southern California," *Shore & Beach* 48(1):3–12.
- Herzberg, A. 1961. "Die Wasserverversorgung Einiger Nordseebader, Munich," *Journal Gasbeleuchtung Wasserversorgung 44*:815–819, 842–844.
- Houston, J. R. 2013. "Global Sea Level Projections to 2100 using Methodology of the Intergovernmental Panel on Climate Change," *Journal of Waterway, Port, Coastal and Ocean Engineering* 139(2):82–87.
- Hulme, M. 2001. "New Tyndall Centre to Encourage Integrated Climate Research," *Ocean Challenge 10*:15–16.
- Hurrell, J. W. 1995. "Decadal Trends in the North Atlantic Oscillation: Regional Temperature and Precipitation," *Science* 269:676--679.
- Inman, D. L. and J. D. Frautschy. 1965. "Littoral Processes and the Development of Shorelines." *Coastal Engineering: Santa Barbara Specialty Conference, October 1995* (pp. 511–553). American Society of Civil Engineers.
- Inman, D. L. and C. E. Nordstrom. 1971. "On the Tectonic and Morphological Classification of Coasts," *Journal of Geology* 79:1–21.
- Inman, D. L. and P. M. Masters. 1991. "Budget of Sediment and Prediction of the Future State of the Coast." In California Storm and Tidal Waves Study, State of the Coast Report (Chapter 9). U.S. Army Corps of Engineers, Los Angeles District. http://escholarship.org/uc/item/0wn3c7kr;jsessionid=75C049257FDF4D2ADEAED6AB48678E0D#page-1.
- Inman, D. L., M.H.S. Elwany, and S. A. Jenkins. 1993. "Shorerise and Bar-berm Profiles on Ocean Beaches," *Journal of Geophysical Research* 98(C10):18,181–18,199.
- IPCC. 1990. "Strategies for Adaptation to Sea Level Rise: Report of the Coastal Management Subgroup." Response Strategies Working Group. Ministry of Transport and Public Works, Rijkswaterstaat, Tidal Waters Division, The Hague.

- IPCC. 1994. "IPCC Technical Guidelines for Assessing Climate Change Impacts and Adaptations." Prepared by Working Group II T. R. Carter, M. L. Parry, H. Harasawa, and S. Nishioka, Eds., and the World Meteorological Association/United Nations Environment Programme. CGER-IO15-'94. University College -London, UK, and Center for Global Environmental Research, National Institute for Environmental Studies, Tsukuba, Japan.
- IPCC. 2001. "Climate Change 2001: Synthesis Report. A Contribution of Working Groups I, II, and III to the Third Assessment Report of the Integovernmental Panel on Climate Change." T. R. Watson and the Core Writing Team, Eds. Cambridge University Press, Cambridge, UK, and New York, NY.
- IPCC. 2007a. "Climate Change 2007. Synthesis Report, Contribution of Working Groups I, II, and III to the Fourth Assessment Report of the Intergovernmental Panel on Climate Change." IPCC, Geneva, Switzerland. http://www.ipcc.ch/ipccreports/assessments-reports.htm.
- IPCC. 2007b. "Climate Change 2007: The Physical Science Basis. Contribution of Working Group I to the Fourth Assessment Report of the Intergovernmental Panel on Climate Change."S. Solomon, D. Qin, and M. Manning, Eds.
- IPCC. 1992. "A Common Methodology for Assessing Vulnerability to Sea Level Rise." In Appendix C in "Global Climate Change and the Rising Challenge of the Sea: Report of the Coastal Zone Management Subgroup." Response Strategies Working Group. Ministry of Transport and Public Works, Rijkswaterstaat, Tidal Waters Division, The Hague.
- Jones, R. N., 2001. An Environmental Risk Assessment/Management Framework for Climate Change Impact Assessments," *Natural Hazards* 23(2-3):197–230.
- Karl, T. R., G. A. Meehl, C. D. Miller, S. J. Hassol, A. M. Waple, and W. L. Murray, Eds. 2008. "Weather and Climate Extremes in a Changing Climate, Regions of Focus: North America, Hawaii, Caribbean, and U.S. Pacific Islands, Synthesis and Assessment Product." Report by the U.S. Climate Change Science Program, and the Subcommittee on Global Change Research, NOAA, National Climatic Data Center, Washington, D.C., downloads.climatescience.gov/sap/sap3-3/sap3-3-final-all.pdf.
- Kasperson, J. X., R. E. Kasperson, and B. L. Turner, II. 2001. "Trajectories of Threat: Assessing Environmental Criticality in Nine Regions." In *Global Environmental Risk (Risk, Society and Policy)*, J. X. Kasperson and R. E. Kasperson, Eds. United Nations University Press, New York, NY.
- Kay, R. and J. Hay. 1993. "A Decision Support Approach to Coastal Vulnerability and Resilience Assessment: A Tool for Integrated Coastal Zone Management," pp. 213–225 R. McLean and N. Mimura (eds), Proceedings of the IPCC Eastern Hemisphere Workshop: Vulnerability Assessment to Sea Level Rise and Coastal Zone Management. World Meteorological Organization (pp. 213–225). 3-6 August, Tsukuba, Japan. World Meteorological Organization/United Nations Environment Programme.
- Kennedy, M. P. and S. S. Tan, 2008. Geologic Map of the San Diego 30' X 60' Quadrangle, California." California Geological Survey, Regional Geologic Map No. 3, scale 1:100000. http://ngmdb.usgs.gov/ngm-bin/ILView.pl?sid=84173_1.sid&vtype=b.
- Kennedy, M. P. 2001. "Geologic Map of the Las Pulgas Canyon 7.5" Quadrangle, San Diego County, California: A Digital Database, Version 1.0." California Department of Conservation, Division of Mines and Geology, scale 1:24,000, 1 plate.

- Kern, P., A. Derrickson, and T. Burke. 1996. Preliminary Geological Map of Quartenary Marine Terraces at Dana Point, Orange County, California." In *The SDAG Field Trip Guidebook*. San Diego Association of Geologists, San Diego, CA.
- Klein, R. J., M. J. Smit, H. Goosen, and C. H. Hulsberge. 1998. "Resilience and Vulnerability: Coastal Dynamics or Dutch Dikes? The Geographical Journal 164(3): 259–268.
- Klein, R.J.T. 2002. "Coastal Vulnerability, Resilience and Adaptation to Climate Change: An Interdisciplinary Perspective." Ph.D. thesis. Christian-Albrechts-Universität zu Kiel.
- Klein, R.J.T. and R. J. Nicholls. 1999. "Assessment of Coastal Vulnerability to Climate Change. *Ambio* 28(2):182–187.
- Kriebel, D. L. and R. G. Dean. 1993. "Convolution Method for Time-dependent Beach Profile Response," *Journal of Waterway, Port, Coastal, and Ocean Eng*ineering 119:204–226.
- Kuhn, G. G. and F. P. Shepard. 1991. Sea Cliffs, Beaches, and Coastal Valleys of San Diego County: Some Amazing Histories and Some Horrifying Implications. University California Press, Berkeley, CA.
- Kuleli, T. 2010. "City-Based Risk Assessment of Sea Level Rise Using Topographic and Census Data for the Turkish Coastal Zone," *Estuaries and Coasts 33*:640–651.
- Lajoie, K. R. 1986. "Coastal Tectonics," *Active Tectonics*:95–124.
- Larson, M. and N. C. Kraus, 1989. "SBEACH: Numerical Model for Simulating Storm-induced Beach Change." Technical Report CERC-89-9, U.S. Army Corps of Engineers, Vicksburg, MS.
- Leatherman, S. P. 1990. "Modeling Shore Response to Sea-Level Rise on Sedimentary Coasts.," *Progress in Physical Geography 14*(4):447–464.
- Leggett, J., W. Pepper, A. Sankovski, J. Smith, R. Tol, and T. Wigley. 2003. Climate Change Risk Analysis Framework (CCRAF) a Probabilistic Tool for Analyzing Climate Change Uncertainties," *Geophysical Research Abstracts* 5:07416.
- LeMehaute, B. and J. D. Wang. 1982. "Wave Spectrum Changes on a Sloped Beach," *Journal of Waterway, Port, Coastal, and Ocean Engineering 108 (WW1)*:33–47.
- Lin, N., K. A. Emanuel, J. A. Smith, and E. Vanmarcke. 2010. Risk Assessment of Hurricane Storm Surge for New York City," *Journal of Geophysical Research* 115:D18121.
- Liverman, D. 2001. "Vulnerability to Global Environmental Change." In *Global Environmental Risk* pp. 201–216, J. X. Kasperson and R. E. Kasperson, Eds. United Nations University Press, Tokyo.
- Longuet-Higgins, M. S. 1957. "On the Transformation of a Continuous Spectrum by Refraction," *Proceedings of the Cambridge Philosophical Society* 53(1):226–229.
- Maas, C. F. and M. D. Albright, 1989. "Origin of the Catalina Eddy," *Monthly Weather Review* 117(11).
- Makkonen, L. 2011. "Reply," Journal of Climate and Applied Meteorology 50:267–270.
- Mantua, N. J., S. R. Hare, Y. Zhang, J. M. Wallace, and R. C. Francis. 1997. "A Pacific Interdecadal Climate Oscillation with Impact on Salmon Production," *Bulletin of the American Meteorological Society* 78:1069–1079.

- Marsden, A. L., M. Wang, J. E. Dennis, and P. Moin. 2004. "Optimal Aeroacoustic Shape Design using the Surrogate Management Framework," *Optimization Engineering* 5(2):235–262, Special Issue: Surrogate Optimization.
- Masters, P. M. and I. W. Aiello. 2007. "Postglacial Evolution of Coastal Environments." In *California Prehistory, Colonization, Culture, and Complexity*, pp. 35–52, T. L. Jones and K. A. Klar, Eds. Alta Mira Press, Landham, MD.
- Maurer, E. P., H. G. Hidalgo, T. Das, M. D. Dettinger, and D. R. Cayan. 2010. "The Utility of Daily Large-Scale Climate Data in the Assessment of Climate Change Impacts on Daily Streamflow in California," *Hydrology and Earth System Sciences* 14(6):1125–1138.
- MCBCP, 2007. "Integrated Natural Resources Management Plan." Marine Corps Base Camp Pendleton, CA.
- MCBCP. 1993. "Camp Pendleton Annual Water Quality Report." 1992. Environmental and Natural Resources Management Office, Water Quality Branch, Marine Corps Base, Camp Pendleton, CA.
- McCarthy, J. J., O. F. Canziani, N. A. Leary, D. J. Dokken, and K. S. White, Eds. 2001. "Climate Change 2001: Impacts, Adaptation and Vulnerability Contribution of Working Group II to the Third Assessment Report of the Intergovernmental Panel on Climate Change." Available online at http://www.grida.no/publications/other/ipcc_tar/ (accessed 08 Sep 2010).
- Merrifield, M. A., S. T. Merrifield, and G. T. Mitchum. 2009. "An Anomalous Recent Acceleration of Global Sea Level Rise," *Journal of Climate* 22:5772–5781, doi: http://dx.doi.org/10.1175/2009JCLI2985.1.
- Messner, S., S. Miranda, K. Green, C. Phillips, J. Dudley, D. Cayan, and E. Young. 2008. "Climate Change Related Impacts in the San Diego Region by 2050: Summary Prepared for the 2008 Climate Change Impacts Assessment." Second Biennial Science Report to the California Climate Action Team. http://www.energy.ca.gov/2009publications/CEC-500-2009-027/CEC-500-2009-027-F.PDF.
- Milankovitch, M. 1920. Theorie Mathematique des Phenomenes Thermiques produits par la Radiation Solaire. Gauthier-Villars, Paris France.
- Miller, A. J., D. R. Cayan, T. P. Barnett, N. E. Graham, and J. M. Oberhuber, 1994. "The 1976–77 Climate Regime Shift of the Pacific Ocean," *Oceanography* 7:21–26.
- Miller, J. K. and R. G. Dean. 2004. "A Simple New Shoreline Change Model," *Coastal Engineering*, 51:531–556.
- Milliman, J. D. and B. U. Haq. 1996. *Sea-Level Rise and Coastal Subsidence: Causes, Consequences and Strategies*. Kluwer Publications, Amsterdam, The Netherlands.
- Mimura. 1999. "Vulnerability of Island Countries in the South Pacific to Sea Level Rise and Climate Change. *Climate Research* 12(2-3):137–143.
- Milne, G. A., A. J. Long and S. E. Bassett. 2005. "Modelling Holocene Relative Sea-Level Observations from the Caribbean and South America," *Quaternary Science Reviews* 24 (10-11):1183–1202.
- Moffatt & Nichol Engineers. 1987. "San Diego Region: Historic Beach Profile Data Report." Report prepared for U.S. Army Corps of Engineers, Los Angeles District. Los Angeles, CA.

- Moore, G. W. and M. P. Kennedy. 1970. "Coastal Geology of the California–Baja California Border Area." In *American Association of Petroleum Geologists Pacific Section Fall 1970 Guidebook*, pp. 4–9.
- Munk, W. H. and M. A. Traylor. 1947. "Refraction of Ocean Waves: A Process Linking Underwater Topography to Beach Erosion," *Journal of Geology* 55(1):1–26.
- Munk, W. H., G. R. Miller, F. E. Snodgrass, and N. F. Barber. 1963. "Directional Recording of Swell from Distant Storms," *Philosophical Transactions of the Royal Society of London* 55(1062) :505–584.
- National Research Council. 1987. Responding to Changes in Sea Level: Engineering Implications. National Academy Press, Washington, D.C. http://www.nap.edu/catalog.php?record_id=1006.
- NAVFAC. 2005. "UFC 4-152-01 Design: Piers and Wharves." Whole Building Design Guide, Port Hueneme, CA.
- NAVFAC. 2011. "UFC 3-701-01 DoD Facilities Pricing Guide." Whole Building Design Guide, Port Hueneme, CA.
- Nerem, R. S. 1999. "Measuring Very Low Frequency Sea Level Variations using Satellite Altimeter Data," *Global and Planetary Change* 20(2-3):57–171.
- Nguyen, X.T., H. Tanaka, and H. Nagabayashi. 2007. "Wave Setup at River and Inlet Entrances Due to an Extreme Event." *Proceedings of International Conference on Violent Flows (VF-2007)*, Kyushu University, Fukuoka, Japan.
- Nicholls, R. J., N. Marinova, J. A. Lowe, S. Brown, P. Vellinga, D. de Gusmão, J. Hinkel and R.S.J. Tol. 2011. "Sea-level Rise and its Possible Impacts Given a 'beyond 4° C World' in the Twenty-first Century," *Philosophical Transactions of the Royal Society A 369*:161–181.
- Nicholls, R. J. 1995. "Synthesis of Vulnerability Analysis Studies." *Proceedings of World Coast* 1993 (pp. 181-216). 1–5 November, Ministry of Transport, Public Works and Water Management, The Netherlands.
- Nicholls, R. J. and N. Mimura. 1998. "Regional Issues Raised by Sea-Level Rise and their Policy Implications," *Climate Research* 11(1):5–18.
- Nicholls, R. J. and R.J.T. Klein. 2000. "Adaptation Frameworks for Sea-Level Rise Impacts." First Meeting for the Implementation of the Recommendations Arising from the Third Ministerial Conference on Environment and Health, London, 1999." European Centre for Environment and Health, World Health Organisation, 26-28 May, Rome, Italy.
- Nicholls, R. J. 2002. Analysis of Global Impacts of Sea-Level Rise: A Case Study of Flooding, Physics and Chemistry of the Earth 27:1455–1466.
- Nicholls, R. J. and A.C. de la Vega-Leinert. 2008. "Implications of Sea-level Rise for Europe's Coasts: An Introduction," *Journal of Coastal Research* 24(2):285–287.
- NOAA. 2009. *Proceedings from the Sea Level Rise and Inundation Community Workshop*. 3–5 December, Lansdowne, VA.
- NOAA. 2011. "Storm Surge Overview: Factors Impacting Surge." http://www.nhc.noaa.gov/ssurge/ssurge_overview.shtml#IMPACT

- North Carolina Division of Emergency Management (NCDEM). 2009. "North Carolina Sea Level Rise Risk Management Study: Potential Impacts, Risk Assessment and Management Strategies." Office of Geospatial and Technology Management Study Plan 3.1 (October 26).
- O'Reilly, W. C. 1993. The Southern California Wave Climate: Effects of Islands and Bathymetry, *Shore & Beach 61(3)*:14–19.
- O'Reilly, W. C., R. T. Guza, and D. Castel. 1993. "Wave Monitoring in the Southern California Bight." *Proceedings of the 2nd International Symposium on Ocean Wave Measurement and Analysis* (448–457). 25-28 July, New Orleans, LA. American Society of Civil Engineers.
- Ocean Protection Council (OPC). 2010. "Resolution of the California Ocean Protection Council on Sea-Level Rise."

 http://www.opc.ca.gov/webmaster/ftp/pdf/agenda_items/20100911/14.%20SLR/1011_COPC _SLR_Draft%20Resolution.pdf.
- O'Reilly, W. C., 1991. "Modeling Surface Gravity Waves in the Southern California Bight." Ph.D. dissertation, University of California, San Diego.
- O'Reilly, W. C. and R. T. Guza, 1991. "A Comparison of Spectral Refraction and Refraction-Diffraction Wave Propagation Models," *Journal of Waterway, Port, Coastal and Ocean Engineering* 117(3):199–215.
- Osborne, R. H., N. J. Darigo, and R. C. Scheidemann, Jr. 1983, "Report of Potential Offshore Sand and Gravel Resources of the Inner Continental Shelf of Southern California." California Department of Boating and Waterways.
- Parry, M. L., Ed. 2007. Climate Change 2007: Impacts, Adaptation and Vulnerability: Working Group II Contribution to the Fourth Assessment Report of the IPCC Intergovernmental Panel on Climate Change. Volume 4. Cambridge University Press, Cambridge, UK.
- Parry, M. L., O.F. Canziani, J. P. Palutikof, P. J. van der Linden, and C.E. Hanson, Eds. 2007. Climate Change 2007: Impacts, Adaptation and Vulnerability. Contribution of Working Group II to the Fourth Assessment Report of the Intergovernmental Panel on Climate Change. Cambridge University Press, Cambridge, UK. Available online at http://www.ipcc.ch/publications_and_data/publications_ipcc_fourth_assessment_report_wg2 _report_impacts_adaptation_and_vulnerability.htm [accessed 08 Sep 2010].
- Patz, J. A. and J. Balbus. 1996. "Methods for Assessing Public Health Vulnerability to Global Climate Change," *Climate Research* 6(2):113–125.
- Pawka, S. S. 1983. "Island Shadows in Wave Directional Spectra," *Journal of Geophysical Research* 88(C4):2579–2591.
- Pilkey, O. H. and J. A. Cooper. 2004. "Society and Sea Level Rise," *Science* 303(5665):1781–1782.
- Poulter, B. and P. N. Halpin. 2008. "Raster Modelling of Coastal Flooding from Sea-level Rise," *International Journal of Geographical Information Science* 22(2):167–182.
- Rahmstorf, S. 2007. "A Semi-Empirical Approach to Projecting Future Sea-Level Rise," *Science* 315(5810):368–370.
- Rahmstorf, S. 2010. "A New View on Sea Level Rise," Nature Reports Climate Change 4:44-45.

- Revell, D., M. Heberger, P. Gleick, B. Battalio, H. Cooley, and J. Vandever. 2009. "An Initial Assessment of the Impacts of Sea Level Rise to the California Coast." Climate Change, Natural Resources, and Coastal Management: A Workshop on the Coastal Ecosystems of California, Oregon and Washington.
- Revell, D. L., R. Battalio, B. Spear, P. Ruggiero, and J. Vandever. 2011. "A Methodology for Predicting Future Coastal Hazards due to Sea-level Rise on the California Coast," *Climatic Change 109 (Supplement 1)*:S251–S276.
- Roelvink, J. A. 1993. "Dissipation in Random Wave Groups Incident on a Beach," *Coastal Engineering 19*:127–150.
- Roelvink, J. A., A. Reniers, A. van Donger, J. van Thiel de Vries, R. McCall, and J. Lescinski. 2009. "Modeling Storm Impacts on Beaches, Dunes and Barrier Islands," *Coastal Engineering* 56: 1133–1152.
- Roff, D. F. 1998. "Injection of Treated Municipal Wastewater into a Coastal Artesian Aquifer." Unpublished Master of Science Thesis, San Diego State University, San Diego, CA.
- Rohde, R. 2013. Image created by Robert A. Rohde/Global Warming Art, based on data from Fleming et al. 1998, Fleming 2000, & Milne et al. 2005. Accessed at http://www.globalwarmingart.com/wiki/File:Post-Glacial_Sea_Level_png on January 12, 2013.
- Runyan, K. and Griggs, G. B. 2003. "The Effect of Armoring Seacliffs on the Natural Sand Supply to the Beaches of California," *Journal of Coastal Research* 19(2):336–347.
- San Diego Association of Governments (SANDAG). 1993. "Shoreline Preservation Strategy for the San Diego Region." SANDAG, San Diego, CA.
- Scheitlin, K. N., J. B. Elsner, S. W. Lewers, J. C. Malmstadt, and T. H. Jagger. 2011. "Risk Assessment of Hurricane Winds for Eglin Air Force Base In Northwestern Florida, USA." *Theoretical and Applied Climatology* 105(3-4):287–296.
- Schlemon, R. J. 1994. "The Christianitos Fault and Quartenary Geology, San Onofre State Beach, California." In *Geology and Natural History Camp Pendleton United States Marine Corps Base San Diego County, California*, pp. 75–84, P. Rosenberd, Ed. San Diego Association of Geologists, San Diego, CA.
- Smit, B., and O. Pilifosova, 2001. "Adaptation to Climate Change in the Context of Sustainable Development and Equity." In *Contribution of the Working Group to the Third Assessment Report of the Intergovernmental Panel on Climate Change*, pp. 879–912. Cambridge University Press, Cambridge, UK.
- Smith, J. B, N. Bhatti, G. V. Menzhulin, R. Benioff, M. Campos, B. Jallow, F. Rijsberman, M. I. Budyoko, and R. K. Dixon, Eds. 1996. *Adapting to Climate Change: An International Perspective*. Springer-Verlag, New York, NY.
- Smith, W. 1986. "The Effects of Eastern North Pacific Tropical Cyclones on the Southwestern United States," NOAA Technical Memorandum NWS WR-197. U.S. Department of Commerce, National Oceanic and Atmospheric Administration, Washington, D.C.
- Snover, A. K., L. Whitely Binder, J. Lopez, E. Willmott, J. Kay, D. Howell, and J. Simmonds. 2007. "Preparing for Climate Change: A Guidebook for Local, Regional, and State Governments." ICLEI Local Governments for Sustainability, Oakland, CA.

- Sterr H., R.J.T. Klein, and S. Reese. 1999. "Climate Change and Coastal Zones: An Overview of the State of the Art on Regional and Local Vulnerability Assessment." In Climate Change and Mediterranean Coastal Systems: Regional Scenarios and Vulnerability Assessment, International workshop, 9–10 December, Fondazione Eni Enrico Mattei, Venice, Italy.
- Stetson Engineering. 2001. "Santa Margarita River Recharge and Recovery Enhancement Program Permit 15000 Feasibility Study for Marine Corps Base Camp Pendleton March 2001." Covina, CA.
- Stockdon, H. F., R. A. Holman, P. A. Howd, and A. H. Sallenger. 2006. "Empirical Parameterization of Setup, Swash, and Runup," *Coastal Engineering* 53(7):573–588.
- Strategic Environmental Research and Development Program (SERDP). 2007. "Assessment of the Impact of Sea Level Rise on Military Infrastructure." SON Number SISON-09-05 (November 8). Alexandria, VA.
- Sunamura, T. 1988. "Projection of Future Coastal Cliff Recession under Sea Level Rise Induced by the Greenhouse Effect: Nii-jima Island, Japan," *Transactions of the Japanese Geomorphical Union*, 9(1):17–33.
- Tan, S. S. 2001. "Geologic map of the San Onofre Bluff 7.5' Quadrangle, San Diego County,California: A Digital Database, Version 1.0. California Department of Conservation, Division of Mines and Geology, scale 1:2400, 1 plate.
- Tawn, J.A. and J.M. Vassie, 1989. Extreme sea levels the joint probabilities method revisited and revised, Proc. Inst. Civil Eng. (Great Britain), Part 2 Research and Theory, 87, 429–442.
- Tawn, J. A. 1988. "An Extreme-value Theory Model for Dependent Observations," *Journal of Hydrology 101*:227–250.
- Tawn, J. A. 1992. "Estimating Probabilities of Extreme Sea-levels," *Applied Statistics* 41(1):77–93.
- Titus, J. G., R. A. Park, S. P. Leatherman, J. R. Weggel, M. S. Greene, P. W. Mausel, M. S. Trehan, S. Brown, C. Grant, and G. W. Yohe. 1991. "Greenhouse Effect and Sea Level Rise: Loss of Land and the Cost of Holding Back the Sea," *Coastal Management 19*:171–204.
- Titus, J. G. and C. Richman. 2001. Maps of Lands Vulnerable to Sea Level Rise: Modeled Elevations along the U.S. Atlantic and Gulf Coasts," *Climate Research* 18:205–228.
- Todd, D. K. 1959. Groundwater Hydrology. John Wiley & Sons, Inc., Hoboken, NJ.
- Tol, R.S.J., S. Fankhauser, and J. B. Smith. 1998. "The Scope for Adaptation to Climate Change: What Can We Learn from the Impact Literature?" *Global Environmental Change* 8(2): 109–123
- Tolman, H. 2002. "User Manual and System Documentation of WAVEWATCH-III Version 2.22," Technical Note. Environmental Modeling Center Marine Modeling Analysis Branch Contribution No. 222 (September). National Oceanic and Atmospheric Administration, National Weather Service, and National Center for Environmental Protection. http://polar.ncep.noaa.gov/mmab/papers/tn222/MMAB_222.pdf.
- Trenberth, K. E. and J. W. Hurrell. 1994. "Decadal Atmosphere-ocean Variations in the Pacific," *Climate Dynamics* 9:303–319.
- Trenberth, K. E. and T. J. Hoar. 1996. "The 1990-1995 El Niño-Southern Oscillation Event: Longest on Record," *Geophysical Research Letters* 23(1):57.

- Turner, B. L. II, R. E. Kasperson, P. A. Matson, J. J. McCarthy, R. W. Corell, L. Christensen, N. Eckley, J. X. Kasperson, A. Luers, M. L. Martello, C. Polsky, A. Pulsipher, and A. Schiller. 2003. "A Framework for Vulnerability Analysis in Sustainability Science," *Proceedings of the National Academy of Science 100 (14)*:8074–8079.
- U.S. Government. 2002. Camp Pendleton Military Installation Map, V795S Edition 3-NIMA, California, 1:50,000.
- UNFCCC (Secretariat of the United Nations Framework Convention on Climate Change). 1999. "Compendium of Decision Tools to Evaluate Strategies for Adaptation to Climate Change Final Report." Prepared by Stratus Consulting Inc. Bonn, Germany.
- U.S. EPA. 1989. "The Potential Effects of Global Climate Change on the United States. Report to Congress." EPA 230-05-89-052. U.S. Environmental Protection Agency, Washington, D.C.
- U.S. EPA. 1991. "Risk Assessment Guidance for Superfund." EPA/540/R-92/003. U.S. Environmental Protection Agency, Washington, D.C.
- U.S. EPA. 1998. "Guidelines for Ecological Risk Assessment." EPA/630/R-95/002F. U.S. Environmental Protection Agency, Washington, D.C.
- U.S. EPA. 2009. "A Framework for Categorizing the Relative Vulnerability of Threatened and Endangered Species to Climate Change." EPA/600/R-09/011. National Center for Environmental Assessment, Washington, D.C. http://www.epa.gov/ncea.
- U.S. EPA. 2010. Climate Change Indicators in the United States." U.S. Environmental Protection Agency. Washington, D.C. http://www.epa.gov/climatechange/science/indicators/oceans/sealevel.html, accessed 11/24/13.
- U.S. EPA. 2013a. "Secondary Drinking Water Regulations: Guidance For Nuisance Chemicals."
 U.S. Environmental Protection Agency. Washington, D.C.
 http://water.epa.gov/drink/contaminants/secondarystandards.cfm, accessed April 16, 2013.
- U.S. EPA. 2013b. "Glossary of Climate Change Terms." U.S. Environmental Protection Agency." Washington, D.C. http://www.epa.gov/climatechange/glossary.html, accessed 8/20/13.
- U.S. Navy. 2010. "Silver Strand Training Complex Environmental Impact Statement." http://www.silverstrandtrainingcomplexeis.com/EIS.aspx.
- U.S. Navy. 2008. "Human Health Risk Assessment Guidance."
- USACE. 1986. "Southern California Coastal Photography and Beach Profile Index." CCSTWS Report 86-2. U.S. Army Corps of Engineers, Los Angeles District.
- USACE. 1988a. "Historic Wave and Sea Level Data Report: San Diego Region." CCSTWS Report 88–6. U.S. Army Corp of Engineers, Los Angeles District.
- USACE. 1988b. "Coastal Cliff Sediments: San Diego Region, Dana Point to the Mexican Border (1887–1947)." CCSTWS Report 88–8. U.S. Army Corp of Engineers, Los Angeles District.
- USACE. 1990. "Sediment Budget Report, Oceanside Littoral Cell." CCSTWS Report 90–2. U.S. Army Corps of Engineers, Los Angeles District.
- USACE. 2006. "Coastal Engineering Manual 1110-2-1100." U.S. Army Corps of Engineers, Washington, D.C.

- USACE. 2009. "Water Resource Policies and Authorities Incorporating Sea-Level Change Considerations in Civil Works Programs." Circular No. 1165–2–211. Department of the Army, U.S. Army Corps of Engineers, Washington, D.C. http://140.194.76.129/publications/eng-circulars/ec1165-2-211/toc.html.
- USACE. 2011. "Sea-level Change Considerations for Civil Works Programs" Circular No. EC 1165-2-212. U.S. Army Corps of Engineers, Washington, DC.
- USAID. 2007. "Adapting to Climate Change Variability and Change: A Guidance Manual for Development Planning." USAID, Washington, D.C.
- USCSP (United States Country Studies Program). 1999. "Climate Change: Mitigation, Vulnerability, and Adaptation in Developing and Transition Countries." U.S. Country Studies Management Team (PO-6), Washington, D.C.
- van Westen, C. J. and P. Y. Georgiadou. 2001. "Spatial Data Requirements And Infrastructure for Geologic Risk Assessment. In *Proceedings Workshop on Natural Disaster Management*, ISPRS Technical Committee VII, Ahmedabad, India.
- Vermeer, M. and S. Rahmstorf. 2009. Global Sea Level Linked to Global Temperature," *Proceedings of the National Academy of Science 106*:21527–21532.
- Voss, C. I. and Provost, A. M. 2002. "SUTRA: A Model for Saturated-unsaturated, Variable-density Ground-water Flow with Solute or Energy Transport." Water Resources Investigations Report 02–4231. U.S. Geological Survey, Reston, VA.
- Walkden, M. and M. Dickson. 2008. "Equilibrium Erosion of Soft Rock Shores with a Shallow or Absent Beach under Increased Sea Level Rise," *Marine Geology* 251(1):75–84.
- Wallace, J. M. and D. S. Gutzler. 1981. "Teleconnections in the Geopotential Height Field during the Northern Hemisphere Winter," *Monthly Weather Review* 109:784–812.
- Wang P. F., R. T. Cheng, K. Richter, E. S. Gross, D. Sutton, and J. W. Gartner. 1998. "Modeling Tidal Hydrodynamics of San Diego Bay, California," *Journal of the American Water Research Association* 34(5):1123–1140.
- White, N. J., J. A. Church, and J. M. Gregory. 2005. "Coastal and Global Averaged Sea Level Rise for 1950 to 2000," *Geophysical Research Letters 32*. L01601, DOI: 10.1029/2004 GL021391.
- Wolinsky, M. A. and A. B. Murray. 2009. "A Unifying Framework for Shoreline Migration: 2. Application to Wave-dominated Coasts," *Journal of Geophysical Research* 114(F1). F01009.
- Woodroffe, C. D. and C. V. Murray-Wallace. 2012. "Sea-level Rise and Coastal Change: The Past as a Guide to the Future," *Quaternary Science Reviews* 54:4–11.
- Worts, G. F., Jr., and R. F. Boss. 1954. "Geology and Ground-water Resources of Camp Pendleton, California." U.S. Geological Survey Administrative Report.
- Yamada, K., P. D. Nunn, N. Mimura, S. Machida, and M. Yamamoto. 1995. "Methodology for the Assessment of Vulnerability of South Pacific Island Countries to Sea-level Rise and Climate Change." *Journal of Global Environmental Engineering* 1:101–125.

- Yates, M. L, R. T. Guza, and W. C. O'Reilly. 2009. "Beach Shoreline Change: Observations and Equilibrium Modeling," Journal Geophysical Research 114. C09014, doi:10.1029/2009JC005359.
- Young, A. P., R. T. Guza, R. E. Flick, W. C. O'Reilly, and R. Gutierrez. 2009. "Rain, Waves, and Short-term Evolution of Composite Seacliffs in Southern California," *Marine Geology* 267:1–7.
- Young, A. P. and Ashford, S. A. 2006. "Application of Airborne LIDAR for Seacliff Volumetric Change and Beach-sediment Budget Contributions," *Journal Coastal Research* 22(2):307–318.
- Young, A. P., R. E. Flick, W. C. O'Reilly, D. B. Chadwick, R. T. Guza, W. C. Crampton, and J. J. Helly. 2014. "Estimating Cliff Retreat in Southern California Considering Sea Level Rise using a Sand Balance Approach," *Marine Geology* 348:15–26.
- Young, A. P., R. T. Guza, W. C. O'Reilly, R. E. Flick, and R. Gutierrez. 2011. "Short-term Retreat Statistics of a Slowly Eroding Coastal Cliff," *Natural Hazard and Earth System Science 11*: 205–217.
- Young, A. P., M. J. Olsen, N. Driscoll, R. E. Flick, R. Gutierrez, R. T. Guza, E. Johnstone, and F. Kuester. 2010b. "Comparison of airborne and terrestrial LiDAR estimates of seacliff erosion in southern California," *Photogrammetric Engineering and Remote Sensors* 76(4):421–428.
- Young, A. P., J. H. Raymond, J. Sorenson, E. A. Johnstone, N. W. Driscoll, R. T. Guza, and R. E. Flick. 2010a. "Coarse Sediment Yields from Seacliff Erosion in the Oceanside Littoral Cell," *Journal of Coastal Research* 26(3):580–585.
- Zetler, B. D. and R. E. Flick. 1985a. "Predicted Extreme High Tides for California, 1983-2000," Journal of Waterway Port, Coastal and Ocean Engineering, American Society of Civil Engineers 111(4):758–765.
- Zetler, B. D. and R. E. Flick. 1985b. "Predicted Extreme High Tides for Mixed-tide Regimes," *Journal of Physical Oceanography* 15(3):357–359.
- Zhang K., B. C. Douglas, and S. P. Leatherman. 2004. "Global Warming and Long-term Sandy Beach Erosion," *Climatic Change* 64(1–2):41–58.
- Zhang, K. 2010. "Analysis of Non-linear Inundation from Sea-level Rise using LIDAR Data: A Case Study for South Florida," *Climatic Change 106(4):537–565*.

APPENDICES

APPENDIX A: SUPPORTING DATA

The supporting data appendices are entirely composed of digital files that represent the key data products that were derived from our models and methodologies, and on which the analysis of the report is based. The following appendices are included on the digital media associated with the report which are available upon request and subject to approval of the report sponsor, the report authors and the installations.

Appendix A1. Sea Level Scenarios

Appendix A2. Baseline Terrain Models

Appendix A3. Installation Infrastructure Models

Appendix A4. Exposed Shoreline Response – Erosion Footprints

Appendix A5. Exposed Shoreline Response – Elevation Models

Appendix A6. Exposed Shoreline Response – Inundation and Flooding Footprints

Appendix A7. Protected Shoreline Response – Inundation and Flooding Footprints

Appendix A8. Groundwater Response – Varying Boundary Condition Results

Appendix A9. Receptor Level Response – Naval Base Coronado

Appendix A10. Receptor Level Response – Marine Corps Base Camp Pendleton

APPENDIX B: LIST OF SCIENTIFIC/TECHNICAL PUBLICATIONS

Publications – Published or Submitted

- Bromirski, P. D., A. J. Miller, R. E. Flick, and G. Auad. 2011. "Dynamical Suppression of Sea Level Rise Along the Pacific Coast of North America: Indications for Imminent Acceleration," *Journal of Geophysical Research C* 116 C07005.
- Chadwick, D. B, R. Flick, J. Helly, T. Nishikawa, P.F. Wang, W. O'Reilly, R. Guza, P. Bromirski, A. Young, W. Crampton, B. Wild, and I. Canner. 2011. "A Framework for Sea Level Rise Vulnerability Assessment for Southwest U.S. Military Installations," *Proceedings of the IEEE Oceanic Engineering Society and The Marine Technology Society (Oceans 11)*, 110426-001.
- Crampton, W. F. and R. E. Flick. 2012. "Wave Runup Study, South Beach Restroom Project, Avenida Del Sol, Coronado, California." TerraCosta Consulting Group Report. Prepared for City of Coronado, Coronado, CA.
- Flick, R. E. 2013. "City of Los Angeles, Coastal Issues Related to Future Mean Sea Level Rise," TerraCosta Consulting Group Report. Prepared for Mayor's Office City of Los Angeles, Los Angeles, CA.
- Flick, R. E., D. B. Chadwick, J. Briscoe, and K. C. Harper. 2012. "Flooding" versus "Inundation." *Eos, Transactions of the American Geophysical Union 93(38)*:365-366.
- Flick, R. E., K. Knuuti, and S. K. Gill. 2013. "Matching Mean Sea Level Rise Projections to Local Elevation Datums," *Journal of Waterway, Port, Coastal and Ocean Engineering 139*(2):142-146. http://dx.doi.org/10.1061/(ASCE)WW.1943-5460.0000145.
- Flick, R. E., W. C. O'Reilly, P. D. Bromirski, A. P. Young, and R. T. Guza. 2010. "A Framework for the Assessment of Sea Level Rise Vulnerability at Coastal Military Installations, Marine Corps Base Camp Pendleton and Naval Station Coronado." TerraCosta Consulting Group Report prepared for Computer Sciences Corporation, San Diego, CA.
- Guza, R. T. and F. Feddersen. 2012. "Effect of Wave Frequency and Directional Spread on Shoreline Runup," *Geophysical Research Letters 39*. L11607.
- Young, A.P., P. N. Adams, W. C. O'Reilly, R. E. Flick, and R. T. Guza. 2011. "Coastal Cliff Ground Motions from Local Ocean Swell and Infragravity Waves in Southern California," *Journal of Geophysical Research C* 116. C09007.
- Young, A. P., R. T. Guza, W. C. O'Reilly, R. E. Flick, and R. Gutierrez. 2011. "Short-term Coastal Cliff Retreat Statistics at Sunset Cliffs Point Loma, California, USA." *Natural Hazard and Earth System Science 11*:1-13.
- Young, A. P., R. E. Flick, W. C. O'Reilly, D. B. Chadwick, R. T. Guza, W. C. Crampton, and J. J. Helly. 2014. "Estimating Cliff Retreat in Southern California Considering Sea Level Rise using a Sand Balance Approach," *Marine Geology* 348:15-26.

In Preparation

Chadwick, D. B., R. E. Flick, J. Helly, T. Nishikawa, I. Canner, W. C. O'Reilly, A. P. Young, P.F. Wang, and M. Brand. In prep. "A Methodology for Assessing the Impact of Sea Level Rise on Representative Military Installations in the Southwestern U.S. SSC Pacific Technical Report.

- Chadwick, D. B., R. E. Flick, A. P. Young, J. J. Helly, W. C. O'Reilly, and R. T. Guza. In prep. "Long- and Short-Term Low-Lying Southern California Shoreline Response to Future Sea Level Rise and Waves Using a Sand Balance Approach, Coastal Engineering."
- Wang, P.F., D. B. Chadwick, R. E. Flick, J. J. Helly, J. McDonald, and W.H. Choi. In prep. "Modeling Wave Runup from Climate Change and Sea Level Rise for Two Southern California Beaches (Naval Base Coronado and Camp Pendleton) Using XBeach Model."

Planned

- Flick, R. E., D. B. Chadwick, W. C. O'Reilly, A. P. Young, R. T. Guza, and J. J. Helly. In prep. "Application of a Cross-shore Equilibrium Beach Width Model to Historical Data Coronado, CA.
- Flick, R. E., W. C. O'Reilly, and W. F. Crampton, J. Strampe, and J. Steinbeck. In prep. "A Decade of Beach Width Change at Avila Beach."
- Young, A. P., R. E. Flick, W. C. O'Reilly, and W. P. Crampton. In prep. "Recent Deep-seated Landsliding at San Onofre State Beach.

APPENDIX C: GLOSSARY

Adaptation: Adaptation is actions that can be implemented or that occur autonomously as a response to changes in the climate that harness and leverage its beneficial opportunities or ameliorate its negative effects (NRC, 2010).

Adaptive Capacity: Represents the "ability of a system to adjust to climate change (including climate variability and extremes) to moderate potential damages, to take advantage of opportunities, or to cope with the consequences" (McCarthy *et al.*, 2001; US EPA, 2013b; Smit and Pilifosova, 2001).

Autonomous Adaptation: Autonomous adaptation is "adaptation that does not constitute a conscious response to climatic stimuli but is triggered by ecological changes in natural systems and by market or welfare changes in human systems". (Jones, 2001; Adaptation Fund, 2013).

Climate Change: Climate change refers to "any significant change in the measures of climate lasting for an extended period of time. In other words, climate change includes major changes in temperature, precipitation, or wind patterns, among others, that occur over several decades or longer". (U.S. EPA, 2013b).

Exposure: Exposure is the degree of climate stress upon a particular unit analysis; it may be represented as either long-term change in climate conditions, or by changes in climate variability, including the magnitude and frequency of extreme events (IPCC, 2001).

Flooding and Inundation: Although "flooding" and "inundation" often have been used interchangeably, some authors (Flick *et al.* 2012) suggest that "flooding" better describes normally dry areas that become wet, but then eventually dry again. For the purposes of this study, we distinguished these terms based on the frequency of the wetting, using inundation to refer to conditions under which the wetting becomes regular (at least weekly to monthly), and flooding to refer to more rare and irregular events (yearly or longer).

Impact: The positive or negative effect on the natural or built environment caused by climate variability or change. Climate variability and change can have multiple impacts on people and communities, infrastructure and the services it provides, and ecosystems and natural resources.

Pathway: In the context of Source-Pathway-Receptor model used in this project, a pathway is the process that forms the connection between a sea-level related hazard (source), and a military installation element that is subject to harm from that hazard (receptor).

Receptor: In the context of Source-Pathway-Receptor model used in this project, a receptor is a military installation element or class of elements that is subject to harm from a sea-level related hazard (source).

Resilience: Resilience represents "a capability to anticipate, prepare for, respond to, and recover from significant multi-hazard threats with minimum damage to social well-being, the economy, and the environment". (US EPA, 2013b; UNFCCC, 1999).

Risk: A qualitative or quantitative measure of the combination of the magnitude of the potential consequence(s) of climate change impact(s) and the likelihood that the consequence(s) will occur (NRC 2010).

Scenario: A plausible and often simplified description of how the future may develop based on a coherent and internally consistent set of assumptions about driving forces and key relationships. (US EPA, 2013b).

Sensitivity: The degree to which a system is affected, either adversely or beneficially, by climate variability or change. (IPCC, 2007b; Smith *et al.*, 2001).

Source: In the context of Source-Pathway-Receptor model used in this project, a source is a sealevel related hazard (source).

Validation: The process of determining the degree to which a model is an accurate representation of the real world from the perspective of the intended uses of the model.

Vulnerability: In general, the degree to which a system is susceptible to, or unable to cope with, the adverse effects of climate change, including climate variability and extremes. Vulnerability is a function of exposure, sensitivity, and adaptive capacity. (NRC, 2010; IPCC, 1992). Research under this statement of need did not focus significantly on adaptation, so in the context of this project we also use vulnerability to describe the combination of exposure and sensitivity without full consideration of adaptive capacity.

REPORT DOCUMENTATION PAGE

Form Approved OMB No. 0704-01-0188

The public reporting burden for this collection of information is estimated to average 1 hour per response, including the time for reviewing instructions, searching existing data sources, gathering and maintaining the data needed, and completing and reviewing the collection of information. Send comments regarding this burden estimate or any other aspect of this collection of information, including suggestions for reducing the burden to Department of Defense, Washington Headquarters Services Directorate for Information Operations and Reports (0704-0188), 1215 Jefferson Davis Highway, Suite 1204, Arlington VA 22202-4302. Respondents should be aware that notwithstanding any other provision of law, no person shall be subject to any penalty for failing to comply with a collection of information.

reformation if it does not display a currently valid OMB control number.

PLEASE DO NOT RETURN YOUR FORM TO THE ABOVE ADDRESS.

1. REPORT DATE (DD-MM-YYYY) April 2015	2. REPORT TYPE Final	3. DATES COVERED (From - To)
4. TITLE AND SUBTITLE	5a. CONTRACT NUMBER	
A Methodology for Assessing the Installation in the Southwestern Un	5b. GRANT NUMBER	
	5c. PROGRAM ELEMENT NUMBER	
	oration with	5d. PROJECT NUMBER
Marissa Brand UCSD Sar	n Consulting Group In Diego Supercomputing Center Ogical Survey	5e. TASK NUMBER
U.S. Geological Survey Moffatt &	Nichol	5f. WORK UNIT NUMBER
7. PERFORMING ORGANIZATION NAM	8. PERFORMING ORGANIZATION REPORT NUMBER	
SSC Pacific, 53560 Hull Street, Sa	TR 2037	
9. SPONSORING/MONITORING AGENCY NAME(S) AND ADDRESS(ES) Strategic Environmental Research and Development Program		10. SPONSOR/MONITOR'S ACRONYM(S)
4800 Mark Center Drive Suite 17D08 Attn: Dr. John Hall Alexandria, VA 22350-3605	11. SPONSOR/MONITOR'S REPORT NUMBER(S)	

12. DISTRIBUTION/AVAILABILITY STATEMENT

Approved for public release.

13. SUPPLEMENTARY NOTES

This is work of the United States Government and therefore is not copyrighted. This work may be copied and disseminated without restriction.

14. ABSTRACT

The objective of the project was to develop an analysis framework and methodologies for evaluation of coastal military installation vulnerabilities and test them under prescribed scenarios of increased local mean sea level (0.5 meters, 1.0 meters, 1.5 meters and 2.0 meters) over the next century. Methodologies were developed to assess the potential scope and magnitude of impacts from physical effects of flooding (wetting that occurs infrequently), inundation (wetting occurs regularly), erosion, seawater intrusion, and alteration of tidal flows. Assessment methodologies targeted potential vulnerabilities of buildings, civil infrastructure, training areas, and waterfront and coastal structures. The project focused on conditions in the southwestern United States (U.S.) and utilized the key coastal military installations at Naval Base Coronado (NBC) and Marine Corps Base Camp Pendleton (MCBCP) to test the approach.

15. SUBJECT TERMS								
Mission Area: Environmental Science sea level rise seawater intrusion sea level variability shoreline erosion		military infrastructure vulnerability assessment		sediment wave models	waterfront structures wave runup			
		17. LIMITATION OF 18. NUMB		19a. NAME OF RESPONSIBLE PERSON				
a. REPORT	b. ABSTRACT	c. THIS PAGE	ABSTRACT	PAGES	Bart Chadwick 19B. TELEPHONE NU	MBER (Include area code)		
U	U	U	U	597	(619) 553-5333			

INITIAL DISTRIBUTION

84300	Library	(2)			
85300	Archive/Stock	(1)			
71750	M. Brand	(1)			
71750	B. Chadwick	(1)			
71750	P. F. Wang	(1)			
	_				
Defense Technical Information Center					
Fort Belvoir, VA 22060–6218					

Approved for public release.



SSC Pacific San Diego, CA 92152-5001